

FOODS

Volume 13
Issue 2
2025

ISSN 2308-4057 (print)

ISSN 2310-9599 (online)

and raw materials



food production technology

food production
processes
and equipment

nutrition

veterinary

biotechnology

biological sciences

chemistry and ecology

standardization,
certification, quality and safety



Foods and Raw Materials reports pioneering research in the food industry and agricultural science. We publish the results of fundamental and applied research as scientific papers, peer reviews, brief scientific reports, etc. The Journal is a single platform for scientific communication.

Foods and Raw Materials has been published in the English language since 2013. Two volumes a year come out in print and online.

All submitted manuscripts are checked for plagiarisms via *antiplagiat.ru* and undergo a double-blind peer review. Authors are responsible for the content of their article. As the Journal is fully supported by the Kemerovo State University, we do not charge for submission, translation, peer-review, or publication.

Foods and Raw Materials is an open access journal (CC BY 4.0). Our open access policy follows the Budapest Open Access Initiative (BOAI), which means that all our articles are available online immediately upon publication. Full-text electronic versions of all published materials appear in open access on *jfrm.ru/en* and *elibrary.ru*

Foods and Raw Materials is included in the following international data-bases: Scopus, Emerging Sources Citation Index (Web of Science Core Collection), DOAJ, CAS, FSTA, ResearchBib, WJCI, Dimensions, LENS.ORG, Scilit, CNKI, ProQuest, CABI, Agricola, Ulrich's, Google Scholar, OCLC WorldCat, and "White list" (Russia) – 1 level.

For submission and subscription instructions, please visit us online at *jfrm.ru/en*

Editor-in-Chief

Alexander Yu. Prosekov, Dr. Sci. (Eng.), Dr. Sci. (Biol.), Professor, Academician of RAS, Kemerovo State University, Kemerovo, Russia.

Deputy Editor-in-Chief

Olga O. Babich, Dr. Sci. (Eng.), Associate Professor, Immanuel Kant Baltic Federal University, Kaliningrad, Russia.

Editorial Board

Levent Bat, Ph.D., Professor Dr., University of Sinop, Sinop, Turkey;

Yogesh Shrinivas Gat, Ph.D., Institute of Chemical Technology, Mumbai, India;

Irina M. Donnik, Dr. Sci. (Biol.), Professor, Academician of RAS, Kurchatov Institute, Moscow, Russia;

Nishant Kumar, Ph.D., National Institute of Food Technology Entrepreneurship and Management, Sonapat, India;

Fatimetuzzehra Küçükbay, Ph.D., Professor Dr., İnönü University, Malatya, Turkey;

Andrey B. Lisitsyn, Dr. Sci. (Eng.), Professor, Academician of RAS, V. M. Gorbатов Federal Research Center for Food Systems of Russian Academy of Sciences, Moscow, Russia;

Yang Li, Dr. Sci. (Eng.), Professor, College of Food Science, Northeast Agricultural University, Harbin, China;

Abdalbasit Adam Mariod, Ph.D., Professor, University of Jeddah, Alkamil, Saudi Arabia;

Philippe Michaud, Ph.D., Professor, Université Clermont Auvergne, Polytech Clermont Ferrand, Aubiere, France;

Mehran Moradi, Doctor of Veterinary Medicine, Ph.D., Urmia University, Urmia, Iran;

Gláucia Maria Pastore, Ph.D., Professor, Campinas University, Campinas, Brazil;

Shirish Hari Sonawane, Ph.D., Professor, National Institute of Technology Warangal, Telangana, India;

Diako Khodaei, Ph.D., Technical University of Dublin, Dublin, Ireland.

Scientific Editor

Galina V. Gurinovich, Dr. Sci. (Eng.), Professor, Kemerovo State University, Kemerovo, Russia;

Tatyana F. Kiseleva, Dr. Sci. (Eng.), Professor, Kemerovo State University, Kemerovo, Russia;

Alexey M. Osintsev, Dr. Sci. (Eng.), Professor, Kemerovo State University, Kemerovo, Russia.

Executive Editor

Anna I. Loseva, Dr. Sci. (Eng.), Kemerovo State University, Kemerovo, Russia.

Founder and Publisher: Kemerovo State University, 6, Krasnaya St., Kemerovo, Kemerovo region – Kuzbass, 650000, Russia

Editorial Office: Kemerovo State University, 6, Krasnaya St., Kemerovo, Kemerovo Region – Kuzbass, 650000, Russia; phone: +7(3842)58-81-19; e-mail: fjournal@mail.ru

Printing Office: Kemerovo State University, 73, Sovetskiy Ave., Kemerovo, Kemerovo Region – Kuzbass, 650000, Russia

Translators: Oxana Yu. Pavlova, Nadezda V. Rabkina

Publishing editors: Ekaterina V. Dmitrieva

Literary editor: Anastasia Yu. Kurnikova

Computer layout and design: Elena V. Volkova

Cover image: image from <https://tr.pinterest.com/cziegler63/getränke/>

Photos credits: contributors

Date of publishing

September 23, 2025

16+

Circulation 500 ex. Open price.

Subscription index in the Ural-Press online catalog – 40539.

The Federal Service for Supervision of Communications, Information Technology, and Mass Media (Roskomnadzor)

Media registration number PI series No. FS77-72606

© Layout, accompanying text, editorial and publishing design,

Kemerovo State University, 2025

Editor's column

Biotechnology is one of the engines of global economic growth. The global biotechnology market was valued at \$1.55 trillion in 2024 and is projected to reach \$4.61 trillion by 2034. The Russian biotechnology market amounted to 300 billion rubles in 2023. According to a May 2025 forecast from the Rosselkhozbank Center for Industry Expertise, the Russian biotechnology market is projected to top 4.2 million tons of produce, i.e., 700 billion rubles, by 2028. So far, it is about 325 billion rubles, which is 29% more than in 2018.

Biotechnology is a knowledge-intensive multidisciplinary industry that integrates life sciences, molecular biology, and engineering to design hi-tech goods and services in the fields of healthcare, production, agriculture, forestry, energy, and ecology. Biomedicine and biopharmaceuticals are its largest segment: 41.73% of the global market. Industrial biotechnology accounts for 24.33% while agrobiotechnology and bioenergy are responsible for 20.78%. Other segments, e.g., bioinformatics, take up 13.16%. According to the BusinesStat analytical agency, the Russian medical and pharmaceutical biotechnology market increased its turnover by 9% between 2023 and 2024 to reach a total of 311 billion rubles. Agriculture accounts for 26% of the Russian biotechnology market, i.e., 149 billion rubles. Food biotechnology is projected to take 14% of Russia's total biotechnology market by 2026.

The current geopolitical situation challenges Russia to develop its own sustainable biotechnologies for the sake of the national healthcare and food security. In addition, independence from imported chemicals is bound to prevent domestic environmental problems. When resources are limited and applications are numerous, the business demand inevitably increases.

Russia's agro-industrial complex uses biotechnology to facilitate its import relief and increase efficiency. Biotechnology significantly boosts crop yields by making biotech crops resistant to pests, diseases, and droughts. It improves the productivity, health, and well-being of farm animals. For example, microbial consortia may prevent feed spoilage while beneficial enzymic preparations improve digestion, thus increasing the nutritional value of the feed. In addition, reproductive and genetic technologies render conventional animal breeds with useful qualities. Russian agriculture sees animal selection and genetics as its strategic priority, integrating them into the National Project on Technological Support for Food Security.

Biotech foods are functional and environmentally friendly. They fortify human diet with such valuable components and

additives as enzymes, probiotics, and proteins. Biotechnologies advance fermentation, as well as clarify juices and wines. They facilitate deep processing of non-traditional and secondary raw materials for cheaper and better finished products.

As Russian biotechnology market keeps growing, so does its share of food technologies. Food biotechnology opens up new opportunities for national food security, expanding the food range and reducing environmental pollution.


Professor Lyubov V. Rimareva, Doctor of Engineering Sciences and Academician of the Russian Academy of Sciences, holds the title of Honored Scientist of the Russian Federation in the field of food biotechnology. Her fundamental and applied research focuses on nanobiotechnology, biosynthesis, and fermentation in food processing.

Professor Rimareva founded a scientific school of industrial enzyme biotechnology and biocatalysis of plant and microbial raw materials. The list of her biotechnological achievements includes commercial strains of yeast and mycelial fungi that produce ethanol, enzymes, and protein. Professor Rimareva and her team design novel biocatalytic and biosynthetic technologies for enzymes, organic acids, and other functional ingredients, as well as bioactive food and feed additives.

Her numerous biotechnological inventions help agricultural storage and processing in Russia and abroad. They have resulted in a wide range of competitive biotechnological productions that yield bioactive functional products. The highly productive microbial strains tested in her laboratories are at work in the enzyme and alcohol industries in the Russian Federation and the CIS. These strains exercise an enormous economic and social effect on agricultural science and technology by reducing heat and energy consumption while optimizing the use of raw materials. New microbial strains boost biotechnological processes, increase production profitability, and create high-quality competitive products.

Professor Rimareva is a respected member of international academia and an exceptional scientific advisor. Her reports on biotechnology, fermentation, alcohol production, bioactive substances, and functional products are the highlight of every scientific conference she participates in.

We congratulate Professor Rimareva on her anniversary, which she celebrates on September 28, and wish her good health, inexhaustible energy, and inspiration for new ideas and scientific achievements, as well as happiness and peace shared with her family, colleagues, and students!

Editor-in-Chief,
Academician of the Russian Academy of Sciences,
Honored Worker of Higher Education of the Russian Federation,
Laureate of the Russian Federation Government Prize in Science and Technology,
Professor A. Yu. Prosekov 





Fermented buttermilk drinks fortified by plant raw materials

Ekaterina I. Reshetnik^{1,*}, Svetlana L. Griбанова¹, Yulia I. Derzhapolskaya¹,
Chun Li², Libo Liu², Guofang Zhang², Nadezhda Yu. Korneva¹, Pavel N. Shkolnikov¹

¹ Far Eastern State Agrarian University^{ROR}, Blagoveshchensk, Russia

² Northeast Agricultural University^{ROR}, Harbin, China

* e-mail: soia-28@yandex.ru

Received 18.03.2024; Revised 02.05.2024; Accepted 04.06.2024; Published online 16.10.2024

Abstract:

The research featured fortified fermented drinks from pasteurized buttermilk with such natural additives as Jerusalem artichoke syrup and beetroot dietary fiber.

The optimal symbiotic culture included *Streptococcus thermophilus* and *Lactobacillus delbrueckii* subsp. *bulgaricus*: it provided rapid fermentation and a creamy, homogeneous structure with delta pH time = 3.5 h. Jerusalem artichoke syrup was added in amounts of 3, 6, and 9%. Its optimal share proved to be 6% by the weight of the finished product. Beet dietary fiber was added in amounts of 2, 4, and 6%, where the optimal amount was 4%. A higher percentage affected the consistency of the finished product but not its clotting or taste. The experimental drinks were produced by the tank method and fermented at $42 \pm 2^\circ\text{C}$ until dense clotting and titratable acidity = $72 \pm 2^\circ\text{T}$. The finished product was stored at $4 \pm 2^\circ\text{C}$. The shelf-life was 12 days for the sample with Jerusalem artichoke syrup and 14 days for the drink fortified with beetroot fiber. The physical and chemical indicators showed that the energy value of the fortified fermented buttermilk drinks was by 45.3% lower compared to conventional fermented dairy drinks.

As a result of research, it has been established that the use of plant components, namely Jerusalem artichoke syrup and beet dietary fiber in the production technology of fermented milk drink from buttermilk makes it possible to obtain a finished product with improved consumer properties.

Keywords: Starter cultures, fermented drinks, buttermilk, plant components, quality indicators, shelf-life

Please cite this article in press as: Reshetnik EI, Griбанова SL, Derzhapolskaya Yul, Li C, Liu L, Zhang G, *et al.* Fermented buttermilk drinks fortified by plant raw materials. Foods and Raw Materials. 2025;13(2):211–218. <https://doi.org/10.21603/2308-4057-2025-2-637>

INTRODUCTION

Healthy diet, food safety, and hygiene have become the main lifestyle concepts as the constantly improving living standards and industrial technologies increase people's health awareness [1–4]. Obesity and cardiovascular diseases are associated with foods that are high in cholesterol and saturated fatty acids. Therefore, plant proteins have good potential regarding healthy nutrition [5–7].

As a result, the food industry gradually turns to plant raw materials [8–11]. For instance, secondary dairy raw materials represent a promising direction. Processing enterprises often use them irrationally. However, secondary dairy raw materials can become part of functional foods if fortified with renewable plant raw materials of high nutritional value [12–14].

The Far Eastern region boasts a wide variety of plants with functional and physiological components. As part of

human diet, they can increase nonspecific resistance to stress and adverse environmental conditions [15, 16].

Buttermilk is a by-product of butter production. It contains all main components of milk, i.e., protein, lactose, milk fat, and minerals. In addition, it also contains vitamins and phospholipids, not to mention macro- and microelements. Buttermilk has an overall beneficial effect on human body. As its calorie content is very small, it can be classified as a dietary drink. However, buttermilk gives so much strength and vigor that it is sometimes regarded as an energy drink. Technological properties of buttermilk depend on its composition and physicochemical parameters [17, 18]. Its physical indicators are similar to those of skimmed milk [19]. The acidity of buttermilk depends on the production method and the type of butter produced. If the buttermilk was obtained by the churning method as a by-product of

sweet cream butter, its titratable acidity ranges between 18 and 20°T while its pH is 6.53–6.59. If the buttermilk came from butter processed by high-fat cream conversion, its titratable acidity and active acidity are 17–18°T and pH 6.52–6.60, respectively.

The market of buttermilk drinks is growing quite rapidly, following the changes in consumption culture. The main market segments have already been occupied; yet, they demonstrate some prospective niches, e.g., fermented milk or buttermilk-based diet drinks.

In the near future, consumers will turn to high-quality products that fortified with functional natural ingredients and contain neither artificial dyes nor preservatives [20–22].

The most probable food plant components for buttermilk drinks are some popular plant additives, e.g., Jerusalem artichoke syrup and beetroot dietary fiber. These plant additives have a natural taste and render the finished product a beautiful color or pleasant aroma [23, 24].

Jerusalem artichoke syrup is a natural sweetener that has a consumer-appealing taste and meets the most rigorous scientific requirements for a healthy diet. Jerusalem artichoke syrup has a low glycemic index of 15: for comparison, the glycemic index of white sugar is 70. Therefore, even patients with diabetes may consume it in moderate quantities, both as a sweetener and for therapeutic and prophylactic purposes. Table 1 illustrates the main properties of Jerusalem artichoke syrup.

Jerusalem artichoke tuber syrup is a highly concentrated natural and environmentally friendly plant extract with physiologically active components. It contains at least 70% solids and more than 60% biologically active reducing substances. Unfiltered syrup is thick and has a sweet caramel flavor. Jerusalem artichoke tuber syrup contains vitamins B₁, B₂, C, PP, pectin, and probiotic inulin. Due to its sweet caramel flavor, Jerusalem artichoke tuber syrup can serve as a healthy natural sugar substitute with a low glycemic index.

Dietary fiber is currently one of the most common ingredients in functional foods. Dietary fiber comes from products of plant origin. It undergoes fermentation in the upper gastrointestinal tract and acts as a prebiotic for healthy intestinal microflora. When regularly consumed, dietary fiber has a beneficial biological effect on people of all ages.

If consumed regularly, beetroot dietary fiber prevents dysfunction of the gastrointestinal tract, as well as various pathological processes. It helps the body to get rid of nitrates and nitrites, bile acids, cholesterol, peroxide compounds, toxic elements, pesticides, radionuclides, and waste. Beetroot dietary fiber normalizes intestinal motility, accelerates intestinal transit, removes pathogenic microflora, and regulates metabolism. It reduces cholesterol, glucose, and urea in the blood while maintaining the antitoxic liver function. In addition, it optimizes fermentation processes in the intestines, as well as prevents cholelithiasis and diabetes. A comparative analysis of beetroot fiber proved that it is superior to all food additives on domestic market. Beetroot fiber

demonstrated high protective, sorption, and mass transfer indicators, as well as good potential for preventing gastrointestinal and cardiovascular diseases [25–27].

Dietary fiber is part of a wide range of products with increased biological value, including functional foods.

Table 2 clearly demonstrates that beetroot fiber is a promising food component.

The research objective was to study the effect of plant components on the quality of fermented milk drinks from secondary dairy raw materials.

We rationalized the possibility of using Jerusalem artichoke syrup and beetroot dietary fiber as functional components in the production of fermented buttermilk drinks. Then, we selected the optimal amount of plant components to render the final product functional properties. Finally, we studied the physicochemical and microbiological indicators of the obtained fermented drinks.

STUDY OBJECTS AND METHODS

The research featured buttermilk, Jerusalem artichoke syrup, beetroot dietary fiber, and starter microorganisms that came in two versions: 1) *Streptococcus thermophilus* (strain No. CNCM I-2980) + *Lactobacillus delbrueckii* subsp. *bulgaricus* and 2) *S. thermophilus* + *L. delbrueckii* subsp. *bulgaricus*. They were lyophilized milk cultures intended for direct addition to the milk base.

The experimental samples were fermented milk drinks with Jerusalem artichoke syrup in amounts of 3, 6 and 9% and fermented drinks with beet dietary fiber in amounts of 2, 4 and 6%. The control sample was a fermented milk drink without plant components.

Table 1 Jerusalem artichoke syrup

Indicator	Content per 100 g
Mass fraction of carbohydrates, %	69.5
Energy value, kcal	254.0

Table 2 Main indicators of bleached beet fibers

Indicator	Value
Mass fraction of fiber, %	23.0–28.0
Mass fraction of lignin, %	7.0–9.0
Mass fraction of pectin substances, %, including:	
water-soluble pectin substances	10.0–12.0
water-insoluble protopectin	8.0–10.0
Protein, %	7.0–8.0
Mass fraction of minerals, % (K – 0.2%; N ₃ – 0.4%; Ca – 0.8%; Mg – 0.4%; P – 0.25%)	3.5–5.0
Moisture-binding coefficient	5.0–5.5
Fat-binding coefficient	1.4–1.5
Color change during mass during hydration	does not change color
pH of water extract	4.3–4.6
Flavor	absent
Taste, aftertaste	sourish
Average fraction size, mm	0.120
Energy value, kcal/100 g	55.0–60.0

In this research, we analyzed the chemical composition, biological value and safety indicators of Jerusalem artichoke syrup and beet fibers as well as the nutritional and energy value of fermented milk drinks based on these plant components. The shelf-life of the finished products was determined using microbiological indicators and sensory assessment.

The research involved standard methods. The sensory, physicochemical, and microbiological methods made it possible to assess the quality of raw materials and product samples. The experiment took into account the chemical composition, physical properties, and microbiological indicators of the plant components.

The synergistic properties of clotting were determined by the amount of whey released by 10 cm³ of a crushed clot during centrifugation at 1000 rpm for 5 min.

We used the formula below to calculate the energy value for 100 g of product based on the coefficients of nutrient absorption:

$$\text{Energy value} = P \times 4.0 + F \times 9.0 + C \times 4.0$$

where *P*, *F*, and *C* mean proteins, fats, and carbohydrates, respectively, contained in g/100 g of the product.

The review of related publications included scientific articles, technical literature, and patent information on fermented milk production.

RESULTS AND DISCUSSION

We studied the acid-forming ability of various starters on Sample 1, which included *Streptococcus thermophilus* (strain No. CNCM I-2980) and *Lactobacillus delbrueckii* subsp. *bulgaricus*, and Sample 2 with *S. thermophilus* and *L. delbrueckii* subsp. *bulgaricus*. The microbial strains were to give the product a pure fermented milk taste and good texture, as well as to facilitate acid formation. The ripening took place on heat-treated buttermilk. The buttermilk was heated at $95 \pm 2^\circ\text{C}$ for 15–20 s. After that, it was normalized to 10% solids and pH 6.60. Since the cultures had been stored at subzero temperatures, the bags were kept at room temperature for 50 min before opening. Before use, we made sure that the culture maintained its powder form. Before adding it to the milk base, we treated the starter with chlorinated water. The temperature of the mix was $42 \pm 2^\circ\text{C}$, i.e., $104\text{--}111.2^\circ\text{F}$. After 30 min of stirring, the samples were fermented at $42 \pm 2^\circ\text{C}$ for 6 h. The acidity accumulation was tested every hour (Table 3).

Figure 1 shows the effect of ripening time on the intensity of acid formation.

Both starter samples increased the titratable acidity in the fermented milk; however, the process proceeded more smoothly in Sample 1. During the entire fermentation period, the samples had a different titratable acidity increase rate. Sample 1 proved to be more efficient because it demonstrated the highest ripening speed and reached the pH delta of 1.35 in 3.5 h. In addition, Sample 1 had a better texture and superior sensory profile. Therefore, we selected the symbiotic starter

Table 3 Acidity accumulation in activated starter cultures

Time, h	pH	
	Sample 1	Sample 2
1	6.42 ± 0.15	6.53 ± 0.10
2	5.56 ± 0.15	5.97 ± 0.15
3	5.28 ± 0.10	5.74 ± 0.15
4	5.07 ± 0.10	5.50 ± 0.10
5	4.86 ± 0.10	5.31 ± 0.10
6	4.68 ± 0.15	4.86 ± 0.10

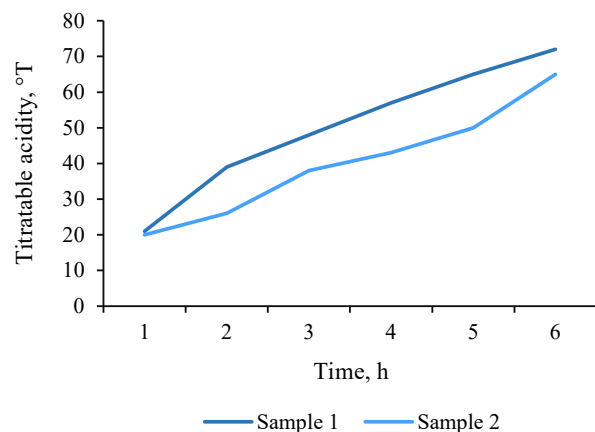


Figure 1 Intensity of acid formation in activated starter cultures

with *S. thermophilus* (strain No. CNCM I-2980) and *L. delbrueckii* subsp. *bulgaricus* for further research.

The amount of plant components in the formulation is known to affect the sensory properties of buttermilk drinks. We chose the optimal share of Jerusalem artichoke syrup, which amounted for 6%.

To evaluate the quality of the finished product, we used sensory indicators based on sight, smell, touch, and taste. The assessment was carried out by panelists and took place in the following order: appearance, consistency, taste, flavor, and color. Table 4 structures the sensory properties of buttermilk drink samples with different contents of Jerusalem artichoke syrup. A sample without Jerusalem artichoke syrup served as control.

The sample with 6% Jerusalem artichoke syrup demonstrated the best sensory characteristics.

To identify the optimal share of beetroot dietary fibers, we studied the synergetic properties of resulting clots. Dietary fibers were added in amounts of 2, 4, and 6%; a sample of fermented buttermilk drink without beetroot dietary fiber served as control (Table 5).

The water-holding capacity increased together with the mass fraction of beetroot dietary fiber in the samples, while the amount of whey released decreased.

We presumed that the increase in the content of beetroot dietary fiber had no effect on the taste of the finished product but changed its consistency. As a result, we added 4% of beetroot fiber by the weight of the finished product, since this amount of beet dietary fiber gave the best consistency to the product.

Table 4 Sensory profile of fermented buttermilk drink fortified with Jerusalem artichoke syrup

Indicator	Fermented buttermilk drink (control)	Fermented buttermilk drink with Jerusalem artichoke syrup in the amount of:		
		3%	6%	9%
Appearance	Homogeneous, moderately viscous	Smooth surface, no stratification	Smooth surface, no stratification	Smooth surface, no stratification
Consistency	Homogeneous, with crushed clots	Homogeneous, with crushed clots, no visible lumps	Homogeneous, with crushed clots, no visible lumps	Homogeneous, with crushed clots, no visible lumps
Taste and flavor	Pure, fermented milk, no atypical tastes or odors	Pure sour milk taste, and flavor	Moderately sweet taste, pure sour milk flavor	Sweet taste, pure sour milk flavor
Color	Milky white	Milky white and uniform	Milky creamy and uniform	Milky creamy and uniform

Table 5 Synergetic clotting properties in fermented buttermilk drink with beetroot dietary fiber

Centrifugation time, min	Whey released, mL			
	Control	Content of beetroot dietary fiber		
		2%	4%	6%
5	5.0	4.95	4.90	4.85
10	6.4	6.3	6.0	5.6
15	6.9	6.1	5.9	5.6
20	7.4	6.9	6.5	6.2
25	7.6	7.1	6.7	6.3
30	7.7	7.3	6.9	6.3

Fermented milk drinks can be produced by thermostatic or tank methods. In this research, we applied the tank method. The buttermilk was pasteurized at $95 \pm 2^\circ\text{C}$ for 15–20 s and cooled to the fermentation temperature of $42 \pm 2^\circ\text{C}$.

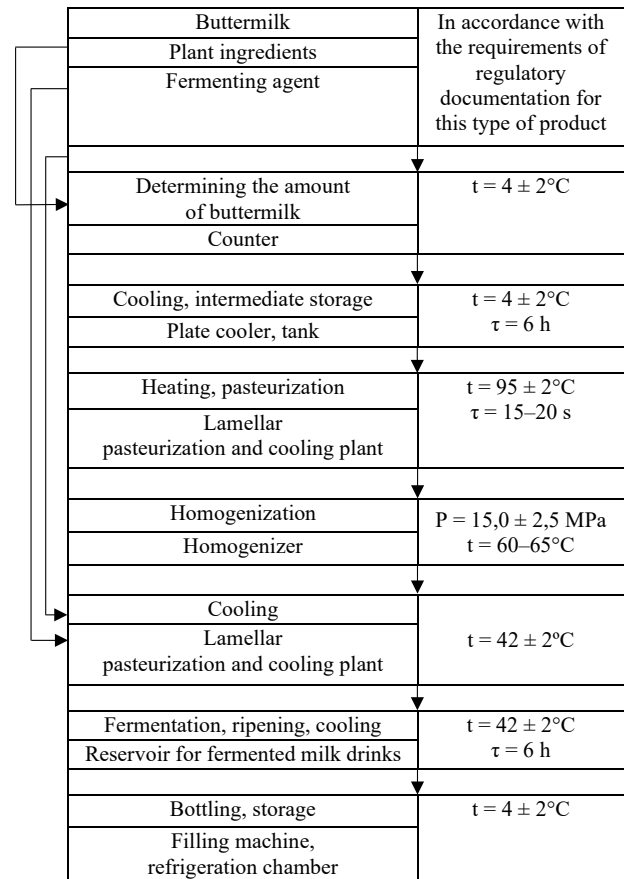
Figure 2 illustrates the technological scheme for fermented buttermilk drinks.

The thermostatic method required plant components to be added cooled down to the ripening temperature. With periodic stirring, the fermented mix was immediately poured into consumer containers and sent to a thermostatic chamber for fermentation. The ripening process ended when the clotting was sufficient and the acidity rose to $72 \pm 2^\circ\text{T}$. Then, the product immediately was moved to a refrigerator for cooling and storage.

Shelf-life characterizes the stability of products during storage. During storage at $4 \pm 2^\circ\text{C}$, we measured the changes in sensory properties, microbiological indicators, and titratable acidity (Table 6).

We counted probiotic microorganisms during 21 days with an interval of three days. On storage day 14, the probiotic microbial count in the experimental samples was higher than in the control sample (3×10^6 CFU/cm³): 1×10^8 CFU/cm³ in the sample with Jerusalem artichoke syrup and 3×10^8 CFU/cm³ in the sample with beetroot fiber.

On storage day 21, the count of lactic acid microorganisms decreased to 2×10^6 CFU/cm³ in the experimental sample with Jerusalem artichoke syrup and to 3×10^6 CFU/cm³ in the sample with beetroot fiber. In the control sample, it dropped down to 1×10^4 CFU/cm³. The results obtained violated the standards mentioned in Technical Regulations of the Customs Union TR CU 033/2013 regarding the amount of probiotic microflora in this type of product.

**Figure 2** Technological scheme for fermented buttermilk drinks**Table 6** Microbiological parameters of fermented buttermilk drinks during storage

Storage time, h	Microbial count, CFU/cm ³		
	Control	Fermented buttermilk drink with Jerusalem artichoke syrup	Fermented buttermilk drink with beetroot fiber
1	4×10^7	5×10^8	7×10^8
4	4×10^7	4×10^8	6×10^8
7	1×10^7	3×10^8	5×10^8
11	6×10^7	2×10^8	4×10^8
14	3×10^6	1×10^8	3×10^8
17	1×10^5	3×10^7	2×10^7
21	1×10^4	2×10^6	3×10^6

Table 7 Chemical composition: buttermilk drinks with Jerusalem artichoke syrup and beetroot fiber vs. industrially produced yogurt

Mass fraction, %	Control	Fermented buttermilk drink with Jerusalem artichoke syrup	Fermented buttermilk drink with beetroot dietary fiber
Fat	2.5	0.5	0.5
Carbohydrates	4.7	8.2	4.8
Protein	3.2	3.2	3.4
Dry skimmed milk residue	9.5	13.0	9.8
Dietary fiber	–	–	4.0

The titratable acidity of the samples met the requirements for this category of fermented milk products and ranged from 75 to 100°T. During the entire period of observation, the acidity in both samples did not exceed the standard values.

The experimental samples also showed sensory stability and good preservation during the entire storage period.

On storage day 17, the sample with beetroot fiber demonstrated signs of deterioration in appearance and consistency. In the sample with Jerusalem artichoke syrup, these processes became visible on storage day 14. In addition, $\geq 3\%$ whey got separated, and the samples started to emit a flavor not typical of fermented milk drinks.

Therefore, dietary fiber in the fermented buttermilk product improved its sensory profile and stabilized its consistency during storage.

The shelf-life of the fermented buttermilk drink with Jerusalem artichoke syrup was defined as 12 days at $4 \pm 2^\circ\text{C}$, and that of the drink with beetroot fiber was 14 days.

We relied on the content of proteins, fats, calcium, phosphorus, vitamins A, B-carotene, and B₂ to define the nutritional value of fermented buttermilk products. However, the nutritional value of fermented milk products mainly depends on the content of microorganisms and their metabolic products that inhibit putrefactive bacteria in the human gastrointestinal tract. It also includes lactic acid, which reduces the pH of the medium. Lactic acid products are digested thrice as fast as milk.

Fermented milk products are popular in clinical nutrition to improve gastric secretion and normalize intestinal motility in the treatment of colitis and gastritis. Lactic acid that enters the intestine with lactic acid products is neutralized, but lactic acid microorganisms endure and ferment food residues to create an acidic environment that kills putrefactive microorganisms.

Fermented milk drinks have a characteristic taste and consistency that meet the taste habits of the population. They differ in the microflora of fermentation starters. Table 7 compares the chemical composition of the experimental functional fermented buttermilk drinks with that of industrially produced yogurt.

Below is the formula we used to calculate the energy value of yogurt:

$$\text{Energy value} = 3.2 \times 4.0 + 0.5 \times 9.0 + 4.7 \times 4.0 = 36.10 \text{ kcal} \\ 36.10 \text{ kcal} \times 4.184 = 151.04 \text{ kJ}$$

The resulting energy value, or calorie content, of yogurt was 36.10 kcal/151.04 kJ.

The energy value of the fermented buttermilk drink with Jerusalem artichoke syrup was calculated as follows:

$$\text{Energy value} = 3.2 \times 4.0 + 0.5 \times 9.0 + 8.2 \times 4.0 = 50.10 \text{ kcal} \\ 50.10 \text{ kcal} \times 4.184 = 209.62 \text{ kJ}$$

The resulting energy value, or calorie content, of the buttermilk drink with Jerusalem artichoke syrup equaled 50.10 kcal/209.62 kJ.

We used the following formula to calculate the energy value of the buttermilk drink with beetroot fiber:

$$\text{Energy value} = 3.4 \times 4.0 + 0.5 \times 9.0 + 4.8 \times 4.0 = 37.30 \text{ kcal} \\ 37.30 \text{ kcal} \times 4.184 = 156.06 \text{ kJ}$$

The resulting energy value, or calorie content, of the fermented buttermilk drink with beetroot dietary fiber appeared to be 37.30 kcal/156.06 kJ.

Compared to a traditional yogurt, the fermented milk drinks based on buttermilk and Jerusalem artichoke syrup had low fat content, the same protein level and higher percentage of carbohydrates, while the milk drinks made from buttermilk with beet dietary fiber contained lower fat content, as well as relatively equal levels of protein and carbohydrates. In addition, the fermented milk drink with beet dietary fiber contained insoluble dietary fiber, which has a positive effect on the digestive system of the human body. The results obtained allow us to consider the developed products as low-calorie containing various nutritional factors.

The mass fraction of carbohydrates in the fermented buttermilk drink with Jerusalem artichoke syrup increased by 74.47% compared to the control sample. Jerusalem artichoke syrup contains such carbohydrates as inulin and fructose. As a result, sweetened fermented buttermilk products can be included in diabetic diets.

Table 8 shows the recipes for the developed fermented milk drinks made from buttermilk with plant ingredients based on 1 ton of the finished product. The recipes were selected based on the results of organoleptic studies.

Thus, Jerusalem artichoke syrup and beetroot dietary fiber improved the quality of fermented drinks from secondary milk raw materials and elevated them to the status of functional products. The amount of plant components in the formulation affected the sensory indicators of the buttermilk drinks. The optimal shares obtained were based on the sensory assessment.

Table 8 Developed recipes for fermented milk drinks made from buttermilk with plant ingredients

Components, kg	Fermented buttermilk drink with Jerusalem artichoke syrup	Fermented buttermilk drink with beetroot dietary fiber
Buttermilk	939.90	959.90
Sourdough (<i>Streptococcus thermophilus</i> (strain No. CNCM I-2980) and <i>Lactobacillus delbrueckii</i> subsp. <i>bulgaricus</i>)	0.10	0.10
Jerusalem artichoke syrup	60.00	–
Beet dietary fiber	–	40.00
Total	1000.00	1000.00

Drinks from secondary dairy raw materials allow for sustainable production; Jerusalem artichoke syrup and beetroot dietary fiber improve the sensory profile and consumer properties of finished products, making them functional. The results obtained were consistent with previous R&D publications on functional dairy products.

The data obtained correlate with the results of previous studies, while supplementing them with new information about the composition of products based on secondary dairy raw materials in the form of buttermilk and plant components.

CONCLUSION

The research rationalized the use of Jerusalem artichoke syrup and beetroot dietary fiber as functional additives. Beetroot dietary fiber had no effect on clotting and taste but changed the consistency of the final product.

The use of Jerusalem artichoke syrup allows you to obtain a fermented milk drink from buttermilk with a uniform consistency, a pleasant sweetish taste and a light creamy tint. Due to the unique chemical composition of Jerusalem artichoke syrup and the beneficial properties of dietary fiber, the developed fermented

milk drinks will have a functional effect on the human body when consumed daily in the diet.

A selected starter consisting of *Streptococcus thermophilus* (strain No. CNCM I-2980) and *Lactobacillus delbrueckii* subsp. *bulgaricus* can let intensify the technological process due to the rapid increase in titratable acidity with the formation of a dense clot.

The shelf-life of the experimental drinks at $4 \pm 2^\circ\text{C}$ was 12 days for the drink with Jerusalem artichoke syrup and 14 days for the drink with beetroot dietary fiber.

Buttermilk drinks can save raw milk resources and reduce the cost of the finished product because dairy by-products are cheap. In addition, they allow expanding the range of competitive products with high-quality sensory profiles and increased biological values.

CONTRIBUTION

All the authors were equally involved in the manuscript and are equally responsible for any potential plagiarism.

CONFLICT OF INTEREST

The authors declared no conflict of interests regarding the publication of this article.








REFERENCES

1. Prosekov AYu, Milent'eva IS, Loseva AI. Bioactive secondary metabolites isolated from plants cultivated *in vitro*. Kemerovo: Kemerovo State University; 2023. 211 p. (In Russ.). <https://www.elibrary.ru/LYZAUW>
2. Poznyakovskiy VM, Shamova MM, Avstriyevskikh AN, Vyalykh EV. Polysystem bioregulator based on the polyprenols for active health management. Food Industry. 2022;7(1):33–38. (In Russ.). <https://doi.org/10.29141/2500-1922-2022-7-1-4>; <https://www.elibrary.ru/XJQMFP>
3. Reshetnik E, Derzhapolskaya Yu, Gribanova S. Study of starter cultures in biotechnology of medical and preventive nutrition products. E3S Web of Conferences. 2020;203:04002. <https://doi.org/10.1051/e3sconf/202020304002>
4. Alloyarova YuV, Kolotova DS, Derkach SR. Nutritional and therapeutic potential of functional components of brown seaweed: A review. Foods and Raw Materials. 2024;12(2):398–419. <https://doi.org/10.21603/2308-4057-2024-2-616>; <https://elibrary.ru/RGPVXQ>
5. Ziaei R, Ghavami A, Khalesi S, Ghiasvand R, Mokari_yamchi A. The effect of probiotic fermented milk products on blood lipid concentrations: A systematic review and meta-analysis of randomized controlled trials. Nutrition, Metabolism and Cardiovascular Diseases. 2021;31(4):997–1015. <https://doi.org/10.1016/j.numecd.2020.12.023>
6. Khamagaeva IS, Zambalova NA, Tsyzhipova AV, Bubeev AT. The development of a biologically active additive to reduce the blood cholesterol level. E3S Web of Conferences. 2020;161:01093. <https://doi.org/10.1051/e3sconf/202016101093>
7. Zakipnaya E, Parfyonova S. Fortified sour-milk beverages with the use of the far eastern region's wild berries. In: Muratov A, Ignateva S, editors. Fundamental and applied scientific research in the development of agriculture

- in the far east (AFE-2021). *Agricultural innovation systems*, Volume 1. Cham: Springer; 2022. pp. 602–610. https://doi.org/10.1007/978-3-030-91402-8_67
8. Tikhonov S, Tikhonova N, Lazarev V, Zhang N. Ultra-high pressure food processing as a promising storage method. *AIP Conference Proceedings*. 2021;2419:050008. <https://doi.org/10.1063/5.0070936>
9. Pei M, Zhao Z, Chen S, Reshetnik EI, Gribova SL, Li C, et al. Physicochemical properties and volatile components of pea flour fermented by *Lactobacillus rhamnosus* L08. *Food Bioscience*. 2022;46:101590. <https://doi.org/10.1016/j.fbio.2022.101590>
10. Liang Z, Yi M, Sun J, Zhang T, Wen R, Li C, et al. Physicochemical properties and volatile profile of mung bean flour fermented by *Lactobacillus casei* and *Lactococcus lactis*. *LWT*. 2022;163:113565. <https://doi.org/10.1016/j.lwt.2022.113565>
11. Maslov AV, Mingaleeva ZSh, Yamashev TA, Starovoytova OV. Effects of a plant-based additive on the properties of flour and dough during fermentation. *Food Processing: Techniques and Technology*. 2023;53(2):347–356. <https://doi.org/10.21603/2074-9414-2023-2-2439>; <https://elibrary.ru/WVUMRP>
12. Nurtayeva Z. Analysis of qualitative and quantitative indicators of milk production and processing at the enterprises of the Akmola region. *Potravinarstvo. Slovak Journal of Food Sciences*. 2022;16:69–79. <https://doi.org/10.5219/1720>
13. Danilov AM, Bazhenova BA, Danilov MB, Gerasimov AV. Study of lysate activity to modify collagen raw materials to use in sausage mixture. *Foods and Raw Materials*. 2018;6(2):256–263. <https://doi.org/10.21603/2308-4057-2018-2-256-263>; <https://www.elibrary.ru/YTJKIP>
14. Bukharev AG, Gavrilova NB, Kriger OV, Chernopolskaya NL. Fermented cream for curd fortified with probiotic cultures: Biotechnological aspects. *Food Processing: Techniques and Technology*. 2021;51(4):664–673. (In Russ.). <https://doi.org/10.21603/2074-9414-2021-4-664-673>; <https://www.elibrary.ru/CYSJHL>
15. Kurbanova M, Voroshilin R, Kozlova O, Atuchin V. Effect of Lactobacteria on bioactive peptides and their sequence identification in mature cheese. *Microorganisms*. 2022;10(10):2068. <https://doi.org/10.3390/microorganisms10102068>
16. Starovoytova KV, Dolgolyuk IV, Tereshchuk LV. Probiotic lactic acid cultures in the production of vegetable cream spread. *IOP Conference Series: Earth and Environmental Science*. 2021;640:022077. <https://doi.org/10.1088/1755-1315/640/2/022077>
17. Tretyak LN, Artyukhova SI, Sarbatova NYu, Aryukhin OV, Zhumanova GT. Evaluation of the stability of the results of studies of beef for lead content using the additive method. *IOP Conference Series: Earth and Environmental Science*. 2021;677:042044. <https://doi.org/10.1088/1755-1315/677/4/042044>
18. Boiarineva IV, Khamagaeva IS, Muruyev IE. Optimization of nutrient medium composition to increase biomass of propionic acid bacteria and acidophilic bacteria. *IOP Conference Series: Earth and Environmental Science*. 2021;640:032059. <https://doi.org/10.1088/1755-1315/640/3/032059>
19. Statsenko ES, Litvinenko OV, Korneva NYu. Development of technology for a fermented soy-milk drink using soy grain varieties of Federal Scientific Centre All-Russian Research Institute of Soybeans Breeding. *Achievements of Science and Technology in Agro-Industrial Complex*. 2023;37(6):86–90. (In Russ.). https://doi.org/10.53859/02352451_2023_37_6_86; <https://www.elibrary.ru/HSPVUC>
20. Praskova YuA, Kiseleva TF, Shkrabak NV, Pomozova VA, Frolova NA. Study of the effect of enzymes on the clarification of juice from the fruits of Amur grapes. *IOP Conference Series: Earth and Environmental Science*. 2022;1052:012099. <https://doi.org/10.1088/1755-1315/1052/1/012099>
21. Rysmukhambetova GE, Beloglazova KE, Ushakova YuV, Kozhushko SYu, Karpunina LV. Development of sour milk products based on goat's milk on the example of yoghurt with dietary fiber. *Proceedings of the Voronezh State University of Engineering Technologies*. 2022;84(3):118–125. (In Russ.). <https://doi.org/10.20914/2310-1202-2022-3-118-125>; <https://www.elibrary.ru/VDIPFZ>
22. Pashina L, Pastushenko S, Reimer V. Innovative-oriented development of AIC complex as an economic priority development vector of the Far Eastern Federal District. *E3S Web of Conferences*. 2020;203:05012. <https://doi.org/10.1051/e3sconf/202020305012>
23. Pakusina A, Platonova T, Parilova T, Parilov M, Malinovsky N, Balan I. Ecological and chemical assessment of the habitats of cranes in the Khingan State Nature Reserve, Russia. In: Muratov A, Ignateva S, editors. *Fundamental and applied scientific research in the development of agriculture in the far east (AFE-2021). Agricultural innovation systems*, Volume 1. Cham: Springer; 2022. pp. 658–666. https://doi.org/10.1007/978-3-030-91402-8_73
24. Lisin PA, Moliboga EA, Trofimov IE. Parametric structural analysis of nutritional value of personalized foods using Microsoft Excel. *IOP Conference Series: Earth and Environmental Science*. 2021;624:012171. <https://doi.org/10.1088/1755-1315/624/1/012171>

25. Lantushenko E, Filipkina N, Dolgolyuk I, Starovoitova K, Tereshchuk L, Kozlova O. Study of properties of bacterial concentrates of lactic acid microorganisms. AIP Conference Proceedings. 2023;2817:020068. <https://doi.org/10.1063/5.0148295>
26. Tsyrendorzhieva SV, Zhamsaranova SD, Syngeyeva EV, Ipatova ND, Khamaganova IV, Badmaeva II. Development of ice cream technology enriched with an encapsulated form of vitamin C. IOP Conference Series: Earth and Environmental Science. 2021;640:032030. <https://doi.org/10.1088/1755-1315/640/3/032030>
27. Reshetnik EI, Griбанова SL, Derzhapolskaya YuI, Li Ch, Li Yu. Effect of soluble dietary fibers from *Larix dahurica* on dairy bioproducts. Dairy Industry. 2023;(6):62–65. (In Russ.). <https://doi.org/10.21603/1019-8946-2023-6-15>; <https://elibrary.ru/IAQFUT>

ORCID IDs

Ekaterina I. Reshetnik  <https://orcid.org/0000-0002-3166-9992>
Svetlana L. Griбанова  <https://orcid.org/0000-0003-1448-4328>
Yulia I. Derzhapolskaya  <https://orcid.org/0000-0002-1851-0063>
Chun Li  <https://orcid.org/0000-0003-1603-7222>
Guofang Zhang  <https://orcid.org/0000-0002-4616-2721>
Nadezhda Yu. Korneva  <https://orcid.org/0000-0001-8180-6070>
Pavel N. Shkolnikov  <https://orcid.org/0000-0003-3587-3082>



The phytochemical composition of Kuzbass medicinal plants

Natalia S. Velichkovich¹, Nina I. Dunchenko²,
Anna A. Stepanova¹, Oksana V. Kozlova¹, Elizaveta R. Faskhutdinova^{1,*},
Vladimir P. Yustratov¹, Sergey L. Luzyanin¹

¹ Kemerovo State University^{ROR}, Kemerovo, Russia

² Russian State Agrarian University – Moscow Timiryazev Agricultural Academy^{ROR}, Moscow, Russia

* e-mail: faskhutdinovae.98@mail.ru

Received 27.04.2024; Revised 02.07.2024; Accepted 06.08.2024; Published online 16.10.2024

Abstract:

Flavonoids are plant polyphenols that exhibit biological activity with antibacterial, antiviral, antioxidant, anti-inflammatory, antimutagenic, and anticarcinogenic effects. The medicinal plants of Kuzbass have high contents of flavonoids and other polyphenolic compounds. Therefore, they can be used in medicinal preparations to prevent or treat serious diseases.

We studied the following plants collected in Kuzbass: common thyme (*Thymus vulgaris* Linn., leaves and stems), woolly burdock (*Arctium tomentosum* Mill., roots), alfalfa (*Medicago sativa* L., leaves and stems), common lungwort (*Pulmonaria officinalis* L., leaves and stems), common yarrow (*Achillea millefolium* L., leaves and stems), red clover (*Trifolium pratense* L., leaves and stems), common ginseng (*Panax ginseng*, roots), sweetvetch (*Hedysarum neglectum* Ledeb., roots), and cow parsnip (*Heracleum sibiricum* L., inflorescences, leaves, and stems). To extract flavonoids, we used ethanol at concentrations of 40, 55, 60, 70, and 75%. Spectrophotometry was used to determine total flavonoids, while high-performance liquid chromatography was employed to study the qualitative and quantitative composition of the extracts.

The highest yield of flavonoids was found in *H. sibiricum* leaves (at all concentrations except 70%), followed by the 55% and 70% ethanol extracts of *T. vulgaris* leaves and stems, as well as the 75% ethanol extract of *A. millefolium* leaves and stems. Thus, these plants have the greatest potential in being used in medicines. High-performance liquid chromatography showed the highest contents of polyphenolic compounds in the samples of *P. officinalis*, *A. millefolium*, *T. vulgaris*, and *T. pratense*.

Our results can be used in further research to produce new medicinal preparations based on the medicinal plants of Kuzbass.

Keywords: Flavonoids, medicinal plants, spectrophotometry, chromatography, HPLC, extraction, plant extracts

Funding: Our study was financially supported by the Russian Science Foundation (RSF)^{ROR} (grant No. 23-16-00113).

Please cite this article in press as: Velichkovich NS, Dunchenko NI., Stepanova AA, Kozlova OV, Faskhutdinova ER, Yustratov VP., *et al.* The phytochemical composition of Kuzbass medicinal plants. *Foods and Raw Materials*. 2025;13(2):219–232. <https://doi.org/10.21603/2308-4057-2025-2-649>

INTRODUCTION

Flavonoids are low-molecular-weight polyphenolic phytochemicals secreted by plants as secondary metabolites in response to stress. Secondary metabolites have a wide range of therapeutic effects that are beneficial to humans. Flavonoids are widely distributed in the plant kingdom and have long been used in various herbal medicines due to their antibacterial, antiviral, antioxidant, anti-inflammatory, antimutagenic, and anticarcinogenic properties [1–3].

There have been many studies on medicinal plants to explore their therapeutic potential in treating disease. Herbal treatments have minimal or no side effects

and are therefore safer than synthetic drugs. Medicinal plants have shown efficiency in treating a number of difficult-to-cure diseases [4, 5]. Ayurveda has successfully used medicinal herbs for many years to prevent and treat serious diseases [6].

Flavonoids protect plants from biotic and abiotic stress. They function as signaling molecules, detoxifiers, UV filters, allopathic compounds, and phytoalexins, as well as play an important role in drought and frost resistance [7].

Acting as antioxidants, flavonoids protect plants, animals, and humans from the effects of reactive oxygen species. They suppress the formation of reactive oxygen

species by either inhibiting the enzyme or chelating trace elements involved in the formation of free radicals, i.e., by removing reactive oxygen species or by enhancing antioxidant protection [8].

Plant flavonoids exhibit antiviral activity helping inhibit various enzymes involved in the viral life cycle [9]. A wide variety of medicinal plants produce antimicrobial effects due to large numbers of flavonoids that are released in response to bacterial infection [10]. Many studies have shown the effectiveness of flavonoids in cardioprotection and prevention of hypertension and atherosclerosis. Flavonoids reduce atrial pressure, enhance the vasorelaxant process, and prevent endothelial dysfunction [11]. Also, flavonoids have antidiabetic properties that regulate carbohydrate digestion, insulin secretion, insulin signaling, glucose uptake, and fat deposition [12]. Finally, flavonoids exhibit anticancerous activity and inhibit the proliferation of tumor cells by suppressing the formation of reactive oxygen species. They also inhibit the enzymes xanthine oxidase, cyclooxygenase-2, and 5-lipoxygenase, which play an important role in tumor development [13].

Plants accumulate different types and amounts of bioactive substances depending on the region of growth, time of collection, plant organs, and other factors. Kemerovo Oblast – Kuzbass is a region that has a variety of soils and climates, with large areas covered by medicinal herbs. In particular, Kuzbass is home to common thyme (*Thymus vulgaris* Linn.), woolly burdock (*Arcium tomentosum* Mill.), alfalfa (*Medicago sativa* L.), common lungwort (*Pulmonaria officinalis* L.), common yarrow (*Achillea millefolium* L.), red clover (*Trifolium pratense* L.), common ginseng (*Panax ginseng*), sweet-vetch (*Hedysarum neglectum* Ledeb.), and cow parsnip (*Heracleum sibiricum* L.) [14, 15]. These plants have great medicinal potential and can be used in medicines against various diseases.

T. vulgaris is a perennial flowering plant belonging to the *Lamiaceae* family, native to southern Europe [16]. *T. vulgaris* is most widely used as a flavoring agent in the food, perfume, and cosmetic industries, as well as a preservative for chicken, meat, and fish. Due to its healing and antiseptic properties, it was used in traditional medicine to treat wounds and skin diseases [17]. It has also been used as essential oil to treat food poisoning due to a high content of polyphenols such as carvacrol and thymol [18]. Modern studies have revealed the effectiveness of *T. vulgaris* in improving oxidative stress and cell-mediated immune response [19, 20]. Studies also confirm the plant's antiparasitic and antihelminthic activity due its content of monoterpenes [21].

A. tomentosum belongs to the *Asteraceae* family and grows in Europe, Asia, and North America [22]. Due to its polyphenolic compounds, the plant is widely applied in traditional medicine. Its root and leaf extracts have a diuretic effect and improve metabolism. They are also used to treat gastrointestinal diseases and diabetes mellitus in the early stages [23, 24]. The leaves and roots of *A. tomentosum* are applied externally to relieve skin in-

flammation. Burdock contains compounds of the lignan group, such as lappaol A, lappaol C, lappaol F, matairesinol, arctiin, arctigenin, and arctigenic acid [22]. Its leaves are rich in flavonoids (luteolin, quercetin, quercitrin, and rutin) and phenolic acids, while its root extracts are rich in dicafoylquinic acid isomers and their derivatives, polysaccharides, and derivatives of polyunsaturated fatty acids [22, 25].

M. sativa is one of the most important forage species that has recently been used for human consumption, mainly due to its content of bioactive phenolic compounds [26]. According to numerous studies, *M. sativa* contains bioactive phytochemicals, such as alkaloids, saponins, phenols, tannins, polysaccharides, and phytoestrogens, which have antioxidant, anti-inflammatory, and anticarcinogenic properties [27–29]. Several classes of alfalfa's phenolic compounds have been described in literature, especially phenolic acids and flavonoids.

P. officinalis is a long-lived, shade-tolerant perennial plant belonging to the *Boraginaceae* family [30]. Although lungwort is native to Central and Eastern Europe, its scattered populations are also found in the UK and Denmark. The plant has emollient, antitussive, expectorant, antimicrobial, diuretic, cleansing, antilithiatic, and anti-inflammatory effects and is used to treat diseases of the respiratory tract and urinary system [31]. The biological properties of *P. officinalis* can be attributed to a diverse set of phytochemicals, such as anthocyanins, alkaloids, flavanones, flavonols, flavones, hydroxycinnamic acid, lignans, polyphenols, polyphenolic acids, and other phytochemicals present in various parts of the plant [31]. The extract of *P. officinalis* leaves contains such compounds as naringin, hesperidin, naringenin, apigenin-7-glucoside, rutin, chlorogenic acid, myricetin, hyperoside, acacetin, and gallic acid [32].

A. millefolium is a herbaceous flowering plant that grows wild in Asia, Africa, Europe, and America [33]. In traditional medicine, its extract is widely used to treat inflammatory, hepatobiliary, cardiovascular, and respiratory diseases, as well as diabetes and diabetes-related diseases [34, 35]. The main phytochemical compounds isolated from *A. millefolium* are essential oil and flavonoid derivatives including apigenin, rutin, lutein, and kaempferol [36].

T. pratense is a valuable forage plant growing in temperate and humid regions [37]. It is used to treat diabetes, as well as cardiovascular, neurodegenerative, and other diseases [38–41]. Isoflavones and flavonoids have been found in *T. pratense*, such as formononetin, biochanin A, genistein, and daidzein.

P. ginseng has been used in traditional medicine since ancient times. It has a positive effect on cardiovascular and neurodegenerative diseases, cancer, and diabetes mellitus [42–46]. Extensive research has associated the biological activities of Korean *P. ginseng* and its products with various functional components, including ginsenosides, polyacetylenes, phenolic compounds, alkaloids, polysaccharides, oligopeptides, and essential oils [47].

H. neglectum is a plant of the legume family [48]. Known in traditional medicine as a “red root,” *H. neglectum* is used as an anti-inflammatory agent, as well as to treat gastrointestinal, cardiovascular, and other diseases. The plant contains polysaccharides, flavonoids, catechins, tannins, alkaloids, and other bioactive substances [49, 50].

H. sibiricum is a perennial taproot plant widespread in the central part of Russia, Central Europe, Ciscaucasia, and Western Siberia [51]. *H. sibiricum* is actively used as a forage plant for cattle, pigs, rabbits, and birds [52]. In medicine, its roots and leaves are used to treat diseases of the nervous and digestive systems, convulsions, and skin diseases. Preparations based on this plant have antimicrobial and anti-inflammatory effects. The leaves are harvested during the flowering period, while the roots are collected and dried in the autumn. Preparations made from the roots of *H. sibiricum* are considered more effective than those based on its leaves [53]. *H. sibiricum* contains essential oils (up to 3%), coumarins (up to 2.5%), tannins, flavonoids, resins, phenols, and other compounds.

Thus, using the medicinal plants of Kuzbass in drugs and preparations can be effective in treating many diseases, including oncological, gastrointestinal, cardiovascular, and neurodegenerative diseases, diabetes, etc. For this, polyphenols in plant materials need to be identified and quantified.

In this study, we aimed to identify phytochemicals in Kuzbass medicinal plants isolated from different plant organs by extractants at various concentrations in order to select the plants rich in bioactive substances to be further extracted and studied by spectrophotometry and high-performance liquid chromatography.

The novelty of our study lies in its focus on medicinal plants that had to adapt to the specific climatic conditions of Kuzbass and therefore developed unique chemical profiles and biological activity. Our data can be further used to develop effective medicines and dietary supplements.

STUDY OBJECTS AND METHODS

Spectrophotometry and high-performance liquid chromatography (HPLC) were employed to analyze medicinal plant materials collected in Kemerovo Oblast – Kuzbass from May to August 2023, namely:

- *Thymus vulgaris* Linn. (leaves and stems) collected in Zhuravlevo village;
- *Arctium tomentosum* Mill. (roots) collected in the Topkinsky Municipal District, Sukhaya Rechka village, and Mamaevsky settlement;
- *Medicago sativa* L. (leaves and stems) collected in Metallploshchadka settlement, Topkinsky Municipal District, Pugachi village, Zhuravlevo village, and Belovsky District;
- *Pulmonaria officinalis* L. (leaves and stems) collected in the Topkinsky Municipal District, Yaya District, Zhuravlevo village;
- *Achillea millefolium* L. (leaves and stems) collected in the Yaya District and Belovsky District;

– *Trifolium pratense* L. (leaves and stems) collected in Kemerovo city, Pugachi village, Mamaevsky settlement, and Zhuravlevo village;

– *Panax ginseng* (roots) collected in Sheregesh village;

– *Hedysarum neglectum* Ledeb. (roots) collected in Sheregesh village; and

– *Heracleum sibiricum* L. (inflorescences, leaves, and stems) collected in the Topkinsky Municipal District, Pugachi village, and Zhuravlevo village.

Morphological identification was carried out by the working group of the grant team.

The plant materials were collected in 2023 and dried according to the State Pharmacopoeia XIII [54]. In particular, the collected materials were washed, crushed, and dried (first, at room temperature in a well-ventilated room and then at 50°C until the samples had a recommended moisture, averaging 6–13%). The samples were stored in bags in a dry, cool place at the Laboratory for Biotesting Natural Nutraceuticals, Kemerovo State University.

Extracts were prepared to isolate flavonoids from the plant materials. For this, we took samples of medicinal plants (1 g each), weighed them in a conical flask, and added 30 mL of ethanol.

Solvents such as mixtures of water with alcohol (methanol or ethanol) are the most suitable systems for polyphenol extraction. Water acts as a swelling agent for the plant material, increasing the contact surface. Pure alcohols dehydrate and disrupt the plant cells, causing the breakdown of the dissolved cell wall bond. Therefore, alcohol is mixed with water for a synergistic effect, and the optimal concentration of alcohol can increase the extraction of flavonoids [55]. We used different concentrations of ethanol (40, 55, 60, 70, and 75%) for all the samples to determine the best yield of flavonoids. For some samples, we used a two-phase extraction system (70% ethanol + oil). Then, the flask was placed in a reflux condenser and heated in a boiling water bath for 30 min, with periodical shaking. The resulting supernatant was filtered into a 100-mL measuring flask, preventing the plant particles from getting on the filter.

Flavonoids were extracted in triplicate for each plant sample with different concentrations of ethanol (30 mL) added to the filtrate. Then the filtered materials were combined and cooled to 20°C. In the volumetric flask, the filtrate was brought to the mark with ethanol.

Spectrophotometry and HPLC were used to determine the mass fraction of flavonoids in the plant extracts, as well as to examine their qualitative and quantitative composition.

Spectrophotometric analysis involved measuring the optical density of the solutions [56]. For this, 5 mL of the extracts was poured into two 25-mL flasks. Then, 4 mL of a 5% solution of aluminum chloride was added to one of the flasks (test solution). Both flasks were brought to the mark with ethanol and thoroughly mixed. To prepare the aluminum chloride solution, 5 g of aluminum chloride was weighed in a 250-mL conical flask and dissolved in 50 g of ethanol; then, the solution was brought

to 100 g with the same alcohol and thoroughly mixed. After 30 min, the optical density of the test solution was determined against the reference solution (without aluminum chloride) at 410 nm (maximum absorption) in cuvettes with a 1-cm optical layer on a UV 1800 spectrophotometer (Shimadzu, Japan).

Then, we determined the amount of rutin in 25 mL of the solution of the state standard reference rutin sample (Sigma-Aldrich) using a calibration graph. To prepare the solution, 0.050 g of rutin was weighed in a 50-mL volumetric flask, mixed with 40 mL of ethanol, and heated to 50–60°C until rutin completely dissolved. Then the solution was cooled to room temperature, brought to the mark with ethanol (at the same concentration as was used to prepare the solutions of medicinal plants), and stirred. To plot the calibration graph, two 25-mL volumetric flasks were filled with 0.2 mL of the prepared rutin solution at a concentration of 1 mg/mL. Then, 4 mL of aluminum chloride solution was added to one of the flasks (test solution), and both flasks were brought to the mark with ethanol and mixed. New solutions were similarly prepared with 0.4, 0.6, 0.8, 1.0, and 1.2 mL of the rutin solution as described above and kept for 30 min. The optical density of the test solutions was measured against the reference solution (without aluminum chloride) at 390–420 nm (maximum absorption) in cuvettes with a 1-cm optical layer.

The mass fraction of flavonoids in terms of rutin (X , %) was determined according to the following Eq. (1):

$$X = C \times 100 \times 100 \times m \times 5 \quad (1)$$

where C is the amount of rutin in 25 mL according to the calibration graph, mg; 100 is the volume of the extracts, mL; 100 is the volume of the extracts, %; m is the mass of the medicinal plant samples, g; and 5 is the volume of the medicinal plant extracts, mL.

Flavonoid compounds were also determined qualitatively and quantitatively by HPLC on an LC-20 Prominence Shimadzu chromatograph with a Shimadzu SPD-20MA diode-matrix detector (Shimadzu, Japan) and a Kromasil C18 chromatographic column (5 μ m, 110 Å, 250×4.6 mm). The conditions included an injection volume of 20 μ L, a column temperature of 400, and a reference wavelength of 254 nm.

Microsoft® Excel was used for statistical data processing. The absolute calibration method with the rutin standard was employed to quantify the flavonoids.

RESULTS AND DISCUSSION

Total flavonoids were spectrophotometrically determined in the following medicinal plant materials: *Thymus vulgaris* Linn. (leaves and stems), *Arctium tomentosum* Mill. (roots), *Medicago sativa* L. (leaves and stems), *Pulmonaria officinalis* L. (leaves and stems), *Achillea millefolium* L. (leaves and stems), *Trifolium pratense* L. (leaves and stems), *Panax ginseng* (roots), *Hedysarum neglectum* Ledeb. (roots), and *Heracleum sibiricum* L. (inflorescences, leaves, and stems). Ethanol extractant was used at different concentrations to identify the highest yield of flavonoid compounds (Figs. 1–4).

The extract of *T. vulgaris* leaves and stems with 55% ethanol showed the highest yield of flavonoids (1.124%). In the study by Malankina *et al.*, this indicator was significantly higher, varying from 1.64 to 2.83% [57]. The authors found that the flavonoid contents tended to increase in the years with lower average daily temperatures during the harvesting period, which might explain the differences. The extracts of *M. sativa* and *A. millefolium* leaves and stems with 75% ethanol had the maximum yields of flavonoids (0.939% each).

Compared to the flavonoid content in the *A. millefolium* extract in our study, Tikhonov *et al.* reported a flavonoid content of 1.28% (0.34% higher) extracted with 40 and 70% ethanol for 24 h [58]. Longer extraction

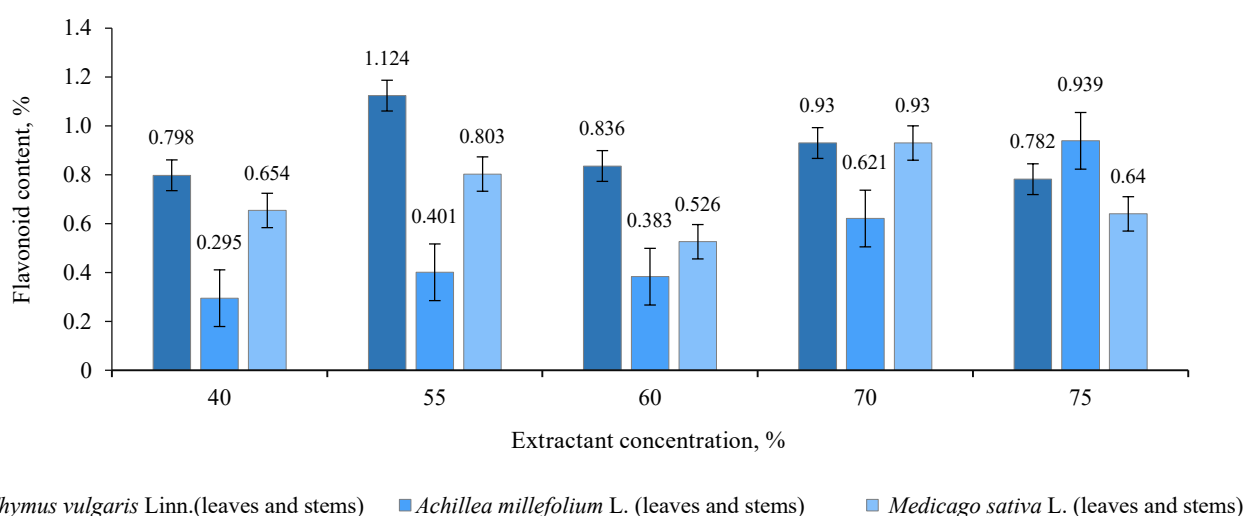


Figure 1 Total flavonoids in the extracts of *Thymus vulgaris* Linn., *Achillea millefolium* L., and *Medicago sativa* L. (leaves and stems)

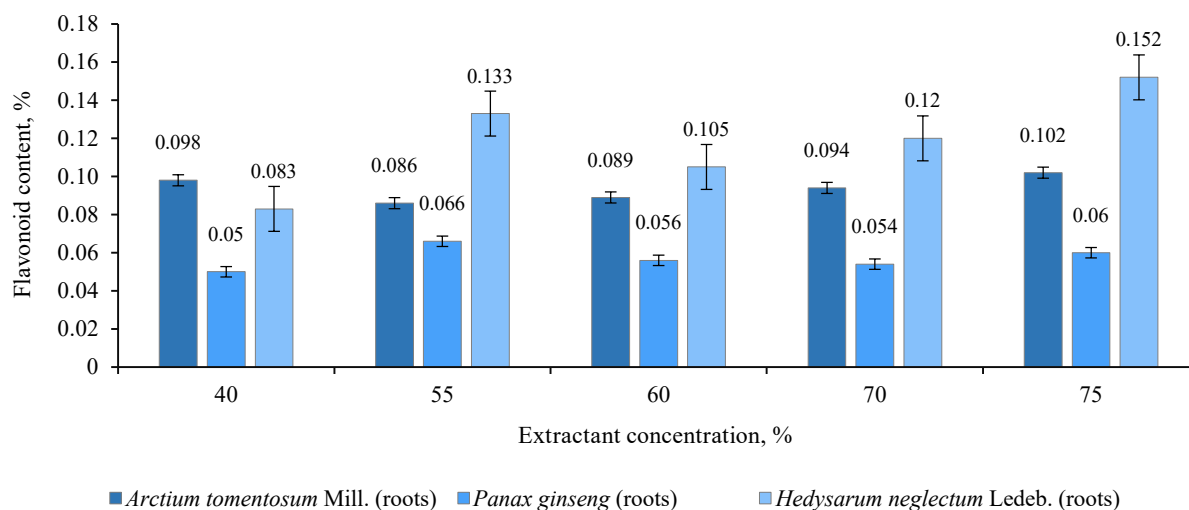


Figure 2 Total flavonoids in the extracts of *Arctium tomentosum* Mill., *Panax ginseng*, and *Hedysarum neglectum* Ledeb. (roots)

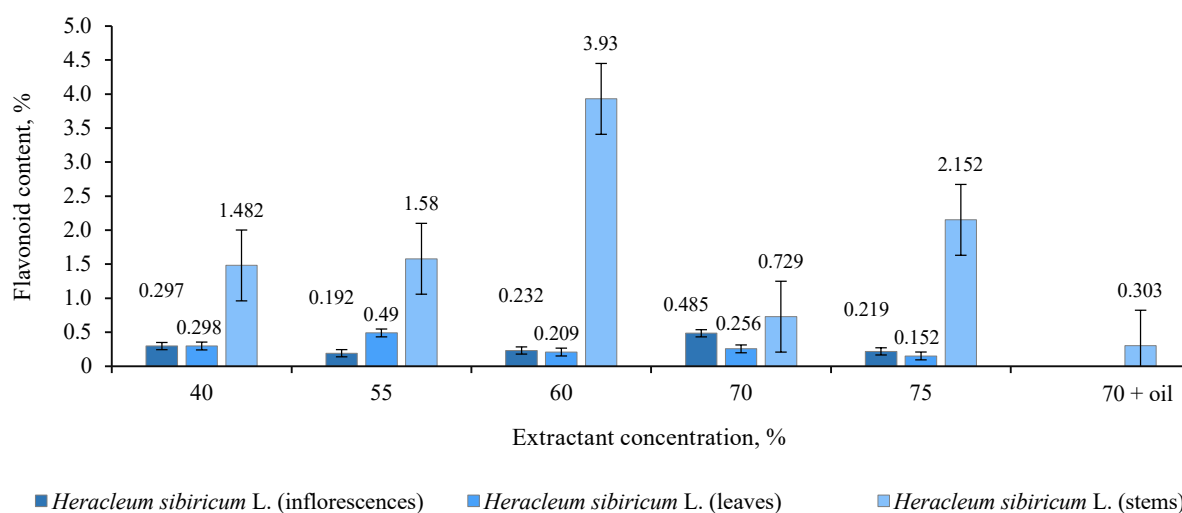


Figure 3 Total flavonoids in the extracts of *Heracleum sibiricum* L. (inflorescences, leaves, stems)

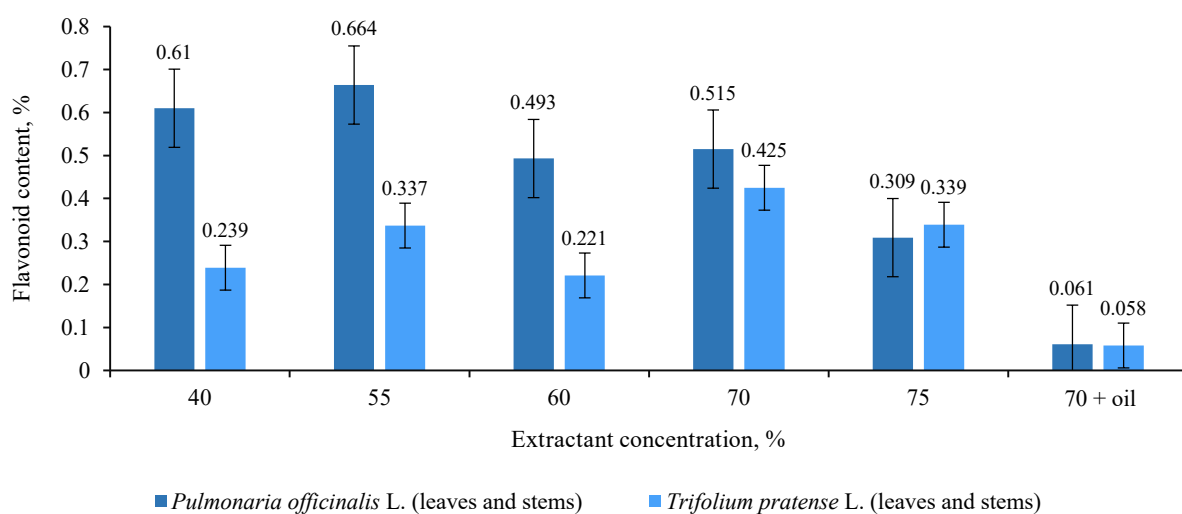


Figure 4 Total flavonoids in the extracts of *Pulmonaria officinalis* L. and *Trifolium pratense* L. (leaves and stems)

can contribute to higher yields of target substances, but it is not always rational for the production process due to high electricity costs. Nevertheless, we are planning to optimize the extraction process in terms of its duration and yield of flavonoids in further research. Another interesting fact is that in the study by Tikhonov *et al.*, the contents of flavonoids were quantitatively the same in the extracts based on 40 and 70% ethanol, while our study showed a 0.33% difference. This can be explained by a number of factors, mainly the difference in the extraction time. It might be that the 24-h extraction in the study by Tikhonov *et al.* ensured the maximum yield of flavonoids regardless of the ethanol concentration. Another possible explanation is the variability in the composition of flavonoids caused by differences in the place of plant growth.

The extracts of *A. tomentosum*, *P. ginseng*, and *H. neglectum* roots extracted with 75, 55, and 75% ethanol had the highest contents of flavonoids, namely 0.102, 0.066, and 0.152%, respectively. In comparison, Shkolnikova *et al.* reported a 0.06% lower flavonoid content (0.09%, in terms of rutin) in the *H. neglectum* roots collected in the Republic of Altai [59]. This is likely due to the difference in the region of growth, including climatic conditions, soil composition, and other environmental factors. Our results indicate great potential of *H. neglectum* grown in Kemerovo Oblast as a source of flavonoids.

The *H. sibiricum* inflorescence, stem, and leaf extracts had the maximum flavonoid contents (0.485, 0.490, and 3.93%, respectively) with 70, 55, and 60% ethanol, respectively. Modern literature lacks information on total flavonoids in different parts of *H. sibiricum*,

so our results contribute significantly to understanding the plant's phytochemical characteristics.

The leaf and stem extracts of *P. officinalis* and *T. pratense* showed the highest yields of flavonoids (0.664 and 0.425%, respectively) with 55 and 70% ethanol, respectively. According to modern literature, the content of flavonoids in *T. pratense* varies greatly depending on the variety and region of cultivation. For example, Konovalenko *et al.* reported 0.58% of flavonoids, while Kasatkina and Nelyubina found 1.3–2.4% of flavonoids in terms of rutin [60, 61]. Our values were significantly lower, which may be due to differences in the methods of extraction and quantification. We used spectrophotometry, while the above studies [60, 61] used thin-layer chromatography, which might affect the accuracy of the results.

According to our spectrophotometric analysis, the highest yield of flavonoids was observed in the *H. sibiricum* leaf extract, followed by the stem and leaf extracts of *T. vulgaris* and *M. sativa*. Therefore, these plants are the most promising for being used in medicinal preparations. We found no correlation between the concentration of the extractant and the yield of flavonoids. However, 55% ethanol produced the maximum yield of flavonoids more often than the other concentrations.

Then, we identified and quantified bioactive substances in the *M. sativa* extract by HPLC (Fig. 5 and Table 1).

As can be seen, the *M. sativa* extract contained significant amounts of tricine and quercetin-3-O-glycoside. Also, we detected 3,3',4,5-tetrahydroxyflavone, formononetin, and naringenin. Karimi *et al.*, who studied the methanol extract of *M. sativa* leaves in Iran, reported

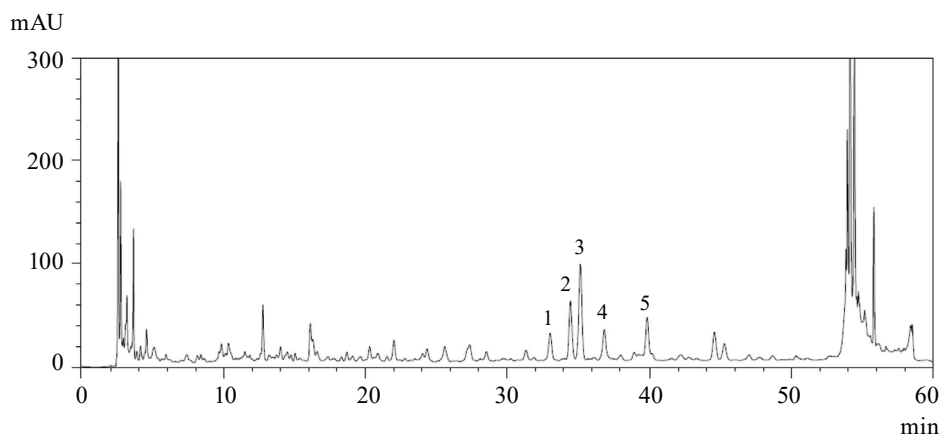


Figure 5 The chromatogram of bioactive substances in the *Medicago sativa* L. extract: 1 – 3,3',4,5-tetrahydroxyflavone, 2 – quercetin-3-O-glycoside, 3 – tricine, 4 – formononetin, 5 – naringenin

Table 1 The contents of bioactive substances in the *Medicago sativa* L. extract

Peak No.	Bioactive substances	Retention time, min	Content, mg/g
1	3,3',4,5-tetrahydroxyflavone	33.0100	0.6400 ± 0.0011
2	Quercetin-3-O-glycoside	34.2100	1.3000 ± 0.0027
3	Tricine	35.1400	2.0900 ± 0.0300
4	Formononetin	36.8900	0.7300 ± 0.0021
5	Naringenin	39.7800	0.9800 ± 0.0026

the phenolic compounds of apigenin (0.214 mg/g), myricetin (0.456 mg/g), naringin (0.738 mg/g), quercetin (0.574 mg/g), and daidzein (0.335 mg/g) [62]. By comparison, the content of naringin in our study was 0.24% higher. The content of tricine, however, has not been previously reported for *M. sativa* extracts. Thus, the flavonoid composition of *M. sativa* differs depending on the region of growth. Further research is needed to identify factors that affect flavonoid contents in the plant and to assess their biological activity.

The results of HPLC analysis of the *P. officinalis* extract are shown in Fig. 6 and Table 2.

As can be seen, the *P. officinalis* extract contained gallic acid, triterpene saponin, ferulic acid, and rosmarinic acid. These results are consistent with those reported by Dushlyuk *et al.* [63]. The authors detected ferulic, gallic, caffeic, rosmarinic, and chlorogenic acids, as well as triterpene saponins, rutin, isorhamnetin, and quercetin in the 70% extract of the *P. officinalis* callus culture. It is worth noting that the contents of caffeic, rosmarinic, and chlorogenic acids were higher in the callus culture than in the above-ground parts of the plant.

The results of HPLC analysis of the *P. ginseng* extract are shown in Fig. 7 and Table 3.

According to HPLC analysis, the *P. ginseng* extract contained syringic acid, ginsenoside LC₁, panaxen, ginsenoside RB₁, panaxoside, and gomisin A.

Ginsenoside RB₁, which showed the highest yield among all the compounds, is one of the most important components of ginseng that contributes to its therapeutic effect [64]. This compound has numerous beneficial effects on human health, including the cardiovascular

and central nervous systems, as well as antidiabetic and antitumorous activity. Notably, we detected significant amounts of syringic acid, which had not been previously reported for *P. ginseng* extracts.

The results of HPLC analysis of the *T. vulgaris* extract are shown in Fig. 8 and Table 4.

The HPLC analysis of the *T. vulgaris* extract determined significant contents of apigenin, thymol, quercetin, and hesperidin, as well as lower contents of gallic and caffeic acids.

Thymol is considered the main component of *T. vulgaris*, which was confirmed by our study. However, apigenin was present in higher contents than thymol. Apigenin has anticarcinogenic, anti-inflammatory, antiviral, and antioxidant properties [65]. Mărculescu *et al.* reported that the *T. vulgaris* extract contained caffeic (436.4 mg/100 g), chlorogenic (25.5 mg/100 g), p-coumaric (19.1 mg/100 g), and ferulic (41.6 mg/100 g) acids, as well as luteolin (658.8 mg/100 g) and apigenin (57.4 mg/100 g) [66].

The results of HPLC analysis of the *A. millefolium* extract are shown in Fig. 9 and Table 5.

As can be seen, the *A. millefolium* extract contained chlorogenic and caffeic acids, apigenin, vicenin-2, luteolin, rutin, hesperidin. Asyakina *et al.*, who studied the chemical composition and biological activity of *A. millefolium* cell cultures, detected caffeic (22.21 mg/mL) and 4,5-dicaffeoylquinic (12.70 mg/mL) acids, as well as coumarosides (14.55 mg/mL), luteolin (9.27 mg/mL), vicenin-2 (4.18 mg/mL), rutin (2.96 mg/mL), and other compounds [67].

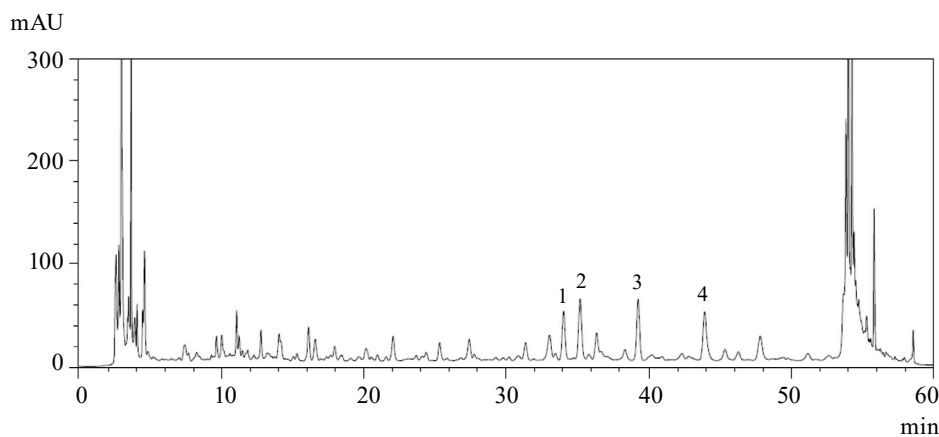


Figure 6 The chromatogram of bioactive substances in the *Pulmonaria officinalis* L. extract: 1 – gallic acid, 2 – triterpene saponin, 3 – ferulic acid, 4 – rosmarinic acid

Table 2 The contents of bioactive substances in the *Pulmonaria officinalis* L. extract

Peak No.	Bioactive substances	Retention time, min	Content, mg/g
1	Gallic acid	34.0500	3.2900 ± 0.0019
2	Triterpene saponin	35.2200	4.3200 ± 0.0031
3	Ferulic acid	39.1000	4.6800 ± 0.0039
4	Rosmarinic acid	43.9500	4.0100 ± 0.0045

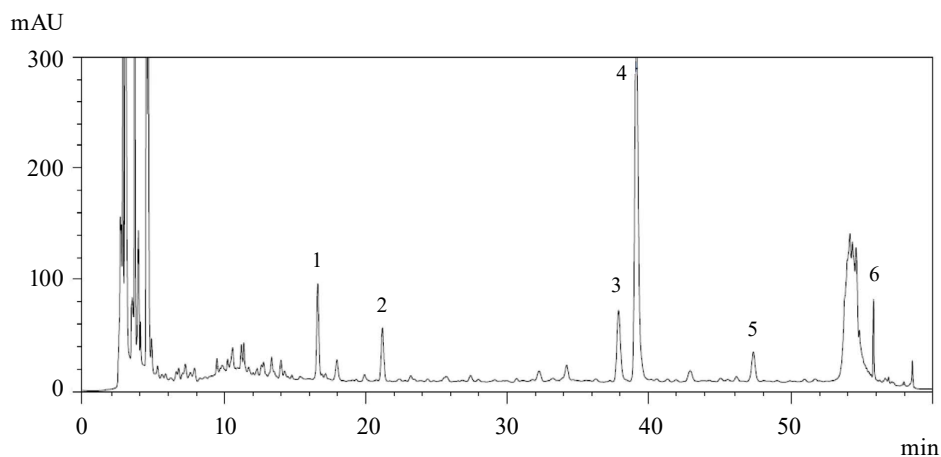


Figure 7 The chromatogram of bioactive substances in the *Panax ginseng* extract: 1 – syringic acid, 2 – ginsenoside LC₁, 3 – panaxen, 4 – ginsenoside RB₁, 5 – panaxoside, 6 – gomisin A

Table 3 The contents of bioactive substances in the *Panax ginseng* extract

Peak No.	Bioactive substances	Retention time, min	Content, mg/g
1	Syringic acid	16.3400	0.9500 ± 0.0020
2	Ginsenoside LC ₁	21.1800	0.5400 ± 0.0012
3	Panaxen	37.9500	0.7100 ± 0.0017
4	Ginsenoside RB ₁	39.1300	0.7100 ± 0.0017
5	Panaxoside	47.1800	0.3400 ± 0.0014
6	Gomisin A	55.9700	0.8300 ± 0.0019

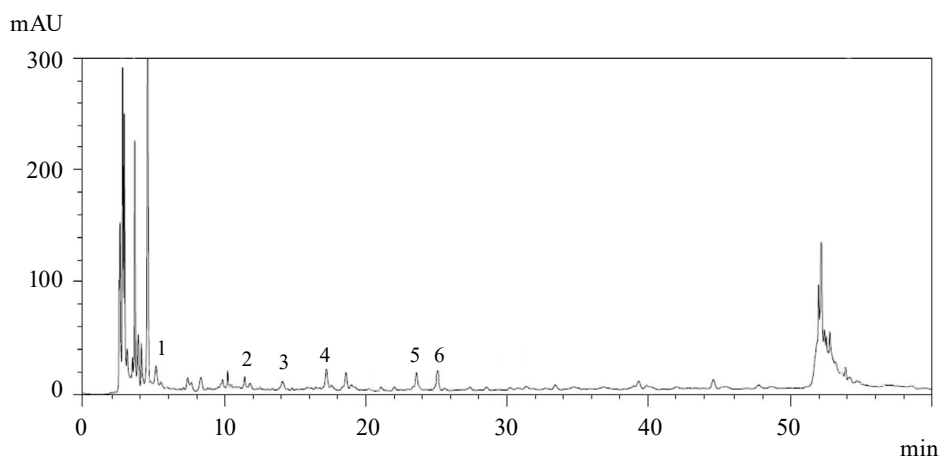


Figure 8 The chromatogram of bioactive substances in the *Thymus vulgaris* Linn. extract: 1 – quercetin, 2 – gallic acid, 3 – caffeic acid, 4 – apigenin, 5 – hesperidin, 6 – thymol

Table 4 The contents of bioactive substances in the *Thymus vulgaris* Linn. extract

Peak No.	Bioactive substances	Retention time, min	Content, mg/g
1	Quercetin	5.1800	1.6000 ± 0.0025
2	Gallic acid	11.3400	1.0900 ± 0.0021
3	Caffeic acid	14.0700	0.3600 ± 0.0013
4	Apigenin	17.0100	2.0700 ± 0.0042
5	Hesperidin	23.6500	1.5600 ± 0.0027
6	Thymol	25.1300	1.8300 ± 0.0034

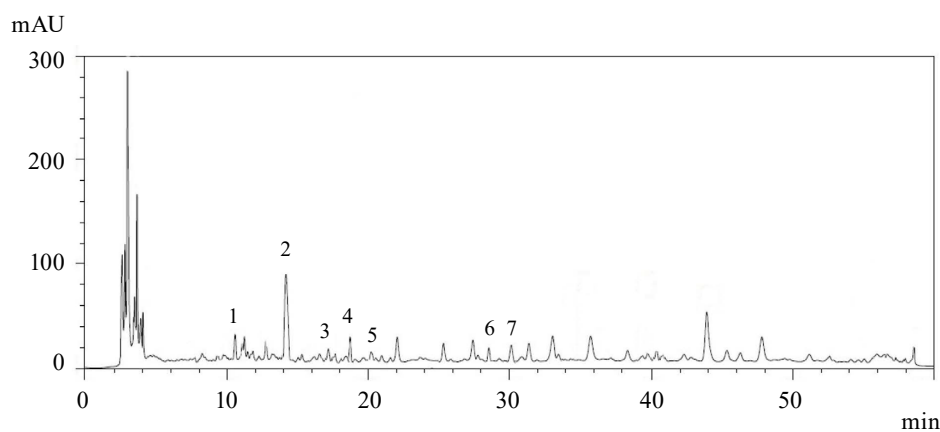


Figure 9 The chromatogram of bioactive substances in the *Achillea millefolium* L. extract: 1 – chlorogenic acid, 2 – caffeic acid, 3 – apigenin, 4 – vicenin-2, 5 – luteolin, 6 – rutin, 7 – hesperidin

Table 5 The contents of bioactive substances in the *Achillea millefolium* L. extract

Peak No.	Bioactive substances	Retention time, min	Content, mg/g
1	Chlorogenic acid	10.2100	1.0300 ± 0.0027
2	Caffeic acid	14.0700	5.2900 ± 0.0059
3	Apigenin	17.0400	0.3900 ± 0.0016
4	Vicenin-2	18.6900	1.0200 ± 0.0023
5	Luteolin	20.3400	0.2400 ± 0.0008
6	Rutin	28.6100	0.4600 ± 0.0010
7	Hesperidin	30.0900	0.7000 ± 0.0022

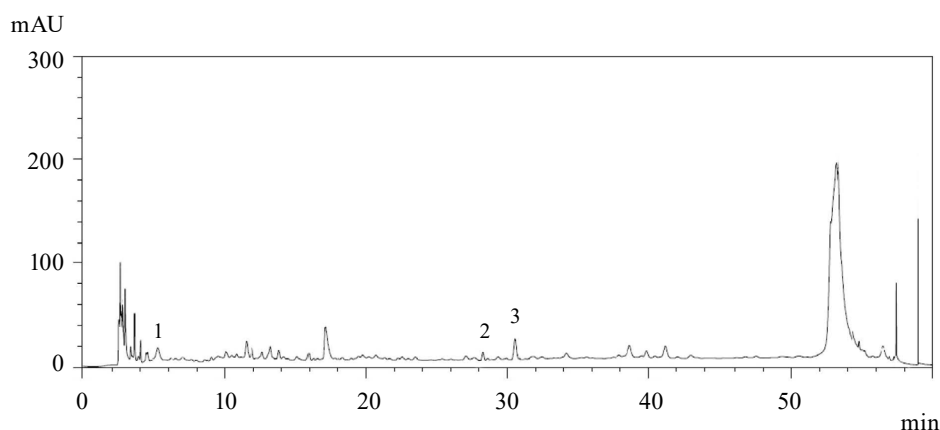


Figure 10 The chromatogram of bioactive substances in the *Hedysarum neglectum* Ledeb. extract: 1 – quercetin, 2 – rutin, 3 – mangiferin

Table 6 The contents of bioactive substances in the *Hedysarum neglectum* Ledeb. extract

Peak No.	Bioactive substances	Retention time, min	Content, mg/g
1	Quercetin	4.9900	0.3800 ± 0.0016
2	Rutin	28.3000	0.1300 ± 0.0007
3	Mangiferin	30.6100	0.7200 ± 0.0021

The results of HPLC analysis of the *H. neglectum* extract are shown in Fig. 10 and Table 6.

According to Table 6, the *H. neglectum* extract contained quercetin, rutin, and mangiferin. Babich *et al.* reported the presence of coumaric acid (0.460 mg/kg), hyperoside/rutin (11.628 mg/kg), and quercetin-3-glycoside (10.410 mg/kg) in the *H. neglectum* extract [68].

The results of HPLC analysis of the *T. pratense* extract are shown in Fig. 11 and Table 7.

According to HPLC results, the *T. pratense* extract contained significant amounts of quercetin, biochanin A, and daidzein. Smaller amounts were detected of genistein, apigenin, rutin, luteolin, formononetin, and naringin. Tundis *et al.* found luteolin (16.7 mg/g),

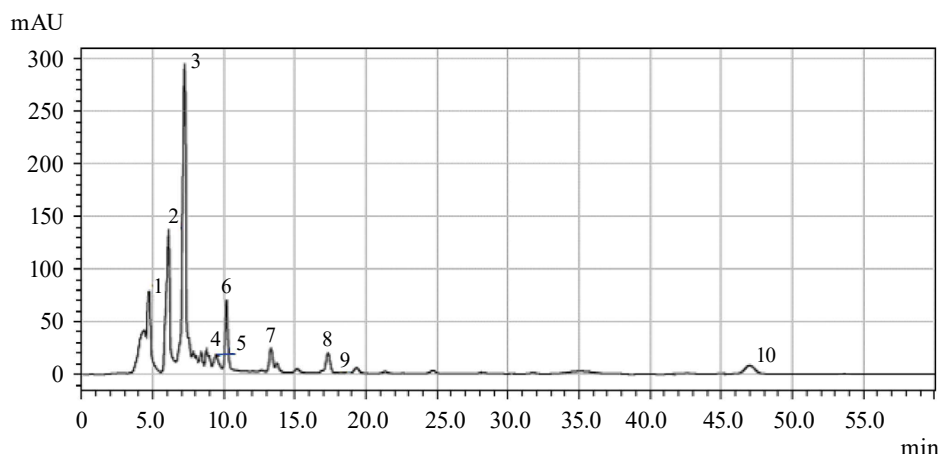


Figure 11 The chromatogram of bioactive substances in the *Trifolium pratense* L. extract: 1 – quercetin, 2 – biochanin A, 3 – daidzein, 4 – genistein, 5 – apigenin, 6 – luteolin, 7 – formononetin, 8 – naringin, 9 – rutin

Table 7 The contents of bioactive substances in the *Trifolium pratense* L. extract

Peak No.	Bioactive substances	Retention time, min	Content, mg/g
1	Quercetin	4.9800	2.8400 ± 0.0048
2	Biokhanin A	6.7300	3.1900 ± 0.0053
3	Daijouin	10.0900	6.3400 ± 0.0076
4	Genistein	15.0000	1.2800 ± 0.0031
5	Apigenin	16.9200	0.4300 ± 0.0012
6	Rutin	28.2900	0.6900 ± 0.0015

kaempferol (0.8 mg/g), and myricetin (0.5 mg/g) in the extract of *T. pratense* flowers [69].

As shown by the tables above, the HPLC analysis revealed the highest contents of polyphenolic compounds in the samples of *P. officinalis*, *A. millefolii*, *T. vulgaris*, and *T. pratense*. Therefore, these plants can be considered the most promising for developing medicinal preparations against various diseases.

CONCLUSION

Flavonoids play a valuable role in human health, which explains their increasing consumption worldwide. The medicinal plants of Kemerovo Oblast – Kuzbass are a rich source of these natural antioxidants. Flavonoids require new methods and technologies to be developed for their study and use in production.

According to the spectrophotometric analysis, the highest yield of flavonoids was determined in the extract of *Heracleum sibiricum* L. leaves with 60% ethanol. Quite high contents were also detected in the 75% ethanol extract of *H. sibiricum* leaves, the 55 and 70%

ethanol extracts of *Thymus vulgaris* Linn. leaves and stems, and in the 75% ethanol extract of *Achillea millefolium* L. leaves and stems.

High-performance liquid chromatography showed the highest contents of polyphenolic compounds in the samples of *Pulmonaria officinalis* L., *A. millefolium*, *T. vulgaris*, and *Trifolium pratense* L.

Thus, our results for the qualitative and quantitative composition of medicinal plants grown in Kemerovo Oblast – Kuzbass can be further used to study the biological activity of the extracts in order to create new medicinal preparations to maintain health and reduce the risk of life-threatening diseases such as diabetes, cancer, stroke, and cardiovascular diseases.

CONTRIBUTION

The authors were equally involved in writing the manuscript and are equally responsible for plagiarism.

CONFLICT OF INTEREST

The authors declare no conflict of interest.

REFERENCES

- Donadio G, Mensitieri F, Santoro V, Parisi V, Bellone ML, De Tommasi N, et al. Interactions with microbial proteins driving the antibacterial activity of flavonoids. *Pharmaceutics*. 2021;13(5):660. <https://doi.org/10.3390/pharmaceutics13050660>
- Roy A, Datta S, Bhatia K, Bhumika, Jha P, Prasad R. Role of plant derived bioactive compounds against cancer. *South African Journal of Botany*. 2022;149:1017–1028. <https://doi.org/10.1016/j.sajb.2021.10.015>








3. Tabakaev AV, Tabakaeva OV, Prikhodko YuV. Functional instant beverages. Foods and Raw Materials. 2023;11(2): 187–196. <https://doi.org/10.21603/2308-4057-2023-2-565>; <https://elibrary.ru/MMKNMH>
4. Kozlova OV, Velichkovich NS, Faskhutdinova ER, Neverova OA, Petrov AN. Methods for extracting immuneresponse modulating agents of plant origin. Food Processing: Techniques and Technology. 2023;53(4):680–688. (In Russ.). <https://doi.org/10.21603/2074-9414-2023-4-2468>; <https://elibrary.ru/EWLVD>
5. Babich O, Prosekov A, Zaushintsena A, Sukhikh A, Dyshlyuk L, Ivanova S. Identification and quantification of phenolic compounds of Western Siberia *Astragalus danicus* in different regions. Heliyon. 2019;5(8):e02245. <https://doi.org/10.1016/j.heliyon.2019.e02245>
6. Perez-Vizcaino F, Fraga C. Research trends in flavonoids and health. Archives of Biochemistry and Biophysics. 2018;646:107–112. <https://doi.org/10.1016/j.abb.2018.03.022>
7. Kaur S, Roy A. A review on the nutritional aspects of wild edible plants. Current Traditional Medicine. 2021;7(4): 552–563. <https://doi.org/10.2174/2215083806999201123201150>
8. Agati G, Azzarello E, Pollastri S, Tattini M. Flavonoids as antioxidants in plants: Location and functional significance. Plant Science. 2012;196:67–76. <https://doi.org/10.1016/j.plantsci.2012.07.014>
9. Khachatoorian R, Arumugaswami V, Raychaudhuri S, Yeh GK, Maloney EM, Wang J, et al. Divergent antiviral effects of bioflavonoids on the hepatitis C virus life cycle. Virology. 2012;433(2):346–355. <https://doi.org/10.1016/j.virol.2012.08.029>
10. Cushnie TPT, Lamb AJ. Antimicrobial activity of flavonoids. International Journal of Antimicrobial Agents. 2005;26(5):343–356. <https://doi.org/10.1016/j.ijantimicag.2005.09.002>
11. Roy A, Khan A, Ahmad I, Alghamdi S, Rajab BS, Babalghith AO, et al. Flavonoids a bioactive compound from medicinal plants and its therapeutic applications. BioMed Research International. 2022;2022(1):5445291. <https://doi.org/10.1155/2022/5445291>
12. Al-Ishaq RK, Abotaleb M, Kubatka P, Kajo K, Büsselberg D. Flavonoids and their anti-diabetic effects: cellular mechanisms and effects to improve blood sugar levels. Biomolecules. 2019;9(9):430. <https://doi.org/10.3390/biom9090430>
13. Maleki SJ, Crespo JF, Cabanillas B. Anti-inflammatory effects of flavonoids. Food Chemistry. 2019;299:125124. <https://doi.org/10.1016/j.foodchem.2019.125124>
14. Belashova OV, Kozlova OV, Velichkovich NS, Fokina AD, Yustratov VP, Petrov AN. A phytochemical study of the clover growing in Kuzbass. Foods and Raw Materials. 2024;12(1):194–206. <https://doi.org/10.21603/2308-4057-2024-1-599>; <https://elibrary.ru/QZBVUI>
15. Faskhutdinova ER, Sukhikh AS, Le VM, Minina VI, Khelef MEA, Loseva AI. Effects of bioactive substances isolated from Siberian medicinal plants on the lifespan of *Caenorhabditis elegans*. Foods and Raw Materials. 2022; 10(2):340–352. <https://doi.org/10.21603/2308-4057-2022-2-544>; <https://elibrary.ru/ZVCUW>
16. Patil SM, Ramu R, Shirahatti PS, Shivamallu C, Amachawadic RG. A systematic review on ethnopharmacology, phytochemistry and pharmacological aspects of *Thymus vulgaris* Linn. Heliyon. 2021;7(5):e07054. <https://doi.org/10.1016/j.heliyon.2021.e07054>
17. Panah KG, Hesarakı S, Farahpour MR. Histopathological evaluation of *Thymus vulgaris* on wound healing. Indian Journal of Fundamental and Applied Life Sciences. 2014;4(S4):3538–3544.
18. da Rosa CG, de Melo APZ, Sganzerla WG, Machado MH, Nunes MR, Maciel MVOB, et al. Application in situ of zein nanocapsules loaded with *Origanum vulgare* Linneus and *Thymus vulgaris* as a preservative in bread. Food Hydrocolloids. 2020;99:105339. <https://doi.org/10.1016/j.foodhyd.2019.105339>
19. El-Nekeety AA, Mohamed SR, Hathout AS, Hassan NS, Aly SE, Abdel-Wahhab MA. Antioxidant properties of *Thymus vulgaris* oil against aflatoxin-induce oxidative stress in male rats. Toxicon. 2011;57(7–8):984–991. <https://doi.org/10.1016/j.toxicon.2011.03.021>
20. Soliman MM, Aldahrani A, Metwally MMM. Hepatoprotective effect of *Thymus vulgaris* extract on sodium nitrite-induced changes in oxidative stress, antioxidant and inflammatory marker expression. Scientific Reports. 2021;11:5747. <https://doi.org/10.1038/s41598-021-85264-9>
21. Isakakroudi N, Talebi A, Allymehr M, Tavassoli M. Effects of essential oils combination on sporulation of Turkey (Meleagris gallopavo) Eimeria oocysts. Archives of Razi Institute. 2018;73(2):113–120. <https://doi.org/10.22092/ari.2017.109255.1102>
22. Skowrońska W, Granica S, Dziedzic M, Kurkowiak J, Ziaja M, Bazyłko A. *Arctium lappa* and *Arctium tomentosum*, Sources of *Arctii radix*: Comparison of anti-lipoxygenase and antioxidant activity as well as the chemical composition of extracts from aerial parts and from roots. Plants. 2021;10(1):78. <https://doi.org/10.3390/plants10010078>

23. Aitynova AE, Ibragimova NA, Shalakhmetova TM, Gapurkhaeva TE, Krasnoshtanov AV, Kenesheva ST. Antimicrobial effect of extract from root of *Arctium tomentosum* Mill. (woolly burdock) against several reference strains. International Journal of Biology and Chemistry. 2022;15(2):10–17. <https://doi.org/10.26577/ijbch.2022.v15.i2.02>
24. Ydyrys A. An overview of medical uses and chemical composition of *Arctium tomentosum* mill. Engineered Science. 2023;26:984. <https://doi.org/10.30919/es984>
25. Strawa J, Wajs-Bonikowska A, Jakimiuk K, Waluk M, Poslednik M, Nazaruk J, et al. Phytochemical examination of woolly burdock *Arctium tomentosum* leaves and flower heads. Chemistry of Natural Compounds. 2020;56:345–347. <https://doi.org/10.1007/s10600-020-03027-w>
26. Horvat D, Viljevac Vuletić M, Andrić L, Baličević R, Kovačević Babić M, Tucak M. Characterization of forage quality, phenolic profiles, and antioxidant activity in alfalfa (*Medicago sativa* L.). Plants. 2022;11(20):2735. <https://doi.org/10.3390/plants11202735>
27. Zagórska-Dziok M, Ziemlewska A, Nizioł-Łukaszewska Z, Bujak T. Antioxidant activity and cytotoxicity of *Medicago sativa* L. seeds and herb extract on skin cells. BioResearch Open Access. 2020;9(1):229–242. <https://doi.org/10.1089/biores.2020.0015>
28. Raeeszadeh M, Beheshtipour J, Jamali R, Akbari A. The antioxidant properties of alfalfa (*Medicago sativa* L.) and its biochemical, antioxidant, anti-inflammatory, and pathological effects on nicotine-induced oxidative stress in the rat liver. Oxidative Medicine and Cellular Longevity. 2022;2022(1):2691577. <https://doi.org/10.1155/2022/2691577>
29. Gatouillat G, Alabdul Magid A, Bertin E, Okiemy-Akeli M-G, Morjani H, Lavaud C, et al. Cytotoxicity and apoptosis induced by alfalfa (*Medicago sativa*) leaf extracts in sensitive and multidrug-resistant tumor cells. Nutrition and Cancer. 2014;66(3):483–491. <https://doi.org/10.1080/01635581.2014.884228>
30. Brys R, Jacquemyn H, Hermy M, Beeckman T. Pollen deposition rates and the functioning of distyly in the perennial *Pulmonaria officinalis* (Boraginaceae). Plant Systematics and Evolution. 2008;273:1–12. <https://doi.org/10.1007/s00606-008-0003-5>
31. Chauhan S, Jaiswal V, Cho Y-I, Lee H-J. Biological activities and phytochemicals of lungworts (genus *Pulmonaria*) focusing on *Pulmonaria officinalis*. Applied Sciences. 2022;12(13):6678. <https://doi.org/10.3390/app12136678>
32. Hawrył MA, Waksmundzka-Hajnos M. Micro 2D-TLC of selected plant extracts in screening of their composition and antioxidative properties. Chromatographia 2013;76:1347–1352. <https://doi.org/10.1007/s10337-013-2490-y>
33. Farhadi N, Babaei K, Farsarae S, Moghaddam M, Ghasemi Pirbalouti A. Changes in essential oil compositions, total phenol, flavonoids and antioxidant capacity of *Achillea millefolium* at different growth stages. Industrial Crops and Products. 2020;152:112570. <https://doi.org/10.1016/j.indcrop.2020.112570>
34. Judzentiene A. Atypical chemical profiles of wild yarrow (*Achillea millefolium* L.) essential oils. Records of Natural Products. 2016;10(2):262–268.
35. Chavez-Silva F, Ceron-Romero L, Arias-Duran L, Navarrete-Vázquez G, Almanza-Pérez J, Román-Ramos R, et al. Antidiabetic effect of *Achillea millefolium* through multitarget interactions: α -glucosidases inhibition, insulin sensitization and insulin secretagogue activities. Journal of Ethnopharmacology. 2018;212:1–7. <https://doi.org/10.1016/j.jep.2017.10.005>
36. Bimbiraite K, Ragazinskiene O, Maruska A, Kornýšova O. Comparison of the chemical composition of four yarrow (*Achillea millefolium* L.) morphotypes. Biologija. 2008;54(3):208–212. <https://doi.org/10.2478/v10054-008-0046-0>
37. Akbaribazm M, Khazaei MR, Khazaei M. Phytochemicals and antioxidant activity of alcoholic/hydroalcoholic extract of *Trifolium pratense*. Chinese Herbal Medicines. 2020;12(3):326–335. <https://doi.org/10.1016/j.chmed.2020.02.002>
38. Khazaei M, Pazhouhi M. Protective effect of hydroalcoholic extracts of *Trifolium pratense* L. on pancreatic β cell line (RIN-5F) against cytotoxicity of streptozotocin. Research in Pharmaceutical Sciences. 2018;13(4):324–331. <https://doi.org/10.4103/1735-5362.235159>
39. Oza MJ, Kulkarni YA. *Trifolium pratense* (red clover) improve SIRT1 expression and glycogen content in high fat diet-streptozotocin induced type 2 diabetes in rats. Chemistry and Biodiversity. 2020;17:e2000019. <https://doi.org/10.1002/cbdv.202000019>
40. Akbaribazm M, Khazaei F, Naseri L, Pazhouhi M, Zamanian M, Khazaei M. Pharmacological and therapeutic properties of the red clover (*Trifolium pratense* L.): An overview of the new findings. Journal of Traditional Chinese Medicine. 2021;41(4):642–649. <https://doi.org/10.19852/j.cnki.jtcm.20210604.001>
41. Al-Shami AS, Essawy AE, Elkader H-TA. Molecular mechanisms underlying the potential neuroprotective effects of *Trifolium pratense* and its phytoestrogen-isoflavones in neurodegenerative disorders. Phytotherapy Research. 2023;37(6):2693–2737. <https://doi.org/10.1002/ptr.7870>
42. Liu H, Lu X, Hu Y, Fan X. Chemical constituents of *Panax ginseng* and *Panax notoginseng* explain why they differ in therapeutic efficacy. Pharmacological Research. 2020;161:105263. <https://doi.org/10.1016/j.phrs.2020.105263>

43. Kim J-H. Cardiovascular diseases and *Panax ginseng*: A review on molecular mechanisms and medical applications. *Journal of Ginseng Research*. 2012;36(1):16–26. <https://doi.org/10.5142/jgr.2012.36.1.16>
44. Kim KH, Lee D, Lee HL, Kim C-E, Jung K, Kang KS. Beneficial effects of *Panax ginseng* for the treatment and prevention of neurodegenerative diseases: past findings and future directions. *Journal of Ginseng Research*. 2018;42(3):239–247. <https://doi.org/10.1016/j.jgr.2017.03.011>
45. Kim S, Kim N, Jeong JY, Lee S, Kim W, Ko S-G, et al. Anti-cancer effect of *Panax ginseng* and its metabolites: From traditional medicine to modern drug discovery. *Processes*. 2021;9(8):1344. <https://doi.org/10.3390/pr9081344>
46. Naseri K, Saadati S, Sadeghi A, Asbaghi O, Ghaemi F, Zafarani F, et al. The efficacy of ginseng (*Panax*) on human prediabetes and type 2 diabetes mellitus: A systematic review and meta-analysis. *Nutrients*. 2022;14(12):2401. <https://doi.org/10.3390/nu14122401>
47. Truong V-L, Jeong W-S. Red ginseng (*Panax ginseng* Meyer) oil: A comprehensive review of extraction technologies, chemical composition, health benefits, molecular mechanisms, and safety. *Journal of Ginseng Research*. 2022;46(2):214–224. <https://doi.org/10.1016/j.jgr.2021.12.006>
48. Vesnina A, Milentyeva I, Minina V, Kozlova O, Asyakina L. Evaluation of the in vivo anti-atherosclerotic activity of quercetin isolated from the hairy roots of *Hedysarum neglectum* Ledeb. *Life*. 2023;13(8):1706. <https://doi.org/10.3390/life13081706>
49. Starostina NP, Durnova NA. Perspectives for the use of plants genus *Hedysarum* in medicine and pharmacy. *Science Diary*. 2021;(4):1–11. (In Russ.). https://doi.org/10.51691/2541-8327_2021_4_4; <https://elibrary.ru/ILGKJW>
50. Dyshlyuk LS, Fotina NV, Milentyeva IS, Ivanova SA, Izgarysheva NV, Golubtsova YuV. Antimicrobial and antioxidant activity of *Panax ginseng* and *Hedysarum neglectum* root crop extracts. *Brazilian Journal of Biology*. 2022;84:e256944. <https://doi.org/10.1590/1519-6984.256944>
51. Popovich SO, Grinets LV. Usage Siberian hogweed. *Youth and Science*. 2023;5:17. (In Russ.). <https://elibrary.ru/MDCVAY>
52. Tkachenko KG. *Heracleum* L. genus – economic plants. *Bulletin of Udmurt University. Series Biology. Earth Sciences*. 2014;(4):27–33. (In Russ.). <https://elibrary.ru/THPRJH>
53. Kolesnikova I, Saparklycheva SE. Spicy wild plants. *Youth and Science*. 2018;(2):13. (In Russ.). <https://elibrary.ru/UUQWYI>
54. The State Pharmacopeia of the Russian Federation. 13th edition [Internet]. [cited 2023 Mar 20]. Available from: <https://pharmacopoeia.regmed.ru/pharmacopoeia/izdanie-13/?ysclid=lx9t2qy4r5104949779>
55. De Luna SLR, Ramírez-Garza RE, Saldívar SOS. Environmentally friendly methods for flavonoid extraction from plant material: Impact of their operating conditions on yield and antioxidant properties. *The Scientific World Journal*. 2020;2020:6792069. <https://doi.org/10.1155/2020/6792069>
56. Adamtseвич NYu, Zakrzheuskaya YeI, Feskova EV, Leontiev VN, Titok VV. Development and validation of the method for the quantification of flavonoids in leaves of *Lithospermum officinale* (Boraginaceae). *Rastitelnye Resursy*. 2022;58(1):100–108. (In Russ.). <https://elibrary.ru/UIEUBR>
57. Malankina EL, Tkacheva EN, Kozlovskaya LN. Medicinal plants of the Lamiaceae family as flavonoids sources. *Problems of Biological, Medical and Pharmaceutical Chemistry*. 2018;21(1):30–35. (In Russ.). <https://doi.org/10.29296/25877313-2018-01-06>; <https://elibrary.ru/YPUTZH>
58. Tikhonov BB, Sidorov AI, Sulman EM, Ozhimkova EV. Glycans and flavonoids from raw materials as functional food components. *Herald of Tver State University. Series: Biology and Ecology*. 2011;(24):68–75. (In Russ.). <https://elibrary.ru/OPIUV>
59. Shkol'nikova MN, Averyanova EV, Tsapalova IE. *Hedysarum* lost – perspective raw material for manufacture of non-alcoholic balsams. *Beer and Beverages*. 2006;(2):66–67. (In Russ.). <https://elibrary.ru/ORNARX>
60. Konovalenko IC, Polovko NP, Bevz NYu. Development of quality control methods of infusion from gynecological medicinal plant collection. *Norwegian Journal of Development of the International Science*. 2019;(10–2):43–48. (In Russ.). <https://elibrary.ru/OYFJBN>
61. Kasatkina NI, Nelyubina ZhS. Biochemical characteristics of *Trifolium pratense* L. varieties in the conditions of the Udmurt Republic. *Chemistry of Plant Raw Materials*. 2022;(1):261–268. (In Russ.). <https://doi.org/10.14258/jcpm.2022019350>; <https://elibrary.ru/JDIWCU>
62. Karimi E, Oskoueian E, Oskoueian A, Omidvar V, Hendra R, Nazeran H. Insight into the functional and medicinal properties of *Medicago sativa* (Alfalfa) leaves extract. *Journal of Medicinal Plants Research*. 2013;7(7):290–297.
63. Dushlyuk LS, Drozdova MYu, Loseva AI. Study on safety profile in extracts of *Pulmonaria officinalis* callus cultures and their phytochemical composition for the presence bioactive substances with the potential geroprotective properties. *Proceedings of Universities. Applied Chemistry and Biotechnology*. 2021;11(2):260–271. (In Russ.). <https://doi.org/10.21285/2227-2925-2021-11-2-260-271>; <https://elibrary.ru/HIEEZU>

64. Lin Z, Xie R, Zhong C, Huang J, Shi P, Yao H. Recent progress (2015–2020) in the investigation of the pharmacological effects and mechanisms of ginsenoside Rb₁, a main active ingredient in *Panax ginseng* Meyer. Journal of Ginseng Research. 2022;46(1):39–53. <https://doi.org/10.1016/j.jgr.2021.07.008>
65. Dauqan EMA, Abdullah A. Medicinal and functional values of thyme (*Thymus vulgaris* L.) herb. Journal of Applied Biology and Biotechnology. 2017;5(2):017–022. <https://doi.org/10.7324/JABB.2017.50203>
66. Mărculescu A, Vlase L, Hanganu D, Drăgulescu C, Antonie I, Neli-Kinga O. Polyphenols analyses from *Thymus* species. Proceedings of the Romanian Academy. Series B: Chemistry, Life Sciences, and Geosciences. 2007;3: 117–121.
67. Asyakina LK, Fotina NV, Izgarysheva NV, Slavyanskiy AA, Neverova OA. Geroprotective potential of *in vitro* bioactive compounds isolated from yarrow (*Achillea millefolium* L.) cell cultures. Foods and Raw Materials. 2021;9(1):126–134. <https://doi.org/10.21603/2308-4057-2021-1-126-134>
68. Babich OO, Samsuev IG, Tcibulnikova AV, Zemlyakova ES, Popov AD, Ivanova SA, et al. Properties of plant extracts and component composition: column chromatography and IR spectroscopy. Foods and Raw Materials. 2024;12(2):373–387. <https://doi.org/10.21603/2308-4057-2024-2-615>
69. Tundis R, Marrelli M, Conforti F, Tenuta MC, Bonesi M, Menichini F, et al. *Trifolium pratense* and *T. repens* (Leguminosae): Edible flower extracts as functional ingredients. Foods. 2015;4(3):338–348. <https://doi.org/10.3390/foods4030338>

ORCID IDs

Natalia S. Velichkovich  <https://orcid.org/0000-0002-9061-1256>
 Nina I. Dunchenko  <https://orcid.org/0000-0002-6158-9854>
 Anna A. Stepanova  <https://orcid.org/0000-0001-7774-8859>
 Oksana V. Kozlova  <https://orcid.org/0000-0002-2960-0216>
 Elizaveta R. Faskhutdinova  <https://orcid.org/0000-0001-9711-2145>
 Vladimir P. Yustratov  <https://orcid.org/0000-0002-1779-4332>
 Sergey L. Luzyanin  <https://orcid.org/0000-0001-9293-4377>



Optimizing the utilization of pomelo (*Citrus maxima* (Brum.) Merr.) seeds as a quality dietary fiber

Budianto^{1,*}, Anik Suparmi², Dewi Susanti³

¹ Institute Science and Technology Al-Kamal^{IROR}, Jakarta, Indonesia

² SMA Negeri 4 Tarakan, Tarakan City, Indonesia

³ Poltekkes Kemenkes Pontianak, Pontianak, Indonesia

* e-mail: budianto_delta@yahoo.com

Received 29.09.2023; Revised 03.11.2023; Accepted 05.12.2023; Published online 18.10.2024

Abstract:

Orange seeds, often overlooked as waste, have hidden potential since fiber derived from them contains numerous biochemical substances that can enhance the nutritional value of food. We aimed to investigate the impact of pomelo seed fiber on the biscuit dough's properties (starch and gluten), physicochemical characteristics, and biochemistry, as well as the product's shelf life.

We studied three types of samples: control (no dietary fiber), biscuits with dietary fiber from pomelo (*Citrus maxima* (Brum.) Merr.) seeds, and biscuits with wheat germ fiber. Scanning electron microscopy was employed to analyze rubbery starch and gluten in the dough, while response surface methods were used to optimize the biscuits' strength via a central composite design. The product's shelf life was determined based on microbial contamination levels. ANOVA test and Tukey's Honestly Significant Difference post hoc test were performed to assess the differences in physicochemical and biochemical properties.

Citrus seed fiber influenced rubbery starch and gluten properties, causing significant differences ($p < 0.05$) in fracturability, total dietary fiber, and Trolox equivalent antioxidant capacity among the three samples. The biscuits enriched with citrus seed fiber contained flavonoid compounds and acylserotonin, with acyl-N ω -methylserotonin dominating in the C22 and C24 homologs. Despite varied evaluations in texture and aroma, the biscuits with citrus seed fiber were well-received for their taste and boasted an extended shelf life (> 12 months).

Dietary fiber obtained from *C. maxima* seeds not only enhanced the nutritional value of the biscuits but also paved the way for innovative healthy food opportunities.

Keywords: Acyl-N ω -methylserotonins, citrus seeds, dietary fiber, N-serotonin, rubbery gluten, rubbery starch, nutritional value

Please cite this article in press as: Budianto, Suparmi A, Susanti D. Optimizing the utilization of pomelo (*Citrus maxima* (Brum.) Merr.) seeds as a quality dietary fiber. Foods and Raw Materials. 2025;13(2):233–241. <https://doi.org/10.21603/2308-4057-2025-2-636>

INTRODUCTION

Orange seeds, often overlooked and dismissed as waste, possess untapped potential waiting to be fully explored. These seeds are a rich source of various biochemical substances, including fatty acids, limonoids, tocopherols, phytosterols, dietary fiber, and flavonoids. Extensive research has revealed their pharmaceutical potential, including anticancer, anti-hematopoiesis, antifertility, and hepatoprotective properties [1–8]. Furthermore, these valuable biochemical compounds can enhance the nutritional value and quality standards of food products [9]. The diverse range of biochemical compounds found in orange seeds makes them a compelling subject for further investigation as potential food additives.

While it is widely acknowledged that biochemical compounds found in orange seeds have potential to enhance the nutritional value and dietary fiber content, there is an ongoing debate among researchers regarding the precise impact of incorporating these ingredients into food products. Notably, the addition of dietary fiber derived from orange seed flour has been shown to influence various properties, including emulsion properties, water absorption in dough, biscuit friability, and the microfibril structure of dough [10–12]. However, there has been a notable absence of research investigating the effects of dietary fiber on the characteristics of rubbery starch and gluten in dough. This represents a significant gap in the existing body of research on the subject.

The production of dietary fiber from orange seeds has traditionally relied on older methods, such as those employed by Akpata & Akubor and Yilmaz & Karaman, involving the removal of seed shells and oil [10, 11]. Orange seed shells and their oil contain a unique compound, N-serotonin, which is relatively rare in the seeds of other plants [13]. In this research, we undertook a novel approach to producing orange seed fiber, which retains the seed shells and oil.

The wealth of antioxidant compounds and pectin fiber in orange seeds becomes particularly evident when they are processed into dietary fiber and subjected to thorough testing. In this research, we assessed their influence on the properties of rubbery starch and gluten in the dough, a concept that has already been extensively studied and well-established [14]. Furthermore, we scrutinized the physicochemical attributes of the final product, namely biscuits. We also conducted optimization trials utilizing the central composite design methodology.

Orange seed oil exhibits potential as an antibacterial agent, although its antimicrobial activity is relatively less potent compared to that of orange fruit and peel oil [15]. Research on *Citrus aurantifolia* seeds using chloroform, methanol, and ethanol has demonstrated robust antibacterial efficacy [16]. Additionally, the ethanol extract of *Citrus paradisi* Macf. seeds from the *Rutaceae* family has exhibited remarkable antifungal activity [17]. However, some studies have suggested that orange seed extract possesses even stronger antibacterial properties [18, 19]. In this study, we assessed the antimicrobial attributes of pomelo (*Citrus maxima* (Brum.) Merr.) seeds. This assessment was designed to determine the shelf life of products by evaluating microorganism contamination levels.

The core focus of our research revolved around the utilization of pomelo seeds to elevate the quality of biscuits. To achieve this, we set two primary objectives: (i) scrutinizing the influence of citrus seed fiber on the properties of rubbery starch and gluten in the dough, and (ii) evaluating the impact of citrus seed fiber on the physicochemical, biochemical, and shelf life characteristics of the biscuits. For this, we employed fiber derived from pomelo seeds along with dietary fiber sourced from wheat seeds as integral components of our study materials.

STUDY OBJECTS AND METHODS

Materials. The following materials were procured from a local grocery store: pomelo seeds (*Citrus maxima* (Brum.) Merr.), wheat flour, and dietary fiber extracted from wheat seeds. Additionally, we obtained various chemical reagents and solutions essential for our experiments, including HOBt solution (N-hydroxybenzotriazole), hexane, 95% alcohol, tetrahydrofuran, EDC (1-ethyl-3-(3-dimethylaminopropyl) carbodiimide), triethylamine, ethyl acetate, NaOH, HCl, dimethylformamide, H_2SO_4 , and Nucleophile. We also acquired specific chemical solutions to conduct tests for flavonoids, phenolics, protein, fat, and ash contents, as well as antioxidant substances.

Producing pomelo (*C. maxima*) seed powder.

First, we thoroughly cleaned and dried pomelo seeds in an oven at 50°C for 4 h. Then, we ground the seeds to break down all of their components, including the outer shell. The resulting product underwent further drying in the oven until its moisture content reached below 10%. To ensure a uniform fineness of the flour, we sifted it through a 100-mesh sieve. Any remaining coarse particles were subjected to additional grinding and sifting until a consistent flour fineness was achieved.

Extracting dietary fiber from pomelo seed powder. The pomelo seed flour was combined with distilled water (1:20) and homogenized at 12 500 rpm for 10 min. To optimize extraction efficiency and product quality, ultrasonic treatment was applied using a UP400St ultrasonic device (Hielscher Ultrasonics) with an amplitude of 90% for 10 min. It was followed by a 5-min break to allow the mixture's temperature to reach 45°C. The resulting mixture was subsequently filtered through a filter cloth with a mesh size of 0.150 mm. Any remaining solid residue was carefully rinsed five times with water before being dried under vacuum conditions at 50°C for 4 days.

Biscuit production. All the ingredients for making biscuits, including wheat flour (40%), shortening (14%), sugar (8%), dietary fiber (3%), and salt (2%), were thoroughly mixed to ensure even distribution. Water (33%) was added to the mixture, and it was blended using a mixer at medium speed for 15 min. The dough was then molded using a biscuit machine with minimal capacity to form wet weights of 7 g per dough portion. These portions were baked in a rotary oven at 160°C (20 rpm) for 30 min. After baking, the biscuits were promptly transferred to a room with a temperature of 14°C and a relative humidity of about 55%. To preserve their freshness, the biscuits were individually wrapped in plastic packaging with resealable zippers as needed.

The samples with dietary fiber were divided into two distinct groups: those containing wheat fiber and those enriched with citrus seed fiber. In addition, we conducted analyses on the control samples that did not contain any dietary fiber.

Physical analysis of the biscuits. The surface color of three randomly selected biscuit samples was evaluated using a WR-10 QC colorimeter (China), while their hardness and brittleness were assessed using PRE MAD-TPA texture analysis (Brookfield Engineering Laboratories, Inc., USA). The physical appearance of the dietary fiber dough and its impact on the adhesive properties of starch and gluten were examined using an Axia Chemi scanning electron microscope (Fisher Scientific, USA). Images displaying the biscuit texture and pores were captured using a cellphone.

Furthermore, we conducted an optimization test using two factors, temperature and heating time, to determine the friability of biscuits with citrus seed fiber. For this test, we employed response surface methods and a central composite design.

Chemical analysis. The extraction of N-acylserotonin. The established protocol for synthesizing N-acylserotonin compounds has been previously executed and subsequently validated by Kruk *et al.* [13, 20]. In this procedure, the fatty acids contained in the dietary fiber were dissolved in 18 mg of HOBT (N-hydroxybenzotriazole) solution and 1 mL of tetra-hydrofuran. Then, 22 μ L of EDC (1-ethyl-3-(3-dimethylaminopropyl) carbodiimide) was added to the mixture and stirred. Concurrently, serotonin hydrochloride was dissolved in 500 μ L of dimethylformamide, and 12 μ L of triethylamine was introduced into the mixture. The resulting mixture was stirred and then subjected to extraction using 5 mL of ethyl acetate and 5 mL of water. The reaction product was subsequently collected, evaporated, and reconstituted in 2 mL of peroxide-free anhydrous tetrahydrofuran.

The hydrolysis of N-acylserotonin. The method of hydrolyzing N-acylserotonin has previously been employed by Kruk *et al.* and Trela-Makowej *et al.* [13, 20]. The compound fractions $C_{33}H_{56}N_2O_2Na^+$ and $C_{35}H_{60}N_2O_2Na^+$ were subjected to hydrolysis in a concentrated solution of HCl and tetrahydrofuran (1:9, v/v) at 105°C for 1 h and subsequently evaporated to dryness. The resultant fatty acids contained in 5-mL Wheaton glass vials were then combined with serotonin. In parallel, 100 mg of lemon seed oil was dissolved in 1 mL of ethanol, followed by the addition of 100 μ L of saturated NaOH in water. The mixture was heated for 1 h at 90°C using a thermoblock. Subsequently, the solution was neutralized with HCl, and the fatty acids were extracted with ethyl acetate after dilution with water. Upon evaporation under a nitrogen atmosphere, the obtained fatty acids were also combined with serotonin.

N-acylserotonin was identified in dietary fiber extracts by assessing peak areas on HPLC chromatograms using a GSYS0002 instrument (Gilson Inc., USA) in conjunction with the synthetic standards of known concentrations. The HPLC setup involved a reverse-phase Nucleophil 100 C18 column and a mobile phase consisting of CAN, MeOH, and H_2O (70:7.5:1, v/v). The chromatographic separation was carried out at a flow rate of 1.4 mL/min.

The nutritional components were analyzed as follows. The moisture content was assessed using an HC103 moisture analyzer (Metler Toledo), while water activity was measured with an MS2100 water activity moisture meter. The crude protein content was determined following method 46–12 of the Association of Official Analytical Chemists (AOAC). The fat and ash contents were quantified using the AOAC's method 30–10 [21]. All the results obtained from these analyses were reported as percentages based on dry weight. Additionally, the Kjeldahl method served as a correction factor for any remaining protein levels.

The capacity of both free and bound phenolic compounds was evaluated by using phenolic extracts. The extract was obtained as outlined in [22] to be subsequently concentrated and reconstituted in 3 mL of deio-

nized water. A membrane filter was utilized to purify the deionized water. Free and bound phenolics were determined by measuring the Trolox equivalent antioxidant capacity (TEAC) as described in [23].

Microbiological test. In our study, we conducted periodic assessments of microbial growth in the three biscuit samples, with observations made once every month over a span of 12 months. These evaluations involved quantitative testing for bacteria using the total plate count method, as well as for yeast and mold [24].

Respondent selection. Randomly selected employees of a biscuit company located in the Bandung region of West Java, Indonesia, were invited to provide their feedback and opinions regarding our research biscuits. The level of respondent acceptance was assessed using the 1–5 Likert scale, with the following interpretations: 1 – “strongly disagree”, 2 – “disagree”, 3 – “neutral”, 4 – “agree”, and 5 – “strongly agree”.

Statistical analysis. The data analyses were conducted using IBM SPSS Statistics, version 26 (SPSS Inc., Chicago, IL, USA). An analysis of variance (ANOVA) was employed, followed by the Tukey Honestly Significant Difference post hoc test to discern variations in the biscuit biochemical levels. The results were presented in the format of mean \pm standard deviation, and statistical significance was determined at a significance level of $p < 0.05$.

RESULTS AND DISCUSSION

Dietary fiber and dough characteristics (starch and gluten granules). Incorporating 3% of dietary fiber and 33% of water into the biscuit dough significantly altered its properties, particularly starch and gluten granules. As illustrated in Fig. 1, the control sample exhibited a strong binding between starch and gluten granules at multiple points. Additionally, liquefied gluten was observed, which effectively bound starch granules from the flour. The control dough sample showed minimal voids, or empty spaces.

The presence of dietary fiber extracted from wheat grain significantly impacted the rubbery starch and gluten phases. The standard practice involves adding water to the mixture to achieve these phases. According to Fig. 1, the rubbery starch and gluten phases were clearly distinguishable in the control dough (without dietary fiber). In contrast, the wheat fiber dough displayed reduced stickiness and elasticity compared to the control sample. A similar behavior was also evident in the dough containing citrus (pomelo) seed fiber.

The incorporation of dietary fiber has a notable impact on the structure of starch and gluten granules within the dough. Blanshard previously indicated that in good bread dough, a water content of over 20%, with no heating, resulted in a rubbery consistency involving both starch and gluten [14]. This state leads to the amalgamation of starch and gluten. In our study, the control samples displayed conditions that align with Blanshard's ideal criteria for bread

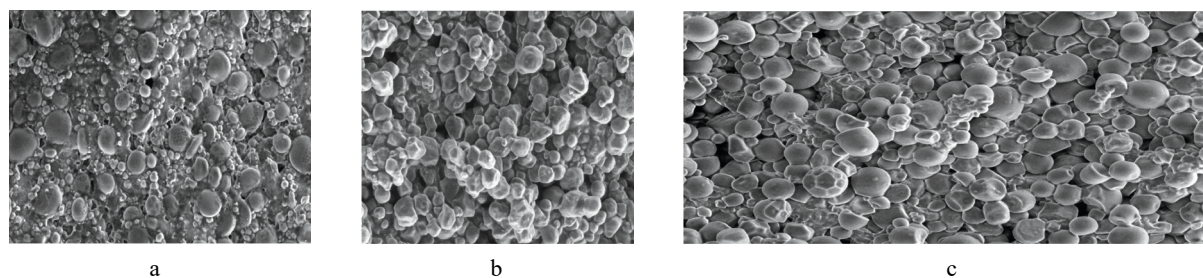


Figure 1 Physical appearance of starch and gluten granules in biscuit dough on Scan Electron Microscopy within 50 μm : a – control; b – wheat dietary fiber; c – citrus seed dietary fiber

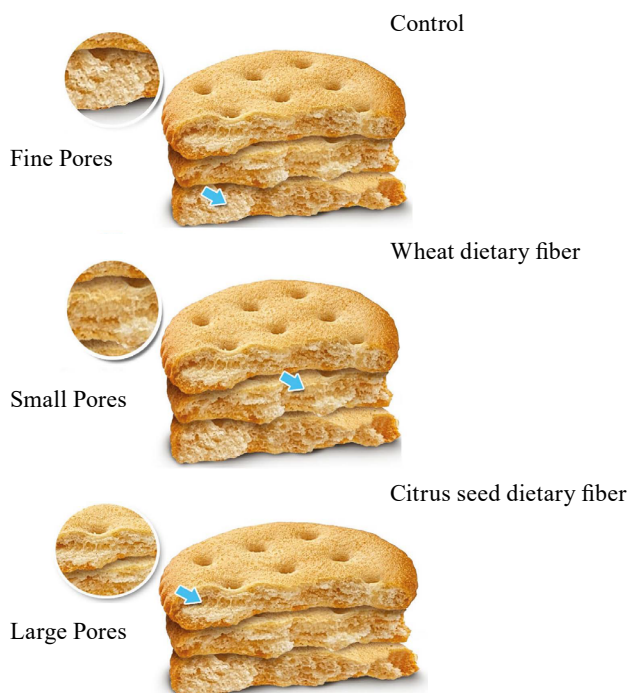


Figure 2 Physical appearance of the biscuits baked at 160°C for 40 min. Biscuit thickness ranged from 5.01 ± 0.15 mm on 50 \times magnification on a cellphone camera

production [14]. Conversely, in the wheat fiber and pomelo seed fiber samples, the liquefaction of starch and gluten was not as evident, resulting in discernible differences in tensile strength and brittleness when the biscuits were subjected to breaking.

Physicochemical chemical analysis and antioxidant composition. The doughs (Fig. 1) were then baked in the oven at 160°C for 40 min. We deliberately enlarged (50 \times) the images of the resulting biscuits (Fig. 2) to see the differences in their pores. As can be seen, the pores of the control sample were small in diameter (0.1 mm) but evenly distributed on all the sides. The wheat fiber sample had large pores (0.2 mm), as well as small ones evenly distributed on all the sides. In the pomelo seed fiber samples, almost all the surfaces were dominated by large pores (± 0.3 mm), with some smaller pores observed as well.

According to Table 1, we observed no notable differences ($p > 0.05$) among the three samples in terms

of weight loss, thickness, or the contents of protein, fat, ash, and soluble dietary fiber. Specifically, no significant disparities were detected between the control and the wheat fiber samples, while a significant difference ($p < 0.05$) was identified in the citrus seed fiber sample. This discrepancy was also evident when examining color (b^*), TEAC (bound), water activity, and moisture.

Significant distinctions ($p < 0.05$) were observed among the three samples in terms of color (a^*), fracturability, total dietary fiber, insoluble dietary fiber, and TEAC (free). We focused our attention on achieving similar levels of fragility in the citrus seed fiber sample as those found in the control and the wheat fiber samples. Maintaining a consistent level of brittleness is crucial to prevent difficulties in the subsequent process, specifically during the packing phase, where powdery characteristics can be problematic.

All the three samples contained antioxidants equivalent to Trolox, with the citrus seed fiber sample exhibiting the highest content of both free (9.11 ± 0.24 $\mu\text{mole Trolox/g}$) and bound (8.21 ± 0.19 $\mu\text{mole Trolox/g}$) TEAC. Additionally, we found that the biscuits enriched with citrus seed fiber also contained flavonoid compounds that were absent in the other two samples. These flavonoid compounds included eriocitrin (free/bound), rutin (free/bound), naringin (free/bound), hesperidin (bound), neohesperidin (free), and naringenin (free). Our findings align closely with the results reported by Yilmaz & Karaman [11].

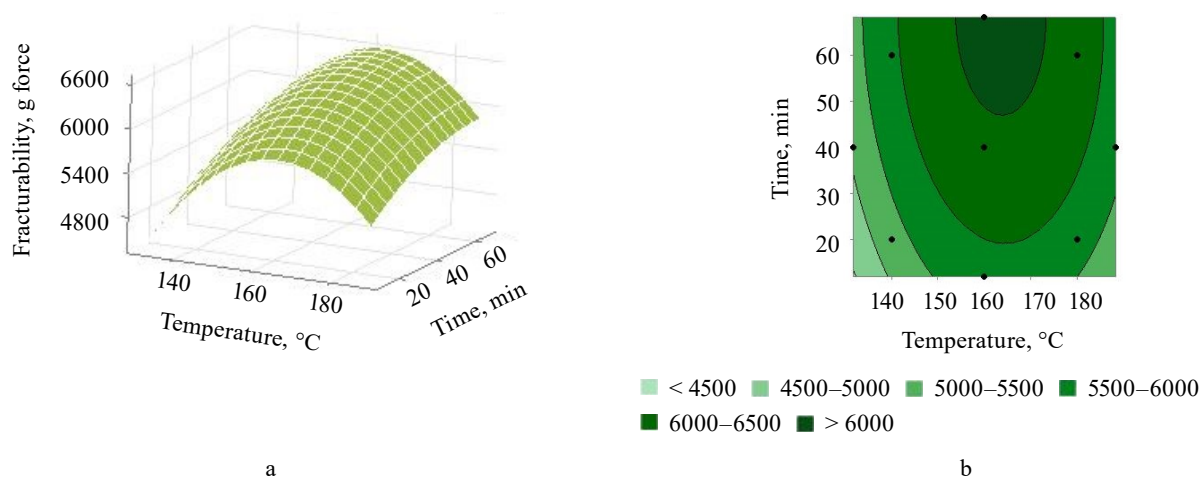
Baking time and temperature optimization for fragile biscuits. We aimed to optimize the baking of biscuits containing citrus seed fiber with a fracturability value of 4326 ± 56 g force. This value was exceptionally high and it was crucial for the packaging process. Therefore, we sought to attain a fracturability value that was equal or close to the values of the control sample (7011 ± 34) and the wheat fiber sample (5990 ± 56). To achieve this, we employed two variables, temperature and time, aiming to establish the standard fracturability values equivalent to those of the control sample. The outcomes of our analysis are presented in Fig. 3.

We conducted a series of experiments utilizing response surface methodology and a central composite design, which were repeated 13 times. In these experiments, we systematically explored a temperature range

Table 1 Physicochemical characteristics and antioxidant composition of the biscuits under study

Property	Control (no fiber)	Wheat fiber	Citrus seed fiber
Weight loss, %	14.58 ± 0.34 ^a	15.21 ± 0.41 ^a	15.01 ± 0.21 ^a
Thickness, mm	4.80 ± 0.10 ^a	4.89 ± 0.12 ^a	5.01 ± 0.15 ^a
Color <i>L</i>	64.32 ± 0.23 ^a	68.21 ± 0.13 ^b	66.64 ± 0.34 ^{ab}
<i>a</i> *	8.90 ± 0.18 ^c	6.70 ± 0.21 ^b	5.54 ± 0.26 ^a
<i>b</i> *	28.86 ± 0.21 ^b	28.27 ± 0.42 ^b	25.32 ± 0.27 ^a
Fracturability, g force	7011 ± 34 ^c	5990 ± 56 ^b	4326 ± 56 ^a
Hardness, g force	4221 ± 35 ^a	6218 ± 65 ^b	5738 ± 47 ^{ab}
Moisture, %	2.65 ± 0.21 ^a	3.01 ± 0.26 ^{ab}	4.03 ± 0.31 ^b
Water activity, <i>A_w</i>	0.15 ± 0.02 ^b	0.13 ± 0.01 ^{ab}	0.10 ± 0.01 ^a
Protein, % dry weight	11.37 ± 0.28 ^a	11.07 ± 0.31 ^a	11.27 ± 0.26 ^a
Fat, % dry weight	14.34 ± 0.29 ^a	14.61 ± 0.45 ^a	14.06 ± 0.36 ^a
Ash, % dry weight	1.54 ± 0.10 ^a	1.62 ± 0.26 ^a	1.59 ± 0.36 ^a
Total dietary fiber, % dry weight	5.12 ± 0.35 ^a	10.28 ± 0.13 ^c	7.42 ± 0.36 ^b
Insoluble dietary fiber, % dry weight	3.23 ± 0.19 ^a	8.04 ± 0.23 ^c	5.23 ± 0.16 ^b
Soluble dietary fiber, % dry weight	3.03 ± 0.15 ^a	2.98 ± 0.23 ^a	3.08 ± 0.14 ^a
TEAC-free, μmole Trolox/g	5.41 ± 0.11 ^b	2.49 ± 0.18 ^a	9.11 ± 0.24 ^c
TEAC-bound, μmole Trolox/g	2.43 ± 0.17 ^a	2.67 ± 0.15 ^a	8.21 ± 0.19 ^b

TEAC – Trolox equivalent antioxidant capacity

**Figure 3** The influence of baking temperature and time on the fracturability of biscuits. The surface visual plot (a) and contour plot (b) of the citrus seed fiber samples

from 140 to 180°C and a time range from 20 to 60 min to analyze their combined impact on fracturability values. Our findings indicated a significant correlation between time and temperature, leading us to identify optimal fracturability values within the time window of 50–60 min and the temperature range of 155–170°C.

As a result of the optimization test conducted with response surface methodology, the fracture strength of the citrus seed fiber samples increased from 4326 to 6000 g force, approaching the values of the control and the wheat fiber samples.

The composition of phenolic acids, flavonoids, and acylserotonin. The phenolic test conducted on the three biscuit samples revealed no statistically significant differences ($p > 0.05$) for various phenolic compounds, including gallic, caffeic, syringic and sy-

ringic (bound), *p*-coumaric and *p*-coumaric (bound), *trans*-ferulic acid, and *trans*-2-hydroxycinnamic acids (Table 2).

When comparing the control with the citrus seed fiber sample, significant differences ($p < 0.05$) were observed in the levels of gallic acid (bound), 3,4-hydroxybenzoic acid, and 3,4-hydroxybenzoic acid (bound). Additionally, vanilic acid was only present in the citrus seed fiber sample. Conversely, vanilic acid (bound) exhibited the opposite trend, with significant differences in its levels between the citrus seed fiber sample and the control.

The citrus seed fiber sample contained several flavonoid biochemicals that were absent in the control and wheat fiber samples. These included eriocitrin, rutin, naringin, hesperidin, neohesperidin, and naringenin,

Table 2 The composition of phenolic acids, acylserotonin, and flavonoids

Biochemical	Control	Wheat fiber	Citrus seed fiber
Phenolic acids, mg/g sample			
Gallic acid	2.70 ± 0.34 ^a	2.42 ± 0.41 ^a	2.20 ± 0.49 ^a
<i>Bound</i>	0.13 ± 0.02 ^a	0.16 ± 0.02 ^a	0.23 ± 0.01 ^b
3,4-Hydroxybenzoic acid	0.410 ± 0.015 ^a	0.470 ± 0.018 ^a	0.74 ± 0.02 ^b
<i>Bound</i>	0.001 ± 0.000 ^a	0.0070 ± 0.0001 ^a	0.037 ± 0.002 ^b
Vanilic acid	n.d.	n.d.	0.028 ± 0.002
<i>Bound</i>	0.019 ± 0.001 ^a	0.020 ± 0.002 ^a	n.d.
Caffeic acid	0.314 ± 0.020 ^a	0.29 ± 0.01 ^a	0.32 ± 0.01 ^a
<i>Bound</i>	0.23 ± 0.01 ^a	0.21 ± 0.01 ^a	n.d.
Syringic acid	0.103 ± 0.001 ^a	0.1060 ± 0.012 ^a	0.115 ± 0.001 ^a
<i>Bound</i>	0.109 ± 0.002 ^a	0.1170 ± 0.013 ^a	0.105 ± 0.002 ^a
<i>p</i> -Coumaric acid	0.118 ± 0.010 ^a	0.108 ± 0.020 ^a	0.115 ± 0.030 ^a
<i>Bound</i>	0.114 ± 0.020 ^a	0.112 ± 0.020 ^a	0.105 ± 0.010 ^a
Sinapic acid	n.d.	n.d.	n.d.
<i>Bound</i>	0.049 ± 0.001 ^a	0.051 ± 0.002 ^a	n.d.
<i>trans</i> -Ferulic acid	4.12 ± 0.40 ^b	2.10 ± 0.21 ^a	n.d.
<i>Bound</i>	2.06 ± 0.12 ^a	2.16 ± 0.21 ^a	1.98 ± 0.01 ^a
<i>trans</i> -2-Hydroxycinnamic acid	0.53 ± 0.01 ^a	0.61 ± 0.02 ^a	0.58 ± 0.01 ^a
<i>Bound</i>	0.12 ± 0.01 ^a	0.14 ± 0.02 ^{ab}	0.16 ± 0.01 ^b
Acylserotonin, mg/g sample			
ai-C21 (18-Methyleicosanoic)	n.d.	n.d.	0.70 ± 0.02
Me-C20	n.d.	n.d.	0.40 ± 0.02
n-C21	n.d.	n.d.	0.30 ± 0.01
Me-C21	n.d.	n.d.	1.90 ± 0.02
n-C22	n.d.	n.d.	1.40 ± 0.40
ai-C23 (20-Methyldocosanoic acid)	n.d.	n.d.	0.70 ± 0.21
Me-C22	n.d.	n.d.	3.30 ± 0.24
n-C23	n.d.	n.d.	1.10 ± 0.13
Me-ai-C23	n.d.	n.d.	0.40 ± 0.02
Me-C23	n.d.	n.d.	3.70 ± 0.21
n-C24	n.d.	n.d.	0.60 ± 0.21
ai-C25 (22-Methyltetracosanoic acid)	n.d.	n.d.	0.50 ± 0.01
Me-C24	n.d.	n.d.	2.20 ± 0.62
n-C25	n.d.	n.d.	1.10 ± 0.02
iso-C26 (24- Methyleicosanoic acid)	n.d.	n.d.	0.90 ± 0.03
Me-C25	n.d.	n.d.	1.90 ± 0.02
n-C26	n.d.	n.d.	1.20 ± 0.02
ai-C27 (25-Methylhexacosanoic acid)	n.d.	n.d.	0.20 ± 0.01
Me-C26	n.d.	n.d.	2.50 ± 0.17
n-C27	n.d.	n.d.	0.10 ± 0.01
iso-C28 (26-Methyleicosanoic acid)	n.d.	n.d.	0.20 ± 0.02
Me-C27	n.d.	n.d.	0.20 ± 0.01
n-C28	n.d.	n.d.	0.40 ± 0.01
Flavonoids, mg/g sample			
Eriocitrin	n.d.	n.d.	0.074 ± 0.004
<i>Bound</i>	n.d.	n.d.	0.1140 ± 0.0005
Rutin	n.d.	n.d.	1.0440 ± 0.0001
<i>Bound</i>	n.d.	n.d.	2.622 ± 0.006
Naringin	n.d.	n.d.	1.455 ± 0.095
<i>Bound</i>	n.d.	n.d.	0.232 ± 0.004
Hesperidin	n.d.	n.d.	n.d.
<i>Bound</i>	n.d.	n.d.	0.250 ± 0.001
Neohesperidin	n.d.	n.d.	0.315 ± 0.006
<i>Bound</i>	n.d.	n.d.	n.d.
Naringenin	n.d.	n.d.	0.129 ± 0.001
<i>Bound</i>	n.d.	n.d.	n.d.

n.d. – not detected

both in their free and bound forms. Notably, naringin exhibited the highest concentration among these compounds. Additionally, the citrus seed fiber sample lacked free hesperidin, bound neohesperidin, and bound naringenin. Phenolic acid compounds, including gallic acid (bound), 3,4-hydroxybenzoic acid (free and bound), and *trans*-2-hydroxycinnamic acid (bound), were prominently present in the citrus seed fiber sample. These results were similar to those reported by Yilmaz & Karaman [11].

The acylserotonin compound was exclusively identified in the citrus seed fiber sample and was absent in the control and wheat fiber samples. These findings reinforced the results of Kruk *et al.*, who reported that citrus seeds contain serotonin (5-hydroxytryptamine, 5-HT) compounds, which are relatively rare in other plant seeds [13]. Having analyzed acylserotonin levels within the citrus seed fiber samples, we found a prevalence of long-chain acyl-methylserotonin. This dominance was evident through the elevated values of such compounds as Methyl-C22-serotonin, Methyl-C23-serotonin, Methyl-C24-serotonin, Methyl-C25-serotonin, and Methyl-C26-serotonin, all of which exceeded 1.5 mg/g in the sample content.

The distribution of acylserotonin compounds in the citrus seed fiber samples indicated that normal-chain acylserotonin came second in terms of prevalence. This was evident through the presence of compounds such as n-C22-serotonin (1.4 mg/g), n-C23-serotonin (1.1 mg/g), n-C25-serotonin (1.1 mg/g), n-C26-serotonin (1.2 mg/g), and other normal-chain acylserotonin compounds with concentrations below 1 mg/g. In contrast, branched-chain acylserotonin compounds were detected in lower quantities, with ai-C21-serotonin present at 0.7 mg/g and ai-C27-serotonin at the lowest concentration of 0.2 mg/g. Additionally, long- and branched-chain acylserotonins

were identified, albeit in very small amounts, exemplified by the compound methyl-anteiso-C23-serotonin (Me-ai-C23) at 0.4 mg/g.

Microorganism contamination analysis. Over the course of 12 months, we conducted regular observations of bacterial contamination, including the total plate count, as well as yeast and mold levels (Fig. 4). These assessments were conducted on a monthly basis. The maximum allowable limits for microbial contamination in biscuits are established by the Indonesian Food and Drug Supervisory Agency [25]. According to their guidelines, the permissible limits are 1×10^4 CFU/g for the total plate count, as well as for the total yeast and mold contamination.

In the control samples, bacterial contamination had peaked at the 11th month, reaching its maximum allowable limit of 1×10^4 CFU/g. By the 12th month, bacterial contamination had further increased to 1.4×10^4 CFU/g. The overall yeast and mold contamination in these samples had already reached 1.2×10^4 CFU/g by the 10th month. Consequently, when considering microbial contamination, the product's effective age in the control samples could be regarded as only 10 months.

The shelf life of the wheat fiber biscuits extended to 12 months, even with a microbial contamination level of 1.15×10^4 CFU/g and total yeast and mold contamination of 1.1×10^4 CFU/g. In contrast, the citrus seed fiber biscuits exhibited lower bacterial contamination at 8.7×10^3 CFU/g by the 12th month, reaching total yeast and mold levels of 9.8×10^3 CFU/g. Notably, the biscuits containing citrus seed fiber boasted a shelf life exceeding 12 months. Thus, citrus seed fiber effectively extended the product's longevity with regards to microbial contamination, as illustrated in Fig. 4a.

While our study did not explicitly focus on microbial aspects, these results bolster the findings from previous

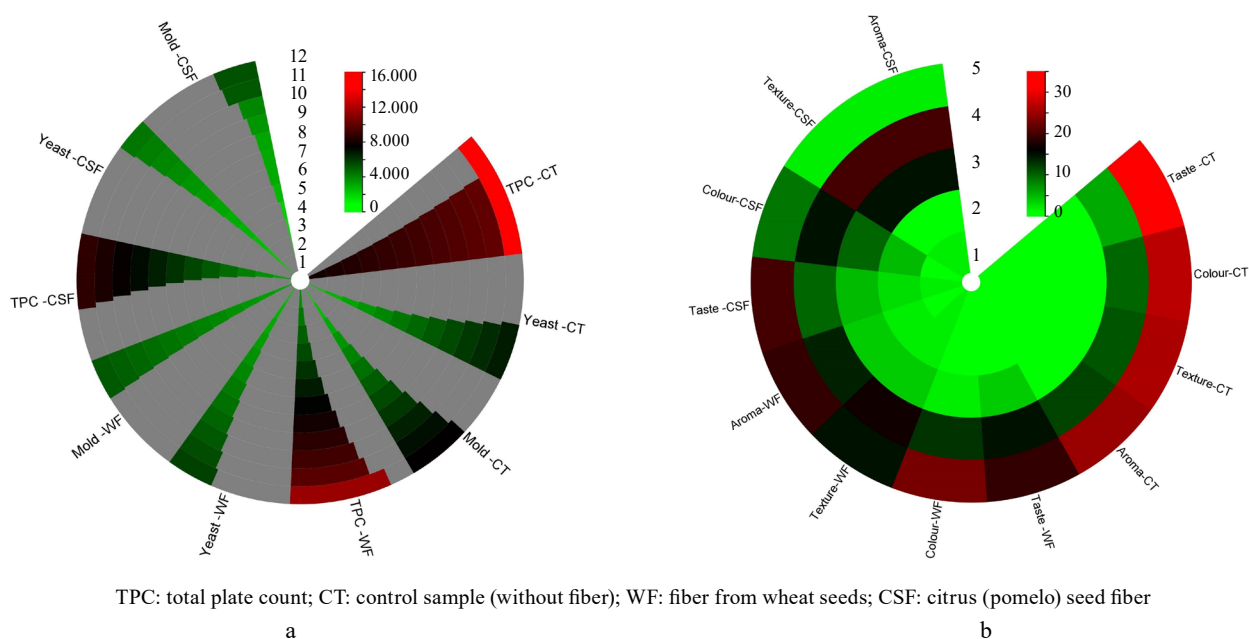


Figure 4 Heatmap diagrams of microorganism contamination (a) and sensory evaluation (b) on the five-point Likert scale

research, indicating the positive impact of citrus seed fiber on the product's longevity and quality [16, 17, 19].

Sensory evaluation of the biscuits. A total of 40 respondents were randomly selected to evaluate the biscuits' quality in terms of taste, color, aroma, and texture. Figure 4b indicates a strong preference for the control biscuits among the respondents, as evidenced by the dominant red color in the chart. In the case of wheat fiber biscuits, the respondents particularly appreciated their color (57.5%) and aroma (47.5%). As for the biscuits with citrus seed fiber, the respondents showed a preference for their taste (50%), with some positive feedback regarding their color (22.5%) and a smaller proportion appreciating their texture (5%) and aroma (5%). While these biscuits may not be as popular as the control or wheat fiber samples, there is still potential for enhancing their quality, especially in terms of texture, aroma, and color.

Despite variations in texture, aroma, and taste among the biscuits enriched with dietary fiber from pomelo seeds, these biscuits continue to receive favorable ratings, particularly in terms of taste. The addition of dietary fiber significantly enhances their nutritional value by incorporating vitamins, minerals, and antioxidants [21]. This not only enriches the product's nutritional profile but also offers consumers the chance to enjoy delicious biscuits while reaping the benefits of plant dietary fiber.

CONCLUSION

Adding citrus dietary fiber to the biscuit dough significantly influenced the structure of starch and gluten, resulting in distinct characteristics. While the typical rubbery texture associated with starch and

gluten was not readily observed in the citrus seed and wheat seed samples, these structural differences had a profound impact on the strength and texture of the biscuits. The samples with citrus seed fiber predominantly had large pores and were very fragile, requiring only 4326 ± 56 g force to break. Their fracture strength was substantially improved to 6000 g force by subjecting them to heating at temperatures between 155–170°C for 50–60 min, thus enhancing their overall texture and strength.

Our research underscores the beneficial impact of incorporating citrus seed fiber into biscuits, particularly in terms of boosting their antioxidant content and TEAC (both free and bound forms). The samples with citrus seed fiber contained flavonoid compounds that were absent in the wheat fiber samples and the control biscuits without dietary fiber. These compounds are believed to possess the potential to inhibit bacterial, mold, and yeast contamination, consequently extending the shelf life of biscuits beyond 12 months.

Pomelo (*Citrus maxima*) seed dietary fiber is a unique source of serotonin, a compound rarely encountered in the seeds of other plants. The predominant forms of serotonin in this fiber were acyl-*N*-methylserotonins, particularly in the C22 and C24 homologues, where long-chain bonds (C20-C28) were prevalent.

CONTRIBUTION

All authors involved in the research analysis and manuscript writing process.

CONFLICT OF INTEREST

There is no conflict of interest between the author.


REFERENCES


1. Rosa An, Era B, Masala C, Nieddu M, Scano P, Fais A, *et al.* Supercritical CO₂ extraction of waste citrus seeds: Chemical composition, nutritional and biological properties of edible fixed oils. *European Journal of Lipid Science and Technology*. 2019;121:1800502. <https://doi.org/10.1002/ejlt.201800502>
2. Rahman MM, Islam F, Parvez A, Azad MAK, Ashraf GM, Ullah MF, *et al.* *Citrus limon* L.(lemon) seed extract shows neuro-modulatory activity in an *in vivo* thiopental-sodium sleep model by reducing the sleep onset and enhancing the sleep duration. *Journal of Integrative Neuroscience*. 2022;21(1):42. <https://doi.org/10.31083/j.jin2101042>
3. Tunjung WAS, Fatonah V, Christy GP, Triono S, Hidayati L, Priyanto D, *et al.* Effect of growth factor in callus induction and bioactive compounds in seed explant of kaffir lime (*Citrus hystrix* DC.). *Indonesian Journal of Pharmacy*. 2020;31(2):61–68. <https://doi.org/10.14499/indonesianjpharm31iss2pp61>
4. Rahman MM, Jahan FI, Mim SA. A brief phytochemical investigation and pharmacological uses of citrus seed – A review. *PharmacologyOnline*. 2019;1:94–103.
5. Kulkarni T, Bodhankar S, Sahasrabudhe R. Reversible anti-fertility effects of lemon seeds (*Citrus limonum*) In female albino rats. *National Journal of Basic Medical Sciences*. 2012;287.
6. Kim J, Jayaprakasha GK, Patil BS. Limonoids and their anti-proliferative and anti-aromatase properties in human breast cancer cells. *Food and Function*. 2013;4:258–265. <https://doi.org/10.1039/C2FO30209H>
7. Mahmoud MF, Hamdan DI, Wink M, El-Shazly AM. Hepatoprotective effect of limonin, a natural limonoid from the seed of *Citrus aurantium* var. bigaradia, on D-galactosamine-induced liver injury in rats. *Naunyn-Schmiedeberg's Archives of Pharmacology*. 2014;387:251–261. <https://doi.org/10.1007/s00210-013-0937-1>
8. Ahsan MT, Maria NN, Tahmida U, Jasmin AA, Chowdhury DUS. Anxiolytic, analgesic and anti-inflammatory effects of *Citrus maxima* (Burm.) Merr. Seed extract in Swiss albino mice model. *Clinical Phytoscience*. 2023;9:2. <https://doi.org/10.1186/s40816-023-00354-7>

9. Zayed A, Badawy MT, Farag MA. Valorization and extraction optimization of *Citrus* seeds for food and functional food applications. *Food Chemistry*. 2021;355:129609. <https://doi.org/10.1016/j.foodchem.2021.129609>
10. Akpata MI, Akubor PI. Chemical composition and selected functional properties of sweet orange (*Citrus sinensis*) seed flour. *Plant Foods for Human Nutrition*. 1999;54:353–362. <https://doi.org/10.1023/A:1008153228280>
11. Yilmaz E, Karaman E. Functional crackers: Incorporation of the dietary fibers extracted from citrus seeds. *Journal of Food Science and Technology*. 2017;54:3208–3217. <https://doi.org/10.1007/s13197-017-2763-9>
12. Karaman E, Yilmaz E, Tuncel NB. Physicochemical, microstructural and functional characterization of dietary fibers extracted from lemon, orange and grapefruit seeds press meals. *Bioactive Carbohydrates and Dietary Fibre*. 2017;11:9–17. <https://doi.org/10.1016/j.bcdf.2017.06.001>
13. Kruk J, Trela-Makowej A, Szymańska R. Acyl- ω -methylserotonins and branched-chain acylserotonins in lemon and other citrus seeds – New lipids with antioxidant properties and potential pharmacological applications. *Biomolecules*. 2022;12(10):1528. <https://doi.org/10.3390/biom12101528>
14. Blanshard JMV. The glass transition, its nature and significance in food processing. In: Beckett ST, editor. *Physico-chemical aspects of food processing*. New York: Springer; 1995. p. 17–48. https://doi.org/10.1007/978-1-4613-1227-7_2
15. Aydeniz Güneşer B, Demirel Zorba NN, Yılmaz E. Antimicrobial activity of cold pressed citrus seeds oils, some citrus flavonoids and phenolic acids. *Rivista Italiana Delle Sostanze Grasse*. 2018;95:119–131.
16. Mohammed RMO, Ayoub SMH. Study of phytochemical screening and antimicrobial activity of *Citrus aurantifolia* seed extracts. *American Journal of Analytical Chemistry*. 2016;7:254–259. <https://doi.org/10.4236/ajac.2016.73022>
17. Cvetnic Z, Vladimir-Knezevic S. Antimicrobial activity of grapefruit seed and pulp ethanolic extract. *Acta Pharmaceutica*. 2004;54(3):243–250.
18. Aladekoyi G, Omosulis V, Orungbemi O. Evaluation of antimicrobial activity of oil extracted from three different citrus seeds (*Citrus limon*, *Citrus aurantifolia* and *Citrus aurantium*). *International Journal of Scientific Research and Engineering Studies*. 2016;3(3):16–20.
19. Atolani O, Adamu N, Oguntoye OS, Zubair MF, Fabiyi OA, Oyegoke RA, et al. Chemical characterization, antioxidant, cytotoxicity, Anti-*Toxoplasma gondii* and antimicrobial potentials of the *Citrus sinensis* seed oil for sustainable cosmeceutical production. *Heliyon*. 2020;6(2):e03399. <https://doi.org/10.1016/j.heliyon.2020.e03399>
20. Trela-Makowej A, Kruk J, Jemioła-Rzemińska M, Szymańska R. Acylserotonins – A new class of plant lipids with antioxidant activity and potential pharmacological applications. *Biochimica et Biophysica Acta (BBA) – Molecular and Cell Biology of Lipids*. 2021;1866(12):159044. <https://doi.org/10.1016/j.bbalip.2021.159044>
21. *Journal of the American Oil Chemists' Society*. Vol. 77. Arlington: AOAC; 2000.
22. Budianto B, Suparmi A. Exploration of the biochemical composition of *Citrus* L. seeds for industrial applications. *Grasas y Aceites*. 2024;75(2):2102. <https://doi.org/10.3989/gya.1204232.2102>
23. Re R, Pellegrini N, Proteggente A, Pannala A, Yang M, Rice-Evans C. Antioxidant activity applying an improved ABTS radical cation decolorization assay. *Free Radical Biology and Medicine*. 1999;26(9–10):1231–1237. [https://doi.org/10.1016/S0891-5849\(98\)00315-3](https://doi.org/10.1016/S0891-5849(98)00315-3)
24. Budianto, Feri ZO, Suparmi A, Arifin MJ. Effect of the chemical composition of fluid foods on the rate of fouling processing during sterilization. *Vitae*. 2023;30(1):349368. <https://doi.org/10.17533/udea.vitae.v30n1a349368>
25. Maximum limits of microbial contamination in processed food by fermented vegetable products. *Indonesian Drug and Food Control*; 2019. 48 p. (In Indonesian).

ORCID IDs

Budianto  <https://orcid.org/0000-0002-8277-6202>

Anik Suparmi  <https://orcid.org/0000-0002-9720-8195>

Dewi Susanti  <https://orcid.org/0009-0008-0604-721X>



UAV imagery, advanced deep learning, and YOLOv7 object detection model in enhancing citrus yield estimation

Mohamed Jibril Daiaeddine^{*ID}, Sara Badrouss^{ID}, Abderrazak El Harti^{ID},
El Mostafa Bachaoui^{ID}, Mohamed Biniz^{ID}, Hicham Mouncif^{ID}

Sultan Moulay Slimane University^{ROR}, Beni Mellal, Morocco

* e-mail: mohamedjibril.daiaeddine@usms.ma

Received 04.01.2024; Revised 14.04.2024; Accepted 07.05.2024; Published online 18.10.2024

Abstract:

Accurate citrus fruit yield and estimation is of utmost importance for precise agricultural management. Unmanned aerial vehicle (UAV) remote-sensing systems present a compelling solution to this problem. These systems capture remote-sensing imagery with both high temporal and spatial resolution, thus empowering farmers with valuable insights for better decision-making. This research assessed the potential application of UAV imagery combined with the YOLOv7 object detection model for the precise estimation of citrus yield.

Images of citrus trees were captured in their natural field setting using a quadcopter-mounted UAV camera. Data augmentation techniques were applied to enhance the dataset diversity; the original YOLOv7 architecture and training parameters were modified to improve the model's accuracy in detecting citrus fruits.

The test results demonstrated commendable performance, with a precision of 96%, a recall of 100%, and an $F1$ -score of 97.95%. The correlation between the fruit numbers recognized by the algorithm and the actual fruit numbers from 20 sample trees provided the coefficient R^2 of 0.98.

The strong positive correlation confirmed both the accuracy of the algorithm and the validity of the approach in identifying and quantifying citrus fruits on sample trees.

Keywords: Agricultural management, unmanned aerial vehicle (UAV), remote-sensing systems, YOLOv7 object detection model, crop yield estimation

Please cite this article in press as: Daiaeddine MJ, Badrouss S, El Harti A, Bachaoui EM, Biniz M, Mouncif H. UAV imagery, advanced deep learning, and YOLOv7 object detection model in enhancing citrus yield estimation. *Foods and Raw Materials*. 2025;13(2):242–253. <https://doi.org/10.21603/2308-4057-2025-2-650>

INTRODUCTION

Crop yield estimation plays a crucial role in effective crop management, enabling farmers to make informed decisions regarding harvesting, transportation, storage, and marketing of their produce. Traditional fruit counting methods, while commonly used, are inherently labor-intensive, time-consuming, and prone to human error; moreover, they often give a higher margin of error than expected [1]. Consequently, fruit farming needs new efficient and automated approaches to crop yield estimation. Automated methods reduce the burden of manual labor while enhancing the accuracy and reliability of yield forecasts.

The recent progress in computer technology, camera capabilities, and image analysis have given rise to a diverse array of fruit count methods [2].

Numerous studies feature image processing techniques and machine learning algorithms in the domain of fruit detection and recognition. Sengupta & Lee harnessed a combination of support vector machines, Canny edge detection, Hough transform, and scale-invariant feature transform, along with the majority voting algorithm, to effectively discern citrus fruits from the background [3]. Maldonado & Barbosa based their approach on the extraction of relevant features from green fruits [4]. The method consisted of a series of steps including color model conversion, thresholding, histogram equalization, spatial filtering with Laplace and Sobel operators, and Gaussian blur. Zhao *et al.* contributed to the field by applying the sum of the absolute transformed difference method to the detection of immature green citrus fruits [5]. The proposed technique effectively identified fruit pixels through the transfor-

mative process. A subsequent support vector machine classifier discerned and eliminated false positives, thereby refining the detection accuracy.

Dorj *et al.* introduced a novel algorithm aimed at automating fruit detection [6]. This algorithm encompassed a series of pivotal steps including the conversion of the RGB (red, green, blue) color space to the hue-saturation-value color space, threshold color detection, fruit segmentation, noise reduction, morphological operations, labeling, feature extraction, and classification.

Liu *et al.* devised a distinctive approach centered on the Cr-Cb color coordinates [7]. They established a multi-elliptical boundary model capable of detecting both citrus fruits and tree trunks in natural light settings. Another contribution by Liu *et al.* introduced a recognition methodology based on regional specifics [8]. The approach hinged on a feature mapping table, which effectively reduced the dimensionality of feature vectors while concurrently enabling the segmentation of citrus fruits, branches, and leaves.

Xu *et al.* pursued the segmentation of target citrus regions within the YUV color space by applying the Otsu adaptive threshold algorithm [9]. Their study incorporated a distinctive *random ring* method which used a greedy algorithm to recognize multiple citrus targets.

In a recent study, Zhang *et al.* introduced a pioneering algorithm that enabled the detection and quantification of citrus fruits within orchards [10]. The proposed methodology leveraged the LAB color space in tandem with the Hough circle transform. While image processing methods demonstrated proficiency in various fruit detection tasks, they encountered challenges when dealing with complex situations, such as occlusion, overlapping objects, and varied illumination [11].

Furthermore, the application of machine learning techniques to large-scale yield estimation often leads to suboptimal outcomes due to their constrained ability to generalize [12].

In recent years, there has been a growing interest in using object detection algorithms based on deep learning as promising tools for fruit detection and yield estimation. These algorithms have remarkably advanced generalization capabilities, which are categorized into one-stage and two-stage algorithms [13–15]. Typically, a one-stage algorithm offers faster inference speeds while a two-stage algorithm achieves better accuracy despite its relatively slower processing pace. The one-stage approach to target detection involves a convolutional neural network (CNN) to directly extract predictions for both the target class and its corresponding location within the input image. Instances of this methodology include the Single Shot MultiBox Detector (SSD) and the You Only Look Once (YOLO) algorithm represented by YOLOv1, YOLOv2, YOLOv3, YOLOv4, YOLOv5, YOLOx, and YOLOv7 [16–23]. As for the two-stage detection approach, the initial step employs a region proposal mechanism to sift through potential candidate regions. This process facilitates the acquisi-

tion of the region of interest, thus enabling the subsequent stages to engage in precise object localization and border regression prediction within the chosen region. Prominent exemplars of the two-stage detection strategy encompass such methods as Fast R-CNN, Faster R-CNN, and Mask R-CNN [24–26].

A cohort of researchers have contributed to the domain of fruit detection by employing deep learning models for object detection. The following researchers focused on the one-stage algorithm, e.g., improved YOLO models. Xu *et al.* introduced HPL-YOLOv4, an innovative approach for detecting citrus fruits [27]. This method employed GhostNet as its foundational backbone network and incorporated a DBM module with depthwise separable convolution and the Mish activation function, replacing the CBL module in the neck segment. The enhancements included integrating the ECA channel attention mechanism and using the soft DIoU-NMS technique to improve detection in overlapping or occluded situations. Yang *et al.* presented BCoYOLOv5, a novel network model for identifying and detecting fruit targets in orchards [28]. The model was based on YOLOv5s architecture and integrated a bidirectional cross attention mechanism for enhanced performance. Lai *et al.* introduced a target detection model based on an enhanced YOLOv7 variant, specifically designed for accurate pineapple detection in field environments [29]. The model incorporated the SimAM attention mechanism, refined the max-pooling convolution architecture, and replaced the conventional NMS with the soft-NMS variant to address detection challenges posed by occlusion and overlapping. Chen *et al.* proposed Citrus-YOLOv7 for citrus detection in orchards [30]. This model enhanced the YOLOv7 architecture with a specialized small object detection layer, lightweight convolution operations, and a convolutional block attention module. Yang *et al.* improved YOLOv7 to enhance apple fruit target recognition in scenarios with dense fruit clusters, occlusion, and overlapping [31]. They integrated a MobileOne module for backbone network establishment and used an altered image fusion strategy; this novel recognition algorithm also had an auxiliary detection head.

Our main objective was to investigate the potential application of unmanned aerial vehicle (UAV) remote-sensing technology and the YOLOv7 object detection model for citrus fruit yield estimation. Our solution will provide farmers with a precise and efficient alternative to traditional manual fruit count, leveraging cutting-edge technology to enhance decision-making in crop management.

STUDY OBJECTS AND METHODS

Study area. The research centered on the use of the *Maroc Late* variety of citrus trees in orchard environment. We obtained the original images of these citrus trees from an orchard located in the Beni Mellal-Khenifra region, Morocco. This region significantly contributes to citrus cultivation, accounting for 14% of

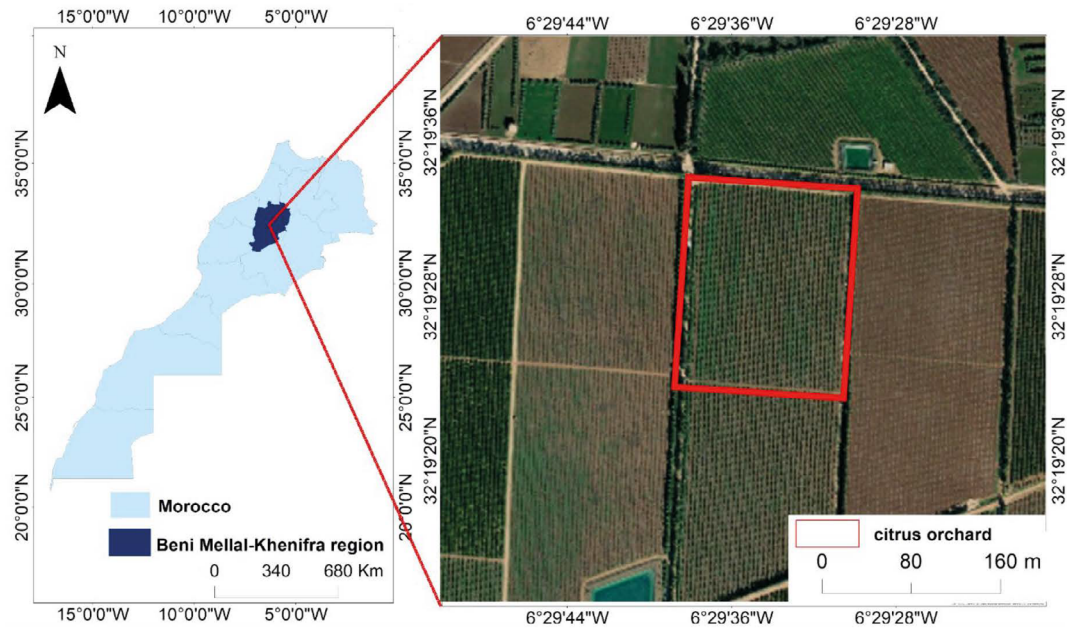


Figure 1 Citrus orchard: geographic location

the country's total citrus farming. The region allocates a substantial 17 426 ha to citrus cultivation, with the Maroc Late variety responsible for 23% of the citrus crops [32]. The central coordinates of the orchard under study are 32°19'28"N and 6°29'36"W (Fig. 1). The orchard, identified by parcel number 20 050, was established on August 18, 2018: it covered an area of 6.11 ha and included a total of 2546 citrus plants. In the standard planting configuration, the rows of citrus trees were separated by a 6-m gap, with each tree spaced approximately 4 m apart.

Sampling citrus trees. The initial tree sampling is crucial before capturing images in the orchard. This process involves selecting a few representative samples from the entire population. These samples should be robust and comprehensive enough to represent the entire orchard. This approach provides a more accurate estimation of the overall yield, thus securing a more precise assessment of the productivity of a particular orchard. This study employed two sampling methods.

The first method was random sampling: it provided a dataset to develop a deep learning model specifically targeting citrus fruit detection. The importance of employing random sampling comes from its ability to unbiasedly select samples from a diverse population. For this research, we selected 200 trees at random to be included in the dataset. The size of the dataset plays a pivotal role, as larger datasets enhance the capacity of deep learning models to recognize more complex patterns, thereby improving their generalization capabilities.

The second sampling method estimated the number of fruits on each citrus tree. We used the traditional method of manual counting to determine the total fruit count across a sample of 20 citrus trees. This sampling relied on the geographical location of the trees in the orchard: it involved four trees in each of the four direc-

Table 1 Imaging system specifications

Parameter	Value
Sensor size, mm	4.87×3.96
Image dimensions, pixels	1600×1300
Focal length, mm	5.74 mm
Shutter type	Global 2 MP shutter

tions (east, west, north, and south) plus another group of four trees in the middle of the orchard. The actual fruit count and the recognized fruit count generated by the algorithm were then paired for each of these trees. Utilizing a linear fitting method, we established a direct correlation between the observed fruit counts and the fruit counts identified by the algorithm created.

Data acquisition and UAV flights. The citrus trees designated for sampling were photographed on March 10 and 15, 2023, during their ripening season. We took the images at various times throughout the day – morning, noon, and afternoon – in the field under natural lighting conditions. The weather conditions during the image capture were ideal for UAV flights, with a wind speed of 9 km/h and a clear, cloudless sky.

This procedure involved the DJI Phantom 4 Multispectral (P4M) Unmanned aerial vehicle (UAV) equipped with a suite of imaging sensors. These sensors included five multispectral sensors representing the blue, green, red, red-edge, and near-infrared bands, along with one RGB sensor. Table 1 demonstrates the parameters of the sensors.

The DJI Pilot application served as the control interface for the P4M-UAV during the data collection process (Fig. 2). We employed manual control mode to navigate the UAV, with the camera angle adjusted to 45°. For each sampling tree, both right-side and left-side images were captured from a consistent distance of 4 m. The flight

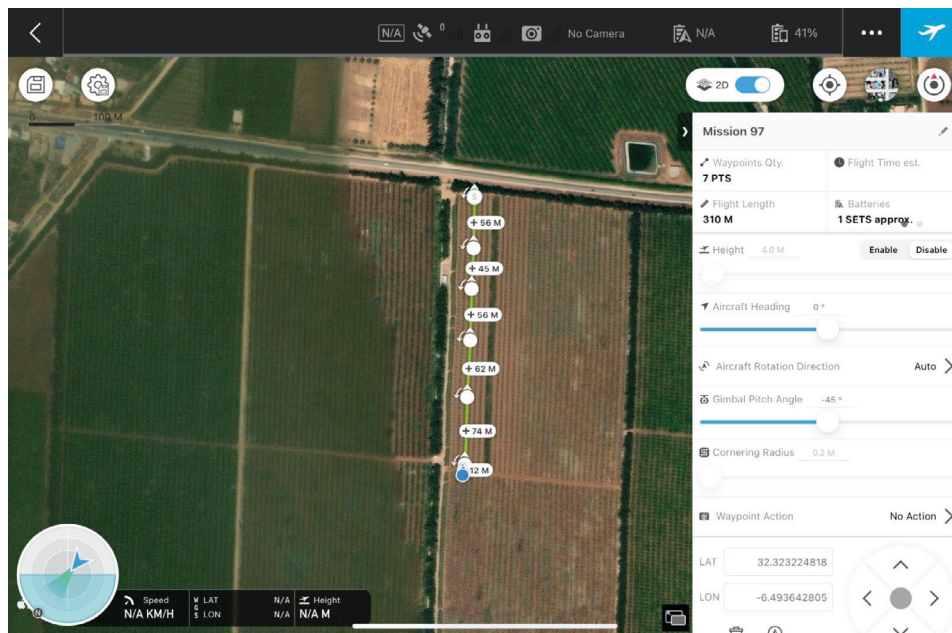


Figure 2 DJI Pilot application interface: examples of image capture locations (white points) and flight path (green line)



Figure 3 Phantom 4 (P4M) UAV imaging: distance from the tree is 4 m; altitude above ground level is 4 m

altitude was maintained at 4 m above ground level, as illustrated in Fig. 3. Consequently, the images obtained boasted a resolution of 0.21 cm/pixel.

We chose manual control instead of automated one to image the trees with a DJI Phantom 4 (P4M) UAV because we needed an accurate and focused data collection. Manual control allows for a high degree of operator engagement, enabling the UAV to maneuver around the selected trees effectively and flexibly. This approach made it possible to take pictures from both the left and right side at a constant height and distance. It provided a high control level, excellent data quality, and thorough coverage.

In the scope of this research, we had several reasons to use RGB sensor-captured images to develop a deep learning model focused on citrus fruit. Firstly, the RGB

images were to be integrated with the deep learning model. As input data, RGB images were more effective in helping the model to identify and classify citrus fruits based on their color and other visual characteristics. Secondly, RGB images streamlined the computational and logistical complexities associated with the development of deep learning models, as opposed to multispectral images. Lastly, citrus fruits stood out clearly in RGB imagery, as illustrated in Fig. 4, thus facilitating the labeling and data verification, which, in turn, enhanced the overall reliability of the research outcomes.

Data preprocessing. In this study, we applied various preprocessing techniques to the original images. Initially, each original image underwent a cropping operation to create sub-images with dimensions of

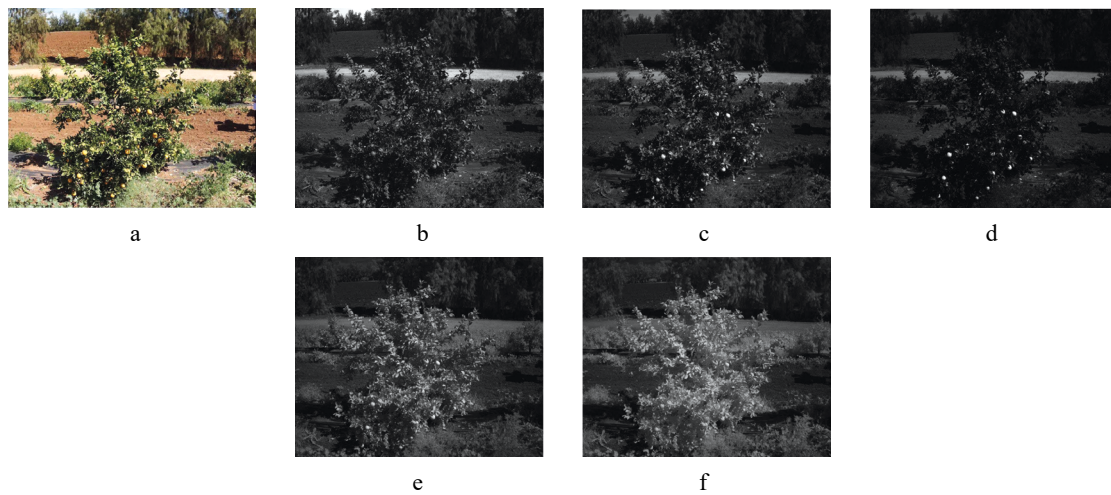


Figure 4 Exemplar citrus tree images captured by Phantom 4 Multispectral (P4M) UAV: (a) RGB (red, green, blue) composite; (b) blue channel; (c) green channel; (d) red channel; (e) red-edge channel; and (f) near-infrared image



Figure 5 Instances of sub-images in the dataset: back lighting (a), front lighting (b), occlusion (c), and overlap (d)

400×433 pixels. This action reduced the background noise and directed the focus towards the areas of particular interest. Consequently, we conducted an elimination process to filter out images devoid of citrus fruits, a measure taken to enhance the precision of the model by eliminating irrelevant data.

The sub-images in question manifested four distinct categories of interference: overlap, occlusion, front lighting, and back lighting. Figure 5 illustrates these types of interference. Overlap interference became evident when multiple citrus fruits partially obscure each other in an image. Occlusion interference arose when segments of a citrus fruit were concealed or shrouded by branches and leaves. Front lighting interference occurred when the illumination on citrus fruits grew intense from the frontal direction. Backlighting interference took place when the light source (the sun) was behind the citrus fruits, causing the fruits to appear as dark silhouettes.

Subsequently, we performed a manual annotation of a total of 1804 sub-images, using the LabelImg software (Fig. 6) to delineate the bounding boxes encompassing citrus fruits within each sub-image. After that, the program generated .txt format files with these annotations.

The dataset was further partitioned into three distinct subsets: a training set, a test set, and a validation set, with a distribution ratio of 70:20:10 (Table 2). The training set was comprised of 1263 sub-images with a

total of 8185 citrus fruits. Meanwhile, the test set encompassed 361 sub-images, featuring 1253 citrus fruits, and the validation set comprised 130 sub-images with a combined total of 747 citrus fruits.

Data augmentation. We used a range of data augmentation strategies to enhance the diversity and size of the dataset. These strategies encompassed morphological operations, including angle rotation, saturation adjustment, image flipping (both vertically and horizontally), and translation. The mosaic data enhancement method involved the amalgamation of four defect images with random scaling, random clipping, and random layout adjustments: it bolstered the classification performance of the model. We also appealed to the mix-up data enhancement method to create mixed samples by proportionally interpolating two images. Additionally, we explored the color space conversion, modifications in picture hue, saturation, and exposure. The primary objective behind the incorporation of these data augmentation techniques was to curb the overfitting tendencies and bolster the model's capacity for generalization.

Object detection framework. YOLOv7 is a computer vision model within the YOLO (You Only Look Once) family of object detection models, renowned for its rapid detection, high precision, and user-friendly nature in both training and deployment. The YOLOv7 model architecture comprises five primary compo-

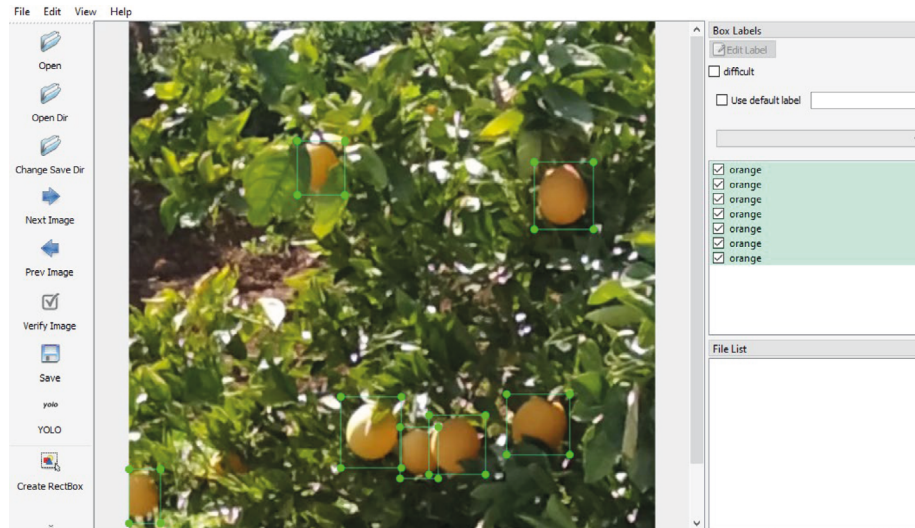


Figure 6 Manual annotation with green rectangles

Table 2 Dataset structure

Data set	Ratio, %	Number of sub-images	Number of fruits
Training se	70	1419	8185
Test set	20	361	1253
Validation set	10	180	747
Total	100	1804	10 185

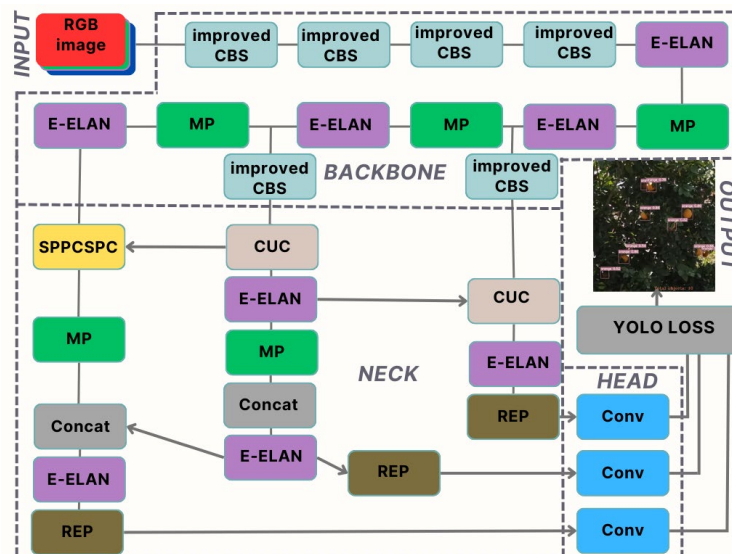


Figure 7 YOLOv7 improved architecture

nents: inputs, backbone network, neck, head, and loss function (Fig. 7). In this study, we applied various modifications to the original YOLOv7 architecture and training parameters to enhance its accuracy in detecting citrus fruits.

The input layer incorporated three techniques to enhance the quality of the data used for citrus fruit detection, i.e., mosaic data augmentation, adaptive anchor box calculation, and adaptive image scaling.

In this research, the backbone network played a crucial role in the feature extraction process. It comprised

several modules, including BConv convolution layers, E-ELAN convolution layers, and MPConv convolution layers [23]. The BConv module, or CBS layer, consisted of a convolution layer, batch normalization (BN) layer, and SiLU activation function. It was specifically designed to extract image features at various scales (Fig. 8).

We conducted a series of experiments to explore different modifications in the backbone network, with a focus on the convolution (Conv) layer. The objective was to enhance the model's performance in citrus fruit detection. The incorporation of a double CBS (Conv-



Figure 8 CBS Layer



Figure 9 Improved CBS layer

BN-SELU-Conv-BN-SiLU) layer instead of a single CBS layer was the most successful change of all modifications tested. Additionally, we replaced the SiLU (sigmoid linear unit) activation function in the first layer with SELU, i.e., scaled exponential linear unit (Fig. 9).

The neck module in the YOLOv7 model architecture played a crucial role in feature fusion and feature pyramids. It served as a bridge between the backbone network and the head module, facilitating the integration of features from different network layers. The neck module consisted of two components: the feature pyramid network module and the path aggregation network module. These modules were responsible for merging and harmonizing the features extracted from multiple layers of the backbone network.

The head module in the YOLOv7 model architecture generated the final detections and predicted the locations and classes of objects within the input image. It was the last component in the YOLOv7 network before the output. Within the head module, the features that had been combined and mixed in the neck module passed through a series of layers that performed the necessary computations for object detection. These layers analyzed the feature representations, as well as made predictions about the bounding boxes and associated object classes. Additionally, the convolutional architecture was updated with the improved CBS to align the head architecture with the backbone architecture and enable the prediction of bounding boxes for small objects.

As for the loss function, YOLOv7 utilized a loss calculation method that consisted of three main components: object confidence loss, classification loss, and coordinate loss. These loss functions were important for training the model and optimizing its performance. The object confidence loss and classification loss in YOLOv7 were computed using the binary cross-entropy loss function. The binary cross-entropy loss measured the dissimilarity between the predicted probabilities and the ground truth labels for both object presence and class predictions. The coordinate loss in YOLOv7 employed the CIoU (complete intersection over union) loss function [33]. The CIoU loss took into account various factors, including the overlapping area, center distance,

and aspect ratio, to measure the localization accuracy of the predicted bounding boxes.

Evaluation metrics. In this work, we used several metrics to assess the YOLOv7 performance, i.e., precision (P), recall, and $F1$ -score ($F1$):

$$\text{Precision} = \frac{TP}{(TP+FP)}$$

$$\text{Recall} = \frac{TP}{(TP+FN)}$$

$$F1 = \frac{2(\text{Precision} + \text{Recall})}{(\text{Precision} + \text{Recall})}$$

where the true positive (TP) was the number of images that the developed model correctly identified as containing citrus fruits; the false positive (FP) was the number of images that the model incorrectly identified as containing citrus fruits when they did not; the false negative (FN) was the number of images that the model incorrectly identifies as not containing citrus fruits when they did.

We used another formula to calculate the percentage of accurate citrus fruit count provided by the YOLOv7 model compared to the actual number of citrus fruits in the dataset:

$$\begin{aligned} \text{Rate of precision in yield estimation} &= \\ &= \frac{\text{Number of citrus fruits by YOLOv7}}{\text{Actual fruit number}} \times 100 \end{aligned}$$

where the number of citrus fruits counted by YOLOv7 was the count of citrus fruits detected by the YOLOv7 model; the actual fruit number was the real, or ground truth, count of citrus fruits in the dataset.

Experimental details. The network model was trained and evaluated on a dedicated laboratory workstation. It included the following hardware components: an Intel i9 13th Gen 13900K processor, an Nvidia RTX 4090 graphics card, 128 GB of 3200 MHz RAM, and a 2 TB Gen 4 SSD for storage. The operating system in use was a 64-bit professional edition of Win-

dows 10. For deep learning tasks, we used a PyTorch 2 with CUDA 11 as a framework; Python 3.8 served as a programming language. Throughout the training process, the input images were maintained at a resolution of 640×640 pixels.

We used the YOLO Evolve hyperparameter optimization method to determine the optimal hyperparameters for the YOLOv7 model. This approach involved 10 trials, each comprising 30 epochs, to assess various hyperparameter combinations and identify the most effective configuration. The relevant hyperparameter values were defined as follows: the model's initial learning rate was set to 0.129, the learning rate momentum was 0.892, the Adam algorithm served as optimizer, and the weight decay value was 0.00052. The training batch size was 32 while the total number of training epochs was 500.

Additionally, we applied transfer learning by utilizing the pre-trained weights from 'yolov7_training.pt,' a standard YOLOv7 model previously trained on the MS COCO dataset.

RESULTS AND DISCUSSION

Training results. Figures 10–14 provide an overview of various training metrics, including box loss, objectness loss, precision, recall, and mAP0.5 values tracked after each training epoch. The box loss assessed the model's accuracy in locating the center of a citrus fruit within an image and drawing a bounding box around it. The objectness gauged the likelihood that a given image region contained the object of interest during detection. Over the training epochs, both box loss and objectness exhibited fluctuations and an overall

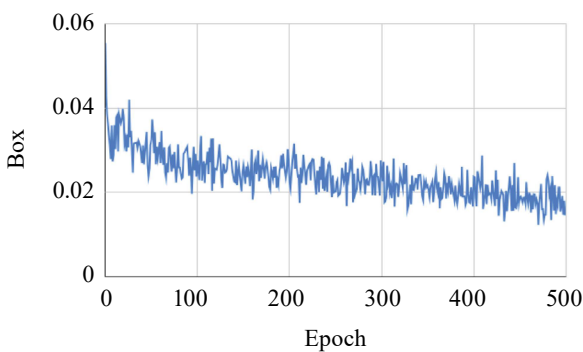


Figure 10 Plot of box loss for the training set

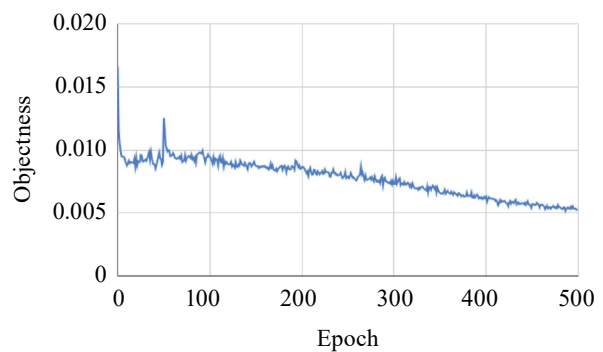


Figure 11 Plot of objectness loss for the training set

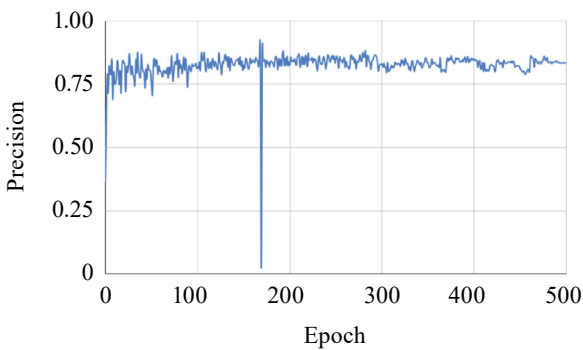


Figure 12 Plot of precision for the training set

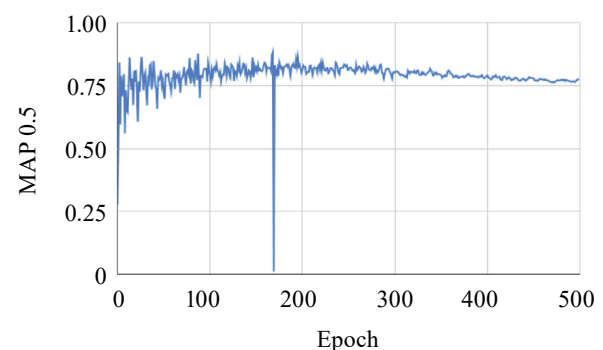


Figure 13 Plot of mean average precision (MAP) for the training set

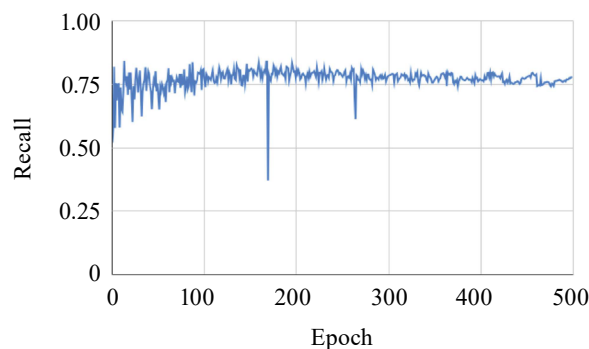


Figure 14 Plot of recall for the training set

		Actual Values	
		Citrus	Background
Predicted Values	Citrus	0.96	0.04
	Background	0	1

Figure 15 Confusion matrix of the test results



Figure 16 Visualizing citrus fruit detection performance in test dataset images

consistent decrease, indicating the progresses of the improved model. In the initial epochs (approximately, epochs 0–10), a rapid decrease signified quick learning. Subsequently, stability with fluctuations might have appeared due to varied data augmentation presenting both complex and simple instances. Towards the end of training (e.g., after epoch 400), stabilization signified that the model reached its learning capacity from the given data.

The metrics, including precision, recall, and mAP0.5 values, demonstrated fluctuations across epochs with an overall upward trend, reflecting improved model performance over training. In the early epochs (e.g., epochs 0–10), these metrics were relatively low but displayed significant improvement as the model learned data patterns. Around epochs 10–50, the rate of improvement slowed down as the model approached a better data representation. Throughout training, occasional fluctuations might

be attributed to data augmentation, offering challenging and straightforward examples. A period of relative stability in precision from epochs 50–150 suggested a performance plateau given the architecture and data. Towards the end (epochs 400–500), a slower but continued improvement highlighted the model's refinement of learned features.

Test results. Figure 15 presents the confusion matrix of the test results, i.e., a critical visual representation of the deep learning model's performance in detecting citrus fruits amidst background objects. The model excelled in accurate identification, achieving a 96% true positive rate, but still exhibited a minor shortcoming with a 4% false positive rate. On the other hand, it effectively identified the background as not containing citrus fruits with a true negative rate of 100%. Figure 16 displays a visualization of selected output from YOLOv7 on several test images from the dataset.

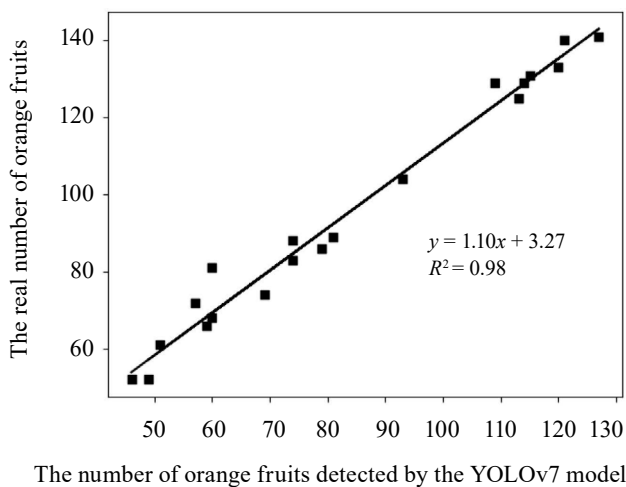
Utilizing YOLOv7 for fruit detection yielded good outcomes, underscoring the model's effectiveness. The achieved results included the precision of 96%, a recall of 100%, and an *F1*-score of 97.95%. Such a high level of detection accuracy could be attributed to a range of strategic approaches, i.e., various modifications to the original YOLOv7 architecture, data augmentation, the careful selection of hyperparameters through the YOLO Evolve method, and the application of transfer learning. Expanding the dataset with additional images of citrus fruits collected from various farms and at different time intervals could prove advantageous to further enhance the performance.

However, despite these optimizations, the model may not attain perfect accuracy due to potential interferences, e.g., leaves and branches obstructing the view. The algorithm relied on a combination of parameters, including color, texture, and various other features. Additionally, the overall detection performance relied on the image quality, which, in its turn, depended on such factors as UAV camera specifications, the time of image capture, lighting conditions, the altitude of the UAV flight, and the horizontal distance between the UAV and the tree.

Yield estimation results. Table 3 illustrates the results of citrus detection achieved by the enhanced YOLOv7 model, conducted across a sample of 20 distinct trees. For each tree, we determined the accuracy rate in estimating the yield. The highest accuracy observed was 94% while the lowest was 74%; the overall average across all trees stood at 87.68%. The improved YOLOv7 model recorded a lower count of citrus fruits compared to the actual count. This disparity between the manual counting and the proposed algorithm could be attributed to several factors, including complete occlusion, shadows, and viewing angles. Manual counting involved capturing fruit numbers from multiple angles whereas the algorithm relied on images taken from two sides of the tree. We performed a regression analysis to assess the correlation between the manual count and the count generated by YOLOv7 for 20 trees (Fig. 17). The resulting regression equation was $y = 1.10 \cdot x + 3.27$.

Table 3 Citrus fruit count results for 20 trees

Tree number	Actual fruit number	Fruit count by YOLOv7	Precision rate in yield estimation
1	52	46	88.46
2	125	113	90.40
3	74	69	93.24
4	131	115	87.70
5	88	74	84.09
6	81	60	74.07
7	140	121	86.42
8	129	109	84.49
9	52	49	94.23
10	61	51	83.60
11	83	74	89.15
12	129	114	88.37
13	141	127	90.07
14	86	79	91.86
15	104	93	89.42
16	72	57	79.16
17	66	59	89.39
18	133	120	90.22
19	89	81	91.01
20	68	60	88.23

**Figure 17** Regression analysis: actual number of citrus fruits vs. citrus fruits detected by the YOLOv7 model

It was accompanied by a high correlation coefficient ($R^2 = 0.98$), which signified a robust correlation within the dataset.

Evaluation. Table 4 compares the proposed approach with previous studies in terms of the algorithm, precision, recall, and $F1$ -score.

In this comparative analysis, we assessed the performance of our approach against the methodologies employed in previous studies that utilized various YOLO (You Only Look Once) variants for citrus fruit detection. Xu *et al.* used HPL-YOLOv4 to achieve the precision, recall, and $F1$ score metrics of 93.45, 94.30, and 94.00%, respectively [27]. Yang *et al.*, who used BCo-

Table 4 Comparative analysis of object detection model performances: precision, recall, and $F1$ -score

Reference	Model	Precision, %	Recall, %	$F1$ -score, %
[27]	HPL-YOLOv4	93.45	94.30	94.00
[28]	BCo-YOLOv5	89.15	97.11	92.96
[30]	Citrus-YOLOv7	94.25	93.37	93.81
This work	YOLOv7	96.00	100.00	97.95

YOLOv5, reported a higher recall at 97.11%, albeit with a slightly lower precision and an $F1$ -score of 89.15 and 92.96% [28]. Chen *et al.* introduced Citrus-YOLOv7: they showcased a well-balanced precision of 94.25%, a recall of 93.37%, and an $F1$ -score of 93.81% [30]. Our results proved remarkable with the precision of 96%, a recall of 100%, and an $F1$ -score of 97.95%. These findings suggest that the method described in this paper may represent a significant advancement in enhancing the accuracy of citrus fruit detection compared to earlier methodologies in this field.

CONCLUSION

In this study, we used unmanned aerial vehicle (UAV) RGB (red, green, blue) remote-sensing imagery and the YOLOv7 object detection model to estimate citrus fruit yield. The innovative modifications to the YOLOv7 model included the introduction of a double CBS (Conv-BN-SELU-Conv-BN-SiLU) layer and the adoption of the SELU activation function. They made it possible to achieve commendable results in citrus fruit detection. The UAV RGB remote-sensing technology enhanced the capabilities of the deep learning model by providing high-resolution, real-time aerial imagery, and, eventually, a more comprehensive assessment of citrus orchards. Hyperparameter optimization with the YOLO Evolve method further improved the performance, resulting in high precision, recall, and $F1$ -score values.

Our findings demonstrated the potential of deep learning object detection models in addressing the challenges associated with traditional fruit counting methods. Cutting-edge technologies, e.g., UAVs, may reduce the labor-intensive and error-prone nature of manual fruit counting, thus providing accurate and efficient estimates for citrus fruit yield.

Our algorithm proved effective in identifying and quantifying citrus fruits, as evidenced by the strong positive correlation between the recognized fruit numbers and the actual fruit numbers from a sample of 20 trees. Our algorithm, combined with UAV RGB remote-sensing, can assist farmers in making informed decisions about crop management.

While the results are promising, we have to acknowledge certain limitations, such as occlusion, that may affect detection accuracy. Further research could expand the dataset to encompass diverse conditions and varieties of citrus fruits, potentially enhancing the model's robustness.

CONTRIBUTION

All the authors were equally involved in the research analysis and manuscript writing.

CONFLICT OF INTEREST




The authors declared no conflict of interests regarding the publication of this article.

REFERENCES

1. Marani R, Milella A, Petitti A, Reina G. Deep neural networks for grape bunch segmentation in natural images from a consumer-grade camera. *Precision Agriculture*. 2021;22:387–413. <https://doi.org/10.1007/s11119-020-09736-0>
2. Gongal A, Amatya S, Karkee M, Zhang Q, Lewis K. Sensors and systems for fruit detection and localization: A review. *Computers and Electronics in Agriculture*. 2015;116:8–19. <https://doi.org/10.1016/j.compag.2015.05.021>
3. Sengupta S, Lee WS. Identification and determination of the number of immature green citrus fruit in a canopy under different ambient light conditions. *Biosystems Engineering*. 2014;117:51–61. <https://doi.org/10.1016/j.biosystemseng.2013.07.007>
4. Maldonado Jr W, Barbosa JC. Automatic green fruit counting in orange trees using digital images. *Computers and Electronics in Agriculture*. 2016;127:572–581. <https://doi.org/10.1016/j.compag.2016.07.023>
5. Zhao C, Lee WS, He D. Immature green citrus detection based on colour feature and sum of absolute transformed difference (SATD) using colour images in the citrus grove. *Computers and Electronics in Agriculture*. 2016;124:243–253. <https://doi.org/10.1016/j.compag.2016.04.009>
6. Dorj U-O, Lee M, Yun S. An yield estimation in citrus orchards via fruit detection and counting using image processing. *Computers and Electronics in Agriculture*. 2017;140:103–112. <https://doi.org/10.1016/j.compag.2017.05.019>
7. Liu T-H, Ehsani R, Toudeshki A, Zou X-J, Wang H-J. Detection of citrus fruit and tree trunks in natural environments using a multi-elliptical boundary model. *Computers in Industry*. 2018;99:9–16. <https://doi.org/10.1016/j.compind.2018.03.007>
8. Liu S, Yang C, Hu Y, Huang L, Xiong L. A method for segmentation and recognition of mature citrus and branches-leaves based on regional features. In: Wang Y, Jiang Z, Peng Y, editors. *Image and graphics technologies and applications*. Singapore: Springer; 2018. pp. 292–301. https://doi.org/10.1007/978-981-13-1702-6_29
9. Xu L, Zhu S, Chen X, Wang Y, Kang Z, Huang P, *et al.* Citrus recognition in real scenarios based on machine vision. *DYNA. Ingeniería e Industria*. 2020;95(1):87–93. <https://doi.org/10.6036/9363>
10. Zhang X, Toudeshki A, Ehsani R, Li H, Zhang W, Ma R. Yield estimation of citrus fruit using rapid image processing in natural background. *Smart Agricultural Technology*. 2022;2:100027. <https://doi.org/10.1016/j.atech.2021.100027>
11. Maheswari P, Raja P, Apolo-Apolo OE, Perez-Ruiz M. Intelligent fruit yield estimation for orchards using deep learning based semantic segmentation techniques – A review. *Frontiers in Plant Science*. 2021;12:684328. <https://doi.org/10.3389/fpls.2021.684328>
12. Yamamoto K, Guo W, Yoshioka Y, Ninomiya S. On plant detection of intact tomato fruits using image analysis and machine learning methods. *Sensors*. 2014;14(7):12191–12206. <https://doi.org/10.3390/s140712191>
13. Loddo A, Loddo M, Di Ruberto C. A novel deep learning based approach for seed image classification and retrieval. *Computers and Electronics in Agriculture*. 2021;187:106269. <https://doi.org/10.1016/j.compag.2021.106269>
14. Han B-G, Lee J-G, Lim K-T, Choi D-H. Design of a scalable and fast YOLO for edge-computing devices. *Sensors*. 2020;20(23):6779. <https://doi.org/10.3390/s20236779>
15. Sivakumar ANV, Li J, Scott S, Psota E, Jhala AJ, Luck JD, *et al.* Comparison of object detection and patch-based classification deep learning models on mid-to late-season weed detection in UAV imagery. *Remote Sensing*. 2020;12(13):2136. <https://doi.org/10.3390/rs12132136>
16. Liu W, Anguelov D, Erhan D, Szegedy C, Reed S, Fu C-Y, *et al.* SSD: Single shot multibox detector. In: Leibe B, Matas J, Sebe N, Welling M, editors. *Computer Vision – ECCV 2016*. Cham: Springer; 2016. pp. 21–37. https://doi.org/10.1007/978-3-319-46448-0_2
17. Redmon J, Divvala S, Girshick R, Farhadi A. You only look once: Unified, real-time object detection. *Proceedings of the 2016 IEEE Conference on Computer Vision and Pattern Recognition*; 2016; Vegas. IEEE; 2016. pp. 779–788. <https://doi.org/10.1109/CVPR.2016.91>
18. Redmon J, Farhadi A. YOLO9000: better, faster, stronger. *Proceedings of the 2017 IEEE Conference on Computer Vision and Pattern Recognition*; 2017; Honolulu. IEEE; 2017. pp. 7263–7271. <https://doi.org/10.1109/CVPR.2017.690>
19. Redmon J, Farhadi A. YOLOv3: An incremental improvement. 2018. <https://doi.org/10.48550/arXiv.1804.02767>
20. Bochkovskiy A, Wang C-Y, Liao H-YM. YOLOv4: Optimal speed and accuracy of object detection. 2020. <https://doi.org/10.48550/arXiv.2004.10934>

21. Jocher G, Chaurasia A, Stoken A, Borovec J, Kwon Y, Fang J, *et al.* ultralytics/yolov5: v6.1 – TensorRT, TensorFlow edge TPU and OpenVINO export and inference. Zenodo. 2022. <https://doi.org/10.5281/zenodo.6222936>
22. Ge Z, Liu S, Wang F, Li Z, Sun J. YOLOX: Exceeding YOLO series in 2021. 2021. <https://doi.org/10.48550/arXiv.2107.08430>
23. Wang C-Y, Bochkovskiy A, Liao H-YM. YOLOv7: Trainable bag-of-freebies sets new state-of-the-art for real-time object detectors. Proceedings of the 2023 IEEE/CVF Conference on Computer Vision and Pattern Recognition; 2023; Vancouver. IEEE; 2023. pp. 7464–7475. <https://doi.org/10.1109/CVPR52729.2023.00721>
24. Girshick R. Fast r-cnn. Proceedings of the 2015 IEEE International Conference on Computer Vision; 2015; Santiago. IEEE; 2015. pp. 1440–1448. <https://doi.org/10.1109/ICCV.2015.169>
25. Ren S, He K, Girshick R, Sun J. Faster R-CNN: Towards real-time object detection with region proposal networks. In: Cortes C, Lawrence N, Lee D, Sugiyama M, Garnett R, editors. Advances in neural information processing systems. Purchase Printed Proceeding; 2015.
26. Lucena F, Breunig FM, Kux H. The combined use of UAV-based RGB and DEM images for the detection and delineation of orange tree crowns with mask R-CNN: An approach of labeling and unified framework. Future Internet. 2022;14(10):275. <https://doi.org/10.3390/fi14100275>
27. Xu L, Wang Y, Shi X, Tang Z, Chen X, Wang Y, *et al.* Real-time and accurate detection of citrus in complex scenes based on HPL-YOLOv4. Computers and Electronics in Agriculture. 2023;205:107590. <https://doi.org/10.1016/j.compag.2022.107590>
28. Yang R, Hu Y, Yao Y, Gao M, Liu R. Fruit target detection based on BCo-YOLOv5 model. Mobile Information Systems. 2022;2022:8457173. <https://doi.org/10.1155/2022/8457173>
29. Lai Y, Ma R, Chen Y, Wan T, Jiao R, He H. A pineapple target detection method in a field environment based on improved YOLOv7. Applied Sciences. 2023;13(4):2691. <https://doi.org/10.3390/app13042691>
30. Chen J, Liu H, Zhang Y, Zhang D, Ouyang H, Chen X. A multiscale lightweight and efficient model based on YOLOv7: Applied to citrus orchard. Plants. 2022;11(23):3260. <https://doi.org/10.3390/plants11233260>
31. Yang H, Liu Y, Wang S, Qu H, Li N, Wu J, *et al.* Improved apple fruit target recognition method based on YOLOv7 model. Agriculture. 2023;13(7):1278. <https://doi.org/10.3390/agriculture13071278>
32. Ministry of Agriculture. <https://www.agriculture.gov.ma>
33. Zheng Z, Wang P, Liu W, Li J, Ye R, Ren D. Distance-IoU loss: Faster and better learning for bounding box regression. AAAI-20 Technical Tracks 7. 2020;34(7):12993–13000. <https://doi.org/10.1609/aaai.v34i07.6999>

ORCID IDs

Mohamed Jibril Daiaeddine  <https://orcid.org/0009-0006-5525-7956>
 Sara Badrouss  <https://orcid.org/0009-0000-2675-4810>
 Abderrazak El Harti  <https://orcid.org/0000-0003-3976-4588>
 El Mostafa Bachaoui  <https://orcid.org/0000-0003-4163-6307>
 Mohamed Biniz  <https://orcid.org/0000-0002-9448-6165>
 Hicham Mouncif  <https://orcid.org/0000-0003-3312-8230>



Stabilizing fish oil during storage with *Satureja bachtiarica* Bunge

Atefeh Matbo¹, Mohammad Mehdi Ghanbari^{1,*}, Seyed Saeed Sekhavatizadeh², Mehdi Nikkhah³

¹ Sarvestan Branch, Islamic Azad University^{ROR}, Sarvestan, Iran

² Fars Research and Academic Center of Agricultural and Natural Resources, AREEO^{ROR}, Shiraz, Fars, Iran

³ Institute of Agricultural Education & Extension, AREEO^{ROR}, Tehran, Iran

* e-mail: m.mehdi.ghanbari@gmail.com

Received 25.12.2023; Revised 01.02.2024; Accepted 05.03.2024; Published online 18.10.2024

Abstract:

Fish oil is highly susceptible to lipid oxidation, which leads to safety loss during storage. Natural antioxidants can prevent lipid oxidation. *Satureja bachtiarica* Bunge, also known as savory, is an endemic species plant that contains the necessary bioactive compounds and possesses antioxidant activity suitable for this purpose. This study featured the effects of savory extract and its essential oil as stabilizing agents on kilka fish oil.

We assessed the oxidative stability of fish oil fortified with of savory extract and essential oil in amounts of 0.5 and 1%. Then we compared their oxidative activity with that of samples treated with a synthetic antioxidant during 35 days at 40°C. The fish oil samples were tested for antioxidant activity, acid degree value, thiobarbituric acid-reactive substances, para-anisidine value, conjugated dienoic acids, peroxide value, total oxidation value, and free fatty acids.

Savory essential oil at the concentration of 1% was more effective than other samples in reducing the rate of lipid oxidation in fish oil. On storage day 35, the control sample yielded the following data: peroxide value = 14.79 mEq O₂/kg, acid degree value = 32.49 mL/g, thiobarbituric acid-reactive substances = 5.82 mg MDA/g, para-anisidine value = 116.03, total oxidation index = 136.27. These results were significantly ($p < 0.05$) higher than those in the sample with 1% savory essential oil: peroxide value = 9.52 mEq O₂/kg, acid degree value = 22.41 mL/g, thiobarbituric acid-reactive substances = 3.46 mg MDA/g, para-anisidine value = 78.3, and total oxidation index = 108.09. The fish oil samples contained more unsaturated fatty acids (66.76–68.83%) than saturated fatty and acids (31.13–32.6%).

Savory essential oil demonstrated good potential as an effective natural antioxidant that extends the shelf life of fish oil.

Keywords: *Satureja bachtiarica* Bunge, *Bachtiarica* spice, *Bakhtiari* savory, essential oil, extract, fish oil, lipid oxidation, natural antioxidant

Please cite this article in press as: Matbo A, Ghanbari MM, Sekhavatizadeh SS, Nikkhah M. Stabilizing fish oil during storage with *Satureja bachtiarica* Bunge. Foods and Raw Materials. 2025;13(2):254–263. <https://doi.org/10.21603/2308-4057-2025-2-645>

INTRODUCTION

Marine fish oils are a source of popular saturated dietary fatty acids, e.g., lauric, palmitic, myristic, and stearic acids [1]. In addition, fish oil yields long-chain ω -3 (n-3) polyunsaturated fatty acids, e.g., eicosapentaenoic acid (EPA, 20:5n-3) and docosahexaenoic acid (DHA, 22:6n-3) [2]. The high content of ω -3 fatty acids promotes its beneficial effects on human health. Fish oil is good for heart, brain, and nervous system, which makes it a valuable functional product. Fish oil fatty acids are effective against obesity, type 2 diabetes, depression, non-alcoholic fatty liver disease, and inflammation. Also, ω -3 fatty acids improve heart rate and reduce the risk of cardiovascular diseases [3]. Unfortunately, ω -3

fatty acids obtained from fish oil are sensitive to oxidation, which limits its use in the food industry. The rate of oil oxidation depends on the oil structure, temperature, and micro components, e.g., pigments, hydroperoxides, and free fatty acids. Therefore, fish oil needs to be protected from oxidation during consumption and storage. Oil oxidation can be prevented or inhibited by antioxidants and special conditions, e.g., thermal processing, exposure to light, oxygen, and storage at $\geq 20^\circ\text{C}$, etc. [3].

Antioxidants prevent oil oxidation by inhibiting the formation of free radicals or by stopping their release. According to Diniz do Nascimento *et al.*, synthetic antioxidants must be limited in animal studies [4]. Therefore, natural antioxidants of plant origin may replace

synthetic substitutes in the food industry to improve the oxidative stability of fish oil [5, 6].

Several compounds used in sufficient concentrations may act as antioxidants, e.g., plant extracts obtained from dried plant materials by steam distillation, cold pressure, or solvent extraction [7]. This list also includes essential oils and aromatic oily liquids that are composed of volatile compounds with low molecular weight [8].

Hrebien-Filisińska & Bartkowiak added 25% (w/w) sage extract to fish oil and managed to reduce the oxidation rate, both during refrigerated storage and at room temperature storage [9].

The genus *Satureja* consists of 30 species. It belongs to aromatic plants that are distributed in the Mediterranean, Africa, Asia, and North America. Iran has 12 wild species of this genus. *Bakhtiari* savory (*Satureja bachtiarica* Bunge) belongs to the *Lamiaceae* family. Its leaves are used as spices, nutrients, and herbal pharmaceuticals. This plant grows in the central part of the Zagros Mountains, Iran. *Bakhtiari* savory is a one-year herbaceous semi-shrub 20–45 cm tall, with numerous stems and short branches covered with gray lashes. Medicinal and aromatic plants are members of the mint family and contain a wide range of bioactive molecules that inhibit free radicals and possess antioxidant activity [10].

Polyphenols are valuable natural products obtained from plant extracts. They can protect cells from damage caused by free radicals. They demonstrate numerous pharmacological properties, e.g., they prevent atherosclerosis, cancer progression, or pathogen growth [11].

Most savory species contain essential oils. Savory varieties are rich in natural preservatives, including monoterpenes, e.g., thymol, carvacrol, and cimen [12]. The major phenolic acid compounds in *Bakhtiari* savory are rosmarinic acid, *p*-coumaric acid, parmen-tin B, 12-hydroxyjasmonic acid, tuberonic acid, β -D-glucopyranoside, methylrosmarinic acid, and caffeic acid ethyl ester [13].

Currently, there is a strong global interest in exploring new sources of natural antioxidants that are both safe and cheap. Natural antioxidants cause no adverse effects typical of their synthetic analogues [14]. As far as we know, no publications have featured *Bakhtiari* savory to enhance the oxidative stability of edible oils. Our research investigated the antioxidant compounds in savory extract and savory essential oil. We also evaluated their antioxidant potential against a synthetic antioxidant, namely tertiary butylhydroquinone. The research parameters assessed during 35 days of storage included peroxide value, acid value, thiobarbituric acid, *p*-anisidine, total oxidation value, and conjugated dienoic acids. In addition, we also studied the antioxidant activity and fatty acid profile of the fish oil samples.

STUDY OBJECTS AND METHODS

Plant and fish oil. *Bakhtiari* savory (*Satureja bachtiarica* Bunge) was gathered from the natural surroundings of the city of Sadra (Shiraz, Fars Province, Iran). This plant was identified using the botanical herbarium

compiled by the Fars Research and Academic Center of Agricultural and Natural Resources. Kilka (*Clupeonella cultriventris caspia*) fish oil was obtained from Apsa Trading Company in Qaimshahr (Mazandaran, Iran) and contained no antioxidants.

Chemicals. 2,2-diphenyl-1-picrylhydrazyl (DPPH), sodium thiosulfate, potassium acetate, gallic acid, Folin-Ciocalteu's reagent, ethanol, chloroform, acetic acid, and aluminum chloride were obtained from Merck (Darmstadt, Germany). Quercetin and methanol came from Applichem (Darmstadt, Germany). Other chemical materials and reagents of analytical grade were purchased from Sigma Aldrich (St. Louis, United States) and Merck (Darmstadt, Germany).

Extracting savory essential oil and savory extract. The savory essential oil and the savory extract were prepared based on the procedures described by Hashemi & Khodaei [15] and Khademvatan *et al.* [16].

Total phenol content. The total phenolic content in the savory essential oil and the savory extract was measured using the Folin-Ciocalteu method. It involved a calibration curve of gallic acid prepared in methanol. The results obtained using a calibration curve regression equation ($Y = 15.575x - 0.0176$, $R^2 = 0.9985$) were expressed as gallic acid in mg/g sample [17].

Total flavonoid content. The total flavonoid content in the savory essential oil and the savory extract was measured based on the aluminum chloride colorimetric method [17]. A calibration curve of quercetin was made in methanol. The results were calculated using a regression calibration curve equation ($Y = 0.0237x + 0.0867$, $R^2 = 0.9886$). It was expressed as quercetin mg/g sample [18].

DPPH analysis. The 2,2-diphenyl-1-picrylhydrazyl (DPPH) method was employed to measure the antioxidant activity concerning free radical inhibition percentage. TBHQ made it possible to construct a standard curve at various concentrations. The equation below served to represent a percentage of scavenging activity:

$$\% \text{ Scavenging} = [(A_0 - A_1) / (A_0)] \times 100 \quad (1)$$

where A_0 is the absorbance of the control and A_1 is the absorbance of the sample.

Finally, we calculated IC_{50} , i.e., the absorbance value of 50% in the reducing power assay [19].

Determining total phenolic content. High-performance liquid chromatography (HPLC) (Agilent Technologies, 1200 series, Germany) was used to determine the number of polyphenolic compounds in the savory extract.

Gas chromatography – mass spectrometry test. We used gas chromatography – mass spectrometry (GC–MS) to identify the chemical components in the savory essential oil (Varian, 450-GC/MS: 1200, USA). The length of column HP-5MS (phenylmethyl silox) was 30 m, its diameter was 250 nm, and its thickness was 0.25 mm. The test involved an electron ionization system with an ionizing energy of 70 eV. The temperature in the oven stayed 50°C for 2 min to be adjusted to 70°C

at 5°C/min and heated to 100°C at 20 and 10°C/min. Finally, it remained 290°C for 2 min. The detector and injector temperatures were 300 and 200°C, respectively. Helium served as carrier gas at a flow degree of 0.8 mL/min, and the 0.5% samples were injected physically in the splitless style. Summits area percents were applied for achieving numerical information. The mass array was determined from 50 m/z to 550 amu. Holding directories were restrained for compounds by homologous types of n-alkanes (C5–C24) injected in circumstances equivalent to those applied to the samples.

In the savory essential oil, chemical components were identified using GC–MS with a similar device. Helium was applied as carrier gas with a persistent flow rate of 1 mL/min. The temperature mode was the same as described above. Four microliters of oil were injected as split; the split relation was 1:100. The MS functional restrictions were as follows: 200°C interface temperature, 70 eV ionization potential, 50–800 mass array acquisition. The oil compounds were determined in line with the protocol described by Fathimoghaddam *et al.* [17]. Table 1 illustrates the gradient program used to measure the polyphenolic compounds in the essential oil.

Preparing fish oil and storage conditions. The fish oil samples and their storage conditions were in line with the method introduced by Lizárraga-Velázquez *et al.* with some modifications [18]. The savory essential oil and the savory extract were added separately to fish oil samples in concentrations of 0.5 and 1% (w/v). Tween 20 (10%, w/v) served as emulsifier for the extract [20]. TBHQ was added (100 ppm) to the fish oil as a synthetic antioxidant. One group contained no antioxidants and served as control. The essential oil, the extract, and the synthetic oxidant were dispersed slowly in the oil and mixed until homogeneous emulsion. The oil samples were poured into dark glass bottles and kept in an incubator at 40°C and 75% relative humidity for 35 days. The samples were evaluated on storage days 0, 7, 14, 21, 28, and 35. Each treatment was performed in triplicate [18].

Peroxide value. To determine the peroxide value in fish oils, we applied the method described by Sarojini *et al.* [21]. The resulting peroxide value, mEq O₂/kg fat, was expressed as milliequivalents of oxygen per 1 kg of fat as in the Eq. (2):

$$\text{Peroxide value} = \frac{(S - B) \times N \times 1000}{W} \quad (2)$$

where S is the sample volume, mL; B is the blank sample volume, mL; N is the normality of sodium thiosulfate solution, mol/L; and W is the sample weight, g [21].

Table 1 Total phenolic, total flavonoid, and IC₅₀ in savory extract and savory essential oil

Sample	Total phenol, mg/g	Total flavonoid, mg/g	IC ₅₀ , mg/mL
Savory extract	104.269	13.825	0.206
Savory essential oil	70.882	0.801	2.865
Gallic acid	–	–	0.025

Acid degree value. We weighed 10 g of the oil sample in a 250-mL Erlenmeyer flask. Then, we added 50 mL of ethanol and diethyl ether (1:1) into the flask, followed by three drops of a phenolphthalein indicator solution. For titration, we applied 0.1 M potassium hydroxide until the mix turned pink. The same conditions were replicated for the blank sample. The acid degree value, mg KOH/g, was determined as follows (ISO 660):

$$\text{Acid degree value} = \frac{(V - b) \times N \times 56.1}{W} \quad (3)$$

where 56.1 is the molecular weight of potassium hydroxide, g/mol; V is the potassium hydroxide volume in for the oil sample, mL; b is the potassium hydroxide volume in the blank sample, mL; N is normality of potassium hydroxide solution, mol/L; and W is the sample weight, g.

The **thiobarbituric acid reactive substances** were measured as proposed by Sarojini *et al.* and represented as mg malonaldehyde (MDA)/kg [21].

The **para-anisidine value** in the fish oil was measured according to the method described by Yeşilisu & Özyurt [22]:

$$\text{Para - anisidine value} = \frac{25 \times (1.2 \times A_s \times A_b)}{m} \quad (4)$$

where A_s is the fat solution absorption; A_b is the absorption of fat solution after its reaction with para-anisidine reagent; and m is the sample weight, g.

Total oxidation value (TOTOX index). We used the TOTOX number, or total oxidation value, to determine the total fat and oil oxidation. It was calculated according to the method described by Jaioun *et al.* [23]:

$$\text{TOTOX index} = (2 \times \text{PV}) + \text{pAV} \quad (5)$$

where pAV is the para-anisidine value and PV is the peroxide value.

Conjugated dienoic fatty acid. We studied the conjugated dienoic fatty acid, %, in the fish oil samples in line with the equation proposed by Na *et al.* [24]:

$$\text{Conjugated dienoic fatty acid} = 0.84 \{A_s / (b \times c) - 0.03\} \quad (6)$$

where A_s is the absorbance observed; b is the cuvette length, cm; and c is the concentration of test sample, g/L.

The **antioxidant activity (DPPH)** was assessed based on the method proposed by Hrebien-Filisińska & Bartkowiak [9].

The **fatty acid profile** of the fish oil was assessed using the method described by Soltaninejad & Sekhavitazadeh [25]. The results were presented as a percentage of the relative peak area.

Statistical analysis. For data analysis, we used a one-way ANOVA and SPSS Statistics 19.0 (Chicago, USA) ($p < 0.05$). To determine the significant difference, we applied Duncan's test. The graphs were constructed in Microsoft Excel 2016.

RESULTS AND DISCUSSION

Identifying chemical compounds by GC–MS.

Table 2 summarizes the gas chromatography – mass spectrometry results for the savory essential oil. The test revealed 12 compounds that made up 100% of the total composition. Carvacrol (58.019%) and γ -terpinene (25.148%) appeared to be the main components. The other compounds were o-cymene (4.836%), α -terpinene (4.361%), β -Myrcene (1.772%), and carvacrol acetate (1.242%). The savory essential oil also contained α -pinene (1.219%), α -Thujene (1.133%), *trans*-anethole (1.009%), β -pinene (0.448%), phellandrene (0.44%), and limonene (0.374%).

Memarzadeh *et al.* identified 28 chemical compounds in savory essential oil, which occupied 98.59% of the total essential oil [10]. They found carvacrol (31.25%) and γ -terpinene (10.65%) to be the most abundant chemical compounds, which was different from our results. In their study, the amount of carvacrol and γ -terpinene was between 28.18–35.71 and 6.05–8.25%, respectively. In addition, o-cimen and thymol were on their list of the main components. The major difference between the results may be related to the number of identified chemical compounds, type, and concentration; however, carvacrol and γ -terpinene proved to be the main components in both studies. Other researchers also reported carvacrol (31.25–14.20%) as the most common chemical component in savory essential oil [15, 17]. The different geographical location, soil structure, consistency, and climate were the most important factors that caused differences in the chemical composition of the savory essential oil [17].

Antioxidant activity, total flavonoid content, and total phenolic content. The results showed that the total flavonoid and phenolic contents in the savory extract were 104.269 and 13.825 mg/g of extract, respectively. These amounts exceeded those detected in the savory essential oil (70.882 and 0.801 mg/g). The IC₅₀ level in the savory essential oil was higher than in the gallic acid sample and the savory extract, which indicates that the antioxidant activity of the savory essential oil was lower than that of the savory extract and the gallic acid sample.

The total phenolic contents were 104.269 and 70.882 mg GAE/g for the extract and the essential oil, respectively. The composition and content of herbal extracts and essential oil are known to depend on various factors, such as temperature, time, extraction method, solvent, etc. The type of solvent is the most important factor due to its polarity and the tendency to combine with different substances [26]. Fathimoghaddam *et al.* measured the total phenolic and flavonoid contents in the savory essential oil as 88.33 ± 1.69 mg GAE/100 g DW and 20.63 ± 1.24 mg QU /100 g DW, respectively [17]. These values were higher than those obtained by us in this research.

These differences may be related to many factors, including extraction method, cultivation conditions, the type of extraction solvent, maturity of plants, geographical location, environment, genetics, variety, part of the plant used, and harvesting season [27].

Table 2 Chemical composition of savory essential oil, GC–MS

Retention time, min	Chemical components	Amount, %
5.592	α -thujene	1.133
5.835	α -pinene	1.219
7.164	β -pinene	0.448
7.396	β -myrcene	1.772
8.067	Phellandrene	0.44
8.446	α -terpinene	4.361
8.785	o-cymene	4.836
8.874	Limonene	0.374
10.138	γ -terpinene	25.148
19.907	<i>trans</i> -anethole	1.009
21.166	Carvacrol	58.019
23.124	Carvacrol acetate	1.242
Total		100.00

In this study, the savory extract had a lower IC₅₀ compared to the savory essential oil: as a result, the antioxidant activity was higher. The IC₅₀ results ranged between 0.025 and 2.865 mg/mL. The lower IC₅₀ content in the savory extract was due to the higher total phenolic and flavonoid contents. It had the highest antioxidant activity compared to the savory essential oil. In this regard, Fathimoghaddam *et al.* linked the high antioxidant effect in savory essential oil to the greater total phenolic and flavonoid contents [17].

In our study, the DPPH radical inhibition was 76.72%. In a similar study, Memarzadeh *et al.* explained the high value of the savory radical scavenging capacity of essential oil by the hydroxyl groups present in the chemical structure of phenolic compounds, which provided a radical scavenger [10].

Table 3 shows the polyphenol content in savory. The essential oil antioxidant activity was probably due to γ -terpinene terpenoids and carvacrol, which were the main contents in savory. Memarzadeh *et al.* also found many polyphenolic compounds in the savory family, especially flavonoids and phenolic acids, including caryophyllene and borneol [10].

Table 3 shows polyphenolic compounds in the savory extract identified by HPLC. Carvacrol (21 250.81 mg/L) proved to be one of the main components in this plant extract. It was followed by rosmarinic acid (3753.279 mg/L), *trans*-ferulic acid (82.60816 mg/L), and catechin (68.24201 mg/L).

In the present study, carvacrol and rosmarinic acid proved to be two major polyphenolic compounds. Phenolic compounds and flavonoids are often reported in scientific publications. For instance, rosmarinic acid and rutin were the most abundant of their kind in *Satureja montana*: 7.85 and 17.29%, respectively. The total polyphenolic content varied from 100.65 to 420.68 mg/100 g among three species [28]. In another research on savory, the total phenolic content was 177.92 mg/100 g [29]. This polyphenolic profile was different from that obtained in our study, probably, due to different HPLC standards and extraction methods [30].

Table 3 Polyphenolic content of savory extract: HPLC

Retention time, min	Polyphenol content	Savory extract, mg/L
3.3	Gallic acid	n.d.
8.3	Catechin	68.24201
11.6	Caffeic acid	n.d.
13.5	Vanilin	n.d.
15.6	<i>p</i> -coumaric acid	n.d.
16.3	<i>trans</i> -ferulic acid	82.60816
16.5	Sinapic acid	n.d.
17.4	Coumarin	n.d.
18.5	Hesperedin	n.d.
19.02	Ellagic acid	n.d.
19.2	Rosmarinic acid	3753.279
21.6	Quercetin	n.d.
22.4	Hesperetin	n.d.
23.7	Eugenol	n.d.
28.4	Carvacrol	21 250.81
28.9	Thymol	n.d.

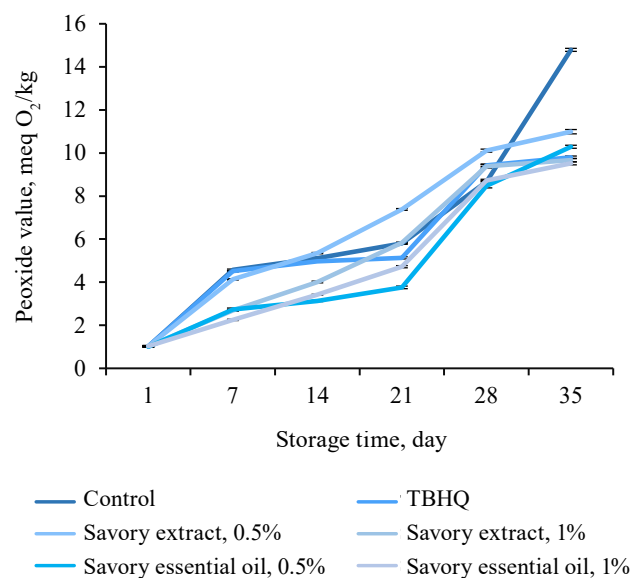
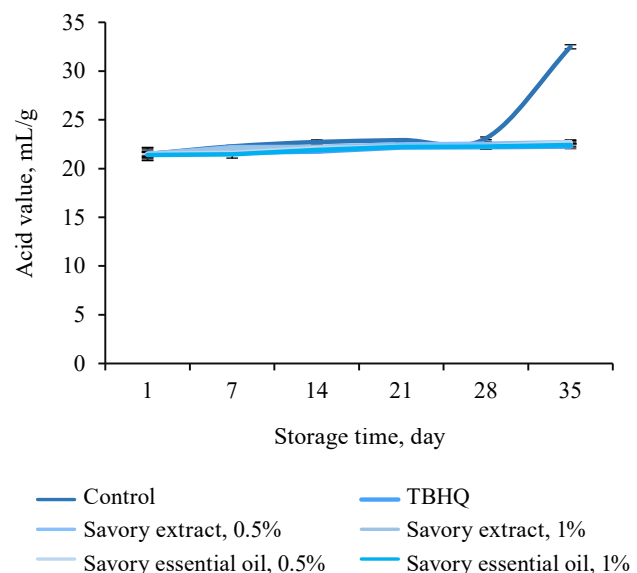
n.d. – not detected

Peroxide value. Figure 1 illustrates the peroxide values in fish oil samples fortified with different concentrations of savory extract and savory essential oil during 35 days of storage. The peroxide values in all fish oil samples increased significantly during the storage period ($p < 0.05$). The initial peroxide value was 1.0–1.3 mEq O₂/kg, but it increased from 9.38 to 14.79 mEq O₂/kg on storage day 35. We detected no significant difference between the fish oil samples with 1% savory extract and the oil sample with TBHQ ($p > 0.05$), but the control sample had the highest peroxide value on storage day 35 ($p < 0.05$).

Therefore, 0.5 and 1% savory essential oil added to fish oil during storage affected its oxidative parameters. Antioxidants usually delay the rate of oxidation due to their ability to chelate metals, quench singlet oxygen, and destroy free radicals [31]. The mint family is known to contain phenolic compounds. For instance, Sayyad & Farahmandfar reported that *Teucrium polium* L. essential oil contained mono and sesquiterpene compounds [32]. They were applied as antioxidants in canola oil and showed higher protective effects than BHA against oxidation during storage.

Acid degree value. Figure 2 demonstrates the changes in acid degree value that occurred in the fish oil samples fortified with different concentrations of savory extract and savory essential oil during 35 days of storage. All samples of fish oil revealed a significant increase ($p < 0.05$) in acid degree value. On storage day 35, the lowest acid degree value belonged to the samples with TBHQ (22.3 ± 0.26 mL/g) and 1% savory essential oil (22.41 ± 0.18 mL/g) ($p < 0.05$).

Acid degree value in the control samples of fish oil increased during storage, except those with TBHQ, savory extract, and savory essential oil. Özkan & Özkan reported that the acid values of oils containing 600 and 1200 ppm of savory (*Satureja thymbra*) and marj-

**Figure 1** Peroxide values in fish oil during storage**Figure 2** Acid degree values in fish oil during storage

oram (*Origanum onites*) extracts were similar to each other [33]. Also, they had a lower acidity compared to the control sample. The presence of monoterpenoid phenolic compounds, e.g., carvacrol, are probably related to the higher number of hydroxyl groups in essential oil molecules.

Thiobarbituric acid index. Figure 3 shows the analysis of the thiobarbituric acid index in the fish oil samples fortified with different concentrations of savory extract and savory essential oil during 35 days of storage. The values of the thiobarbituric acid index in all fish oil samples demonstrated a significant increase ($p < 0.05$) and rose from 1.19–1.28 to 3.46–5.82 mg MDA/kg during storage time. On storage day 35, the lowest thiobarbituric acid index belonged to the sample with 0.5 and 1% savory essential oil (4.19 ± 0.09 and 3.46 ± 0.08 mg MDA/kg, respectively).

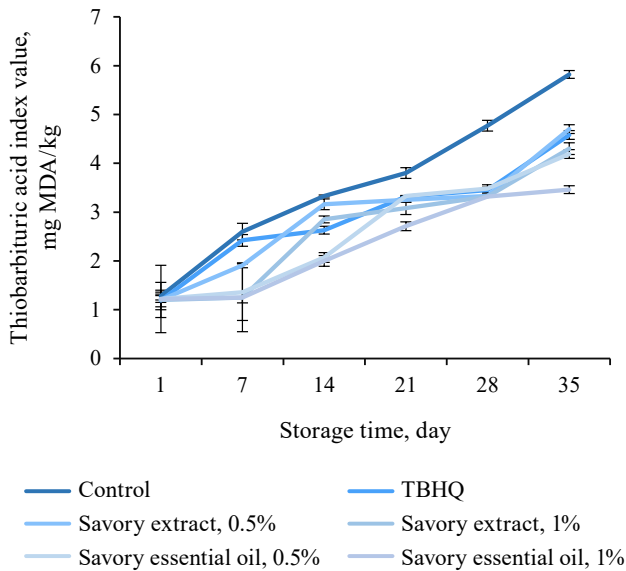


Figure 3 Thiobarbituric acid index in fish oil during storage

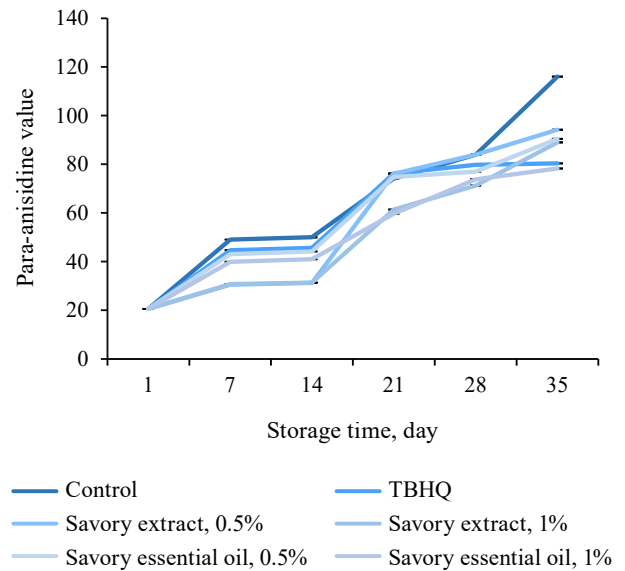


Figure 4 Para-anisidine values in fish oil during storage

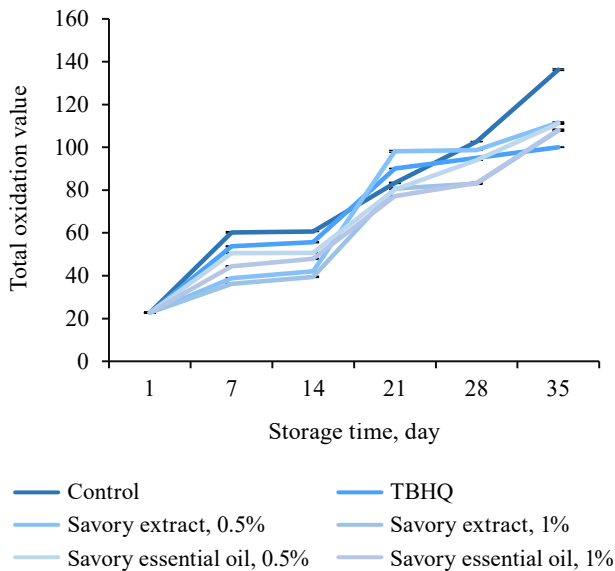


Figure 5 Total oxidation index in fish oil during storage

In our research, the thiobarbituric acid index increased during the storage time. However, the thiobarbituric acid index in all samples treated with savory extract and savory essential oil was lower compared to the control and the samples with tertiary butylhydroquinone, which can be related to their phenolic compound [17]. Kamkar *et al.* added methanolic and ethanolic extracts of summer savory (*Satureja hortensis* L.) to soybean oil to increase its oxidation stability [34]. García-Pérez *et al.* added *Bryophyllum* plant extracts to fish oil to increase the antioxidant efficiency due to the incorporation of polyphenols [35].

Para-anisidine value. Figure 4 reports para-anisidine values in the fish oil samples. The para-anisidine values increased significantly in all fish oil samples during the storage period. On storage day 35, the highest

value was observed in the control oil sample (116.05 ± 0.23). In our study, para-anisidine values increased significantly ($p < 0.05$) with storage. Santos *et al.* linked para-anisidine increase to the degradation of primary lipid oxidation products (hydroperoxides) that turned to secondary oxidation products (carbonyls) [36]. On storage day 35, the lowest para-anisidine values belonged to the sample with TBHQ (76.22 ± 0.22) and 1% savory extract (78.00 ± 0.23). Hwang *et al.* reported an increase in para-anisidine when they raised the concentration of coffee acetone extract (0.1, 0.25, and 0.5%) added to fish oil as antioxidant during 14 days of storage [37].

Total oxidation value (TOTOX index). Figure 5 shows the changes in the total oxidation value. The TOTOX index ranged from 22.64 to 22.85 on the first day and increased to 100.01–136.27 on storage day 35. At the end of the storage time, the highest total oxidation value belonged to the control sample (136.27 ± 0.38). The lowest was observed in the samples with TBHQ (100.01 ± 0.09) and 1% savory essential oil (108.09 ± 0.40).

In a similar study, low concentrations of sage extract (5, 10, 25, and 50%) in cod fish liver oil caused a significant decrease ($p < 0.05$) in the TOTOX index due to the appropriate amount of antioxidant polyphenols [38]. However, in our research, this parameter increased significantly ($p < 0.05$) during the storage period.

Conjugated dienoic acid. Figure 6a illustrates the contents of conjugated dienoic acids in the fish oil samples fortified with different concentrations of savory extract and savory essential oil. The amount of conjugated dienoic acid increased significantly in all fish oil samples during storage ($p < 0.05$), rising from 0.64–1.01 to 1.7–1.75%. We detected no significant difference in conjugated dienoic acid between the samples at the end of storage ($p > 0.05$).

In the present study, synthetic and natural antioxidants produced no significant effect on conjugated dienoic acid. However, other scientists reported that

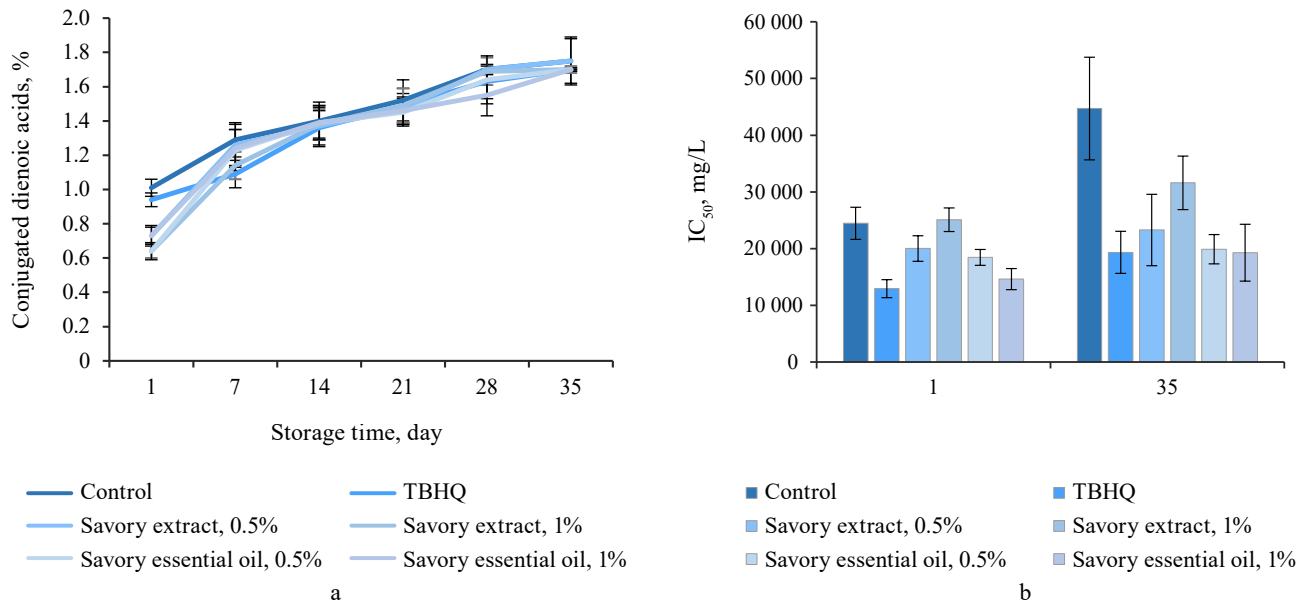


Figure 6 Conjugated dienoic acid (a) and antioxidant activity (b) in fish oil during storage

Table 4 Fatty acids in fish oil during storage

Fatty acid, type	Fatty acid, name	Day 1	Day 35		
		Control	Control	Savory extract (1%)	Savory essential oil (1%)
Saturated fatty acids (SFA)					
C12:0	Lauric acid	0.13	0.12	0.06	0.07
C14:0	Myristic acid	3.24	3.23	3.39	3.66
C15:0	Pentadecylic acid	0.63	0.63	0.64	0.66
C16:0	Palmitic acid	19.58	19.18	19.82	20.31
C17:0	Margaric acid	1.52	1.46	1.48	1.48
C18:0	Stearic acid	4.86	4.86	4.71	4.95
C20:0	Arachidic acid	0.31	0.27	0.40	0.33
C22:0	Behenic acid	0.74	0.72	0.76	0.72
C24:0	Lignoceric acid	0.63	0.66	0.14	0.42
Monounsaturated fatty acids (MUFA)					
C14:1	Myristoleic acid	0.51	0.53	0.54	0.49
C15:1	Pentadecenoic acid	0.16	0.16	0.16	0.14
C16:1	Palmitoleic acid	5.82	6.33	6.27	5.97
C17:1	heptadecenoic acid	0.77	0.77	0.78	0.75
C18:1 $trans$	Vaccenic acid	0.22	0.22	0.26	0.63
C18:1 cis	Oleic acid (ω -9)	36.80	37.07	35.50	36.61
C20:1	Gondoic acid	1.93	1.94	1.90	1.88
C22:1	Erucic acid	0.20	0.19	0.18	–
C24:1	Nervonic acid	0.47	0.45	0.58	0.43
Polyunsaturated fatty acids (PUFA)					
C18:2 cis	linoleic acid (ω -6)	1.91	2.00	1.91	2.29
C18:3 cis	α -Linolenic acid (ω -3)	1.66	1.70	1.59	1.66
C20:2	Eicosadienoic acid	–	0.10	0.19	0.18
C22:5	docosapentaenoic acid (DPA)	0.44	0.50	0.44	–
C20:5	Eicosapentaenoic acid (EPA)	6.46	6.30	6.55	6.01
C22:6	Docosahexaenoic acid (DHA)	11.00	10.57	11.19	9.72
ω -6/ ω -3		1.15	1.17	1.20	1.37
Σ SFA		31.64	31.13	31.4	32.60
Σ MUFA		46.88	47.66	46.17	46.90
Σ PUFA		21.47	21.17	21.87	19.86
Σ UFA		68.35	68.83	68.04	66.76
Σ PUFA/ Σ SFA		0.67	0.68	0.69	0.60
Polyene index (EPA + DHA)/palmitic acid)		0.89	0.87	0.89	0.77

synthetic and natural antioxidants curbed the amount of conjugated dienoic acid produced. The list of substances that reduced the amount of conjugated dienoic acid in fish oil included different concentrations of such plant extracts as rosemary, garlic, and bryophyllum, as well as 5% roasted or unroasted pumpkin seed oil [35, 39, 40].

Antioxidant activity (DPPH). Figure 6b demonstrates antioxidant activity in the fish oil samples during storage. The sample with lower IC_{50} revealed the highest antioxidant activity. In our study, the samples with TBHQ and 1% savory essential oil had the highest antioxidant activity on storage days 1 and 35. In general, the antioxidant activity in all samples decreased during the storage period.

The IC_{50} in all oil samples increased significantly after 35 days of storage ($p < 0.05$), which indicated a gradual decrease in antioxidant activity during storage. Thus, the storage time had a significant effect on the antioxidant activity of kilka fish oil. The sample with 1% savory essential oil was not significantly different from the sample with TBHQ ($p > 0.05$). Other samples with natural antioxidants, except for the 1% savory extract sample, had a significant difference with the TBHQ sample on storage day 35. Other reports on the high antioxidant activity of different savory species confirm the results obtained in this study [41]. Moreover, Jafari *et al.* linked the total antioxidant capacity not only to phenolic compounds but also to enzyme systems, vitamins, organic acids, and other compounds in the plant [42].

Fatty acid profile. Table 4 gives data on the fatty acid profile. During storage, the fatty acid content was in the range of 31.13–32.6% (saturated fatty acids), 46.17–47.66% (monounsaturated fatty acids), and 19.86–21.87% (polyunsaturated fatty acids). Monounsaturated fatty acids proved to be the most abundant of their kind both in the control sample and in the samples fortified with savory extract and savory essential oil.

Golmakani *et al.* reported the fatty acid composition of kilka oil as mainly composed of monounsaturated fatty acids, followed by saturated fatty acids and polyunsaturated fatty acids, which was in line with our research [43]. In the present research, the n-6 to n-3 ratio in the fish oil samples was 1.15–1.37%.

In this regard, Golmakani *et al.* also reported that the ratio of polyunsaturated to saturated fatty acids in kilka fish oil was 0.54%, which also confirmed our results [44].

CONCLUSION

In the present study, we obtained *Bakhtiari* savory extract and *Bakhtiari* savory essential oil using traditional methods and added them separately to kilka fish oil in concentrations of 0.5 and 1%.

Satureja bachtiarica Bunge proved to be rich in bioactive compounds, including active phenolic ones, e.g., carvacrol with its high antioxidant activity and oxygenated monoterpenes.

Fish oil, which is highly susceptible to oxidative degradation, was mixed with the savory extract and savory essential oil with high antioxidant content. As a result, the oxidative stability of fish oil increased. Savory essential oil in a higher concentration (1%) inhibited the oxidation process more effectively than the samples fortified with savory extract and 0.5% savory essential oil. In addition, 1% savory essential oil had the same potential as TBHQ in delaying the formation of secondary oxidation products. As a result, savory essential oil could be used as an effective natural antioxidant to increase the shelf-life of kilka fish oil.

CONTRIBUTIONS

Mohammad Mehdi Ghanbari supervised the project. Atefeh Matbooe performed the research, as well as collected and interpreted the data. Seyed Saeed Sekhavatizadeh drafted the manuscript and proofread the final version. Mehdi Nikkhah proofread the manuscript.

CONFLICT OF INTEREST

The authors declare that there is no conflict of interests related to the publication of this article.

ACKNOWLEDGMENTS

The authors thank the Head of Fars Agriculture Research and Education Center for support and encouragement.


REFERENCES


1. Kapoor B, Kapoor D, Gautam S, Singh R, Bhardwaj S. Dietary polyunsaturated fatty acids (PUFAs): Uses and potential health benefits. *Current Nutrition Reports*. 2021;10:232–242. <https://doi.org/10.1007/s13668-021-00363-3>
2. Tocher DR, Betancor MB, Sprague M, Olsen RE, Napier JA. Omega-3 long-chain polyunsaturated fatty acids, EPA and DHA: Bridging the gap between supply and demand. *Nutrients*. 2019;11(1):89. <https://doi.org/10.3390/nu11010089>
3. Jamshidi A, Cao H, Xiao J, Simal-Gandara J. Advantages of techniques to fortify food products with the benefits of fish oil. *Food Research International*. 2020;137:109353. <https://doi.org/10.1016/j.foodres.2020.109353>
4. Nascimento LD, de Moraes AAB, da Costa KS, Galúcio JMP, Taube PS, Costa CML, *et al.* Bioactive natural compounds and antioxidant activity of essential oils from spice plants: New findings and potential applications. *Biomolecules*. 2020;10(7):988. <https://doi.org/10.3390/biom10070988>
5. Gebremeskel AF, Ngoda PN, Kamau-Mbuthia EW, Mahungu SM. The effect of roasting, storage temperature, and ethanoic basil (*Ocimum basilicum* L.) extract on the oxidative stability of crude sesame (*Sesamum indicum* L.) oil. *Food Science and Nutrition*. 2022;10:2736–2748. <https://doi.org/10.1002/fsn3.2877>


6. Blasi F, Cossignani L. An overview of natural extracts with antioxidant activity for the improvement of the oxidative stability and shelf life of edible oils. *Processes*. 2020;8(8):956. <https://doi.org/10.3390/pr8080956>
7. Yolci Omeroglu P, Acoglu B, Özdal T, Tamer CE, Çopur ÖU. Extraction techniques for plant-based bio-active compounds. In: Swamy MK, Akhtar MS, editors. *Natural bio-active compounds. Volume 2: Chemistry, pharmacology and health care practices*. Singapore: Springer; 2019. pp. 465–492. https://doi.org/10.1007/978-981-13-7205-6_18
8. Bhavaniramy S, Vishnupriya S, Al-Aboody MS, Vijayakumar R, Baskaran D. Role of essential oils in food safety: Antimicrobial and antioxidant applications. *Grain and Oil Science and Technology*. 2019;2(2):49–55. <https://doi.org/10.1016/j.gaost.2019.03.001>
9. Hrebien-Filisińska AM, Bartkowiak A. Antioxidative effect of sage (*Salvia officinalis* L.) macerate as “green extract” in inhibiting the oxidation of fish oil. *Antioxidants*. 2021;11(1):100. <http://dx.doi.org/10.3390/antiox11010100>
10. Memarzadeh SM, Gholami A, Ghasemi Pirbalouti A, Masoum S. Bakhtiari savory (*Satureja bachtiarica* Bunge.) essential oil and its chemical profile, antioxidant activities, and leaf micromorphology under green and conventional extraction techniques. *Industrial Crops and Products*. 2020;154:112719. <https://doi.org/10.1016/j.indcrop.2020.112719>
11. Rana A, Samtiya M, Dhewa T, Mishra V, Aluko RE. Health benefits of polyphenols: A concise review. *Journal of Food Biochemistry*. 2022;46:e14264. <https://doi.org/10.1111/jfbc.14264>
12. Ejaz A, Waliat S, Arshad MS, Khalid W, Khalid MZ, Suleria HAR, et al. A comprehensive review of summer savory (*Satureja hortensis* L.): promising ingredient for production of functional foods. *Frontiers in Pharmacology*. 2023;14:1198970. <https://doi.org/10.3389/fphar.2023.1198970>
13. Rahmani Samani M, D’Urso G, Nazzaro F, Fratianni F, Masullo M, Piacente S. Phytochemical investigation and biofilm-inhibitory activity of bakhtiari savory (*Satureja bachtiarica* Bunge) aerial parts. *Plants*. 2024;13(1):67. <https://doi.org/10.3390/plants13010067>
14. Novais C, Molina AK, Abreu RMV, Santo-Buelga C, Ferreira ICFR, Pereira C, et al. Natural food colorants and preservatives: A review, a demand, and a challenge. *Journal of Agricultural and Food Chemistry*. 2022;70(9):2789–2805. <https://doi.org/10.1021/acs.jafc.1c07533>
15. Hashemi SMB, Khodaei D. Antimicrobial activity of *Satureja Khuzestanica* Jamzad and *Satureja bachtiarica* Bunge essential oils against *Shigella flexneri* and *Escherichia coli* in table cream containing *Lactobacillus plantarum* LU5. *Food Science and Nutrition*. 2020;8:5907–5915. <https://doi.org/10.1002/fsn3.1871>
16. Khademvatan S, Eskandari A, Nejad BS, Najafi S. *In vitro* anti-leishmanial activity of *Satureja khuzestanica* Jamzad and *Oliveria decumbens* Vent. Extracts on *Leishmania major* and *Leishmania infantum* promastigotes. *Journal of Reports in Pharmaceutical Sciences*. 2019;8(2):149–154. https://doi.org/10.4103/jrptps.JRPTPS_39_18
17. Fathimoghaddam E, Shakerian A, Sharafati Chaleshtori R, Rahimi E. Chemical composition and antioxidant properties and antimicrobial effects of *Satureja bachtiarica* Bunge and *Echinophora platyloba* DC. essential oils against *Listeria monocytogenes*. *Journal of Medicinal Plants and By-product*. 2020;9:47–58. <https://doi.org/10.22092/jmpb.2020.121750>
18. Lizárraga-Velázquez CE, Hernández C, González-Aguilar GA, Heredia JB. Effect of hydrophilic and lipophilic antioxidants from mango peel (*Mangifera indica* L. cv. Ataulfo) on lipid peroxidation in fish oil. *CyTA – Journal of Food*. 2018;16(1):1095–1101. <https://doi.org/10.1080/19476337.2018.1513425>
19. Rahpeyma E, Sekhavatizadeh SS. Effects of encapsulated green coffee extract and canola oil on liquid kashk quality. *Foods and Raw Materials*. 2020;8(1):40–51. <https://doi.org/10.21603/2308-4057-2020-1-40-51>
20. Kumari A, Venkateshwarlu G, Choukse MK, Anandan R. Effect of essential oil and aqueous extract of ginger (*Zingiber officinale*) on oxidative stability of fish oil-in-water emulsion. *Journal of Food Processing and Technology*. 2014;6(1):1000412. <https://doi.org/10.4172/2157-7110.1000412>
21. Sarojini A, Raju CV, Lakshmisha IP, Amitha, Gajendra. Effect of pomegranate (*Punica granatum*) peel extract on lipid oxidation in sardine fish oil. *Journal of Entomology and Zoology Studies*. 2019;7(2):140–144.
22. Yeşilsu AF, Özyurt G. Oxidative stability of microencapsulated fish oil with rosemary, thyme and laurel extracts: A kinetic assessment. *Journal of Food Engineering*. 2019;240:171–182. <https://doi.org/10.1016/j.jfoodeng.2018.07.021>
23. Jairoun AA, Shahwan M, Zyoud SH. Fish oil supplements, oxidative status, and compliance behaviour: Regulatory challenges and opportunities. *PLoS ONE*. 2020;15(12):e0244688. <https://doi.org/10.1371/journal.pone.0244688>
24. Na HS, Mok CK, Lee JH. Effects of plasma treatment on the oxidative stability of vegetable oil containing antioxidants. *Food Chemistry*. 2020;302:125306. <https://doi.org/10.1016/j.foodchem.2019.125306>
25. Soltaninejad F, Sekhavatizadeh SS. Effects of encapsulated black caraway extract and sesame oil on kolompeh quality. *Foods and Raw Materials*. 2019;7(2):311–320. <https://doi.org/10.21603/2308-4057-2019-2-311-320>
26. Ali A, Chua BL, Chow YH. An insight into the extraction and fractionation technologies of the essential oils and bioactive compounds in *Rosmarinus officinalis* L.: Past, present and future. *TrAC Trends in Analytical Chemistry*. 2019;118:338–351. <https://doi.org/10.1016/j.trac.2019.05.040>


27. Aminzare M, Hashemi M, Afshari A, Mokhtari MH, Noori SMA. Impact of microencapsulated *Ziziphora tenuior* essential oil and orange fiber as natural-functional additives on chemical and microbial qualities of cooked beef sausage. Food Science and Nutrition. 2022;10:3424–3435. <https://doi.org/10.1002/fsn3.2943>
28. Jakovljević M, Vladić J, Vidović S, Pastor K, Jokić S, Molnar M, et al. Application of deep eutectic solvents for the extraction of rutin and rosmarinic acid from *Satureja montana* L. and evaluation of the extracts antiradical activity. Plants. 2020;9(2):153. <https://doi.org/10.3390/plants9020153>
29. Rahimmalek M, Afshari M, Sarfaraz D, Miroliaei M. Using HPLC and multivariate analyses to investigate variations in the polyphenolic compounds as well as antioxidant and antiglycative activities of some *Lamiaceae* species native to Iran. Industrial Crops and Products. 2020;154:112640. <https://doi.org/10.1016/j.indcrop.2020.112640>
30. Casoni D, Olah N, Soran L, Cobzac SCA. Comparison of different extraction techniques for the evaluation of polyphenols content in Summer savory extracts. Studia Universitatis Babeş-Bolyai Chemia. 2017;62(3):45–56. <https://doi.org/10.24193/subbchem.2017.3.04>
31. Grosshagauer S, Steinschaden R, Pignitter M. Strategies to increase the oxidative stability of cold pressed oils. LWT. 2019;106:72–77. <https://doi.org/10.1016/j.lwt.2019.02.046>
32. Sayyad R, Farahmandfar R. Influence of *Teucrium polium* L. essential oil on the oxidative stability of canola oil during storage. Journal of Food Science and Technology. 2017;54:3073–3081. <https://doi.org/10.1007/s13197-017-2743-0>
33. Özkan G, Özcan MM. Antioxidant activity of some medicinal plant extracts on oxidation of olive oil. Journal of Food Measurement and Characterization. 2017;11:812–817. <https://doi.org/10.1007/s11694-016-9452-7>
34. Kamkar A, Tooriyan F, Jafari M, Bagherzade M, Saadatjou S, Molaei Aghaei E. Antioxidant activity of methanol and ethanol extracts of *Satureja hortensis* L. in soybean oil. Journal of Food Quality and Hazards Control. 2014;1:113–119.
35. García-Pérez P, Losada-Barreiro S, Bravo-Díaz C, Gallego PP. Exploring the use of *Bryophyllum* as natural source of bioactive compounds with antioxidant activity to prevent lipid oxidation of fish oil-in-water emulsions. Plants. 2020;9(8):1012. <https://doi.org/10.3390/plants9081012>
36. Santos MMF, Lima DAS, Madruga MS, Silva FAP. Lipid and protein oxidation of emulsified chicken patties prepared using abdominal fat and skin. Poultry Science. 2020;99(3):1777–1787. <https://doi.org/10.1016/j.psj.2019.11.027>
37. Hwang H-S, Winkler-Moser JK, Kim Y, Liu SX. Antioxidant activity of spent coffee ground extracts toward soybean oil and fish oil. European Journal of Lipid Science and Technology. 2019;121(4):1800372. <https://doi.org/10.1002/ejlt.201800372>
38. Hrebien-Filisińska AM, Bartkowiak A. The use of sage oil macerates (*Salvia officinalis* L.) for oxidative stabilization of cod liver oil in bulk oil systems. International Journal of Food Science. 2020;2020:4971203. <https://doi.org/10.1155/2020/4971203>
39. Jung H, Kim I, Jung S, Lee J. Oxidative stability of chia seed oil and flaxseed oil and impact of rosemary (*Rosmarinus officinalis* L.) and garlic (*Allium cepa* L.) extracts on the prevention of lipid oxidation. Applied Biological Chemistry. 2021;64:6. <https://doi.org/10.1186/s13765-020-00571-5>
40. Gashi A, Chernev G, Symoniuk E, Jankulovski Z, de Souza CK, Rexhepi F. Evaluation of the oxidative thermal stability of fish oil with the addition of pumpkin seed oil or rosemary extract. Journal of Chemical Technology and Metallurgy. 2024;59(1):61–72. <https://doi.org/10.59957/jctm.v59.i1.2024.7>
41. Fatemi F, Abdollahi MR, Mirzaie-Asl A, Dastan D, Papadopoulou K. Phytochemical, antioxidant, enzyme activity and antifungal properties of *Satureja khuzistanica* in vitro and in vivo explants stimulated by some chemical elicitors. Pharmaceutical Biology. 2020;58(1):286–296. <https://doi.org/10.1080/13880209.2020.1743324>
42. Jafari SA, Khorshidi J, Morshedloo MR, Houshidari F. Comparative study on the quantity and chemical composition of essential oil, antioxidant activity and total phenol content of some Iranian native *Satureja* species under the same conditions. Journal of Medicinal Plants and By-product. 2022;58(3):259–266. <https://doi.org/10.22092/JMPB.2022.356164.1406>
43. Golmakani M-T, Keramat M, Moosavi-Nasab M, Moosavian B. Oxidative stability of common kilka (*Clupeonella cultriventris caspia*) oil supplemented with microwave extracted Ghure (unripe grape) marc extract. Journal of Aquatic Food Product Technology. 2017;26(9):1022–1031. <https://doi.org/10.1080/10498850.2017.1375589>
44. Golmakani M-T, Moosavi-Nasab M, Keramat M, Mohammadi M-A. *Arthrospira platensis* extract as a natural antioxidant for improving oxidative stability of common kilka (*Clupeonella cultriventris caspia*) oil. Turkish Journal of Fisheries and Aquatic Sciences. 2018;18:1315–1323. https://doi.org/10.4194/1303-2712-v18_11_08

ORCID IDs

Atefeh Matbo  <https://orcid.org/0009-0001-5226-7642>

Mohammad Mehdi Ghanbari  <https://orcid.org/0000-0003-4955-4883>

Sayed Saeed Sekhavatizadeh  <https://orcid.org/0000-0003-1055-646X>

Mehdi Nikkhah  <https://orcid.org/0000-0002-0157-794X>



BOX-PCR and ERIC-PCR evaluation for genotyping Shiga toxin-producing *Escherichia coli* and *Salmonella enterica* serovar Typhimurium in raw milk

Lesley Maurice Bilung^{1,*}, Ernie Suhaiza Radzi¹, Ahmad Syatir Tahar¹,
Azham Zulkharnain², Romano Ngui¹, Kasing Apun¹

¹ University of Malaysia Sarawak, Kota Samarahan, Malaysia

² Shibaura Institute of Technology, Tokyo, Japan

* e-mail: mblesley@unimas.my

Received 24.09.2023; Revised 01.02.2024; Accepted 05.03.2024; Published online 18.10.2024

Abstract:

Over the past decade, the occurrence of milk-borne infections caused by Shiga toxin-producing *Escherichia coli* (STEC) and *Salmonella enterica* serovar Typhimurium (*S. Typhimurium*) has adversely affected consumer health and the milk industry. We aimed to detect and genotype the strains of *E. coli* and *S. Typhimurium* isolated from cow and goat milks using two genotyping tools, BOX-PCR and ERIC-PCR. A total of 200 cow and goat milk samples were collected from the dairy farms in Southern Sarawak, Malaysia.

First, *E. coli* and *Salmonella* spp. detected in the samples were characterized using PCRs to identify pathogenic strains, STEC and *S. Typhimurium*. Next, the bacterial strains were genotyped using ERIC-PCR and BOX-PCR to determine their genetic relatedness. Out of 200 raw milk samples, 46.5% tested positive for non-STEC, 39.5% showed the presence of *S. Typhimurium*, and 11% were positive for STEC. The two genotyping tools showed different discrimination indexes, with BOX-PCR exhibiting a higher index mean (0.991) compared to ERIC-PCR (0.937). This suggested that BOX-PCR had better discriminatory power for genotyping the bacteria.

Our study provides information on the safety of milk sourced from dairy farms, underscoring the importance of regular inspections and surveillance at the farm level to minimize the risk of *E. coli* and *Salmonella* outbreaks from milk consumption.

Keywords: Food safety, epidemiology, public health, *Escherichia coli*, *Salmonella* spp., milk-born infections, genotyping

Funding: This project was funded by the Ministry of Higher Education in Malaysia (MOHE) under the Research Acculturation Collaboration Effort (RACE Grant Scheme, RACE/b(3)/1095/2013(3)).

Please cite this article in press as: Maurice Bilung L, Radzi ES, Tahar AS, Zulkharnain A, Ngui R, Apun K. BOX-PCR and ERIC-PCR evaluation for genotyping Shiga toxin-producing *Escherichia coli* and *Salmonella enterica* serovar Typhimurium in raw milk. *Foods and Raw Materials*. 2025;13(2):264–275. <https://doi.org/10.21603/2308-4057-2025-2-639>

INTRODUCTION

Escherichia coli is generally known as normal microflora in the intestines of birds and mammals. However, not all of its strains are commensal to humans. Enteric *E. coli* is clustered into six pathotypes based on its pathogenicity profiles (virulence factors, clinical manifestation, and phylogenetic profile). They are enteropathogenic *E. coli* (EPEC), enterohaemorrhagic *E. coli* (EHEC), enterotoxigenic *E. coli* (ETEC), enteroaggregative *E. coli* (EAEC), enteroinvasive *E. coli* (EIEC), and diffusely adherent *E. coli* (DAEC) [1]. Among many *E. coli* pathogenic strains, *E. coli* O157:H7 is the most

notable serotype associated with food poisoning [2]. *E. coli* O157:H7 is one of EHECs that harbors and expresses the genes for Shiga toxins type 1 (*Stx1*) and 2 (*Stx2*) that result in hemorrhagic colitis (HC) in humans. A life-threatening sequel of hemorrhagic colitis is hemolytic uremic syndrome (HUS). *Salmonella* is a causative agent of severe foodborne disease worldwide, with most of the infections caused by *Salmonella enterica* [3, 4]. The symptoms of salmonellosis are headache, fever, diarrhea, nausea, vomiting, and abdominal cramp. These symptoms usually start 12 to 72 h after the ingestion and can last up to four to seven days, depending on the

severity of the infection. Infants, the elderly, and immune-compromised groups are generally more susceptible to salmonellosis [5]. In Malaysia, it is difficult to evaluate the status of salmonellosis due to the lack of detailed epidemiological studies by the public health and veterinary sector.

Molecular typing is crucial in studying outbreaks, identifying transmission routes, detecting pathogen cross-transmission, and determining sources of infection [6]. The enterobacterial repetitive intergenic consensus (ERIC)- and the BOX repetitive sequence (BOX)-polymerase chain reaction (PCR) are examples of genotyping tools. We used these tools to discriminate the strains of *E. coli* and *Salmonella enterica* serovar Typhimurium (*S. Typhimurium*), as well as investigate their power in clustering according to the origin of bacterial isolates.

BOX-PCR was first used for the genetic characterization of *Streptococcus pneumoniae*. It produced amplicons based on repetitive sequences in the bacterial genome and was later used to discriminate many bacterial species [7]. This tool employs the BOX A1R primer for the repetitive element sequence-based PCR to amplify the repetitive regions of the bacterial genome. This primer has been found in many microbial genomes in previous studies. The band profiles of the amplified repetitive regions are unique among the species or even between the species. Thus, different species can be identified through their band patterns [8].

ERIC-PCR is commonly used for the genetic characterization of *E. coli*. It is more powerful than other molecular fingerprinting tools such as PCR ribotyping, RAPD-PCR, or PFGE [9, 10]. Its other advantages include fast speed, sensitivity, and reliability [11]. BOX sequences are highly conserved, but their chromosomal locations differ between the species [7]. Thus, ERIC sequences are used in the PCR as practical primer binding sites to produce fingerprints of different bacterial genomes. They differ from the sequences from other bacterial repeats assays (e.g. BOX-PCR) due to their more comprehensive species distribution range [12].

Raw milk is defined as milk that has not been processed, e.g., via pasteurization and homogenization. Unprocessed milk is perceived to have more nutritional benefits than processed milk. Consumers believe that foods in their natural and unprocessed form are safer and healthier, although such beliefs have not been proven and remain the subject of ongoing debate [13]. The

practice of raw milk consumption is prevalent and linked to consumers' educational level, socioeconomic factors, and living on dairy farms. This is of public health concern since there is an 850 times higher risk of acquiring infections from consuming raw dairy products compared to pasteurized milk [14]. Thus, the risk of infection by pathogenic bacteria far outweighs the theoretical potential benefits. Milk-borne diseases cause unsurmountable economic losses, not to mention the resulting public health consequences. For example, in the United States of America (USA) and France, separate outbreaks of *E. coli* and *Salmonella* in retailed dairy products made from raw milk have caused national and international recalls. The concern about the safety of raw milk is more apparent when small, individual farms grow into larger, commercial-scale productions to meet the increased demand for milk. Since the prevalence of milk-borne *E. coli* and *Salmonella* in East Malaysia (Sarawak) has not been investigated, we aimed to: a) enumerate *E. coli* and *Salmonella* spp., and b) detect and evaluate the genetic-relatedness of Shiga toxin-producing *E. coli* and *S. Typhimurium* strains of the isolates.

STUDY OBJECTS AND METHODS

Sample collection. Samples of cow and goat raw milk were purchased from six farms in the southern region of Sarawak (Table 1). A total of 200 raw cow and goat milk samples were purchased over ten months, during 17 trips between April 2014 and January 2015. All the samples (50–200 mL per sample) were purchased in sterile plastic bottles and kept in an ice box to be transported to the Molecular Microbiology Laboratory at the University of Malaysia, Sarawak.

Enrichment and enumeration of *Escherichia coli* and *Salmonella* spp. by the MPN method. *E. coli* were isolated and enriched by the most probable number (MPN) method, as previously described with some modification [15]. For this, 10 mL of raw milk was transferred into a sterile Stomacher bag and mixed with 90 mL of Tryptone Soy Broth. The mixture was homogenized for 60 s and incubated at 37°C for 24 h. The enriched cultures were subjected to a three-tube MPN method. The MPN index was calculated based on 95% confidence limits for various combinations of positive tubes in a three-tube dilution series using 1, 0.1, and 0.01 mL for *E. coli* and *Salmonella* spp. detection in the samples. As indicated with tube turbidity, positive samples were cultured

Table 1 Raw milk samples from different dairy farms

Farm	Farm feature	Type of raw milk	Total number of samples
A	Small dairy goat and horse farm	Goat	65
B	Small dairy goat farm	Goat	6
C	Small dairy goat farm	Goat	17
D	Mixed dairy farm comprising cattle, goats, buffaloes, and horses	Goat	5
E	Small dairy goat farm	Goat	7
F	Large cow farm	Cow	100
			Total: 200

on EMB (Oxoid, USA) and XLD (Oxoid, USA) agars for *E. coli* and *Salmonella* spp., respectively. The grown colonies were picked and used in molecular analysis.

Genomic DNA extraction. Bacterial DNA was extracted using the boiling extraction method [16, 17]. For this, an aliquot of 1.5 mL of an overnight MPN suspension was centrifuged (Hettich EBA21 Zentrifugen, Germany) at 10 000 rpm for 5 min. Then, the suspension was boiled for 20 min and promptly chilled in ice for 20 min. Afterwards, it was centrifuged at 10 000 rpm for 5 min. The final supernatant containing bacterial DNA was collected and stored at -20°C for further use.

Detection of Shiga toxin-producing *E. coli* and *E. coli* O157:H7. The Multiplex-PCR was conducted to detect *E. coli* strains in the raw milk samples using four primer pairs that target the *Stx1* and *Stx2* genes (encoding Shiga-like toxins 1 and 2), *rfbE* gene (encoding the somatic antigen, or O-antigen), and *fliC_{H7}* (encoding the flagellar antigen, or H7-antigen) (Table 1) [18, 19]. The PCR was conducted using GoTaq® DNA polymerase (Promega, USA) with PCR conditions comprising a cycle of initial denaturation at 94°C for 2 min, 35 cycles of denaturation at 94°C for 1 min, annealing at 55°C for 1 min, extension at 72°C for 1 min, and a final extension at 72°C for 10 min. The DNA of *E. coli* O157:H7 was used as a positive control. The PCR product was analyzed by using agarose (1.5%) gel electrophoresis.

Specific-PCR for detecting *Salmonella enterica* serovar Typhimurium. The Specific-PCR assay was carried out to detect *Salmonella enterica* serovar Typhimurium (*S. Typhimurium*), by using the *Fli15* and *Tym* primers that are specific to the *fliC* gene of *S. Typhimurium*, with minor modifications (Table 2) [20]. The PCR was conducted using GoTaq® DNA Polymerase (Promega, USA) with PCR conditions comprising a cycle of initial denaturation of 95°C for 5 min, 35 cycles of denaturation at 94°C at 60 s, annealing at 56°C for 30 s, extension at 72°C for 30 s, and a cycle of final extension at 72°C for 1 min. The DNA of *S. Typhimurium* strain ATCC 14028 was used as a positive control. The PCR product was analyzed by using agarose (1.5%) gel electrophoresis.

BOX-PCR genotyping of *E. coli* and *S. Typhimurium* isolates. The BOX-PCR was conducted on *E. coli* and *S. Typhimurium* using a single BOXA1R primer: (5'-CTACGGCAAGGCGACGCTGACG-3'), as well as a TopTaq PCR Master Mix Kit (Qiagen, Germany) [8]. The PCR conditions comprised a cycle of initial denaturation at 94°C for 5 min, 35 cycles of denaturation at 94°C for 1 min, annealing at 53°C for 1 min, extension at 72°C for 1 min, and a cycle of final extension at 72°C for 10 min. The PCR product was analyzed with the help of agarose (1%) gel electrophoresis.

ERIC-PCR genotyping of *E. coli* and *S. Typhimurium* isolates. The ERIC-PCR was conducted on *E. coli* and *S. Typhimurium* using the primers ERIC-1 (5'-ATG TAAGCTCCTGGGGATTAC-3') and ERIC-2 (5'-AAGTAAGTGACTGGGGTGAGCG-3'), as well as GoTaq® DNA Polymerase (Promega, USA) [8]. The

PCR conditions comprised a cycle of initial denaturation at 95°C for 5 min, 35 cycles of denaturation at 90°C for 30 s, annealing at 50°C for 1 min, extension at 72°C for 5 min, and a cycle of final extension at 72°C for 15 min. The PCR product was analyzed by agarose (1%) gel electrophoresis.

Phylogenetic data analysis. DNA fragments amplified in BOX-PCR and ERIC-PCR were analyzed for their electrophoretic profile [8]. RAPDistance and PyElph 1.3 gel analysis softwares were employed to determine the respective clonal relatedness of *E. coli* and *S. Typhimurium*. Normalization steps were included in the analysis to ensure adequate gel-to-gel banding pattern comparison. A band-scoring procedure identified bands in each lane that made a fingerprint based on the threshold of stringency and optimization settings. Utilizing PyElph 1.3 software, the positions of the marker run in BOX-PCR and ERIC-PCR were normalized from lane-to-lane and gel-to-gel variations. The unweighted pair group method with arithmetic mean (UPGMA) cluster analysis was performed in combination with the neighbor-joining tree (NJTREE) method and displayed in dendrograms.

The discriminatory index (D) of both BOX-PCR and ERIC-PCR was calculated based on Simpson's Diversity Index. A value of 0 (zero) indicates an identical pattern between isolates, whereas a value of 1 indicates a complete dissimilarity between isolates, corresponding to the higher Simpson's Diversity Index, the greater the discriminatory power of the typing tool [8].

$$D = 1 - \left(\frac{1}{N(N-1)} \right) \sum_{j=1}^s n_j(n_j - 1)$$

where N is the total number of colonies in the sample population; s is the total number of clusters described; and n_j is the number of colonies belonging to the cluster.

RESULTS AND DISCUSSION

Occurrence and concentration of *Escherichia coli* and *Salmonella enterica* serovar Typhimurium in the fresh raw milk samples. We examined 200 samples of raw milk from six dairy farms, including 100 cow milk and 100 goat milk samples, for the presence of *E. coli* and *S. Typhimurium*. *E. coli* colonies appeared on EMB agar as dark blue-black growth with a green-metallic sheen, while *S. Typhimurium* colonies appeared on XLD agar in shiny and small-to-medium colorless shape after 24 h. Out of the total milk samples, 83.5% (167/200) and 65.5% (131/200) showed MPN values greater than 1100 MPN/mL for the presence of *E. coli* and *Salmonella* spp., respectively (Table 2).

Detection of Shiga toxin-producing *E. coli* and *S. Typhimurium* by PCR. Out of 200 raw milk samples tested, only 1.5% (3 samples) were found to be positive for *E. coli* O157:H7. However, a higher prevalence (9.5%; 19 samples) was found to be Shiga toxin-producing *E. coli* (STEC) of different serogroups which carried the *Stx1* and/or *Stx2* genes but did not possess *rfbE*⁺ or *fliC_{H7}*

Table 2 Most probable numbers of *Escherichia coli* and *Salmonella* spp. in raw milk samples

Raw milk type	Bacteria	Number of samples	MPN/mL	95% confidence level	
				Lower	Upper
Goat milk	<i>E. coli</i>	1	20	0.45	4.2
Goat milk	<i>E. coli</i>	1	21	0.45	4.2
Goat milk	<i>E. coli</i>	1	28	0.87	9.4
Goat milk	<i>E. coli</i>	1	35	0.87	9.4
Goat milk	<i>E. coli</i>	2	36	0.87	9.4
Goat milk	<i>E. coli</i>	5	93	1.8	42
Goat milk	<i>E. coli</i>	5	150	3.7	42
Goat milk	<i>E. coli</i>	5	210	4.0	43
Goat milk	<i>E. coli</i>	1	240	4.2	100
Goat milk	<i>E. coli</i>	2	460	9.0	200
Goat milk	<i>E. coli</i>	9	1100	18	410
Goat milk	<i>E. coli</i>	67	> 1100	42	–
Goat milk	<i>Salmonella</i> spp.	1	21	0.45	4.2
Goat milk	<i>Salmonella</i> spp.	6	28	0.87	9.4
Goat milk	<i>Salmonella</i> spp.	5	36	0.87	9.4
Goat milk	<i>Salmonella</i> spp.	6	93	1.8	42
Goat milk	<i>Salmonella</i> spp.	6	150	3.7	42
Goat milk	<i>Salmonella</i> spp.	10	210	4.0	43
Goat milk	<i>Salmonella</i> spp.	6	240	4.2	100
Goat milk	<i>Salmonella</i> spp.	2	460	9.0	200
Goat milk	<i>Salmonella</i> spp.	15	1100	18	410
Goat milk	<i>Salmonella</i> spp.	43	> 1100	42	–
Cow milk	<i>E. coli</i>	100	> 1100	42	–
Cow milk	<i>Salmonella</i> spp.	3	150	3.7	42
Cow milk	<i>Salmonella</i> spp.	9	1100	18	410
Cow milk	<i>Salmonella</i> spp.	88	> 1100	42	–

The MPN/mL values in boldface indicate concentrations of the bacteria in the samples > 1100 MPN/mL

Table 3 Numbers of raw cow and goat milk samples positive for the targeted genes of *Escherichia coli* and *Salmonella enterica* serovar Typhimurium

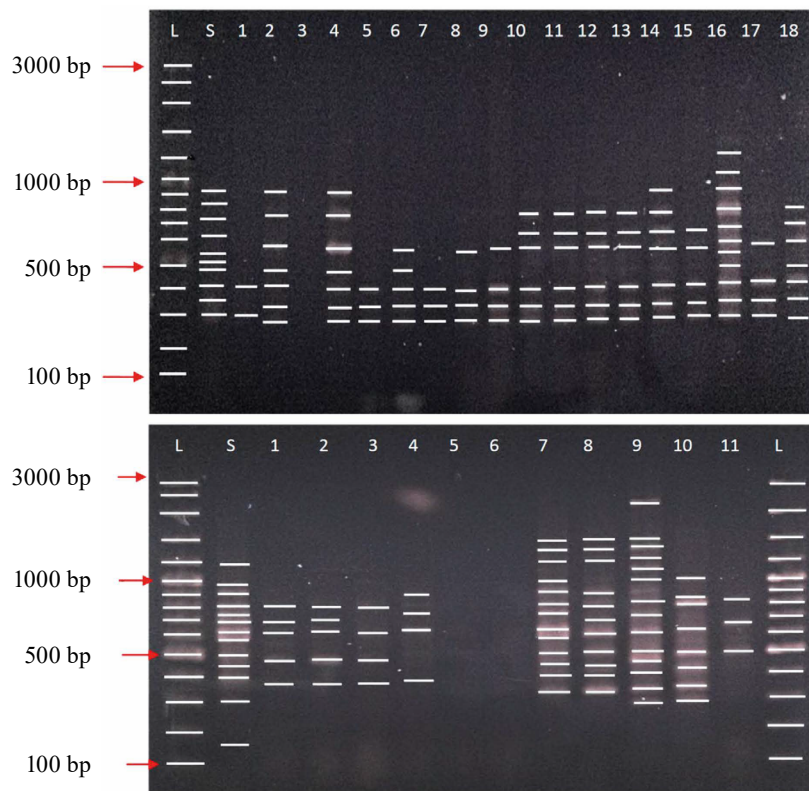
Bacteria	Virulence genes	Cow milk	Goat milk	Serogroup	Total
<i>E. coli</i>	<i>Stx1/Stx2/rfbE+/fliC_{h7}</i>	1	0	STEC O157:H7	3/200 (1.5%)
	<i>Stx2/rfbE+/fliC_{h7}</i>	2	0		
	<i>Stx2/fliC_{h7}</i>	4	1	STEC of other serogroups	19/200 (9.5%)
	<i>Stx2/rfbE+</i>	14	0		
	<i>Stx1/Stx2</i>	0	0		
	<i>Stx1</i>	1	0		
	<i>Stx2</i>	2	1		
	<i>rfbE+/fliC_{h7}</i>	9	1	Non-STEC O157:H7	10/200 (5%)
	<i>rfbE+</i>	42	10	Non-STEC of other serogroups	83/200 (41.5%)
	<i>fliC_{h7}</i>	15	16		
<i>S. Typhimurium</i>	<i>fliC</i>	11	68	–	79/200 (39.5%)

Other than that, 5% (10 samples) and 41.5% (83 samples) were found to be non-STEC O157:H7 and non-STEC of other serogroups, respectively, because they lacked the *Stx* genes. Finally, 39.5% (79 samples) of the milk samples tested positive for *S. Typhimurium* (Table 3).

Virulence profiles of *E. coli* and *S. Typhimurium*. *E. coli* were classified into four groups based on the presence of Shiga-toxin genes (*Stx1* and *Stx2*) and the *rfbE* and *fliC_{h7}* genes, namely STEC O157:H7, STEC of

other serogroups, non-STEC O157:H7, and non-STEC. STEC indicates Shiga toxin-producing *E. coli*.

Genotyping of *E. coli* and *S. Typhimurium* using BOX-PCR and ERIC-PCR. The BOX-PCR genotyping for *E. coli* produced 2–11 bands for the raw cow milk samples (Fig. 1) and 3–14 bands for the raw goat milk samples (figure not shown). Simpson's Diversity Index (SID) was utilized to measure the species diversity in a community. This index was adjusted to generate a



E. coli isolated from Farm F (top). L: 100 bp ladder, Lane S: Standard, Lane 1: EC-CM83, Lane 2: EC-CM84, Lane 3: EC-CM85, Lane 4: EC-CM86, Lane 5: EC-CM87, Lane 6: EC-CM88, Lane 7: EC-CM89, Lane 8: EC-CM90, Lane 9: EC-CM91, Lane 10: EC-CM92, Lane 11: EC-CM93, Lane 12: EC-CM94, Lane 13: EC-CM95, Lane 14: EC-CM96, Lane 15: EC-CM97, Lane 16: EC-CM98, Lane 17: EC-CM99, Lane 18: EC-CM100. “EC” denotes *E. coli*, “CM” denotes cow milk sample

S. Typhimurium from Farm A (bottom). L: 100 bp ladder, Lane S: Standard, Lane 1: ST-CM3, Lane 2: ST-CM5, Lane 3: ST-CM56, Lane 4: ST-CM58, Lane 5: ST-CM59, Lane 6: ST-CM67, Lane 7: ST-CM70, Lane 8: ST-CM77, Lane 9: ST-CM78, Lane 10: ST-CM82, Lane 11: ST-CM83. “ST” denotes *Salmonella enterica* serovar Typhimurium, “CM” denotes cow milk sample

Figure 1 Gel electrophoresis of BOX-PCR

numerical index for the discriminatory ability of single or combined typing systems. For raw cow milk, the SID among *E. coli* isolates was 0.989, which indicated an average genetic similarity of 40% between 100 isolates. For raw goat milk, the SID among *E. coli* isolates was 0.992, indicating an average genetic similarity of 45% between 40 isolates.

The BOX-PCR for *S. Typhimurium* in goat milk showed that only 9 out of 11 samples were successfully genotyped, producing 5–10 bands for raw cow milk (Fig. 1) and 4–14 bands for raw goat milk (figure not shown). The SID among *S. Typhimurium* isolates was $D = 0.985$ for raw cow milk, indicating an average genetic similarity of 35% between 100 isolates. For raw goat milk, the SID was $D = 0.999$, indicating an average genetic similarity of 30% between 40 isolates.

The dendrograms of the BOX-PCR for *E. coli* and *S. Typhimurium* isolates in both cow and goat milk were grouped into two clusters (A and B). Each of the clusters was further subdivided into several sub-clusters (Fig. 2). *E. coli* isolates were randomly grouped into different clusters and sub-clusters, indicating greater

heterogeneity in the BOX-PCR DNA profiling compared to *S. Typhimurium*.

The ERIC-PCR for *E. coli* produced 2 to 13 bands in the raw cow milk samples (Fig. 3) and 2 to 11 bands in the raw goat milk samples (figure not shown). Simpson’s Diversity Index (SID) for *E. coli* isolates was $D = 0.997$ in the cow milk samples, indicating an average genetic similarity of 40% among 100 isolates, and $D = 0.980$ in the goat milk samples, indicating an average genetic similarity of 40% among 40 isolates.

The ERIC-PCR for *S. Typhimurium* produced 3 to 14 bands in the raw cow milk samples (Fig. 3) and 2 to 4 bands in the raw goat milk samples (figure not shown). The SID of *S. Typhimurium* isolates was $D = 0.900$ in raw cow milk, indicating a 35% genetic similarity between 100 isolates, and $D = 0.872$ in raw goat milk, indicating a 50% genetic similarity between 40 isolates.

Based on the dendrograms (Fig. 4), *E. coli* and *S. Typhimurium* isolates were grouped into two clusters (A and B) for both cow and goat milk samples. *E. coli* isolates were randomly grouped into different clusters and subclusters. Despite sharing the same

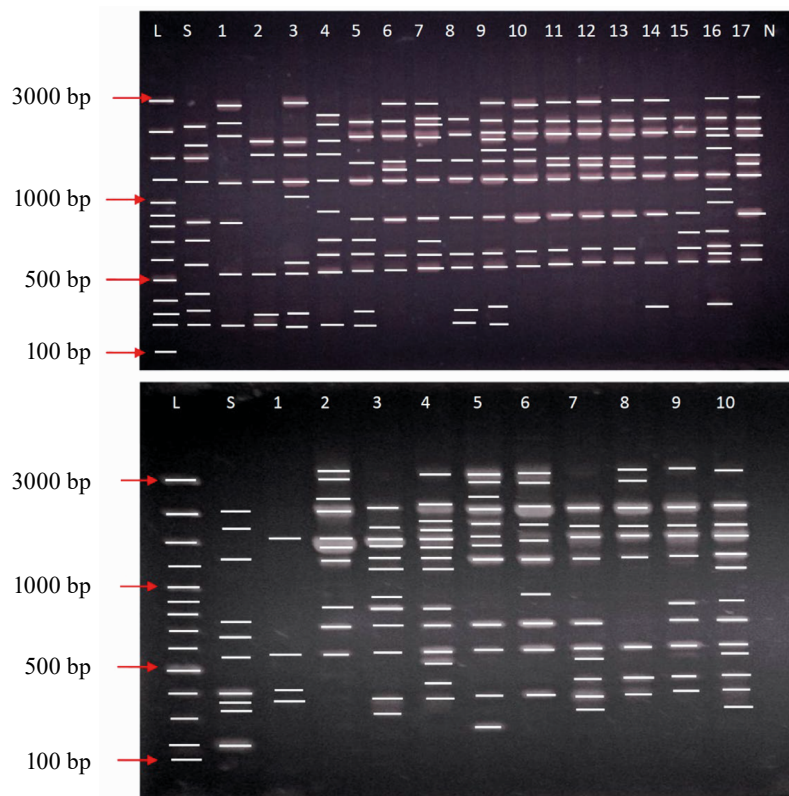
genotype from the same sampling sites, they showed more heterogeneity in the ERIC-PCR profiling compared to *S. Typhimurium*.

The discriminatory power of genotyping tools is indicated by Simpson's Diversity Index (D). In particular, the higher the D, the greater the effectiveness of a particular fingerprinting method in strain discrimination. The D of 1 represents maximum diversity where no isolates are similar. As shown in Table 4, the BOX-PCR demonstrated better discriminatory power (for both *E. coli* and *S. Typhimurium*) than the ERIC-PCR, with D ranging from 0.985 to 0.999 (mean: 0.991) and from 0.872 to 0.997 (mean: 0.937), respectively.

Our study revealed high concentrations of *E. coli* and *Salmonella* spp. in both milks since large numbers of the samples had bacterial concentrations exceeding 1100 MPN/mL. In particular, out of all cow milk samples, 100 were positive for *E. coli* and 88 for *Salmonella* spp., while among the goat milk samples, 67 were positive for *E. coli* and 43 for *Salmonella* spp. The prevalence of high bacterial concentrations was found to be greater in cow milk (150 to > 1100 MPN/mL) than goat milk (20 to > 1100 MPN/mL).

In Malaysia, the permissible limits of total plate and coliform counts in pasteurized milk are 10^5 and 5×10 per mL, respectively, with no specified detection limit for *Salmonella*. In Australia and New Zealand, raw milk must undergo stringent controls and meet the microbial limits for *E. coli* (3 organisms/mL) and *Salmonella* (undetected in 25 mL). If retailed milk products exceed these limits, they must be recalled. While infectious concentrations of foodborne bacteria differ depending on their serovars, they are determined as 10–100 organisms for *E. coli* O157:H7 and 10^7 – 10^9 CFU/g for *Salmonella* [21]. However, given the lipid-dependent nature of infection, these concentrations can be lower in high-fat milk, with 1–5 cells potentially able to cause infection [22].

In this study, we could not rule out a possibility of contamination due to various factors contributing to milk spoilage. *E. coli* and *Salmonella* spp. may be introduced into milk directly from cow's blood (systemic infection), due to mastitis (udder infection) or cross-contamination among cows during milking, as well as from environmental sources (feces, water, pasture) [23]. However, these risks can be reduced by exercising good

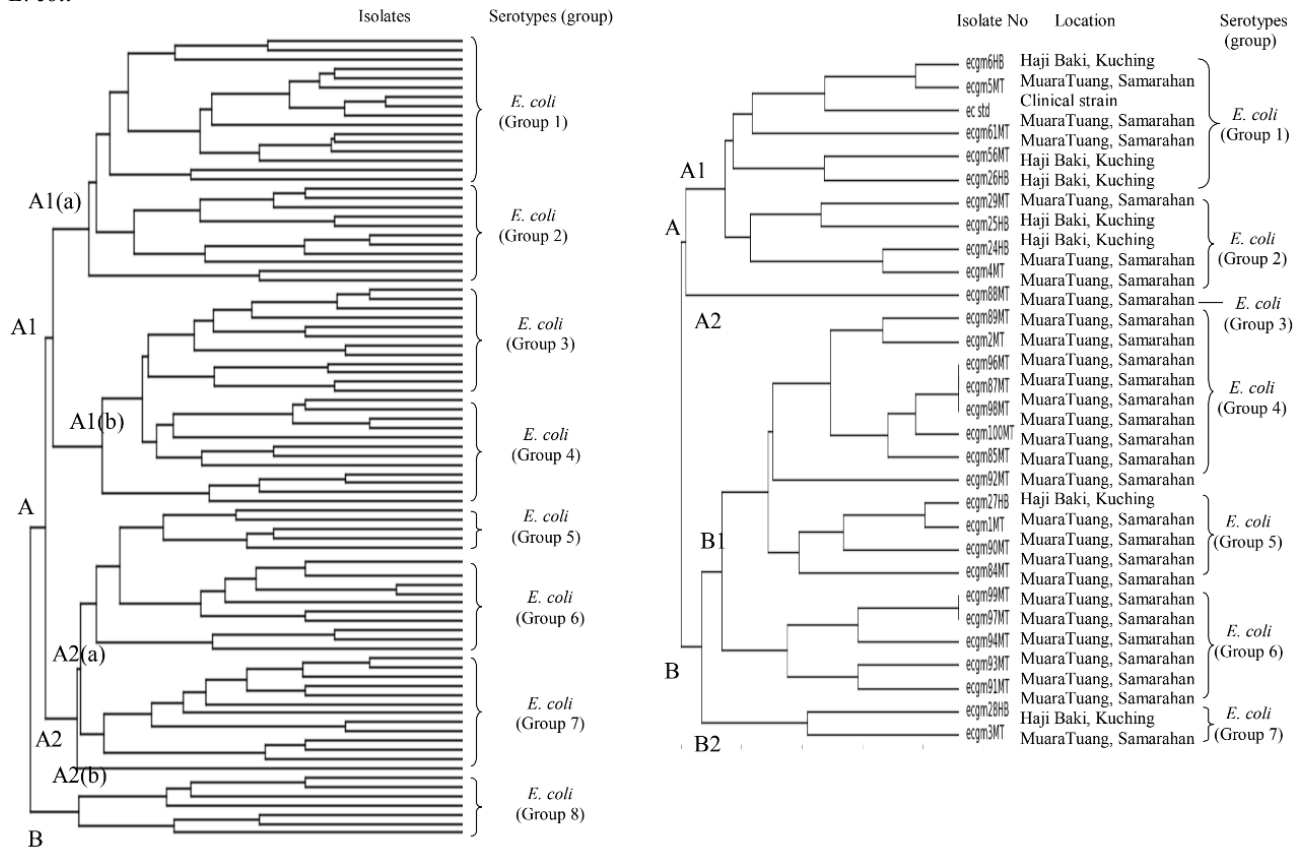


E. coli from Farm F (top). L: 100 bp ladder, Lane S: Standard, Lane 1: EC-CM84, Lane 2: EC-CM85, Lane 3: EC-CM86, Lane 4: EC-CM87, Lane 5: EC-CM88, Lane 6: EC-CM89, Lane 7: EC-CM90, Lane 8: EC-CM91, Lane 9: EC-CM92, Lane 10: EC-CM93, Lane 11: EC-CM94, Lane 12: EC-CM95, Lane 13: EC-CM96, Lane 14: EC-CM97, Lane 15: EC-CM98, Lane 16: EC-CM99, Lane 17: EC-CM100, Lane N: Negative control. "EC" denotes *E. coli*, "CM" denotes cow milk sample

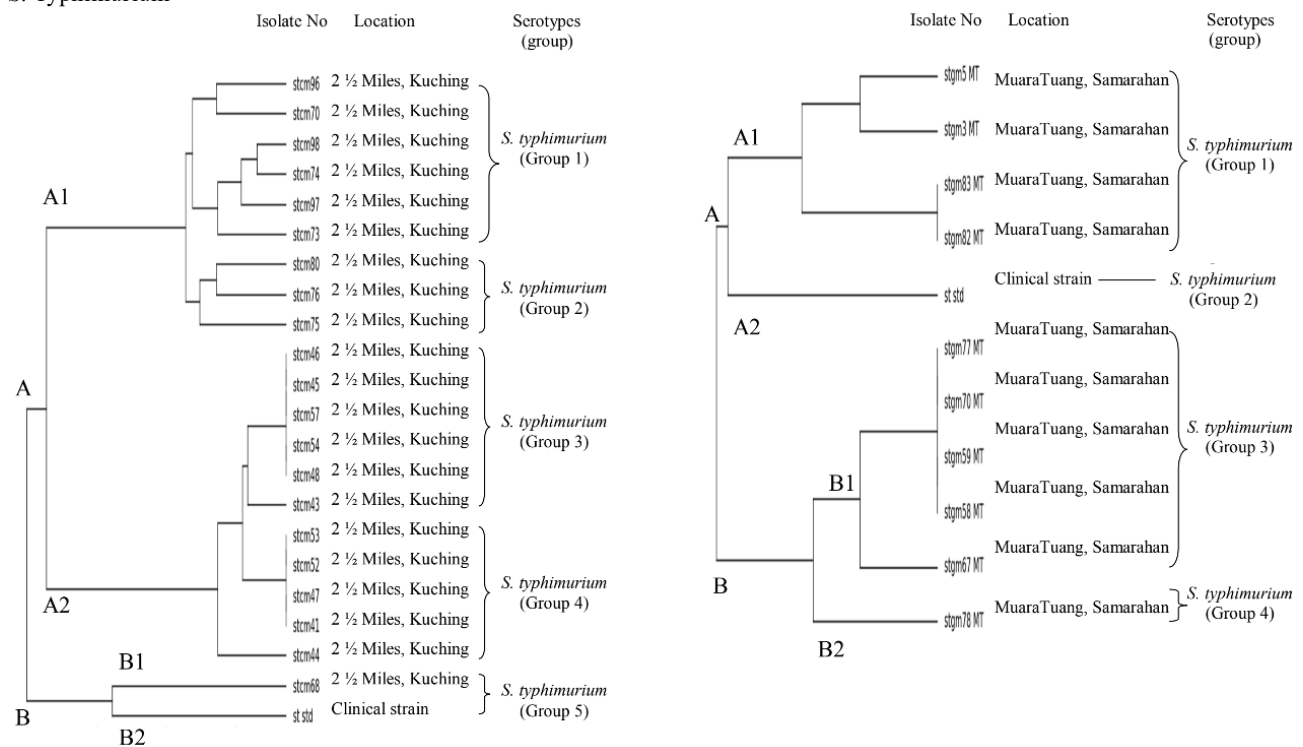
S. Typhimurium from Farm A (bottom). L: 100 bp ladder, Lane S: Standard, Lane 1: ST-CM68, Lane 2: ST-CM70, Lane 3: ST-CM73, Lane 4: ST-CM74, Lane 5: ST-CM75, Lane 6: ST-CM76, Lane 7: ST-CM80, Lane 8: ST-CM96, Lane 9: ST-CM97, Lane 10: ST-CM98. "ST" denotes *Salmonella enterica* serovar Typhimurium, "CM" denotes cow milk sample

Figure 3 Gel electrophoresis of ERIC-PCR

E. coli



S. Typhimurium



E. coli (top). The left side is the dendrogram for cow milk samples from Farm F (2 1/2 Miles, Kuching), while the right side is the dendrogram for goat milk samples from Farms A (Muara Tuang, Samarahan) and B (Haji Baki, Kuching)

S. Typhimurium (bottom). The left side is the dendrogram for cow milk samples from Farm F (2 1/2 Miles, Kuching), while the right side is the dendrogram for goat milk samples from Farm A (Muara Tuang, Samarahan)

Figure 4 Dendrograms of ERIC-PCR

Table 4 Summary of discriminatory power for ERIC-PCR and BOX-PCR

Genotyping method	Sample type	Bacteria	Number of types	Simpson's Diversity Index (D)
BOX-PCR	Cow milk	<i>E. coli</i>	34	0.989
	Goat milk	<i>E. coli</i>	22	0.992
	Cow milk	<i>S. Typhimurium</i>	19	0.985
	Goat milk	<i>S. Typhimurium</i>	10	0.999
ERIC-PCR	Cow milk	<i>E. coli</i>	41	0.997
	Goat milk	<i>E. coli</i>	24	0.980
	Cow milk	<i>S. Typhimurium</i>	13	0.900
	Goat milk	<i>S. Typhimurium</i>	11	0.872

hygienic practices. Pathogenic *E. coli* and *Salmonella* spp. are among common bacterial contaminants in raw milk, as well as *Campylobacter* spp., *Yersinia enterocolitica*, *Listeria monocytogenes*, and *Staphylococcus aureus* [24]. To prevent disease, it is important to ensure safe milk production from healthy animals. In addition, farm owners and milking workers should be trained to adhere to hygienic practices, and collected milk should be pasteurized immediately. However, this does not eliminate the risk of unsuccessful inactivation of *E. coli*, especially due to suboptimal pasteurization or post-contamination from milk-contact surfaces. Several outbreaks have been reported to be linked to pasteurized milks [25, 26]. Heat-resistant *E. coli* can refold and repair the denatured proteins by maintaining the integrity of cell envelopes and elevating the synthesis of heat shock proteins and chaperones after high temperatures [27]. Since *E. coli* can survive in processed pasteurized milk, and even grow faster due to less antagonistic interaction with pre-existing bacteria, processed milk should be stored at 5°C or below to avoid post-processing contamination [26, 28].

The higher prevalence of STEC in cow milk than in goat milk was due to cattle being a major reservoir of STEC [29]. Martin and Beutin found similar concentrations of STEC in the food products as in the original animal species, indicating that the contamination was likely to come from the animals rather than from humans or the environment [30]. Our study detected three *E. coli* O157:H7 isolates (1.5%; 3/200) in the cow milk samples (Farm F). Specific virulence factors such as Shiga-toxin and adherent fimbriae are linked to frequent cases of hemolytic uremic syndrome (HUS) and bloody diarrhea. O-antigen has high levels of chemical composition and variation structure, thus exhibiting different survivability and virulence across different strains [31]. The O serogrouping of *E. coli* strains provides important information for identifying pathogenic clonal groups. For example, O157 is a leading O serogroup associated with enterohemorrhagic *E. coli* (EHEC) and related to foodborne diseases worldwide. The most important strain detected in our study was *E. coli* O157:H7 that possessed a single *Stx2* gene, since this strain is more highly associated with causing hemolytic uremic syndrome than the strains that produce both *Stx1* and *Stx2* [29]. Although *E. coli* is inactivated at tem-

peratures exceeding 63°C, the milk containing thermostable Shiga toxins can still pose health problems [32]. Even though a large proportion of the milk samples were not positive for STEC (Table 3), there remains concern if the other serogroups, which we did not analyze, could contain other important pathogens such as ETEC or EPEC.

S. Typhimurium, a contaminant that frequently degrades raw milk quality, was found in 39.5% (79/200) of the samples in our study. Similar to STEC, cow milk had a higher occurrence of *S. Typhimurium* than goat milk. Wang *et al.* detected *S. Typhimurium* in the PCR by targeting the flagellin gene, *fliC*, which encodes a major component of flagellum in the *S. Typhimurium* [33]. The flagellum of *S. enterica* is made up of a single protein called “flagellin”, which consists of about 490 amino acids varying among the serovars. Flagellin is the main structural protein for flagella that is important during the initial stage of infection, involving mortality and invasion [34].

We analyzed the genetic relatedness of the *E. coli* strains isolated on the basis of the BOX-PCR fingerprinting patterns and found that the isolates were genetically heterogeneous, with average similarities of 40 and 45% in the cow and goat milk samples, respectively. The *S. Typhimurium* isolates showed genetic heterogeneity too, with average similarities of 30 and 35% in the cow and goat milk samples, respectively (Table 4). A previous study analyzed 211 strains of *E. coli* collected from dairy farms, calves, feces, pigs, primates, humans, and food products by the repetitive-element polymerase chain reaction using the BOXA1 primer. The similarity of 65% suggested that the BOX-PCR had good discriminatory power and was effective in clustering *E. coli* strains according to the sources [35].

The *E. coli* strains isolated on the basis of the ERIC-PCR fingerprinting patterns showed genetic heterogeneity among all the samples (Fig. 4). The *S. Typhimurium* isolates were genetically heterogeneous too, with average similarities of 35 and 50% in the cow and goat milk samples, respectively. A previous study, which examined *Salmonella* isolates from a variety of sources (humans, animals, food, and environment) using the ERIC primer set, found each of five serotypes clustered together, with a minimum similarity of 74% [36]. We determined that both genotyping tools (BOX-PCR and ERIC-PCR) can discriminate both bacteria spe-

cies (*E. coli* and *S. Typhimurium*) with varying degrees of discriminatory power.

CONCLUSION

We examined the safety of milk from the dairy farms in Southern Sarawak, specifically looking at the presence of bacteria associated with Shiga toxin-producing *Escherichia coli* and *Salmonella enterica* serovar Typhimurium (*S. Typhimurium*). Our results showed that regular inspections and surveillance are necessary to minimize the risk of bacterial contamination in milk at the farms. Additionally, our study demonstrated the usefulness of the BOX-PCR as a tool for genotyping *E. coli* and *S. Typhimurium*. This tool showed better discriminatory power than the ERIC-PCR as a fingerprinting method to discriminate different strains.

CONTRIBUTION

L. Maurice Bilung, A. Zulkharnain, K. Apun, and E.S. Radzi designed the research. E.S. Radzi conducted the experiment. E.S. Radzi and A.S. Tahar validated the data. L. Maurice Bilung, K. Apun, R. Nguai, and A.S. Tahar drafted the manuscript.

CONFLICT OF INTEREST

The authors declare that there is no conflict of interest.

ACKNOWLEDGEMENTS

We would like to thank the dairy farms' owners for granting us permission to carry out this study.

ABBREVIATIONS

BOX-PCR: BOX repetitive sequence-polymerase chain reaction; DAEC: diffusely adherent *Escherichia coli*; EAEC: enteroaggregative *E. coli*; EHEC: enterohaemorrhagic *E. coli*; EIEC: enteroinvasive *E. coli*; EMB: Eosin Methylene Blue; EPEC: enteropathogenic *E. coli*; ERIC-PCR: enterobacterial repetitive intergenic consensus-polymerase chain reaction; ETEC: enterotoxigenic *E. coli*; HUS: hemolytic uremic syndrome; MPN: Most Probable Number; PCR: polymerase chain reaction; Shiga toxin-producing *E. coli*; SID: Simpson's Diversity Index; TSB: Tryptone Soy Broth; XLD: Xylose Lysine Deoxycholate.

DATA AVAILABILITY

All the data are available in this manuscript.







REFERENCES

1. Pakbin B, Brück WM, Rossen JWA. Virulence factors of enteric pathogenic *Escherichia coli*: A review. International Journal of Molecular Sciences. 2021;22(18):9922. <https://doi.org/10.3390/ijms22189922>
2. Oluwarinde BO, Ajose DJ, Abolarinwa TO, Montso PK, Preez ID, Njom HA, et al. Safety properties of *Escherichia coli* O157:H7 specific bacteriophages: Recent advances for food safety. Foods. 2023;12(21):3989. <https://doi.org/10.3390/foods12213989>
3. Mkangara M. Prevention and control of human *Salmonella enterica* infections: An implication in food safety. International Journal of Food Science. 2023;2023:8899596. <https://doi.org/10.1155/2023/8899596>
4. Zenu F, Bekele T. Major food-borne zoonotic bacterial pathogens of livestock origin: A review. Foods and Raw Materials. 2024;12(1):179–193. <https://doi.org/10.21603/2308-4057-2024-1-595>
5. Lamichhane B, Mawad AMM, Saleh M, Kelley WG, Harrington II PJ, Lovestad CW, et al. Salmonellosis: An overview of epidemiology, pathogenesis, and innovative approaches to mitigate the antimicrobial resistant infections. Antibiotics. 2024;13(1):76. <https://doi.org/10.3390/ANTIBIOTICS13010076>
6. Humphreys H, Coleman DC. Contribution of whole-genome sequencing to understanding of the epidemiology and control of methicillin-resistant *Staphylococcus aureus*. The Journal of Hospital Infection. 2019;102(2):189–199. <https://doi.org/10.1016/j.jhin.2019.01.025>
7. El-Badawy MF, El-Far SW, Althobaiti SS, Abou-Elazm FI, Shohayeb MM. The first Egyptian report showing the co-existence of *bla*_{NDM-25}, *bla*_{OXA-23}, *bla*_{OXA-181}, and *bla*_{GES-1} among carbapenem-resistant *K. pneumoniae* clinical isolates genotyped by BOX-PCR. Infection and Drug Resistance. 2020;13:1237–1250. <https://doi.org/10.2147/IDR.S244064>
8. Maurice Bilung L, Sin Chai L, Tahar AS, Ted CK, Apun K. Prevalence, genetic heterogeneity, and antibiotic resistance profile of *Listeria* spp. and *Listeria monocytogenes* at farm level: A highlight of ERIC- and BOX-PCR to reveal genetic diversity. BioMed Research International. 2018;2018:3067494. <https://doi.org/10.1155/2018/3067494>
9. van Kessel JS, Karns JS, Gorski L, Perdue ML. Subtyping *Listeria monocytogenes* from bulk tank milk using automated repetitive element-based PCR. Journal of Food Protection. 2005;68(12):2707–2712. <https://doi.org/10.4315/0362-028X-68.12.2707>
10. Nath G, Maurya P, Gulati AK. ERIC PCR and RAPD based fingerprinting of *Salmonella* Typhi strains isolated over a period of two decades. Infection, Genetics and Evolution. 2010;10(4):530–536. <https://doi.org/10.1016/j.meegid.2010.02.004>
11. Movahedi M, Zarei O, Hazhirkamal M, Karami P, Shokoohizadeh L, Taheri M. Molecular typing of *Escherichia coli* strains isolated from urinary tract infection by ERIC-PCR. Gene Reports. 2021;23:101058. <https://doi.org/10.1016/j.genrep.2021.101058>

12. Bakhshi B, Afshari N, Fallah F. Enterobacterial repetitive intergenic consensus (ERIC)-PCR analysis as a reliable evidence for suspected *Shigella* spp. outbreaks. *Brazilian Journal of Microbiology*. 2018;49(3):529–533. <https://doi.org/10.1016/j.bjm.2017.01.014>
13. O’Callaghan TF, Sugrue I, Hill C, Ross RP, Stanton C. Nutritional aspects of raw milk: A beneficial or hazardous food choice. In: Nero LA, De Carvalho AF. *Raw milk: Balance between hazards and benefits*. Academic Press; 2019. pp. 127–148. <https://doi.org/10.1016/B978-0-12-810530-6.00007-9>
14. Kapoor S, Goel AD, Jain V. Milk-borne diseases through the lens of one health. *Frontiers in Microbiology*. 2023;14:1041051. <https://doi.org/10.3389/fmicb.2023.1041051>
15. Lee E, Radu S, Jambari NN, Abdul-Mutalib NA. Prevalence and antibiogram profiling of extended-spectrum beta-lactamase (ESBL) producing *Escherichia coli* in raw vegetables, in Malaysia. *Biology and Life Sciences Forum*. 2021;6(1):44. <https://doi.org/10.3390/foods2021-10960>
16. Yew CS, Fan CS, Kira R, Tahar AS, Bilung LM. Occurrence of *Listeria monocytogenes* and *Salmonella* Typhimurium in fruit juices from local stalls and restaurant in Kuching, Sarawak. *Trends in Undergraduate Research*. 2018;1(1): a1–7. <https://doi.org/10.33736/tur.1133.2018>
17. Bilung LM, Tesfamariam F, Andriesse R, San FYK, Ling CY, Tahar AS. Presence of *Bacillus cereus* from local unhusked (Rough) rice samples in Sarawak, Malaysia. *Journal of Sustainability Science and Management*. 2018;13(1):181–187.
18. Bilung LM, Ling KK, Apun K, Abdullah MT, Rahman MA, Ming CY, et al. Occurrence of *Escherichia coli* in wildlife from different habitats of Sarawak, Malaysia. *Borneo Journal of Resource Science and Technology*. 2014;4(1):19–27. <https://doi.org/10.33736/bjrst.240.2014>
19. Tarazi YH, El-Sukhon SN, Ismail ZB, Almestarehieh AA. Molecular characterization of enterohemorrhagic *Escherichia coli* isolated from diarrhea samples from human, livestock, and ground beef in North Jordan. *Veterinary World*. 2021;14(10):2827–2832. <https://doi.org/10.14202/vetworld.2021.2827-2832>
20. Jamshidi A, Ghasemi A, Mohammadi A. The effect of short-time microwave exposures on *Salmonella typhimurium* inoculated onto chicken drumettes. *Iranian Journal of Veterinary Research*. 2009;10(4):378–382. <https://doi.org/10.22099/IJVR.2009.1730>
21. Kuruwita DP, Jiang X, Darby D, Sharp JL, Fraser AM. Persistence of *Escherichia coli* O157:H7 and *Listeria monocytogenes* on the exterior of three common food packaging materials. *Food Control*. 2020;112:107153. <https://doi.org/10.1016/j.foodcont.2020.107153>
22. Khan MAS, Rahman SR. Use of phages to treat antimicrobial-resistant *Salmonella* infections in poultry. *Veterinary Sciences*. 2022;9(8):438. <https://doi.org/10.3390/vetsci9080438>
23. Singha P, Kaushik G, Hussain CM, Chel A. Food safety issues associated with milk: A review. In: Grumezescu AM, Holban AM. *Safety issues in beverage production*. Volume 18: the science of beverages. Academic Press; 2020. pp. 399–427. <https://doi.org/10.1016/B978-0-12-816679-6.00012-7>
24. Fusco V, Chieffi D, Fanelli F, Logrieco AF, Cho G-S, Kabisch J, et al. Microbial quality and safety of milk and milk products in the 21st century. *Comprehensive Reviews in Food Science and Food Safety*. 2020;19. <https://doi.org/10.1111/1541-4337.12568>
25. Jenkins C, Bird PK, Wensley A, Wilkinson J, Aird H, Mackintosh A, et al. Outbreak of STEC O157:H7 linked to a milk pasteurisation failure at a dairy farm in England, 2019. *Epidemiology and Infection*. 2022;150:e114. <https://doi.org/10.1017/S0950268822000929>
26. Sebastianski M, Bridger NA, Featherstone RM, Robinson JL. Disease outbreaks linked to pasteurized and unpasteurized dairy products in Canada and the United States: A systematic review. *Canadian Journal of Public Health*. 2022;113:569–578. <https://doi.org/10.17269/s41997-022-00614-y>
27. Rosario AILS, Castro VS, Santos LF, Lisboa RC, Vallim DC, Silva MCA, et al. Shiga toxin – producing *Escherichia coli* isolated from pasteurized dairy products from Bahia, Brazil. *Journal of Dairy Science*. 2021;104(6):6535–6547. <https://doi.org/10.3168/jds.2020-19511>
28. Quinto EJ, Marín JM, Caro I, Mateo J, Schaffner DW. Modelling growth and decline in a two-species model system: Pathogenic *Escherichia coli* O157:H7 and psychrotrophic spoilage bacteria in milk. *Foods*. 2020;9(3):331. <https://doi.org/10.3390/foods9030331>
29. Gonzalez GMA, Cerqueira MFA. Shiga toxin-producing *Escherichia coli* in the animal reservoir and food in Brazil. *Journal of Applied Microbiology*. 2020;128(6):1568–1582. <https://doi.org/10.1111/jam.14500>
30. Martin A, Beutin L. Characteristics of Shiga toxin-producing *Escherichia coli* from meat and milk products of different origins and association with food producing animals as main contamination sources. *International Journal of Food Microbiology*. 2011;146(1):99–104. <https://doi.org/10.1016/j.ijfoodmicro.2011.01.041>
31. Liu B, Furevi A, Perepelov AV, Guo X, Cao H, Wang Q, et al. Structure and genetics of *Escherichia coli* O antigens. *FEMS Microbiology Reviews*. 2020;44(6):655–683. <https://doi.org/10.1093/femsre/fuz028>

32. Hughes AC, Zhang Y, Bai X, Xiong Y, Wang Y, Yang X, et al. Structural and functional characterization of Stx2k, a new subtype of Shiga toxin 2. *Microorganisms*. 2020;8(1):4. <https://doi.org/10.3390/microorganisms8010004>
33. Wang F, Deng L, Huang F, Wang Z, Lu Q, Xu C. Flagellar motility is critical for *Salmonella enterica* serovar typhimurium biofilm development. *Frontiers In Microbiology*. 2020;11:499150. <https://doi.org/10.3389/fmicb.2020.01695>
34. Das C, Mokashi C, Mande SS, Saini S. Dynamics and control of flagella assembly in *Salmonella tyhimurium*. *Frontiers in Cellular and Infection Microbiology*. 2018;8:252000. <https://doi.org/10.3389/fcimb.2018.00036>
35. Cesaris L, Gillespie BE, Srinivasan V, Almeida RA, Zeconi A, Oliver SP. Discriminating between strains of *Escherichia coli* using pulsed-field gel electrophoresis and BOX-PCR. *Foodborne Pathogens and Disease*. 2007;4(4): 473–480. <https://doi.org/10.1089/fpd.2007.0038>
36. Rasschaert G, Houf K, Imberechts H, Grijspeerdt K, de Zutter L, Heyndrickx M. Comparison of five repetitive-sequence-based PCR typing methods for molecular discrimination of *Salmonella enterica* isolates. *Journal of Clinical Microbiology*. 2005;43(8):3615–3623. <https://doi.org/10.1128/JCM.43.8.3615-3623.2005>

ORCID IDs

Lesley Maurice Bilung  <https://orcid.org/0000-0001-5653-0463>
 Ernie Suhaiza Radzi  <https://orcid.org/0009-0009-9841-8280>
 Ahmad Syatir Tahar  <https://orcid.org/0000-0002-0442-0729>
 Azham Zulkharnain  <https://orcid.org/0000-0001-9173-8171>
 Romano Ngui  <https://orcid.org/0000-0002-3520-579X>
 Kasing Apun  <https://orcid.org/0000-0001-8042-2972>



Multi-objective development of novel egg free cakes using quinoa protein and its quality attributes

Rasha K. Mohamed^{ID}, Zahra S. Ahmed^{*ID}, Safaa S. Abozed^{ID}

National Research Centre^{ROR}, Cairo, Egypt

* e-mail: Zahra3010@hotmail.com

Received 08.08.2023; Revised 15.10.2023; Accepted 07.11.2023; Published online 23.10.2024

Abstract:

This study explores the potential of utilizing quinoa protein as an egg substitute in bakery products for customers with health, culture/religion, or dietary restrictions.

Quinoa protein was prepared from quinoa seed by alkaline solubilization followed by isoelectric precipitation and drying. Four different formulations of egg-free cakes were prepared by incorporating quinoa protein in egg equivalents of 50 g (Formulation 1), 75 g (Formulation 2), 100 g (Formulation 3), and 150 g (Formulation 4). The research involved Fourier-transform infrared spectroscopy and revealed such functional properties as proximate composition, physical properties, color, texture, microstructure, and sensory characteristics for the batters and the cakes.

The incorporation of different quinoa protein concentrations significantly ($p < 0.05$) affected all the functional properties of the batters and the cakes. Such variables as crude protein and ash increased while moisture and fat contents decreased. The baking loss went down as the share of quinoa protein went up. The structural analysis showed an increase in gumminess and chewiness accompanied by a decrease in cohesiveness and elasticity. The analysis also revealed hardness and non-uniform changes. The lightness (L^*) and yellowness (b^*) of the cake surface and crumb decreased while the redness (a^*) increased.

The cakes prepared according to Formulation 4 with the greatest share of quinoa protein had a high nutritional value with reasonable concentrations of essential amino acids in general and a high level of lysine in particular. The same sample also received the highest score for overall sensory properties. The sensory assessment proved that quinoa protein could meet consumer expectations of egg-free cakes.

Keywords: Quinoa protein isolate, functional cake, egg-free products, microstructure, functional and physicochemical attributes, amino acid composition

Please cite this article in press as: Mohamed RK, Ahmed ZS, Abozed SS. Multi-objective development of novel egg free cakes using quinoa protein and its quality attributes. 2025;13(2):276–286. <https://doi.org/10.21603/2308-4057-2025-2-638>

INTRODUCTION

Quinoa (*Chenopodium quinoa* Willd.) and its products have been gaining more and more scientific attention since 2013, which was proclaimed the international year of quinoa by the Food and Agriculture Organization. As a result, production and consumption of quinoa increased exponentially worldwide [1]. This pseudo-cereal grows on marginal soils, tolerates salinity as well as drought, and adapts well to extreme or changeable weather conditions [2]. Quinoa is richer in protein than other cereals and boasts a better distribution of essential amino acids. In addition, quinoa protein contains more lysine (5.1–6.4%) than cereals and more methionine (0.4–1.0%) than legumes [2, 3]. Quinoa protein has a balanced amino acid profile and can be used as an alternative to milk or egg proteins in bakery products [4].

Eggs are an indispensable part of cake formulation and affect the quality of the final product. Eggs give the cake its soft texture while their foaming and emulsifying properties provide moistness. Egg proteins assist in entrapping air during mixing, thus improving aeration [5]. The gelling properties of egg protein are responsible for the cake volume while egg lipoproteins provide good emulsification [6]. In addition, eggs contribute to the color and aroma [7]. For customers who suffer from egg allergy, the availability of egg-free products can be quite a challenge. Vegetarianism, religious reasons, or personal lifestyle have also increased the demand for egg-free cakes [4]. Quinoa proteins with their diverse bioactive components, good functional properties, and low anti-nutritional content may offer a solution to the abovementioned problems [2].

A lot of studies introduce proteins of whey, soya, pea, and lupine as an egg substitute [7–10]. Other baking additives include xanthan gum, soya lecithin baking powder, mono- and di-glycerides, or combinations of two protein concentrates, e.g., lupine and whey [10, 11]. Unfortunately, the quality of egg-free cakes is almost always inferior to traditional samples. For example, the replacement may result in such undesirable changes as low cake volume, coarse structure, or poor foaming stability [12].

Quinoa protein concentrate in bakery and cakes represents a novel hypoallergenic egg substitute and creates niche products with unique sensory characteristics that meet contemporary consumer expectations and needs. Our study responds to the growing demand of egg-free products by exploring quinoa proteins as an egg substitute in egg-free cakes with a conventional sensory profile. This work explored the potential benefits of utilizing quinoa protein as part of formulation of egg-free cakes. This multi-objective formulation was developed so as to improve nutritional quality, preserve sensory properties, and respond to the growing demand for allergen-free bakery products. In addition, quinoa proteins could contribute to a more environmentally friendly and sustainable food industry.

STUDY OBJECTS AND METHODS

Materials. Cake ingredients involved all-purpose wheat flour, eggs, milk, oil, sugar, vanilla, and baking powder, all purchased from a local market. The quinoa seeds were obtained from the Desert Research Center (Egypt). Other reagent-grade chemicals came from the Network of Central Laboratories and Centers of Excellence.

Methods. Preparing quinoa flour. The flour was defatted by shaking for 12 h with hexane to the ratio of 1:4 (w/v), filtered, and air-dried at 40°C for 8 h. The defatted flour was stored in a polyethylene film bag at 4°C until further use.

Preparing quinoa protein concentrate. The quinoa protein concentrate was prepared according to the method described in [13]. The defatted quinoa flour was suspended in water 1:20 (w/v). We adjusted its pH to 11 using 2N NaOH, stirred it for 150 min, and centrifuged at 4500 g at 36°C for 30 min. After bringing the pH down to 4.0 with 1N HCl, we centrifuged the mix at 4500 g for 20 min to precipitate the protein. The precipitates were resuspended in water, neutralized to pH 7.0, dried, and stored at –20°C until further use. The protein concentration was measured by the micro-Kjeldahl method in line with method 920.152 developed by the American Association of Cereal Chemists (% N×6.25).

Determining functional properties of quinoa protein. The functional properties of quinoa protein to be tested included protein swelling capacity, bulk density, water-holding capacity, oil-holding capacity, emulsifying capacity, whippability, and foaming stability.

The protein swelling capacity was determined according to the method described by Robertson *et al.* and reflected the ease with which quinoa proteins increased

in volume under water excess [14]. This variable was calculated as X mL of water retained per 1 g of dry sample for 18 h.

We measured the bulk density in line with the method suggested by Wani *et al.* [15]. We put a sample of 50 g in a 100-mL graduated cylinder and tapped 20–30 times. To calculate the bulk density, we divided the weight of the sample by its volume (g/mL).

The water-holding capacity and the oil-holding capacity were determined based on the procedure proposed by Fallah-Delavar & Farmani and calculated as the difference between the weight of the sample before and after we added water/oil by gram [16].

To determine the emulsifying capacity, we turned to the methodology described by Shahidi *et al.*, who expressed it as the volume of the emulsified layer vs. the total volume [17].

The procedure for foam stability followed the protocols described by Shao & Kao, who expressed it as the difference between the initial and the final foam volumes measured after settling for 30 min [18].

The whippability was calculated as the percent increase in volume [18]. For each test, the measurements were conducted in triplicates.

Fourier-transform infrared spectroscopy (FTIR).

The study involved a Fourier-transform infrared spectrometer coupled to an attenuated total reflectance (ATR) accessory (FTIR-ATR Bruker Vertex 80v). We placed the powdered samples on the surface of the ATR crystal and pressed with a flat-tip plunger. An average of 32 scans were performed between 4000 and 400 cm^{–1} at a resolution of 4 cm^{–1}. The analysis was carried out at room temperature.

Preparing batter and cake. The cake batter samples were made according to the formulations represented in Table 1. They included wheat flour (100 g), sugar (100 g), oil (40 mL), milk (90 mL), whey protein (6.6 g), and baking powder (1.1 g). The control contained a liquid whole egg (50 g) while the test samples included 2.87, 4.30, 5.74, and 8.61 g of quinoa protein. These ratios were derived from a set of preliminary experiments conducted in our lab. After mixing wheat flour, sucrose, and baking powder with eggs/quinoa protein, milk, and oil, we whipped the ingredients to avoid lumps. The obtained smooth and uniform batter was poured in aluminum cake molds and baked at 200°C for 20 min. After baking, the cakes were removed from molds, allowed them to cool at room temperature for 30 min, and wrapped in polyethylene bags for further analysis.

Determining physical properties of batter. The batter density in the finished cakes was tested in line with the method proposed by Özhamamci *et al.*, who divided certain weight of batter by volume [19]. The specific gravity was measured and calculated by dividing the weight of a certain batter volume by the weight of the same volume of distilled water. The viscosity of each batter sample was measured at room temperature using a Brookfield digital viscometer (USA) equipped

Table 1 Batter formulations: control vs. egg-free cakes

Ingredients	Batter composition, %				
	Control	Formulation 1 (50 g quinoa protein in egg equivalent)	Formulation 2 (75g quinoa protein in egg equivalent)	Formulation 3 (100 g quinoa protein in egg equivalent)	Formulation 4 (150 g quinoa protein in egg equivalent)
Wheat flour	100	100	100	100	100
Liquid whole egg	50	–	–	–	–
Quinoa protein	–	2.87	4.30	5.74	8.61
Whey protein	–	6.6	6.6	6.6	6.6
Sugar	100	100	100	100	100
Milk	90	90	90	90	90
Oil	40	40	40	40	40
Emulsifier	–	1.75	1.75	1.75	1.75
Vanilla	0.1	0.1	0.1	0.1	0.1
Baking powder	1.1	1.1	1.1	1.1	1.1

with a So4 spindle. The samples were subjected to shear rates of 0–30 s^{−1} [19].

Determining physical properties of cake. The weight loss was represented as the difference between the weight of cake batter in each cake mold and the weight of finished cake after 4 h of cooling at room temperature. The weight loss, %, was calculated using the following Eq. (1):

$$\text{Weight loss} = (\text{weight}_{\text{batter}} - \text{weight}_{\text{cake}}) / \text{weight}_{\text{batter}} \times 100 \quad (1)$$

The density, g/cm³, was calculated as cake weight divided by cake volume:

$$\text{Density} = \text{weight}_{\text{cake}} / \text{volume}_{\text{cake}} \quad (2)$$

The specific volume, cm³/g, of cake samples made according to different formulations was evaluated by the seed replacement method and calculated using the following Eq. (3):

$$\text{Specific volume} = \text{volume}_{\text{cake}} / \text{weight}_{\text{cake}} \quad (3)$$

To measure the cake volume index (B+C), we cut it into equal halves and made cross-sectional tracings. The symmetry index (2C – B – D) and uniformity index (B–D) were calculated from the height at the center and at the distance between the center and each edge according to method 10-91 described by the American Association of Cereal Chemists (2000) [20].

Proximate analyses. The proximate composition analyses of cakes formulations were carried out according to the method described by the American Association of Cereal Chemists (2010) [21]. We also determined such variables as moisture content, crude protein, ash, and crude fiber. The carbohydrate amount was represented as the difference between 100 and the sum of protein, lipids, ash, fiber, and moisture content.

Color assessment. We used the HunterLab scan XE and the CIELAB color scale to define the color of the four samples [22]. The white and black tiles of HunterLab color standards served as equipment standardization,

after which we evaluated the lightness (*L**), redness (*a**), and yellowness (*b**) of every sample. The total color difference (*ΔE*) was calculated according to the following Eq. (4):

$$\Delta E = [(\Delta L)^2 + (\Delta a)^2 + (\Delta b)^2]^{1/2} \quad (4)$$

where $\Delta L = L_{\text{sample}} - L_{\text{control}}$; $\Delta a = a_{\text{sample}} - a_{\text{control}}$; and $\Delta b = b_{\text{sample}} - b_{\text{control}}$.

Texture profile analysis of cake crumb. We used a TA-CT3 Brookfield texture analyzer (USA) to determine the texture parameters, i.e., hardness, springiness, cohesiveness, gumminess, and chewiness of cake samples according to method 74-09 developed by the American Association of Cereal Chemists (2000) [20]. The samples were cut into 25-mm cubic pieces of cake crumbs. All the experiments were performed in triplicates; the results were expressed as mean ± SD values.

Microstructural analysis. After cutting the cake samples into 0.5×0.5 cm cubes, we froze them in liquid nitrogen and freeze-dried. After drying, the surface of the sample was sputter-coated with a thin layer of gold palladium. The microstructure of the sample was scanned with a QUANTA FEG250 Scanning Electron Microscope.

Sensory properties. The sensory profile included taste, color, softness, flavor, cell size uniformity, and overall acceptability. The panelists evaluated the samples in 6 h after baking using the nine-point hedonic test, i.e., from 1 (most disliked) to 9 (most liked). The panel consisted of seven men and eight women, who were selected randomly. The samples were served in white plastic containers in random order. The panelists were provided with drinking water to wash their mouths between samples. Each panelist signed a consent approved by the National Research Council ethical committee in 2022.

Statistical analysis. We used the Duncan test to identify significant differences between the control and the egg-free samples. The experiment involved a one-way analysis of variance (ANOVA) and a SPSS Statistics 20.0 package for Windows (SPSS Inc., USA). The

alpha level was 0.05 ($p < 0.05$). All the experiments were performed in triplicates, except for the sensory evaluation. The results were presented as mean \pm standard deviation (SD). Statistically significant differences were indicated by superscripts.

RESULTS AND DISCUSSION

Proximate analysis and functional properties of quinoa protein. Table 2 shows the approximate composition of quinoa protein prepared using the alkaline precipitation technique. The protein content was 72.21%, which confirmed the data published in [5–7]. Quinoa protein showed water holding capacity of 2.9 g/g and oil holding capacity of 2.05 g/g. Foaming capacity was 71.12%. Foaming stability reached 94.61% after 30 min whereas whippability was 63.33%. These results reflected the functional properties of quinoa protein that are linked to its physicochemical properties, i.e., those that govern the behavior of protein in foods and affect the choice of protein to be used in an industrial process. Emulsifying capacity and emulsion stability are two important functional properties of proteins that affect the structure of adhesives [23]. Emulsion capacity and stability can affect tension in the water-and-oil interface and help prevent coalescence [24]. Proteins stabilize emulsions due to the membrane matrix that surrounds the oil drop and prevents coalescence [25].

Quinoa protein showed good foaming properties that suggested it could be used as an egg replacer in food processing. In other publications, the foaming capacity of egg albumin ranged between 156 and 200% while the foaming stability was 33–54%, which makes it an excellent foaming agent [26]. Consequently, quinoa pro-

tein demonstrated poorer foaming properties compared to egg albumin but exhibited a good foaming stability. Dakhili *et al.* compared the foaming stability of quinoa protein to soybean protein and egg white protein: it was similar or significantly higher in foaming stability than soybean protein but lower than egg white protein [27]. Such results support its use in bakery products [28].

Amino acid profile of quinoa protein. The amino acid profile of quinoa protein (Table 3) confirmed previous results where quinoa protein proved to be a complete protein. Unlike some other plant proteins, quinoa protein contained all nine essential amino acids that human body cannot synthesize on their own. From highest to lowest mean content, the most abundant essential amino acids ($n = 8$) were lysine, isoleucine, tryptophan, leucine, histidine, methionine valine, and phenylalanine (Table 3). The most abundant non-essential amino acids ($n = 8$), from highest to lowest, were alanine, aspartic acid, glutamic acid, tyrosine, serine, proline, arginine, and glycine.

The mean values for such amino acids as histidine, isoleucine, lysine, sulfur amino acids, aromatic amino

Table 2 Functional properties of quinoa protein

Properties	Value
Bulk density, g/mL	0.77 \pm 0.01
Swelling capacity, mL/g	1.31 \pm 0.08
Water holding capacity, g/g	2.90 \pm 0.13
Oil holding capacity, g/g	2.05 \pm 0.05
Emulsifying capacity, %	71.12 \pm 1.02
Foaming stability after 30 min, %	94.61 \pm 1.47
Whippability, %	63.33 \pm 2.08
Protein content, %	72.21 \pm 1.78

Table 3 Amino acid content in quinoa protein

Amino acids	g/100 g dry weight	%	Amino acid requirements for adults, mg/kg of body weight/day (WHO/FAO)
Essential amino acids			
Histidine	3.17	4.96	
Isoleucine	6.39	9.97	9.5
Leucine	3.82	5.97	12.5
Lysine	7.40	11.55	9.4
Methionine	3.15	4.91	12.1 (methionine + cysteine)
Phenylalanine	2.93	4.57	12.1 (phenylalanine + tyrosine)
Tryptophan	3.97	6.21	2.9
Valine	2.97	4.63	10.7
Non-essential amino acids			
Alanine	7.81	12.19	
Aspartic	4.09	6.38	
Arginine	2.94	4.59	
Glycine	2.92	4.55	
Glutamic	3.16	4.94	
Proline	2.95	4.61	
Serine	3.10	4.84	
Tyrosine	3.23	5.05	
Total essential amino acids	33.84	52.81	
Total non-essential amino acids	30.23	47.18	
Total amino acids	64.07		

acids, threonine, tryptophan, and valine met the daily requirements set by the World Health Organization or the Food and Agriculture Organization (mg/kg of body weight/day). Quinoa protein isolates were reported as similar to casein and other milk proteins [29]. Quinoa protein is high in lysine, methionine, and threonine, which are the limiting amino acids in wheat and maize. Our results confirmed that quinoa protein has a good amino acid profile and can be used as a reliable source of protein [30, 31].

Fourier-transform infrared spectroscopy (FTIR).

Fourier-transform infrared spectroscopy is a useful method that defines the secondary structure of certain proteins via the unique vibrations of their structural units. The infrared region showed three distinct absorption bands: amide I band, amide II band, and amide III band (Fig. 1). The secondary structure of proteins and peptides mainly contains three absorption bands in the infrared region, i.e., amide I band, amide II band, and amide III band. Amide I accounts for $\approx 80\%$ of peptide links, i.e., C=O stretch [29]. Amide I band ($1700\text{--}1600\text{ cm}^{-1}$) is also considered the most sensitive spectral region of protein secondary structural components.

This band appeared at 1630 cm^{-1} with C=O vibrations predominating, followed by C-N. The Fourier-transform infrared spectra of quinoa protein also showed some in-plane N-H bending contributed to amide I. Amide II band exhibited less sensitivity than amide I band and appeared at 1534 cm^{-1} . Amide III band was coupled with C-N stretching, as well as C-H and N-H deformation vibrations. It appeared at $\approx 1234\text{ cm}^{-1}$ and was associated with the N-H plane. Amide A band appeared at 3276 cm^{-1} and arose from N-H stretching. We also observed the presence of residual carbohydrates in the spectrum between 1158 and $1023\text{--}900\text{ cm}^{-1}$.

Physical properties of control vs. quinoa protein

cake batter. The list of physical properties to be tested included density, specific gravity, and viscosity. The increasing ratios of quinoa protein affected the physical profile of batter as presented in Table 4. The density of cake batter ranged between 0.8209 ± 0.0100 and 1.0856 ± 0.0000 . Quinoa protein significantly decreased the density of the batter ($p < 0.05$). The density of cake batter usually depends on the air content. As a result, a lower density can be associated with a decrease in the air volume incorporated into the batter [26].

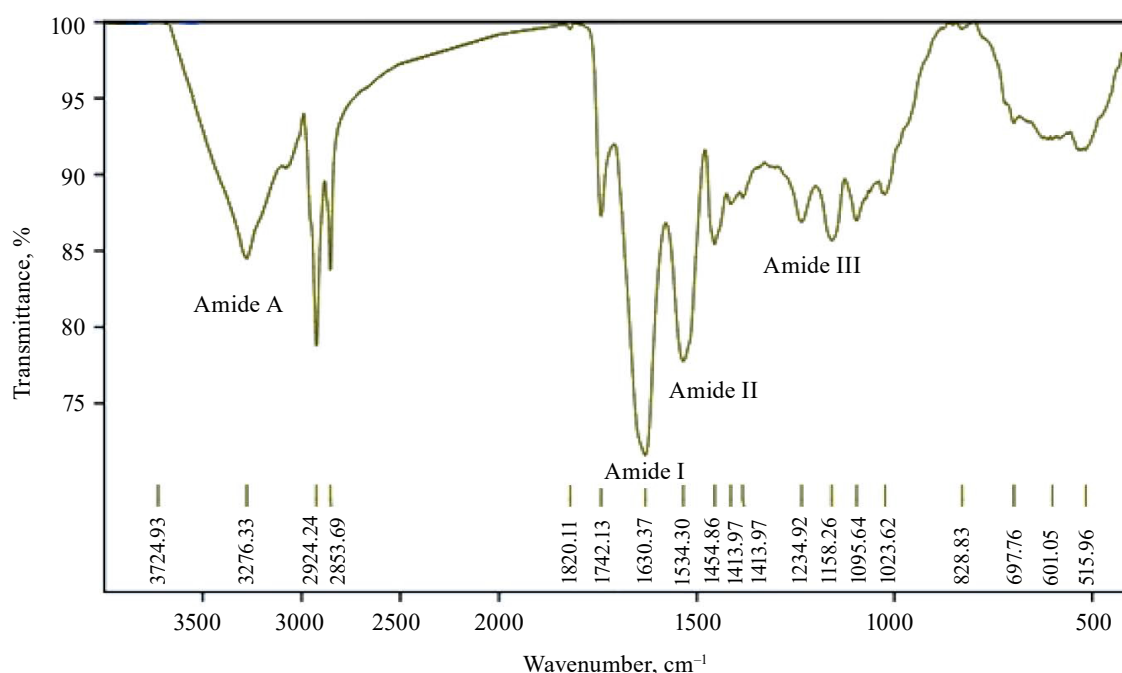


Figure 1 Fourier-transform infrared spectroscopy spectra of quinoa protein

Table 4 Physical properties of cake batter samples with different shares of quinoa protein

Sample	Batter density, g/cm ³	Specific gravity	Viscosity, CPs				
			5	6	10	20	30
Control	1.0856 ± 0.0000^a	1.1428 ± 0.0100^b	29.000	19.500	15.300	11.640	10.570
Formulation 1 (50 g quinoa protein)	0.8209 ± 0.0100^c	1.5006 ± 0.3400^a	93.000	70.800	46.800	33.900	28.400
Formulation 2 (75 g quinoa protein)	0.9076 ± 0.0100^d	1.2341 ± 0.0200^{ab}	158.000	100.800	84.700	72.000	65.200
Formulation 3 (100 g quinoa protein)	0.9315 ± 0.0200^e	1.2783 ± 0.0400^{ab}	172.400	139.700	113.700	86.900	76.800
Formulation 4 (150 g quinoa protein)	0.9730 ± 0.0100^b	0.9878 ± 0.0100^c	385.300	227.700	143.600	114.00	97.200

Values with different superscripts in the same line are significantly different at $p < 0.05$

The specific gravity in the control batter (1.14) was significantly lower than in the egg-free samples, except for Formulation 4, which contained the highest share of quinoa protein. We discovered the same trend for batter density. By incorporating quinoa protein into the control cakes, we obtained the highest specific gravity value of 1.50, which suggested heavier batter without proper aeration. As the quantity of quinoa protein kept increasing in Formulations 2, 3, and 4, the specific gravity of the egg-free cake batter went down as 1.23, 1.28, and 0.99, respectively. The specific gravity measures revealed the total air holding capacity. It was inversely proportional to the air holding capacity, i.e., high values indicated less air incorporated into the batter and vice versa. However, if the batter entraps a lot of air bubbles, it provides a better cake structure.

Figure 2 shows that viscosity and the flow properties of the control and the experimental samples remained

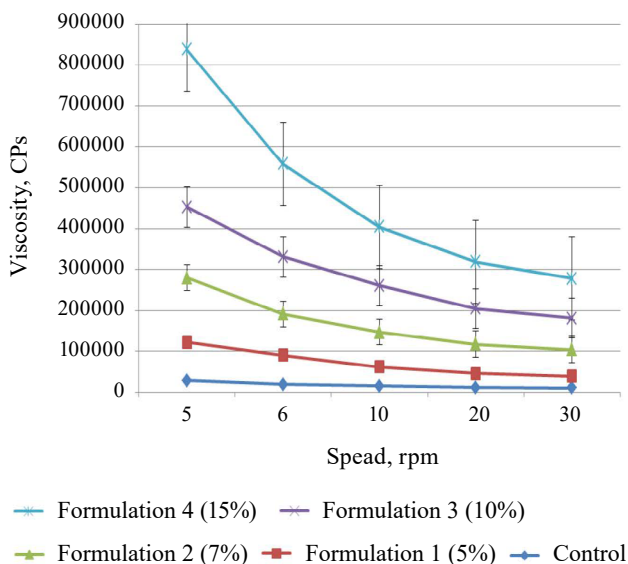


Figure 2 Rheological properties of cake batters; flow ramp curves of control and egg-free batter samples (curves are represented as a mean of at least two replicates)

within the $0.01\text{--}100\text{ s}^{-1}$ shear rate. When quinoa protein was incorporated, it resulted in an inverse relationship, where a greater quinoa protein share corresponded to a lower viscosity value. This effect can be explained by the fact that the incorporation of quinoa protein decreased the batter density whereas the high viscosity obstructed air incorporation during mixing [27]. The increase in the viscosity of the batter could be related to the quantity of available water in the system absorbed by the flour, which is known to depend on the quantity of proteins [26]. For instance, Mu *et al.* recommended to keep high viscosity as a favorable factor for batter stability and quality of the final product [28].

Proximate compositions of control and quinoa protein cake samples. Proximate compositions for cakes include moisture, ash, crude protein, crude fat, and crude fiber. We determined these variables according to the recommendations given by the American Association of Cereal Chemists (2010). The total carbohydrates content was estimated as the following difference: total carbohydrate = $100 - (\text{moisture} + \text{ash} + \text{crude protein} + \text{crude fat})$. The moisture contents of the egg-free samples decreased as the share of quinoa protein increased (Table 5). Harisha *et al.* reported the same trend: when they incorporated pea protein isolate, the moisture content went down [30]. We also detected a significant incremental increase in the crude protein (6.45–7.90%) and ash (0.46–0.96%) in the egg-free samples. When the concentration of quinoa protein in the cake formulations increased, the crude fat decreased from 13.01 to 9.56% whereas the crude fiber content showed no significant differences. The total carbohydrate calculated by differences increased together with the share of quinoa protein.

Physical property of cakes. Table 6 illustrates the impact of quinoa protein on the physical properties of cake, i.e., baking loss, density, specific volume, volume index, symmetric index, and uniformity index. The baking loss of the control cake (15.61%) was quite higher than that of the egg-free samples. As the percentage of quinoa protein increased, the weight loss increased

Table 5 Proximate compositions: quinoa protein samples vs. control

Sample	*Parameters						
	Moisture, %	Ash, %	Fat, %	Fiber, %	Protein, %	**Total carbohydrates, %	***Energy, kcal/100 g
Control	24.39 ± 0.27^a	0.46 ± 0.01^b	13.01 ± 0.52^a	3.46 ± 0.43^a	6.45 ± 0.07^d	52.22	365.81
Formulation 1 (50 g quinoa protein)	17.53 ± 0.30^c	0.90 ± 0.05^a	11.22 ± 0.27^b	3.05 ± 0.12^a	6.05 ± 0.01^c	61.25	383.18
Formulation 2 (75 g quinoa protein)	17.61 ± 0.18^c	0.98 ± 0.04^a	10.61 ± 0.54^b	3.34 ± 0.18^a	6.60 ± 0.02^c	60.85	378.65
Formulation 3 (100 g quinoa protein)	18.10 ± 0.43^c	0.97 ± 0.59^a	9.59 ± 0.33^c	3.16 ± 0.14^a	6.82 ± 0.06^b	61.36	374.91
Formulation 4 (150 g quinoa protein)	18.60 ± 0.49^b	0.96 ± 0.06^a	9.56 ± 0.42^c	3.50 ± 0.24^a	7.90 ± 0.07^a	59.47	369.88

*The values are mean \pm SD; values marked by different superscripts in the same column are significantly different ($p \leq 0.05$);

By difference; *Calculated

Table 6 Physical properties of cakes with different shares of quinoa protein

Samples	Baking loss, %	Density, g/cm ³	Specific volume, cm ³ /g	Volume index, mm	Symmetric index, mm	Uniformity index, mm
Control	15.61 ± 0.14 ^a	0.338 ± 0.000 ^b	2.96 ± 0.02 ^c	3.04 ± 0.78 ^{ab}	175.98 ± 0.21 ^c	0.857 ± 0.180 ^a
Formulation 1 (50 g quinoa protein)	13.02 ± 0.32 ^c	0.323 ± 0.000 ^c	3.10 ± 0.02 ^b	4.05 ± 0.40 ^a	184.45 ± 0.37 ^c	0.053 ± 0.070 ^d
Formulation 2 (75 g quinoa protein)	13.92 ± 0.15 ^b	0.343 ± 0.000 ^a	2.92 ± 0.01 ^c	2.58 ± 0.43 ^b	176.73 ± 0.51 ^d	0.403 ± 0.010 ^b
Formulation 3 (100 g quinoa protein)	12.86 ± 0.14 ^c	0.321 ± 0.000 ^c	3.11 ± 0.02 ^b	3.80 ± 0.33 ^a	190.88 ± 0.35 ^b	0.357 ± 0.040 ^c
Formulation 4 (150 g quinoa protein)	12.94 ± 0.17 ^c	0.313 ± 0.000 ^d	3.20 ± 0.03 ^a	2.60 ± 0.58 ^b	194.42 ± 0.24 ^a	0.347 ± 0.030 ^c

Table 7 Texture analysis of cakes with different shares of quinoa protein

Sample	Hardness, g	Cohesiveness	Resilience, mm	Gumminess, g	Chewiness, g
Control	657.00 ± 0.00 ^b	0.60 ± 0.02 ^b	8.75 ± 0.07 ^a	369.62 ± 0.22 ^c	3,283.16 ± 2.70 ^c
Formulation 1 (50 g quinoa protein)	716.00 ± 4.24 ^a	0.61 ± 0.03 ^b	8.30 ± 0.14 ^{ab}	443.06 ± 3.87 ^a	3,451.68 ± 2.61 ^a
Formulation 2 (75 g quinoa protein)	636.00 ± 4.24 ^c	0.82 ± 0.06 ^a	8.20 ± 0.42 ^{ab}	402.91 ± 5.82 ^b	3,417.35 ± 3.13 ^b
Formulation 3 (100 g quinoa protein)	605.00 ± 1.41 ^d	0.56 ± 0.06 ^b	8.20 ± 0.14 ^{ab}	351.14 ± 0.49 ^d	2,888.23 ± 8.62 ^d
Formulation 4 (150 g quinoa protein)	512.50 ± 0.71 ^c	0.58 ± 0.01 ^b	8.10 ± 0.14 ^b	283.06 ± 3.92 ^c	2,286.41 ± 4.45 ^c

Means with different superscripts in the same column are significantly different at $p \leq 0.05$

accordingly. The foaming capacity and the stability of quinoa protein can explain the reducing baking loss in the egg-free samples. The density decreased as the share of quinoa protein grew; the lowest value was reported for Formulation 4 with the highest quinoa protein concentration. However, Formulation 3 had a higher density value than the control. The specific volume significantly improved as the proportion of quinoa protein grew larger.

Specific volume affects consumer preference, which makes it one of the most important quality parameters for baked products. Table 6 shows that the control sample without quinoa protein exhibited the lowest specific volume, whereas the sample baked according to Formulation 4 had the highest specific volume. Samples with more quinoa protein had a greater specific volume ($p < 0.05$), which could be explained by the higher protein content. Thus, proteins increase the volume of cakes by increasing the viscoelasticity of batter and the time it takes the batter to become semisolid. This phenomenon is, in turn, related to the protein-starch interaction and transition [31]. Therefore, the cake volume depended not on the initial air quantity but on the capacity of retaining air during baking [32].

Texture analysis. Table 7 compares the texture quality of the control sample cake and the egg-free cakes with different shares of quinoa protein. The incorporation affected the hardness of the cake, its lowest value corresponding to Formulation 4 with the highest quinoa protein content (150 g). So, the degree of hardness depended on the protein content. Our findings contradict those reported in some previous publications, where, for instance, chickpea flour raised the initial firmness in cake [33]. Probably, the water binding capacity of quinoa protein made the cake softer and affected the crumb firmness as well. Regarding the cohesiveness values, we detected no significant difference between the control cake and the cake prepared with quinoa protein,

the only exception being Formulation 2 (75 g quinoa protein), which exhibited the maximal value (0.61). Meanwhile, Formulation 4 showed significantly higher resilience compared to the other test samples and the control. In general, hardness and firmness had an impact on the cake structure and its compression resistance. These qualities are mirrored by the development of internal bonding in a three-dimensional protein network and affect consumer acceptance.

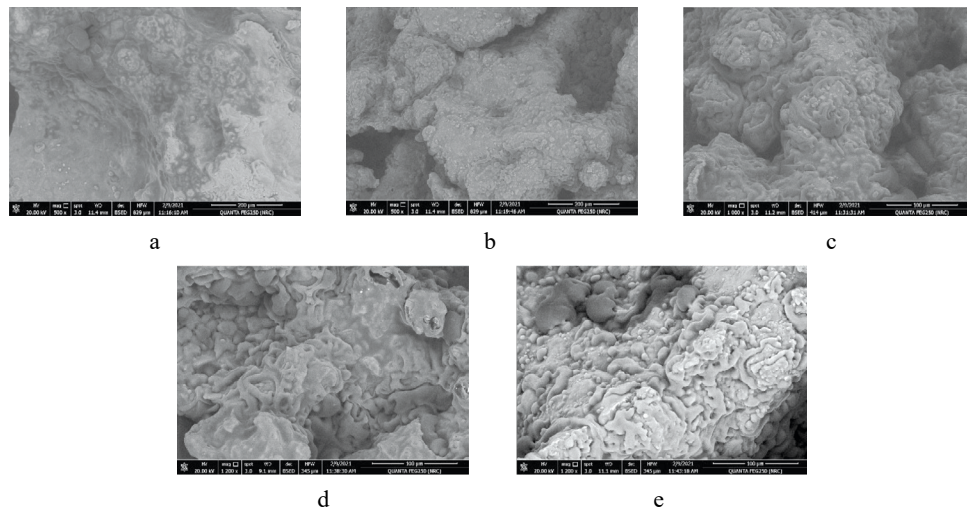
The egg-free samples demonstrated greater gumminess and chewiness than the control. Formulations 3 and 4 showed a more distinguish pattern where greater quinoa protein shares increased the gumminess and chewiness. Both values followed the same pattern as the one that was reported for hardness.

Color. The type of ingredients and interactions between them affect the final color of baked products. Color attributes include lightness (L^*), redness (a^*), and yellowness (b^*) of the surface and crumb (Table 8). By incorporating quinoa protein in different proportions, we changed the color of both crust and crumb. The lightness (L^*) and yellowness (b^*) decreased whereas the redness (a^*) increased. The minimal lightness and yellowness were registered for the cake baked according to Formulation 4 with the highest quinoa protein concentration. The redness grew together with the ratio of quinoa protein. As a rule, the increase in the redness in cake crust is associated with caramelization and the Maillard reaction. The larger amount of quinoa protein increased the protein content in the cakes and consequently stimulated the Maillard reaction, thus producing dark-brown components. Gallego *et al.* reported that protein increased the redness in muffin crust [34]. Our findings confirm those observed by Blanco Canalis *et al.*, who also reported an increase in redness (a^*) and significant reduction in lightness (L^*) as a result of increasing protein level in cake [35].

Table 8 Color parameters of cakes with different shares of quinoa protein

	Crust			Total color difference	Crumb			Total color difference
	L^*	a^*	b^*		L^*	a^*	b^*	
Control	47.10 ± 0.56 ^c	8.61 ± 0.05 ^c	22.16 ± 0.22 ^b		69.67 ± 0.01 ^a	0.50 ± 0.01 ^c	20.91 ± 0.02 ^a	
Formulation 1 (50 g quinoa protein)	51.08 ± 0.05 ^a	11.80 ± 0.01 ^c	23.62 ± 0.02 ^a	18.37 ± 0.06 ^d	68.47 ± 0.13 ^b	0.22 ± 0.02 ^c	17.95 ± 0.10 ^c	6.78 ± 0.02 ^c
Formulation 2 (75 g quinoa protein)	48.12 ± 0.01 ^b	12.86 ± 0.01 ^a	21.44 ± 0.01 ^c	22.11 ± 0.01 ^c	67.34 ± 0.05 ^c	0.29 ± 0.07 ^d	19.90 ± 0.11 ^b	6.54 ± 0.03 ^d
Formulation 3 (100 g quinoa protein)	43.10 ± 0.27 ^d	10.50 ± 0.05 ^d	20.00 ± 0.11 ^c	27.00 ± 0.03 ^b	63.42 ± 0.03 ^d	0.78 ± 0.01 ^b	18.43 ± 0.02 ^d	10.61 ± 0.02 ^b
Formulation 4 (150 g quinoa protein)	42.51 ± 0.17 ^e	12.34 ± 0.01 ^b	20.34 ± 0.08 ^d	27.52 ± 0.19 ^a	62.44 ± 0.04 ^e	0.94 ± 0.01 ^a	18.97 ± 0.01 ^c	11.30 ± 0.03 ^d

Values are represented as mean ± SD. Values with different superscripts in the same column are significantly different at $p \leq 0.05$

**Figure 3** Scanning electron microscopy images (200×): a – control; b – Formulation 1 (50 g quinoa protein); c – Formulation 2 (75 g quinoa protein); d – Formulation 3 (100 g quinoa protein); e – Formulation 4 (150 g quinoa protein)**Table 9** Sensory scores of cakes with different shares of quinoa protein

Treatment	Taste	Color	Softness	Flavor	Cells size uniformity	Overall acceptability
Control	8.30 ± 0.95 ^{ab}	8.20 ± 0.92 ^a	8.80 ± 1.16 ^a	8.00 ± 0.94 ^{ab}	8.70 ± 0.82 ^{ab}	8.100 ± 0.744 ^b
Formulation 1 (50 g quinoa protein)	7.40 ± 0.84 ^{bc}	8.20 ± 0.92 ^a	8.20 ± 0.63 ^{ab}	7.90 ± 0.99 ^{abc}	8.20 ± 0.63 ^{bc}	7.70 ± 0.67 ^b
Formulation 2 (75 g quinoa protein)	7.90 ± 0.99 ^{abc}	9.00 ± 0.94 ^a	7.60 ± 1.43 ^b	7.40 ± 1.17 ^{bc}	7.90 ± 0.74 ^c	7.70 ± 0.95 ^b
Formulation 3 (100 g quinoa protein)	7.00 ± 1.41 ^c	7.20 ± 1.14 ^b	7.90 ± 1.52 ^{ab}	6.80 ± 1.40 ^c	7.80 ± 0.92 ^c	7.35 ± 1.38 ^b
Formulation 4 (150 g quinoa protein)	8.80 ± 1.135 ^a	6.70 ± 1.16 ^b	9.00 ± 0.94 ^a	8.70 ± 1.34 ^a	9.00 ± 0.94 ^a	9.00 ± 0.96 ^a

Values with different superscripts in the same line are significantly different at $p \leq 0.05$

Microstructure analysis. We appealed to scanning electron microscopy to study the microstructure of the control cake and the samples with different shares of quinoa protein (Fig. 3). The impact of the quinoa protein on the batter microstructure was determined in order to investigate the network or structure-forming potential of quinoa protein as a safe ingredient. The scanning electron microscopy revealed the preliminary structural properties of the egg-free cakes, which showed alterations in the microstructure. The experimental samples exhibited a distinct protein matrix with embedded starch granules. However, the size distribution of the micro-particles was wide. This appearance was similar to that

of the dough described in [36]. During mixing, the diverse bonds in the proteins started to interact with each other via hydrogen, ionic, hydrophobic, and covalent bonds, thus developing a cross-linked network [37]. Romano *et al.* reported gelatinized starch granules surrounded by a continuous protein matrix in a scanning electron microscopy image of cakes with quinoa protein [38].

Sensory properties. A descriptive sensory test made it possible to define and evaluate the sensory properties. Table 9 shows the sensory assessment of color, softness, flavor, cell size uniformity, and overall acceptance. The cakes with quinoa protein were significantly ($p < 0.05$) different from the control in all sensory aspects. The

color sensory score decreased as the share of quinoa protein grew. Formula 4 with the greatest quinoa protein content received the highest score for overall acceptability sensory.

CONCLUSION

Quinoa is a non-conventional source of protein rich in essential amino acids and with an excellent nutritional value. This study featured cakes with different shares of quinoa protein with improved nutritional properties and microstructure. Our results underscored the unique features of egg-free cakes, e.g., a higher protein value. The balanced amino acid profile could make quinoa protein a potential egg replacer in bakery products designed for people with allergy to eggs. The new product also demonstrated an acceptable overall sensory profile.

Quinoa protein proved to be a prospective nutritive source, a food supplement, and a functional food ingredient. With the rapidly developing processing technology and ingredient functionality, the mass production of

quinoa protein can overcome the challenge of cost effectiveness as a competitive egg replacer and may become available in the near future. Yet, advanced research is needed to prove and improve its functional properties and versatility as a food ingredient. In addition, more work is required to better understand quinoa protein and its potential for the food industry in general, functional foods, and special dietary foods.

CONTRIBUTION

Rasha K. Mohamed and Safaa S. Abozed carried out the experiment, prepared the materials, and analyzed the obtained data. Zahra S. Ahmed aided in interpreting the results and drafted the manuscript. All the authors contributed to the study conception and design, as well as read and approved the final manuscript.

CONFLICT OF INTEREST

The authors declare no conflict of interests regarding the publication of this article.


REFERENCES


1. Bazile D, Baudon F. The dynamics of the global expansion of quinoa growing in view of its high biodiversity. In: Bazile D, Bertero D, Nieto C, editors. State of the art report of quinoa in the world in 2013. Rome: FAO & CIRAD; 2013. pp. 42–55.
2. Agarwal A, Rizwana, Tripathi AD, Kumar T, Sharma KP, Patel SKS. Nutritional and functional new perspectives and potential health benefits of quinoa and chia seeds. *Antioxidants*. 2023;12(7):1413. <https://doi.org/10.3390/antiox12071413>
3. Gojković Cvjetković VS, Škuletić DM, Marjanović-Balaban ŽR, Vujadinović DP, Rajić DZ, Tomović VM. Gliadin proteins in muffins with quinoa flour. *Food Processing: Techniques and Technology*. 2024;54(1):82–92. <https://doi.org/10.21603/2074-9414-2024-1-2490>
4. Angeli V, Silva PM, Massuela DC, Khan MW, Hamar A, Khajehei F, et al. Quinoa (*Chenopodium quinoa* Willd.): An overview of the potentials of the “golden grain” and socio-economic and environmental aspects of its cultivation and marketization. *Foods*. 2020;9(2):216. <https://doi.org/10.3390/foods9020216>
5. Yang X, Zhu K, Guo H, Geng Y, Lv W, Wang S, et al. Characterization of volatile compounds in differently coloured *Chenopodium quinoa* seeds before and after cooking by headspace-gas chromatography-ion mobility spectrometry. *Food Chemistry*. 2021;348:1290086. <https://doi.org/10.1016/j.foodchem.2021.129086>
6. Li X, Chen S, Yao Y, Wu N, Xu M, Zhao Y, et al. The quality characteristics formation and control of salted eggs: A review. *Foods*. 2022;11(19):2949. <https://doi.org/10.3390/foods11192949>
7. Komerowski MR, de Oliveira VR. Influence of the amount and type of whey protein on the chemical, technological, and sensory quality of pasta and bakery products. *Foods*. 2023;12(14):2801. <https://doi.org/10.3390/foods12142801>
8. Godefroidt T, Ooms N, Pareyt B, Brijs K, Delcour JA. Ingredient functionality during foam-type cake making: A review. *Comprehensive Reviews in Food Science and Food Safety*. 2019;18:1550–1562. <https://doi.org/10.1111/1541-4337.12488>
9. Yazici GN, Ozer MS. A review of egg replacement in cake production: Effects on batter and cake properties. *Trends in Food Science and Technology*. 2021;111:346–359. <https://doi.org/10.1016/j.tifs.2021.02.071>
10. Erfanian A, Rasti B. Effects of soy milk on physical, rheological, microbiological and sensory properties of cake. *International Food Research Journal*. 2019;26(1):237–245.
11. Boukid F, Gagaoua M. Vegan egg: A future-proof food ingredient? *Foods*. 2022;11(2):161. <https://doi.org/10.3390/foods11020161>
12. Nastaj M, Mleko S, Terpiłowski K, Tomczyńska-Mleko M. Effect of sucrose on physicochemical properties of high-protein meringues obtained from whey protein isolate. *Applied Sciences*. 2021;11(11):4764. <https://doi.org/10.3390/app11114764>


13. Guerreiro-Ochoa MR, Pedreschi R, Chirinos R. Optimised methodology for the extraction of protein from quinoa (*Chenopodium quinoa* Willd.). *International Journal of Food Science and Technology*. 2015;50(8):1815. <https://doi.org/10.1111/ijfs.12834>
14. Robertson JA, de Monredon FD, Dysseler P, Guillon F, Amado R, Thibault J-F. Hydration properties of dietary fibre and resistant starch: A European collaborative study. *LWT – Food Science and Technology*. 2000;33(2):72–79. <https://doi.org/10.1006/fstl.1999.0595>
15. Wani AI, Sogi D, Gill SB. Physicochemical and functional properties of flours from three Black gram (*Phaseolus mungo* L.) cultivars. *International Journal of Food Science and Technology*. 2013;48(4):771. <https://doi.org/10.1111/ijfs.12025>
16. Fallah-Delavar M, Farmani J. Recovery and characterization of enzymatic protein hydrolysates and fat from chicken skin. *Journal of the American Oil Chemists' Society*. 2018;95:1151–1161. <https://doi.org/10.1002/aocs.12131>
17. Shahidi F, Han X-O, Synowiecki J. Production and characteristics of protein hydrolysates from capelin (*Mallotus villosus*). *Food Chemistry*. 1995;53(3):285–293. [https://doi.org/10.1016/0308-8146\(95\)93934-J](https://doi.org/10.1016/0308-8146(95)93934-J)
18. Shao Y, Kao J. Foaming properties of soy protein isolates and concentrates. *International Conference on Food Security and Nutrition*. 2014.
19. Özhamamci I, Çakiroglu K, Ertugay MF. The effects of emulsifiers and their different forms on the physical, chemical and textural properties of sponge cakes. *International Journal of Engineering Trends and Technology*. 2019;67(1). <https://doi.org/10.14445/22315381/IJETT-V67I1P201>
20. Approved Method of the American Association of Cereal Chemists. American Association of Cereal Chemists; 2000. 1200 p.
21. Officials Methods of Analysis, 17th Edn. Association of Official Analytical Chemists; 2000.
22. Polachini TC, Morales SAV, Filho LRP, Ribeiro EF, Saraiva LS, Basso RC. Physical properties and molecular interactions applied to food processing and formulation. *Processes*. 2023;11(7):2181. <https://doi.org/10.3390/pr11072181>
23. Zhang Y, Hou R, Zhu B, Yin G, Zhang J, Zhao W, et al. Changes on the conformational and functional properties of soybean protein isolate induced by quercetin. *Frontiers in Nutrition*. 2022;9:966750. <https://doi.org/10.3389/fnut.2022.966750>
24. Mizutani Y, Shibata M, Yamada S, Nambu Y, Hirotsuka M, Matsumura Y. Effects of heat treatment under low moisture conditions on the protein and oil in soybean seeds. *Food Chemistry*. 2019;275:577–584. <https://doi.org/10.1016/j.foodchem.2018.09.139>
25. Hedayati S, Tehrani MM. Effect of total replacement of egg by soymilk and lecithin on physical properties of batter and cake. *Food Science and Nutrition*. 2018;6:1154. <https://doi.org/10.1002/fsn3.656>
26. Li X, Wang Y-M, Sun C-F, Lv J-H, Yang Y-J. Comparative study on foaming properties of egg white with yolk fractions and their hydrolysates. *Foods*. 2021;10(9):2238. <https://doi.org/10.3390/foods10092238>
27. Dakhili S, Abdolalizadeh L, Hosseini SM, Shojaee-Aliabadi S, Mirmoghtadaie L. Quinoa protein: Composition, structure and functional properties. *Food Chemistry*. 2019;299:125161. <https://doi.org/10.1016/j.foodchem.2019.125161>
28. Mu J, Qi Y, Gong K, Chen Z, Brennan MA, Qianyun M, et al. Effects of quinoa flour (*Chenopodium quinoa* Willd) substitution on wheat flour characteristics. *Current Research in Food Science*. 2023;7:100556. <https://doi.org/10.1016/j.crfs.2023.100556>
29. Tian Y, Rao H, Zhang K, Tao S, Xue W-T. Effects of different thermal processing methods on the structure and allergenicity of peanut allergen Ara h 1. *Food Science and Nutrition*. 2018;6:1706. <https://doi.org/10.1002/fsn3.742>
30. Harisha R, Singh SK, Ahlawat AK, Narwal S, Jaiswal JP, Sin JB, et al. Elucidating the effects on polyphenol oxidase activity and allelic variation of polyphenol oxidase genes on dough and whole wheat-derived product color parameters. *International Journal of Food Properties*. 2023;26(2):2716–2731. <https://doi.org/10.1080/10942912.2023.2252196>
31. Rashwan AK, Osma AI, Abdelshafy AM, Mo J, Chen W. Plant-based proteins: Advanced extraction technologies, interactions, physicochemical and functional properties, food and related applications, and health benefits. *Critical Reviews in Food Science and Nutrition*. 2023. <https://doi.org/10.1080/10408398.2023.2279696>
32. Khalid II, Elharadallou SB. Functional properties of cowpea (*Vigna unguiculata* L. Walp), and lupin (*Lupinus termis*) flour and protein isolates. *Journal of Nutrition and Food Sciences*. 2023;3:234–240. <https://doi.org/10.4172/2155-9600.1000234>
33. Salehi F. Improvement of gluten-free bread and cake properties using natural hydrocolloids: A review. *Food Science and Nutrition*. 2019;7:3391–3402. <https://doi.org/10.1002/fsn3.1245>

34. Gallego C, Belorio M, Guerra-Oliveira M, Gomez M. Effects of adding chickpea and chestnut flours to layer cakes. *International Journal of Food Science and Technology*. 2022;57:4840–4846. <https://doi.org/10.1111/ijfs.15719>
35. Blanco Canalis MS, Valentinuzzi MC, Acosta RH, León AE, Ribotta PD. Effects of fat and sugar on dough and biscuit behaviours and their relationship to proton mobility characterized by TD-NMR. *Food and Bioprocess Technology*. 2018;11:953–965. <https://doi.org/10.1007/s11947-018-2063-z>
36. Bieniek B, Buksa K. Properties and functionality of cereal non-starch polysaccharides in breadmaking. *Applied Sciences*. 2023;13(4):2282. <https://doi.org/10.3390/app13042282>
37. Vidal L, Ewigmann H, Schuster C, Alpers T, Scherf K, Jekle M, et al. Microscopic analysis of gluten network development under shear load-combining confocal laser scanning microscopy with rheometry. *Journal of Texture Studies*. 2023;54(4). <https://doi.org/10.1111/jtxs.12796>
38. Romano A, Masi P, Bracciale A, Aiello A, Nicolai MA, Ferranti P. Effect of added enzymes and quinoa flour on dough characteristics and sensory quality of a gluten-free bakery product. *European Food Research and Technology*. 2018;244:1595–1604. <https://doi.org/10.1007/s00217-018-3072-x>

ORCID IDs

Rasha K. Mohamed  <https://orcid.org/0000-0002-7290-5533>

Zahra S. Ahmed  <https://orcid.org/0000-0002-6543-0584>

Safaa S. Abozed  <https://orcid.org/0000-0002-8992-364X>



Ultra-high-pressure homogenization in chicory root juice production

Muhammet Irfan Aksu^{1,*}, Halil İbrahim Erkovan², Sule Erkovan²

¹ Atatürk University^{ROR}, Erzurum, Türkiye

² Eskişehir Osmangazi University^{ROR}, Eskişehir, Türkiye

* e-mail: miaksu@atauni.edu.tr

Received 05.12.2023; Revised 05.02.2024; Accepted 05.03.2024; Published online 23.10.2024

Abstract:

The demand for freshly squeezed natural fruit juices has increased in recent years, however their shelf life is quite short. Thermal processes applied to extend the shelf life of such products and increase their storage stability cause significant losses in color and other sensory properties, depending on the temperature applied. Therefore, the preference for high-pressure homogenization as an alternative to thermal processes is on the rise. We aimed to determine effects of ultra-high-pressure homogenization and production stages on some quality properties of chicory root juice.

Ultra-high-pressure homogenization was applied at the pressure levels of 0 (control), 50, 100, 150, and 200 MPa. The samples also included juice after homogenization with an ULTRA-TURRAX disperser and after a water bath.

Ultra-high-pressure homogenization affected such quality characteristics of chicory root juice as total soluble solids ($p < 0.01$), pH ($p < 0.01$), L^* ($p < 0.01$), a^* ($p < 0.01$), b^* ($p < 0.01$), a^*/b^* ($p < 0.01$), chroma ($p < 0.01$), hue angle ($p < 0.01$), and total color difference ΔE ($p < 0.01$). Higher levels of ultra-high-pressure homogenization pressure increased pH ($p < 0.05$), a^* values ($p < 0.05$), and the a/b^* ratio ($p < 0.05$) but reduced L^* ($p < 0.05$), b^* ($p < 0.05$), chroma ($p < 0.05$), and hue angle ($p < 0.05$) values of the juice samples. Thus, the use of ultra-high-pressure homogenization (100 and 200 MPa) contributed to improving the total soluble solids and redness values of chicory root juice.

Our study showed that the ultra-high-pressure homogenization process improved the quality of chicory root juice.

Keywords: Chicory root juice, ultra-high pressure, homogenization, color characteristics, pH, total soluble solids

Funding: This study was funded by the authors, with no support from any funding agency. The study was carried out in the research laboratories of the Department of Field Crops and Food Engineering, the Faculty of Agriculture, Eskişehir Osmangazi University (ESOGU)^{ROR}.

Please cite this article in press as: Aksu MI, Erkovan Hİ, Erkovan S. Ultra-high-pressure homogenization in chicory root juice production. *Foods and Raw Materials*. 2025;13(2):287–295. <https://doi.org/10.21603/2308-4057-2025-2-640>

INTRODUCTION

Chicory is a tuberous taproot with rosette leaves that grows widely under cool conditions. Although increasingly cultivated for different purposes around the world, chicory is not grown in Turkey. The genus *Chicory* (*Asteraceae*) contains six species, two of which are of economic importance, namely *Cichorium intybus* and *Cichorium endivia*. These two species are morphologically similar. However, *C. intybus* can be distinguished from *C. endivia* by its short pappus (extension at the end of the fruit), as well as other perennial and self-sustainable characteristics. *C. intybus* is the most prevalent and varied species of the genus *Chicory* in the world [1].

Chicory roots are one of the most important plant resources used in the production of inulin [2, 3]. Inulin

contains less energy compared to other carbohydrates. It stimulates the growth of bifidobacteria in the intestines, reducing the risk of developing heart disease, diabetes, osteoporosis, and cancer [4]. European countries are increasing the consumption of inulin as a dietary lithium and producing up to one million metric tons of indigestible Chicory for the food industry [5]. Inulin is resistant to digestion and passes directly into the colon without being absorbed in the small intestine. Chicory sticks contain another sugar group, oligofructose (5–10), which has similar effects to inulin. It is found in glucose and sucrose, which are sugar groups [6]. The content of raw protein and raw fiber in Chicory shoot and root after industrialized extraction are higher than that in corn grain. It is therefore regarded as a valuable industrial plant in

terms of its economic yield and quality [7]. Furthermore, spruce-type chicory varieties are also used as coffee additives after processing [8].

Chicory is rich in water, low in calories, and contains a significant amount of dietary fiber, particularly inulin, which is a prebiotic. It also has a modest amount of proteins, low level of fats, and is a good source of several minerals like potassium, calcium, magnesium, and iron, as well as vitamins such as vitamin C and some B vitamins [9, 10]. Chicory is known for its high content of bioactive compounds including inulin, sesquiterpene lactones (such as lactucin and lactucopicrin), caffeic acid derivatives, and various phenolic compounds [11]. These compounds are associated with various health benefits, including antioxidant, anti-inflammatory, and hepatoprotective effects [12]. Chicory and its extracts are generally considered safe for consumption, with inulin from chicory recognized for its prebiotic properties that support gut health. The potential health benefits of chicory include its role in reducing post-prandial glycaemic responses and promoting bowel function, as well as its antioxidant and anti-inflammatory properties. These health benefits make chicory an attractive ingredient and a source of inulin for functional foods aimed at improving health and preventing disease [13]. Chicory is used in various food products, including salads, and as a coffee substitute. Food scientists are trying to optimize the extraction of chicory's bioactive compounds for their application in food products on an industrial scale [14]. Chicory presents a promising potential as a functional food ingredient due to its rich nutritional profile, bioactive compounds, and associated health benefits for humans and animals [15, 16]. Its application in the food industry could contribute to the development of health-promoting functional foods, aligning with the consumer demand for natural and beneficial food ingredients [17].

There has been a recent increase in the demand for freshly squeezed fruit juices as natural products. However, the shelf life of such products is quite limited due to microbiological and enzymatic spoilage. In order to reduce these negative effects, thermal processes (60–90°C, < 1 min) are frequently used. However, these temperature applications may cause a significant loss in color and other sensory properties, depending on the temperature and duration [18]. Therefore, in recent years, alternative non-thermal techniques have been widely used in food technology to overcome these disadvantages and enhance the product's quality [19–22]. One of such techniques is high-pressure homogenization applied as an alternative to thermal processing in the fruit juice and beverage technology.

High-pressure homogenization can improve the rheological properties of foods and their emulsion capacity, as well as reduce their particle size. This technology can also inactivate microbial growth and extend the shelf life of the products. Most importantly, it provides a better protection of nutrients and bioactive components whose structures are damaged by thermal processes. In this context, high-pressure homogenization can be used

in the fruit juice technology to reduce pulp precipitation, increase physical stability, and improve product's physical properties [22, 23].

Ultra-high-pressure homogenization is used in different areas of food processing, e.g., to improve the rheological properties of citrus fiber or the functional properties of gelatin, as well as to develop functional foods and produce juice [24–28]. A previous study, which applied ultra-high-pressure homogenization (60, 80, 100, 120, 140, and 160 MPa) to native rice starches, found that the viscosity of starch increased between 60 and 120 MPa, while higher pressure applications produced the opposite effect [29].

In summary, ultra-high-pressure homogenization is a method that has been widely applied and studied in recent years to improve the techno-functional properties of fluid foods. Many of its effects have been proven, such as microbial inactivation, changing the physical properties of liquid foods and viscous properties of liquids, homogenization, and enzyme inactivation [23, 30]. Previous studies have generally used fruits as raw materials to determine the effects of ultra-high-pressure homogenization on fruit juice quality. However, we know of no research into the quality of juice produced from the roots of plants. Therefore, we aimed to determine the effects of ultra-high-pressure homogenization at different pressure levels on some quality properties of chicory root juice.

STUDY OBJECTS AND METHODS

Study objects. In our research we tested juice samples after homogenization with an ULTRA-TURRAX disperser, samples after homogenization and keeping in a water bath, and samples treated by ultra-high-pressure homogenization at different pressure levels, namely 0 (control), 50, 100, 150, and 200 MPa.

Preparation of chicory root juice and ultra-high-pressure homogenization. For this research, chicory roots were obtained from the Ertuğrulgazi gardens (Eskişehir, Turkey). They were separated from the soil by washing with tap water and used as material for producing chicory juice (Fig. 1). The chicory juice was passed through an ultra-high-pressure homogenization system (50, 100, 150, and 200 MPa) using a table-top homogenizer (GEA Homogenizer Panda PLUS 2000, Parma, Italy). High-pressure homogenization-untreated chicory juice was considered a control group. The maximum flow rate of the high-pressure homogenization system was 9 L/h. The inlet temperature of the juice was about 4–6°C, while the outlet temperature was in the range of 30.5–36.8°C. For this reason, the chicory juices coming out of the high-pressure homogenization system were immediately cooled and analyzed.

Analysis of chicory juices. Determination of total soluble solids. Total soluble solids in the control and high-pressure-homogenized samples of chicory juice were determined using a digital refractometer (Hanna HI 96801, USA). A constant temperature of 20°C was used in all the measurements.

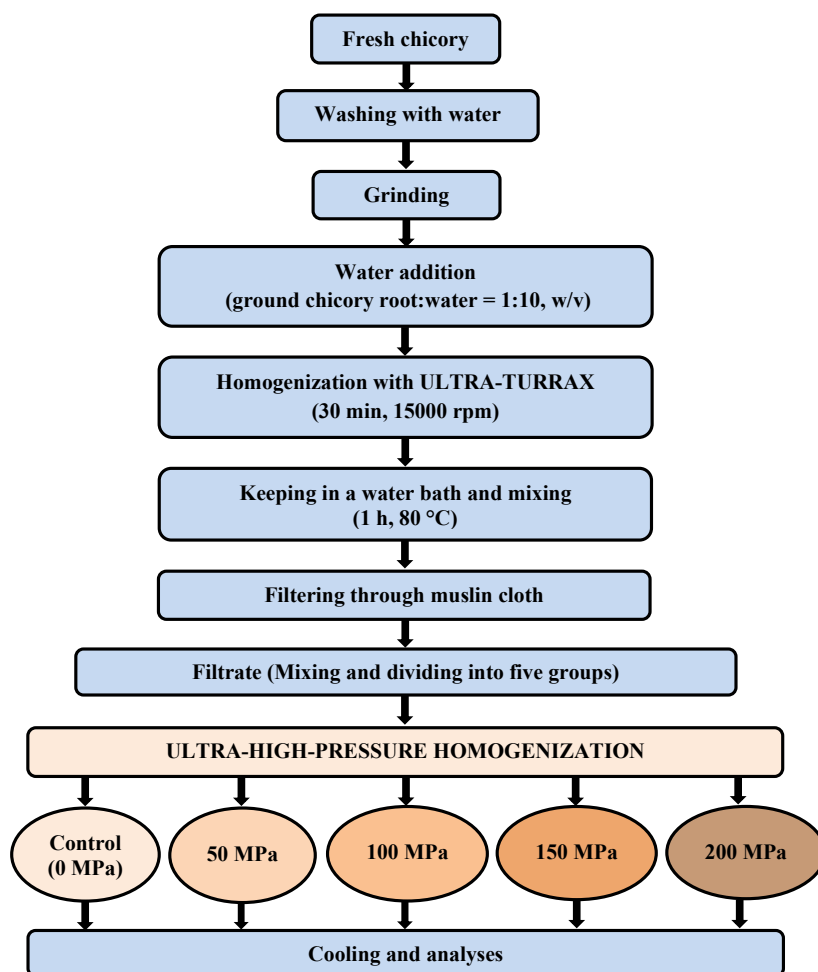


Figure 1 Chicory juice production from fresh chicory root by ultra-high-pressure homogenization

Determination of pH. The pH values of the chicory juice samples were determined using a benchtop pH meter (Hanna Instruments, USA). Measurements were made after the samples were thoroughly homogenized. Before use, a pH meter was calibrated with 3 different buffer solutions with pH of 4.0, 7.0, and 10.0.

Determination of instrumental color values. First, we measured L^* (darkness: $L^* = 0$; lightness: $L^* = 100$), a^* (redness: $+a^*$; greenness: $-a^*$), and b^* (yellowness: $+b^*$; blueness: $-b^*$) values and then, chroma (C^*) and hue angle (h°) values [31]. In addition, the total color difference (ΔE) was calculated in the samples treated by ultra-high-pressure homogenization versus the control.

Statistical analysis. The study was carried out according to a completely randomized design with two replications. An analysis of variance was performed using the SPSS package program (SPSS 23.0). The mean values of the main sources of variation were compared with the Duncan Multiple Comparison Test (95% confidence interval, $p < 0.05$).

RESULTS AND DISCUSSION

We found that the chicory root juice samples treated by ultra-high-pressure-homogenization had higher values of total soluble solids compared to the samples after

Table 1 Effects of treatments on total soluble solids and pH values of chicory root juices

Treatment	Total soluble solids, °Brix	pH
ULTRA-TURRAX	0.875 ± 0.071	6.82 ± 0.02
Water bath	0.875 ± 0.046	7.47 ± 0.20
Control (0 MPa)	0.925 ± 0.046	7.44 ± 0.01
50 MPa	0.937 ± 0.052	7.54 ± 0.01
100 MPa	1.050 ± 0.053	7.63 ± 0.04
150 MPa	0.975 ± 0.046	7.66 ± 0.03
200 MPa	1.012 ± 0.064	7.75 ± 0.02
SEM	0.020	0.029
<i>p</i> -value	< 0.0001	< 0.0001

the ULTRA-TURRAX homogenization and keeping in a water bath (Table 1). There was no statistical difference ($p > 0.05$) in total soluble solids between the control and the 50 MPa treatment groups (Fig. 2). However, we observed a statistically significant ($p < 0.05$) increase in the 100 MPa group compared to the 150 and 200 MPa groups (Fig. 2). The amount of total soluble solids mainly refers to soluble sugars in fruit or fruit juices and varies depending on the amount of soluble sugar in the raw material and the applied process [32]. The increase we found in total soluble solids might be due to the

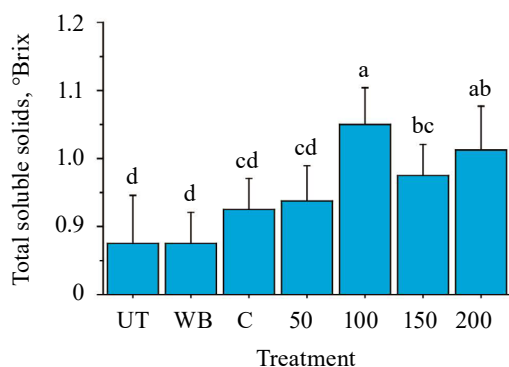


Figure 2 Effects of ultra-high-pressure homogenization on total soluble solids of chicory root juice samples. UT – after homogenization with ULTRA-TURRAX; WB – after keeping in a water bath and mixing; C – control (0 MPa). Different letters indicate statistical difference ($p < 0.05$)

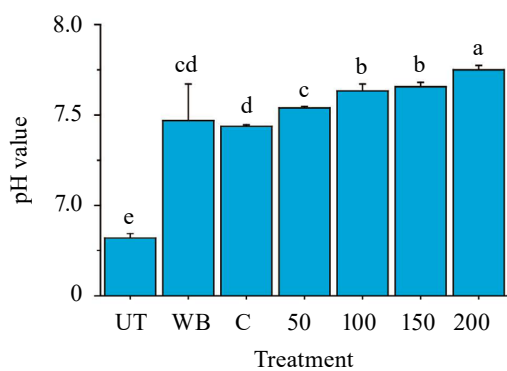


Figure 3 Effects of ultra-high-pressure homogenization on pH value of chicory root juice samples. UT – after homogenization with ULTRA-TURRAX; WB – after keeping in a water bath and mixing; C – control (0 MPa). Different letters indicate statistical difference ($p < 0.05$)

disintegration of macromolecules in chicory root juice under the influence of ultra-high-pressure homogenization. Similarly, Yan *et al.* reported that high-pressure homogenization causes an increase in the amount of water-soluble cell materials and pectin, which might be a cause of the increasing in total soluble solids [33]. A similar change was detected in the study that determined the effects of high-pressure homogenization on the quality of Ottoman strawberry (*Fragaria × ananassa*) juice [34]. Contrary to our current findings, we have previously determined that high-pressure homogenization applied to juices produced from different pomegranate genotypes reduced the amount of total soluble solids [35]. This difference could be explained by the difference in the composition and properties of fruit tissue and root properties since plant root parts contain more complex macromolecules than stems and leaves.

Table 1 also shows the effects of the production stages and ultra-high-pressure homogenization treatments at 0, 50, 100, 150, and 200 MPa on the pH values of chicory root juice. As can be seen, the pH values ranged from 6.82 ± 0.02 to 7.75 ± 0.02 , with significant ($p < 0.05$) dif-

ferences between the treatments. We observed that ultra-high-pressure homogenization increased the pH values of the samples, especially at 200 MPa pressure, i.e. the higher the homogenization pressure, the higher the pH values. Lower pH values were determined in the ULTRA-TURRAX stage of the process (Table 1). Among the production stages and high-pressure homogenization processes, the highest pH increase occurred after the ULTRA-TURRAX stage (Fig. 3). This increase could be due to the heat treatment at 80°C for 1 h after the ULTRA-TURRAX process (Fig. 1). The pH probably increased due to an increase in, or a release of, alkaline components by tissue dissolution in the ULTRA-TURRAX process. In line with our current findings, Gul *et al.* and Wellala *et al.* stated that high-pressure homogenization increased pH value, and this was due to breakdown of pectin and proteins into cellular materials [36, 37].

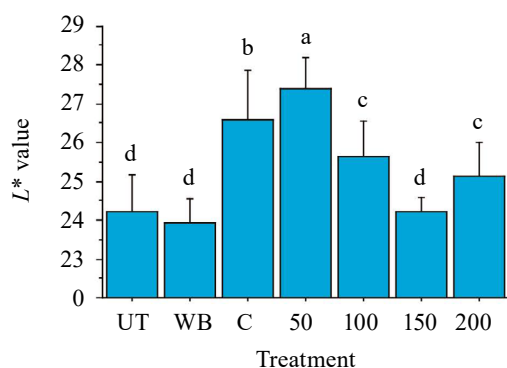
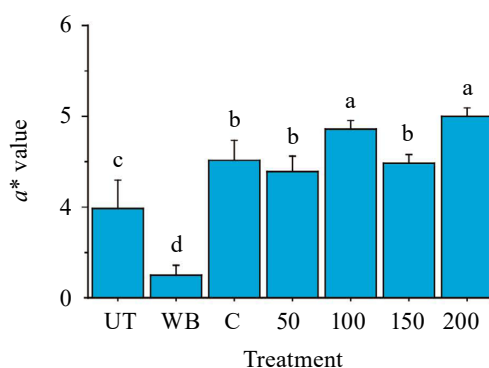
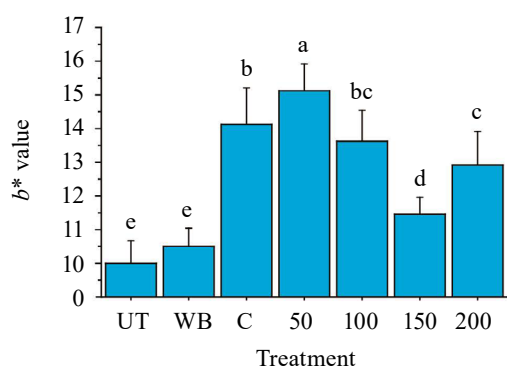
In another study, Liu *et al.* determined the effects of ultra-high-pressure homogenization (50, 100, 150, and 200 MPa) on the pH of pear juice at different temperatures (4, 20, 30, 40, 60, and 80°C) [30]. Contrary to our findings, the researchers reported that different pressures applied at the same temperature did not affect pH. However, the pH value decreased due to the disintegration of cells and the dissolution of organic acids and other substances under the influence of ultra-high-pressure homogenization at high temperatures (especially at 60 and 80°C). These differences among the studies show that the effect of ultra-high-pressure homogenization on pH may vary depending on the matrix of raw material from which the juice is produced, as well as production conditions and the treatment applied.

Table 2 demonstrates the effects of different treatments on L^* , a^* , b^* , C^* , and °h of the chicory root juices under study. As can be seen, pressure application increased the L^* value ($p < 0.01$, Table 2). However, as the pressure level increased, the L^* (lightness) value decreased, so among all the treatments, the highest value was determined in the 50 MPa group, while the lowest value was determined in the 150 MPa group ($p < 0.05$, Fig. 4). In a study on cloudy honey peach juice, the applied pressure of 20–40 MPa significantly increased the L^* value [33]. The researchers stated that this increase was due to the stabilization of the product by decreasing the centrifugation precipitating rates (13.49–24.22%) and the mean particle diameter (from 1853.67 nm to 501.10–665.27 nm) at this pressure compared to the control. Our results clearly show a negative effect of high levels of pressure (over 50 MPa) on the L^* value.

An important color criterion that varies depending on fruit juice characteristics is the $+a^*$ value, which indicates redness. This value is associated with the structure and form of phenolic components in the fruit or its roots. Phenolic components, especially anthocyanins, affect the $+a^*$ value depending on pH [38]. The leaves of *Cichorium intybus* L. are a good source of phenolic compounds of high medicinal importance [39]. High-pressure application, which is a non-thermal technique, also increases the redness value by providing more release of

Table 2 Effects of different treatments on instrumental color values of chicory root juice samples

Treatment	L^*	a^*	b^*	a^*/b^*	Chroma (C^*)	Hue angle (h°)
ULTRA-TURRAX	24.23 ± 0.95	3.99 ± 0.30	9.94 ± 0.67	0.40 ± 0.04	10.76 ± 0.64	68.19 ± 2.24
Water bath	23.94 ± 0.63	3.24 ± 0.11	10.49 ± 0.55	0.31 ± 0.02	10.98 ± 0.53	72.80 ± 0.98
Control (0 MPa)	26.59 ± 1.28	4.51 ± 0.23	14.11 ± 1.09	0.32 ± 0.03	14.84 ± 0.12	72.13 ± 1.58
50 MPa	27.38 ± 0.82	4.38 ± 0.17	15.12 ± 0.79	0.29 ± 0.02	15.75 ± 0.74	73.80 ± 1.13
100 MPa	25.64 ± 0.92	4.86 ± 0.09	13.61 ± 0.98	0.36 ± 0.03	14.46 ± 0.87	70.26 ± 1.38
150 MPa	24.21 ± 0.39	4.48 ± 0.10	11.45 ± 0.51	0.39 ± 0.01	12.29 ± 0.51	68.61 ± 0.52
200 MPa	25.15 ± 0.88	4.99 ± 0.09	12.92 ± 0.94	0.39 ± 0.03	13.86 ± 0.94	68.80 ± 1.26
SEM	0.262	0.057	0.273	0.008	0.253	0.416
p -value	< 0.0001	< 0.0001	< 0.0001	< 0.0001	< 0.0001	< 0.0001

**Figure 4** Effects of ultra-high-pressure homogenization on the L^* value of chicory root juice samples. UT – after homogenization with ULTRA-TURRAX; WB – after keeping in a water bath and mixing; C – control (0 MPa). Different letters indicate statistical difference ($p < 0.05$)**Figure 5** Effects of ultra-high-pressure homogenization on the a^* value of chicory root juice samples. UT – after homogenization with ULTRA-TURRAX; WB – after keeping in a water bath and mixing; C – control (0 MPa). Different letters indicate statistical difference ($p < 0.05$)**Figure 6** Effects of ultra-high-pressure homogenization on the b^* value of chicory root juice samples. UT – after homogenization with ULTRA-TURRAX; WB – after keeping in a water bath and mixing; C – control (0 MPa). Different letters indicate statistical difference ($p < 0.05$)

anthocyanins from the tissue [34, 40]. In line with this literature, we also found that high-pressure homogenization affected the a^* value ($p < 0.01$, Table 2). Even higher a^* values were determined in the chicory root juices subjected to 100 and 200 MPa pressure treatments compared to the control ($p < 0.05$, Fig. 5). No significant difference was observed between the control, 50 and 150 MPa groups ($p > 0.05$). Another study determined

the effects of ultra-high-pressure homogenization and low temperature on the quality of fresh pomegranate juice [40]. The researchers stated that the a^* value increased from 5.31 ± 0.38 in the control to 5.61 ± 0.55 and 6.35 ± 0.23 in the 100 and 150 MPa groups, respectively.

Different levels of high-pressure homogenization of chicory root juices also affected their b^* values ($p < 0.01$, Table 2). The highest b^* values were detected in the 50 MPa group, while lower values were determined in the 100, 150, and 200 MPa groups compared to the control ($p < 0.05$, Fig. 6). As expected, ultra-high-pressure homogenization had very significant effects on the a^*/b^* ratio in the chicory root juices ($p < 0.01$, Table 2). This ratio was significantly higher in the 150 and 200 MPa groups than in the 50 MPa and the control groups ($p < 0.05$, Fig. 7).

Chroma, hue angle (h°), and total color difference (ΔE) parameters are calculated using L^* , a^* , and b^* values. In food science, these parameters are generally used to determine color changes in fresh food and food processed by different methods. In our study, ultra-high-pressure homogenization affected the chroma values of the chicory root juice samples ($p < 0.01$, Table 2), which indicate the degree of intensity or purity of color. We found that the chroma values decreased according to the applied pressure level ($p < 0.05$), with the lowest value recorded in the 150 MPa treatment group (Fig. 8). As

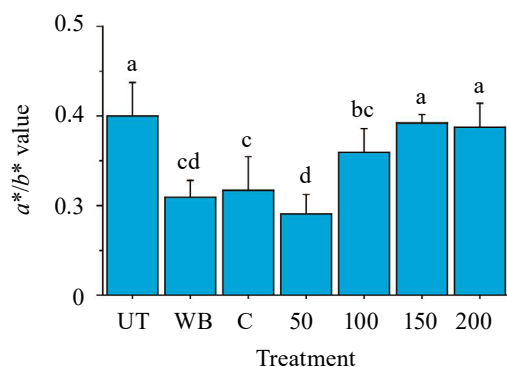


Figure 7 Effects of ultra-high-pressure homogenization on the a^*/b^* ratio of chicory root juice samples. UT – after homogenization with ULTRA-TURRAX; WB – after keeping in a water bath and mixing; C – control (0 MPa). Different letters indicate statistical difference ($p < 0.05$)

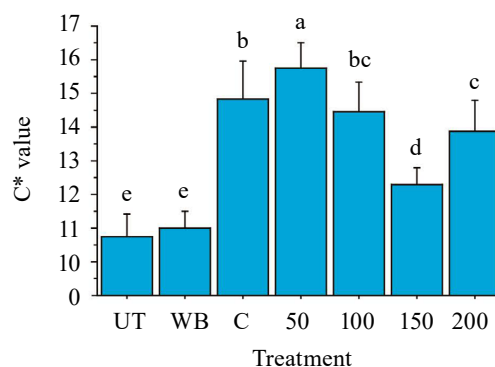


Figure 8 Effects of ultra-high-pressure homogenization on the Chroma (C^*) value of chicory root juice samples. UT – after homogenization with ULTRA-TURRAX; WB – after keeping in a water bath and mixing; C – control (0 MPa). Different letters indicate statistical difference ($p < 0.05$)

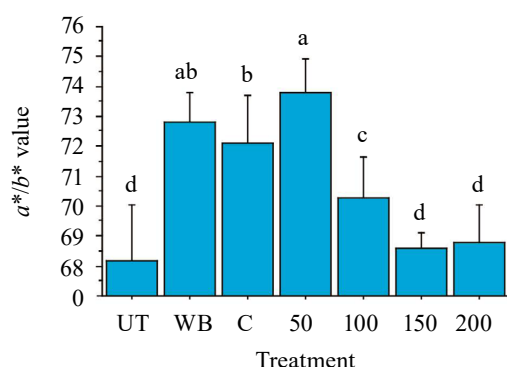


Figure 9 Effects of ultra-high-pressure homogenization on the hue angle (h°) value of chicory root juice samples. UT – after homogenization with ULTRA-TURRAX; WB – after keeping in a water bath and mixing; C – control (0 MPa). Different letters indicate statistical difference ($p < 0.05$)

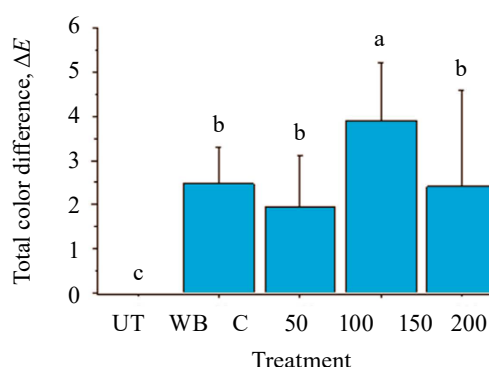


Figure 10 Effects of ultra-high-pressure homogenization on total color difference values of chicory root juice samples. UT – after homogenization with ULTRA-TURRAX; WB – after keeping in a water bath and mixing; C – control (0 MPa). Different letters indicate statistical difference ($p < 0.05$)

Table 3 Effects of ultra-high-pressure homogenization on total color difference values of chicory root juice samples

Treatment	Total color difference (ΔE)
Control (0 MPa)	0
50 MPa	2.47 ± 0.84
100 MPa	1.94 ± 1.19
150 MPa	3.91 ± 1.32
200 MPa	2.41 ± 2.17
SEM	0.252
p -value	< 0.0001

SEM: Standard error of the mean

with the chroma parameter, ultra-high-pressure homogenization also affected the h° value very significantly ($p < 0.01$, Table 2). Generally, a gradual decrease in h° values was determined in the groups according to the levels of pressure ($p < 0.05$), indicating decoloration from red to yellow. However, this decrease was less pronounced in the 50 MPa group, compared to the control, because the 50 MPa group had the highest h° values among all the samples ($p < 0.05$, Fig. 9).

The total color difference (ΔE) between the control group (0 MPa) and the samples homogenized with high pressure is presented in Table 3. This parameter is mostly used to detect color changes in processed foods. Compared to the control sample, higher ΔE values indicate higher color differences [41, 42]. In this study, we found significant differences in ΔE between the control and high-pressure treatment groups ($p < 0.01$, Table 3). The highest value was determined in the 150 MPa group ($p < 0.05$), with no statistical difference between the other treatment groups ($p > 0.05$, Fig. 8).

Another study determined the combined effects of short-wave ultraviolet radiation and ultra-high-pressure homogenization on the properties of cloudy apple juice [43]. The authors reported that the ΔE value increased with the pressure applied to apple juice. Changes in the structure of pigments cause visible color changes during food processing, especially in fruits, vegetables, and beverages. In our study, the increase in the a^* value is an important cause for the change in ΔE . Tiwari *et al.* and Patras *et al.* classified the differences in perceptible color as very distinct ($\Delta E > 3$), distinct ($1.5 < \Delta E < 3$), and minor differences ($0.5 < \Delta E < 1.5$) [44, 45].

According to our results, there were significant changes in the 150 MPa treatment group and significant changes in the 50, 100, and 200 MPa treatments (Fig. 10). Similarly, Saricaoglu *et al.* found that the ΔE value increased depending on the applied pressure and multi-pass high-pressure homogenization in rosehip (*Rosa canina* L.) nectar [46]. Also, a research on pear juice found that when the total color difference (ΔE) was less than 2, there was no visually noticeable color change in the product [30]. These results show that the effect of ultra-high-pressure homogenization on the total color difference (ΔE) may vary depending on the raw material, the density of color pigments in the raw material, the temperature applied, and the process conditions.

CONCLUSION

In this research, we determined the effects of ultra-high-pressure homogenization on some quality characteristics of chicory root juice. An important result was the increase in total soluble solids, depending on the pressure level applied, due to the disintegration of macromolecules in chicory juice. Since chicory roots are a good source of inulin, its extraction can be increased by applying ultra-high-pressure homogenization. Based on our results, the quality characteristics of chicory root juice treated with

ultra-high-pressure homogenization should be determined in detail with different analyses (total sugar, reducing sugar, particle size, inulin, phenolic components, etc.). In addition, it would be useful to further investigate the color and storage stability of chicory root juice prepared by using ultra-high-pressure homogenization.

CONTRIBUTION

M.I. Aksu and H.I. Erkovan developed the research concept and design, collected and analyzed the material, processed the data statistically, as well as wrote and edited the manuscript. S. Erkovan performed the analysis, and all the authors approved the final version of the article.

CONFLICT OF INTEREST

The authors declare that there is no conflict of interest.

FUNDING

This study was funded by the authors, with no support from any funding agency. The study was carried out in the research laboratories of the Department of Field Crops and Food Engineering, the Faculty of Agriculture, Eskişehir Osmangazi University.

REFERENCES


1. Kiers AM, Mes THM, van der Meijden R, Bachmann K. Morphologically defined *Cichorium* (Asteraceae) species reflect lineages based on chloroplast and nuclear (ITS) DNA data. *Systematic Botany*. 1999;24(4):645–659. <https://doi.org/10.2307/2419648>
2. Franck A, de Leenheer L. Inulin. *Biopolymers Online*. Weinheim: Wiley-VCH Verlag GmbH and Co. KGaA; 2005.
3. Kusova IU, Ildirova SK, Fedotova NA, Bystrov DI. Pâté with inulin supplement. *Food Processing: Techniques and Technology*. 2022;52(2):344–349. (In Russ.). <https://doi.org/10.21603/2074-9414-2022-2-2368>
4. Chen J, Chen X, Ho CL. Recent development of probiotic *Bifidobacteria* for treating human diseases. *Frontiers in Bioengineering and Biotechnology*. 2021;9:770248. <https://doi.org/10.3389/fbioe.2021.770248>
5. Yin H, Lin X. Research progress of inulin and oligofructose. *China Food Additives*. 2008;3:97–101.
6. Cabezas MJ, Rabert C, Bravo S, Shene C. Inulin and sugar contents in *Helianthus tuberosus* and *Cichorium intybus* tubers: Effect of postharvest storage temperature. *Journal of Food Science*. 2002;67(8):2860–2865. <https://doi.org/10.1111/j.1365-2621.2002.tb08829.x>
7. Wu H, Li W, Dai Z, Hu T. A review of research and the development of chicory products in China. *Forum of Development on Pratacultura Science in China 2008*, Xiameng, China. 2008.
8. Raulier P, Maudoux O, Notte C, Draye X, Bertin P. Exploration of genetic diversity within *Cichorium endivia* and *Cichorium intybus* with focus on the gene pool of industrial chicory. *Genetic Resources and Crop Evolution*. 2016; 63:243–259. <https://doi.org/10.1007/s10722-015-0244-4>
9. Nwafor IC, Shale K, Achilonu MC. Chemical composition and nutritive benefits of chicory (*Cichorium intybus*) as an ideal complementary and/or alternative livestock feed supplement. *The Scientific World Journal*. 2017;2017:7343928. <https://doi.org/10.1155/2017/7343928>
10. Figueira GM, Park KJ, Brod RPF, Honorio SL. Evaluation of desorption isotherms, drying rates and inulin concentration of chicory roots (*Cichorium intybus* L.) with and without enzymatic inactivation. *Journal of Food Engineering*. 2004;63(3):273–280. <https://doi.org/10.1016/j.jfoodeng.2003.06.001>
11. Kam N, Kanberoglu GS. Chemical analysis and fatty acid composition of the chicory plants (*Cichorium intybus* L.) by GC-MS. *Journal of Engineering Technology and Applied Sciences*. 2019;4(2):51–62. <https://doi.org/10.30931/jetas.588102>
12. Khalaf AH, El-Saadani RM, El-Desouky AI, Abdeldaiem HM, Elmehy EM. Antioxidant and antimicrobial activity of gamma-irradiated chicory (*Cichorium intybus* L.) leaves and roots. *Journal of Food Measurement and Characterization*. 2018;12:1843–1851. <https://doi.org/10.1007/s11694-018-9798-0>


13. Chandra K, Khan W, Jetty S, Ahmad S, Jain SK. Antidiabetic, toxicological, and metabolomic profiling of aqueous extract of *Cichorium intybus* seeds. *Pharmacognosy Magazine*. 2018;14:S377–S383.
14. Saeed M, El-Hack MEA, Alagawany M, Arain MA, Arif M, Mirza MA, et al. Chicory (*Cichorium intybus*) herb: Chemical composition, pharmacology, nutritional and health applications. *International Journal of Pharmacology*. 2017;13(4):351–360. <https://doi.org/10.3923/ijp.2017.351.360>
15. Fan H, Chen J, Lv H, Ao X, Wu Y, Ren B, et al. Isolation and identification of terpenoids from chicory roots and their inhibitory activities against yeast α -glucosidase. *European Food Research and Technology*. 2017;243:1009–1017. <https://doi.org/10.1007/s00217-016-2810-1>
16. Foster JG, Fedders JM, Clapham WM, Robertson JW, Bligh DP, Turner KE. Nutritive value and animal selection of forage chicory cultivars grown in Central Appalachia. *Agronomy Journal*. 2002;94:1034–1042. <https://doi.org/10.2134/AGRONJ2002.1034>
17. Lightowler H, Thondre S, Holz A, Theis S. Replacement of glycaemic carbohydrates by inulin-type fructans from chicory (oligofructose, inulin) reduces the postprandial blood glucose and insulin response to foods: report of two double-blind, randomized, controlled trials. *European Journal of Nutrition*. 2018;57:1259–1268. <https://doi.org/10.1007/s00394-017-1409-z>
18. Cilla A, Perales S, Lagarda MJ, Barberá R, Clemente G, Farré R. Influence of storage and in vitro gastrointestinal digestion on total antioxidant capacity of fruit beverages. *Journal of Food Composition and Analysis*. 2011;24(1): 87–94. <https://doi.org/10.1016/j.jfca.2010.03.029>
19. Alexandre EMC, Silva S, Santos SAO, Silvestre AJD, Duarte MF, Saraiva JA, et al. Antimicrobial activity of pomegranate peel extracts performed by high pressure and enzymatic assisted extraction. *Food Research International*. 2019;115:167–176. <https://doi.org/10.1016/j.foodres.2018.08.044>
20. Aksu MI, Turan E. Effects of lyophilized black carrot (*Daucus carota* L.) water extract on the shelf life, physico-chemical and microbiological quality of high-oxygen modified atmosphere packaged (HiOx-MAP) ground beef. *Journal of Food Science and Technology*. 2021;58:3514–3524. <https://doi.org/10.1007/s13197-021-05044-1>
21. Cheng J, Li J, Xiong R-G, Wu S-X, Huang S-Y, Zhou D-D, et al. Bioactive compounds and health benefits of pomegranate: An updated narrative review. *Food Bioscience*. 2023;53:102629. <https://doi.org/10.1016/j.fbio.2023.102629>
22. Augusto PED, Tribst AAL, Cristianini M. High hydrostatic pressure and high-pressure homogenization processing of fruit juices. In: Rajauria G, Tiwari BK. *Fruit juices. Extraction, composition, quality and analysis*. Academic Press; 2018. pp. 393–421. <https://doi.org/10.1016/B978-0-12-802230-6.00020-5>
23. Levy R, Okun Z, Shpigelman A. High-pressure homogenization: Principles and applications beyond microbial inactivation. *Food Engineering Reviews*. 2021;13:490–508. <https://doi.org/10.1007/s12393-020-09239-8>
24. Su D, Zhu X, Wang Y, Li D, Wang L. Effect of high-pressure homogenization on rheological properties of citrus fiber. *LWT*. 2020;127:109366. <https://doi.org/10.1016/j.lwt.2020.109366>
25. Malik T, Sharma R, Ameer K, Bashir O, Amin T, Manzoor S, et al. Potential of high-pressure homogenization (HPH) in the development of functional foods. *International Journal of Food Properties*. 2023;26(1):2509–2531. <https://doi.org/10.1080/10942912.2023.2249262>
26. Heidary A, Soltanizadeh N. The effects of high-pressure homogenization on physicochemical and functional properties of gelatin. *Food and Bioprocess Technology*. 2024;17:100–122. <https://doi.org/10.1007/s11947-023-03113-1>
27. Zheng X, Chen Z, Guo Z, Chen M, Xie B, Sun Z, et al. Effect of novel processing techniques on the carotenoid release during the production of red guava juice. *Molecules*. 2024;29(2):487. <https://doi.org/10.3390/molecules29020487>
28. Dave J, Kumar N, Upadhyay A, Purba DT, Kudre T, Nukthamna P, Sa-nguanpuag S, et al. Sustainable fish oil extraction from catfish visceral biomass: A comparative study between high-shear homogenization and high-frequency ultrasound on wet rendering process. *Foods and Raw Materials*. 2025;13(1):94–106. <https://doi.org/10.21603/2308-4057-2025-1-627>
29. Sun C, Hu Y, Yu X, Zhu Z, Hao S, Du X. Morphological, structural and physicochemical properties of rice starch nanoparticles prepared via ultra-high pressure homogenization. *International Journal of Food Engineering*. 2021; 17(12):981–988. <https://doi.org/10.1515/ijfe-2021-0186>
30. Liu Y, Liao M, Rao L, Zhao L, Wang Y, Liao X. Effect of ultra-high pressure homogenization on microorganism and quality of composite pear juice. *Food Science and Nutrition*. 2022;10:3072–3084. <https://doi.org/10.1002/fsn3.2906>
31. Aksu MI, Turan E, Gülbandır A, Tamtürk F. Utilization of spray-dried raspberry powder as a natural additive to improve oxidative stability, microbial quality and overcome the perception of discoloration in vacuum-packed ground beef during chilled storage. *Meat Science*. 2023;197:109072. <https://doi.org/10.1016/j.meatsci.2022.109072>
32. Liu Q, Huang G, Ma C, Li G, Wang R. Effect of ultra-high pressure and ultra-high temperature treatments on the quality of watermelon juice during storage. *Journal of Food Processing and Preservation*. 2021;45:e15723. <https://doi.org/10.1111/jfpp.15723>

33. Yan C, Jiayan G, Xiaoting X, Xudong L, Haitao S, Wenwen D, et al. Effect of high pressure homogenization on the stability and quality of not-from-concentrate cloudy honey peach (*Prunus persica* L.) juice. *Science Technology Food Industry*. 2022;18:322–330. <https://doi.org/10.13386/j.issn1002-0306.2021110085>
34. Karacam CH, Sahin S, Oztop MH. Effect of high pressure homogenization (microfluidization) on the quality of Ottoman Strawberry (*F. Ananassa*) juice. *LWT – Food Science and Technology*. 2015;64(2):932–937. <https://doi.org/10.1016/j.lwt.2015.06.064>
35. Turan E, Aslantaş R, Bilgin J, Aksu MI. High pressure homogenization of pomegranate juice: Impact on physico-chemical, antioxidant, antimicrobial and in vitro bioaccessibility properties. *Food Science & Nutrition*. 2024; <https://doi.org/10.1002/fsn3.4571>
36. Gul O, Saricaoglu FT, Mortas M, Atalar I, Yazici F. Effect of high pressure homogenization (HPH) on microstructure and rheological properties of hazelnut milk. *Innovative Food Science and Emerging Technologies*. 2017;41:411–420. <https://doi.org/10.1016/j.ifset.2017.05.002>
37. Wellala CKD, Bi J, Liu X, Liu J, Lyu J, Zhou M. Effect of high-pressure homogenization on mixed juice stability, rheology, physicochemical properties and microorganism reduction. *Journal of Food Science and Technology*. 2020;57:1944–1953. <https://doi.org/10.1007/s13197-019-04230-6>
38. Aksu MI, Turan E, Sat IG. Effects of lyophilized red cabbage water extract and pH levels on the quality properties of pastırma cemen paste during chilled storage. *Journal of Stored Products Research*. 2020;89:101696. <https://doi.org/10.1016/j.jspr.2020.101696>
39. Dzharov VV, Mishra AP, Shariati MA, Atanassova MS, Plygun S. Phytochemical contents in solid–liquid extraction of aqueous alcoholic extract of chicory (*Cichorium intybus* L.) leaves. *Foods and Raw Materials*. 2016;4(2):32–37. <https://doi.org/10.21179/2308-4057-2016-2-32-37>
40. Benjamin O, Gamrasni D. Microbial, nutritional, and organoleptic quality of pomegranate juice following high pressure homogenization and low temperature pasteurization. *Journal of Food Science*. 2020;85(3):592–599. <https://doi.org/10.1111/1750-3841.15032>
41. Shewale SR, Hebbar HU. Effect of infrared pretreatment on low-humidity air drying of apple slices. *Drying Technology*. 2017;35(4):490–499. <https://doi.org/10.1080/07373937.2016.1190935>
42. Bahriye G, Dadashi S, Dehghannya J, Ghaffari H. Influence of processing temperature on production of red beetroot powder as a natural red colorant using foam-mat drying: Experimental and modeling study. *Food Science and Nutrition*. 2023;11:6955–6973. <https://doi.org/10.1002/fsn3.3621>
43. Saucedo-Galvez JN, Codina-Torrella I, Martinez-Garcia M, Hernández-Herrero MM, Gervilla R, Roig-Sagués AX. Combined effects of ultra-high pressure homogenization and short-wave ultraviolet radiation on the properties of cloudy apple juice. *LWT*. 2021;136:110286. <https://doi.org/10.1016/j.lwt.2020.110286>
44. Tiwari BK, Muthukumarappan K, O'Donnell CP, Cullen PJ. Effects of sonication on the kinetics of orange juice quality parameters. *Journal of Agricultural Food Chemistry*. 2008;56(7):2423–2428. <https://doi.org/10.1021/jf073503y>
45. Patras A, Brunton NP, Tiwari BK, Butler F. Stability and degradation kinetics of bioactive compounds and colour in strawberry jam during storage. *Food and Bioprocess Technology*. 2011;4:1245–1252. <https://doi.org/10.1007/s11947-009-0226-7>
46. Saricaoglu FT, Atalar I, Yilmaz VA, Odabas HI, Gul O. Application of multi pass high pressure homogenization to improve stability, physical and bioactive properties of rosehip (*Rosa canina* L.) nectar. *Food Chemistry*. 2019;282: 67–75. <https://doi.org/10.1016/j.foodchem.2019.01.002>

ORCID IDs

Muhammet Irfan Aksu  <https://orcid.org/0000-0001-9391-6955>

Halil İbrahim Erkovan  <https://orcid.org/0000-0001-8511-0791>

Sule Erkovan  <https://orcid.org/0000-0001-6235-6000>



Aurelia aurita jellyfish collagen: Recovery properties

Noora Barzkar¹, Stanislav A. Sukhikh^{2,*}, Anastasiia V. Zhikhreva²,
Elizaveta Yu. Cheliubeeva², Anastasia I. Kapitunova², Danil I. Malkov²,
Olga O. Babich², Yuliya V. Kulikova²

¹ University Malaysia Sabah, Kota Kinabalu, Malaysia

² Immanuel Kant Baltic Federal University, Kaliningrad, Russia

* e-mail: stas-asp@mail.ru

Received 02.05.2024; Revised 28.05.2024; Accepted 04.06.2024; Published online 23.10.2024

Abstract:

Wound and burn healing is a complex physiological process that can be facilitated by medications based on marine collagen. In this regard, biomass of the *Aurelia aurita* jellyfish is a promising alternative source of medical collagen. As the global incidence of burns and wounds continues to grow, new healing methods have become a relevant area of medical science.

This study featured acetic acid as a means of marine collagen extraction from *A. aurita* biomass. The physical and chemical properties of jellyfish collagen were determined gravimetrically and included such indicators as water solubility and water holding capacity. The molecular weight was defined by gel electrophoresis. The spectral studies relied on the method of UV spectroscopy. The regenerative experiments included such parameters as cytotoxicity, antioxidant properties, adhesion, and wound healing rate, as well as a quantitative PCR analysis.

The optimal conditions for maximal collagen yield were as follows: 0.5 M acetic acid and 48 h extraction time. However, the collagen yield was very low ($\leq 0.0185\%$). The high water holding capacity showed good prospects for *A. aurita* collagen to be used as hemostatic sponge. The acid-soluble collagen sample had a molecular weight of 100–115 kDa, which made it possible to classify it as type I. *A. aurita* jellyfish collagen revealed no cytotoxic properties; it had no effect on adhesion, migration, and proliferation of keratinocytes, neither did it affect the expression of cell differentiation markers.

The wound healing model proved that the marine collagen had regenerative properties as it was able to increase the wound healing rate by 24.5%. Therefore, collagen extracted from the biomass of *A. aurita* jellyfish demonstrated good prospects for cosmetology and regenerative medicine.

Keywords: *Aurelia aurita*, jellyfish, marine collagen, biological activity, regenerative properties, cytotoxicity, extraction, regenerative medicine

Funding: The research was supported by the Ministry of Science and Higher Education of the Russian Federation (Minobrnauki), contract no. 075-15-2023-601 (external no. 13.2251.21.0219).

Please cite this article in press as: Barzkar N, Sukhikh SA, Zhikhreva AV, Cheliubeeva EYu, Kapitunova AI, Malkov DI, *et al.* *Aurelia aurita* jellyfish collagen: Recovery properties. Foods and Raw Materials. 2025;13(2):296–305. <https://doi.org/10.21603/2308-4057-2025-2-648>

INTRODUCTION

Burn injuries and wounds are a major global health issue. High temperatures, accidents, surgery, and infections damage skin structure and function, which makes wound healing a complex physiological process [1].

Silver sulfadiazine and mafenide acetate are popular medications against wounds and burns. However, they are expensive and may cause severe side effects. Moreover, they are not effective against deep burn wounds and often cause scarring. As a result, novel burn-treating substances are a relevant medical issue [2].

The second half of the XX century witnessed a great progress in regenerative medicine and burn therapy. For instance, pharmacotherapy with tissue scaffolds promote the formation of new viable human tissues, offering an alternative to donor tissues. Unfortunately, the use of skin substitutes is limited by immunogenicity, postoperative infections, and donor site area [3].

Collagen is a promising wound healing biomaterial. However, collagen and its derivatives are usually obtained from swine and bovine skins and bones, which means a certain risk of transmissible spongiform

encephalopathy. Religious restrictions also limit the use of biomaterials obtained from pigs and cows [4].

Fish, jellyfish, sponges, and other marine invertebrates can serve as an alternative source of collagen. Their biocompatibility is quite high, and they do not transmit diseases to humans [5]. Collagens isolated from marine organisms make excellent scaffolds with high biodegradability and low immunogenicity [6].

Jellyfish is a biomass that consists of proteins organized into a complex polymer, i.e., collagen. Fibrillar collagen is the most abundant component in most jellyfish [7]. Jellyfish tissue structure resembles that of human skin tissue, which makes marine jellyfish a popular subject of scientific research [8]. Unlike mammalian collagens, jellyfish collagen does not transmit spongiform encephalopathy. Jellyfish collagen extracts are known to stimulate the immune response *in vivo* without causing allergy [1].

In addition, jellyfish collagen peptides accelerate the healing of skin wounds. In the future, they may render new wound treatment medications [9]. Jellyfish collagen peptides are a source of bioactive compounds, polysaccharide structures, and extracts, which makes jellyfish a potential raw material in medical therapy and tissue engineering, e.g., biomaterials, new pharmaceuticals, and nutraceuticals [1].

Despite all their numerous benefits, modern medicine still possesses very limited data on collagen peptides derived from *Aurelia aurita* or their effect on wound healing. *A. aurita* is a species of *Scyphozoa* jellyfish [10]. These marine creatures have a translucent pinkish body that consists of a flat bell of up to 40 cm across and numerous short tentacles [11]. They inhabit sea waters with consistent currents and temperatures from -6 to 31°C , the optimal temperatures being 9 – 19°C . *A. aurita* are so common in Russia that they may affect human activities in coastal areas [12–14]. For instance, they sting tourists, thus causing harm to local tourism

when their population increases as a result of climate change, eutrophication, or life cycle patterns [1]. Jellyfish are often discarded as waste in commercial fishing. Therefore, *A. aurita* biomass can become a valuable raw material for collagen without causing damage to the environment.

This study assesses the most popular method of collagen extraction from *A. aurita*, as well as the physicochemical composition and biochemical properties of collagen obtained.

STUDY OBJECTS AND METHODS

Research objects. The study featured *Aurelia aurita* fished in the coastal areas of the Baltic Sea, Kaliningrad Region, Russia, where they migrate to, following seasonal patterns. Previously, vacationers and residents reported that this type of jellyfish washed on shore in masses in the third decade of August or early in September. As the weather pattern changes, mass strandings of *A. aurita* now occur in different periods. In 2020, it happened in December; in 2023, it occurred in the third decade of September.

We obtained 140 kg raw jellyfish biomass manually in the sea near the town of Pionersky (Fig. 1), using a fish net (Fig. 2). The samples were placed in sealed ten-liter containers and delivered to the laboratory within 2 h. There, we washed the jellyfish with fresh water to remove sand and foreign matter and weighed the total mass within 0.1 g. We measured the average bell size since the bell is responsible for up to 97% of biomass. We decided not to separate oral arms as this manipulation was found too labor-intensive for commercial processing. After washing, the jellyfish were frozen at -79°C in plastic containers or zip-bags.

Collagen extraction methods. Obtaining acid-soluble collagen from *Aurelia aurita* jellyfish. Collagen was extracted with acid following the protocol

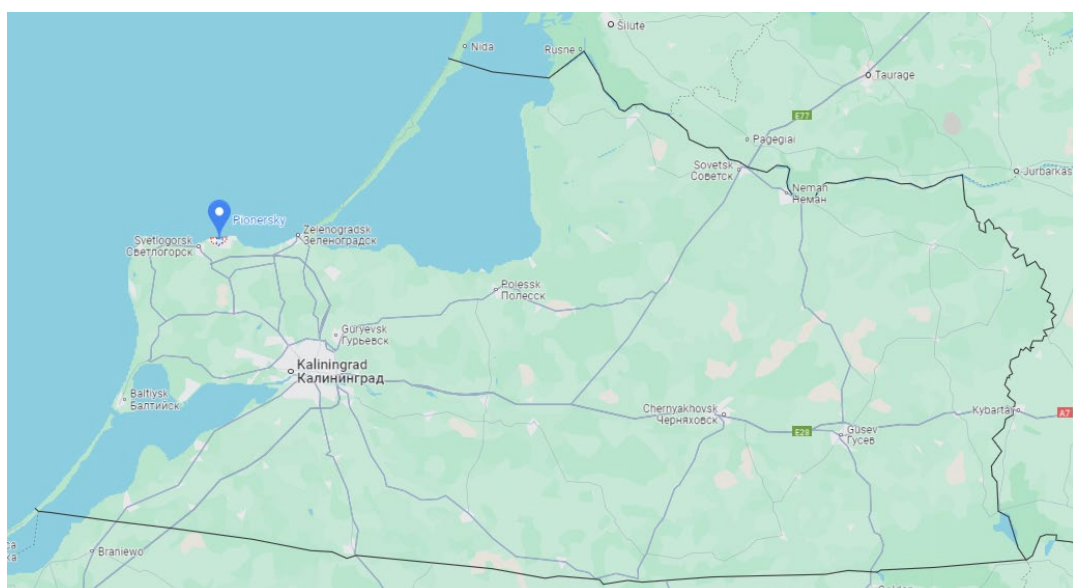


Figure 1 *Aurelia aurita* catching site on the Baltic Sea coast near the town of Pionersky (54.955098, 20.227932)

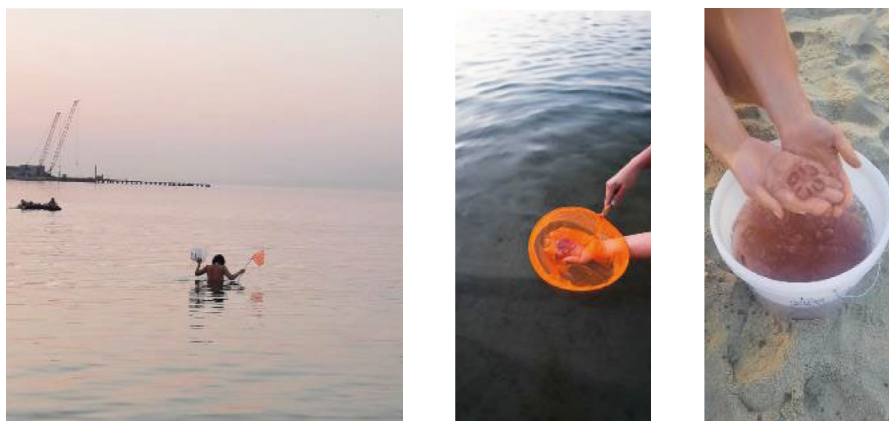


Figure 2 Fishing for *Aurelia aurita*



Figure 3 Filtering post-hydrolysis solution through gauze

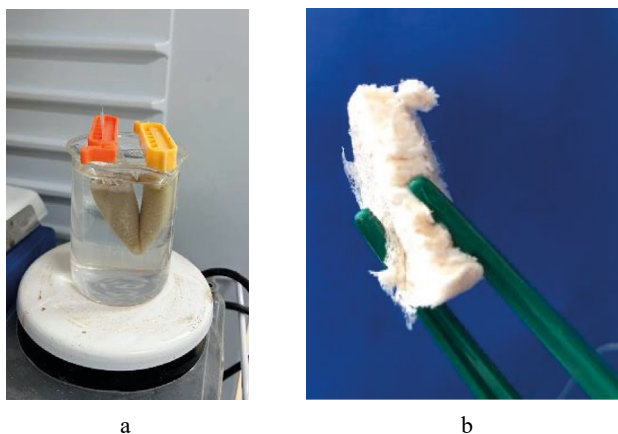


Figure 4 Dialysis of the resulting collagen against a solution of acetic acid (a) and the sponge obtained after freeze-drying (b)

described by Nagai *et al.* [15]. Crushed jellyfish biomass was placed in a flask and subjected to extraction with 0.5 M acetic acid in a ratio of 1:10 (w/v). The extraction process lasted three days at 4°C. After filtration, the insoluble residue underwent another extraction. After two extractions, we brought the filtrates (Fig. 3) to 0.9% with sodium chloride and separated precipitate by centrifugation at 3600 g for 15 min. After dissolving it in 0.5 M acetic acid, we dialyzed the obtained samples using 0.1 M acetic acid for three days, followed by

dialysis with distilled water for another three days (Fig. 4a). The final solution was lyophilized to obtain acid-soluble collagen (Fig. 4b).

Assessing collagen properties. Solubility. The lyophilized collagen samples were dispersed at room temperature in such solvents as 96% ethanol, methanol, ethyl acetate, n-hexane, methylene chloride, double-distilled water, 0.5 M acetic acid, aqueous solutions of sodium hydroxide (pH 12), 37% hydrochloric acid, as well as 0.5 M acetic acid with ultrasonic treatment.

Water-holding capacity. We placed 0.05 g of lyophilized collagen in 15-mL centrifuge tubes and added 5 mL of distilled water. The resulting solution was suspended in a shaking incubator at 150 rpm for 15 min followed by a five-minute centrifugation. After removing supernatant with a dispenser, we weighed the tubes with wet collagen.

The water-holding capacity was calculated by the formula below:

$$\text{Water holding capacity} = \frac{m_{\text{wet}} - m_{\text{dry}}}{m_{\text{dry}}} \quad (1)$$

where m_{wet} is the mass of wet collagen and m_{dry} is the mass of dry collagen.

UV spectroscopy. Dry collagen was dissolved in 0.5 M acetic acid at room temperature at a concentration of 1 mg/mL. The spectral scanning involved a UV-1800 dual-beam spectrophotometer (Shimadzu, Japan) at 220–600 nm.

Molecular weight analysis. To measure the molecular weight, we dissolved 1 mL of dialyzed collagen in 0.5 M Tris-HCl buffer (pH 6.8, 1% SDS, 10% glycerol, 0.01% bromophenol blue). After denaturing the solution at 70–80°C for 5 min, we put 15 µL denatured sample and 7 µL marker with a molecular weight of 10–250 kDa into the wells at the top of the polyacrylamide gel (Protein Dual Color Standards, BioRad, USA). The polyacrylamide gel consisted of one-millimeter layers of 4% concentrating gel and 12.5% separating gel. In order to observe the separation of proteins by size, we raised the initial voltage of 15 mA (30 min) to 30 mA (1 h) after the proteins reached the separating layer. Upon separation, the gels were stained overnight with a dye solution, which consisted of 0.25% Coomassie Brilliant Blue

G-250 (JT Baker, USA), 10% acetic acid, 40% ethanol, and 50% de-ionized water. After being washed with a solution of 10% acetic acid, 40% ethanol, and 50% de-ionized water, the gels were incubated for 1 h.

Antioxidant activity. We applied two types of radicals, i.e., 2,2-diphenyl-1-picrylhydrazyl (DPPH) and 2,2'-azino-bis(3-ethylbenzothiazoline-6-sulfonic acid (ABTS). The procedure involved a CLARIOstar microplate reader (BMG Labtech GmbH, Germany). A Trolox solution (6-hydroxy-2,5,7,8-tetramethylchroman-2-carboxylic acid) of known concentration served as control. The test results were expressed in milligrams of Trolox equivalents per one gram of dry weight (mg TE/g).

To determine the antioxidant activity by the DPPH method, we mixed 20 µL of collagen solution with 300 µL of fresh 2,2-diphenyl-1-picrylhydrazyl solution (0.1 mM). The optical density was recorded at 515 nm.

To determine the antioxidant activity by the ABTS method, we added 20 µL of extract to 300 µL of ABTS radical cation. The ABTS radical included aliquots of a 7.0 mM ABTS solution (2,2'-azino-bis(3-ethylbenzothiazolino-6-sulfonic acid) and a 2.45 mM potassium persulfate solution. The incubation occurred in the dark at room temperature and lasted for 16 h. The optical density was measured at 734 nm.

Wound healing test in vitro. The lyophilized collagen was dissolved in 0.07% acetic acid at the rate of 2 µg per 1 mL of solution. Ten minutes of ultrasonic bath at room temperature improved the solubility.

To study the collagen sorption on cultural surface, we added collagen solutions in a volume sufficient to cover 2–3 mm of the wells and incubated them at 37°C for 15 min. After draining the collagen solution, we washed the wells three times with Hanks' solution with phenol red (PanEco, Russia).

HaCaT fibroblasts and keratinocytes were cultivated in a culture medium that consisted of Dulbecco's Modified Eagle Medium (DMEM) (PanEco, Russia), 10% fetal bovine serum (Hyclon, USA), 1% Glutamax (Gibco, USA), and 1% PenStrep (Gibco, USA). The cultivation process involved a CO₂ incubator (37°C). The medium changed every 2–3 days. Cultures were removed from the surface of culture flasks with a trypsin solution and Versene solution (1:2) (PanEco, Russia) as soon as the confluent layer was reached, i.e., every 3–4 days. The cell seeding had a ratio of 1:3 or 1:5, depending on the

growth rate. The experiments involved cultures of primary fibroblasts obtained at early (< 5) passages.

The scratch test was triplicated as follows: 155 000 HaCaT cells were planted in a 12-well plate with collagen. Type I collagen from rat tail tendons in 0.1% acetic acid served as positive control while empty wells served as negative control. On day 4, as the cell culture reached 100% confluence, we imitated a wound by scratching vertical lines with a Pasteur pipette in the center of each well, thus disrupting the integrity of the epithelial layer.

To assess the healing rate, we made phase contrast photographs of the cell culture immediately after scratching and on days 1, 2, and 3. We used an Olympus IX73 inverted microscope equipped with an Olympus U-TV0.63XC camera. The images were processed using Olympus cellSens Dimension, and the size of the wounds in the photographs was measured with ImageJ.

Quantitative polymerase chain reaction analysis (PCR). We applied ExtractRNA reagent (Evrogen, Russia) to isolate RNA and followed the protocol recommended by the manufacturer. The reverse transcription involved 1 µg of RNA. For the reverse transcription PCR test (RT-PCR), we used a standard qPCRmix-HS SYBR+LowROX kit (Evrogen, Russia) and a LightCycler 96 amplifier (Roche). The test pattern was triplicated as follows: 50 ten-minute cycles at 95°C; each cycle included 10 s at 95°C, 10 s at 60°C, and 20 s at 72°C. The content of products in each sample was determined by the 2-ΔΔCq method; the results were referenced to GAPDH (glyceraldehyde 3-phosphate dehydrogenase) expression (see Table 1 for primers).

Assessing cytotoxicity and adhesive properties. Primary human fibroblasts at a concentration of 66 000 cells per 1 mL were planted in a 24-well plate with collagen solution at the rate of 33 000 cells per well.

The cytotoxicity test presupposed live and dead cell counts after 48 h and involved a Luna-II counter (Logos Biosystems, South Korea) and staining with trypan blue.

After 10, 20, 30, 60 min, and 24 h, we conducted a cell count to define adhesive properties using the same Luna-II counter (Logos Biosystems, South Korea).

RESULTS AND DISCUSSION

Optimal extraction parameters. Acetic acid with a concentration of 0.2–0.5 M proved to be the most popular means of collagen extraction from marine

Table 1 Primer sequences

Gene	Forward primer	Reverse primer
KRT1	ACTTGATTGCTCCCTTTCTCG	TATGGTCCTGTCTGCCCTCC
KRT 5	CTCCTCGGTCCTCACCTCT	GGCTTTCCTGTCTGCCCTCC
KRT10	AAAGAGCCACCACTGAACCC	GGAGGAGTGTATCCCTAAGAA
KRT14	ATCTTGTA CTCTGGTTCTGCTG	GAGACCAAAGGTCGCTACTGC
FLG	CCAAACGCACTTGCTTTACAGATA	AGACATGGCAGCTATGGTAGTG
IVL	TTCCTCCTCCAGTCAATACCC	CATTCTTGCTCAGGCAGTCC
ITGA6	AAGCAGGAATCCCGAGACAT	TCTCAATCGCCCATCACAAA
ITGB4	TCCTTTGAGCAGCCTGAGTTC	CGGTAGGAGACCTGGGACTTC
GAPDH	CATCAAGAAGGTGGTGAAGCAG	TCAAAGGTGGAGGAGTGGGT

animal biomass; the most common extraction time was 24–72 h [15–19].

Table 2 shows the limits for acid concentration and treatment time.

Table 2 and Figs. 5–6 illustrate the results of acid extraction. The collagen yield grew from 143.5 ± 7.8 to 150.1 ± 5.4 mg/kg at 0.2 and 0.5 M acetic acid, respectively. A further increase in acid concentration by 0.1 M reduced the economic efficiency by 8000 rubles/g.

The maximal yield of 156.2 ± 8.8 mg collagen per 1 kg wet biomass occurred at 0.5 M acetic acid after 96 h.

The extraction time was an important variable: when it grew from 24 to 48 h, we observed a 17.4% increase in the yield. A further increase in extraction time, however, had no significant effect.

In this study, the maximal collagen yield reached 0.0156% jellyfish dry weight, which is in line with the data obtained by Addad *et al.*, who reported 0.01% collagen yield [20].

Physicochemical properties of collagen. Solubility.

No solvent used in this study was able to dissolve jellyfish collagen completely. The ultrasonic treatment was the only method that transformed collagen in acetic acid into a yellow cloudy solution, which eventually produced some precipitate of collagen. The tests with acidic media demonstrated partial dissolution of collagen.

Other researchers reported similar collagen properties. Swatschek *et al.* failed to dissolve sponge collagen in any of the solutions they applied [21]. They mentioned slight dispersion in solutions with pH 8–10 and hydrolysis of collagen fragments in an acidic environment. Ahmed *et al.* tested the solubility of collagen obtained from big-eyed tuna (*Thunnus obesus*) at different pH values with the Lowry protein assay [22]. They reported the highest solubility at pH = 6.

Water holding capacity. Collagen owes its water holding capacity properties due to its porous structure, which traps moisture in the fibers. Potentially, this parameter can be used to assess the hemostatic properties of jellyfish collagen [23]. In this research, the water holding capacity of *Aurelia aurita* collagen was 4.194 g/g. This value exceeds that for medical gauze (2 g/g) but comes short of collagen sponges from *Rhopilema esculentum* [24].

UV spectroscopy. Collagen has an absorption maximum in the range of 210–240 nm because it contains mainly glycine and hydroxyproline but no tryptophan. The collagen we obtained from *A. aurita* had its absorption maximum at 232 nm (Fig. 7), which is in line with other similar publications. The peak was quite homogeneous, which indicates purity.

In [25], collagen obtained from the skin of Pacific cod demonstrated its maximal absorption at 231 nm. In [26], collagen from catfish skin had it at 235 nm.

In collagen, absorption in the UV region is associated with COOH, CONH₂, and C=O in polypeptide chains. Tyrosine, tryptophan, and phenylalanine have their absorption maxima at 250–285 nm. The spectrum we obtained had no clear peak in this region, which indicates a low content of these amino acids.

Table 2 Extracting collagen with acid: experimental results

No.	Concentration of CH ₃ COOH and treatment time	Collagen yield, mg/kg wet jellyfish biomass
1	0.2 M, 48 h	143.5 ± 7.8
2	0.3 M, 48 h	144.7 ± 6.6
3	0.5 M, 48 h	150.1 ± 5.4
4	0.5 M, 24 h	127.8 ± 4.7
5	0.5 M, 72 h	153.3 ± 9.2
6	0.5 M, 96 h	156.2 ± 8.8

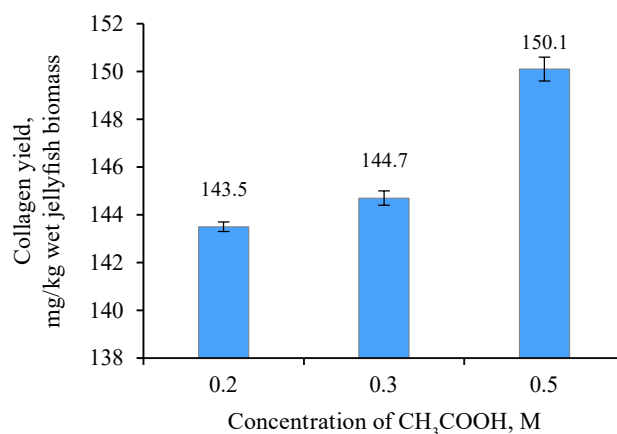


Figure 5 Collagen yield after acid extraction depending on acetic acid concentration

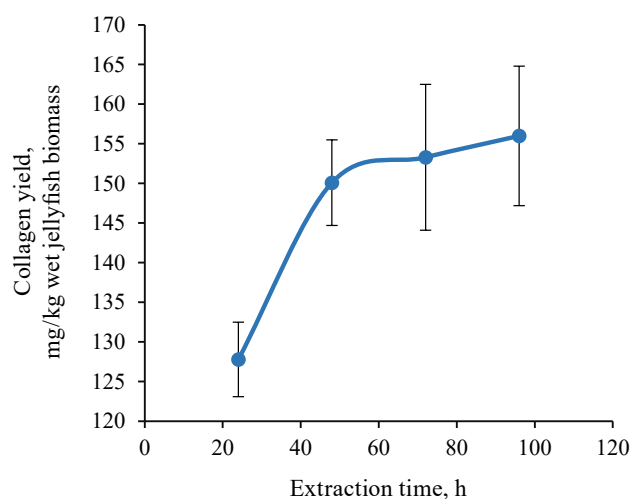


Figure 6 Collagen yield from acid extraction depending on extraction time

Molecular weight. Figure 8 illustrates the molecular weight of *A. aurita* collagen samples. For this test, we used native collagen, i.e., a sample dissolved in water, and a collagen solution obtained by sonicating a mix of collagen and 0.2 M acetic acid for 2 min.

The molecular weight of native collagen exceeded 250 kDa, which prevented the sample from advancing in the gel. The sample with acetic acid demonstrated two clear bands of 100 and 110 kDa.

To compare the proteins, we used PhotoMetrix 1.2.1, a free application that we downloaded from the Play Store

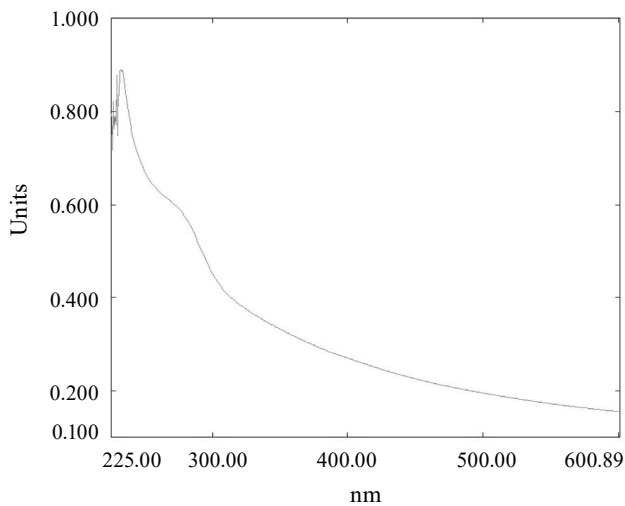


Figure 7 UV spectral profile of *Aurelia aurita* collagen

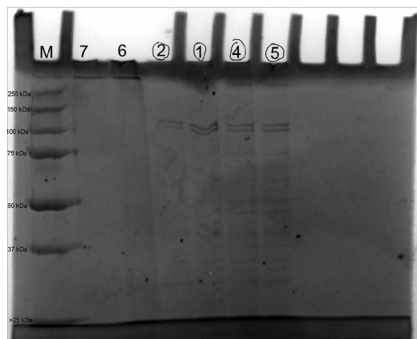


Figure 8 Electropherogram of *Aurelia aurita* collagen samples: the leftmost line is a protein marker with components of a known molecular weight (kDa); lines 7 and 6 are native collagen; lines 1–5 are *Aurelia aurita* collagen treated with ultrasound and 0.2 M acetic acid

to install on a smartphone (POCO ×3 Pro, China) [27]. The images were montaged; each band was quantified by the size of images captured from an area of 64×64 pixel. The application provided calibration curves by pre-entering the amount of protein at each point. A protein-free gel band was used for analytical testing. For accuracy, we scanned the same gel in Image Lab 6.0.1 (BioRad, USA) [28]. Then, we built a plot that demonstrated the effect of protein amount on band volume. The resulting linear regression produced calibration curves that made it possible to calculate the amount of protein in the sample. The calibration curves relied on albumin used at concentrations of 0–10 µg (Table 3).

The molecular weight of native collagen exceeded 250 kDa (lines 6 and 7), which made it insoluble in phosphate buffer (pH = 7.4). Samples 1–5 were essentially identical but with different concentrations of collagen solution in gel pockets: Table 3 shows the difference in the intensity of collagen bands of various masses.

We also analyzed the results of *A. aurita* mesoglea collagen electrophoresis. The samples consisted of $\alpha 1$ and $\alpha 2$ chains of 110 kDa at a ratio of approximately 2:1.

Table 3 Shares of proteins with different molecular weights in *Aurelia aurita* biomass

Molecular weight, kDa	Protein share by PhotoMetrix, %	Protein share by ImageLab, %
> 250	13.75	22.7
110	14.67	19.6
100	15.16	7.5
75	7.12	5.4
70	7.1	8.7
50	7.1	9.5
43	7.1	3.9
39	7.0	3.7
35	7.0	1.1
34	7.0	5.1
31	7.0	12.8

As for β and γ chains, they were located in the high molecular weight region of ≥ 250 kDa. As a result, the collagen samples could be classified as type I. Our results confirmed those obtained by other scientists, who also reported collagen of *Rhopilema esculentum* and *Nemopilema nomurai* as type I [24, 29]. Acid-soluble collagen had a molecular weight of 100–115 kDa.

Biological activity of collagen. Antioxidant properties. Collagen owes its antioxidant activity to its amino acid composition. In this study, however, *A. aurita* collagen demonstrated no antioxidant activity, probably, because we did not use collagen hydrolysate. Li *et al.*, who studied collagen hydrolysate from Spanish mackerel skin, reported good radical scavenging properties [30]. According to Gautam *et al.*, hydrolysis increased the antioxidant activity in collagen [31].

Adhesive and cytotoxic properties of collagen on primary human fibroblasts. The cytotoxicity assay showed that fibroblasts continued to grow for three days (Fig. 9).

Table 4 presents the results of a live cell count performed on an automatic counter by the trypan blue method.

A. aurita collagen improved the survival rate of fibroblast cells by 45.6%, probably, by activating different types of cellular receptors. Besides, the interaction of collagen with cells is known to depend on various growth factors and other modulations of the cytoskeletal complex [32].

In our case, the test on adhesive properties revealed no significant difference between the two samples (Table 5).

In this study, *A. aurita* collagen had no effect on the share of free cells, compared to the control sample. However, the method was not entirely accurate. In our future research, we will need to determine the number of attached live cells.

Regenerative properties of collagen on immortalized keratinocytes of HaCaT cells. Figure 10 shows that wound healing occurred in all collagen samples.

The wound healing rate represented as an average rate of cell migration into the wound had no significant difference between the *A. aurita* collagen sample and the control sample (Table 6).

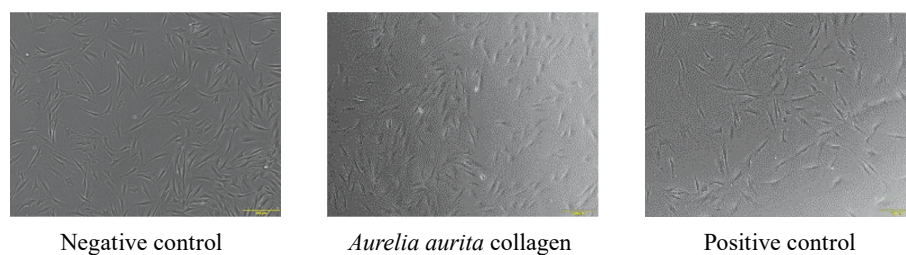


Figure 9 Fibroblasts growing on surfaces adsorbed with different collagen samples on cultivation day 3, phase contrast

Table 4 Live cell count, day 3

Sample	Live cells, %
<i>Aurelia aurita</i> collagen	65.87
Positive control	54.97
Negative control	45.23

Table 5 Free cell count after collagen incubation

Incubation time	<i>Aurelia aurita</i> collagen			Positive control			Negative control		
	Concentration, cells/mL $\times 10^4$	Total cells, $\times 10^4$	% Total cells	Concentration, cells/mL $\times 10^4$	Total cells, $\times 10^4$	% Total cells	Concentration, cells/mL $\times 10^4$	Total cells, $\times 10^4$	% Total cells
10 min	4.92	2.46	74.58	4.28	2.14	64.88	4.64	2.32	70.23
20 min	2.01	1.00	30.42	2.46	1.23	37.29	1.97	0.98	29.82
30 min	1.23	0.62	18.65	1.48	0.74	22.40	1.13	0.57	17.15
60 min	1.15	0.57	17.41	0.90	0.45	13.67	0.86	0.43	13.05
24 h	0.99	0.50	15.00	0.60	0.30	9.09	0.74	0.37	11.21

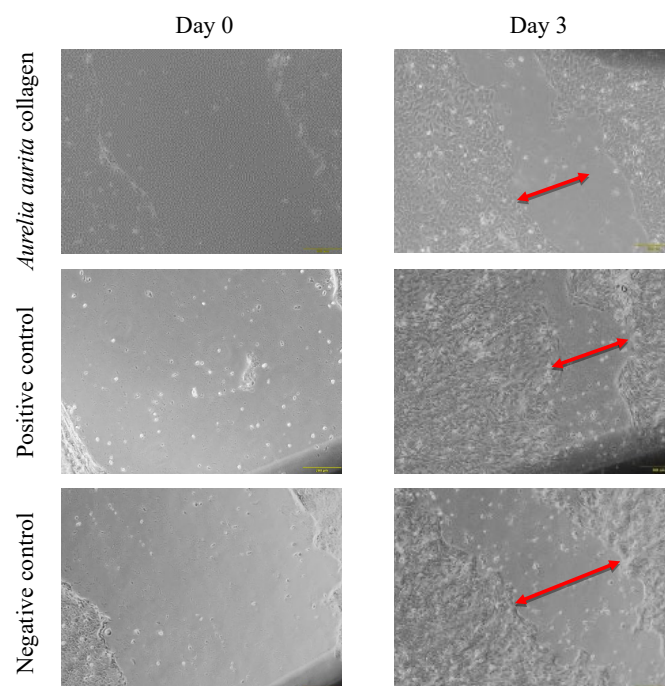


Figure 10 Wound model on HaCaT cell line *in vivo* on day 0 and day 3, phase contrast

Table 6 Wound healing assay, day 3

<i>Aurelia aurita</i> collagen	Healing rate, day 3		Average wound healing rate	
	μm	% from initial wound size	$\mu\text{m/day}$	% wound healing per day (from initial wound size)
Test sample	810.23	70.20	270.08	23.40
Positive control	1087.44	69.92	362.48	23.31
Negative control	712.87	56.18	237.62	18.73

Table 7 Keratinocyte differentiation markers referenced to GAPDH

Sample	KRT1	KRT10	KRT 14	KRT5	FLG	IVL	ITGA6	ITGB4
<i>Aurelia aurita</i> collagen	0.70	0.68	0.97	0.74	0.68	0.70	0.68	0.67
Positive control	0.78	0.75	0.97	0.79	0.76	0.75	0.73	0.73
Negative control	0.84	0.80	0.95	0.84	0.77	0.79	0.74	0.75

Differential gene expression in an immortalized keratinocyte HaCaT model after cultivation on collagen samples. The expression of KRT1, KRT10, FLG, and IVL served as markers of late differentiation while the expression of KRT5, KRT14, ITGA6, and ITGB4 served as basal differentiation. Different collagen samples showed no significant difference in these markers (Table 7), which means that *A. aurita* collagens did not affect the differentiation status of keratinocytes.

CONCLUSION

In this research, the maximal collagen extraction yield during acetic acid treatment was 185 mg/kg wet *Aurelia aurita* biomass. It was obtained in a 0.5 M solution after 48 h.

When the concentration of acetic acid increased from 0.2 to 0.5 M, the collagen yield grew from 143.5 ± 7.8 to 150.1 ± 5.4 mg/kg. A further increase in acid concentration by 0.1 M reduced the economic efficiency of the process by 8000 rubles/g.

Extraction time also had a significant effect on collagen yield: when it increased from 24 to 48 h, the yield grew by 17.4% with no effect thereafter.

The native collagen samples showed very low solubility in water and organic solvents, which is quite natural. However, it dissolved in a high-concentrated solution of acetic acid (≥ 0.5 M). This property is no disadvantage because some collagen sponges should be resistant to biological fluids.

The water holding capacity of *A. aurita* collagen was 4.194, i.e., twice as high as that of medical gauze.

The UV spectroscopy showed that the collagen had a high degree of purity, as evidenced by a clear peak at 230–235 nm, i.e., in the region of glycine and hydroxyproline. The molecular weight of acid-soluble collagen was 100–115 kDa, which made it possible to classify *A. aurita* collagen as type I, typical of animal biomass.

A. aurita collagen demonstrated no cytotoxic properties. It had no effect on cell adhesion, migration, and proliferation, neither did it affect the expression of cell differentiation markers.

The wound-healing assay demonstrated regenerative properties: *A. aurita* collagen was able to increase the healing rate by 24.5%.

The high biological activity of collagen obtained from the *A. aurita* jellyfish renders it suitable for regenerative medicine. However, the product yield appeared to be very low ($\leq 0.02\%$). As a result, *A. aurita* is a potential source of collagen but the method described in this research will be economically justified only by large-scale fishing, e.g., to increase the recreational attractiveness of a coastal area during mass stranding or to eliminate a certain negative effect of *A. aurita* mass migration on human economic activity.

CONTRIBUTION

The authors were equally involved in the research and are equally responsible for any potential plagiarism.

CONFLICT OF INTEREST

The authors declared no conflict of interests related to the publication of this article.








REFERENCES

- Cadar E, Pesterau A-M, Sirbu R, Negreanu-Pirjol BS, Tomescu CL. Jellyfishes – Significant marine resources with potential in the wound-healing process: A review. *Marine Drugs*. 2023;21(4):201. <https://doi.org/10.3390/md21040201>
- Hu Z, Yang P, Zhou C, Li S, Hong P. Marine collagen peptides from the skin of Nile Tilapia (*Oreochromis niloticus*): Characterization and wound healing evaluation. *Marine Drugs*. 2017;15(4):102. <https://doi.org/10.3390/md15040102>
- Lahmar A, Rjab M, Sioud F, Selmi M, Salek A, Kilani-Jaziri S, et al. Design of 3D hybrid plant extract/marine and bovine collagen matrixes as potential dermal scaffolds for skin wound healing. *The Scientific World Journal*. 2022;2022:8788061. <https://doi.org/10.1155/2022/8788061>
- Pozzolini M, Millo E, Oliveri C, Mirata S, Salis A, Damonte G, et al. Elicited ROS scavenging activity, photoprotective, and wound-healing properties of collagen-derived peptides from the marine sponge *Chondrosia reniformis*. *Marine Drugs*. 2018;16(12):465. <https://doi.org/10.3390/md16120465>
- Geahchan S, Baharlouei P, Rahman A. Marine collagen: A promising biomaterial for wound healing, skin anti-aging, and bone regeneration. *Marine Drugs*. 2022;20(1):61. <https://doi.org/10.3390/md20010061>
- Davison-Kotler E, Marshall WS, García-Gareta E. Sources of collagen for biomaterials in skin wound healing. *Bioengineering*. 2019;6(3):56. <https://doi.org/10.3390/bioengineering6030056>
- D'Ambra I, Merquiol L. Jellyfish from fisheries by-catches as a sustainable source of high-value compounds with biotechnological applications. *Marine Drugs*. 2022;20(4):266. <https://doi.org/10.3390/md20040266>

8. Fernández-Cervantes I, Rodríguez-Fuentes N, León-Deniz LV, Quintana LEA, Cervantes-Uc JM, Kao WAH, et al. Cell-free scaffold from jellyfish *Cassiopea andromeda* (Cnidaria; Scyphozoa) for skin tissue engineering. Materials Science and Engineering: C. 2020;111:110748. <https://doi.org/10.1016/j.msec.2020.110748>
9. Felician FF, Yu R-H, Li M-Z, Li C-J, Chen H-Q, Jiang Y, et al. The wound healing potential of collagen pepti-desderived from the jellyfish *Rhopilema esculentum*. Chinese Journal of Traumatology. 2019;22(1):12–20. <https://doi.org/10.1016/j.cjtee.2018.10.004>
10. Miyake H, Iwao K, Kakinuma Y. Life history and environment of Aurelia aurita. South Pacific Study. 1997;17(2): 273–285.
11. Tardent P. Coelenterata, Cnidaria. In: Seidel T, editor. Morphogenesis der Tiere. New York: Gustav Fischer Verlag; 1978. pp. 71–391.
12. Zavolokin AV. Jellyfish of the Far Eastern Seas of Russia. 1. Species composition and spatial distribution. Izvestiya TINRO. 2010;163:45–46. (In Russ.). <https://elibrary.ru/NTEWYR>
13. Brodeur RD, Sugisaki H, Hunt Jr GL. Increases in jellyfish biomass in the Bering Sea: Implications for the ecosystem. Marine Ecology Progress Series. 2002;233:89–103. <https://doi.org/10.3354/meps233089>
14. Aleksandrov SV, Gusev AA, Dmitrieva OA, Semenova AS, Chukalova NN. Planktonic and benthic communities of the Baltic Sea of the northern coast of the Sambian Peninsula in summer and autumn 2017. Trudy AtlantNIRO. 2019;3(2):38–58. (In Russ.). <https://elibrary.ru/WWD AJN>
15. Nagai T, Worawattanamateekul W, Suzuki N, Nakamura T, Ito T, Fujiki K, et al. Isolation and characterization of collagen from rhizostomous jellyfish (*Rhopilema asamushi*). Food Chemistry. 2000;70(2):205–208. [https://doi.org/10.1016/S0308-8146\(00\)00081-9](https://doi.org/10.1016/S0308-8146(00)00081-9)
16. Dong J, Sun M, Wang B, Liu H. Comparison of life cycles and morphology of *Cyanea nozakii* and other scyphozoans. Plankton and Benthos Research. 2008;3:118–124. <https://doi.org/10.3800/pbr.3.118>
17. Liu D, Nikoo M, Boran G, Zhou P, Regenstein JM. Collagen and gelatin. Annual Review of Food Science and Technology. 2015;6:527–557. <https://doi.org/10.1146/annurev-food-031414-111800>
18. Wahyuningsih R, Rusman, Nurliyani, Pertiwinigrum A, Rohman A, Fitriyanto NA, et al. Optimization of acid soluble collagen extraction from Indonesian local “Kacang” goat skin and physico-chemical properties characterization. Chemical Engineering Transactions. 2018;63:703–708. <https://doi.org/10.3303/CET1863118>
19. Hakim TR, Pratiwi A, Jamhari J, Fitriyanto NA, Rusman R, Abidin MZ, et al. Extraction of collagen from the skin of Kacang goat and production of its hydrolysate as an inhibitor of angiotensin converting enzyme. Tropical Animal Science Journal. 2021;44(2):222–228. Google Scholar. CrossRef. <https://doi.org/10.5398/tasj.2021.44.2.222>
20. Addad S, Exposito J-Y, Faye C, Ricard-Blum S, Lethias C. Isolation, characterization and biological evaluation of jellyfish collagen for use in biomedical applications. Marine Drugs. 2011;9(6):967–983. <https://doi.org/10.3390/md9060967>
21. Swatschek D, Schatton W, Kellermann J, Müller WEG, Kreuter J. Marine sponge collagen: Isolation, characterization and effects on the skin parameters surface-pH, moisture and sebum. European Journal of Pharmaceutics and Biopharmaceutics. 2002;53(1):107–113. [https://doi.org/10.1016/S0939-6411\(01\)00192-8](https://doi.org/10.1016/S0939-6411(01)00192-8)
22. Ahmed R, Haq M, Chun B-S. Characterization of marine derived collagen extracted from the by-products of bigeye tuna (*Thunnus obesus*). International Journal of Biological Macromolecules. 2019;135:668–676. <https://doi.org/10.1016/j.ijbiomac.2019.05.213>
23. Neuffer MC, McDivitt J, Rose D, King K, Cloonan CC, Vayer JS. Hemostatic dressings for the first responder: A review. Military Medicine. 2004;169(9):716–720. <https://doi.org/10.7205/MILMED.169.9.716>
24. Cheng X, Shao Z, Li C, Yu L, Raja M, Liu C. Isolation, characterization and evaluation of collagen from jellyfish *Rhopilema esculentum* Kishinouye for use in hemostatic applications. PLoS ONE. 2017;12(1):e0169731. <https://doi.org/10.1371/journal.pone.0169731>
25. Kittiphattanabawon P, Benjakul S, Visessanguan W, Shahidi F. Isolation and properties of acid-and pepsin-soluble collagen from the skin of blacktip shark (*Carcharhinus limbatus*). European Food Research and Technology. 2010;230:475–483. <https://doi.org/10.1007/s00217-009-1191-0>
26. Nurubhasha R, Sampath Kumar NS, Thirumalasetti SK, Simhachalam G, Dirisala VR. Extraction and characterization of collagen from the skin of *Pterygoplichthys pardalis* and its potential application in food industries. Food Science and Biotechnology. 2019;28:1811–1817. <https://doi.org/10.1007/s10068-019-00601-z>
27. Helfer GA, Magnus VS, Böck FC, Teichmann A, Ferrão MF, da Costa AB. PhotoMetrix: An application for univariate calibration and principal components analysis using colorimetry on mobile devices. Journal of the Brazilian Chemical Society. 2017;28(2):328–335. <https://doi.org/10.5935/0103-5053.20160182>

28. Maurer MH. Software analysis of two-dimensional electrophoretic gels in proteomic experiments. *Current Bioinformatics*. 2006;1(2):255–262. <https://doi.org/10.2174/157489306777011969>
29. Qiu L, Wang B, Zou S, Wang Q, Zhang L. Isolation and characterization of collagen from the jellyfish *Nemopilema nomurai*. *Journal of Pharmaceutical Practice and Service*. 2020;38(6):509–515. <https://doi.org/10.12206/j.issn.1006-0111.202008078>
30. Li J, Li Y, Li Y, Yang Z, Jin H. Physicochemical properties of collagen from *Acaudina molpadioides* and its protective effects against H₂O₂-induced injury in RAW264. 7 cells. *Marine Drugs*. 2020;18(7):370. <https://doi.org/10.3390/md18070370>
31. Gautam RK, Kakatkar AS, Mishra PK, Kumar V, Chatterjee S. Marine peptides: Potential applications as natural antioxidants. In: Kim S-K, Shin K-H, Venkatesan J, editors. *Marine antioxidants. Preparations, syntheses, and applications*. Academic Press; 2023. pp. 395–408. <https://doi.org/10.1016/B978-0-323-95086-2.00028-X>
32. Elango J, Hou C, Bao B, Wang S, Maté Sánchez de Val JE, Wenhui W. The molecular interaction of collagen with cell receptors for biological function. *Polymers*. 2022;14(5):876. <https://doi.org/10.3390/polym14050876>

ORCID IDs

Noora Barzkar  <https://orcid.org/0000-0001-9694-9138>
 Stanislav A. Sukhikh  <https://orcid.org/0000-0001-7910-8388>
 Anastasiia V. Zhikhreva  <https://orcid.org/0000-0002-5640-3533>
 Elizaveta Yu. Cheliubeeva  <https://orcid.org/0009-0005-7055-3641>
 Anastasia I. Kapitonova  <https://orcid.org/0000-0003-0958-6338>
 Olga O. Babich  <https://orcid.org/0000-0002-4921-8997>
 Yuliya V. Kulikova  <https://orcid.org/0000-0002-0896-4571>



Red wines from the Mostar area: Physicochemical, antioxidative, and antimicrobial properties

Tatjana Jovanović-Cvetković*^{OR}, Aleksandar Savić^{OR},
Ljiljana Topalić-Trivunović^{OR}, Ana Velemir^{OR}, Rada Grbić^{OR}

University of Banja Luka^{OR}, Banja Luka, Bosnia and Herzegovina

* e-mail: tatjana.jovanovic-cvetkovic@agro.unibl.org

Received 16.11.2023; Revised 05.12.2023; Accepted 09.01.2024; Published online 25.10.2024

Abstract:

Wines are complex alcoholic beverages. Apart from alcohol, they also contain other compounds, including those that have a beneficial effect on human health.

This paper features the basic physicochemical properties of four red grape varieties (Blatina, Vranac, Cabernet Sauvignon, Merlot) from the Mostar area, Bosnia and Herzegovina, as well as the antioxidant and antimicrobial properties of wines made of these grape varieties. The wines were produced in a standard way; the results were observed during two consecutive seasons of 2020 and 2021. The physicochemical properties were analyzed by standard methods recommended by the International Organization of Vine and Wine. The study involved tests for total phenolics, flavonoids, and anthocyanins, as well as for antioxidant activity. The methodology included FRAP, DPPH, and ABTS assays. The antimicrobial activity was tested by agar dilution method, which made it possible to determine the minimum inhibitory and bactericidal values. The list of pathogenic and opportunistic bacteria consisted of *Escherichia coli*, *Pseudomonas aeruginosa*, *Staphylococcus aureus*, and *Bacillus cereus*. Pathogenic yeasts were represented by *Candida albicans*. *Lactobacillus plantarum* and *Saccharomyces boulardii* were selected as probiotic cultures.

The physicochemical characteristics of grapes, i.e. must, depended on the harvest year, variety, and their interaction. The best antioxidant effect and the highest total phenolic content belonged to the Vranac wine, vintage 2020. *B. cereus* appeared to be the most sensitive bacteria. The Blatina wines of both harvest years demonstrated the lowest antimicrobial and the antioxidant activities. Probiotic cultures proved to be resistant to the effects of wine. Pearson's test revealed a reliable correlation between the antioxidant properties and the antimicrobial effect on *B. cereus* and, in one case, on *S. aureus* and *P. aeruginosa*. All grapevine varieties in this research proved to be suitable for the production of quality wines in the Mostar area.

Keywords: Red grape varieties, wine, must, physicochemical properties, antioxidant activity, antimicrobial activity

Funding: This work was partially supported by the Ministry of Scientific and Technological Development, Higher Education and Information Society of the Republic of Srpska (contract number: 19.032/961-70/19, December 31, 2019).

Please cite this article in press as: Jovanović-Cvetković T, Savić A, Topalić-Trivunović L, Velemir A, Grbić R. Red wines from the Mostar area: Physicochemical, antioxidative, and antimicrobial properties. *Foods and Raw Materials*. 2025;13(2): 306–319. <https://doi.org/10.21603/2308-4057-2025-2-646>

INTRODUCTION

The quality of grapes and wine depends on the variety, the agro-ecological conditions of the vineyard, and the production technologies. The structural and physicochemical characteristics of grape clusters and berries define the ampelographic and technological properties of grape varieties [1, 2].

Wine is one of the oldest and most widespread alcoholic beverages. As a rule, it contains alcohol, sugars, acids, tannins, minerals, proteins, organic acids, vola-

tile compounds, and phenolic compounds [3]. Antioxidant activity is one of the most important properties of red wines. It is associated with polyphenols, e.g., flavonoids, phenolic acids, stilbenes, coumarins, etc. [4]. The polyphenol content of wine depends on the grape variety, vineyard location, cultivation system, climate, soil type, grapevine production practices, harvesting time, production process, and ageing. The polyphenol molecules behave as antioxidants against free radicals. They increase the antioxidant capacity in the human body.

In addition, they affect the sensory profile of wines [5]. Anthocyanins contribute to color while flavan-3-ols are responsible for bitterness and astringency [5, 6]. Vintage has a different effect on antioxidant properties of red wines, even if they share the same production conditions, vineyard location, cultivation system, climate, soil type, harvesting time, and ageing [5].

The antimicrobial activity of red wines against pathogenic and opportunistic microorganisms is well documented and mostly associated with the content of various polyphenolic compounds in red wine, e.g., anthocyanins, flavonoids, stilbenes, catechins, and phenolic acids [7, 8]. The inhibitory effect also depends on the type of bacteria. The content of phenolic acids, resveratrol, and some flavonoids was found to correlate with the inhibitory activity of wine against *Clostridium perfringens* and *Micrococcus flavus* [9]. Antimicrobial activity of wine against *Listeria inocua* and *Proteus vulgaris* was reported to depend on the catechin content. However, none of the abovementioned components correlated with the activity against *Klebsiella pneumonia* strains. Apart from polyphenols, the antimicrobial effect of wines is known to depend on other components and variables, e.g., organic acids, low pH, alcohol, and acetates [10]. In relation to pathogenic microorganisms, wine components do not inhibit the digestive tract microbiota: plant phenols actually have a stimulating effect on their growth [11].

The physicochemical characteristics of grapes from Bosnia and Herzegovina, especially those from the region of Mostar, remain as understudied as the antioxidant and antimicrobial properties of the local wines. This research aimed at analyzing the effect of grapevine variety and production season on these properties.

STUDY OBJECTS AND METHODS

The study involved grapes and wine varieties of Blatina, Vranac, Cabernet Sauvignon, and Merlot, harvested in the area of Mostar (43°20'N; 17°48'E) in Bosnia and Herzegovina in 2020–2021.

Climate indicators. Mostar is located in the southwestern part of Bosnia and Herzegovina. The area owes its warm Mediterranean climate to the Adriatic Sea [12]. Figures 1a and b give the basic meteorological data, average monthly temperatures, extreme daily temperatures, and total monthly precipitation during the growing seasons of April – October 2020–2021 [13]. Both research years were similar in terms of air temperature, with occasional extreme daily temperatures as high as $\geq 30^{\circ}\text{C}$ in May – September. The amount of precipitation was quite low, especially in June – July 2021.

Physical characteristics of grape clusters and berries. The analysis included examination of the basic physical characteristics of grape clusters and berries. The average weights of 10 grape clusters and 100 grape berries, g, were measured using a digital scale (KERN 440, Germany).

Physicochemical characteristics of must and wine. The quality analysis of the basic physicochemical parameters of the must took place during the first stage of

microvinification. It covered the following parameters. The percentage of total soluble solids – sugar (TSS, °Brix) was measured with a digital refractometer (Atago-Pal-3, Japan). The total titratable acidity was determined by the neutralization method. The pH value of the must was measured with a pH-meter (Hanna HI2211, USA).

Microvinification was the same for all grape varieties and followed the classic protocol for red wines. After crushing the grapes, we protected the resulting must from oxidation by adding Vulcasulph, a commercial preparation produced by Vulcascot, Austria, in the amount of 10 g/100 kg. After that, we added Vitamon Combi yeast food (Erbslöh, Germany). The inoculation involved the Oenoferm Color selection yeast culture (Erbslöh, Germany) in the quantities recommended by the manufacturer. Fermentation took place at $20\text{--}23^{\circ}\text{C}$, with must submersion performed twice a day until the

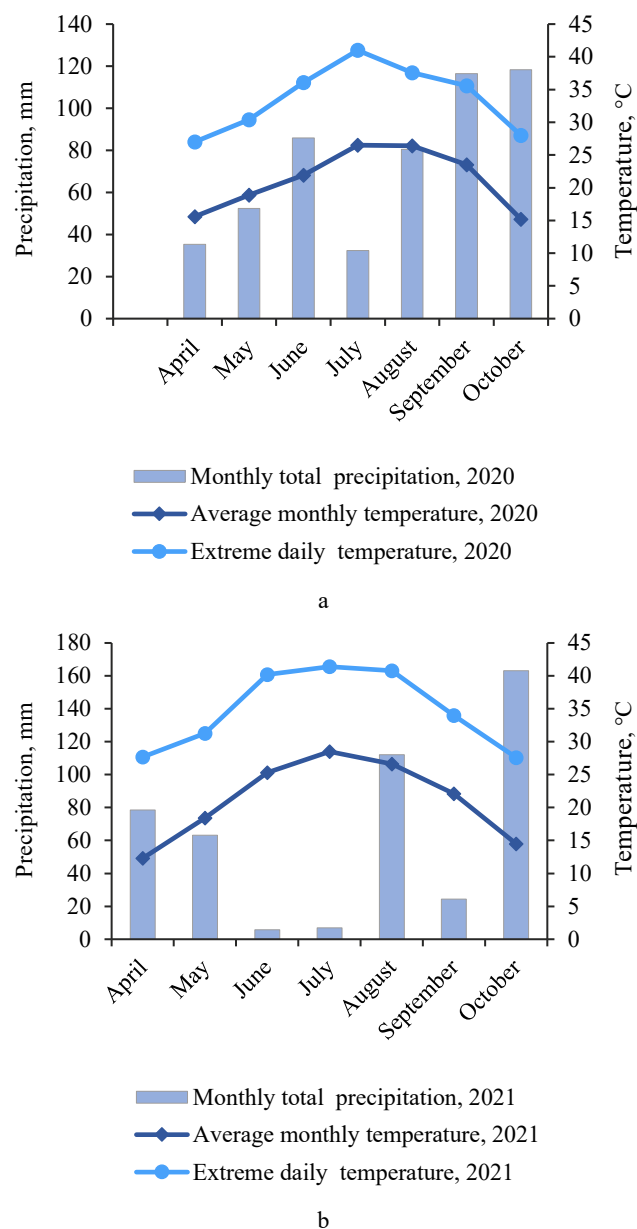


Figure 1 Meteorological data in 2020 (a) and in 2021 (b)

level of remaining sugar in the wine was between 1.0 and 2.0 g/L. The young wine was analyzed after five months of storage in stainless steel tanks. The analysis followed standard procedures and covered the following physicochemical parameters: ethanol, total extract, sugar-free extract, reducing sugars, total acidity, volatile acidity, and pH value [14].

Antioxidant activity of wines. The total phenolic content was determined by the Folin-Ciocalteu colorimetric method [15]. The non-flavonoid content was determined by the formaldehyde method whereas the flavonoid content was calculated as the difference between total phenols and non-flavonoids [16]. The antioxidant activity analysis involved DPPH, ABTS, and FRAP assays [17, 18]. The total anthocyanin content was determined by the spectrophotometric method as described by Mitrevska et al. [19].

Antimicrobial activity of wines. The antimicrobial activity test included the following nutrient media: Mueller Hinton agar, Mueller Hinton broth, Nutrient agar, Sabouraud agar, De Man Rogosa and Sharpe agar, and agar (1.5%).

Microbial cultures: the experiment involved five bacterial cultures, namely *Escherichia coli* WDCM 00013, *Pseudomonas aeruginosa* WDCM 00024, *Staphylococcus aureus* WDCM 00034, *Bacillus cereus* WDCM 00151, *Lactobacillus plantarum* 299v, as well as two yeast cultures (*Candida albicans* WDCM 00054 and *Saccharomyces boulardii* DBVPG 6763).

Microbial culture media preparation: the bacterial cultures of *E. coli*, *P. aeruginosa*, *S. aureus*, and *B. cereus*, as well as the *Candida albicans* yeast culture, were prepared from the logarithmic phase by the direct colony suspension method (M07. Methods for dilution antimicrobial susceptibility tests for bacteria that grow aerobically; M11. Methods for antimicrobial susceptibility testing of anaerobic bacteria) [20].

Preparing standardized inoculum from the logarithmic phase (*E. coli*, *P. aeruginosa*, and *B. cereus*). The cultures inoculated on Nutrient agar slant and Mueller Hinton broth agar plates were incubated for 24 h at 37°C. After incubation, we transferred 3–5 isolated colonies from the agar plate to a test tube with 5 mL of Mueller Hinton Broth. The tubes with the inoculated bacteria were left to incubate for 2–6 h. The culture incubation time was the same for each experiment.

Preparing standardized inoculum for *S. aureus* and *C. albicans*. *S. aureus* and *C. albicans* were inoculated from agar slant (nutrient agar for *S. aureus* and Sabouraud agar for *C. albicans*) on the corresponding agar plates (Mueller Hinton agar for *S. aureus* and Sabouraud agar for *C. albicans*) with an inoculation loop. The agar plates were left to incubate at 37°C (*S. aureus*) and 30°C (*C. albicans*) for 24 h. After incubation, we collected two or three colonies directly from the Mueller Hinton agar and Sabouraud agar to be transferred to the Mueller Hinton broth (*S. aureus*) and the physiological solution (*C. albicans*). The density of the microbial cultures was determined spectrophotometrically (625 nm for bacteria and 530 nm

for yeast), and 0.5 McFarland standard (1.5×10^8 CFU/mL) was used for comparison. By diluting the cultures, we adjusted their density to 1.5×10^6 CFU/mL.

Preparing *L. plantarum* inoculum. A capsule of Flo-bian (Abela Pharm, Belgrade) was added to 99.9 mL of saline solution and vortexed at 300 rpm for 30 min. The density of the culture for inoculation was adjusted to 1.5×10^6 CFU/mL by dilution [21].

Preparing *S. boulardii* inoculum. A capsule of Bular-di Probiotic (Abela Pharm, Belgrade) was suspended in 40 mL of saline solution, shaken, and adjusted to a density of 1.5×10^6 CFU/mL by dilution [22].

Antimicrobial activity testing. To determine the antimicrobial activity of wine, we used the agar dilution method to obtain minimum inhibitory, minimum bactericidal, and minimum fungicidal concentrations (M07 and M11) [20–22]. We performed a series of dilutions on agar by adding an appropriate amount of wine to the previously dissolved and cooled (45°C) Mueller Hinton agar, so that the final concentration of wine in the media would be 10, 20, and 30% (v/v). After shaking the media with wine, we poured the samples into sterile Petri dishes. Upon media setting, the microbial cultures were inoculated onto the surface of the agar plates in drops of 10 µL. The Petri dishes with *L. plantarum* were covered with a layer of 1.5% agar, dissolved, and cooled to 45°C. The inoculated Petri dishes were then incubated at 37°C for 24 h. After incubation, we measured the growth of the cultures on the media with wine. The lowest concentration of wine in the media with no visible culture growth was determined as minimum inhibitory. All Petri dishes with no visible culture growth underwent re-inoculation. After scraping the inoculated spots with a sterile inoculation loop, we re-inoculated them on Nutrient agar, Sabouraud agar, De Man Rogosa, and Sharpe agar. The petri dishes were incubated at 37°C for 24 h. The lowest wine concentrations with no growth of inoculated colonies were determined as minimum bactericidal or fungicidal concentrations. A medium without wine was used as positive control, and ethanol served as negative control in concentrations that corresponded to the concentration of ethanol in the wine.

Statistical analysis. The results were expressed as means \pm standard deviation. The statistical analysis involved a one-way analysis of variance (ANOVA). Significant differences between the results were determined by the Duncan's multiple range test. The differences were considered significant at $p < 0.05$. Relationships between antioxidant and antimicrobial activity were established using the Pearson correlation test.

RESULTS AND DISCUSSION

Basic physical characteristics of grapes. The quality and typicality of the wine depend on, among other things, the variety and the quality of berries. This research featured two domestic (Blatina and Vranac) and two international (Cabernet Sauvignon and Merlot) grape varieties. The study of intervarietal differences included the basic physical indicators of grape clusters and

berries (average weight of 10 representative grape clusters and 100 grape berries), as well as how these qualities depended on the production year, variety, and the interaction of these two factors.

Table 1 shows that the average grape cluster weight was statistically higher in 2021. An inter-varietal comparison showed that the Blatina variety had the highest grape cluster weight (463.97 g), followed by the Vranac variety (414.17 g); in 2021, their weights were statistically significantly higher than those of the other varieties. The Cabernet Sauvignon variety had the lowest grape cluster weight in both years. The mentioned parameter strongly depended on both year and variety, as well as on their interaction. The highest weight of 100 grape berries also belonged to the Blatina variety (330.00 g), followed by the Vranac variety (290.04 g), while the lowest weight was recorded in Cabernet Sauvignon in both research years (120.63 and 126.30 g, respectively). In contrast to the grape cluster weight, the berry weight depended only on the variety. The research period showed no statistically significant difference between the varieties regarding the average weight of 100 grape berries (232.75 and 226.35 g).

The varietal differences were best illustrated by the lowest values of grape cluster and grape berry weights in the Cabernet Sauvignon variety, which did not contradict the description of the technological potential for this variety published in the official catalog of grapevine varieties [23]. Similar results were found by

Ivanišević *et al.* while Russian research teams reported somewhat lower grape mass [24–26]. However, the large variation in the grape cluster weight for the Blatina variety during the research period could be linked to varietal specificity. Functionally female flower causes poor fertilization, which results in a lower percentage of fruit setting and, therefore, leads to a lower grape cluster weight [27, 28]. In the case of the Vranac variety, the locality also had a positive effect on the above-mentioned variables. Our results for this variety were in accordance with a recent multi-year qualitative study of Vranac grapes in Herzegovina [29]. In fact, our results were very close to those published for another study that took place in Montenegro, i.e., the primary production region for Vranac [30, 31]. Similarly, the results we obtained for the Merlot variety indicated a positive effect of the environment. Our values were higher compared to those reported for other regions [32, 33].

Basic physicochemical properties of must. The composition and sensory profile of wine depend on the composition and the ratio of primary and secondary metabolites in grapes. Table 2 sums up the basic physicochemical parameters, total soluble solids, total titratable acidity, and pH values of the musts for each variety and harvest year, as well as their interaction.

The statistical analysis of total soluble solids in the must revealed a statistically significant ($p < 0.001$) difference between the grape varieties. For all varieties, the total amount of soluble solids was significantly ($p < 0.001$)

Table 1 Basic physical parameters of grape clusters and grape berries

Variety	Grape cluster weight, g	Weight of 100 grape berries, g
2020		
Blatina	229.01 ± 22.27 ^{bcd}	320.00 ± 1.07 ^{ab}
Vranac	379.22 ± 28.75 ^a	280.41 ± 0.97 ^b
Cabernet Sauvignon	192.93 ± 10.73 ^{cd}	120.63 ± 0.32 ^d
Merlot	325.91 ± 37.79 ^{ab}	200.06 ± 0.71 ^c
2021		
Blatina	463.97 ± 27.51 ^a	330.00 ± 1.33 ^a
Vranac	414.17 ± 31.72 ^a	290.04 ± 1.02 ^b
Cabernet Sauvignon	149.53 ± 11.18 ^d	126.30 ± 0.31 ^d
Merlot	283.52 ± 11.26 ^{bc}	150.87 ± 0.39 ^d
Year (Y)	9.59**	1.08 ^{ns}
Variety (V)	58.97***	223.12***
Y×V	17.55***	3.76*
Mean values (± standard error)		
Year		
2020	281.77 ± 18.98 ^b	232.75 ± 1.27 ^{ns}
2021	327.69 ± 21.34 ^a	226.35 ± 1.44 ^{ns}
Variety		
Blatina	346.49 ± 28.65 ^b	326.00 ± 0.84 ^a
Vranac	396.70 ± 21.21 ^a	285.23 ± 0.69 ^b
Cabernet Sauvignon	171.23 ± 7.55 ^c	126.30 ± 0.22 ^d
Merlot	304.72 ± 20.55 ^b	179.38 ± 0.62 ^c

^{a–d} – different letters within the same column indicate statistically significant difference at $p < 0.05$ by Duncan's test

***, **, * – significant at $p < 0.001$, $p < 0.01$, and $p < 0.05$, respectively

^{ns} – not significant

Table 2 Basic physicochemical parameters of grape musts

Year	Variety	Total soluble solids, %			Total titratable acidity, g/L			pH		
		\bar{x}	\pm	SE	\bar{x}	\pm	SE	\bar{x}	\pm	SE
2020	Blatina	18.71	\pm	0.14	6.95	\pm	0.04	3.01	\pm	0.01
	Vranac	26.02	\pm	0.05	4.21	\pm	0.09	3.29	\pm	0.03
	Cabernet Sauvignon	24.42	\pm	0.09	4.96	\pm	0.04	3.71	\pm	0.02
	Merlot	25.48	\pm	0.22	4.60	\pm	0.04	3.44	\pm	0.02
2021	Blatina	17.24	\pm	0.17	8.05	\pm	0.05	3.28	\pm	0.01
	Vranac	22.59	\pm	0.09	5.59	\pm	0.07	3.54	\pm	0.01
	Cabernet Sauvignon	23.82	\pm	0.09	4.83	\pm	0.06	3.56	\pm	0.04
	Merlot	24.11	\pm	0.12	5.80	\pm	0.05	3.35	\pm	0.01
$F_{\text{year}}, p_{\text{year}}$		290.86**, $p < 0.001$			403.22**, $p < 0.001$			17.77**, $p < 0.001$		
$F_{\text{variety}}, p_{\text{variety}}$		135.71**, $p < 0.001$			877.66**, $p < 0.001$			134.08**, $p < 0.001$		
$F_{\text{year*variety}}, p_{\text{year*variety}}$		36.16**, $p < 0.001$			50.54**, $p < 0.001$			44.41**, $p < 0.001$		
LSD _{year*variety}		0.37			0.16			0.06		

higher in 2020 than in 2021. The highest value of total soluble solids was observed in the Vranac must in 2020. Regarding the total titratable acidity in the must, the varieties also showed a statistically significant ($p < 0.001$) difference. In general, the total titratable acidity values for all musts were lower ($p < 0.001$) in 2020 than in 2021, with the exception of the Cabernet Sauvignon must, which had a higher total titratable acidity in 2020. The statistical analysis of pH values also revealed a statistically significant ($p < 0.001$) difference between the varieties under analysis. The pH values for all varieties were significantly ($p < 0.001$) higher in 2021 than in 2020. The lowest pH belonged to the musts obtained from the Blatina and Vranac varieties in 2020.

The harvest year had a statistically significant effect ($p < 0.001$) on all variables. The interaction between the variety and the harvest year also proved highly significant ($p < 0.001$). To sum up, the variety factor affected all physicochemical quality indicators. Other studies, which included a greater number of varieties, also confirmed that the content and composition of sugar and acids in grapes largely depended on the variety [34, 35].

Although the effect of climatic factors was not the subject of this research, we reviewed the specifics of the weather conditions during the research period. According to the meteorological data in Figs. 1a and b, the average monthly air temperatures during the research period were relatively high, with occasional extreme daily temperatures as early as in May and low precipitation during the ripening period.

Warm environment was reported to raise sugar concentration and reduce the content of malic acid salts in grapes [36]. However, according to the same author, temperatures $\geq 33^\circ\text{C}$ could lead to a decrease in sugar concentration although low acidity could also be manifested under lower temperatures. The higher temperatures recorded during our research were probably one of the factors that triggered an increase in total soluble solids (23.82–26.02°Brix) and a decrease in total titratable

acidity (4.21–5.59 g/L) in most varieties except Blatina. The low content of total soluble solids was registered for all must samples obtained in 2021, which was particularly evident in the case of the Vranac variety. This phenomenon could also be linked to the stressful weather conditions in June and August 2021 when the monthly precipitation was as low as 5.7 and 7.0 mm, respectively, and the extreme daily temperatures were as high as 40.8 and 41.4°C, respectively [13].

In addition to the climatic conditions, the quality of all grape varieties in this research was affected by pedological and agrotechnical methods, as well as by the ampelotechnical measures in the production years. The total soluble solids we obtained for the Blatina must were relatively consistent with those reported in [37, 38] whereas our total titratable acidity data were higher. Maraš *et al.* also confirmed the low total titratable acidity demonstrated by the Vranac variety, which also grows in warmer climates, e.g., in Montenegro [39]. Banjanin, who studied grapes in Trebinje, Herzegovina, in 2016–2018, reported lower total soluble solids in Cabernet Sauvignon grape juice (22.8%) and a significantly higher total titratable acidity (6.83–9.15 g/L) compared to our results [29]. This difference illustrates, to some extent, the effect of the harvest year on the parameters under study. Other authors, who compared different Merlot clones or the yield and quality of Merlot grapes grafted onto different rootstocks, reported a higher total titratable acidity (5.77–10.00 g/L) but lower total soluble solids (15.61–22.20°Brix) [40, 41].

Basic physicochemical characteristics of wine.

Table 3 shows the basic physicochemical parameters of wine quality in the harvest years. The ethanol content in all wines was higher in 2020, which was quite predictable from the total soluble solids in the must. The same situation was observed with the total extract. Alcohol determines the stability and sensory properties of wine, but the content of the extract is also significant [42]. This parameter makes it possible to divide wines into light

Table 3 Basic chemical composition of Blatina, Vranac, Cabernet Sauvignon, and Merlot wines

Parameters	Blatina, 2020	Blatina, 2021	Vranac, 2020	Vranac, 2021	Cabernet Sauvignon, 2020	Cabernet Sauvignon, 2021	Merlot, 2020	Merlot, 2021
Ethanol, % (v/v)	9.91 ± 0.04	9.54 ± 0.04	15.43 ± 0.04	13.36 ± 0.04	15.16 ± 0.04	14.28 ± 0.00	15.20 ± 0.00	14.43 ± 0.04
Total extract, g/L	25.80 ± 0.00	22.55 ± 0.15	31.80 ± 0.00	28.00 ± 0.10	33.90 ± 0.00	29.40 ± 0.00	30.60 ± 0.10	24.50 ± 0.00
Sugar-free extract, g/L	25.70 ± 0.00	22.55 ± 0.15	31.00 ± 0.00	27.50 ± 0.16	31.86 ± 0.00	29.15 ± 0.00	29.96 ± 0.10	24.48 ± 0.01
Reducing sugar, g/L	1.10 ± 0.00	0.80 ± 0.00	1.80 ± 0.00	1.50 ± 0.06	3.04 ± 0.00	1.25 ± 0.00	1.64 ± 0.00	1.02 ± 0.01
Total acidity, g tartaric acid/L	6.34 ± 0.00	6.94 ± 0.02	5.23 ± 0.00	6.96 ± 0.00	4.50 ± 0.02	7.30 ± 0.00	5.27 ± 0.00	6.37 ± 0.02
Volatile acidity, g acetic acid/L	0.20 ± 0.01	0.18 ± 0.01	0.22 ± 0.00	0.31 ± 0.01	0.30 ± 0.01	0.26 ± 0.00	0.25 ± 0.01	0.24 ± 0.01
pH	3.57 ± 0.00	3.36 ± 0.00	3.50 ± 0.00	3.58 ± 0.00	3.83 ± 0.01	3.52 ± 0.00	3.91 ± 0.01	3.40 ± 0.00

(≤ 20 g/L) and full-bodied (≥ 30 g/L) [43]. Given that the total extract content in our research ranged from 31.1 to 33.9 g/L, all the wine samples, except Blatina, could be characterized as full-bodied.

The largest variations were recorded for the total acidity for most wine samples. The total acidity of wine correlated with the initial (observed) values of the total titratable acidity of must. This phenomenon was especially pronounced in Cabernet Sauvignon (2021), closely followed by Vranac and Merlot. The acidity of the wine usually depends on the most abundant organic acids, i.e., L-tartaric, L-malic, and citric acids. Their level is known to change during fermentation [44, 45]. In addition to these acids, other acids also appear during fermentation, but in lower quantities. They are the products of different strains of wine yeasts and/or bacteria activity (succinic, lactic, acetic, etc.).

In addition to all these factors, the wines in our research came from grapes produced in warm Mediterranean climate. As a result, the volatile acidity in all wines was low (0.18–0.31 g/L) and stayed within permissible limits [46]. The increase in total acidity in certain wines and years might be linked to the higher content of some other acids that developed during fermentation. Contrary to the above, the Blatina wine samples showed a decrease in the total acidity in both years, compared to the initial values of the total titratable acidity in the must. According to certain literary references, such phenomena are associated with malolactic fermentation, which can go unnoticed – simultaneously or subsequently with alcoholic fermentation [47, 48]. Additionally, the Blatina wine samples demonstrated a lower total acidity caused by longer maceration [49]. However, the Blatina samples had a higher pH. In our research, the pH values in all wine samples were more or less higher than those in the must samples, except for the Cabernet Sauvignon wine sample (2021). The values of reducing sugars ranged from 0.80 to 3.04 g/L, which made it possible to define the wine samples as dry wines [46].

The lowest ethanol content belonged to the Blatina wine harvested in both research years (9.91 and 9.54%, respectively). However, other Blatina studies performed

in Herzegovina managed to achieve a higher alcohol content (12.1–13.2%) because the level of total soluble solids in the must was quite high [50, 51].

The wines of the Vranac variety were particularly high in alcohol in 2020. These data exceeded the alcohol content in wines of this variety reported by several authors from Montenegro and Serbia, which ranged from 13.00 to 15.38% (v/v) [52–54]. However, the alcohol content in certain Vranac wines from the Tikveš region, North Macedonia, was as high as 15.83–16.44% [55]. Some other authors reported a lower alcohol content in wines of this variety, which was confirmed by our results for 2021 [39, 56]. Although the total extract content and the total acidity of the Vranac wine samples depended on the research year, our values stayed within the framework reported by the previously mentioned authors, excluding the higher wine total acidity in 2021. Regarding the pH of the Vranac wine, the differences between the research years were defined as insignificant (3.50 and 3.58, respectively).

The analysis of Cabernet Sauvignon indicated the high oenological potential of this international variety grown in the conditions of the Herzegovinian vineyards. Cabernet Sauvignon showed the highest total extract content and sugar-free extract, as well as a very high average alcohol content. On the other hand, we observed large annual variations in total acidity (4.50 and 7.30 g/L). The initial concentrations of total titratable acidity in the must (4.96 and 4.81 g/L) demonstrated a significantly larger deviation in the second research year. The pH of the wine did not change significantly compared to the pH of the must. The relatively high content of alcohol and total extract in Cabernet Sauvignon wines was also reported by other authors [57, 58]: the total acidity and pH ranged from 5.40 to 6.70 g/L and from 3.22 to 3.73 g/L, respectively. Their results only partially corresponded with ours, excluding the lower total acidity of Cabernet Sauvignon in 2020. Considering the global presence of Cabernet Sauvignon, a Russian research team managed to increase the content of alcohol and extract in wine made from grapes grown in the Krasnodar Region [59].

In this research, the average alcohol content in the Merlot wine sample (14.82%) was higher than the average alcohol content in all other wines. The year of 2020 showed a relatively high content of the total extract in the wine. The differences in the total titratable acidity of must between the harvest years (4.60 and 5.80 g/L, respectively) also manifested themselves in the total acidity of the wine (5.27 and 6.37 g/L, respectively). In addition, a slight increase in the pH value of the wine correlated with the pH value of the must in 2020. The year of 2021, on the contrary, demonstrated much more uniform values. Our research yielded higher values of alcohol, extract, and total acidity for Merlot grapes and wine than a recent study on other Merlot grapes from Herzegovina and a multi-year study of Merlot clones [60, 61].

Antioxidant activity. Table 4 illustrates the content of total phenolics, non-flavonoids, flavonoids, and total anthocyanins. The total phenolic content was 2.69–5.77 g GAE/L in 2020 and 2.37–4.17 g GAE/L in 2021. The average total phenolics showed the same order for both years: Vranac > Cabernet Sauvignon > Merlot > Blatina. The content of polyphenolic compounds in grapes and wine depends on several factors, e.g., climate, location, and agricultural conditions of grape production and origin, as well as on the winemaking phase [3, 5, 62–64]. The total phenolics for Vranac and

Cabernet Sauvignon varied between 1623 and 2485 mg/L in the 2015 vintage, and between 1551 and 2227 mg/L in the 2016 vintage [64]. For Merlot wines, these values varied between 1.51 and 7.55 mmol GAE/L in the 2017 vintage, and from 4.07 to 5.28 mmol GAE/L in the 2018 vintage [65]. For Blatina, the range was from 1786.71 to 2235.59 mg GAE/L [48].

In our study, the content of non-flavonoids and flavonoids ranged from 0.83 to 3.20 g GAE/L in 2020 and from 0.29 to 3.90 g GAE/L in 2021. The difference was probably caused by the grape composition. Flavonoids and non-flavonoids shape the sensory profile of wine by giving it either the typical long-aged taste or the astringency and bitterness of young wines [19].

Anthocyanins are responsible for the bright red color [66]. The total anthocyanins ranged from 194.65 to 376.17 mg/L in 2020 and from 223.95 to 532.66 mg/L in 2021. The lowest content belonged to Blatina while the highest belonged to Vranac and Cabernet Sauvignon.

As for the effect of maceration time, the maximal value of total anthocyanins was 200.23 mg/L: it was registered in the Blatina wine samples after 12 days of skin maceration [48]. Pajović Šćepanović R *et al.* reported values from 439 to 586 mg/L for red wines of the 2008–2010 vintages [63]. These differences in the total anthocyanin content might be explained by the

Table 4 Total phenolics, non-flavonoids, flavonoids, and total anthocyanins

Year	Variety	Total phenolics, g GAE/L			Non-flavonoids, g GAE/L			Flavonoids, g GAE/L			Total anthocyanins, mg/L		
		\bar{x}	\pm	SE	\bar{x}	\pm	SE	\bar{x}	\pm	SE	\bar{x}	\pm	SE
2020	Blatina	2.69 ^{aA}	\pm	0.05	2.40 ^{aA}	\pm	0.08	0.29 ^{aA}	\pm	0.13	194.65 ^{aA}	\pm	0.10
	Vranac	5.77 ^{bB}	\pm	0.09	1.87 ^{bB}	\pm	0.07	3.90 ^{bB}	\pm	0.07	366.15 ^{bB}	\pm	0.77
	Cabernet Sauvignon	4.80 ^{cC}	\pm	0.03	3.20 ^{cC}	\pm	0.04	1.59 ^{cC}	\pm	0.07	376.17 ^{cC}	\pm	0.50
	Merlot	3.96 ^{dD}	\pm	0.04	1.48 ^{dD}	\pm	0.04	2.48 ^{dD}	\pm	0.08	279.40 ^{dD}	\pm	0.25
2021	Blatina	2.37 ^{aE}	\pm	0.07	0.83 ^{aE}	\pm	0.01	1.54 ^{aC}	\pm	0.08	223.95 ^{aC}	\pm	0.62
	Vranac	4.17 ^{bF}	\pm	0.06	0.88 ^{aE}	\pm	0.05	3.29 ^{bE}	\pm	0.12	532.66 ^{bE}	\pm	0.38
	Cabernet Sauvignon	3.95 ^{cD}	\pm	0.09	1.17 ^{bF}	\pm	0.06	2.77 ^{cF}	\pm	0.03	513.02 ^{cF}	\pm	0.86
	Merlot	3.07 ^{dG}	\pm	0.02	0.84 ^{aE}	\pm	0.09	2.23 ^{dG}	\pm	0.10	233.42 ^{dG}	\pm	0.41

^{a–d} – Different letters within the same column indicate statistically significant difference at $p < 0.05$ by Duncan's test for the same year;

^{A–E} – Different capital letters within the same column indicate statistically significant difference at $p < 0.05$ by Duncan's test

Table 5 Antioxidant activity of wines

Year	Variety	FRAP, mmol Fe ²⁺ /L			DPPH (IC ₅₀ , %), μ L			ABTS (IC ₅₀ , %), μ L		
		\bar{x}	\pm	SE	\bar{x}	\pm	SE	\bar{x}	\pm	SE
2020	Blatina	10.57 ^{aA}	\pm	0.24	2.40 ^{aA}	\pm	0.07	0.78 ^{aA}	\pm	0.06
	Vranac	53.25 ^{bB}	\pm	0.62	1.21 ^{bB}	\pm	0.08	0.37 ^{bB}	\pm	0.09
	Cabernet Sauvignon	19.88 ^{cC}	\pm	0.61	1.46 ^{cC}	\pm	0.06	0.41 ^{bB}	\pm	0.05
	Merlot	29.91 ^{dD}	\pm	0.64	1.64 ^{dD}	\pm	0.06	0.59 ^{cC}	\pm	0.07
2021	Blatina	17.22 ^{aE}	\pm	0.43	3.14 ^{aE}	\pm	0.09	0.86 ^{aA}	\pm	0.05
	Vranac	31.40 ^{bF}	\pm	0.81	1.39 ^{bC}	\pm	0.06	0.38 ^{bB}	\pm	0.02
	Cabernet Sauvignon	34.26 ^{cG}	\pm	0.65	1.69 ^{cD}	\pm	0.05	0.37 ^{bB}	\pm	0.02
	Merlot	21.58 ^{dH}	\pm	0.41	2.21 ^{dF}	\pm	0.07	1.02 ^{dD}	\pm	0.04

^{a–d} – Different letters within the same column indicate statistically significant difference at $p < 0.05$ by Duncan's test for the same year;

^{A–H} – Different letters within the same column indicate statistically significant difference at $p < 0.05$ by Duncan's test

variations under weather conditions between the growing seasons, especially in rainfall.

The antioxidant activities of wines were analyzed by FRAP, DPPH, and ABTS assays (Table 5).

Total antioxidant activity determined by FRAP assay ranged from 10.57 to 53.25 mmol Fe²⁺/L for the year of 2020, and from 17.22 to 31.40 mmol Fe²⁺/L for the year of 2021. In fact, red wines tend to demonstrate a wide range of FRAP values, which means it depends on the total phenolic content [5]. The effect of phenolic compounds on the antioxidant activity of red wines had a high correlation, and the FRAP assay results reported in [5] as 10.54–62.77 mmol Fe²⁺/L were in accordance with ours (Table 5).

The DPPH (IC₅₀, %) activity ranged from 1.21 to 3.14 µL. Đorđević *et al.* reported 37–62.1% anti-DPPH radical activity for Vranac wines [66]. Radonjić *et al.* also reported stronger DPPH scavenging and reducing ability in Vranac wines [6]. Mitić *et al.* determined slightly higher values of 71.30–83.53% for Cabernet Sauvignon wines from the Balkan region [67]. Many authors consider that DPPH radical activity correlates with the total phenolic content [5, 66, 67].

According to the ABTS assay, the values ranged from 0.37 to 1.02 µL. Cabernet Sauvignon showed stronger antioxidant activity than Vranac and Kratošija red wines as reported by Pajović Šćepanović *et al.*, who considered that the total phenolic content correlated with the ABTS scavenging activity [66].

Antimicrobial activity: minimum inhibitory, bactericidal, and fungicidal concentrations. Table 6 illustrates the agar dilution method. The antimicrobial activity was tested on four types of pathogenic and opportunistic bacteria. The most pronounced antimicrobial activity, i.e., the lowest minimum inhibitory concentration of ≤ 10%, belonged to Vranac, Cabernet Sauvignon, and Merlot in relation to *Bacillus cereus* while the minimum bactericidal concentration was ≥ 30%. The Blatina wine samples showed the weakest antimicrobial activity

on all microorganisms in this test. Gram-positive *Staphylococcus aureus* and Gram-negative *Pseudomonas aeruginosa* showed similar sensitivity in relation to the analyzed wines with the minimum inhibitory concentration of 20%. Gram-negative *Escherichia coli* was the least sensitive to all analyzed wine varieties, compared to other pathogenic and opportunistic bacteria, with the minimum inhibitory concentration of 20 and 30% and the minimum bactericidal concentration of ≥ 30%. Probiotic cultures of *Lactobacillus plantarum* and *Saccharomyces boulardii* were not sensitive to the wine samples.

The antimicrobial effect of red wines on Gram-positive and Gram-negative pathogens is associated with phenolics [9]. According to many authors, phenolic components are more effective against Gram-positive bacteria than against Gram-negative ones [7]. In our research, Gram-positive *B. cereus* had the highest sensitivity to the tested wine concentrations; the lowest minimum inhibitory concentrations belonged to Vranac, Cabernet Sauvignon, and Merlot. These wines had a higher total phenolic content than Blatina, which had a weaker effect on *B. cereus*. Minimum bactericidal concentrations exceeded 30% in all wines, except for Vranac 2021 with its 30%. Our results were in agreement with those published by other authors [68]. However, these authors linked the inhibitory effect of wine on *B. cereus* to organic acids in the wine rather than to phenolic components. The content of gallic acid, caffeic acid, resveratrol, quercetin, quercetin-3-glucoside, and malvidin-3-glucoside also correlated with the antimicrobial activity of Vranac wine against Gram-negative bacteria, including *E. coli* and *P. aeruginosa* [9]. In our experiment, *P. aeruginosa* and *S. aureus* were both sensitive to the wines. The antimicrobial activity was similar in all samples, regardless of the contents of phenolics, alcohol, and organic acids.

The exact mechanism of antimicrobial activity of wine has not been fully explained [10]. Wine contains alcohols, organic acids, and various phenolic components; in addition, its pH is low. The combination of organic

Table 6 Antimicrobial activity of the wines under study

Microorganisms	Concentrations, % (v/v)	Blatina, 2020	Blatina, 2021	Vranac, 2020	Vranac, 2021	Cabernet Sauvignon, 2020	Cabernet Sauvignon, 2021	Merlot, 2020	Merlot, 2021
<i>Staphylococcus aureus</i>	MIC	20	20	20	20	20	20	20	20
	MBC	> 30	30	30	30	20	> 30	20	> 30
<i>Bacillus cereus</i>	MIC	20	20	< 10	< 10	< 10	< 10	10	< 10
	MBC	> 30	> 30	> 30	30	> 30	> 30	> 30	30
<i>Escherichia coli</i>	MIC	20	30	30	20	30	20	30	20
	MBC	> 30	> 30	> 30	> 30	> 30	> 30	> 30	> 30
<i>Pseudomonas aeruginosa</i>	MIC	20	20	20	20	20	20	20	20
	MBC	30	30	30	30	30	20	30	30
<i>Lactobacillus plantarum</i>	MIC	> 30	> 30	> 30	> 30	> 30	> 30	> 30	> 30
	MBC	> 30	> 30	> 30	> 30	> 30	> 30	> 30	> 30
<i>Candida albicans</i>	MIC	> 30	> 30	> 30	> 30	> 30	> 30	30	> 30
	MBC	> 30	> 30	> 30	> 30	> 30	> 30	> 30	> 30
<i>Saccharomyces boulardii</i>	MIC	> 30	> 30	> 30	> 30	> 30	> 30	> 30	> 30
	MBC	> 30	> 30	> 30	> 30	> 30	> 30	> 30	> 30

MIC – minimum inhibitory concentration; MBC – minimum bactericidal concentration

Table 7 Pearson's correlation coefficient of antioxidant and antimicrobial activity of wine

MIC	<i>Staphylococcus aureus</i>		<i>Bacillus cereus</i>		<i>Escherichia coli</i>		<i>Pseudomonas aeruginosa</i>		<i>Lactobacillus plantarum</i>		<i>Candida albicans</i>		<i>Saccharomyces boulardii</i>	
	MBC	MIC	MBC	MIC	MBC	MIC	MBC	MIC	MBC	MIC	MBC	MIC	MBC	MIC
Total phenolic content	Pearson's correlation	0.029	−0.458*	−0.722**	0.124	0.356	−0.010	0.029	−0.033	−0.010	−0.043	−0.010	0.214	0.214
	Sig. (2-tailed)	0.891	0.024	0.000	0.565	0.088	0.964	0.891	0.877	0.964	0.843	0.964	0.314	0.314
	N	24	24	24	24	24	24	24	24	24	24	24	24	24
Total nitrogen content	Pearson's correlation	0.017	−0.281	0.004	0.517**	0.323	−0.025	0.017	0.187	−0.025	0.048	−0.025	−0.183	−0.183
	Sig. (2-tailed)	0.937	0.184	0.985	0.010	0.123	0.909	0.937	0.381	0.909	0.825	0.909	0.391	0.391
	N	24	24	24	24	24	24	24	24	24	24	24	24	24
Total flavonoid content	Pearson's correlation	0.016	−0.242	−0.724**	−0.272	0.107	0.009	0.016	−0.177	0.009	−0.079	0.009	0.353	0.353
	Sig. (2-tailed)	0.939	0.255	0.000	0.198	0.620	0.966	0.939	0.408	0.966	0.714	0.966	0.091	0.091
	N	24	24	24	24	24	24	24	24	24	24	24	24	24
FRAP	Pearson's correlation	0.007	−0.215	−0.615**	0.036	0.226	−0.008	0.007	−0.210	−0.008	−0.081	−0.008	0.279	0.279
	Sig. (2-tailed)	0.976	0.313	0.001	0.867	0.289	0.970	0.976	0.325	0.970	0.708	0.970	0.186	0.186
	N	24	24	24	24	24	24	24	24	24	24	24	24	24
DPPH	Pearson's correlation	0.034	0.317	0.803**	0.085	−0.046	−0.049	0.034	0.117	−0.049	0.157	−0.049	−0.171	−0.171
	Sig. (2-tailed)	0.876	0.131	0.000	0.694	0.830	0.821	0.876	0.585	0.821	0.464	0.821	0.424	0.424
	N	24	24	24	24	24	24	24	24	24	24	24	24	24
ABTS	Pearson's correlation	−0.090	0.388	0.524**	−0.239	−0.154	0.066	−0.090	0.353	0.066	0.020	0.066	−0.213	−0.213
	Sig. (2-tailed)	0.675	0.061	0.009	0.261	0.473	0.760	0.675	0.090	0.760	0.926	0.760	0.317	0.317
	N	24	24	24	24	24	24	24	24	24	24	24	24	24
Total acidity	Pearson's correlation	−0.001	−0.111	−0.677**	−0.204	−0.231	0.002	−0.001	−0.523**	0.002	0.187	0.002	0.249	0.249
	Sig. (2-tailed)	0.995	0.605	0.000	0.340	0.277	0.994	0.995	0.009	0.994	0.381	0.994	0.241	0.241
	N	24	24	24	24	24	24	24	24	24	24	24	24	24

** – Correlation is significant at the 0.01 level (2-tailed);

* – Correlation is significant at the 0.05 level (2-tailed);

MIC – minimum inhibitory concentration; MBC – minimum bactericidal concentration

acids and alcohol with a low pH has a significantly better antibacterial effect than each of these factors separately [10]. Different phenolic components are known to exhibit a synergistic effect that contributes to a better antimicrobial activity of wine than individual phenolic compounds. Phenolic compounds were also reported to exhibit a synergistic effect with a low pH, alcohol, and organic acids [10]. All these factors mean that the antimicrobial activity of wine depends on the variety, growing conditions, concentration, and type of microorganism.

Candida albicans, *L. plantarum*, and *S. boulardii* showed no sensitivity to the wines in our research. Although *C. albicans* is known to be sensitive to some phenolic components, it was reported resistant to most wines and wine extracts [68]. Plant polyphenols and phenolic components have a stimulating effect on microorganisms that are part of the intestinal microbiome, e.g., *L. plantarum* and *S. boulardii* [11]. Dueñas *et al.* studied phenolic compounds in wine and red wine extracts, e.g., (+) catechin, anthocyanins, etc. [69]. They found out that these substances could stimulate the growth of bacteria of the *Lactobacillus* – *Enterococcus* spp. group. Vilela *et al.* revealed that *S. boulardii* has a high tolerance to alcohol and organic acids [70].

Table 7 illustrates the degree of correlation between the measured antioxidant and antimicrobial activity of wines using Pearson's test. The correlation was proven in the case of *B. cereus* bacteria (the largest number of cases), as well as *S. aureus* and *P. aereginosa* bacteria (one case each). This finding once again confirms that the antimicrobial activity of wine does not come only from the content of phenolic compounds, but is a combination of several different factors.

CONCLUSION

The statistical analyses confirmed a strong effect of the harvest year and variety, as well as their interaction, on the physicochemical properties of grape must. The highest total phenolic content, as well as the best antioxidant properties, belonged to Vranac wines of both vintages (2020 and 2021). All wines showed satisfactory antimicrobial properties, and the strongest activity was recorded against *Bacillus cereus*. The probiotic strains used in this research showed resistance to all wines. The Pearson test revealed a correlation between antioxidant and antimicrobial effects against *B. cereus*, as well as against *Staphylococcus aureus* and *Pseudomonas aeruginosa* (one case each), while other cases demonstrated no correlation. All grapevine varieties in this study (Blatina, Vranac, Cabernet Sauvignon, Merlot) proved to be suitable for the production of quality wines from grapes grown in the area of Mostar.

CONTRIBUTION

Conceptualization: T. Jovanović-Cvetković and A. Savić. Methodology: T. Jovanović-Cvetković, A. Savić, L. Topalić-Trivunović, A. Velemir, and R. Grbić. Investigation: A. Savić, L. Topalić-Trivunović, A. Velemir, and R. Grbić. Data curation: T. Jovanović-Cvetković, L. Topalić-Trivunović, A. Velemir, and R. Grbić. Original draft: T. Jovanović-Cvetković, A. Savić, L. Topalić-Trivunović, A. Velemir, and R. Grbić. All authors read and approved of the final manuscript.

CONFLICT OF INTEREST

The authors declared no conflict of interests regarding the publication of this article.

REFERENCES

1. Jovanović-Cvetković T, Sredojević M, Natić M, Grbić R, Akšić MF, Ercisli S, *et al.* Exploration and comparison of the behavior of some indigenous and international varieties (*Vitis vinifera* L.) grown in climatic conditions of Hercegovina: The influence of variety and vintage on physico-chemical characteristics of grapes. *Plants*. 2023;12(4):695. <https://doi.org/10.3390/plants12040695>
2. Gnilomedova NV, Anikina NS, Kolesnov AY. A review of methodological approaches to authenticating the geographical origin of wines. *Food Processing: Techniques and Technology*. 2023;53(2):231–246. (In Russ.). <https://doi.org/10.21603/2074-9414-2023-2-2429>: <https://elibrary.ru/AUQCPD>
3. Gutiérrez-Escobar R, Aliaño-González MJ, Cantos-Villar E. Wine polyphenol content and its influence on wine quality and properties: A review. *Molecules*. 2021;26(3):718. <https://doi.org/10.3390/molecules26030718>
4. Kubyshekin A, Ogai Y, Fomochkina I, Chernousova I, Zaitsev G, Shramko Yu. Polyphenols of red grape wines and alcohol-free food concentrates in rehabilitation technologies. In: Wong J, editor. *Polyphenols*. IntechOpen; 2018. pp. 99–120. <https://doi.org/10.5772/intechopen.76655>
5. Kesić A, Smajlović B, Ibršimović Mehmedinović N, Hodžić Z, Šestan A, Dedić J, *et al.* The content of total polyphenols of the selected red wines from the territory of Tuzla canton in correlation with antioxidant activity. *International Journal of Research Methodology*. 2019;2(1):141–151.
6. Radonjić S, Maraš V, Košmerl T. The importance of total polyphenols content in red wine. *Third International Mediterranean Congress on Natural Sciences, Health Sciences and Engineering*; 2019; Podgorica. Podgorica; 2019. p. 231–240.
7. Kauffmann AC, Castro VS. Phenolic compounds in bacterial inactivation: A perspective from Brazil. *Antibiotics*. 2023;12(4):645. <https://doi.org/10.3390/antibiotics12040645>

8. Santoro HC, Skroza D, Dugandžić A, Boban M, Šimat V. Antimicrobial activity of selected red and white wines against *Escherichia coli*: In vitro inhibition using fish as food matrix. *Foods*. 2020;9(7):936. <https://doi.org/10.3390/foods9070936>
9. Radovanović AN, Jovančičević BS, Radovanović BC, Mihajilov-Krstev T. Antimicrobial effectiveness of selected Vranac wines against six gram-positive and six gram-negative bacterial strains. *Tropical Journal of Pharmaceutical Research*. 2014;13(5):819–824. <https://doi.org/10.4314/tjpr.v13i5.24>
10. Boban N, Tonkić M, Budimir D, Modun D, Sutlović D, Punda-Polic V, et al. Antimicrobial effects of wine: Separating the role of polyphenols, pH, ethanol, and other wine components. *Journal of Food Science*. 2010;75(5):M322–M326. <https://doi.org/10.1111/j.1750-3841.2010.01622.x>
11. Milutinović M, Dimitrijevic-Branković S, Rajilić-Stojanović M. Plant extracts rich in polyphenols as potent modulators in the growth of probiotic and pathogenic intestinal microorganisms. *Frontiers in Nutrition*. 2021;8:688843. <https://doi.org/10.3389/fnut.2021.688843>
12. The climate of Bosnia and Herzegovina [Internet]. [cited 2023 Oct 10]. Available from: <https://www.fhmzbih.gov.ba/latinica/KLIMA/klimaBIH.php>
13. Federal hydrometeorological institute of Bosnia and Herzegovina [Internet]. [cited 2023 Oct 10]. Available from: <http://www.fhmzbih.gov.ba>
14. Compendium of international methods of wine and must analysis. Paris; 2021. 673 p.
15. Kupina S, Fields C, Roman MC, Brunelle SL. Determination of total phenolic content using the Folin-C assay: Single-laboratory validation, first action 2017.13. *Journal of AOAC International*. 2018;101(5):1466–1472. <https://doi.org/10.5740/jaoacint.18-0031>
16. Correa Uriburu FM, Cattaneo F, Maldonado LM, Zampini IC, Alberto MR, Isla MI. *Prosopis alba* seed as a functional food waste for food formulation enrichment. *Foods*. 2022;11(18):2857. <https://doi.org/10.3390/foods11182857>
17. Rodríguez-Vaquero MJ, Vallejo CV, Aredes-Fernández PA. Antibacterial, antioxidant and antihypertensive properties of polyphenols from Argentinean red wines varieties. *Open Journal of Pharmacology and Pharmacotherapeutics*. 2020;5(1):001–006. <https://doi.org/10.17352/ojpp.000010>
18. Rumpf J, Burger R, Schulze M. Statistical evaluation of DPPH, ABTS, FRAP, and Folin-Ciocalteu assays to assess the antioxidant capacity of lignins. *International Journal of Biological Macromolecules*. 2023;233:123470. <https://doi.org/10.1016/j.ijbiomac.2023.123470>
19. Mitrevska K, Grigorakis S, Loupassaki S, Calokerinos AC. Antioxidant activity and polyphenolic content of North Macedonian wines. *Applied Sciences*. 2020;10(6):2010. <https://doi.org/10.3390/app10062010>
20. Kowalska-Krochmal B, Dudek-Wicher R. The minimum inhibitory concentration of antibiotics: Methods, interpretation, clinical relevance. *Pathogens*. 2021;10(2):165. <https://doi.org/10.3390/pathogens10020165>
21. Geng D-H, Liu L, Zhou S, Sun X, Wang L, Zhou X, et al. Effects of *Lactobacillus plantarum* inoculum on the fermentation rate and rice noodle quality. *Journal of Oleo Science*. 2020;69(9):1031–1041. <https://doi.org/10.5650/jos.ess20003>
22. Chelliah R, Kim E-J, Daliri EB-M, Antony U, Oh D-H. In vitro probiotic evaluation of *Saccharomyces boulardii* with antimicrobial spectrum in a *Caenorhabditis elegans* model. *Foods*. 2021;10(6):1428. <https://doi.org/10.3390/foods10061428>
23. Catalogue of grapevines cultivated in France [Internet]. [cited 2023 Oct 15]. Available from: <https://www.plantgrape.fr/en>
24. Ivanišević D, Kalajdžić M, Drenjančević M, Puškaš V, Korać N. The impact of cluster thinning and leaf removal timing on the grape quality and concentration of monomeric anthocyanins in Cabernet-Sauvignon and Probus (*Vitis vinifera* L.) wines. *OENO One*. 2020;54(1):63–74. <https://doi.org/10.20870/oeno-one.2020.54.1.2505>
25. Aleinikova N, Didenko P, Shaporenko V, Didenko L, Belash S. The effect of mineral nutrition systems as an element of cultivation technology of wine grape varieties on their productivity in the conditions of Crimea. *IOP Conference Series: Earth and Environmental Science*. 2023;1206:012026. <https://doi.org/10.1088/1755-1315/1206/1/012026>
26. Arestova N, Ryabchun I. Influence of biostimulants on productivity and quality of grapes. *E3S Web of Conferences*. 2020;210:05001. <https://doi.org/10.1051/e3sconf/202021005001>
27. Jovanovic-Cvetkovic T, Micic N, Djuric, G, Cvetkovic M. Pollen morphology and germination of indigenous grapevine cultivars Žilavka and Blatina (*Vitis vinifera* L.). *AgroLife Scientific Journal*. 2016;5(1):105–109.
28. Jovanović-Cvetković T, Šutalo V, Kupe M, Ercisli S, Životić A, Pašalić B. Influence of interaction effects of the different pollenizers on the Blatina variety (*Vitis vinifera* L.) grape cluster and seed characteristics. *Plants*. 2022;11(3):420. <https://doi.org/10.3390/plants11030420>

29. Banjanin T. Characterization of quantitative and qualitative characteristics of Blatina vine variety in agroecological conditions of Trebinje. Ph.D. Thesis. Belgrade; 2022.
30. Maras V, Tomic M, Kodzulovic V, Knezevic B, Raicevic D, Cizmovic M. Yield and quality of grapes and wine of the cultivars “Vranac”, “Primitivo” and “NegroAmaro”. *Acta Horticulturae*. 2012;931. <https://doi.org/10.17660/ActaHortic.2012.931.43>
31. Popović T, Raičević D. Yield and quality of grapes of autochthonous variety Vranac in agroecological conditions of Podgorica subregion. In: Jacimovic M, editor. *The First International Conference on Vranac and Other Montenegrin Indigenous Sorts of Grapevine*. Podgorica: Montenegrin Academy of Sciences and Art; 2021. pp. 197–206.
32. Gombau J, Pons-Mercadé P, Conde M, Asbiro L, Pascual L, Gómez-Alonso S, et al. Influence of grape seeds on wine composition and astringency of Tempranillo, Garnacha, Merlot and Cabernet Sauvignon wines. *Food Science and Nutrition*. 2020;8:3442–3455. <https://doi.org/10.1002/fsn3.1627>
33. Bubola M, Rossi S, Váczy KZ, Hegyi ÁI, Persic M, Zdunić G, et al. Modification of cv. Merlot berry composition and wine sensory characteristics by different leaf area to fruit ratios. *Applied Sciences*. 2023;13(9):5456. <https://doi.org/10.3390/app13095465>
34. Liu H-F, Wu B-H, Fan P-G, Li S-H, Li L-S. Sugar and acid concentrations in 98 grape cultivars analyzed by principal component analysis. *Journal of the Science of Food and Agriculture*. 2006;86:1526–1536. <https://doi.org/10.1002/jsfa.2541>
35. Zhong H, Yadav V, Wen Z, Zhou X, Wang M, Han S, et al. Comprehensive metabolomics based analysis of sugar composition and content in berries of 18 grape varieties. *Frontiers in Plant Science*. 2023;14:1200071. <https://doi.org/10.3389/fpls.2023.1200071>
36. Coombe BG. Influence of temperature on composition and quality of grapes. *Acta Horticulturae*. 1987;206. <https://doi.org/10.17660/ActaHortic.1987.206.1>
37. Banjanin T, Lisov N, Petrović A, Ranković-Vasić Z, Blesić M. The quality of grape and wine of Merlot and Blatina varieties in the agroecological conditions of the Trebinje vineyard. VIII International Symposium on Agricultural Sciences. Banja Luka: Faculty of Agriculture University of Banja Luka; 2019. p. 69–75.
38. Jovanović-Cvetković T, Grbić R, Grobelnik Mlakar S, Bosančić B, Cvetković M. Physicochemical evaluation of the grape and wine of the Blatina, Trnjak and Vranac in different vintage. *AgroLife Scientific Journal*. 2023;12(1):105–115. <https://doi.org/10.17930/AGL2023113>
39. Maraš V, Kodžulović V, Mugoša M, Raičević J, Gazivoda A, Šućur S, et al. Clonal selection of autochthonous grape variety Vranac in Montenegro. In: Badnjevic A, editor. *Proceedings of the International Conference on Medical and Biological Engineering 2017*. Singapore: Springer; 2017. pp. 787–790. https://doi.org/10.1007/978-981-10-4166-2_118
40. Sivcev B, Rankovic-Vasic Z, Petrovic A, Jancis R, Milisic K. Fruit characteristics of the Merlot clones in Belgrade wine Growing Region, Serbia. *Journal of Advancements in Plant Science*. 2018;1(2).
41. Tecchio MA, da Silva MJR, Sanchez CAPC, Callili D, Vedoato BTF, Hernandez JL, et al. Yield performance and quality of wine grapes (*Vitis vinifera*) grafted onto different rootstocks under subtropical conditions. *Crop Production and Management*. 2022;81:e1622. <https://doi.org/10.1590/1678-4499.20210214>
42. Yang J, Lee J. Current research related to wine sensory perception since 2010. *Beverages*. 2020;6(3):47. <https://doi.org/10.3390/beverages6030047>
43. Zoecklein BW, Fugelsang KC, Gump BH, Nury FS. Alcohol and extract wine. In: Zoecklein B, Fugelsang KC, Gump BH, Nury FS, editors. *Wine analysis and production*. Springer; 1999. pp. 97–113.
44. Lima MMM, Choy YY, Tran J, Lydon M, Runnebaum RC. Organic acids characterization: Wines of Pinot noir and juices of “Bordeaux grape varieties”. *Journal of Food Composition and Analysis*. 2022;114:104745. <https://doi.org/10.1016/j.jfca.2022.104745>
45. Vicente J, Baran Y, Navascués E, Santos A, Calderón F, Marquina D, et al. Biological management of acidity in wine industry: A review. *International Journal of Food Microbiology*. 2022;375:109726. <https://doi.org/10.1016/j.ijfoodmicro.2022.109726>
46. International Code of Oenological Practices. Paris; 2022. 393 p. (In French).
47. Ribéreau-Gayon P, Dubordieu D, Donèche B, Lonvaud A. *Treatise on oenology – Microbiology of wine, Vinifications*. Paris: Dunod; 2004. 498 p. (In French).
48. Paramithiotis S, Stasinou V, Tzamourani A, Kotseridis Y, Dimopoulou M. Malolactic fermentation – Theoretical advances and practical considerations. *Fermentation*. 2022;8(10):521. <https://doi.org/10.3390/fermentation8100521>


49. Herjavec S, Jeromel A, Maslov L, Jagatić Korenika AM, Mihaljević M, Prusina T. Influence of different maceration times on the anthocyanin composition and sensory properties of blatina wines. *Agriculturae Conspectus Scientificus*. 2012;77(1):41–44.
50. Lavrić M, Prusina T. The influence of the vintage year on Blatina wine quality. *Proceedings of 55th Croatian & 15th International Symposium on Agriculture*; 2020; Vodice. Zagreb: University of Zagreb; 2020. p. 501–504.
51. Jagatić Korenika A-M, Tomaz I, Preinar D, Lavrić M, Šimić B, Jeremol A. Influence of *L. thermotolerans* and *S. cerevisiae* commercial yeast sequential inoculation on aroma composition of red wines (Cv Trnjak, Babic, Blatina and Frankovka). *Fermentation*. 2021;7(4):4. <https://doi.org/10.3390/fermentation7010004>
52. Gašović B, Đaković J, Radonjić S, Maraš V, Kodžulović V. Characteristics and quality of grapes and wines of the Vranac variety. In: Jacimovic M, editor. *The First International Conference on Vranac and Other Montenegrin Indigenous Sorts of Grapevine*. Podgorica: Montenegrin Academy of Sciences and Art; 2021. pp. 267–277.
53. Jakšić D, la Notte P, Giannini PB, Perović V, Cagnazzo A. Montenegrin Vranac vine variety in the most eastern point of the Vranac cultivation area – Knjaževac wine-growing region (Serbia). In: Jacimovic M, editor. *The First International Conference on Vranac and Other Montenegrin Indigenous Sorts of Grapevine*. Podgorica: Montenegrin Academy of Sciences and Art; 2021. pp. 207–225.
54. Sošić S, Pajović-Šćepanović R, Raičević D, Popović T. Quality of wines Vranac and Kratošija in the vintage 2021. *Agriculture and Forestry*. 2023;69(1):127–137. <https://doi.org/10.17707/AgricultForest.69.1.11>
55. Ivanova-Petropulos V, Ricci A, Nedelkovski D, Dimovska V, Parpinello GP, Versari A. Targeted analysis of bioactive phenolic compounds and antioxidant activity of Macedonian red wines. *Food Chemistry*. 2015;171:412–420. <https://doi.org/10.1016/j.foodchem.2014.09.014>
56. Raičević D, Mijović S, Popović T, Pajović-Šćepanović R. The influence of variety and vintage on the chemical composition and sensory properties of red wines in Podgorica subregion (Montenegro). *Journal of Agricultural, Food and Environmental Sciences*. 2017;71(1):157–164.
57. Eder R, Pajović Šćepanović R, Raičević D, Popović T, Korntheuer K, Wendelin S, et al. Study of the effects of climatic conditions on the phenolic content and antioxidant activity of Austrian and Montenegrin red wines. *OENO One*. 2023;57(3):69–85. <https://doi.org/10.20870/oeno-one.2023.57.3.7450>
58. Xu S, Zhu J, Zhao Q, Gao J, Zhang H, Hu B. Quality evaluation of Cabernet Sauvignon wines in different vintages by ¹H nuclear magnetic resonance-based metabolomics. *Open Chemistry*. 2021;19(1):385–399. <https://doi.org/10.1515/chem-2020-0126>
59. Antonenko MV, Guguchkina TI, Prakh AV, Kolesnov AYU, Zenina MA. Research of physical and chemical characteristics of grapes from different regions of Krasnodar territory for their use as standards of authenticity of wine production. *Fruit Growing and Viticulture of South Russia*. 2019;55(1):95–106. <https://doi.org/10.30679/2219-5335-2019-1-55-95-106>
60. Banjanin T, Ranković-Vasić Z, Nikolić D, Anđelić B. Influence of climatic factors on the quality of Merlot grapevine variety in Trebinje region vineyards (Bosnia and Herzegovina). *Agrofor*. 2019;4(2):95–101. <https://doi.org/10.7251/AGRENG1902094B>
61. Miele A. Wine composition of Merlot and Cabernet Sauvignon vine clones under the environmental conditions of Serra Gaúcha, Brazil. *Food Science and Technology*. 2021;41(Suppl.1):116–122. <https://doi.org/10.1590/fst.10520>
62. Muñoz-Bernal ÓA, Vazquez-Flores AA, de la Rosa LA, Rodrigo-García J, Martínez-Ruiz NR, Alvarez-Parrilla E. Enriched red wine: Phenolic profile, sensory evaluation and in vitro bioaccessibility of phenolic compounds. *Foods*. 2023;12(6):1194. <https://doi.org/10.3390/foods12061194>
63. Pajović Šćepanović R, Madžgalj V, Vukoslavljević V. Assay of polyphenolic in Montenegrin Vranac wines. *Mitteilungen Klosterneuburg*. 2019;69:65–75.
64. Pajović Šćepanović R, Wendelin S, Raičević D, Eder R. Characterization of the phenolic profile of commercial Montenegrin red and white wines. *European Food Research and Technology*. 2019;245:2233–2245. <https://doi.org/10.1007/s00217-019-03330-z>
65. Tzanova M, Atanassova S, Atanasov V, Grozeva N. Content of polyphenolic compounds and antioxidant potential of some Bulgarian red grape varieties and red wines, determined by HPLC, UV, and NIR spectroscopy. *Agriculture*. 2020;10(6):193. <https://doi.org/10.3390/agriculture10060193>
66. Đorđević N, Novaković M, Pejin B, Živković M, Savić A, Mutić J, et al. An insight into chemical composition and biological activity of Montenegrin *Vranac* red wine. *Scientia Horticulturae*. 2018;230:142–148. <https://doi.org/10.1016/j.scienta.2017.11.033>


67. Mitić MN, Kostic DA, Pavlović AN, Micić RJ, Stojanović BT, Paunović DĐ, *et al.* Antioxidant activity and polyphenol profile of Vranac red wines from Balkan region. *Chemical Industry*. 2016;70(3):265–275. <https://doi.org/10.2298/HEMIND150130032M>
68. Čomić LR, Radojević ID, Vasić SM, Mladenović KG, Grujović MŽ. Traditionally made red wines produced from an autochthonous grapevine variety as a source of biologically active compounds and their antioxidant potential. *Journal of Food and Nutrition Research*. 2020;59(4).
69. Dueñas M, Cueva C, Muñoz-González I, Jiménez-Girón A, Sánchez-Patán F, Santos-Buelga C, *et al.* Studies on modulation of gut microbiota by wine polyphenols: From isolated cultures to omic approaches. *Antioxidants*. 2015;4(1):1–21. <https://doi.org/10.3390/antiox4010001>
70. Vilela A, Fernanda Cosme F, Inês A. Wine and non-dairy fermented beverages: A novel source of pro- and prebiotics. *Fermentation*. 2020;6(4)113. <https://doi.org/10.3390/fermentation6040113>


ORCID IDs

Tatjana Jovanović-Cvetković  <https://orcid.org/0000-0001-5767-1698>

Aleksandar Savić  <https://orcid.org/0000-0002-2475-6764>

Ljiljana Topalić-Trivunović  <https://orcid.org/0000-0002-7988-0025>

Ana Velemir  <https://orcid.org/0000-0003-2152-5183>

Rada Grbić  <https://orcid.org/0000-0002-6696-0552>



Physicochemical, rheological, and microbiological properties of honey-fortified probiotic drinkable yogurt

Zehra Albay^{1,*}, Mehmet Çelebi², Bedia Şimşek¹

¹ Süleyman Demirel University, Isparta, Türkiye

² Aydın Adnan Menderes University, Aydın, Türkiye

* e-mail: zehraalbay32@gmail.com

Received 16.10.2023; Revised 29.12.2023; Accepted 09.01.2024; Published online 25.10.2024

Abstract:

This study aimed to investigate the physicochemical, rheological, and microbiological attributes of drinkable yogurts prepared with three distinct types of honey (flower, pine, and thyme) in amounts of 10 and 20% and probiotic cultures (*Lactobacillus acidophilus* and *Bifidobacterium* spp.).

The control sample was brighter while the yogurt containing 20% pine honey was more yellow during storage (21 days). The samples' serum separation quantities rose together with the honey ratio. All the honey-fortified drinkable yogurts were found to be non-Newtonian pseudoplastic liquids that are thixotropic. However, as the honey ratio increased, the apparent viscosity and consistency coefficients increased, too. After 21 days of storage, *L. acidophilus* and *Bifidobacterium* spp. counts rose to more than 5.0 log CFU/mL in the experimental yogurts containing honey (except for the sample with 20% flower honey). The panelists preferred the 10% honey-fortified drinkable yogurts over the others. The yogurts with flower honey were mostly favored, followed by pine and thyme honeys. Although honey contributed to the properties of drinkable yogurt, adding more than 10% of honey degraded the product's quality and acceptability.

In conclusion, 10% is an optimal amount for flower and pine honey, with a smaller amount recommended for thyme honey. More research is needed on honey-fortified drinkable yogurt for its commercial production.

Keywords: Drinkable yogurt, flower honey, pine honey, thyme honey, functional foods, dairy drinks

Funding: This study was financially supported by the Süleyman Demirel University's Scientific Research Project Coordination Unit through Project No. BAP- 4607-YL1-16.

Please cite this article in press as: Albay Z, Çelebi M, Şimşek B. Physicochemical, rheological, and microbiological properties of honey-fortified probiotic drinkable yogurt. *Foods and Raw Materials*. 2025;13(2):320–329. <https://doi.org/10.21603/2308-4057-2025-2-641>

INTRODUCTION

Functional foods such as yogurt and honey are crucial to human health. Yogurt has already demonstrated its functional efficacy against a variety of human illnesses, including diabetes, chronic diseases, and metabolic syndrome risk factors such as hyperglycemia [1, 2]. Recently, a few highly diverse dairy drinks, such as drinkable yogurt, fermented milk, and other milk-based beverages, have been added to the dairy production program to increase dairy consumption [3]. Drinkable yogurt is a non-alcoholic fermented milk product. Traditionally, it is produced by adding water (30–50%) and salt (0.5–1%) to yogurt. Starter bacteria (*Streptococcus thermophilus* and *Lactobacillus delbrueckii* subsp. *bulgaricus*) are used to facilitate the fermentation process

in industrial production [4, 5]. Probiotic bacteria have recently become more prevalent in fermented milk products such as drinkable yogurt. *Lactobacilli* and *Bifidobacteria* are the most popular strains of the microbial genera linked to drinkable probiotic yogurts. Probiotics are live microorganisms that have health benefits for the host and regulate microbial activity in the gastrointestinal system [6, 7]. They help restore the balance of beneficial intestinal microflora while also preventing dangerous enteropathogens. Probiotics lower blood cholesterol, boost the body immunity, and have antimutagenic and anticarcinogenic properties. They also regulate lactose intolerance symptoms, reduce antibiotic side effects, and prevent gut infections by creating organic acids and antibacterial compounds. In addition to their health

benefits, probiotics help dairy products last longer and have better sensory characteristics. To produce health-benefitting effects, dairy products must contain at least $6\text{--}7 \log \text{CFU/g}$ of live probiotic bacteria. Their growth and activity are usually improved by prebiotics. In particular, prebiotics selectively stimulate the growth of bacterial species such as *Bifidobacterium* spp. and *Lactobacilli* spp. while inhibiting the proliferation of bacteria such as *Salmonella* spp. and *Escherichia coli* [8].

Recent years have seen a widespread intake of dairy drinks containing flavorings, sugar syrup, and water. Various ingredients, including chocolate, honey, and strawberries, are used to enhance the flavor of dairy-based healthy drinks [3]. Honey has been regarded a better alternative to artificial sweeteners in new dairy products [9]. This natural nutritious sweetener is one of the most popular foods around the world. In 2019, the global output of honey was 1.9 million tons, with China accounting for 24% of total production (444 100 tons), followed by Türkiye (109 330 tons), Canada (80 345 tons), Argentina (78 927 tons), Iran (75 463 tons), and the United States (71 179 tons) [1]. Honey has traditionally played an important role in diets due to its superior flavor and many other beneficial characteristics.

There is a wide variety of natural bee honeys, depending on many factors such as botanical and geographical (regional or local) origins and bee species [10, 11]. The botanical origin (honey harvest) distinguishes between flower and honeydew honeys [10]. Furthermore, the honey's botanical and geographical origins determine its quality criteria, such as color, moisture, acidity, and phenolic content. Other important factors include the climate, environmental conditions, and the processes that honey goes through [11]. Additionally, two types of honey are generally defined: multifloral or monofloral, which are made from a combination of numerous botanical species or a single flower variety, respectively. Monofloral honey has a higher market value due to its physicochemical properties [12]. Türkiye boasts a large variety of monofloral honeys because of its geographic position [11].

The natural organic material known as honey is created by honeybees (*Apis mellifera* L.) from flower nectar [1]. Pine honey is made by honeybees processing the secretions of *Marchalina hellenica*. This insect lives on *Pinus brutia*, which grows in Türkiye, particularly in the Aegean, Western Mediterranean, and Southern Marmara regions [9]. Thyme honey, on the other hand, is produced by bees from thyme (*Thymus* spp.) blossoms and has a high sensory value [12]. Honey provides body cells with a significant amount of energy [11]. It generally consists of 70–80% sugar, 10–20% water, and such components as proteins, free amino acids, vitamins, mineral salts, phenolics, and organic acids. Monosaccharides, glucose, and fructose are the main sugars present in honey [13]. In addition, honey contains 25 oligosaccharides, including hybridose, panose, and raffinose. These oligosaccharides are reported to have similar effects to those of fructooligosaccharides and glucooligosaccharides. Honey also contains antioxidants (such as caro-

tenoids, flavonoids, and phenolics) and Maillard reaction products. Together with its acidity and sugar profile, they provide honey with special sensory qualities [14]. Non-peroxide substances (such as glucose oxidase, catalase, hydrogen peroxide, and lysozyme) and phenolic substances found in honey exhibit antimicrobial properties [15]. Furthermore, honey contains probiotics and prebiotics, has immunomodulatory and antiviral properties, and is used to treat cancer and neurological illnesses. Honey has always held a unique position in the human diet due to its functional and therapeutic qualities [10].

In this study, honey was added to drinkable yogurts, which have a slightly salty and sour flavor, to improve their functional characteristics. We aimed to see how different types (flower, pine, and thyme) and ratios (10 and 20%) of honey added to drinkable yogurts containing probiotic culture (*Lactobacillus acidophilus* and *Bifidobacterium* spp.) affected their physicochemical, rheological, and microbiological properties. We expect this study to benefit industry, science, and consumers.

STUDY OBJECTS AND METHODS

Materials. In this study, floral, pine, and thyme honeys were added to drinkable probiotic yogurts at two different ratios (10 and 20%). Raw cow milk ($4 \pm 1^\circ\text{C}$) was provided by the Ünsüt Dairy Products Plant (Isparta, Türkiye) and the Isparta Cattle Breeders' Association. To prepare drinkable yogurt, *Streptococcus thermophilus* and *Lactobacillus delbrueckii* subsp. *bulgaricus* were mixed with the yogurt culture (YC380) and the probiotic cultures *Lactobacillus acidophilus* and *Bifidobacterium* spp. (LA-5 and BB-12) obtained from Peyma-Chr. Hansen (Istanbul, Türkiye). Thyme honey was acquired from the regional honey producers in Isparta, while the honeys sold in the market (Anavarza Honey) were supplied by Sezen Gıda Ltd. Şti. (Istanbul, Türkiye).

Drinkable yogurt production. Homogenized cow's milk was pasteurized at 90°C for 15 min and then cooled to $43 \pm 2^\circ\text{C}$. The yogurt culture (1%) and the probiotic culture (2%) were used as inoculants. The drinkable yogurts were normalized with water once the pH level was 4.6 and the dry matter was 7.5%. Then, 0.3% of table salt was added to the samples. The yogurts were divided into seven groups, namely two samples with flower honey (10 and 20%), two samples with pine honey (10 and 20%), two samples with thyme honey (10 and 20%), and the control yogurt without any honey. The yogurts were placed in sterilized glass jars and kept chilled ($4 \pm 1^\circ\text{C}$) for storage. Physicochemical, microbiological, and rheological analyses were performed on days 1, 10, and 21 of storage.

Applied analyses. Raw milk and honey analysis. Raw milk's dry matter, fat, titration acidity, and total nitrogen were calculated according to AOAC [16]. A WTW pH 315 digital meter (Weilheim, Germany) was used to monitor pH readings. A Hanna HI 96801 digital refractometer (Hanna Instruments Inc., USA) was used to measure the total soluble solids content (Brix) in the honeys.

Physicochemical analysis. Dry matter, fat, titration acidity (ISO/TS 11869:2012) and salt analyses were carried out. The micro-Kjeldahl method was employed to measure protein contents [16]. Serum separation was performed as described in [17]. A WTW pH 315 digital meter (Weilheim, Germany) was used to monitor pH readings.

Color properties. The Hunter method was employed to analyze the color properties of the honey-fortified drinkable yogurts [18]. A CR-400 Minolta chroma meter (Konica Minolta, Inc., Japan) was used to determine the L^* , a^* , and b^* values representing bright/dark (0 black, 100 white), green/red (−60 green, 60 red), and blue/yellow (−60 blue, 60 yellow), respectively. The colors were examined by utilizing cells of 9 cm in diameter and 4 cm in height. Calibration was performed on a white plate ($Y = 92.7$, $x = 0.3160$, $y = 0.3321$). The L^* , a^* , and b^* values were measured in triplicate.

Rheological properties. A Brookfield DV-II+Pro Extra viscometer (Brookfield Engineering Laboratories Inc., USA) was employed to determine the rheological characteristics of the drinkable yogurt and honey samples. The yogurt's flow type was ascertained by using a tiny sample adaptor, and the honey's viscosity was assessed by using a 0.6-mm spindle tip. The samples were recorded and plotted using the RHEOCAL[®] application software (Brookfield Engineering Laboratories Inc., USA). The yogurt samples were stored at 4°C and examined on days 1, 10, and 21 of storage.

Microbiological analysis. Under aseptic conditions, 10 mL of a drinkable yogurt sample was added to 90 mL of a sterile Ringer's solution (1/10), and 1 mL of this dilution was transferred to 9 mL of a sterile Ringer's solution. Then, serial dilutions were carried out. The materials were microbiologically analyzed using the spread plate method. During storage, the contents of *L. delbrueckii* subsp. *bulgaricus* and *S. thermophilus* in the yogurts were detected on MRS (de Man, Rogosa, and Sharpe) and M17 agars, respectively (Merck, Germany) [19]. Petri dishes were incubated at 37°C for 48 and 72 h to enumerate *S. thermophilus* and *L. delbrueckii* subsp. *bulgaricus* counts, respectively.

The Plate Count Agar was used to determine the total number of mesophilic bacteria. Petri dishes were incubated for 72 h at 30°C under aerobic conditions [20]. The numbers of *Bifidobacterium* spp. and *L. acidophilus* were determined on MRS-NNLP and MRS-sorbitol agars, respectively [21, 22]. The MRS-NNLP agar medium contained nalidixic acid (50 mg/L), neomycin sulphate (100 mg/L), lithium chloride (3000 mg/L), and paronomycin sulphate (200 mg/L). The NNLP was mixed with the MRS agar medium, which had been sterilized with a 0.45- μ m disposable sterile filter just before pouring into Petri plates. For *L. acidophilus* enumeration, the MRS agar (90 mL) was sterilized and mixed with 10% (w/v) D-sorbitol solution (10 mL) using a sterile 0.45- μ m filter. For the enumeration of both probiotics, the Petri dishes were incubated for 72 h at 37°C in anaerobic jars (Merck, Germany). For yeast-mold counting, 1 mL of the prepared 1:10 dilution was inoculated

into the PDA (Potato Dextrose Agar) medium (Merck, Germany). The cultivated petri dishes were incubated at 25°C for 4–5 days [23]. Then, 1 mL of a 1:10 dilution was obtained and put into the EMB (Eosin Methylene-Blue Lactose Sucrose) medium (Merck, Germany) for coliform bacteria detection. The Petri dishes were incubated at 37°C for 24–48 h [24]. The results were expressed as log transformed data in CFU/g.

Sensory analysis. Until their sensory evaluation, the drinkable yogurts were kept in sterile glass jars at $4 \pm 1^\circ\text{C}$ in the refrigerator. On days 1, 10, and 21 of storage, they were evaluated by 10 panelists (6 women and 4 men aged 20–40). Although the panelists had a prior experience with sensory analysis, they were given two two-hour training sessions on evaluating drinkable yogurts. Three-digit numbers were chosen at random to code the samples. The panelists tasted the samples that were very good and very bad in terms of the indicated sensory qualities, and they were instructed to use those samples as a benchmark for evaluating the test samples. With the use of a less-to-more indicator across 10 points, the sensory qualities of the drinkable yogurts were assessed in accordance with five criteria: appearance (yellowness, general color, etc.), texture (fluidity, consistency, etc.), taste (sweetness, saltiness, etc.), odor (aroma, honey-like odor, etc.), and general acceptance [25].

Statistical analysis. Three parallel analyses were set up in triplicate. The SPSS 17.0 program was used to statistically examine the analysis outcomes. The Duncan multiple comparison test ($p < 0.05$) was used to interpret the samples where there was a statistically significant variation in storage times for the analysis results and differences between the samples [26].

RESULTS AND DISCUSSION

Raw milk and honey analysis. The average specific gravity, pH, titration acidity (% lactic acid), dry matter, fat, and total nitrogen values of raw cow's milk used in drinkable yogurt production were found as 1.031 g/cm³, 6.72, 0.18, 11.99, 3.75, and 3.35%, respectively.

The average L^* , a^* and b^* values were 23.63, 2.64, and 8.29, respectively, in the flower honey; 22.91, 3.23, and 6.74, respectively, in the pine honey; and 25.29, 1.16, and 9.42, respectively, in the thyme honey. These results were different from those found in other studies [27, 28]. The color differences may be due to the type of honey used. In general, the color is light in honeys with a low value and dark in honeys with a high value. The color of honey is essentially related to the total mineral content. It is derived from plant pigments that include unknown amounts of chlorophyll, carotene, xanthophyll, as well as yellow and green hues [27]. In our study, the total soluble solid contents (brix) in the flower, pine, and thyme honeys were 79.533 ± 1.357 , 78.633 ± 1.422 , and 79.500 ± 0.264 , respectively ($n = 3$). Since there are few studies on thyme honey, we compared the brix values for flower, pine, and thyme honeys with those for different types of honey. We found that our results were similar to those reported by some other studies [13, 27].

Physicochemical analysis. Table 1 shows the results of the physicochemical and color analyses of the probiotic drinkable yogurts on days 1, 10, and 21. We found a statistically significant ($p < 0.05$) difference in the samples' pH values but no statistical difference between the storage times and the samples in terms of titration acidity (% lactic acid). On day 1, the control group had the lowest pH levels (4.19) compared to the other samples. After 21 days, however, the pH values of the samples became close to each other. The control group had the highest (0.60) lactic acid content among the samples. In a study by Özünlü on drinkable yogurt, lactic acid levels were found between 0.495 and 0.817% [29]. In another study, yogurts made with flower honey had the lowest pH value (4.13), while yogurts made with chestnut honey had the highest pH value (4.20) [30]. Since there are few studies on honey-fortified drinkable yogurt, we compared our results with those for different types of honey. Coskun and Dirican reported that the titration acidity of yogurts with pine honey increased during storage, while their pH values decreased [9]. The titration acidity of honey yogurts is believed to be affected by the organic acids that honey contains [30]. These acids include for-

mic, acetic, butyric, lactic, oxalic, succinic, tartaric, maleic, pyruvic, pyroglutamic, alpha-ketoglutaric, glycolic, citric, malic, 2- or 3-phosphoglyceric, α - or β -glycerophosphate, glucose-6-phosphate, and others.

The serum separation values showed a statistically significant difference between the samples under study ($p < 0.05$). Later during storage, more serum separated from all the samples (Table 1). The highest rise in serum separation (from 3.70 to 14.12 mL/25 g) was recorded in the sample containing 10% flower honey. We also found that the yogurts with larger amounts of honey had higher serum separation values. Özünlü determined that the serum separation values of drinkable yogurts increased gradually during 14 days [29].

In our study, the average dry matter content in the control group was 7.22% (Table 2), which was lower than in the yogurts with different types and amounts of honey added. The samples with larger amounts of honey (20%) had higher dry matter values. We compared our results with those found in some honey-supplemented kefir studies since kefir is a probiotic-containing drink. For example, in a study by Dogan, the dry matter contents in the kefir samples were directly proportionate to

Table 1 Physicochemical and color characteristics of drinkable yogurts ($n = 3$)

Parameter	Storage day	Samples						
		Control	Flower honey (10%)	Flower honey (20%)	Pine honey (10%)	Pine honey (20%)	Thyme honey (10%)	Thyme honey (20%)
pH	1	4.19 \pm 0.03 ^{bcd}	4.27 \pm 0.03 ^{a-d}	4.32 \pm 0.09 ^{ab}	4.25 \pm 0.03 ^{a-d}	4.31 \pm 0.06 ^{abc}	4.24 \pm 0.01 ^{a-d}	4.30 \pm 0.09 ^{a-d}
	10	4.10 \pm 0.02 ^{bcd}	4.11 \pm 0.05 ^{bcd}	4.15 \pm 0.01 ^{a-d}	4.11 \pm 0.08 ^{bcd}	4.14 \pm 0.11 ^{a-d}	4.14 \pm 0.08 ^{a-d}	4.17 \pm 0.09 ^{a-d}
	21	4.05 \pm 0.05 ^d	4.06 \pm 0.06 ^d	4.10 \pm 0.01 ^{bcd}	4.10 \pm 0.08 ^{bcd}	4.11 \pm 0.11 ^{bcd}	4.06 \pm 0.09 ^{cd}	4.08 \pm 0.11 ^{bcd}
Lactic acid, %	1	0.56 \pm 0.07	0.55 \pm 0.04	0.53 \pm 0.09	0.54 \pm 0.03	0.53 \pm 0.02	0.54 \pm 0.03	0.53 \pm 0.04
	10	0.60 \pm 0.03	0.58 \pm 0.02	0.57 \pm 0.07	0.59 \pm 0.06	0.58 \pm 0.05	0.59 \pm 0.04	0.58 \pm 0.06
	21	0.59 \pm 0.02	0.57 \pm 0.01	0.56 \pm 0.03	0.57 \pm 0.05	0.54 \pm 0.06	0.58 \pm 0.05	0.57 \pm 0.07
Serum separation, mL/25 g	1	2.72 \pm 0.32 ^{fg}	3.70 \pm 0.80 ^{ef}	4.27 \pm 0.27 ^{def}	3.35 \pm 0.20 ^{efg}	4.25 \pm 0.40 ^{def}	3.47 \pm 0.97 ^{efg}	4.40 \pm 0.50 ^{def}
	10	3.25 \pm 0.75 ^{efg}	5.15 \pm 0.10 ^{cde}	6.20 \pm 0.05 ^{cd}	4.90 \pm 0.30 ^{def}	5.75 \pm 0.10 ^{cde}	6.67 \pm 0.37 ^{cd}	7.15 \pm 0.60 ^{cd}
	21	6.02 \pm 0.42 ^{cd}	14.12 \pm 0.12 ^a	14.55 \pm 0.60 ^a	12.67 \pm 0.27 ^{abc}	13.00 \pm 0.50 ^{ab}	12.70 \pm 0.25 ^{abc}	13.47 \pm 0.75 ^{ab}
L^*	1	82.08 \pm 0.06 ^a	77.92 \pm 0.50 ^{bc}	74.47 \pm 0.27 ^{cd}	77.01 \pm 0.11 ^{bcd}	72.89 \pm 0.09 ^{gh}	78.10 \pm 0.03 ^b	74.94 \pm 0.14 ^{ef}
	10	81.50 \pm 0.16 ^a	76.82 \pm 0.74 ^{bcd}	74.32 \pm 0.42 ^d	76.40 \pm 0.23 ^d	72.75 \pm 0.31 ^{gh}	77.99 \pm 0.22 ^{bc}	74.77 \pm 0.17 ^{ef}
	21	80.83 \pm 0.82 ^a	76.68 \pm 0.60 ^{a-d}	73.64 \pm 0.71 ^{de}	75.77 \pm 0.61 ^{de}	72.01 \pm 0.61 ^h	76.82 \pm 0.64 ^{bcd}	74.09 \pm 0.44 ^{fg}
a^*	1	-2.80 \pm 0.27 ^d	-2.03 \pm 0.29 ^{bc}	-1.73 \pm 0.23 ^{ab}	-1.74 \pm 0.39 ^{ab}	-1.21 \pm 0.35 ^a	-2.14 \pm 0.27 ^{bcd}	1.77 \pm 0.26 ^{ab}
	10	-2.80 \pm 0.03 ^d	-2.04 \pm 0.20 ^{bc}	-1.74 \pm 0.12 ^{ab}	-1.71 \pm 0.28 ^{ab}	-1.13 \pm 0.13 ^{gh}	-2.04 \pm 0.28 ^{bcd}	-1.70 \pm 0.27 ^{ab}
	21	-2.74 \pm 0.35 ^d	-1.98 \pm 0.35 ^{bc}	-1.66 \pm 0.03 ^{ab}	-1.65 \pm 0.08 ^{ab}	-1.14 \pm 0.22 ^a	-2.01 \pm 0.08 ^{bcd}	-1.66 \pm 0.10 ^{ab}
b^*	1	3.69 \pm 0.08 ^h	7.69 \pm 0.25 ^f	10.38 \pm 0.05 ^b	9.20 \pm 0.14 ^c	12.40 \pm 0.04 ^a	6.45 \pm 0.10 ^g	8.34 \pm 0.04 ^{de}
	10	3.72 \pm 0.03 ^h	7.46 \pm 0.78 ^f	10.49 \pm 0.01 ^b	9.41 \pm 0.01 ^c	12.42 \pm 0.05 ^a	6.52 \pm 0.11 ^g	8.38 \pm 0.18 ^{de}
	21	3.71 \pm 0.15 ^h	7.67 \pm 0.02 ^f	10.07 \pm 0.17 ^b	9.32 \pm 0.03 ^c	12.10 \pm 0.03 ^a	6.03 \pm 0.04 ^g	8.27 \pm 0.05 ^{de}

*a-h — Different letters indicate statistical significance between the groups ($p < 0.05$)

Table 2 Physicochemical parameters of drinkable yogurts ($n = 3$)

Parameter, %	Samples						
	Control	Flower honey (10%)	Flower honey (20%)	Pine honey (10%)	Pine honey (20%)	Thyme honey (10%)	Thyme honey (20%)
Dry matter	7.22 \pm 0.02 ^c	13.61 \pm 0.03 ^{ab}	19.73 \pm 0.03 ^a	13.33 \pm 0.01 ^{ab}	19.32 \pm 0.08 ^a	13.82 \pm 0.05 ^{ab}	19.23 \pm 0.03 ^a
Fat	1.25 \pm 0.05 ^a	1.15 \pm 0.00 ^{ab}	1.00 \pm 0.00 ^b	1.15 \pm 0.05 ^{ab}	1.00 \pm 0.00 ^b	1.15 \pm 0.02 ^{ab}	1.10 \pm 0.00 ^b
Salt	0.51 \pm 0.13 ^a	0.47 \pm 0.13 ^{ab}	0.45 \pm 0.12 ^{ab}	0.47 \pm 0.11 ^{ab}	0.45 \pm 0.12 ^{ab}	0.48 \pm 0.11 ^{ab}	0.44 \pm 0.11 ^b
Protein	2.35 \pm 0.26 ^a	2.11 \pm 0.16 ^a	1.95 \pm 0.11 ^a	2.12 \pm 0.14 ^a	2.04 \pm 0.11 ^a	2.10 \pm 0.12 ^a	1.98 \pm 0.14 ^a

*a-c — Different letters indicate statistical significance between the groups ($p < 0.05$)

the amount of honey added [31]. This was because honey contains a large amount of total soluble solids, most of which are sugars.

Our study revealed that the fat content was the highest (1.25) in the control group and the lowest (1.00) in the samples with 20% flower honey and 20% pine honey. The fat content decreased as the honey concentration increased. The fat content in our yogurts was lower than that reported by Şanlı [32].

The salt content was the highest in the control group (Table 2). In the study by Şanlı, salt ranged from 0.74 to 0.79% [32]. Salt is known to enhance flavor and increase sweetness, hide any metallic or chemical flaws, and speed up the product's processing [33]. Therefore, the honey-fortified samples in our study were minimally salted, resulting in lower salt values compared to other studies.

The protein contents in the yogurt samples decreased with larger amounts of honey added. The lowest protein content was detected in the yogurt with 20% flower honey. Chapagain *et al.* reported that a yogurt beverage with 7.5% honey had a protein content of 2.25% [34]. Our samples containing 10% honey had slightly higher protein contents. Protein production is stimulated by proline, lysine, phenylalanine, GABA, glutamine, serine, as well as glutamic and aspartic acids present in honey. However, storing honey for a long time in unfavorable conditions significantly decreases the number of amino acids [35].

The L^* values showed a statistically significant ($p < 0.05$) difference between the drinkable yogurt samples (Table 1). The control group had the highest brightness (L^*) value. The samples with 20% honey had a lower L^* value than those with 10% honey, and these values dropped throughout the storage time.

The a^* values increased with larger amounts of honey in all the samples. The samples with 10% thyme and 10% floral honey had the closest a^* values to those in the control group. Also, we found no statistically significant changes in the a^* values between the control and any other samples throughout the storage time.

The samples with pine honey had higher b^* values than those with floral and thyme honeys, while the samples with thyme honey had the lowest b^* values (apart from the control group). The b^* values partially dropped during storage, with no statistically significant changes.

In the study by İnce, the samples with flower and pine honeys had their L^* values ranging between 74.57 and 81.14, a^* values of -2.17 to -2.88 , and b^* values ranging from 4.54 to 8.58 during storage [36]. Similarly, Machado *et al.* found that the L^* values of yogurt decreased with larger amounts of honey, but the a^* and b^* values increased [14]. They noted that the bright white color of goat milk combined with high gloss values made the honey appear brighter in the honey-containing samples. The L^* , a^* , and b^* values found in our study differed from those in other studies due to the coloring properties of honey, the natural proteolytic activity in yogurt or drinkable yogurt, and the oxidation of fatty acids [14].

Rheological properties. Thyme honey had the maximum viscosity (970.5 mPa·s) at various rotational speeds,

followed by pine and flower honeys (Fig. 1). Durmuş found the greatest viscosity values at 50 rpm, namely 11.50 Pa·s in flower honey and 9.15 Pa·s in pine honey [28]. In another study, the viscosity values measured at 25°C at 5 rpm ranged between 1866 and 31 600 mPa·s for floral honeys and between 3033 and 40 600 mPa·s for pine honeys [27]. The honey samples were found to exhibit Newtonian behavior over the whole shear rate range, and their viscosity reduced as the temperature rose [13]. The viscosity of honey is affected by the brix value, the types of sugars, as well as their amounts and ratios in honey [27].

The Power Law model was selected because the threshold shear stress (τ_0) was zero for probiotic drinkable yogurt fortified with honey. The graph in Fig. 2 displays the apparent viscosity measurements for the probiotic yogurts taken at 100 rpm. The results from different storage times were found to be statistically similar. The

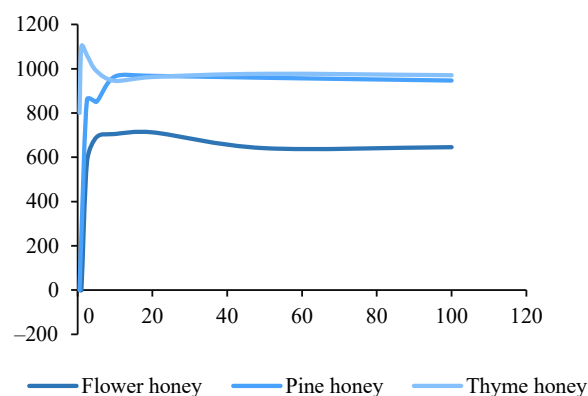
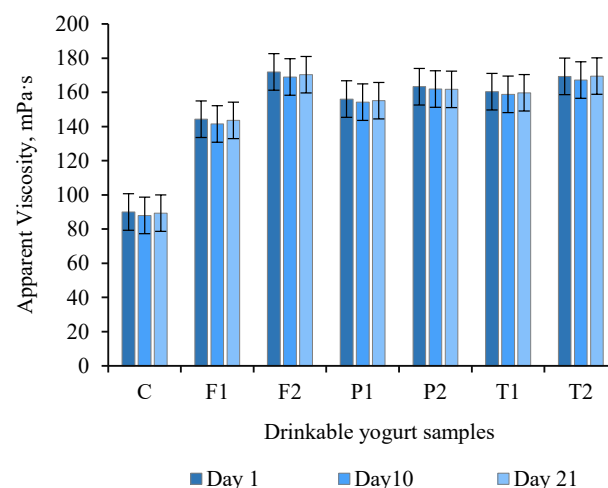


Figure 1 Viscosity values of honey samples (cP) ($n = 3$)



C – Probiotic drinkable yogurt without honey (Control group); F1 – Probiotic drinkable yogurt with 10% flower honey, F2 – Probiotic drinkable yogurt with 20% flower honey, P1 – Probiotic drinkable yogurt with 10% pine honey, P2 – Probiotic drinkable yogurt with 20% pine honey, T1 – Probiotic drinkable yogurt with 10% thyme honey, T2 – Probiotic drinkable yogurt with 20% thyme honey

Figure 2 Apparent viscosity values of drinkable yogurts at 100 rpm

sample with 10% flower honey had the closest apparent viscosity value to that of the control.

According to İnce, the apparent viscosity of drinkable yogurt with 20% flower honey was 247.5 ± 10 mPa·s on the 10th day and that of the sample with 20% pine honey was 170 ± 30 mPa·s on the first day [36]. Another study found that goat yogurt without honey showed a decrease in perceived viscosity during storage ($p \leq 0.05$), whereas all the formulations with various honey contents showed an increase in perceived viscosity over time ($p \leq 0.05$) [14]. The addition of honey increased the yogurt's dry matter content and consistency, causing an initial rise in apparent viscosity proportional to the amount added. However, the viscosity values of yogurt formulations with honey became more unstable during storage, possibly due to honey's ability to act as a pseudoplastic liquid and resist the force applied to fluids.

According to Table 3, the flow indexes of the samples decreased during storage. The consistency coefficients were higher in the samples with larger amounts of honey

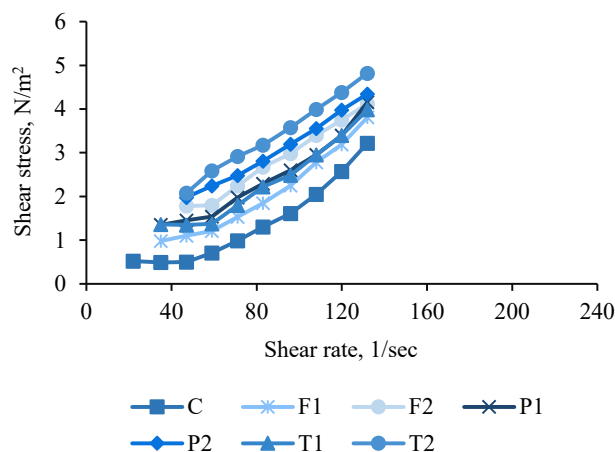
(20%). Additionally, the yogurt fortified with thyme honey had the highest consistency coefficient. The confidence coefficients of the samples ranged from 97.1 to 99.3.

Figures 3 and 4 illustrate the relationship between the shear stress (N/m^2) and the shear rate ($1/\text{s}$) for the drinkable yogurt samples (first day). In both figures, the flow of all the samples was identified as pseudoplastic because the shear stress increased with the shear rate in response to the form. The apparent viscosity of the samples was found to decrease as the shear rate increased (Fig. 4). This decrease in viscosity characterizes the flow as both thixotropic and non-Newtonian.

Microbiological analysis. Not all the samples were found to have coliform bacteria or yeast-mold during storage (Table 4). The control yogurt had the lowest number of mesophilic bacteria ($7.39 \log \text{CFU/mL}$), while the sample containing 20% pine honey had the highest number ($8.35 \log \text{CFU/mL}$) on the first day of storage. The total mesophilic bacteria count decreased over time for all the samples. On day 21, the honey yogurts had a lower

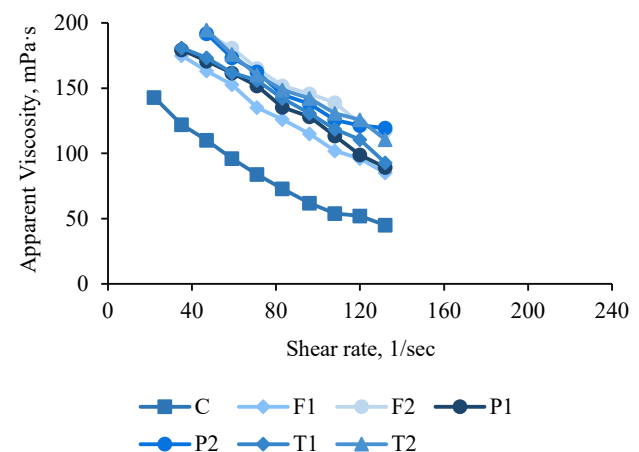
Table 3 Flow indexes, consistency and confidence coefficients of drinkable yogurts according to the Power Law model ($n = 3$)

Samples	Storage, day								
	1			10			21		
	Flow index (n)	Consistency coefficient, mPa·s	Confidence coefficient, %	Flow index (n)	Consistency coefficient, mPa·s	Confidence coefficient, %	Flow index (n)	Consistency coefficient, mPa·s	Confidence coefficient, %
Control	0.52	1670	98.4	0.29	1705	99.2	0.28	1820	98.2
Flower honey (10%)	0.44	1703	97.2	0.36	1785	98.7	0.21	1975	98.7
Flower honey (20%)	0.42	1888	99.0	0.38	1956	99.1	0.40	2125	99.2
Pine honey (10%)	0.35	2189	98.4	0.40	2293	98.4	0.39	2498	98.4
Pine honey (20%)	0.41	2571	99.3	0.33	2746	97.2	0.30	2869	99.2
Thyme honey (10%)	0.42	2193	97.1	0.37	2256	98.8	0.38	2787	98.9
Thyme honey (20%)	0.47	2557	98.2	0.43	2673	99.1	0.33	2917	97.3



C – Probiotic drinkable yogurt without honey (Control group); F1 – Probiotic drinkable yogurt with 10% flower honey, F2 – Probiotic drinkable yogurt with 20% flower honey, P1 – Probiotic drinkable yogurt with 10% pine honey, P2 – Probiotic drinkable yogurt with 20% pine honey, T1 – Probiotic drinkable yogurt with 10% thyme honey, T2 – Probiotic drinkable yogurt with 20% thyme honey

Figure 3 Shear stress/shear rate graph for drinkable yogurt samples (day 1) ($n = 3$)



C – Probiotic drinkable yogurt without honey (Control group); F1 – Probiotic drinkable yogurt with 10% flower honey, F2 – Probiotic drinkable yogurt with 20% flower honey, P1 – Probiotic drinkable yogurt with 10% pine honey, P2 – Probiotic drinkable yogurt with 20% pine honey, T1 – Probiotic drinkable yogurt with 10% thyme honey, T2 – Probiotic drinkable yogurt with 20% thyme honey

Figure 4 Apparent viscosity/shear rate graph for drinkable yogurt samples (day 1) ($n = 3$)

count than the control group. There was a significant variation in the total mesophilic bacteria count between the samples and over time ($p < 0.05$). Ince *et al.* reported the total counts of 7.13 to 8.51 log CFU/mL for the samples with pine and floral honeys [37].

On day 1, the highest amount of *Lactobacillus delbrueckii* subsp. *bulgaricus* was found in the control sample, while the lowest was registered in the yogurt with 20% thyme honey (Table 4). According to the results, storage decreased the amount of *L. delbrueckii* subsp. *bulgaricus* in all the samples. The samples with 20% honey had lower concentrations of these bacteria compared to those with 10% honey. According to Mercan, drinkable yogurts with karakovan honey (100% raw honey unique to Anatolia) had the highest concentration of *L. delbrueckii* subsp. *bulgaricus* [30]. The decrease in these bacteria was also significant in all the samples after storage.

An increase in the amount of *Streptococcus thermophilus* was seen in all the samples except for the control group at the end of storage. Thus, adding honey promoted the growth of these bacteria. According to Coskun and Dirican, probiotic drinkable yogurts with pine honey contained more *S. thermophilus* than the control sample during storage [9].

Our results revealed the presence of *Lactobacillus acidophilus* in the samples containing probiotic culture (Table 4). On day 1, the control sample had 6.95 log CFU/mL of *L. acidophilus*. The lowest and highest concentrations of these bacteria were 6.02 and 7.65 log CFU/mL, respectively, in the sample with 20% flower honey. After 21 days of storage, the quantity of *L. acidophilus* decreased in all the samples. Coskun and Dirican reported that adding and storing honey had a significant impact on *L. acidophilus* populations [9]. In the study by Machado *et al.*, goat yogurt fortified with honey (*Melipona scutellaris* Latrelle-Urucu) had

6.0 log CFU/g of *L. acidophilus* La-05 during 28 days of storage, and the addition of honey maintained their count and the quantity of yogurt starter germs [14].

Bifidobacterium spp. counts ranged from 5.22 to 6.45 log CFU/mL on day 1 and from 4.92 to 6.04 log CFU/mL on day 21. They were higher at the start of storage in the samples fortified with 10% of thyme honey and 20% of each honey, but decreased throughout storage. Fiorda *et al.* found that honey has good potential as a stimulating ingredient to produce probiotic beverages and that honey-based kefir can prevent microbial DNA damage [38]. We believe that adding honey to drinkable yogurt during its manufacture can enhance the product's functional qualities.

Sensory analysis. The control sample was rated the highest in appearance, texture, taste, odor, and general acceptability (Table 5). After 21 days of storage, the sample with 10% honey (flower, thyme) had higher sensory scores, and was more similar in appearance to the control, than the sample with 20% honey. The structural scores of the samples with 20% flower honey and 10% flower, pine, and thyme honeys were like those of the control. The samples with 10% honey (flower, pine, and thyme) were rated higher in taste than those with 20% honey. The general acceptability scores during storage were between 2.6 to 9.17, with higher scores given to the samples with 10% honey (flower, pine, and thyme). This might suggest that a honey concentration of 20% is too high for drinkable yoghurts. Additionally, the adult panelists might prefer yogurt with the usual salty taste or a less sweet taste than that of honey yogurt. Studies show that fruit yogurts appeal more to children than adults. Therefore, we think that honey-fortified drinkable yogurt may be more suitable for children.

In Mercan's study, the yogurts with karakovan honey had the highest scores, while those with thyme

Table 4 Microbiological parameters of drinkable yogurt samples (n = 3)

Parameter, CFU/mL	Day	Samples						
		Control	Flower honey (10%)	Flower honey (20%)	Pine honey (10%)	Pine honey (20%)	Thyme honey (10%)	Thyme honey (20%)
Total mesophilic bacteria	1	7.39 ± 0.02 ^{a-c}	8.16 ± 0.68 ^{abc}	8.28 ± 0.68 ^{ab}	7.68 ± 1.06 ^{a-d}	8.35 ± 0.78 ^a	7.46 ± 1.46 ^{a-c}	8.15 ± 0.75 ^{abc}
	10	6.37 ± 0.28 ^{c-f}	5.80 ± 0.58 ^{efg}	5.80 ± 0.90 ^{efg}	6.59 ± 0.60 ^{c-f}	6.47 ± 0.15 ^{b-f}	6.06 ± 0.25 ^{d-g}	6.06 ± 0.28 ^{d-g}
	21	6.07 ± 0.40 ^{d-g}	4.41 ± 0.29 ^g	4.29 ± 0.37 ^g	5.10 ± 0.02 ^{fg}	4.72 ± 0.03 ^{fg}	5.03 ± 0.10 ^{fg}	4.45 ± 0.11 ^g
<i>Lactobacillus</i> <i>delbrueckii</i> subsp. <i>bulgaricus</i>	1	6.99 ± 0.08 ^a	6.19 ± 0.07 ^{abc}	6.17 ± 0.42 ^{abc}	6.31 ± 0.09 ^{abc}	5.94 ± 0.35 ^{abc}	6.07 ± 0.04 ^{abc}	5.91 ± 0.81 ^{abc}
	10	6.92 ± 0.09 ^{ab}	6.04 ± 0.08 ^{abc}	6.12 ± 0.43 ^{abc}	6.22 ± 0.16 ^{abc}	5.76 ± 0.40 ^c	6.04 ± 0.03 ^{abc}	5.41 ± 0.64 ^c
	21	5.80 ± 0.80 ^{abc}	5.98 ± 0.12 ^{abc}	5.91 ± 0.35 ^{abc}	6.01 ± 0.04 ^{abc}	5.67 ± 0.34 ^{abc}	6.03 ± 0.01 ^{abc}	5.39 ± 0.82 ^{abc}
<i>Streptococcus</i> <i>thermophilus</i>	1	7.07 ± 0.17 ^{a-d}	7.63 ± 0.13 ^{a-d}	8.08 ± 0.42 ^{abc}	7.66 ± 0.84 ^{a-d}	6.91 ± 0.95 ^{a-d}	6.49 ± 0.60 ^{cd}	6.60 ± 0.53 ^{bcd}
	10	6.81 ± 0.25 ^{a-d}	8.04 ± 0.05 ^{abc}	8.13 ± 0.09 ^{abc}	7.83 ± 1.35 ^{a-d}	6.96 ± 0.77 ^{a-d}	6.66 ± 0.39 ^{bcd}	6.45 ± 0.30 ^{cd}
	21	7.02 ± 0.18 ^{a-d}	8.08 ± 0.01 ^{abc}	8.19 ± 0.23 ^{abc}	8.42 ± 0.19 ^{ab}	7.40 ± 1.00 ^{a-d}	7.38 ± 1.08 ^{a-d}	7.36 ± 0.24 ^{a-d}
<i>Lactobacillus</i> <i>acidophilus</i>	1	6.95 ± 0.23 ^{bc}	6.90 ± 0.03 ^c	7.65 ± 0.14 ^a	7.01 ± 0.02 ^{bc}	7.14 ± 0.12 ^{ab}	6.02 ± 0.01 ^{efg}	6.88 ± 0.01 ^c
	10	6.44 ± 0.58 ^{c-f}	6.18 ± 0.43 ^{d-g}	6.56 ± 0.35 ^{cde}	6.84 ± 0.04 ^c	6.92 ± 0.14 ^{bc}	5.85 ± 0.06 ^{fg}	6.75 ± 0.04 ^{cd}
	21	5.59 ± 0.03 ^g	5.63 ± 0.02 ^g	4.68 ± 0.03 ^h	5.69 ± 0.10 ^g	5.87 ± 0.10 ^{fg}	5.71 ± 0.03 ^g	5.80 ± 0.04 ^g
<i>Bifidobacterium</i> spp.	1	5.41 ± 0.02 ^{c-f}	5.22 ± 0.07 ^{efg}	6.40 ± 0.08 ^a	5.24 ± 0.12 ^{ef}	5.23 ± 0.07 ^{efg}	6.45 ± 0.06 ^a	5.81 ± 0.01 ^{bcd}
	10	5.52 ± 0.15 ^{cde}	5.06 ± 0.10 ^{c-f}	5.22 ± 0.26 ^{efg}	4.71 ± 0.58 ^g	4.92 ± 0.13 ^{fg}	5.88 ± 0.08 ^{bc}	5.13 ± 0.17 ^{efg}
	21	6.04 ± 0.03 ^{ab}	5.04 ± 0.05 ^{efg}	4.92 ± 0.13 ^{fg}	5.00 ± 0.10 ^{fg}	5.09 ± 0.13 ^{efg}	5.44 ± 0.01 ^{c-f}	5.19 ± 0.07 ^{efg}

*a-h — Different letters indicate statistical significance between the groups ($p < 0.05$)

Table 5 Sensory evaluation of drinkable yogurt samples (n = 3)

Parameter	Day	Samples						
		Control	Flower honey (10%)	Flower honey (20%)	Pine honey (10%)	Pine honey (20%)	Thyme honey (10%)	Thyme honey (20%)
Appearance	1	9.52 ± 0.19 ^{ab}	7.68 ± 0.18 ^{bc}	5.05 ± 0.38 ^{c-i}	5.95 ± 0.38 ^{c-g}	4.05 ± 0.38 ^{g-j}	7.06 ± 0.77 ^{cde}	4.57 ± 0.57 ^{f-j}
	10	9.75 ± 0.25 ^{ab}	7.17 ± 0.50 ^{cd}	5.33 ± 1.00 ^{d-h}	5.42 ± 0.75 ^{d-h}	3.42 ± 0.58 ^{hij}	6.42 ± 0.58 ^{c-f}	4.42 ± 0.42 ^{f-j}
	21	9.83 ± 0.03 ^a	7.37 ± 1.23 ^{cd}	3.76 ± 0.04 ^{hij}	4.46 ± 0.26 ^{f-j}	2.91 ± 0.51 ⁱ	6.17 ± 0.97 ^{c-f}	2.99 ± 1.59 ^{ij}
Texture	1	8.68 ± 0.18 ^{ab}	7.80 ± 0.37 ^{a-c}	6.26 ± 0.40 ^{d-g}	7.08 ± 0.25 ^{b-g}	6.01 ± 0.15 ^{d-h}	5.98 ± 0.31 ^{d-h}	5.08 ± 0.08 ^{gh}
	10	9.17 ± 0.50 ^a	7.92 ± 0.25 ^{a-d}	7.33 ± 0.33 ^{a-f}	6.33 ± 0.67 ^{c-g}	5.89 ± 0.61 ^{c-h}	7.33 ± 0.33 ^{a-f}	6.08 ± 0.58 ^{d-g}
	21	8.31 ± 0.11 ^{abc}	7.50 ± 0.50 ^{a-f}	7.04 ± 0.24 ^{b-g}	6.34 ± 0.94 ^{c-g}	5.56 ± 1.16 ^{gh}	6.46 ± 0.26 ^{c-g}	4.00 ± 2.00 ^h
Taste	1	8.78 ± 0.19 ^a	6.93 ± 0.54 ^{abc}	4.73 ± 0.44 ^{cde}	4.90 ± 0.76 ^{cde}	4.25 ± 0.25 ^{cde}	4.33 ± 0.33 ^{cde}	3.17 ± 1.97 ^c
	10	8.83 ± 0.33 ^a	6.25 ± 0.75 ^{a-d}	4.92 ± 0.42 ^{cde}	4.67 ± 0.50 ^{cde}	4.08 ± 0.25 ^{cde}	4.37 ± 0.17 ^{cde}	2.96 ± 0.08 ^c
	21	8.93 ± 1.07 ^a	6.96 ± 1.19 ^{abc}	5.19 ± 0.79 ^{cde}	5.16 ± 0.56 ^{cde}	5.01 ± 2.41 ^{cde}	4.36 ± 1.36 ^{cde}	2.92 ± 0.54 ^c
Odor	1	9.06 ± 0.23 ^a	7.77 ± 0.06 ^{ab}	4.96 ± 0.53 ^{cd}	5.11 ± 0.39 ^{cd}	4.61 ± 0.11 ^d	4.88 ± 0.55 ^{cd}	3.85 ± 0.01 ^{def}
	10	9.25 ± 0.25 ^a	6.50 ± 0.50 ^{bc}	5.58 ± 0.42 ^{cd}	5.50 ± 0.17 ^{cd}	4.75 ± 0.25 ^d	3.92 ± 0.08 ^{def}	2.83 ± 0.01 ^{ef}
	21	8.71 ± 1.29 ^a	5.57 ± 0.57 ^{cd}	5.13 ± 0.73 ^{cd}	4.54 ± 0.74 ^{de}	4.30 ± 0.70 ^{de}	4.13 ± 0.27 ^{def}	2.46 ± 1.26 ^f
General acceptability	1	9.13 ± 1.82 ^a	7.50 ± 1.75 ^{abc}	4.90 ± 0.76 ^{d-g}	5.00 ± 0.67 ^{d-g}	4.09 ± 1.48 ^{fg}	4.46 ± 0.04 ^{efg}	3.14 ± 0.14 ^{fg}
	10	9.17 ± 0.50 ^a	6.86 ± 0.14 ^{a-d}	5.33 ± 1.00 ^{c-f}	4.69 ± 0.89 ^{d-g}	4.08 ± 0.75 ^{fg}	4.39 ± 0.19 ^{fg}	2.92 ± 0.08 ^g
	21	8.73 ± 0.87 ^{ab}	6.75 ± 0.75 ^{b-c}	4.80 ± 1.20 ^{d-g}	4.45 ± 0.88 ^{efg}	3.86 ± 0.14 ^{fg}	3.83 ± 0.17 ^{fg}	2.67 ± 1.47 ^g

*a-j – Different letters indicate statistical significance between the groups ($p < 0.05$)

honey were disliked the most. The general acceptability ratings reportedly dropped at the end of storage [30].

CONCLUSION

Our results showed a significant difference ($p < 0.05$) in the total dry matter, fat, salt, pH, and serum separation values among the drinkable yogurts. The samples with floral and thyme honeys had similar serum separation values. The samples with 20% honey had a lower L^* value than those with 10% honey. The samples' viscosity decreased throughout storage, assigning drinkable yogurts to the class of thixotropic and non-Newtonian pseudoplastic liquids. As the honey content increased, so did the apparent viscosity and consistency coefficients. The samples fortified with 20% thyme honey had the greatest consistency coefficient on day 21 of storage.

We found that *Lactobacillus delbrueckii* subsp. *bulgaricus* were more abundant in the yogurts containing 10% honey compared to those with 20% honey at the end of 21 days of storage. However, the count of *Streptococcus thermophilus* increased only with a higher flower honey ratio at the end of storage. After 21 days of storage, the probiotic bacteria levels in the honey-contain-

ing samples were adequate ($> 5 \log \text{CFU/mL}$) for consumer health, except for the samples with 20% floral honey. The sensory evaluation showed a preference for the yogurts with 10% honey (flower, pine, and thyme) over those with 20% honey. Based on the probiotic levels at the end of storage and consumer preference, 10% was determined as an optimal amount of flower or pine honey for drinkable yogurt, with 10% flower honey being particularly favored. We also expect that limiting the amount of thyme honey to less than 10% will produce drinkable yogurt with more desirable sensory characteristics. Our study showed that honey improves the functional properties of drinkable yogurt by promoting the growth of probiotic bacteria.

CONTRIBUTION

The authors contributed equally to this work.

CONFLICT OF INTEREST

The authors declare that they have no known competing financial interests or personal relationships that could have appeared to influence the work reported in this paper.


REFERENCES


- Prokisch J, Badgar K, El-Ramady H. Fortification of functional foods for human health: A case study of honey and yogurt for diabetes. *Environment, Biodiversity and Soil Security*. 2021;5:331–340. <https://doi.org/10.21608/jenvbs.2021.110812.1154>
- Abdolmaleki F, Rezaei Mokarram R, Daneshniya M, Maleki MH. Iranian grape syrup used as a prebiotic and its effect on the physicochemical, microbiological, and sensory properties of probiotic yogurt. *Foods and Raw Materials*. 2025;13(1):202–210. <https://doi.org/10.21603/2308-4057-2025-1-634>
- Jafarpour D, Amirzadeh A, Maleki M, Mahmoudi MR. Comparison of physicochemical properties and general acceptance of flavored drinking yogurt containing date and fig syrups. *Foods and Raw Materials*. 2017;5(2):36–43. <https://doi.org/10.21603/2308-4057-2017-2-36-43>


4. Sarhir ST, Amanpour A, Selli S. Characterization of Ayran aroma active compounds by solvent-assisted flavor evaporation (SAFE) with gas chromatography-mass spectrometry-olfactometry (GC-MS-O) and aroma extract dilution analysis (AEDA). *Analytical Letters*. 2019;52(13):2077–2091. <https://doi.org/10.1080/00032719.2019.1594244>
5. Baskar N, Varadharajan S, Rameshbabu M, Ayyasamy S, Velusamy S. Development of plantbased yogurt. *Foods and Raw Materials*. 2022;10(2):274–282. <https://doi.org/10.21603/2308-4057-2022-2-537>
6. López-Prieto A, Rodríguez-López L, Rincón-Fontán M, Moldes AB, Cruz JM. Effect of biosurfactant extract obtained from the corn-milling industry on probiotic bacteria in drinkable yogurt. *Journal of the Science of Food and Agriculture*. 2018;99:824–830. <https://doi.org/10.1002/jsfa.9251>
7. Sibirtsev VS, Kuzmin AG, Titov YuA, Zaitseva AY, Sherstnev VV. Gas mass spectrometry of industrial yogurts. *Food Processing: Techniques and Technology*. 2024;54(2):285–297. (In Russ.). <https://doi.org/10.21603/2074-9414-2024-2-2507>
8. Albay Z. The effect of inulin and wheat fiber addition to low-fat milk on some properties of probiotic Tulum cheese. PhD Thesis. Isparta: Süleyman Demirel University; 2022. 307 p.
9. Coskun F, Karabulut Dirican L. Effects of pine honey on the physicochemical, microbiological and sensory properties of probiotic yoghurt. *Food Science and Technology*. 2019;39(Suppl.2):616–625. <https://doi.org/10.1590/fst.24818>
10. Kostenko O. Beekeeping and honey production in Russia. *BIO Web of Conferences*. 2022;48:02007. <https://doi.org/10.1051/bioconf/20224802007>
11. Karaçelik AA, Sahin H. Determination of enzyme inhibition and antioxidant activity in some chestnut honeys. *Foods and Raw Materials*. 2018;6(1):210–218. <https://doi.org/10.21603/2308-4057-2018-1-210-218>
12. Sánchez-Martín V, Morales P, González-Porto AV, Iriando-DeHond A, López-Parra MB, Del Castillo MD, et al. Enhancement of the antioxidant capacity of thyme and chestnut honey by addition of bee products. *Foods*. 2022;11(19):3118. <https://doi.org/10.3390/foods11193118>
13. Oroian M. Measurement, prediction and correlation of density, viscosity, surface tension and ultrasonic velocity of different honey types at different temperatures. *Journal of Food Engineering*. 2013;119(1):167–172. <https://doi.org/10.1016/j.jfoodeng.2013.05.029>
14. Machado TADG, de Oliveira MEG, Campos MIF, de Assis POA, de Souza EL, Madruga MS, et al. Impact of honey on quality characteristics of goat yogurt containing probiotic *Lactobacillus acidophilus*. *LWT*. 2017;80:221–229. <https://doi.org/10.1016/j.lwt.2017.02.013>
15. Silici S, Sagdic O, Ekici L. Total phenolic content, antiradical, antioxidant and antimicrobial activities of *Rhododendron* honeys. *Food Chemistry*. 2010;121(1):238–243. <https://doi.org/10.1016/j.foodchem.2009.11.078>
16. Official methods of analysis of the Association of Official Analytical Chemists. 16th Edition. Washington: AOAC; 1997.
17. Ozunlu TB, Kocak C, Aydemir S. Factors affecting the stability of ayran. Ankara: Food Technology Association; 2007. (In Turkish).
18. Meals SE, Schiano AN, Drake MA. Drivers of liking for Cheddar cheese shreds. *Journal of Dairy Science*. 2020;103(3):2167–2185. <https://doi.org/10.3168/jds.2019-16911>
19. Akgun A, Yazici F, Gulec HA. Effect of reduced fat content on the physicochemical and microbiological properties of buffalo milk yoghurt. *LWT*. 2016;74:521–527. <https://doi.org/10.1016/j.lwt.2016.08.015>
20. Gocer EMC, Ergin F, Küçükçetin IO, Küçükçetin A. In vitro gastrointestinal resistance of *Lactobacillus acidophilus* in some dairy products. *Brazilian Journal of Microbiology*. 2021;52:2319–2334. <https://doi.org/10.1007/s42770-021-00590-4>
21. Fathy HM, Abd El-Maksoud AA, Cheng W, Elshaghabee FMF. Value-added utilization of citrus peels in improving functional properties and probiotic viability of *Acidophilus-bifidus-thermophilus* (ABT)-type synbiotic yoghurt during cold storage. *Foods*. 2022;11(17):2677. <https://doi.org/10.3390/foods11172677>
22. Sharma S, Sekhon AS, Unger P, Lampien A, Galland AT, Bhavnani K, et al. Impact of ultrafine bubbles on the survivability of probiotics in fermented milks. *International Dairy Journal*. 2023;140:105591. <https://doi.org/10.1016/j.idairyj.2023.105591>
23. Güllü M, Beyaz D, Demirpençe H. Determination of chemical and microbiological quality of strained yoghurt samples marketed in Aydın Province. *Animal Health Production and Hygiene*. 2023;12(2):13–19. <https://doi.org/10.53913/aduveterinary.1297717>
24. Astawan M, Wresdiyati T, Suliantari, Arief II, Septiawan R. Production of synbiotic yogurt-like using indigenous lactic acid bacteria as functional food. *Media Peternakan*. 2012;35(1):9–14. <https://doi.org/10.5398/medpet.2012.35.1.9>
25. Akarca G, Denizkara AJ. Changes of quality in yoghurt produced under magnetic field effect during fermentation and storage processes. *International Dairy Journal*. 2024;150:105841. <https://doi.org/10.1016/j.idairyj.2023.105841>

26. Yazıcıoğlu Y, Erdoğan S. SPSS applied scientific research methods. Detay; 2011. (In Turkish).
27. Polat G. Determination of the rheological, physicochemical characteristics and mineral contents of different floral honeys obtained from different locations. Master Thesis. Konya: Selçuk University; 2007. 51 p.
28. Durmuş R. Determination of glass transition temperature and some physicochemical properties of several honeys produced my country. Master Thesis. Erzurum: Atatürk University; 2013. 57 p.
29. Özünlü TB. Studies on some parameters affecting the quality of Ayran (drinking yoghurt). Ph.D. Thesis. Ankara: Ankara University; 2005. 127 p.
30. Mercan E. Determination of changes on some physicochemical and microbiological properties of set type yogurt produced from using different origins honeys during refrigerated storage. Master Thesis. Konya: Selçuk University; 2013. 85 p.
31. Dogan M. Rheological behaviour and physicochemical properties of kefir with honey. *Journal für Verbraucherschutz und Lebensmittelsicherheit*. 2011;6:327–332. <https://doi.org/10.1007/s00003-010-0643-6>
32. Şanlı T. A Study on some properties of Ayrans produced from milk, the protein of which is modified by transglutaminase enzyme. Ph.D. Thesis: Ankara University; 2009. 114 p.
33. Nosrat S. Salt, fat, acid, heat: Mastering the elements of good cooking. New York: Simon and Schuster; 2017. 469 p.
34. Chapagain K, Karki TB, Ojha P. Development and quality assessment of functional probiotic yoghurt drink from sweet cream buttermilk. *Journal of Food Science and Technology Nepal*. 2013;8:52–59. <https://doi.org/10.3126/jfstn.v8i0.11750>
35. Karadal F, Yıldırım Y. The quiality parameters and nutritional and health effect of honey. *Journal of The Faculty of Veterinary Medicine Erciyes University*. 2012;9(3):197–209. (In Turkish).
36. İnce YN. Determination of some properties in drinkable yogurt (Ayran) produced with different floral sources of honey. Master Thesis. Isparta: Suleyman Demirel University; 2019. 92 p.
37. İnce YN, Çelebi M, Şimşek B. Some chemical and sensory properties of Ayran produced by adding honeydew honey and flower honey. *OKU Journal of The Institute of Science and Technology*. 2022;5(3):1407–1418.
38. Fiorda FA, de Melo Pereira GV, Thomaz-Soccol V, Medeiros AP, Rakshit SK, Soccol CR. Development of kefir-based probiotic beverages with DNA protection and antioxidant activities using soybean hydrolyzed extract, colostrum and honey. *LWT – Food Science and Technology*. 2016;68:690–697. <https://doi.org/10.1016/j.lwt.2016.01.003>

ORCID IDs

Zehra Albay  <https://orcid.org/0000-0002-5090-8151>

Mehmet Çelebi  <https://orcid.org/0000-0002-0769-299X>

Bedia Şimşek  <https://orcid.org/0000-0002-7497-1542>



Lycopene from tomato biomass: Extraction and stabilization

Rosa Nallely Murillo Vázquez¹, Fermín Paul Pacheco Moisés¹,
Verónica Nardello-Rataj², Gregorio Guadalupe Carbajal Arízaga^{1,*}

¹ University of Guadalajara^{ROR}, Guadalajara, Mexico

² University of Lille^{ROR}, Lille, France

* e-mail: gregoriocarbjal@yahoo.com.mx

Received 17.10.2023; Revised 27.02.2024; Accepted 05.03.2024; Published online 29.10.2024

Abstract:

Lycopene and other carotenoids have a significant added value in the food and cosmetic industries due to their nutraceutical properties and antioxidant activity. The extraction and stabilization of these compounds remain challenging due to their sensitivity to light, temperature fluctuations, and oxidation. This article introduces a sustainable method of extracting lycopene from tomato waste (*Solanum lycopersicum* L.) using layered double hydroxide nanoparticles to stabilize lycopene.

We used tomato juice and lycopene as a positive control, while ZnAl was a negative control. The experimental samples included 75 and 100 mg of zinc salt per 1 mL of tomato juice, which were labeled as ZnAl75J and ZnAl100J.

Zinc and aluminum salts developed insoluble hydroxides, which precipitated lycopene from tomato juice, thus forming composites. The composites proved to be efficient means of encapsulating lycopene as they recovered 97% lycopene present in tomato juice. The physicochemical properties of the organic material enhanced resistance to thermal degradation and acted as an extended-release antioxidant. ZnAl100J, which contained a lot of lycopene, inhibited 89% of DPPH[•] in 24 h and showed a value higher than IC₅₀ for ABTS^{•+}, which was 0.02 µg/mL of TEAC ABTS^{•+}. ZnAl75J composites showed a higher protection against oxidation and a higher sun protection factor value (3.08) at 15% concentration.

The composites could be used as an active ingredient in a wide range of formulations that require antioxidant and photosensitizing properties, or simply as encapsulators and carriers of lycopene.

Keywords: Lycopene, composites, hydroxides, zinc salts, aluminum salts, layered nanoparticles, antioxidant activity

Funding: This research was supported by the National Council for Humanities, Sciences, and Technologies (CONAHCYT)^{ROR}, México, due to the doctoral scholarship given to Rosa Nallely Murillo Vázquez (CVU number: 486681).

Please cite this article in press as: Murillo Vázquez RN, Pacheco Moisés FP, Nardello-Rataj V, Carbajal Arízaga GG. Lycopene from tomato biomass: Extraction and stabilization. *Foods and Raw Materials*. 2025;13(2):330–340. <https://doi.org/10.21603/2308-4057-2025-2-644>

INTRODUCTION

Lycopene is a nutraceutical ingredient that helps prevent diseases or minimize their symptoms. As an excellent antioxidant, it is highly demanded in the cosmetic industry. Tomatoes, which are cultivated worldwide, are extremely rich in lycopene and serve as the main source of this valuable substance [1]. Even tomato waste may be used as raw material [2, 3]. In fact, tomato waste biomass can generate lycopene, a high-value-added ingredient, to be used as a nutraceutical or cosmetic [4]. However, isolated lycopene has a major disadvantage: it degrades easily when exposed to light and ambient oxygen.

Our research team has already reported that tomato juice can be used as a reaction medium to produce

layered double hydroxide nanoparticles and a composite that could serve as a carrier powder for lycopene [5]. Layered double hydroxide particles are crystalline particles with a layered structure containing a combination of M(II) and M(III) cations coordinated by hydroxyl groups. The M(III) cation generates an excess charge in the layers that is balanced with interlayer anions. As a result, a layered double hydroxide particle represents a stacking of layers of metallic hydroxides that retain interlayer anions [6, 7]. Considering that various elements can form layered double hydroxide, those with low toxicity can be selected to design particles to be used in food or cosmetics [8]. For instance, we used Mg₃Al(OH)₈(CO₃)_{0.5}·XH₂O [5]. Zinc and aluminum are

also widely studied for layered double hydroxide formulations in pharmacy and cosmetics [9–11]. This variant is useful for topical applications in cosmetics. In this study, we reported an experiment modification of crystalline layered double hydroxide formation with $\text{Zn}_3\text{Al}(\text{OH})_8(\text{CO}_3)_{0.5}\cdot\text{XH}_2\text{O}$ composition in tomato juice. However, our modification resulted in amorphous compounds that possessed the same efficiency in lycopene removal and stabilization.

The research objective was to study the properties of the material and determine its application in the food industry, food packaging, or cosmetics.

STUDY OBJECTS AND METHODS

We used the coprecipitation technique to synthesize the composites. First, we dissolved zinc and aluminum salts in 100 mL of tomato juice and alkalized them with NaOH 1 M to reach pH 8.5. After that, we dissolved sodium carbonate in 20 mL of water and added it to the suspension. After stirring the suspension for 2 h at room temperature and air atmosphere, we centrifuged it at 1380 rpm, washed the red solid with water until the washing liquid reached the desired pH, and dried at 50°C. Table 1 illustrates the samples and reagents involved. As a positive control, we used tomato juice and lycopene. The ZnAl sample, which contained zinc and aluminum cations, was a negative control. ZnAl75J and ZnAl100J were the samples with 75 and 100 mg of zinc salt used per milliliter of tomato juice.

To calculate the yield percentage, we used the final weight of the dry composites as in Eq. (1):

$$W = \frac{(W_f \times 100)}{W_o} \quad (1)$$

where W is the percentage of weight, %; W_f is the final weight of the dry composites; and W_o is the expected theoretical weight considering the inorganic phase corresponded to layered double hydroxide particles.

The X-ray diffraction profiles were collected from 100 mg of the sample pressed onto a holder to produce a smooth surface. The procedure involved a D8 ADVANCE Bruker analytical diffractometer with Cu-K α radiation. The data were collected within the 5–70° range in 2-Theta mode with steps of 0.02° and scanned at 30 s per step. The X-ray photoelectron spectra were obtained in a SPECS spectrometer with an 1D DLD detector with a Phoibos 150 analyzer. The device employed AlK α radiation (1486.7 eV) generated at 250 W

and 12.5 kV; the spectra were collected at a pressure $\leq 2.12 \times 10^{-9}$ mbar. The charge of operation was adjusted at 20 μA of emission and 2 eV. The samples were applied on glass. The infrared spectra were obtained from 2 mg of sample with an iS50 ATR Thermo Scientific spectrometer. The spectra were collected with 15 scans with a resolution of 4 cm^{-1} at room temperature. The scanning electron microscopy analysis involved a JEOL JSM 5400 LV microscope. The images were obtained using secondary electrons generated with a voltage of 20 kV. The energy dispersive X-ray spectroscopy maps were acquired with an X-Max detector (Oxford Instruments) at 20 mm^2 , which was assembled to a JEOL JSM-6610LV microscope at 15 kV. The dynamic light scattering required 2 mg of each sample added to 2 mL of 0.9% NaCl solution and 0.1M HCl. The suspensions were dispersed with ultrasound for 10 min. The hydrodynamic size and the zeta potential were measured with a Nano ZS Malvern device. A refractive index of 1.2 was loaded to the software with 15 readings per sample. The Discovery thermogravimetric device included 2 mg of each sample at 25–900°C with steps of 20°C per 1 min under a nitrogen flow of 20 mL/min.

Quantification of lycopene content in composites. To quantify the amount of lycopene contained in the composites, we performed a solvent extraction using 5 mL toluene per 1 g composite, which was then agitated for 30 min at 1500 rpm. After that, the samples were centrifuged, and the supernatant was read in a Cary 60 UV-Vis spectrometer (Agilent Technologies) within the range of 50–500 nm. The reads were interpolated with a calibration curve.

Antioxidant activity. A stock solution of 2,2-diphenyl-1-picrylhydrazyl (DPPH \cdot) was prepared as follows. A solution of 20 mg of DPPH \cdot in 300 mL of ethanol was agitated for 10 min, after which we measured its initial absorbance at 517 nm and verified that the read stayed below 3.0 absorbance units. Then, we weighed about 70 mg of the samples in 2 mL Eppendorf tubes and poured 1 mL DPPH \cdot solution into each tube, leaving the samples to incubate for 30 min in the dark [12]. After that, we centrifuged the samples to ensure sedimentation of the powders and immediately measured the absorbance in a Perkin Elmer Lambda EZ 150UV-vis spectrometer. To quantify the percentage of the remaining DPPH \cdot , we used Eq. (2):

$$\% \text{ DPPH} \cdot = \frac{A_t}{A_i} \times 100 \quad (2)$$

Table 1 Samples used to synthesize composites

ZnCl $_2$ ·6H $_2$ O, g	AlCl $_3$ ·6H $_2$ O, g	Na $_2$ CO $_3$, g	Medium, 100 mL	Final weight expected, g	Sample
–	–	–	Tomato juice	3.86	Tomato juice
5.25	3.10	1.59	Water	5.00	ZnAl
–	–	–	–	0.50	Lycopene
7.88	4.65	2.39	Tomato juice	11.36	ZnAl75J
10.50	6.20	3.19	Tomato juice	13.86	ZnAl100J
0.53	0.31	0.16	Lycopene	1.00	ZnAlLyc

where A_f is the stands for the final absorbance of each sample; and A_i is the corresponds to the initial absorbance of DPPH $^{\cdot}$.

We assessed the antioxidant kinetics with DPPH $^{\cdot}$ by placing 50 mg of particles in 20 mL tubes, which had been protected from light with aluminum foil. In this experiment, the stock solution was diluted to set the absorbance at 0.8 units. After that, we added 10 mL of the DPPH $^{\cdot}$ diluted solution to each tube and agitated them. The UV-Vis measurements were carried out in 0, 5, 15, 30, 60, 90, 123, 180, 240, 360, and 1440 min in triplicate. With the values obtained, the percentage of inhibited DPPH $^{\cdot}$ in the solution was calculated as follows:

$$\% \text{ inhibition DPPH}^{\cdot} = \frac{(A_o - A_s)}{A_o} \times 100 \quad (3)$$

where A_o is the initial absorbance of DPPH $^{\cdot}$ without antioxidant added and A_s is the absorbance of the sample.

A solution of ABTS $^{+}$ (2,2'-azino-di-3-ethyl-benzthiazoline sulphonate) in ethanol was prepared with an absorbance of 0.740 ± 0.050 at a wavelength of 732 nm. Separately, we weighed 10.0 ± 0.5 mg of each sample in Eppendorf tubes in triplicate. Then, we added 1 mL of ABTS $^{+}$ solution to each sample and left for incubation for 5 min to take time readings in triplicate at a wavelength of 732 nm. The inhibition of ABTS $^{+}$ was calculated according to Eq. (4):

$$\% \text{ inhibition ABTS}^{+} = \frac{(A_o - A_s)}{A_o} \times 100 \quad (4)$$

where A_o is the initial absorbance of the ABTS $^{+}$ solution (0.740 ± 0.050) and A_s is the absorbance of the sample.

Antioxidant capacity on copper (CUPRAC method). This experiment involved three solutions: $\text{NH}_4(\text{CH}_3\text{COO})$ buffer (pH = 7.1), CuCl_2 (10 mM), and neocuproine (7.5 mM in ethanol). In this order, 0.33 mL of each solution was added to each vial; the samples were shaken and left for incubation in the dark for 30 min. After that, the liquid part was extracted and read using the UV-Vis spectrometer at 450 nm. Each test was done in triplicate.

RapidOxy oxidation stability test. The RapidOxy assay was conducted with 0.01, 0.03, and 0.05 g of each sample added to 1 mL of purified linseed oil. After homogenization, we placed the mix in Teflon capsules inside a PetrOXY 13-3006 device to measure the induction period and the oxidation stability until reaching $\Delta\text{PO}_2 = 50\%$. The oxygen consumption, mol, was calculated using Eq. (5):

$$\text{Oxygen Consumption} = \frac{[P(\text{O}_2)_{\text{max}} - P(\text{O}_2)_t] V(\text{O}_2)}{R T} \quad (5)$$

where $P(\text{O}_2)_{\text{max}}$ is the maximal pressure of O_2 inside the equipment chamber; $P(\text{O}_2)_t$ represents the pressure of O_2 upon reaching ΔP of 50%; $V(\text{O}_2)$ is the volume of O_2 contained inside the equipment chamber; R corresponds to

the universal constant of perfect gases (8.314 J/(K·mol); and T is the temperature of the system at $P(\text{O}_2)_t$.

Evaluating the solar protection factor. This part of the experiment required a neutral moisturizing cream, 1 mL of which was placed in a test tube followed by three different particle concentrations: 5, 10, and 15%. This mix was centrifuged at 13 000 rpm for 3 min using an IKA T18 digital Ultra Turrax homogenizer.

The solar protection factor was measured using a Cary 60 UV-Vis device (Agilent Technologies) within the range of 290–320 nm. According to the prescribed procedure, 2 mg/cm 2 of the mix was weighed on a 1×2 cm quartz plate and dispersed, leaving a homogeneous layer. This layer was placed in the UV-Vis device to take the corresponding readings.

The absorbance readings made it possible to calculate the solar protection factor value:

$$\text{Solar protection factor} = CF \sum_{290}^{320} EE(\lambda) I(\lambda) ABS(\lambda) \quad (6)$$

where CF is the correction factor of 10, $EE(\lambda)$ is the erythema effect spectrum, $I(\lambda)$ defines the solar intensity spectrum, and $ABS(\lambda)$ stands for the absorbance of the sample. The experiment was performed in triplicate.

RESULTS AND DISCUSSION

Figure 1 presents yields of the products and their relationship with their theoretical yield, considering that all the organic matter from the tomato juice was removed by the idealized layered double hydroxide of ZnAl (Table 1). The lyophilized tomato juice produced 3.86 g of powder, considered as 100% of the organic matter. The reference ZnAl had a yield of 60.5%, which is common when the synthesis is conducted at pH 8.5, according to our personal observations. The composites, ZnAl75J and ZnAl100J, had a yield of 50.67 and 50.30%, respectively. ZnAl100J had the highest yield (72.84%), indicating that the yield was proportional to the amount of the salts added. Another cause of the low yield was

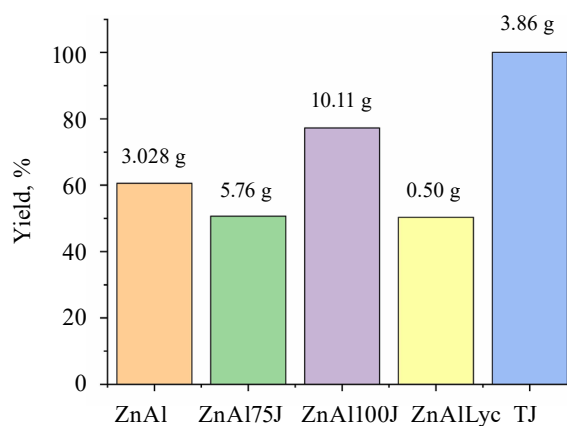


Figure 1 Solid yield obtained considering the mass of the tomato juice and the total formation of the ideal layered double hydroxide of ZnAl. TJ is tomato juice

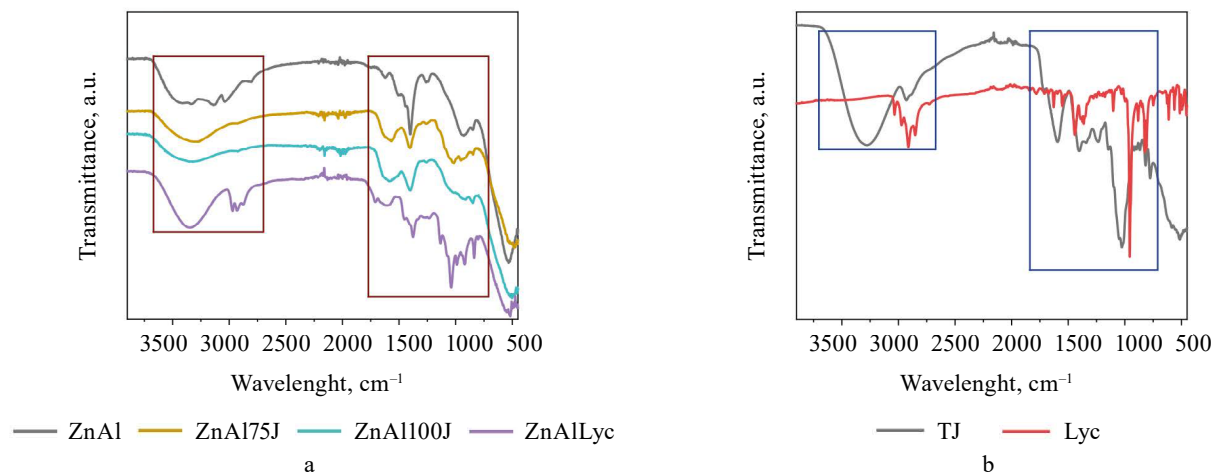


Figure 2 Infrared spectra of: the composites (a) and tomato juice and lycopene (b)

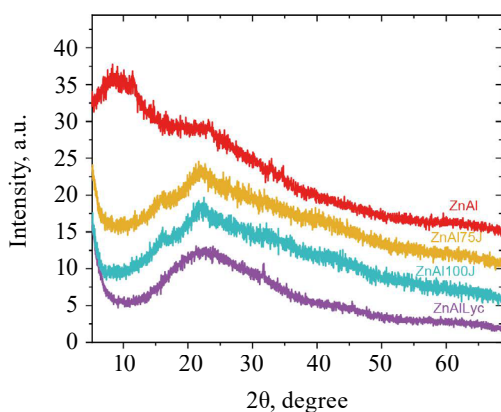


Figure 3 X-ray diffraction pattern of composites synthesized using tomato juice as reaction medium

that the expected layered double hydroxide structure was not obtained (see the X-ray diffraction section).

Figure 2 shows the infrared spectra of the composites and their respective references, i.e., tomato juice and lycopene. They exhibited bands between 3090 and 2800 cm^{-1} , which is typical of lycopene methyl groups. The band at 3400 cm^{-1} was attributed to the stretching of O-H hydroxyl bonds while the band at 994 cm^{-1} corresponded to C-H vibrations, and the band at 820 cm^{-1} was related to lycopene vinyl bonds ($\text{R}_2\text{-C}=\text{C-R}$) [13, 14].

Regarding the composites ZnAl75J and ZnAl100J, the weak band at 1630 cm^{-1} could be attributed to the water (H_2O) bending vibration. The band at 1027 cm^{-1} corresponded to C-O stretching, and the bands at 550 cm^{-1} were attributed to the M-O groups, corresponding to Al-O or Zn-O. Another phenomenon was registered in the region around 1460 cm^{-1} and manifested itself as an increase in the signal of methyl groups combined with the carbonyl signal [15]. This information suggested the possible presence of lycopene in both composites.

The band at around 1365 cm^{-1} could be attributed to the asymmetric stretching mode of the carbonate, as confirmed by the bands at 870 and 680 cm^{-1} , which cor-

responded to weak bending and angular bending modes of the carbonate, respectively [16, 17]. In the ZnAl spectrum, we observed signals related to O-H stretching at 3440, 3330, and 3144 cm^{-1} , which were probably associated with water or metallic hydroxides [18].

The diffractograms of all the products showed broad signals (Fig. 3), indicating that the structure of the ZnAl reference and the composites were predominantly amorphous. A weak but clear signal was recorded at 14.4° , which coincided with the most intense signal of boehmite, i.e., $\text{AlO}(\text{OH})$, as described in the International Centre for Diffraction Data, 83 by 1505. Although this weak signal was the only evidence of crystalline particles, other zinc and aluminum compounds might have been formed in an amorphous phase. We performed an elemental analysis by energy-dispersive X-ray spectroscopy to identify them. The spectra revealed the presence of Zn, Al, C, and O in the sample, consistent with the presence of boehmite as confirmed by X-ray diffraction, carbonates in agreement with the IR spectrum, and zinc, probably amorphous. The composites ZnAl75J and ZnAl100J rendered the same results, indicating the presence of presumably amorphous zinc. Other elements detected were C, O, P, Na, and Cl, which corresponded to the elements from the tomato juice. In all cases, the elements were uniformly distributed throughout the matrix, as indicated by the energy-dispersive X-ray spectroscopy maps (Fig. 4). The formation of ZnAl layered double hydroxide was affected by the initial reagents, pH, and even temperature, as reported in [19]. Unlike our previous work, here we started with chloride salts instead of nitrate, with the aim of using reagents authorized for the food and cosmetics industry. Although the composites were amorphous, they were even better at developing fine powders which could be easily dispersed in the sun protection factor assays. The X-ray photoelectron spectra (Fig. 5) provided detailed information about the spectra of the Zn2p levels, indicating the presence of two types of zinc atoms in the ZnAl reference and the composites. One signal at 1020.9 eV and another at 1026.0 eV, both with a spin-splitting of

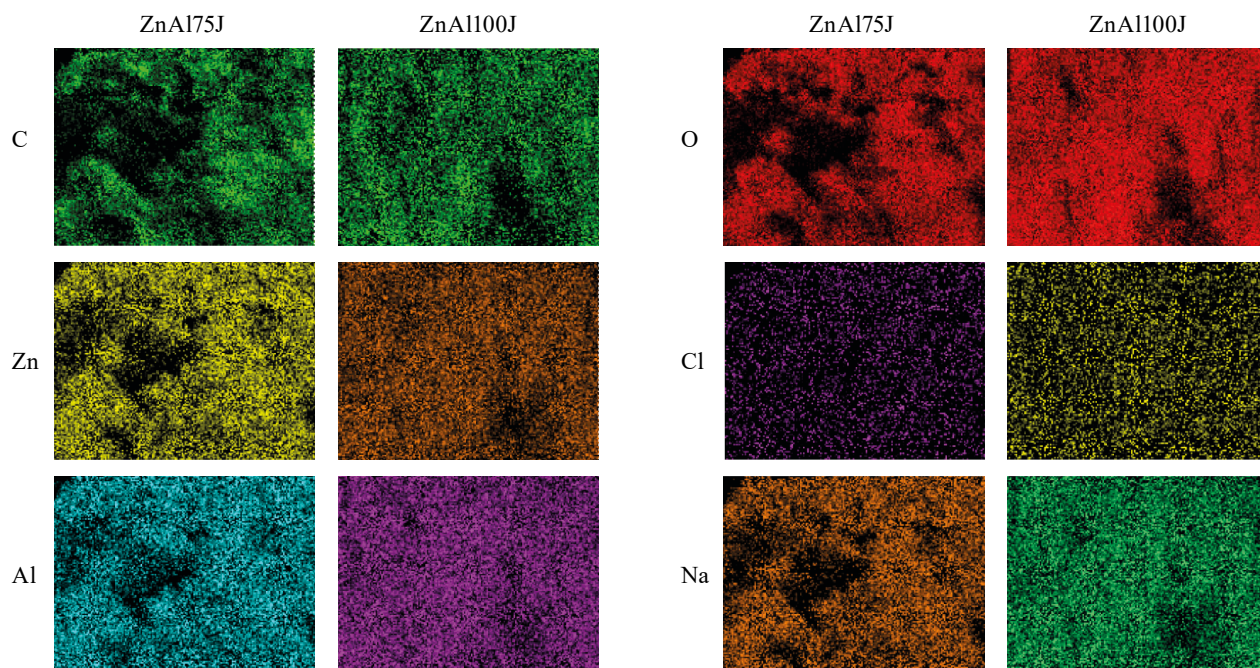


Figure 4 Elemental composition maps obtained by electron dispersive spectroscopy in composites

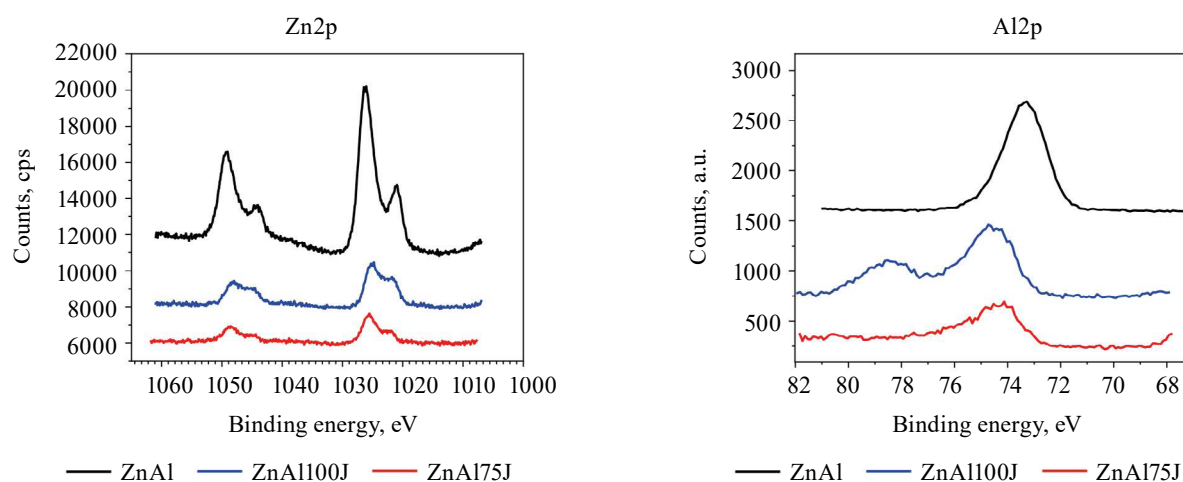


Figure 5 X-ray photoelectron spectra of Zn2p and Al2p in composites vs. ZnAl reference

23.1 eV, corresponded to Zn^{2+} , commonly found in ZnO and $\text{Zn}(\text{OH})_2$ [20]. The signal at 1020.9 eV is typical of crystalline or amorphous ZnO [21, 22]. The signal at 1026.0 eV has not been reported in scientific literature. However, it was close to high values in salts with highly electronegative counterions, e.g., halides and sulfates, suggesting that Zn^{2+} may be attributed to anions present in tomato juice [23]. On the other hand, the $\text{Al}2p$ spectrum of the ZnAl reference contained a signal at 73.3 eV, which is characteristic of aluminum oxides or hydroxides [23]. The composites also demonstrated a shift to 74.2 eV, consistent with the spectrum reported for aluminum hydroxide, which supported the X-ray diffraction data [24]. ZnAl100J exhibited an additional signal at 78.5 eV. Although it was not registered in databases, it approached the binding energy reported for Al

with halides hydroxides, suggesting coordination with such highly negatively charged anions as Cl [23]. Therefore, the powders consisted of organic compounds from tomato pulp and amorphous zinc, aluminum oxides, or hydroxides.

The scanning electron micrographs of all the composites (Fig. 6) demonstrated ZnAl, ZnAl175J, and ZnAl100J with a rough surface and multiple cavities. Additionally, a more spherical morphology was present in clusters with smooth surfaces. The absence of defined crystalline structures could be indicative of a higher amount of organic or amorphous material, as detected by the X-ray diffraction. ZnAlLyc demonstrated different structures in the form of layers corresponding to aluminum hydroxides [25, 26]. In all cases, particles tended to be spherical in ZnAl, ZnAl175J, and ZnAl100J, while ZnAl-

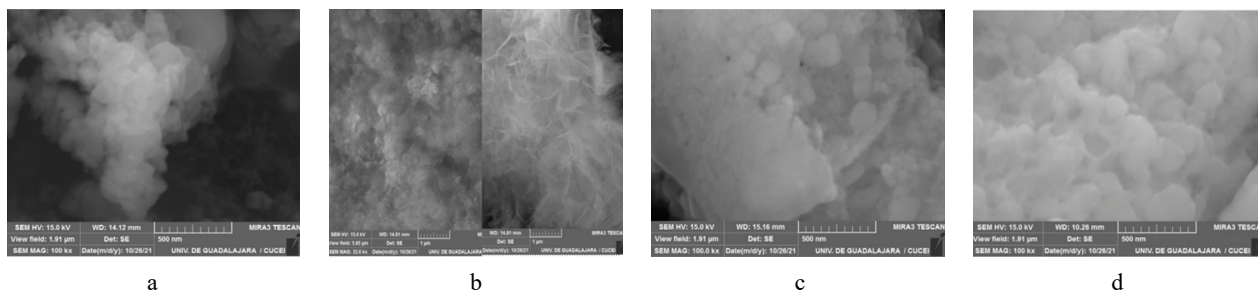


Figure 6 Micrographs obtained by scanning electron microscopy: (a) ZnAl, (b) ZnAlLyc, (c) ZnAl75J, and (d) ZnAl100J

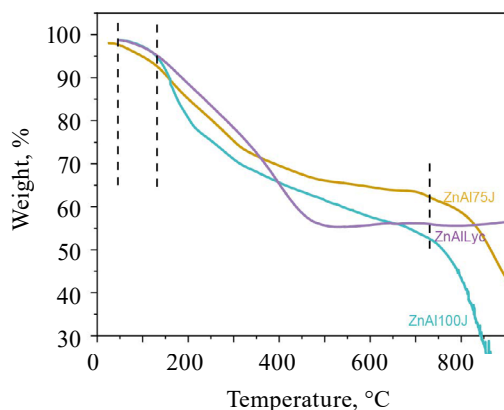


Figure 7 Thermogravimetric analysis for composites ZnAl75J, ZnAl100J, and ZnAlLyc

Lyc formed needle-like structures. All particles were 400–800 nm in size; however, the particle size in the liquid medium was different (see the dynamic light scattering section).

Thermogravimetric analysis. Figure 7 illustrates the decomposition of the composites as a function of temperature. Regarding ZnAlLyc, the degradation was continuous with the first step at 250°C and the second at 450°C. The first event might correspond to the removal of water and the burning of organic matter whereas the second event might correspond to the decomposition of metal hydroxides, possibly producing oxides at $\geq 500^\circ\text{C}$. The 50% of compounds that did not degrade could be metallic oxides of amorphous nature as they were not observed in the X-ray diffraction analysis.

ZnAl75J and ZnAl100J revealed a step that culminated at 150°C due to evaporation of approximately 5% water [26, 27]. That step was followed by another event ending at 200°C, which probably corresponded to the combustion of organic material and partial dihydroxylation. The third step was at 330–750°C, where the combustion of organic matter and the formation of metal oxides were completed [27].

Comparing the degradation profile with our previous composites with layered double hydroxide phases, this profile formed a lower slope, which indicated a slower degradation [5]. In addition, the amorphous phases in the current work provided a slightly greater thermal stability.

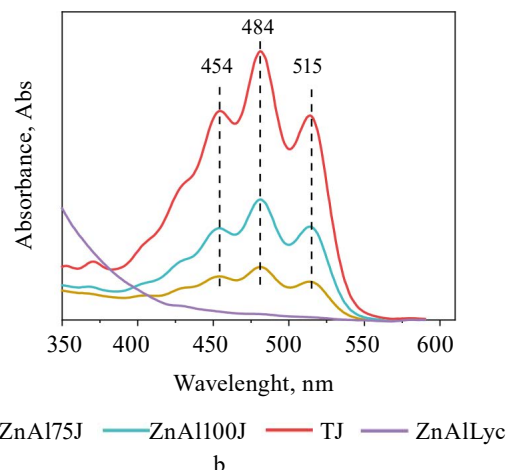
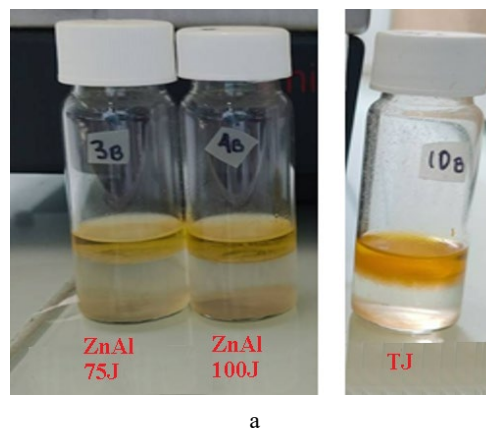


Figure 8 Extraction of encapsulated lycopene in composites (a) and UV-Vis spectra of lycopene extracted from composites with toluene (b). TJ is tomato juice

Quantification of lycopene. The quantification was possible due to the easy release of lycopene from the composites (Fig. 8a) because adsorption forces between the metal-organic composition in these composites were not strong enough to prevent organic solvents from removing lycopene with simple agitation. Figure 8a shows the red phase containing lycopene. The identification was done by comparing the UV-Vis absorption profile of the red pigment released by the samples with a standard lycopene solution (Fig. 8b), with peaks at 454, 484, and 515 nm [28]. The easy release may suggest that the nanoparticles somehow broke the pericarp and chromoplasts to let the lycopene out.

Using the quantified lycopene in tomato juice as a reference, we compared it with the lycopene released from the composites to determine recoveries per volume of tomato juice and yield. The ZnAl100J composite recovered 0.717 mg per 1 mL of tomato juice (Fig. 9a), and this amount corresponded to the yield of 95.92% (Fig. 9b). This value exceeded the highest values reported in [29, 30], which ranged between 0.43 and 0.50 mg/mL of tomato juice. ZnAl75J recovered only 26.6% of the lycopene, suggesting that the synthesis conditions of ZnAl100J require additional research.

Hydrodynamic particle size. We used a liquid medium to study the particle size of the composites because liquid is a more representative environment for their use, e.g., in foods or cosmetics. The hydrodynamic size detected by the dynamic light scattering test (Fig. 10) for ZnAl75J was 615 nm while that for ZnAl100J it was 1720 nm. Comparing these results with the scanning electron micrographs, ZnAl75J particles were completely dispersed in water. However, the aggregation was two particles on average for ZnAl100J.

Regarding the zeta potential, the composites were subjected to acidic and saline media. Figure 11 shows

that the ZnAl particles maintained the positive potential in HCl and saline solution while the composites with tomato juice changed the values to negative when they were in saline solution. The positive values in HCl suggested that H^+ ions were adsorbed on the surface of the composites while Cl^- ions were retained in saline solutions. Stable suspension preparation often requires high values of the zeta potential, e.g., $\geq \pm 30$ mV [31]. However, the low aggregation detected by the dynamic light scattering indicated that these types of composites were easily dispersible in liquid formulations.

Antioxidant capacity. Figure 12 presents the results of total antioxidant capacity expressed as a percentage of DPPH \cdot inhibition in 2 and 24 h. In 2 h, the inhibition was 31% for ZnAl75J and ZnAl100J. ZnAl showed 18% inhibition, which seemed to have a significant contribution from the inorganic particles. In ZnAlLyc, the inhibition slightly increased to 42% whereas the tomato juice and lycopene references showed superior activity of $\geq 90\%$. This phenomenon indicated that the antioxidant components in tomato juice and lycopene were more available in 2 h than those in all the composites. However, the activity of the tomato juice and lycopene

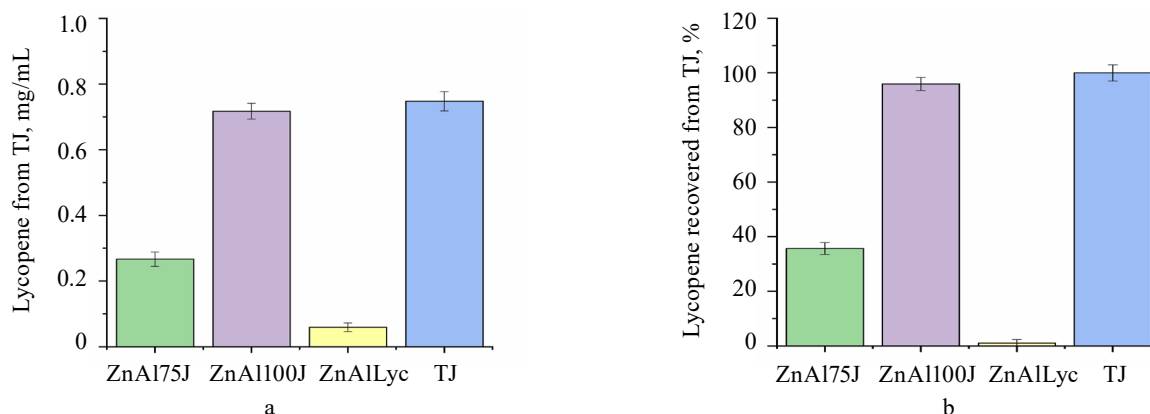


Figure 9 Lycopene recovered from tomato juice (a) and corresponding yield regarding the lycopene in tomato juice as reference (b). The bars correspond to standard deviation. TJ is tomato juice

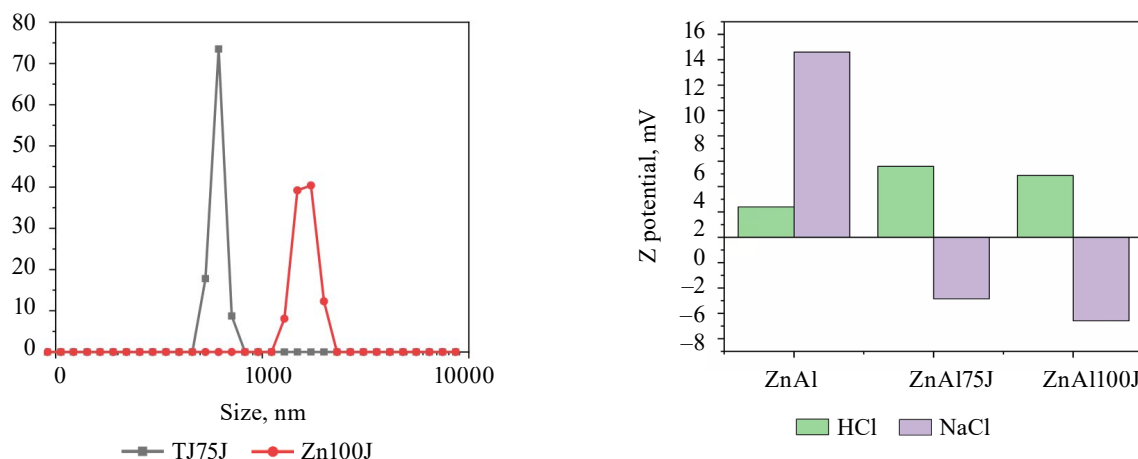


Figure 10 Dynamic light scattering test: particle size histogram

Figure 11 Zeta potential for composites in acidic (green) and saline (purple) media. TJ is tomato juice

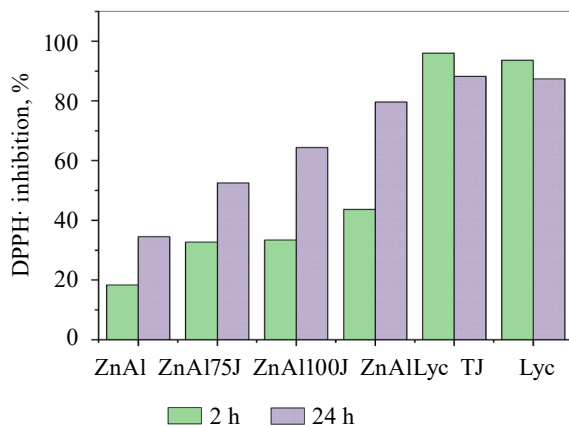


Figure 12 Percentage of DPPH• inhibition in 2 and 24 h (standard deviation $\leq \pm 0.05$, $n = 3$)

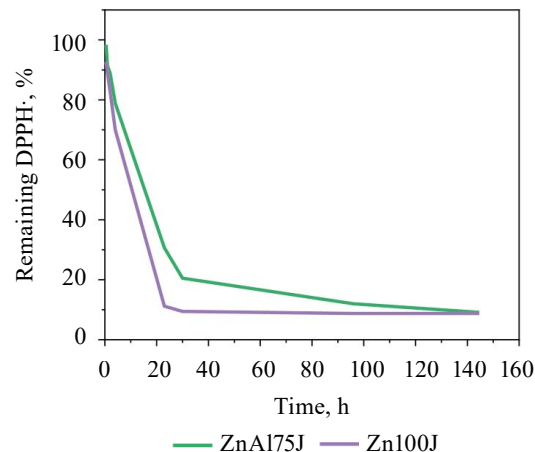


Figure 13 Percentage of remaining DPPH• over time (standard deviation $\leq \pm 0.08$, $n = 3$)

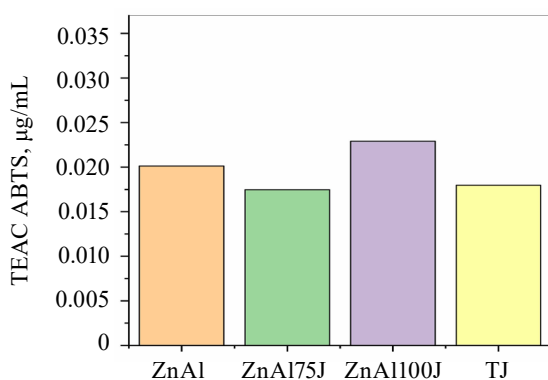


Figure 14 Trolox equivalent antioxidant capacity (TEAC) in the ABTS•+ assay (standard deviation $\leq \pm 0.05$, $n = 3$)

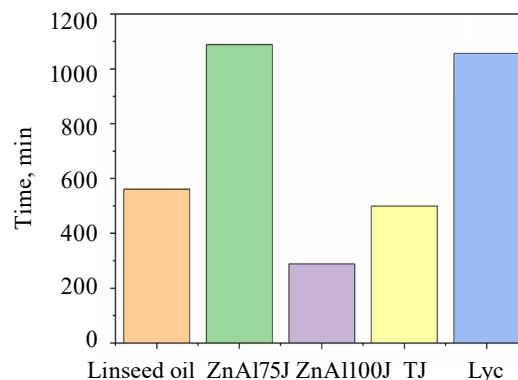


Figure 15 Time to consume $\Delta\text{PO}_2 = 50\%$ of composites and their references at 37°C and 101 KPa. TJ is tomato juice

references slightly decreased in 24 h while all composites and the ZnAl reference increased their activity. ZnAl75J reached 52% inhibition, ZnAl100J reached 64%, and ZnAlLyc reached 82%. Probably, the inorganic particles were the ones contributing to the long-term inhibition, presumably because the Zn and Al oxides/hydroxides slowed down the release of lycopene into the reaction medium.

Antioxidant kinetics with DPPH•. Figure 13 illustrates the kinetics of antioxidant activity. Tomato juice retained 6.6% of the remaining DPPH• 5 min after the start of the experiment. Due to the fast decay it was not plotted. Using this data as a reference point, we observed that the consumption of DPPH• decreased rapidly: ZnAl100J consumed 89% of DPPH• in 23 h (remaining 11%) while ZnAl75J consumed 80% of DPPH• in 30 h (remaining 20%). Probably, the higher lycopene removal efficiency observed for ZnAl100J indicated that lycopene allowed for greater antioxidant activity in this assay.

In the ABTS•+ assay, the composites demonstrated a value of IC_{50} 0.012 $\mu\text{g/mL}$ of ABTS with trolox equivalent antioxidant capacity. All the samples obtained a value higher than that after 5 min of incubation (Fig. 14), indicating a greater antioxidant activity towards ABTS•+ than towards DPPH•. This result could be explained by

the type and number of charges. In ABTS•+, the SO_3^- group had a negative charge. Most likely, this anion was attracted to the charges of zinc or aluminum, just as it happened with the chlorides that shifted the zeta potential to negative values.

In the RapidOxy experiment, the results represented the time required to consume 0.4 mol of O_2 , corresponding to $\Delta P = 50\%$.

We used purified linseed oil as the oily medium reference in this experiment, which needed 555 min for oxidation. In this experiment, the concentration of linseed oil was 0.03 g/mL. Figure 15 shows that ZnAl75J and lycopene had the longest time of O_2 consumption with 1089 and 1057 min, respectively, which means they provided stronger protection against oxidation. On the other hand, ZnAl100J consumed oxygen faster than tomato juice, taking 287 min. Thus, the protection time was reduced in spite of the fact that this assay had more organic material.

As for the sun protection factor, the values presented in Fig. 16 indicated that ZnAl75J at 15% (SPF 3.08) was the mix with the highest value, followed by ZnAl at 15% (SPF 2.58) and ZnAl100J at 5% (SPF 2.5). Therefore, no high photoprotective synergy occurred between the Zn compounds and the organic material.

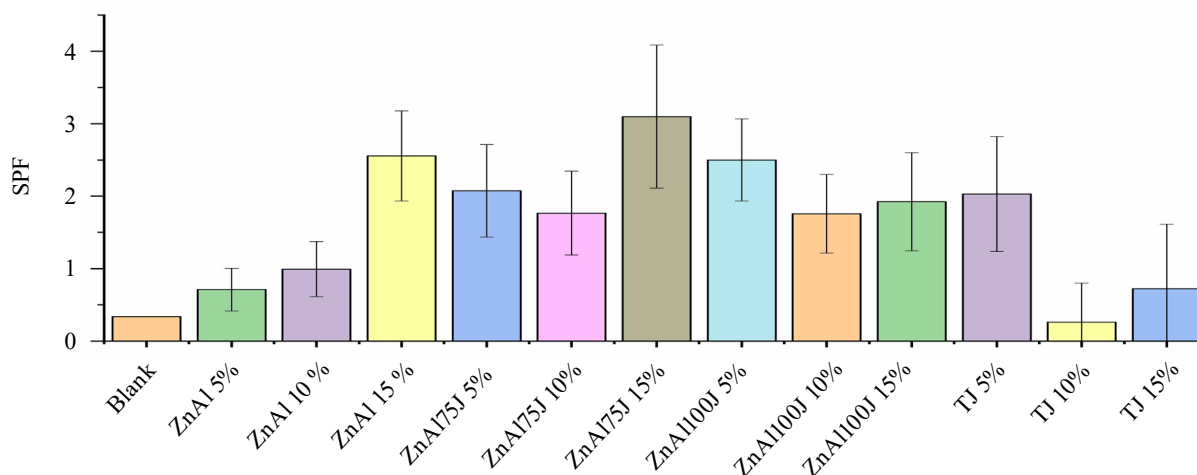


Figure 16 Sun protection factor for composites and references at different concentrations. Each experiment was performed in triplicate, the bars correspond to standard deviations

The sun protection factor values of ZnAl75J and ZnAl100J stayed within the range reported for these compounds [32–34]. Similarly, the sun protection factor of 1 obtained with ZnAl was lower than the values reported for ZnO in [35] as approximately 5 SPF.

Previous studies showed that human skin increases the quantity of carotenoids by approximately 25% during summer and autumn [36]. These composites could then be an alternative to meet the increased need for carotenoids in the skin when applied topically. Corresponding with the obtained zeta potential values, these composites show stability in oil-in-water emulsions [37].

CONCLUSION

The synthesized composites were found to be amorphous, indicating that the reaction did not produce layered double hydroxide crystals when the synthesis was carried out using zinc and aluminum chlorides with tomato juice as a reaction medium. The powdered material was composed of amorphous zinc and aluminum oxides or hydroxides, which removed 97% of the available lycopene in tomato juice under the synthesis conditions of ZnAl100J. Although ZnAl75J removed a smaller amount of lycopene, its antioxidant activity and sun protection factor were sufficient for it to be used as an antioxidant ingredient in food, food packaging, or cosmetics. In addition, its lack of aggregation in water allows for uniform dispersion.

ZnAl100J showed higher antioxidant activity against free radicals while ZnAl75J exhibited the best results for oxidation resistance.

Regarding the sun protection factor, the composites showed no high values; however, they could be considered as substitutes for increasing carotenoids in human

skin. Finally, these composites seem to be a promising option for sustainable extraction of lycopene, as well as for encapsulating organic material obtained from tomato juice because they provided protection against degradation and antioxidant loss.

CONTRIBUTIONS

Rosa Nallely Murillo Vázquez designed and conducted the experiments, organized the data, and wrote the draft of the article. Fermín Paul Pacheco Moisés analyzed and processed the results, as well as supervised the work. Verónica Nardello-Rataj provided the conceptualization, supervision, and discussion. Gregorio Guadalupe Carbajal Arízaga provided conceptualization, formal analysis, supervision, and revision.

CONFLICT OF INTEREST

The authors declared no conflict of interests regarding the publication of this article.

ACKNOWLEDGMENTS

The authors acknowledge the technical assistance of José Antonio Rivera Mayorga for collecting the X-ray photoelectron spectra and the Transdisciplinary Institute of Research and Services – ITRANS at the University of Guadalajara for collecting the energy dispersive X-ray spectra. This manuscript is dedicated to the memory of Rosa Nallely Murillo Vázquez, who left this world during the peer review of her manuscript.

INFORMED CONSENT

Informed consent was obtained from all individual participants included in the study.


REFERENCES


1. Heriyanto S, Romulo A. Tomato pomace ketchup: Physicochemical, microbiological, and sensory characteristics. *Food Processing: Techniques and Technology*. 2023;53(4):766–774. <https://doi.org/10.21603/2074-9414-2023-4-2477>

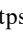
2. Madia VN, de Vita D, Ialongo D, Tudino V, de Leo A, Scipione L, et al. Recent advances in recovery of lycopene from tomato waste: A potent antioxidant with endless benefits. *Molecules*. 2021;26(15):4495. <https://doi.org/10.3390/molecules26154495>
3. Méndez-Carmona JY, Ascacio-Valdes JA, Alvarez-Perez OB, Hernández-Almanza AY, Ramírez-Guzman N, Sepúlveda L, et al. Tomato waste as a bioresource for lycopene extraction using emerging technologies. *Food Bioscience*. 2022;49:101966. <https://doi.org/10.1016/j.fbio.2022.101966>
4. Yasmeen N, Sameer AS, Nissar S. Lycopene. In: Kour J, Nayik GA, editors. *Nutraceuticals and health care*. Academic Press; 2022. pp. 115–134. <https://doi.org/10.1016/B978-0-323-89779-2.00009-0>
5. Hernández DE, Magallon AP, Arizaga GGC. Green extraction of lycopene from tomato juice with layered double hydroxide nanoparticles. *Micro and Nano Letters*. 2019;14(3):230–233. <https://doi.org/10.1049/mnl.2018.5437>
6. Chen Z, Fan Q, Huang M, Cölfen H. Synthesis of two-dimensional layered double hydroxides: A systematic overview. *CrystEngComm*. 2022;24(26):4639–4655. <https://doi.org/10.1039/D2CE00511E>
7. Min L, Duan J, Song C, Chen Y, Zhang W, Wang Y. Decarbonating layered double hydroxides using a carbonated salt solution. *Dalton Transactions*. 2023;52(21):7330–7335. <https://doi.org/10.1039/D3DT01079A>
8. Kesavan Pillai S, Kleyi P, de Beer M, Mudaly P. Layered double hydroxides: An advanced encapsulation and delivery system for cosmetic ingredients – An overview. *Applied Clay Science*. 2020;199:105868. <https://doi.org/10.1016/j.clay.2020.105868>
9. Mosangi D, Moyo L, Kesavan Pillai S, Ray SS. Acetyl salicylic acid-ZnAl layered double hydroxide functional nanohybrid for skin care application. *RSC Advances*. 2016;6(107):105862–105870. <https://doi.org/10.1039/C6RA22172F>
10. Cheng H-M, Gao X-W, Zhang K, Wang X-R, Zhou W, Li S-J, et al. A novel antimicrobial composite: ZnAl-hydrotalcite with *p*-hydroxybenzoic acid intercalation and its possible application as a food packaging material. *New Journal of Chemistry*. 2019;43(48):19408–19414. <https://doi.org/10.1039/C9NJ03943K>
11. Egambaram OP, Kesavan Pillai S, Ray SS, Goosen M. Structural and photoprotective characteristics of Zn-Ti, Zn-Al, and Mg-Al layered double hydroxides – A comparative study. *Cosmetics*. 2023;10(4):100. <https://doi.org/10.3390/cosmetics10040100>
12. Szerlauth A, Muráth S, Szilagyi I. Layered double hydroxide-based antioxidant dispersions with high colloidal and functional stability. *Soft Matter*. 2020;16(46):10518–10527. <https://doi.org/10.1039/D0SM01531H>
13. Singh A, Ahmad S, Ahmad A. Green extraction methods and environmental applications of carotenoids – A review. *RSC Advances*. 2015;5(77):62358–62393. <https://doi.org/10.1039/C5RA10243J>
14. Ma Y, Zhong L, Peng Z, Liu X, Ouyang D, Guan S. Development of a highly water-soluble lycopene cyclodextrin ternary formulation by the integrated experimental and modeling techniques. *AAPS PharmSciTech*. 2021;22:5. <https://doi.org/10.1208/s12249-020-01861->
15. Aghel N, Ramezani Z, Amirfakhrian S. Isolation and quantification of lycopene from tomato cultivated in Dezfool, Iran. *Jundishapur Journal of Natural Pharmaceutical Products*. 2011;6(1):9–15.
16. Benítez JJ, Castillo PM, del Río JC, León-Camacho M, Domínguez E, Heredia A, et al. Valorization of tomato processing by-products: Fatty acid extraction and production of bio-based materials. *Materials*. 2018;11(11):2211. <https://doi.org/10.3390/ma11112211>
17. Gordeeva A, Hsu Y-J, Jenei IZ, Brant Carvalho PHB, Simak SI, Andersson O, et al. Layered zinc hydroxide dihydrate, $\text{Zn}_5(\text{OH})_{10} \cdot 2\text{H}_2\text{O}$, from hydrothermal conversion of $\epsilon\text{-Zn}(\text{OH})_2$ at gigapascal pressures and its transformation to nanocrystalline ZnO. *ACS Omega*. 2020;5(28):17617–17627. <https://doi.org/10.1021/acsomega.0c02075>
18. Bastianini M, Faffa C, Sisani M, Petracci A. Caffeic acid-layered double hydroxide hybrid: A new raw material for cosmetic applications. *Cosmetics*. 2018;5(3):51. <https://doi.org/10.3390/cosmetics5030051>
19. Bukhtiyarova MV. A review on effect of synthesis conditions on the formation of layered double hydroxides. *Journal of Solid State Chemistry*. 2019;269:494–506. <https://doi.org/10.1016/j.jssc.2018.10.018>
20. Wang T, Jin B, Jiao Z, Lu G, Ye J, Bi Y. Photo-directed growth of Au nanowires on ZnO arrays for enhancing photoelectrochemical performances. *Journal of Materials Chemistry A*. 2014;2(37):15553–15559. <https://doi.org/10.1039/C4TA02960G>
21. Chen H, Deng H, Zhong X, Zhou H, Zhan J, Zhou X. Highly dispersed amorphous ZnO on a petal-like porous silica-clay composite with enhanced antimicrobial properties. *Colloids and Surfaces B: Biointerfaces*. 2022;220:112978. <https://doi.org/10.1016/j.colsurfb.2022.112978>
22. Xiao S, Zhao L, Leng X, Lang X, Lian J. Synthesis of amorphous TiO_2 modified ZnO nanorod film with enhanced photocatalytic properties. *Applied Surface Science*. 2014;299:97–104. <https://doi.org/10.1016/j.apsusc.2014.01.192>

23. Naumkin AV, Kraut-Vass A, Gaarenstroom SW, Powell CJ. NIST X-ray photoelectron spectroscopy database. Gaithersburg: National Institute of Standards and Technology; 2000. <https://doi.org/10.18434/T4T88K>
24. Rotole JA, Sherwood PMA. Nordstrandite (Al(OH)₃) by XPS. *Surface Science Spectra*. 1998;5:32–38. <https://doi.org/10.1116/1.1247854>
25. Pooresmaeil M, Behzadi Nia S, Namazi H. Green encapsulation of LDH(Zn/Al)-5-Fu with carboxymethyl cellulose biopolymer; new nanovehicle for oral colorectal cancer treatment. *International Journal of Biological Macromolecules*. 2019;139:994–1001. <https://doi.org/10.1016/j.ijbiomac.2019.08.060>
26. Zhang Y, Chang J, Zhao J, Fang Y. Nanostructural characterization of Al(OH)₃ formed during the hydration of calcium sulfoaluminate cement. *Journal of the American Ceramic Society*. 2018;101(9):4262–4274. <https://doi.org/10.1111/jace.15536>
27. Guo X, Tang M, Wang N, Li L, Wu Y, Chen X, et al. The synthesis of organically modified layered double hydroxide and its effect on the structure and physical properties of low-density polyethylene/ethylene–vinyl acetate blends. *Polymers and Polymer Composites*. 2019;27(5):287–298. <https://doi.org/10.1177/0967391119846218>
28. Adriany A, Jéssica S, Ana O, Raimunda S, Andreanne V, Luan S, et al. Anti-inflammatory and antioxidant activity improvement of lycopene from guava on nanoemulsifying system. *Journal of Dispersion Science and Technology*. 2021;42(5):760–770. <https://doi.org/10.1080/01932691.2020.1728300>
29. Cámara M, de Cortes Sánchez-Mata M, Fernández-Ruiz V, Cámara RM, Manzoor S, Caceres JO. Lycopene: A review of chemical and biological activity related to beneficial health effects. *Studies in Natural Products Chemistry*. 2013;40:383–426. <https://doi.org/10.1016/B978-0-444-59603-1.00011-4>
30. Guerra AS, Hoyos CG, Molina-Ramírez C, Velásquez-Cock J, Vélez L, Gañán P, et al. Extraction and preservation of lycopene: A review of the advancements offered by the value chain of nanotechnology. *Trends in Food Science and Technology*. 2021;116:1120–1140. <https://doi.org/10.1016/j.tifs.2021.09.009>
31. Zhang C, Li C, Zhu Y, Cui H, Lin L. Stability of a novel glycosylated peanut protein isolate delivery system loaded with gallic acid. *Food Chemistry*. 2024;437:137790. <https://doi.org/10.1016/j.foodchem.2023.137790>
32. Joshi H, Hegde AR, Shetty PK, Gollavilli H, Managuli RS, Kalthur G, et al. Sunscreen creams containing naringenin nanoparticles: Formulation development and in vitro and in vivo evaluations. *Photodermatology Photoimmunology and Photomedicine*. 2018;34(1):69–81. <https://doi.org/10.1111/phpp.12335>
33. Aloanis AA, Karundeng M, Paat VI, Tengker SMT, Siwu O. Sun protecting factor value of the Ficus benjamina Linn. fruits extract. *Journal of Physics: Conference Series*. 2021;1968:012009. <https://doi.org/10.1088/1742-6596/1968/1/012009>
34. Rohmah J, Wulandari FE, Rini CS. In vitro: Sunscreen activity of red lettuce extract (*Lactuca sativa* var. *crispa* L.). *IOP Conference Series: Earth and Environmental Science*. 2020;519:012009. <https://doi.org/10.1088/1755-1315/519/1/012009>
35. Fogaça LA, Feuser PE, Ricci-Júnior E, Hermes de Araújo PH, Sayer C, da Costa C. ZnO and quercetin encapsulated nanoparticles for sun protection obtained by miniemulsion polymerization using alternative co-stabilizers. *Materials Research Express*. 2020;7:015096. <https://doi.org/10.1088/2053-1591/ab6c8e>
36. Lademann J, Meinke M, Sterry W, Darvin M. Carotenoids in human skin. *Experimental Dermatology*. 2011;20:377–382. <https://doi.org/10.1111/j.1600-0625.2010.01189.x>
37. Low LE, Siva SP, Ho YK, Chan ES, Tey BT. Recent advances of characterization techniques for the formation, physical properties and stability of Pickering emulsion. *Advances in Colloid and Interface Science*. 2020;277:102117. <https://doi.org/10.1016/j.cis.2020.102117>

ORCID IDs

Rosa Nallely Murillo Vázquez  <https://orcid.org/0000-0001-7881-6649>

Fermín Paul Pacheco Moisés  <https://orcid.org/0000-0002-3769-5649>

Verónica Nardello-Rataj  <https://orcid.org/0000-0001-8065-997X>

Gregorio Guadalupe Carbajal Arízaga  <https://orcid.org/0000-0003-3120-0243>



Innovative physical techniques in freeze-drying

Oksana I. Andreeva^{ID}, Ivan A. Shorstkii*^{ID}

Kuban State Technological University^{ROR}, Krasnodar, Russia

* e-mail: i-shorstky@mail.ru

Received 25.12.2023; Revised 09.02.2024; Accepted 05.03.2024; Published online 29.10.2024

Abstract:

Malnutrition is a global problem that is caused by insufficient sources of vitamins, microelements, and other nutrients. This creates a need for developing long-term preservation techniques. One of the solutions is to pre-treat food materials before freeze-drying by applying advanced and safe electrophysical techniques instead of traditional thermomechanical methods.

We reviewed three of the most promising electrophysical techniques (low-temperature plasma, ultrasound, and pulsed electric field) which have proven effective for a wide range of food materials. In particular, we focused on their mechanism of action and the equipment required, drawing on successful laboratory and large-scale studies in Russia and abroad.

The electrophysical techniques under review had an etching effect on the material, caused electroporation, and changed the material's internal structure. In addition to these effects, we described their process and technology, as well as their advantages and disadvantages in industrial applications.

Based on literature analysis, we stressed the importance of developing innovative electrophysical techniques for the food industry. These techniques should ensure high energy efficiency of the freeze-drying process and maintain good quality characteristics of food products.

Keywords: Freeze-drying, physical treatment, food product, ultrasound, pulsed electric field, low-temperature plasma

Funding: The research was funded by the Kuban Scientific Foundation within Scientific Project No. MFI-20.1/42. The modeling was carried out at the facilities of the Scientific Research Center for Food and Chemical Technologies, the Kuban State University of Technology (KubSTU)^{ROR} (SKR_3111), with the support from the Ministry of Science and Higher Education of the Russian Federation (Minobrnauki)^{ROR} (Agreement No. 075-15-2021-679).

Please cite this article in press as: Andreeva OI, Shorstkii IA. Innovative physical techniques in freeze-drying. *Foods and Raw Materials*. 2025;13(2):341–354. <https://doi.org/10.21603/2308-4057-2025-2-643>

INTRODUCTION

Russia's food industry prioritizes a transition to highly productive and green agriculture and aquaculture, efficient processing, and formulation of safe and high-quality products, including functional foods [1]. This requires advanced technology for processing, production, and preservation of foods and raw materials [2, 3].

Drying is one of the oldest techniques to preserve food and its vitamins, trace elements, and other macro- and micronutrients. The quality and safety of the resulting product depend on the drying method applied [4]. Freeze-drying is a highly effective method of dehydrating pre-frozen food by sublimating ice in a vacuum under gentle temperature conditions. The resulting product is of much higher quality than that provided by other conventional drying techniques [5].

Energy saving is of major importance in freeze-drying [6]. The duration and high energy costs of freeze-drying are the main technological barriers to its widespread use [5]. Energy saving is a global trend in all processing industries, including food and agriculture (Industry 4.0).

Today, Russian and international research groups are looking for ways to save energy used in the freeze-drying process. Some are developing better facilities, while others focus on various techniques for both food preparation and the process itself [7–11].

Shorstkij described the main technical solutions to improve freeze-drying such as intensified heat supply, better vapor removal, and the recycling of thermal resources, including secondary ones [2]. These solutions also cover the stage of freezing raw materials.

Physical pre-processing techniques allow for energy saving and better quality of the resulting product. For example, the conventional thermomechanical blanching process inactivates enzymes, removes intracellular air, reduces the loss of color and taste, and increases the drying rate [12]. Another technique is osmotic dehydration, which involves introducing a food matrix into a hypertonic solution [13]. The resulting loss of water reduces the subsequent drying time and the amount of dry matter, thus improving the product's sensory and functional properties [14]. However, these thermomechanical techniques provide insufficient energy efficiency, especially during the freeze-drying of berries [15].

In recent years, new electrophysical techniques have been introduced as a pre-treatment before freeze-drying, including ultrasound, pulsed electric fields, and low-temperature plasma. Without using high temperatures, these innovative techniques help reduce the drying time and improve the quality of the resulting product. They are also quite economical due to low energy consumption.

We aimed to review the current uses of innovative physical techniques for freeze-drying food products.

STUDY OBJECTS AND METHODS

In this review, we presented the most effective physical techniques used in the freeze-drying process, briefly describing their mechanism of action, application, and equipment requirements. For this, we retrospectively analyzed scientific papers published in 2010–2024 and indexed in the Scopus, Web of Science, and eLIBRARY.RU databases. The search was based on the keywords “freeze-drying” and “emerging technology”.

RESULTS AND DISCUSSION

Physical techniques in freeze-drying. Low-temperature plasma (LTP) results from gas ionization by an electric discharge using various media (air, argon, oxygen, etc.). The LTP jet generates cations, anions, free and excited electrons, and a number of volatile atoms and molecules [16]. They can be divided into reactive oxygen species and reactive nitrogen species. Their interaction with a food product causes complex physical and chemical reactions. These reactions produce various effects, including sterilization, enzyme inactivation,

surface changes, as well as an effect on the anatomical integrity of plant cells [17, 18]. The variety of active LTP particles indicates their high chemical (including bactericidal) activity, which is why LTP was initially used to sterilize food products.

As technology developed, LTP began to be used to modify the surface structure of raw materials and produce an “etching” effect, which changed the capillary-porous structure of the material [19]. This treatment was later used to prepare seeds for sowing to improve their germination [20].

Surface etching effect. Numerous studies show that the surface effect of low-temperature plasma (LTP) accelerates the freeze-drying of plant materials [21–26]. The mechanism of this effect is shown in Fig. 1. As can be seen, particles of reactive oxygen species and reactive nitrogen species bombard, and interact with, the surface (shell and upper layer) of a food material. The etching effect is mainly due to the decomposition of the material's waxy shell, which causes cracks and channels to form [27]. This waxy shell, commonly present in most foods exposed to freeze-drying (e.g., berries), is a “diffusion barrier” to moisture removal [28]. Exposure to LTP helps remove this barrier and increase drying efficiency. Miraei *et al.* found that the LTP treatment of grapes changed the angle at which water wetted their surface [29]. The etching effect of LTP on the grape's waxy shell increased its hydrophilicity by 40%. This study showed that changing the structure of a plant material's waxy shell leads to higher wettability and moisture absorption. Similarly, Shorstkij and Mounassar reported a rise in moisture absorption when wheat seeds were treated with LTP [30]. In addition, micropores were seen on the surfaces of grapes and wheat seeds, as shown by the scanning electron microscope images. Dharini *et al.* provide more detail about the chemical reactions in the food product's shell [31].

The size of temporary pores formed as a result of LTP treatment may change over time [29]. The size of pores has a direct effect on the efficiency of moisture diffusion onto the surface of the material during freeze-drying. Therefore, further research is needed to maximize the etching effect of LTP. Sosnin and Shorstkij exposed apple slices to LTP, with a pore diameter set at 100 μm [28]. They found that electrically-induced pores

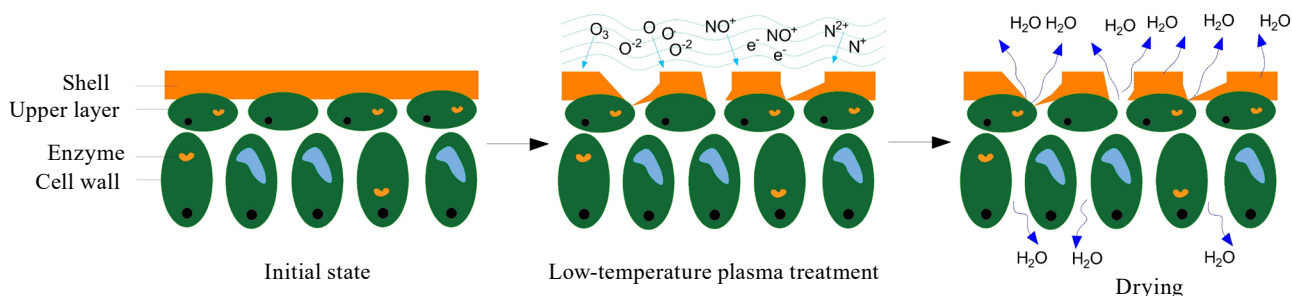


Figure 1 Effect of low-temperature plasma on the surface of plant material: ROS – reactive oxygen species, RNS – reactive nitrogen species

accelerated drying by 15–20%. Similar findings are presented in a study on honeysuckle berries [21]. Also, pores and channels form not only on the surface of fruits but also on other parts of plants, for example, tobacco stem and leaf or common hyssop [32, 33].

The etching effect of LTP treatment directly depends on the material's moisture, as well as the composition and concentration of active substances involved in reactions on the surface of the plant material. Longer treatment and higher moisture significantly increase the number of micropores on the treated surface, which affects the drying time [28]. In other words, the efficiency of etching is one of the main factors for improving the efficiency of freeze-drying.

Changes in the internal structure. As noted above, the surface effects of low-temperature plasma (LTP) can accelerate freeze-drying processes. However, the internal structure of plant materials is modified as well. Since moisture is distributed throughout the volume of the material, it is not enough to only remove the diffuse barrier of the waxy shell. Another barrier to effective mass transfer is the plant cell membrane. There have been few recent studies on improving the drying process by modifying the plant's internal structure [21–26]. Huang *et al.* reported a modified internal structure of grapes, with similar results obtained by Miraei *et al.* using a spark discharge [29, 34].

Li *et al.* reported a high efficiency of treating honeysuckle berries with LTP before freeze-drying [21]. In particular, the LTP pre-treatment for 75 s reduced the freeze-drying time by 27% and increased the permeability of plant cell membranes by 15%. In a study on strawberries, exposure to LTP maintained their quality and improved their sensory characteristics [35]. Yu-Hao *et al.* reported that the cell walls of wolfberry became thinner and more permeable after LTP treatment [36]. Based on the microscopic analysis, the authors assumed that

these changes promoted the release of phenolic compounds through the pores formed after extraction. However, it remains unknown whether this might contribute to a loss of the target component during freeze-drying. Therefore, these changes need to be correlated with varying sizes of the channels formed on the plant's surface and cell membranes. To sum up, changes in the structure of the plant cell membrane are a second factor that affects the efficiency of freeze-drying.

Pectin and cellulose are the main components of a plant cell wall. Based on [37], we can assume that pectin molecules may break down due to the cleavage of the C₄–O covalent bond during oxidation processes induced by LTP. In other words, the LTP treatment of plant materials can promote the breaking of covalent bonds in the cell walls, thereby increasing the rate of water diffusion.

Thus, etching and electroporation of plant cell walls are the main effects of the LTP treatment that have been confirmed by most studies, despite the complexity of LTP's action on multi-component foods. Important factors include the depth of LTP's penetration into the plant structure, the nature of its propagation, as well as the size of pores and channels formed in the material. Saengrayap *et al.* found that the drying efficiency is also determined by the time of the material's relaxation after the treatment [38]. In the study on apple slices, LTP promoted the release of intracellular fluid on the surface of the material, with higher moisture transfer during the drying process [39].

Generation of low-temperature plasma and drying efficiency. The effectiveness of low-temperature plasma (LTP) depends on the method of its generation, among other things (Fig. 2). In particular, LTP can be obtained via a dielectric barrier discharge (two oppositely charged plates), an arc discharge, a microplasma jet, a corona discharge, and a microplasma jet supported by thermionic emission [35, 40].

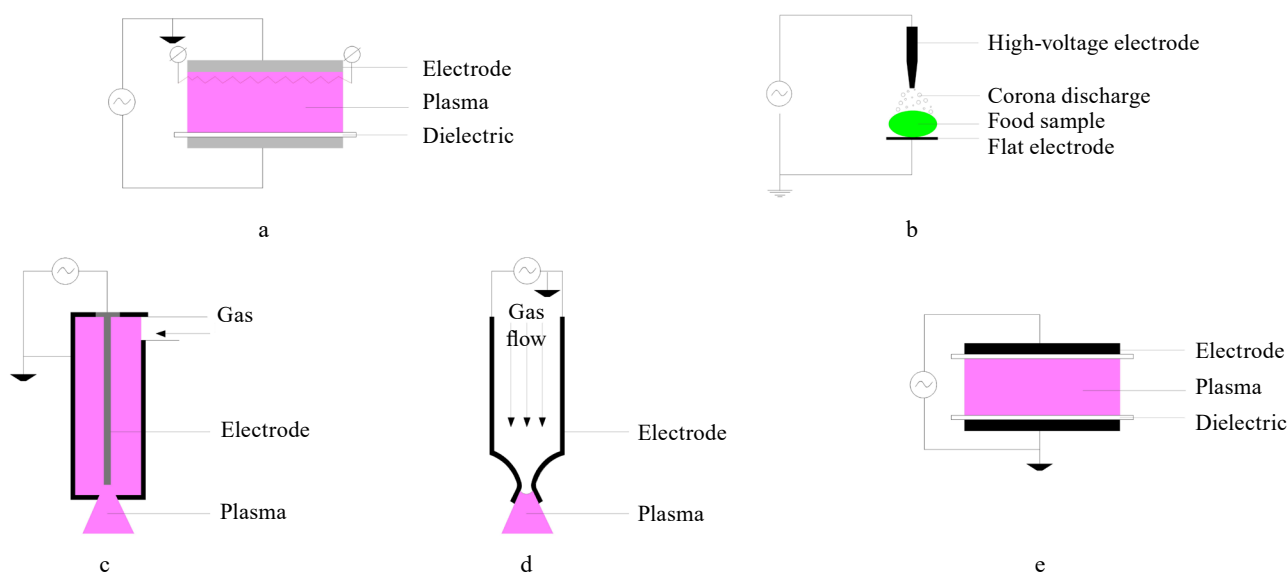


Figure 2 Low-temperature plasma generation schemes: (a) low-temperature plasma supported by thermionic emission; (b) corona discharge; (c) a low-temperature plasma jet with working gas; (d) an arc discharge; and (e) a dielectric barrier discharge

LTP supported by thermionic emission produces a thin string of charged particles that have a directed effect on the object of treatment. Due to thermionic emission, the electric field strength ranges from 6 to 8 kV/cm, in contrast to the range of 15–20 kV/cm for other methods of LTP generation [28]. This method reduces overall energy consumption and provides a better control of the process. The material is hardly heated and the process can be scaled up [28].

With a corona discharge, LTP is generated by using point-plane electrodes set up 3–10 cm apart from each other. Low energy consumption is an obvious advantage of this method. However, the corona discharge does not penetrate into the internal structure of the material, causing only an etching effect on its surface.

A low-temperature plasma jet with pressurized gas supply is the most widely used LTP generation system. The intensity of plasma depends on the generator's power and the flow rate of the gas [41]. Compared to other methods, the plasma jet is more flexible and not limited to a space between the electrodes. Its main disadvantage, however, is a limited impact area and low permeability.

In the dielectric barrier discharge method, the object of treatment is placed between metal electrodes (plane-parallel plates), with at least one of them coated with a dielectric material [42]. To ensure discharge stability, the distance between the two electrodes is limited to a few millimeters, and a high voltage sine wave or switching power supply is required to obtain discharge at atmospheric pressure. The main advantage of this method is that it can be used to treat food materials in dielectric packaging such as polyethylene film. However, given the treatment area of several millimeters, this method can be used mainly for powders.

“Jacob’s Ladder” exemplifies the generation of a traveling arc in the air. When two slightly diverging electrodes are placed vertically and exposed to high-frequency high-voltage power, an arc is first ignited in the narrowest gap between the electrodes and then it slides

along them due to convection [43]. The sliding arc discharge has high energy and gas consumption, with most of the energy used to stimulate chemical reactions rather than heat the gas. Compared to other plasma generating methods, the sliding arc discharge has a larger impact area, which is good for drying [29]. For example, Miraei *et al.* reported that the grapes treated for 50 s at an air flow of 10 L/min had their effective water conductivity at 60°C increased by 30% and their drying time decreased by 26% [29]. However, the devices based on the sliding arc discharge are too complex and sometimes unstable. This disadvantage makes scaling the technology difficult. Yet, this method of generating plasma has high potential in the food industry.

Liu *et al.* showed that treating brown rice with LTP generated by a dielectric barrier discharge had a positive effect on the product’s stability during a short storage period [23]. The treatment maintained the levels of aldehydes and alkanes and increased the content of volatile substances. In another study, LTP pre-treatment (200 and 800 Hz) improved the safety of tucum fruits during storage, causing changes in their tissue structure and improving dehydration [24].

Zhang *et al.* observed no significant changes in the color of red pepper depending on the time of LTP treatment [26]. Yet, the treatment of 30 s improved the recovery of color pigments during further processing. Table 1 summarizes the effects of pre-treating plant materials with LTP on the efficiency of their freeze-drying. As can be seen, most studies aim to assess the energy efficiency of the freeze-drying process with LTP pre-treatment. For example, Miraei *et al.* reported electrically induced pores on the surface of grapes, with no numerical correlations [29].

Industrial application of low-temperature plasma for freeze-drying. Figure 3 shows a tray-type commercial unit for pre-treating raw materials with low-temperature plasma (LTP) created by the Kuban State University of Technology in partnership with manufacturing companies [45].

Table 1 Effects of low-temperature plasma pre-treatment of food materials on the efficiency of their freeze-drying

Material and mode of treatment	Treatment efficiency	References
Honeysuckle Low-temperature plasma jet in the reactor	Drying rate increased by 27%, cell permeability increased by 15%	[21]
Strawberry Low-temperature plasma jet in the reactor (3 kV, 1 MHz)	Enhanced aroma at zero/average pressure	[22]
Brown rice Low-temperature plasma jet (30–100 kV)	Free fatty acids reduced by 25.2%	[23]
Tucum Corona discharge (200, 500, and 800 Hz)	Higher drying and rehydration rates, more phenolic compounds retained at 500 and 800 Hz	[24]
Mushrooms Corona discharge	Higher drying rate, accelerated mass transfer, the largest number of phenolic compounds preserved (463.30 mg/100 g)	[25]
Chili pepper Plasma flow (3 L/min, 20 kHz, 750 W, treatment time: 15, 30, 45, and 60 s)	Higher drying rate; longer treatment may result in pigment loss due to degradation of bioactive compounds	[26]
Plums	Drying time reduced by 5–6 h	[44]



Figure 3 A commercial unit for low-temperature plasma treatment based at Kuban State Technological University



Figure 4 An industrial machine for low-temperature plasma treatment of foods for sterilization [47]: 1 – a discharge chamber, 2 – an electrode unit, 3 – a control panel, 4 – an ozonation chamber, 5 – a belt conveyor

This LTP unit can treat up to 100 kg of raw materials per hour, with their subsequent transfer to the freeze-drier. Recent years have seen a steady rise in the number of patents on the use of LTP in the food industry [46]. For example, Pańka *et al.* presented a pilot machine based on a belt conveyor to treat food products (such as ground spices) with LTP for sterilization [47]. This unit can be easily adapted for treatment prior to freeze-drying (Fig. 4).

Advantages and disadvantages of low-temperature plasma. The main advantages of treating plant materials with low-temperature plasma (LTP) to improve the efficiency of their drying are as follows:

1. LTP treatment reduces the diffusion barrier of the food's shell and produces an etching effect that facilitates subsequent freeze-drying.
2. The product retains high sensory characteristics because LTP treatment reduces the drying time.
3. Various methods of generating LTP to treat materials under atmospheric pressure reduce the cost of processing (no need for vacuum units) and allow for conveyor-type processing with a continuous flow of materials.

However, there are a few downsides to LTP application, namely:

1. LTP equipment used for drying is expensive and unstable. The cost of applying LTP to dry food products

starts from 50 000 US dollars [17]. There is a lack of commercial LTP equipment.

2. Scientists do not have a full understanding of how pre-treating raw materials with LTP affects the properties of the final product. Drying efficiency varies greatly depending on different parameters. Finding the optimal dose of LTP and controlling the pretreatment process are still challenging.

3. LTP has a low penetrating ability. This limits its application to mainly overcoming the surface diffusion barrier.

4. The quality of LTP treatment depends on the surface of the material. If the surface is not homogeneous and has some irregularities or protrusions, some areas may remain untreated.

To introduce LTP treatment into commercial food technologies, we need combined efforts of interdisciplinary scientists, manufacturers, and suppliers of agricultural products. This can also be helped by advanced research and equipment design.

Ultrasonic treatment. Effect of ultrasonic treatment on the structure of plant materials. Ultrasonic treatment is a technology for non-thermal processing of the food matrix that is used in a wide range of processes. Ultrasound propagates due to a series of compression and extension cycles induced by an ultrasonic wave at a frequency from 2×10^4 to 1×10^9 Hz. Cavitation bubbles form when the power of an ultrasonic wave exceeds the power of attraction between the molecules in a medium [48]. When the natural frequency of vibration of the bubbles coincides with the frequency of the ultrasonic wave, the bubbles collapse quickly at the compression stage and release energy with a subsequent increase in pressure (Fig. 5). High pressure from the collapse of the bubbles, which can reach 100 MPa, can rupture the cell membranes and damage the cell microstructure [49, 50]. This process may also cause water molecules to dissociate and free radicals (H^+ and OH^-) to form. These free radicals are capable of reacting with other molecules.

The above effects of ultrasonic treatment can cause a number of physical and chemical effects that can be used to prepare food materials for freeze-drying. Unlike low-temperature plasma (LTP), ultrasonic treatment can affect the size of ice crystals during the freezing stage. This accelerates the freezing rate and, subsequently, reduces the total duration of freeze-drying [50].

Effects of ultrasonic treatment on freeze-drying. Ultrasonic treatment was used to accelerate the freeze-drying of bell pepper in [51]. The authors found that ultrasonic water removal required lower temperatures and shorter time. In particular, ultrasonic treatment lasting 10% of the total freeze-drying time reduced the drying time by 11.5%, ensuring a high-quality product. The findings were based on the bulk density, color characteristics, ascorbic acid content, and rehydration parameters.

In another study, the ultrasonic treatment of strawberry slices decreased their drying time by 15.25–50.00%, compared to the untreated samples [52]. Semenov *et al.* reported that applying mechanical vibrations was as ef-

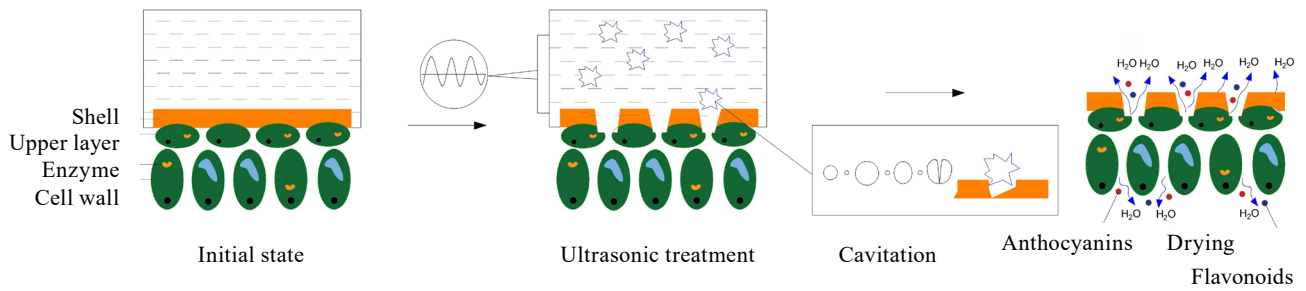


Figure 5 The process of ultrasonic treatment

Table 2 Effects of ultrasonic pre-treatment of food materials on the efficiency of their freeze-drying

Material and mode of treatment	Treatment efficiency	References
Red beetroot 40 kHz, 180 W, 5–10 min	Lower water activity, greater shrinkage of the resulting product	[55]
Barley tops 10, 30, 45, and 60 W/L, 10 min	Energy consumption reduced by 19%	[49]
Pear 20 kHz, 360 and 960 W	Moisture content reduced to 0.12–0.08 g/g dry material	[56]
Bell pepper 76, 90, and 110 W	Total drying time reduced by 11.5%, the product's color preserved	[51]
Hawthorn 37 kHz, 70 W, 20 min	Shorter drying time	[57]
Potato 30 kHz, 200, 400, and 600 W, 30 min	Drying time reduced by 7.2–17.8%, energy consumption reduced by 12–18%, taste and nutritional properties preserved	[58]
Melon 25 kHz, intensity 4870 W/m ²	Overall carotenoid loss reduced, softer texture, and better color retention	[59]
Carrot 25 kHz, 41 W/L, 30–60 min	Drying time reduced due to cell destruction, microchannel formation, and cell swelling	[60]
Apples 400 W/L, 10 min	Internal water diffusion increased by 93%, external mass transfer increased by 10%	[61]
Strawberry 20 and 40 kHz	Drying time reduced by 15.25–50.00%	[52]
Apples 1 kW, 40 kHz, 26–40°C	Minimum moisture (5% by weight), rehydration rate increased by 45%	[62]
Rowan Piezoelectric emitter, 8 kW	Drying time reduced 1.28 times	[63]

efficient as ultrasonic treatment [53]. They also found that ultrasound treatment at 20 and 40 kHz reduced the drying time more greatly than at a single frequency. This most likely indicated the collapse of bubbles of various sizes. Finally, the ultrasonically treated samples had better quality indicators, including vitamin C content, rehydration parameters, density, color, aroma, total anthocyanins and phenols, as well as antioxidant activity.

According to [54], the average rate of freeze-drying was higher for ultrasonically pre-treated apple samples than for the control group. In particular, the pre-treatment at 100 kHz for 5 min at 25°C increased the average drying rate 1.25 times, compared to the control. This might be because ultrasound destroys cell membranes, increasing their permeability to water. As a result, moisture is more easily removed from the cells, accelerating the freeze-drying process.

Table 2 summarizes the effects of ultrasonic pretreatment on the efficiency of freeze-drying of food materials.

To improve the penetration of ultrasonic radiation into the product, the wave resistance needs to be reduced at the medium-product interface. For this purpose, ultrasonic pre-treatment is often carried out in a liquid medium (distilled water or osmotic solution). As a result, the product may lose or gain water during ultrasonic pre-treatment depending on the direction of the concentration gradient at the interface. For example, Oliveira *et al.* found that apples absorbed water from the external medium during their ultrasonic pre-treatment in distilled water and an osmotic solution [64]. When sugar was added, water absorption decreased. This was because sugar increased the resistance to moisture transfer on the surface of the apple. Therefore, the medium parameters are just as important as the frequency, duration, and power of ultrasonic treatment.

Industrial application of ultrasonic treatment for freeze-drying. Continuous-flow ultrasonic treatment is mainly applied to liquid and paste-like materials. Ultra-

sonic treatment is carried out directly in the working chamber or in an ultrasonic bath of a freeze-drying equipment [65, 66].

The industrial application of ultrasonic treatment is described in [67]. The apparatus consists of a stationary ultrasonic bath supplied with all necessary utilities (Fig. 6).

Huang *et al.* combined ultrasonic treatment with the drying process [68]. According to the authors, the formation of a pressure gradient at the gas/liquid phase interface during drying intensified moisture evaporation. As a result, the water went out of the sample without coming back during the positive pressure phase. However, ultrasonic treatment cannot be combined with freeze-drying, since this would require a medium conducting acoustic waves. Vacuum-free freeze-drying can be an alternative to this method [69].

Advantages and disadvantages of ultrasonic treatment. The main advantages of ultrasonic treatment of plant materials are as follows:

1. Ultrasound pre-treatment greatly aids the freeze-drying technology.



Figure 6 An industrial ultrasonic treatment apparatus for food sterilization [67]

2. Ultrasonic waves activate the rate of heat and mass transfer, reducing the drying time.

3. The cost of ultrasound pre-treatment equipment starts from 10 000 US dollars, which is significantly lower than the cost of low-temperature plasma machinery.

However, there are a few downsides to ultrasonic treatment, namely:

1. To reduce wave resistance, ultrasonic treatment should be carried out in a liquid medium. However, this may change the composition of the freeze-dried product since enlarged pores ease the release of the product's target components into the liquid medium, causing their loss.

2. Despite its relatively low cost, ultrasonic treatment is not widely used in the food industry due to several technological challenges. For example, it is important to set the optimal frequency and such medium characteristics as temperature, pH, electrical conductivity, and others. Moreover, the treatment can accidentally destroy the shell of the freeze-dried product, reducing its consumer appeal.

Pulsed electric field treatment. Effects of pulsed electric field on the structure of plant material.

Pulsed electric field (PEF) treatment is an application of short, high-voltage electrical pulses to a liquid or solid product placed between two electrodes in a conductive medium. During this treatment, the cell membrane becomes polarized, which makes the cell wall more permeable. The cell wall can even rupture at certain levels of electric field strength [70]. This mechanism is known as electroporation (Fig. 7). When exposed to an electrical impulse, hydrophilic channels are formed in the lipid bilayer of the cell membrane. Moving along the electric field lines to the membrane boundary, polarized molecules create their internal electrical potential on both sides. The membrane ruptures when the electrical potential reaches a critical level. Thus, this method can enhance mass and heat transfer without causing undesirable changes in the food quality [71]. The electrical conductivity of membranes, as well as pore formation, depends on the critical strength of the electric field (1–2 kV/cm), the size of

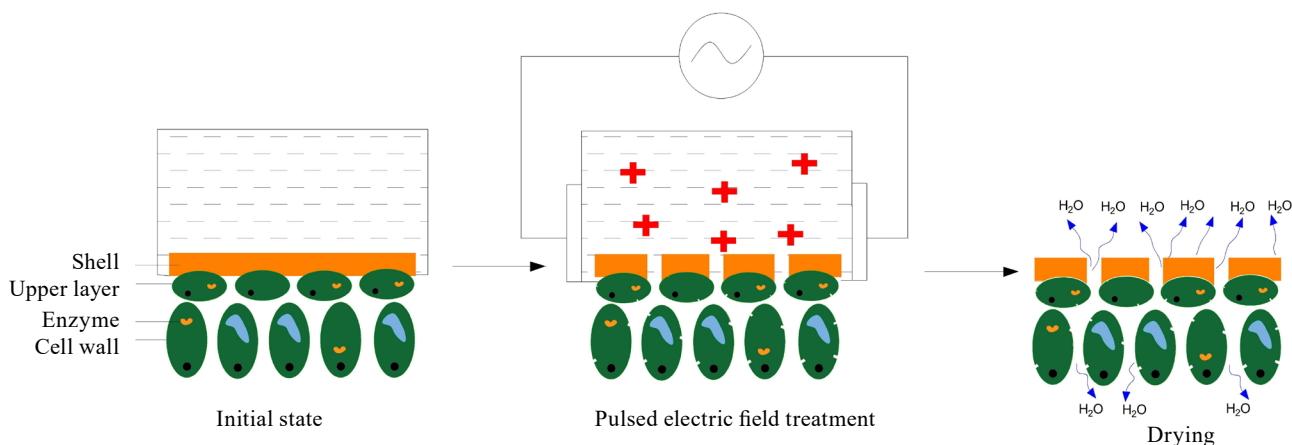


Figure 7 The process of pulsed electric field treatment

a treated cell (40–200 μm), and its electrical characteristics [72]. Electroporation does not occur if the electric field strength and pulse duration are less than critical. Temporary (reversible) pores may form if the electric field strength is close to the critical level, but does not exceed it. In this case, the electrical conductivity of the membranes may change but only temporarily, with a possibility of returning to the original state [73]. This method is used in medicine to introduce target components into the cell. Food scientists, however, are more interested in electroporation caused by the field strength. If the field strength is higher than the critical level, with high specific energy costs, electroporation can become irreversible and the formed electrical pores can cause cell destruction.

The critical levels of electric field strength vary greatly, depending on the material's tissue structure, the size of its cells, and their electrical characteristics [74].

Pulsed electric field treatment for freeze-drying of food products. In a research by Lammerskitten *et al.*, freeze-dried strawberry cubes pre-treated with pulsed electric field (PEF) better retained their shape and volume, as well as had a dense and compact structure [75]. In another study, PEF treatment significantly improved the freeze-drying process due to better mass transfer from the electroporation effect [76]. PEF pre-treatment destroyed the anatomical integrity of cell membranes and accelerated further moisture transfer [77]. Importantly, PEF treatment is performed throughout the material, which promotes further scaling.

Table 3 shows the effects of pre-treating food materials with PEF on the efficiency of freeze-drying. As can be seen, in addition to lower energy consumption due to a shorter drying time, PEF treatment can im-

prove the textural characteristics and quality indicators of the resulting product [76]. The extent of shrinkage during freeze-drying and the preservation of useful target components are important for consumer acceptance. Lammerskitten *et al.* reported that PEF treatment preserved the shape and color of the resulting product and contributed to an even distribution of sugar and moisture inside the material [78]. This had a significant impact on the shock freezing stage, since the channels formed were not clogged with sugar. Witrowa-Rajchert and Lewicki noted an improved reducing ability of plant raw materials after PEF treatment and freeze-drying [79]. This confirms that PEF treatment causes changes in the internal structure of the material.

However, the external product evaluation revealed lower shrinkage of the PEF-treated material. What still needs exploring is the relation between PEF's uniform effect on the internal structure of the material and its shrinkage during freeze-drying. For example, Parniakov *et al.* found that PEF-treated samples retained lower temperature in their core for a longer time, compared to untreated samples [80]. This means that frozen water inside the sample retains its original shape, which impairs further heat and mass transfer processes.

Industrial application of pulsed electric field for freeze-drying. According to Google Scholar, there are over 15 000 publications on pulsed electric field (PEF) treatment and over 55 research groups exploring this technology [85]. However, its industrial application has only become possible recently thanks to the advancement of reliable electronics and high-voltage equipment. In particular, this treatment is mainly used in the production of juices (1500 L/h, PulseMaster, the Nether-

Table 3 Effects of pulsed electric field pre-treatment of food raw materials on the efficiency of freeze-drying

Material and mode of treatment	Treatment efficiency	References
Strawberry Unipolar pulses with an interval of 0.5 s, pulse duration 40 μs ; $E = 1 \text{ kV/cm}$	Preserved shape, color, and taste; more porous structure with evenly distributed pores; greater crunchiness	[75]
Strawberry, bell pepper $E = 1.0 \text{ kV/cm}$; specific energy 0.3–6.0 kJ/kg, treatment time 2.0–28.6 ms	Reduced shrinkage, increased rehydration, improved mass transfer	[76]
Apples $E = 800 \text{ V/cm}$	Drying time reduced, pore size increased to 86 μm , rehydration capacity increased by 1.3 times, shape preserved	[80]
Apples $E = 0.3, 0.6, 0.9, \text{ and } 1.2 \text{ kV/cm}$; 5, 10 or 15 pulses	Changes in the integrity of the cellular structure, reduced content of water suitable for freezing	[81]
Apples $E = 1.07 \text{ kV/cm}$, specific energy 0.5, 1, and 5 kJ/kg	Reduced shrinkage, preserved shape, improved porosity, greater retention of phenols, antioxidant activity reduced by 60%	[78]
Red bell pepper 1 and 3 kJ/kg, $E = 1.07 \text{ kV/cm}$	Drying time reduced by 70 %, appearance preserved	[78]
Apples $E = 1000, 1250, \text{ and } 1500 \text{ V/cm}^{-1}$	Energy consumption reduced by 17.74%, freeze-drying time reduced by 22.50%, productivity per unit area increased by 28.50%	[82]
Potato $E = 0.2\text{--}1.1 \text{ kV/cm}$; pulse duration 20 μs , specific energy 1–10 kJ/kg	Uneven changes in cell viability and microstructure, increased cell rupture at a constant frequency and higher electric field strength	[83]
Potato $E = 600 \text{ V/cm}$; total treatment time $t_{\text{PEF}} = 0.1 \text{ s}$	Drying time reduced by 22–27% at $T_d = 40\text{--}70^\circ\text{C}$, significant changes in the texture and microstructure	[84]

lands), French fries (50 t/h, Elea, Germany), and milk (350 L/h, EnergyPulse) [86].

The application of PEF to plant materials (apples, potatoes, red peppers, etc.) during drying processes started in the early 2000s [75–77]. Since then, its efficiency has been experimentally confirmed by many studies. PEF is industrially applied in Germany, Italy, the USA, and some other countries. High-performance PEF apparatuses have been developed for potato processing and juice production [87]. Figure 8 shows one of such systems for preparing various food materials (such as berries and fruits) for freeze-drying. The apparatus has a belt conveyor passing through a bath with a medium where an electrode unit is installed. PEF pre-treatment significantly reduces undesirable shrinkage of plant materials. This improves the rehydration ability of the freeze-dried product, which is especially important for instant soups or whole berries [80, 88].

Advantages and disadvantages of pulsed electric field treatment. The main advantages of pulsed electric field (PEF) treatment of plant materials are as follows:

1. PEF treatment occurs throughout the material, which is why both whole and sliced products can be treated.
2. The use of cooling systems makes up for increasing product temperatures during PEF treatment.
3. The size of channels formed on the surface of plant cell membranes can be controlled by changing PEF's electrophysical characteristics.

However, PEF has a few downsides and technological challenges, namely:



Figure 8 An industrial pulsed electric field apparatus for pre-treatment of solid materials (Elea, Germany) [89]

1. PEF treatment requires a conductive medium, which is usually a liquid electrolyte.
2. PEF treatment consumes a lot of energy due to the use of high-ampere Marx generators.
3. The use of high voltage and high currents during PEF treatment requires more effective protection of equipment and personnel.
4. The liquid medium used for PEF treatment may erode the metal electrodes, with metal traces entering the final product.

Although the cost of a PEF system starts from 200 000 US dollars (10 t/h), this technology boasts wider commercial application than low-temperature plasma and ultrasonic treatment systems described above. Quite a few companies manufacture PEF systems for industrial use.

Promising areas of research. Industry 4.0, or the fourth industrial revolution, and the emerging Industry 5.0 require that we move away from the traditional thermomechanical processing systems and look for alternative techniques. They include autonomous intelligent systems that make use of advanced robotics and smart technologies at all stages of the food supply chain [90]. In addition, we need to ensure the safety of nutritious food products, low energy consumption, and environmentally clean production.

Introducing advanced electrophysical techniques into the food production chain is a promising area for drying technologies (Fig. 9). This approach involves a synergistic effect which can help produce sufficient amounts of high-quality freeze-dried products.

In this paper, we discussed three innovative physical techniques that can be applied to prepare materials for freeze-drying processes, namely low-temperature plasma, ultrasonic treatment, and pulsed electric field. Before these techniques can be used on a wider scale, we need to address a few technological challenges.

For low-temperature plasma to be introduced widely, we need to:

1. understand how chemically active plasma particles interact with, and affect, individual food components (such as lipids, proteins, carbohydrates, etc.);
2. optimize ways of generating low-temperature plasma in order to reduce overall energy costs; develop atmospheric treatment without the use of vacuum; unify methods for calculating energy indicators; and
3. analyze the effect of low-temperature plasma on the size of pores and channels so that this technique can be used to produce products with a desirable appearance.

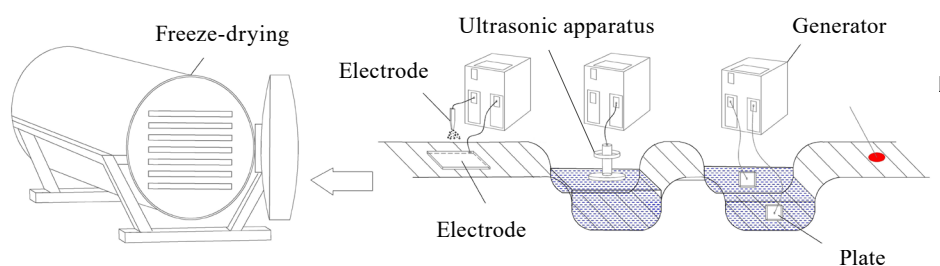


Figure 9 Preparation of food raw materials for freeze-drying within Industry 4.0

To promote ultrasonic pre-treatment, it is important to:

1. establish ranges of ultrasonic frequencies for materials that differ in moisture, size, and composition, as well as for different treatment media;
2. optimize ways of ultrasonic treatment for continuously supplied raw materials; and
3. develop mechanisms to reduce the loss of target components after ultrasonic treatment and further freeze-drying.

For pulsed electric field to be applied more widely, we need to:

1. optimize energy costs in order to increase the efficiency of freeze-drying; determine the effects of pulsed electric field treatment on the freezing stage, where moisture distribution throughout the material is an important factor;
2. reduce the cost of pulsed electric field equipment, as well as search for analogues of the Marx generator for generating high voltage pulses.

CONCLUSION

Vacuum freeze-drying is one of the most effective and one of the most expensive methods of food preservation. Low-temperature plasma, ultrasound, and pulsed electric field are innovative physical techniques that can

be used to pre-treat raw materials before freeze-drying. These techniques can significantly reduce the drying time and enhance the quality of freeze-dried products.

In particular, they can improve heat and mass transfers during the drying process by causing an etching effect and electroporation. They also help preserve the quality characteristics of freeze-dried products. However, pulsed electric field and low-temperature plasma are quite expensive techniques, while ultrasonic treatment needs to be optimized for continuously supplied raw materials.

Freeze-drying is an energy-intensive process, although numerous studies have sought to speed it up while preserving the nutritional and sensory properties of the final products. Therefore, further research is needed to optimize pretreatment conditions for different types of raw materials.

CONTRIBUTION

O.I. Andreeva collected information for the review and designed the graphics. I.A. Shorstkii collected additional information and wrote the manuscript.

CONFLICT OF INTEREST

The authors declare that there is no conflict of interest.

REFERENCES

1. Egorov EA, Kuizheva SK, Lisovaya EV, Viktorova EP. The current state and prospects for the development of food production and food additives in the Russian Federation. *New Technologies*. 2022;18(2):53–61. (In Russ.). <https://doi.org/10.47370/2072-0920-2022-18-2-53-61>; <https://elibrary.ru/UJTLUY>
2. Shorstkii IA. Use of electrophysical methods when processing oil raw materials. *Izvestiya vuzov. Food Technology*. 2019;(4):11–16. (In Russ.). <https://doi.org/10.26297/0579-3009.2019.4.3>; <https://elibrary.ru/PIFPWV>
3. Artyukhova SI, Kozlova OV, Tolstoguzova TT. Developing freeze-dried bioproducts for the Russian military in the Arctic. *Foods and Raw Materials*. 2019;7(1):202–209. <https://doi.org/10.21603/2308-4057-2019-1-202-209>
4. Waghmare R, Kumar M, Yadav R, Mhatre P, Sonawane S, Sharma S, *et al.* Application of ultrasonication as pre-treatment for freeze drying: An innovative approach for the retention of nutraceutical quality in foods. *Food Chemistry*. 2023;404:134571. <https://doi.org/10.1016/j.foodchem.2022.134571>
5. Semenov GV, Krasnova IS. *Freeze-drying*. Moscow: DeLi; 2021. 325 p. (In Russ.).
6. Menon A, Stojceska V, Tassou SA. A systematic review on the recent advances of the energy efficiency improvements in non-conventional food drying technologies. *Trends in Food Science and Technology*. 2020;100:67–76. <https://doi.org/10.1016/j.tifs.2020.03.014>
7. Semenov GV, Bulkin AB, Kuzenkov MS. Modern research trends and technical solutions for the intensification of the process of freeze-drying in the food industry, pharmaceutical production and applied biotechnology (Part 1). *Processes and Food Production Equipment*. 2015;(1):187–202. (In Russ.). <https://elibrary.ru/TIJTMH>
8. Semenov GV, Ermakov SA, Krasnova IS. Vacuum freeze drying of food products: Temperature limits for rational use in industrial production. *Izvestiya vuzov. Food Technology*. 2022;(2–3):51–57. (In Russ.). <https://doi.org/10.26297/0579-3009.2022.2-3.10>; <https://elibrary.ru/BZOIXG>
9. Gorobtsov EI. The development of energy saving technology for the fruit and fruit crop sublimation drying using microwave and ultrasonic radiation. *Bulletin of KSAU*. 2013;(10):235–239. (In Russ.). <https://elibrary.ru/RDCOPD>
10. Belwal T, Cravotto C, Prieto MA, Venskutonis PR, Dagila M, Devkota HP, *et al.* Effects of different drying techniques on the quality and bioactive compounds of plant-based products: A critical review on current trends. *Drying Technology*. 2022;40(8):1539–1561. <https://doi.org/10.1080/07373937.2022.2068028>
11. Antipov ST, Shakhov AS. Modelling of the granular products vacuum freeze-dried process. *Proceedings of the Voronezh State University of Engineering Technologies*. 2016;(3):56–60. (In Russ.). <https://doi.org/10.20914/2310-1202-2016-3-56-60>; <https://elibrary.ru/XWNJWF>

12. Deng L-Z, Pan Z, Mujumdar AS, Zhao J-H, Zheng Z-A, Gao Z-J, *et al.* High-humidity hot air impingement blanching (HHAIB) enhances drying quality of apricots by inactivating the enzymes, reducing drying time and altering cellular structure. *Food Control*. 2019;96:104–111. <https://doi.org/10.1016/j.foodcont.2018.09.008>
13. Yadav AK, Singh SV. Osmotic dehydration of fruits and vegetables: A review. *Journal of Food Science and Technology*. 2014;51:1654–1673. <https://doi.org/10.1007/s13197-012-0659-2>
14. Prosapio V, Norton I. Influence of osmotic dehydration pre-treatment on oven drying and freeze drying performance. *LWT*. 2017;80:401–408. <https://doi.org/10.1016/j.lwt.2017.03.012>
15. Bhatta S, Janezic TS, Ratti C. Freeze-drying of plant-based foods. *Foods*. 2020;9(1):87. <https://doi.org/10.3390/foods9010087>
16. Pan Y, Cheng J-H, Sun D-W. Cold plasma-mediated treatments for shelf life extension of fresh produce: A review of recent research developments. *Comprehensive Reviews in Food Science and Food Safety*. 2019;18(5):1312–1326. <https://doi.org/10.1111/1541-4337.12474>
17. Du Y, Yang F, Yu H, Xie Y, Yao W. Improving food drying performance by cold plasma pretreatment: A systematic review. *Comprehensive Reviews in Food Science and Food Safety*. 2022;21(5):4402–4421. <https://doi.org/10.1111/1541-4337.13027>
18. Tarasov A, Bochkova A, Muzyukin I, Chugunova O, Stozhko N. The effect of pre-treatment of arabica coffee beans with cold atmospheric plasma, microwave radiation, slow and fast freezing on antioxidant activity of aqueous coffee extract. *Applied Sciences*. 2022;12(12):5780. <https://doi.org/10.3390/app12125780>
19. Shorstkii I, Mounassar EHA. Atmospheric microplasma treatment based on magnetically controlled Fe–Al dynamic platform for organic and biomaterials surface modification. *Coatings*. 2023;13(8):1362. <https://doi.org/10.3390/coatings13081362>
20. Vasilyev MM, Naumov EV, Petrov OF, Gladysheva OV, Gureeva EV, Ushakova EYu, *et al.* The increase of cereal crops resistance to frost, low temperature and moisture deficit after low-temperature plasma treatment of the seeds. *Agrochemistry and Ecology Problems*. 2016;(2):26–33. (In Russ.). <https://elibrary.ru/WICCCZZ>
21. Li J, Zhou Y, Lu W. Enhancement of haskap vacuum freeze-drying efficiency and quality attributes using cold plasma pretreatment. *Food and Bioprocess Technology*. 2023;17:1059–1071. <https://doi.org/10.1007/s11947-023-03186-y>
22. Warne GR, Lim M, Wilkinson K, Hessel V, Williams PM, Coad B, *et al.* Radiofrequency cold plasma – A novel tool for flavour modification in fresh and freeze-dried strawberries. *Innovative Food Science and Emerging Technologies*. 2023;90:103497. <https://doi.org/10.1016/j.ifset.2023.103497>
23. Liu Q, Wu H, Luo J, Liu J, Zhao S, Hu Q, *et al.* Effect of dielectric barrier discharge cold plasma treatments on flavor fingerprints of brown rice. *Food Chemistry*. 2021;352:129402. <https://doi.org/10.1016/j.foodchem.2021.129402>
24. Loureiro AC, Souza FCA, Sanches EA, Bezerra JA, Lamarão CV, Rodrigues S, *et al.* Cold plasma technique as a pretreatment for drying fruits: Evaluation of the excitation frequency on drying process and bioactive compounds. *Food Research International*. 2021;147:110462. <https://doi.org/10.1016/j.foodres.2021.110462>
25. Shishir MRI, Karim N, Bao T, Gowd V, Ding T, Sun C, *et al.* Cold plasma pretreatment – A novel approach to improve the hot air drying characteristics, kinetic parameters, and nutritional attributes of shiitake mushroom. *Drying Technology*. 2020;38(16):2134–2150. <https://doi.org/10.1080/07373937.2019.1683860>
26. Zhang X-L, Zhong C-S, Mujumdar AS, Yang X-H, Deng L-Z, Wang J, *et al.* Cold plasma pretreatment enhances drying kinetics and quality attributes of chili pepper (*Capsicum annuum* L.). *Journal of Food Engineering*. 2019;241:51–57. <https://doi.org/10.1016/j.jfoodeng.2018.08.002>
27. Du Y, Yang F, Yu H, Xie Y, Yoa W. Improving food drying performance by cold plasma pretreatment: A systematic review. *Comprehensive Reviews in Food Science and Food Safety*. 2022;(5). <https://doi.org/10.1111/1541-4337.13027>
28. Sosnin MD, Shorstkii IA. Cold atmospheric gas plasma processing of apple slices. *Food Processing: Techniques and Technology*. 2023;53(2):368–383. (In Russ.). <https://doi.org/10.21603/2074-9414-2023-2-2442>; <https://elibrary.ru/WPBYMS>
29. Miraei Ashtiani S-H, Rafiee M, Mohebi Morad M, Khojastehpour M, Khani MR, Rohani A, *et al.* Impact of gliding arc plasma pretreatment on drying efficiency and physicochemical properties of grape. *Innovative Food Science and Emerging Technologies*. 2020;63:102381. <https://doi.org/10.1016/j.ifset.2020.102381>
30. Shorstkii IA, Mounassar EH. Effect of low current cold atmospheric plasma on grains surface structure and water absorption capacity. *Proceedings of the Voronezh State University of Engineering Technologies*. 2023;85(2):23–31. (In Russ.). <https://doi.org/10.20914/2310-1202-2023-2-23-31>; <https://elibrary.ru/QOSXAQ>
31. Dharini M, Jaspin S, Mahendran R. Cold plasma reactive species: Generation, properties, and interaction with food biomolecules. *Food Chemistry*. 2023;405:134746. <https://doi.org/10.1016/j.foodchem.2022.134746>


32. Khudyakov DA, Shorstkii IA, Ulyanenko EE, Gnuchykh EV. Influences of cold atmospheric plasma pretreatment on drying kinetics, structural, fractional and chemical characteristics of tobacco leaves. *Drying Technology*. 2022;40(15):3285–3291. <https://doi.org/10.1080/07373937.2021.2021230>
33. Ahmadian S, Esmailzadeh Kenari R, Raftani Amiri Z, Sohbatzadeh F, Haddad Khodaparast MH. Effect of ultrasound-assisted cold plasma pretreatment on cell wall polysaccharides distribution and extraction of phenolic compounds from hyssop (*Hyssopus officinalis* L.). *International Journal of Biological Macromolecules*. 2023;233:123557. <https://doi.org/10.1016/j.ijbiomac.2023.123557>
34. Huang C-C, Wu JS-B, Wu J-S, Ting Y. Effect of novel atmospheric-pressure jet pretreatment on the drying kinetics and quality of white grapes. *Journal of The Science of Food and Agriculture*. 2019;99:5102–5111. <https://doi.org/10.1002/jsfa.9754>
35. Campêlo RA, Casanova MA, Guedes DO, Laender AHF. A brief survey on replica consistency in cloud environments. *Journal of Internet Services and Applications*. 2020;11:1.
36. Zhou Y-H, Vidyarthi SK, Zhong C-S, Zheng Z-A, An Y, Wang J, et al. Cold plasma enhances drying and color, rehydration ratio and polyphenols of wolfberry via microstructure and ultrastructure alteration. *LWT*. 2020;134:110173. <https://doi.org/10.1016/j.lwt.2020.110173>
37. Cao Y, Hua H, Yang P, Chen M, Chen W, Wang S, et al. Investigation into the reaction mechanism underlying the atmospheric low-temperature plasma-induced oxidation of cellulose. *Carbohydrate Polymers*. 2020;233:115632. <https://doi.org/10.1016/j.carbpol.2019.115632>
38. Saengrayap R, Tansakul A, Mittal GS. Effect of far-infrared radiation assisted microwave-vacuum drying on drying characteristics and quality of red chilli. *Journal of Food Science and Technology*. 2015;52:2610–2621. <https://doi.org/10.1007/s13197-014-1352-4>
39. Sosnin MD, Shorstky IA. Evaluation of hydrodynamic flows of cellular fluid in artificially formed continuums of plant material structure. *New Technologies*. 2023;19(2):72–82. (In Russ.). <https://doi.org/10.47370/2072-0920-2023-19-2-72-82>; <https://elibrary.ru/WOXLIV>
40. Khudyakov D, Sosnin M, Shorstkii I, Okpala COR. Cold filamentary microplasma pretreatment combined with infrared dryer: Effects on drying efficiency and quality attributes of apple slices. *Journal of Food Engineering*. 2022;329:111049. <https://doi.org/10.1016/j.jfoodeng.2022.111049>
41. Chen Y-Q, Cheng J-H, Sun D-W. Chemical, physical and physiological quality attributes of fruit and vegetables induced by cold plasma treatment: Mechanisms and application advances. *Critical Reviews in Food Science and Nutrition*. 2020;60(16):2676–2690. <https://doi.org/10.1080/10408398.2019.1654429>
42. Klockow PA, Keener KM. Safety and quality assessment of packaged spinach treated with a novel ozone-generation system. *LWT – Food Science and Technology*. 2009;42(6):1047–1053. <https://doi.org/10.1016/j.lwt.2009.02.011>
43. Almazova KI, Belonogov AN, Borovkov VV, Gorelov EV, Dubinov AE, Morozov IV, et al. dynamics of gliding arc climbing in a unipolar Jacob’s ladder. *Technical Physics*. 2020;90(7):1076–1079. (In Russ.). <https://doi.org/10.21883/JTF.2020.07.49439.408-19>; <https://elibrary.ru/GRLTGZ>
44. Meliboyev M, Mamatov S, Ergashev O, Eshonturaev A. Improving of the process freeze drying of plums. In: Khasanov SZ, Muratov A, Ignateva S, editors. *Fundamental and applied scientific research in the development of Agriculture in the Far East (AFE-2022)*. Agricultural cyber-physical systems, Volume 2. Cham: Springer; 2023. pp. 173–179. https://doi.org/10.1007/978-3-031-36960-5_21
45. Equipment for the preparation of food raw materials [Internet]. [cited 2023 Dec 10]. Available from: <https://tehplasma.ru>
46. Hernández-Torres CJ, Reyes-Acosta YK, Chávez-González ML, Dávila-Medina MD, Verma DK, Martínez-Hernández JL, et al. Recent trends and technological development in plasma as an emerging and promising technology for food biosystems. *Saudi Journal of Biological Sciences*. 2022;29(4):1957–1980. <https://doi.org/10.1016/j.sjbs.2021.12.023>
47. Pańka D, Jeske M, Łukanowski A, Batur-Cieśniewska A, Prus P, Maitah M, et al. Can cold plasma be used for boosting plant growth and plant protection in sustainable plant production? *Agronomy*. 2022;12(4):841. <https://doi.org/10.3390/agronomy12040841>
48. Mokhova E, Gordienko M, Menshutina N, Gurskiy I, Tvorogova A. Ultrasonic freezing of polymers of various compositions before freeze drying: Effect of ultrasound on freezing kinetics and ice crystal size. *Drying Technology*. 2023;41(10):1663–1685. <https://doi.org/10.1080/07373937.2023.2173226>
49. Cao X, Zhang M, Mujumdar AS, Zhong Q, Wang Z. Effects of ultrasonic pretreatments on quality, energy consumption and sterilization of barley grass in freeze drying. *Ultrasonics Sonochemistry*. 2018;40:333–340. <https://doi.org/10.1016/j.ultsonch.2017.06.014>
50. Cheng X, Zhang M, Xu B, Adhikari B, Sun J. The principles of ultrasound and its application in freezing related processes of food materials: A review. *Ultrasonics Sonochemistry*. 2015;27:576–585. <http://dx.doi.org/10.1016/j.ultsonch.2015.04.015>

51. Schössler K, Jäger H, Knorr D. Novel contact ultrasound system for the accelerated freeze-drying of vegetables. *Innovative Food Science and Emerging Technologies*. 2012;16:113–120. <https://doi.org/10.1016/j.ifset.2012.05.010>
52. Xu B, Chen J, Sylvain Tiliwa E, Yan W, Roknul Azam SM, Yuan J, et al. Effect of multi-mode dual-frequency ultrasound pretreatment on the vacuum freeze-drying process and quality attributes of the strawberry slices. *Ultrasonics Sonochemistry*. 2021;78:105714. <https://doi.org/10.1016/j.ultsonch.2021.105714>
53. Semenov GV, Krasnova IS, Khvyliia SI, Balabolin DN. Freezing and freeze-drying of strawberries with an additional effect of micro-vibrations. *Journal of Food Science and Technology*. 2021;58:3192–3198. <https://doi.org/10.1007/s13197-020-04822-7>
54. Ren Z, Bai Y. Ultrasound pretreatment of apple slice prior to vacuum freeze drying. *Advances in Engineering Research*. 2018;169:112–117. <https://doi.org/10.2991/mseee-18.2018.20>
55. Ciurzyńska A, Falacińska J, Kowalska H, Kowalska J, Galus S, Marzec A, et al. The effect of pre-treatment (Blanching, ultrasound and freezing) on quality of freeze-dried red beets. *Foods*. 2021;10(1):132. <https://doi.org/10.3390/foods10010132>
56. Islam MN, Zhang M, Liu H, Xinfeng C. Effects of ultrasound on glass transition temperature of freeze-dried pear (*Pyrus pyrifolia*) using DMA thermal analysis. *Food and Bioproducts Processing*. 2015;94:229–238. <https://doi.org/10.1016/j.fbp.2014.02.004>
57. Ergün AR. The effects of electric field and ultrasound pretreatments on the drying time and physicochemical characteristics of the zucchini chips. *Annals of the Brazilian Academy of Sciences*. 2022;94(3):e20210349. <https://doi.org/10.1590/0001-376520220210349>
58. Wu X, Zhang M, Ye Y, Yu D. Influence of ultrasonic pretreatments on drying kinetics and quality attributes of sweet potato slices in infrared freeze drying (IRFD). *LWT*. 2020;131:109801. <https://doi.org/10.1016/j.lwt.2020.109801>
59. Dias da Silva G, Barros ZMP, de Medeiros RAB, de Carvalho CBO, Rupert Brandão SC, Azoubel PM. Pretreatments for melon drying implementing ultrasound and vacuum. *LWT*. 2016;74:114–119. <https://doi.org/10.1016/j.lwt.2016.07.039>
60. Ricce C, Rojas ML, Miano AC, Siche R, Augusto PED. Ultrasound pre-treatment enhances the carrot drying and rehydration. *Food Research International*. 2016;89:701–708. <https://doi.org/10.1016/j.foodres.2016.09.030>
61. Magalhães ML, Cartaxo SJM, Gallão MI, García-Pérez JV, Cárcel JA, Rodrigues S, et al. Drying intensification combining ultrasound pre-treatment and ultrasound-assisted air drying. *Journal of Food Engineering*. 2017;215:72–77. <https://doi.org/10.1016/j.jfoodeng.2017.07.027>
62. Kahraman O, Malvandi A, Vargas L, Feng H. Drying characteristics and quality attributes of apple slices dried by a non-thermal ultrasonic contact drying method. *Ultrasonics Sonochemistry*. 2021;73:105510. <https://doi.org/10.1016/j.ultsonch.2021.105510>
63. Anisimova KV, Porobova OB, Anisimov AB. Intensification of non-vacuum sublimation drying of fruit by sound field. *Bulletin of Altai State Agricultural University*. 2013;(2):103–106. (In Russ.). <https://elibrary.ru/PWPVND>
64. Oliveira FIP, Gallão MR, Rodrigues S, Fernandes FAN. Dehydration of malay apple (*Syzygium malaccense* L.) using ultrasound as pre-treatment. *Food and Bioprocess Technology*. 2010;4:610–615. <https://doi.org/10.1007/s11947-010-0351-3>
65. Kasatkin VV, Shumilova ISh. Continuous drying equipment for thermolabile materials. *Food Industry*. 2006;(10):12–13. (In Russ.). <https://elibrary.ru/TLOYSX>
66. Alvarez C, Ospina Corral S, Orrego C. Effects of ultrasound-assisted blanching on the processing and quality parameters of freeze-dried guava slices. *Journal of Food Processing and Preservation*. 2019;43. <https://doi.org/10.1111/jfpp.14288>
67. Chemat F, Zill-E-Huma, Khan MK. Applications of ultrasound in food technology: Processing, preservation and extraction. *Ultrasonics Sonochemistry*. 2011;18(4):813–835. <https://doi.org/10.1016/j.ultsonch.2010.11.023>
68. Huang D, Men K, Li D, Wen T, Gong Z, Sunden B, et al. Application of ultrasound technology in the drying of food products. *Ultrasonics Sonochemistry*. 2020;63:104950. <https://doi.org/10.1016/j.ultsonch.2019.104950>
69. Anisimova KV, Porobova OB, Anisimov AB. Intensification of non-vacuum sublimation drying of fruit by sound field. *Bulletin of Altai State Agricultural University*. 2013;(2):103–106. (In Russ.). <https://elibrary.ru/PWPVND>
70. Zhang C, Lyu X, Arshad RN, Aadil RM, Tong Y, Zhao W, et al. Pulsed electric field as a promising technology for solid foods processing: A review. *Food Chemistry*. 2023;403:134367. <https://doi.org/10.1016/j.foodchem.2022.134367>
71. Gudmundsson M, Hafsteinsson H. Effect of high-intensity electric field pulses on solid foods. In: Sun D-W, editor. *Emerging technologies for food processing*. Academic Press; 2014. pp. 147–153. <https://doi.org/10.1016/B978-012676757-5/50008-6>
72. Demir E, Tappi S, Dymek K, Rocculi P, Gómez GF. Reversible electroporation caused by pulsed electric field – Opportunities and challenges for the food sector. *Trends in Food Science and Technology*. 2023;139:104120. <https://doi.org/10.1016/j.tifs.2023.104120>

73. Genovese J, Kranjc M, Serša I, Petracci M, Rocculi P, Miklavčič D, *et al.* PEF-treated plant and animal tissues: Insights by approaching with different electroporation assessment methods. *Innovative Food Science and Emerging Technologies*. 2021;74:102872. <https://doi.org/10.1016/j.ifset.2021.102872>
74. Raso J, Heinz V, Alvarez I, Toepfl S. Pulsed electric fields technology for the food industry. Fundamentals and applications. Cham: Springer; 2022. 561 p. <https://doi.org/10.1007/978-3-030-70586-2>
75. Lammerskitten A, Wiktor A, Mykhailik V, Samborska K, Gondek E, Witrowa-Rajchert D, *et al.* Pulsed electric field pre-treatment improves microstructure and crunchiness of freeze-dried plant materials: Case of strawberry. *LWT*. 2020;134:110266. <https://doi.org/10.1016/j.lwt.2020.110266>
76. Fauster T, Giancaterino M, Pittia P, Jaeger H. Effect of pulsed electric field pretreatment on shrinkage, rehydration capacity and texture of freeze-dried plant materials. *LWT*. 2020;121:108937. <https://doi.org/10.1016/j.lwt.2019.108937>
77. Donsi F, Ferrari G, Maresca P, Pataro G. Effects of emerging technologies on food quality. In: Medina DA, Laine AM, editors. *Food quality: Control, analysis and consumer concerns*. Hauppauge: Nova Science Publishers; 2011. pp. 505–554.
78. Lammerskitten A, Wiktor A, Siemer C, Toepfl S, Mykhailik V, Gondek E, *et al.* The effects of pulsed electric fields on the quality parameters of freeze-dried apples. *Journal of Food Engineering*. 2019;252:36–43. <https://doi.org/10.1016/j.jfoodeng.2019.02.006>
79. Witrowa-Rajchert D, Lewicki PP. Rehydration properties of dried plant tissues. *International Journal of Food Science and Technology*. 2006;41(9):1040–1046. <https://doi.org/10.1111/j.1365-2621.2006.01164.x>
80. Parniakov O, Bals O, Lebovka N, Vorobiev E. Pulsed electric field assisted vacuum freeze-drying of apple tissue. *Innovative Food Science and Emerging Technologies*. 2016;35:52–57. <https://doi.org/10.1016/j.ifset.2016.04.002>
81. Tylewicz U, Aganovic K, Vannini M, Toepfl S, Bortolotti V, Dalla Rosa M, *et al.* Effect of pulsed electric field treatment on water distribution of freeze-dried apple tissue evaluated with DSC and TD-NMR techniques. *Innovative Food Science and Emerging Technologies*. 2016;37:352–358. <https://doi.org/10.1016/j.ifset.2016.06.012>
82. Wu Y, Guo Y. Experimental study of the parameters of high pulsed electrical field pretreatment to fruits and vegetables in vacuum freeze-drying. In: Li D, Liu Y, Chen Y, *et al.* *Computer and computing technologies in agriculture IV*. Heidelberg: Springer Berlin; 2011. pp. 691–697. https://doi.org/10.1007/978-3-642-18333-1_83
83. Faridnia F, Burritt DJ, Bremer PJ, Oey I. Innovative approach to determine the effect of pulsed electric fields on the microstructure of whole potato tubers: Use of cell viability, microscopic images and ionic leakage measurements. *Food Research International*. 2015;77:556–564. <https://doi.org/10.1016/j.foodres.2015.08.028>
84. Liu C, Grimi N, Lebovka N, Vorobiev E. Effects of pulsed electric fields treatment on vacuum drying of potato tissue. *LWT*. 2018;95:289–294. <https://doi.org/10.1016/j.lwt.2018.04.090>
85. Toepfl S, Heinz V, Knorr D. High intensity pulsed electric fields applied for food preservation. *Chemical Engineering and Processing: Process Intensification*. 2007;46(6):537–546. <https://doi.org/10.1016/j.cep.2006.07.011>
86. Toepfl S, Siemer C, Saldaña-Navarro G, Heinz V. Overview of pulsed electric fields processing for food. In: Sun D-W, editor. *Emerging technologies for food processing*. Academic Press; 2014. pp. 93–114. <https://doi.org/10.1016/B978-0-12-411479-1.00006-1>
87. Moens LG, van Wambeke J, de Laet E, van Ceunebroeck J-C, Goos P, van Loey AM, *et al.* Effect of postharvest storage on potato (*Solanum tuberosum* L.) texture after pulsed electric field and thermal treatments. *Innovative Food Science and Emerging Technologies*. 2021;74:102826. <https://doi.org/10.1016/j.ifset.2021.102826>
88. Jalté M, Lanoisellé J-L, Lebovka NI, Vorobiev E. Freezing of potato tissue pre-treated by pulsed electric fields. *LWT – Food Science and Technology*. 2009;42(2):576–580. <https://doi.org/10.1016/j.lwt.2008.09.007>
89. Using pulsed electric field (PEF) in potato production [Internet]. [cited 2023 Dec 10]. Available from: <https://potatosystem.ru/ispolzovanie-impulsnogo-elektricheskogo>
90. Hassoun A, Jagtap S, Trollman H, Garcia-Garcia G, Abdullah NA, Goksen G, *et al.* Food processing 4.0: Current and future developments spurred by the fourth industrial revolution. *Food Control*. 2023;145:109507. <https://doi.org/10.1016/j.foodcont.2022.109507>

ORCID IDs

Oksana I. Andreeva  <https://orcid.org/0009-0008-4265-9651>

Ivan A. Shorstkii  <https://orcid.org/0000-0001-5804-7950>



Extraction methods: Effects on the contents of bioactive compounds and anti-oxidant activity of *Coriolopsis aspera* mycelia

Le Minh Thu^{ID}, Nguyen Ngoc Thuan^{ID}, Luu Thao Nguyen^{ID}, Dam Sao Mai^{ID}, Do Viet Phuong^{*ID}

Industrial University of Ho Chi Minh City^{ROR}, Ho Chi Minh, Vietnam

* e-mail: dovietphuong@iuh.edu.vn

Received 24.11.2023; Revised 18.01.2024; Accepted 06.02.2024; Published online 02.11.2024

Abstract:

Coriolopsis aspera has been known as a medicinal mushroom commonly used in Vietnam, China, and certain regions in South Asia. It has many health-beneficial effects, namely anti-inflammatory, anti-cancerous, and anti-antioxidant. Despite these advantages, the rigid and durable cell walls of *C. aspera* pose challenges during chemical or mechanical extraction processes. We aimed to identify the optimal method for extracting bioactive compounds from *C. aspera* among hot-water extraction, ultrasound-assisted extraction, microwave-assisted extraction, ultrasound-assisted alkali extraction, and ultrasound-assisted liquid nitrogen extraction.

Among these methods, a combination of liquid nitrogen treatment (with a material-to-nitrogen ratio of 1:6) and ultrasound-assisted extraction (15 min) proved to be the most effective. This method yielded the highest concentrations of polyphenols (4.69 ± 0.02 mg GAE/g dry weight), flavonoids (0.88 ± 0.01 mg QE/g dry weight), and triterpenoids (1.28 ± 0.01 mg OAE/g dry weight). Additionally, it exhibited a notable antioxidant activity of 3.48 ± 0.01 μ g ascorbic acid/g dry weight. The scanning electron microscope images indicated that ultrasound-assisted liquid nitrogen extraction was the only method able to effectively disrupt the cell walls of *C. aspera*.

Our study contributes to the potential application of *C. aspera* in developing functional foods. It emphasizes the importance of effective extraction techniques in discovering medicinal properties of the mushroom.

Keywords: Anti-oxidant activity, *Coriolopsis aspera*, flavonoids, mycelia, triterpenoids, ultrasound-assisted extraction

Please cite this article in press as: Thu LM, Thuan NN, Nguyen LT, Mai DS, Phuong DV. Extraction methods: Effects on the contents of bioactive compounds and anti-oxidant activity of *Coriolopsis aspera* mycelia. Foods and Raw Materials. 2025; 13(2):355–365. <https://doi.org/10.21603/2308-4057-2025-2-642>

INTRODUCTION

Fungal species on earth have been estimated to number around 140 000 to 160 000. However, only 10% of them have been identified, and only about 2000 species are considered safe for humans as edible or medicinal mushrooms [1, 2]. For example, *Coriolopsis aspera*, a member of the *Polyporaceae* family, is a medicinal mushroom commonly used in Vietnam, China, and some regions in South Asia. It has been reported to exhibit health-promoting effects, including anti-inflammatory, anti-oxidant, and anti-cancerous activities [3]. Several other strains belonging to the *Polyporaceae* family are also used to treat diabetes, oxidative stress-related diseases, or bacterial infections. They include *Coriolopsis rigida*, *Coriolopsis gallica*, and *Coriolopsis polyzona* [4–6]. These fungi are a promising source of valuable compounds, such as anti-oxidant (polyphenols, flavonoids),

immuno-chemotherapy (polysaccharide Krestin, lentinan, and schizophyllan), as well as anti-inflammatory and anti-cancerous (triterpene) compounds [7, 8].

Fungal cell walls possess complex components and textures. They mainly contain chitins, glucans, and some proteins, including hydrophobins and mannoproteins [9]. For instance, the cell wall of *Agaricus bisporus*, a common edible mushroom, is composed of 12.0–14.3% of protein, 33.0–37.0% polysaccharides, and 15.8–17.4% chitin [10]. Furthermore, the cell walls of *Ganoderma resinaceum*, a medicinal mushroom, possess manogalactan, β -D-glucans, (1 \rightarrow 3)- α -D-glucan, (1 \rightarrow 3)- β -D-glucan, chitin, and β -D-glucan complex, O-2- β -D-mannosyl-(1 \rightarrow 6)- α -D-galactan and (1 \rightarrow 3)(1 \rightarrow 4)(1 \rightarrow 6)- β -D-glucan [11]. These components and their arrangement in fungal cell walls provide the cell shape and rigidity. In addition, they protect fungal cells from chemical or mechanical destruction, which in turn lowers the

extraction yield of bioactive compounds in medicinal mushrooms. Aside from the traditional hot-water extraction, some new extraction techniques have been developed recently to break down fungal cell walls and enhance the efficiency of extracting active ingredients from plant and fungal materials. They include chemical treatments (enzymatic hydrolysis, acid hydrolysis, ethanol-acid treatment, and alkaline extraction) and mechanical methods (high-speed centrifugal shearing pulverization, ultrasound-assisted extraction, microwave-assisted extraction, and cavitation-based extraction) [12–14]. The ultrasound- and microwave-assisted extractions have been reported to increase the extraction yield of bioactive compounds. They were also considered as green technologies with many advantages, such as a shorter extraction time, as well as solvent and energy saving [15]. Sun *et al.* used a method of pulverizing plant materials with liquid nitrogen that punctured the fibers of *Astragalus mongholicus*, thus improving the extraction yield of bioactive compounds [16]. In another study, Liang *et al.* revealed that pulverization with liquid nitrogen significantly changed the physical properties of the raw material, benefiting the extraction of bioactive substances in *Astragalus mongholicus* [17].

Although there has been extensive research into the bioactivities of *C. aspera*, an optimal method of extracting bioactive components from this species has not been found so far. Therefore, we aimed to study a range of methods (hot-water extraction, ultrasound- and microwave-assisted extraction, NaOH treatment coupled with ultrasound-assisted extraction, and liquid nitrogen treat-

ment coupled with ultrasound-assisted extraction) to select an optimal method for extracting bioactive compounds (polyphenol, flavonoids, and triterpenoids) from *C. aspera* to ensure its antioxidant activity.

STUDY OBJECTS AND METHODS

Chemicals and reagents. Most chemicals and reagents, such as the Folin-Ciocalteu reagent, gallic acid, oleanolic acid, ascorbic acid, quercetin, and 2,2-Diphenylpicrylhydrazyl (DPPH) were purchased from Sigma Aldrich (Sigma Chemicals Co., St. Louis, MO, USA), while others were obtained commercially and were of analytical grade.

Fungal materials. Fresh mycelia of *Coriolopsis aspera* were obtained from the Experimental Garden, Institute of Biotechnology and Food Technology, Industrial University of Ho Chi Minh City (Fig. 1). The specimens were dried at 45°C in the oven to less than 6% moisture prior to being ground into a fine powder using a hammer mill. The powder was then sifted through a 20-mesh sieve and distributed into polyethylene bags, with 2 g of powder per bag. The samples were stored at 4°C in a refrigerator for further analysis.

Ultrasound equipment (Fig. 2). Product type: ultrasonic processor. Model: GE 750. Power: 750 W. Freq: 20 kHz. Min Sample Size (mL): 0.25. Max Sample Size (mL): 1900. Amplitude: 0–100%.

Ultrasound-assisted extraction (USE). Single factor experimental designs were employed to investigate the effects of ultrasonic power and extraction time on

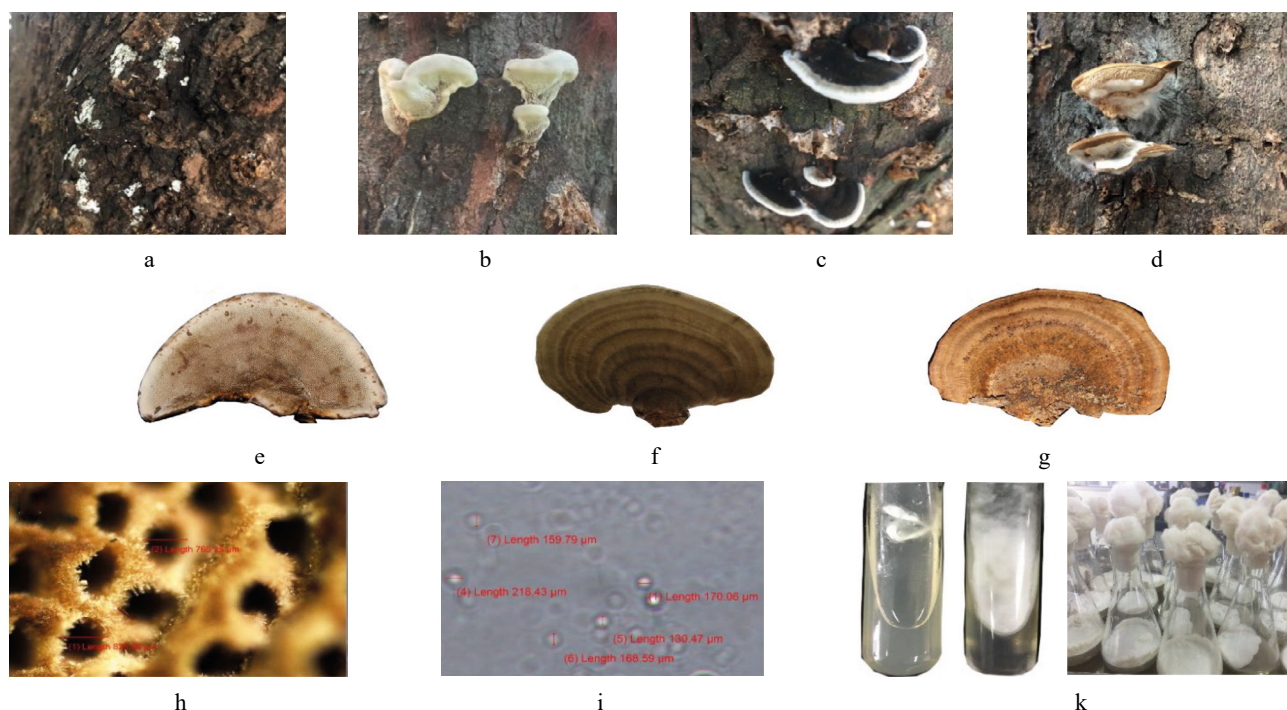


Figure 1 Natural samples of *Coriolopsis aspera* on wood and its laboratory-cultivated samples. Mycelia (a) and immature fruiting bodies after 3 days (b), 7 days (c), and 10 days (d). Lower (e) and upper (f) surface of a fruiting body after 15–18 days. The mature fruiting body (g) and microscopic images of pores in lower surface (h) and spores (i). Laboratory-cultivated *Coriolopsis aspera* strains and mycelia (k)



Figure 2 Ultrasonic processor equipment GE 750

the extraction yield of bioactive compounds. In particular, we determined the effect of different ultrasonic power levels on the contents of polyphenols (TPC), flavonoids (TFC), triterpenoids (TTC), and antioxidant activity (radical scavenging activity, RSA) of the extracts. For this, a *C. aspera* sample, with a material-to-water ratio of 1:60 (w/v), was treated with a range of ultrasonic power levels (150–525 W, equivalent to an amplitude range of 20–70% at 20 kHz) for 25 min at 30°C to break down the cell walls. Following this, an extract was collected through centrifugation at 6000 rpm. The solid residue of the sample was then dried until 6% moisture was reached. Upon drying out, the sample was extracted twice with 96% ethanol for 30 min each time. All fractioned extracts were combined to obtain the final extract. The effect of extraction time on the contents of polyphenols, flavonoids, triterpenoids, and antioxidant activity of the extracts was determined using the same procedure with minor modifications. In particular, the extraction time ranged from 5 to 35 min, while the constant ultrasonic power was obtained from the above experiment. The control sample was treated with the same procedure without ultrasound-assisted extraction. The M1 (USE-treated) sample was considered an optimal sample since it possessed the highest values of TPC, TFC, TTC, and RSA.

Microwave-assisted extraction (MAE). Single factor experimental designs were employed to clarify the effect of microwave energy and extraction time on the extraction yield of bioactive compounds. In particular, we determined the effect of different microwave power levels on the contents of polyphenols (TPC), flavonoids (TFC), triterpenoids (TTC), and antioxidant activity (radical scavenging activity, RSA) of the extracts. For this, a *C. aspera* sample, with a material-to-water ratio of 1:60 (w/v) set as constant, was treated with a range of microwave power levels (110–140 W) for 10 min. Following this, an extract was collected through centrifugation at 6000 rpm. The solid residue of the samples was then dried until 6% moisture was reached. Upon drying out, the sample was extracted twice with 96% ethanol for 30 min each time. All fractioned extracts were combined to obtain the final extract. The effect of extraction time on the TPC, TFC, TTC, and RSA of the extracts was determined using the same procedure with minor modifications. In particular, the extraction time ranged

from 5 to 35 min, while the constant microwave power was obtained from the above experiment. The control sample was treated with the same procedure without microwave-assisted extraction. The M2 (MAE-treated) sample was considered an optimal sample since it possessed the highest values of TPC, TFC, TTC, and RSA.

Hot-water extraction (HWE). Single factor experimental designs were employed to clarify the effect of extraction temperature and time on the extraction yield of bioactive compounds. In particular, we determined the effect of different extraction temperatures on the contents of polyphenols (TPC), flavonoids (TFC), triterpenoids (TTC), and antioxidant activity (radical scavenging activity, RSA) of the extracts. For this, a *C. aspera* sample, with a material-to-water ratio of 1:60 (w/v) set as constant, was treated with a range of temperatures (70–100°C) for 10 min. Following this, an extract was collected through centrifugation at 6000 rpm. The solid residue of the samples was then dried until 6% moisture was reached. Upon drying out, the sample was extracted twice with 96% ethanol for 30 min each time. All fractioned extracts were combined to obtain the final extract. The effect of extraction time on the TPC, TFC, TTC, and RSA of the extracts was determined using the same procedure with minor modifications. In particular, the extraction time ranged from 5 to 35 min while the constant temperature was obtained from the above experiment. The control sample (M0) was treated with the same procedure without hot-water extraction. The M3 (HWE-treated) sample was considered an optimal sample since it possessed the highest values of TPC, TFC, TTC, and RSA.

Alkali treatment coupled with ultrasound-assisted extraction (AKE). The effect of different alkali treatments on the contents of polyphenols (TPC), flavonoids (TFC), triterpenoids (TTC), and antioxidant activity (radical scavenging activity, RSA) of the extracts was determined by pre-treating the materials with NaOH solutions at concentrations ranging from 3 to 9% for 20 min. For this, a *C. aspera* sample, with a material-to-water ratio of 1:60 (w/v) set as constant, was treated with ultrasonic power at 375 W and 30°C for 15 min. Following this, an extract was collected through centrifugation at 6000 rpm. The solid residue of the samples was dried until 6% moisture was reached. Upon drying out, the sample was extracted twice with 96% ethanol for 30 min

each time. All the fractions were combined and adjusted to the neutral pH to obtain the final extract. The effect of extraction time on the TPC, TFC, TTC, and RSA of the extracts was performed using the same procedure with minor modifications. In particular, the extraction time ranged from 5 to 35 min, while the NaOH solution at the constant concentration was obtained from the above experiment. The control sample was treated with the same procedure without liquid nitrogen pre-treatment and ultrasound-assisted extraction. The M4 (AKE-treated) sample was considered an optimal sample since it possessed the highest values of TPC, TFC, TTC, and RSA.

Liquid nitrogen treatment coupled with ultrasound-assisted extraction (LNE). The effect of different liquid nitrogen pre-treatments on the contents of polyphenols (TPC), flavonoids (TFC), triterpenoids (TTC), and antioxidant activity (radical scavenging activity, RSA) was determined by pulverizing the materials using liquid nitrogen with a material-to-liquid nitrogen ratio of 1:2–1:8. For this, a *C. aspera* sample, with a material-to-water ratio of 1:60 (w/v) set as constant, was treated with ultrasonic power at 375 W and 30°C for 15 min. Following this, an extract was collected through centrifugation at 6000 rpm. The solid residue of the samples was dried until 6% moisture was reached. Upon drying out, the sample was extracted twice with 96% ethanol for 30 min each time. All the fractions were then combined and adjusted to the neutral pH to obtain the final extract. The effect of extraction time on the TPC, TFC, TTC, and RSA of the extracts was determined using the same procedure with minor modifications. In particular, the extraction time ranged from 5 to 35 min, while the constant material-to-liquid nitrogen ratio was obtained from the above experiment. The control sample was treated with the same procedure without liquid nitrogen pre-treatment and ultrasound-assisted extraction. The M5 (LNE-treated) sample was considered an optimal sample since it possessed the highest values of TPC, TFC, TTC, and RSA.

Determining the total polyphenol content (TPC) of the extract. The total polyphenol content of the extracts was evaluated by colorimetric assay with a Folin-Ciocalteu reagent and a UV-Vis spectrophotometer. A 1 mL aliquot of a diluted extract was added into a test tube containing 0.5 mL of the Folin-Ciocalteu reagent. The mixture was vortexed and maintained at room temperature for 5 min. The mixture was neutralized with 2.5 mL of a saturated Na_2CO_3 solution before it was brought to 10 mL with distilled water and vigorously shaken. After 30 min of incubation in the darkness, the absorbance of the solution at 765 nm was recorded and the polyphenol content was calculated from the standard curve of gallic acid with a concentration range of 0–100 ppm. The results were expressed as mean \pm standard deviation of triplicate experiments and the unit was set as mg gallic acid equivalent per one gram of dry weight of the sample (mg GAE/g dry weight) [18].

Determining the total flavonoids content (TFC) of the extract. The total flavonoid content of the ex-

tracts was evaluated by aluminum chloride assay [19]. For this, a 1 mL aliquot of a diluted extract was mixed with 0.3 mL of a 5% NaNO_2 solution in a test tube and maintained at room temperature for 5 min. The mixture was then mixed with 0.3 mL of a 10% AlCl_3 solution and maintained at room temperature for 5 min. It was then mixed with 2 mL of a 1M NaOH solution, brought to 10 mL with distilled water, and vigorously shaken. The absorbance of the mixture at 510 nm was recorded and the flavonoid content was calculated from the standard curve of quercetin with a concentration range of 0–100 ppm. The results were expressed as mean \pm standard deviation of triplicate experiments and the unit was set as mg quercetin equivalent per one gram of dry weight of the sample (mg QE/g dry weight) [18].

Determining the triterpenoid content (TTC) of the extract. The triterpenoid content of the extracts was evaluated by colorimetric assay using a UV-Vis spectrophotometer, as described in previous studies [20]. For this, a 0.2 mL aliquot of a sample was mixed with 0.2 mL of a 5% vanillin-glacial acetic acid solution and 1.2 mL of perchloric acid (70–72%) in a test tube. Subsequently, the mixture was briefly vortexed and incubated in a thermostatic water bath at 70°C for 15 min. The reaction mixture was rapidly cooled down for 2 min and brought to 5 mL with ethyl acetate. The absorbance of the solution at 550 nm was recorded and the triterpenoid content was calculated from the standard curve of oleonic acid with a concentration range of 0–10 ppm. The results were expressed as mean \pm standard deviation of triplicate experiments and the unit was set as mg oleonic acid equivalent per one gram of dry weight of the sample (mg OAE/g dry weight) [18].

Determining the antioxidant activity (RSA) of the extract. The antioxidant activity of the extracts was evaluated by DPPH radicals scavenging assay according to the procedure described by Chu *et al.* with minor modifications [21]. For this, 0.1 mL aliquot of an extract was mixed with 4 mL of a 0.1 mM DPPH solution and 0.9 mL of ethanol in a test tube. The reaction mixture was kept in the darkness at room temperature for 30 min before the absorbance was measured at 517 nm. Ascorbic acid was used as a reference substance with a concentration range of 0–10 ppm and the antioxidant activity of the extract (DDPH radical scavenging activity, RSA) was estimated from the standard curve between various concentrations of ascorbic acid and changes in the absorbance of the samples. The results were expressed as mean \pm standard deviation of triplicate experiments and the unit was set as μg ascorbic acid equivalent per one gram of dry weight of the sample (μg AAE/g dry weight) [18].

Statistical analysis. The statistical analysis of all analytic experiments was implemented using Statgraphics Centurion XV. The differences among the treatments were determined by ANOVA One-way analysis, followed by Multiple Sample Comparison and Fisher's Least Significant Difference procedures. The statistical significance threshold was set as $p < 0.05$.

RESULTS AND DISCUSSION

The effects of ultrasonic power levels and extraction time on bioactive compounds and antioxidant activity of the extracts. Table 1A presents the effects of ultrasonic power levels on the contents of polyphenols (TPC), flavonoids (TFC), triterpenoids (TTC), and antioxidant activity (radical scavenging activity, RSA) of the samples treated with ultrasound-assisted extraction (UAE). The results indicate that the samples treated with ultrasound at 150, 225, 300, 375, 450, and 525 W had higher values of TPC, TFC, TTC, and RSA than the untreated samples. The increase in ultrasonic power levels was associated with higher contents of TPC, TFC, and TTC, as well as greater antioxidant activity (RSA) of the extracts. For example, the TPC, TFC, TTC, and RSA of the samples treated with 525 W were 1.2, 1.5, 1.5, and 1.1 fold higher, respectively, than those of the samples treated with 150 W. Notably, there was no significant difference among the ultrasound-treated samples at higher power levels (375, 450, and 525 W). Among those levels, 375 W was considered an optimal UAE power level in terms of cost and energysaving issues.

Data were expressed as Mean \pm SD of three experiments, and different lowercase letters (a, b, c, d, e) indicated statistically significant differences among the treatments ($p < 0.05$). TPC is total polyphenol content, TFC is total flavonoid content, TTC is total triterpenoid content, and RSA is antioxidant activity

Table 1B presents the effects of different UAE times on the TPC, TFC, TTC, and RSA of the samples. There was an increase in the TPC, TFC, TTC, and RSA values with longer extraction times. For example, the TPC, TFC, TTC, and RSA of the samples treated for 35 min were respectively 1.6, 2.5, 2.1, and 1.5 fold higher than those of the samples treated for 5 min. Notably, we found no significant difference between the samples

treated for 30 and 35 min ($p > 0.05$). Taken together, the optimal UAE conditions were 375 W power and 30 min extraction time (UAE-treated M1 sample).

Medicinal mushrooms are a rich source of bioactive ingredients and precious natural products but they possess hard, rigid, and durable cell walls which protect them from mechanical or chemical treatment. Therefore, rupturing fungal cell walls to improve bioactive compound extraction is a challenge for food and pharmaceutical industries. UAE is a modern and green technology for natural product extraction. In addition to saving the extraction time and energy, it is eco-friendlier compared to other conventional extraction methods, such as organic solvent extraction. Our data are in line with several previous studies, which indicated the effectiveness of UAE, especially for bioactive compound extraction [22, 23]. For example, Machado-Carvalho *et al.* suggested that UAE could be a better choice for bioactive compound isolation [22]. According to the authors, the optimal conditions for extracting polyphenols and antioxidants from the medicinal mushroom *Inonotus hispidus* were a 1:75 (w/v) ratio of material and 40% ethanol solution and an extraction time of 20 min.

In a study by Zheng *et al.*, the optimal extraction procedure involved using UAE with ultrasonic power of 210 W, a 1:50 (w/v) ratio of material to 50% ethanol solution, and extraction at 80°C for 100 min [24, 25]. Notably, these findings implied that prolonging the extraction time was a more efficient strategy for bioactive compound extraction than increasing ultrasonic power levels. Although the thermal effect of ultrasound was minimized by using a thermostatic water bath (30°C), the higher power of ultrasound can also degrade bioactive compounds (antioxidants, polyphenols, flavonoids, and triterpenoids) or generate too many bubbles, leading to a decline in cavitation effect, which in turn may decrease the extraction yield [26].

Table 1 Changes in bioactive compounds and antioxidant activity of the extracts under different ultrasonic power levels and ultrasound-assisted extraction times

(A)	Ultrasonic power, W							
	0	150	225	300	375	450	525	
TPC, mg GAE/g DW	1.12 ± 0.01 ^a	2.60 ± 0.01 ^b	2.70 ± 0.01 ^c	2.81 ± 0.01 ^d	3.13 ± 0.01 ^c	3.14 ± 0.03 ^c	3.15 ± 0.01 ^c	
TFC, mg QE/g DW	0.15 ± 0.01 ^a	0.18 ± 0.01 ^b	0.21 ± 0.02 ^c	0.23 ± 0.01 ^d	0.26 ± 0.02 ^c	0.27 ± 0.01 ^c	0.27 ± 0.01 ^c	
TTC, mg OAE/g DW	0.11 ± 0.02 ^a	0.36 ± 0.01 ^b	0.48 ± 0.01 ^c	0.49 ± 0.01 ^c	0.54 ± 0.01 ^d	0.54 ± 0.02 ^d	0.55 ± 0.01 ^d	
RSA, µg ascorbic acid/g DW	0.37 ± 0.02 ^a	1.52 ± 0.05 ^b	1.61 ± 0.01 ^c	1.68 ± 0.01 ^c	1.71 ± 0.03 ^d	1.73 ± 0.02 ^d	1.74 ± 0.01 ^d	
(B)	Extraction times, min							
	0	5	10	15	20	25	30	35
TPC, mg GAE/g DW	1.12 ± 0.01 ^a	2.12 ± 0.01 ^b	2.13 ± 0.01 ^b	2.26 ± 0.01 ^c	2.31 ± 0.04 ^d	3.13 ± 0.01 ^c	3.41 ± 0.03 ^f	3.42 ± 0.02 ^f
TFC, mg QE/g DW	0.15 ± 0.01 ^a	0.12 ± 0.02 ^b	0.26 ± 0.02 ^c	0.26 ± 0.01 ^c	0.26 ± 0.01 ^c	0.26 ± 0.02 ^c	0.30 ± 0.01 ^d	0.30 ± 0.02 ^d
TTC, mg OAE/g DW	0.11 ± 0.02 ^a	0.31 ± 0.01 ^b	0.54 ± 0.01 ^c	0.54 ± 0.01 ^c	0.55 ± 0.02 ^c	0.54 ± 0.01 ^c	0.66 ± 0.02 ^d	0.66 ± 0.01 ^d
RSA, µg ascorbic acid/g DW	0.37 ± 0.02 ^a	1.58 ± 0.01 ^b	1.71 ± 0.03 ^c	1.70 ± 0.02 ^c	1.72 ± 0.02 ^c	1.71 ± 0.03 ^c	2.43 ± 0.02 ^d	2.44 ± 0.02 ^d

Data were expressed as Mean \pm SD of three experiments, and different lowercase letters (a, b, c, d, e) indicated statistically significant differences among the treatments ($p < 0.05$). TPC is total polyphenol content, TFC is total flavonoid content, TTC is total triterpenoid content, and RSA is antioxidant activity. DW is dry weight.

Table 2 Changes in bioactive compounds and antioxidant activity of the extracts under different microwave power and microwave-assisted extraction times

(A)	Microwave power, W					
	0	110	120	130	140	
TPC, mg GAE/g DW	1.12 ± 0.01 ^a	1.73 ± 0.03 ^b	1.96 ± 0.02 ^c	2.08 ± 0.01 ^d	2.10 ± 0.01 ^d	
TFC, mg QE/g DW	0.05 ± 0.01 ^a	0.19 ± 0.02 ^b	0.24 ± 0.01 ^c	0.27 ± 0.02 ^d	0.28 ± 0.01 ^d	
TTC, mg OAE/g DW	0.11 ± 0.02 ^a	0.39 ± 0.02 ^b	0.47 ± 0.03 ^c	0.57 ± 0.03 ^d	0.59 ± 0.01 ^d	
RSA, µg ascorbic acid/g DW	0.37 ± 0.02 ^a	1.89 ± 0.04 ^b	2.02 ± 0.01 ^c	2.10 ± 0.02 ^d	2.18 ± 0.02 ^d	
(B)	Extraction times, min					
	0	5	10	15	20	25
TPC, mg GAE/g DW	1.12 ± 0.01 ^a	2.00 ± 0.01 ^b	2.08 ± 0.01 ^c	3.17 ± 0.01 ^d	3.17 ± 0.03 ^d	3.19 ± 0.02 ^d
TFC, mg QE/g DW	0.05 ± 0.01 ^a	0.19 ± 0.01 ^b	0.27 ± 0.02 ^c	0.29 ± 0.01 ^c	0.29 ± 0.01 ^c	0.30 ± 0.02 ^c
TTC, mg OAE/g DW	0.11 ± 0.02 ^a	0.46 ± 0.01 ^b	0.57 ± 0.03 ^c	0.66 ± 0.02 ^d	0.66 ± 0.01 ^d	0.67 ± 0.01 ^d
RSA, µg ascorbic acid/g DW	0.37 ± 0.02 ^a	1.65 ± 0.01 ^b	2.10 ± 0.02 ^c	2.21 ± 0.01 ^d	2.21 ± 0.02 ^d	2.22 ± 0.01 ^d

Data were expressed as Mean ± SD of three experiments, and different lowercase letters (a, b, c, d, e) indicated statistically significant differences among the treatments ($p < 0.05$). TPC is total polyphenol content, TFC is total flavonoid content, TTC is total triterpenoid content, and RSA is antioxidant activity. DW is dry weight.

The effects of microwave power levels and extraction time on bioactive compounds and antioxidant activity of the extracts. As shown in Table 2A, microwave could effectively extract bioactive compounds from the medical mushroom. The contents of polyphenols (TPC), flavonoids (TFC), triterpenoids (TTC), and antioxidant activity (radical scavenging activity, RSA) of the samples treated with microwave at 110 W were remarkably higher those of the untreated samples ($p < 0.05$). Additionally, there was an increase in TPC, TFC, TTC, and RSA depending on the microwave power level. For example, the samples treated with microwave-assisted extraction (MAE) at 130 W yielded the highest TPC, TFC, TTC, and RSA, followed by the samples treated with MAE at 120 W, 110 W, and the untreated samples ($p < 0.05$). We observed that the MAE level of 140 W did not improve the TPC, TFC, TTC, and RSA as compared to 130 W ($p > 0.05$). The microwave power of 130 W was therefore identified as the optimal power for extraction.

Aside from the microwave power, the extraction time was also found to enhance the extraction efficacy (Table 2B). There was a positive correlation between the MAE time and bioactive compound extraction efficacy (TPC, TFC, TTC, and RSA). The MAE-treated samples obtained their maximal values of TPC, TTC, and RSA after 15 min ($p < 0.05$), with no noticeable differences observed under the longer extraction time. Notably, the TFC of the samples reached a plateau at 10 min and remained constant until 25 min. These results indicated that the duration of 15 min was the sufficient time to extract bioactive compounds (MAE-treated M2 sample).

MAE has been one of the green extraction techniques widely used in bioactive compound extraction, especially from medicinal mushrooms. As microwave heats and dries fungal cells, increasing temperature and aqueous vapor inside the cells cause their walls to stretch and break down, which in turn facilitates the extraction process [27]. According to Maeng *et al.*, MAE

is a better practice to obtain the maximal values of polyphenols and antioxidants from turkey tail or Yun Zhi mushroom in contrast to the aqueous-based reflux method [28]. Smiderle *et al.* also used MAE to extract β -D-glucan, a bioactive constituent of cell walls acting as an immuno-stimulant, from two medicinal mushrooms, *Ganoderma lucidum* and *Pleurotus ostreatus* [29]. They found some slight differences in the optimal conditions between a previous study (125 W, 3.8 min, 40% ethanol) and the present study (130 W, 15 min, water), which could be mainly due to the different solvents used for extraction in these experiments. The selection of optimal conditions for MAE is a critical requirement for bioactive constituent extraction, since high microwave power and long extraction time are often accompanied by a higher risk of loss of bioactive compounds, especially in the substances susceptible to thermal degradation [27].

The effects of hot-water extraction temperature and time on bioactive compounds and antioxidant activity of the extracts. The effects of hot-water extraction (HWE) temperature on the extraction efficacy are presented in Table 3A. Briefly, we found a positive correlation between the extraction temperature and the contents of polyphenols (TPC), flavonoids (TFC), triterpenoids (TTC), and antioxidant activity (radical scavenging activity, RSA) of the extracts. For example, the samples treated at 90°C exhibited a noticeable increase in the TPC, TFC, TTC, and RSA (1.6, 3.2, 2.8, and 3.6 fold, respectively, $p < 0.05$) in comparison with the control treated at room temperature (25°C). The TPC, TFC, TTC, and RSA continuously increased until reaching the maximal values at 100°C. Our findings were consistent with a previous study by Sharma and Tulsawani, where higher extraction temperatures were associated with a greater amount of TPC and TFC. Noteworthy, the temperature higher than 100°C could lead to a degradation of some antioxidants [30]. Therefore, we chose the extraction temperature of 100°C for further experiments. We also observed that longer extraction

Table 3 Changes in bioactive compounds and antioxidant activity of the extracts under different hot-water extraction temperatures and times

(A)	Extraction temperature, °C				
	25	70	80	90	100
TPC, mg GAE/g DW	1.12 ± 0.01 ^a	1.55 ± 0.01 ^b	1.66 ± 0.01 ^c	1.81 ± 0.02 ^d	2.08 ± 0.01 ^e
TFC, mg QE/g DW	0.05 ± 0.01 ^a	0.08 ± 0.01 ^b	0.12 ± 0.01 ^c	0.16 ± 0.01 ^d	0.19 ± 0.02 ^e
TTC, mg OAE/g DW	0.11 ± 0.02 ^a	0.23 ± 0.01 ^b	0.31 ± 0.02 ^c	0.31 ± 0.01 ^c	0.36 ± 0.01 ^d
RSA, µg ascorbic acid/g DW	0.37 ± 0.02 ^a	1.04 ± 0.02 ^b	1.14 ± 0.01 ^c	1.28 ± 0.02 ^d	1.34 ± 0.02 ^e
(B)	Extraction time, min				
	0	5	10	15	20
TPC, mg GAE/g DW	1.12 ± 0.01 ^a	1.43 ± 0.01 ^b	2.08 ± 0.02 ^c	2.35 ± 0.01 ^d	2.37 ± 0.01 ^d
TFC, mg QE/g DW	0.05 ± 0.01 ^a	0.09 ± 0.02 ^b	0.19 ± 0.01 ^c	0.24 ± 0.02 ^d	0.25 ± 0.01 ^d
TTC, mg OAE/g DW	0.11 ± 0.02 ^a	0.24 ± 0.02 ^b	0.34 ± 0.01 ^c	0.38 ± 0.01 ^d	0.39 ± 0.01 ^d
RSA, µg ascorbic acid/g DW	0.37 ± 0.02 ^a	1.20 ± 0.01 ^b	1.34 ± 0.01 ^c	1.51 ± 0.01 ^d	1.52 ± 0.02 ^d

Data were expressed as Mean ± SD of three experiments, and different lowercase letters (a, b, c, d, e) indicated statistically significant differences among the treatments ($p < 0.05$). TPC is total polyphenol content, TFC is total flavonoid content, TTC is total triterpenoid content, and RSA is antioxidant activity. DW is dry weight.

Table 4 Changes in bioactive compounds and antioxidant activity of the extracts pretreated with different NaOH concentrations and at different ultrasound extraction times

(A)	NaOH concentration, %				
	0	3	5	7	9
TPC, mg GAE/g DW	1.19 ± 0.02 ^a	2.19 ± 0.01 ^b	2.48 ± 0.01 ^c	2.49 ± 0.01 ^c	2.49 ± 0.02 ^c
TFC, mg QE/g DW	0.08 ± 0.01 ^a	0.16 ± 0.01 ^b	0.21 ± 0.02 ^c	0.22 ± 0.02 ^c	0.22 ± 0.01 ^c
TTC, mg OAE/g DW	0.17 ± 0.02 ^a	0.53 ± 0.01 ^b	0.88 ± 0.02 ^c	0.89 ± 0.02 ^c	0.90 ± 0.02 ^c
RSA, µg ascorbic acid/g DW	0.40 ± 0.02 ^a	1.23 ± 0.01 ^b	2.15 ± 0.01 ^c	2.15 ± 0.02 ^c	2.16 ± 0.02 ^c
(B)	Ultrasound extraction time, min				
	0	5	10	15	20
TPC, mg GAE/g DW	1.19 ± 0.02 ^a	2.12 ± 0.03 ^b	2.22 ± 0.02 ^c	2.48 ± 0.01 ^d	2.49 ± 0.01 ^d
TFC, mg QE/g DW	0.08 ± 0.01 ^a	0.11 ± 0.01 ^b	0.17 ± 0.02 ^c	0.21 ± 0.01 ^d	0.22 ± 0.01 ^d
TTC, mg OAE/g DW	0.17 ± 0.02 ^a	0.22 ± 0.02 ^b	0.61 ± 0.01 ^c	0.88 ± 0.02 ^d	0.89 ± 0.01 ^d
RSA, µg ascorbic acid/g DW	0.40 ± 0.02 ^a	1.29 ± 0.01 ^b	1.46 ± 0.02 ^c	2.15 ± 0.02 ^d	2.15 ± 0.01 ^d

Data were expressed as Mean ± SD of three experiments, and different lowercase letters (a, b, c, d, e) indicated statistically significant differences among the treatments ($p < 0.05$). TPC is total polyphenol content, TFC is total flavonoid content, TTC is total triterpenoid content, and RSA is antioxidant activity. DW is dry weight.

times improved the TPC, TFC, TTC, and RSA of the extracts (Table 3B). Among five times of extraction (0–20 min), all of bioactive compound contents obtained a plateau at 15 min ($p < 0.05$) and remained unchanged until 20 min. Thus, the HWE temperature of 100°C and HWE time of 15 min (HWE-treated M3 sample) were found to be optimal conditions to extract polyphenols, flavonoids, triterpenoids, and antioxidants.

HWE is a conventional method for extracting plant bioactive components. It shortens the extraction time and improves the yield, compared to cold-water extraction [31]. For some particular phenolic substances, such as gallic acid and *p*-hydroxybenzoic acid, hot-water extraction had a greater efficacy than methanol extraction [32]. However, its efficacy for natural product extraction was less than that of some modern techniques, such as ultrasound-assisted extraction [24, 25]. In this study, the maximal extraction yields of HWE in terms of TPC, TFC, TPC, and RSA were lower than those of

ultrasound- or microwave-assisted extraction. For example, the TPC of the UAE-treated sample (M1) was the highest, followed by that of the MAE-treated (M2) and HWE-treated (M3) samples ($p < 0.05$). Therefore, ultrasound-assisted extraction was considered the most appropriate extraction method for *C. aspera*.

The effects of NaOH pretreatment and ultrasound extraction time on bioactive compounds and antioxidant activity of the extracts. The effects of NaOH concentration (alkali pretreatment) and ultrasound extraction time on the extraction efficacy are presented in Table 4. As can be seen, alkali treatment (AKE) remarkably increased the contents of bioactive compounds in the extracts (Table 4A). For example, the samples treated with a 3% NaOH solution improved the extraction efficacy of polyphenols (TPC), flavonoids (TFC), triterpenoids (TTC), and antioxidant activity (radical scavenging activity, RSA) (1.84, 2.00, 3.11, and 3.07 fold, respectively), as compared to the untreated samples. Since the maxi-

mal values of TPC, TFC, TTC, and RSA were obtained in 5% NaOH pretreatment, this concentration was used in the further optimization experiment. We also observed that longer extraction times (0–20) increased the TPC, TFC, TTC, and RSA, which subsequently reached a plateau at the time point of 15 min. These results indicated that the optimal AKE conditions were 5% NaOH, 375 W, and 15 min extraction (AKE-treated M4 sample). The samples treated under the optimal AKE conditions possessed higher TPC and TTC, compared to those treated with ultrasound only (375 W, 25 min) (Table 1). This suggested that the alkali pretreatment facilitated the extraction of bioactive compounds.

Alkali treatment is one of the most popular methods for extracting polysaccharides, a group of bioactive compounds found in mushrooms [33]. Medicinal mushroom cell walls are rich in polysaccharides, most of which are easily dissolved under alkaline conditions [33]. The alkaline solution not only punctures the fugal cell walls but also breaks down cellular fibers and links within peptides, as well as glucan [33, 34]. Therefore, alkali pretreatment effectively enhances the extraction yield of bioactive compounds from medicinal mushrooms, which was also demonstrated in this study. However, the maximal values of TPC, TTC, and RSA of the ultrasound-treated samples under the optimal conditions (375 W, 25 min) were higher than those of the AKE-treated samples. This indicated that ultrasound-assisted extraction was a better method to extract these bioactive compounds.

The effects of different ratios of material to liquid nitrogen and ultrasound extraction times on bioactive compounds and antioxidant activity of the extracts. The effects of liquid nitrogen pre-treatment and ultrasound extraction times on the extraction efficacy are presented in Table 5. As shown in Table 5A, pulverizing the samples with liquid nitrogen significantly increased their contents of polyphenols (TPC), flavonoids (TFC), triterpenoids (TTC), and antioxidant activity

(radical scavenging activity, RSA) compared to the control sample ($p < 0.05$). We also found a positive correlation between the material-to-liquid nitrogen ratio (w/v) and the TPC, TFC, TTC, and RSA. For example, the samples pre-treated with liquid nitrogen in the ratio of 1:8 had their TPC, TFC, TTC, and RSA increased by 94.2, 128.2, 112.5, and 17.9%, respectively, compared to the samples pre-treated with liquid nitrogen in the ratio of 1:2. Among four ratios under study, the maximal values of TPC, TFC, TTC, and RSA were obtained with the ratios of 1:6 and 1:8 (w/v). In addition, there was no significant difference between the optimal ratios of 1:6 and 1:8 ($p > 0.05$). We also found that longer ultrasound extraction times increased the efficacy of bioactive compound extraction in terms of TPC, TFC, TTC, and RSA, which reached the optimal values at 15 min (Table 5B). Therefore, the material-to-liquid nitrogen ratio of 1:6 for pulverizing materials and the ultrasound extraction time of 15 min were identified as the optimal conditions for extracting polyphenols, flavonoids, triterpenoids, and antioxidants.

Our results were consistent with some previous studies. For example, in a study by Razumov *et al.*, pulverizing the Chaga mushroom, *Inonotus obliquus*, with liquid nitrogen enhanced the extraction of such bioactive compounds as methionine, leucine, melanin, asparagine, glutamine, and flavonoids [35]. Furthermore, cryogenic grinding with liquid nitrogen is a common method used in the food industry due to its effectiveness in producing super-fine materials. Besides, the low temperature during the grinding process accelerates the extraction of natural products, especially in phytosterols, soluble dietary fiber, and glucosinolate [36, 37]. Our findings proved the efficacy of pulverization in liquid nitrogen coupled with ultrasound-assisted extraction. In particular, the samples pretreated with liquid nitrogen (1:4) and treated with ultrasound extraction (375 W, 15 min) possessed higher TPC, TFC, TTC, and RSA, compared to the samples treated with ultrasound only (375 W, 15 min,

Table 5 Changes in bioactive compounds and antioxidant activity of the extracts under different ratios of material to liquid nitrogen and ultrasound extraction times

(A)	Ratios of material to liquid nitrogen, w/v				
	0	1:2	1:4	1:6	1:8
TPC, mg GAE/g DW	1.13 ± 0.04 ^a	2.43 ± 0.02 ^b	3.59 ± 0.01 ^c	4.69 ± 0.02 ^d	4.72 ± 0.01 ^d
TFC, mg QE/g DW	0.06 ± 0.01 ^a	0.39 ± 0.01 ^b	0.61 ± 0.03 ^c	0.88 ± 0.01 ^d	0.89 ± 0.01 ^d
TTC, mg OAE/g DW	0.12 ± 0.02 ^a	0.56 ± 0.01 ^b	0.82 ± 0.02 ^c	1.18 ± 0.01 ^d	1.19 ± 0.01 ^d
RSA, µg ascorbic acid/g DW	0.38 ± 0.03 ^a	2.96 ± 0.02 ^b	3.18 ± 0.02 ^c	3.48 ± 0.01 ^d	3.49 ± 0.01 ^d
(B)	Ultrasound extraction time, min				
	0	5	10	15	20
TPC, mg GAE/g DW	1.13 ± 0.04 ^a	3.10 ± 0.02 ^b	4.01 ± 0.01 ^c	4.69 ± 0.02 ^d	4.71 ± 0.01 ^d
TFC, mg QE/g DW	0.06 ± 0.01 ^a	0.38 ± 0.01 ^b	0.64 ± 0.02 ^c	0.88 ± 0.01 ^d	0.87 ± 0.01 ^d
TTC, mg OAE/g DW	0.12 ± 0.02 ^a	0.60 ± 0.02 ^b	0.96 ± 0.01 ^c	1.28 ± 0.01 ^d	1.29 ± 0.01 ^d
RSA, µg ascorbic acid/g DW	0.38 ± 0.03 ^a	2.91 ± 0.02 ^b	3.24 ± 0.02 ^c	3.48 ± 0.01 ^d	3.48 ± 0.02 ^d

Data were expressed as Mean ± SD of three experiments, and different lowercase letters (a, b, c, d, e) indicated statistically significant differences among the treatments ($p < 0.05$). TPC is total polyphenol content, TFC is total flavonoid content, TTC is total triterpenoid content, and RSA is antioxidant activity. DW is dry weight.

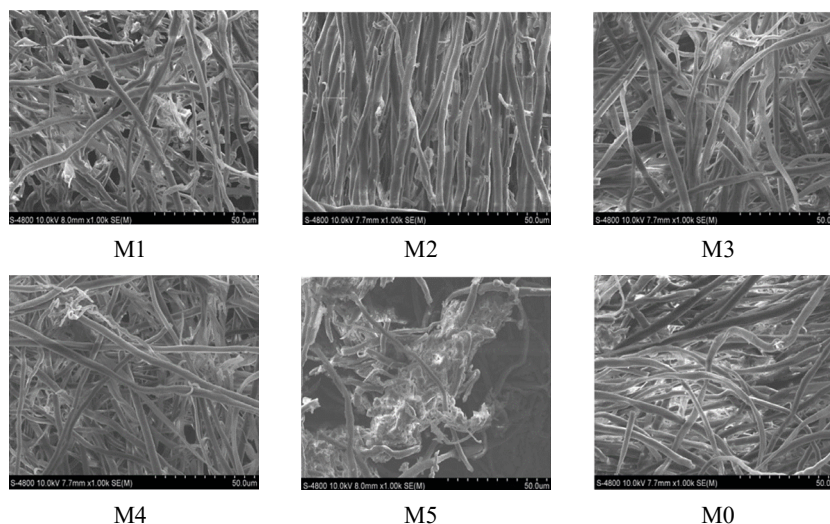


Figure 3 SEM images of *Coriolis aspera* mycelia after treatments. The mycelia of the control samples (M0) are intact, complex, and compactly organized, while those of the samples treated with ultrasound-assisted extraction (M1), microwave-assisted extraction (M2), hot-water extraction (M3), and alkali extraction (M4) are partly destroyed. Only the mycelia of the samples treated with liquid nitrogen (M5) have visible damages

Table 1). This implied the superior effect of liquid nitrogen pretreatment coupled with UAE (LNE) against purely ultrasound-assisted extraction (UAE).

Among the five treatments under study, LNE was the best extraction method for TPC, TFC, TTC, and RSA. In the optimal LNE conditions with the material-to-liquid nitrogen ratio of 1:6 (w/v) and UAE (15 min), the extract contained the highest amounts of polyphenols (4.69 ± 0.02 mg GAE/g dry weight), flavonoids (0.88 ± 0.01 mg QE/g dry weight), triterpenoids (1.28 ± 0.01 mg OAE/g dry weight), and antioxidant activity (3.48 ± 0.01 μ g acid ascorbic/g dry weight). These results were consistent with the SEM analysis of the mycelia of the LNE-treated samples (M5, Fig. 3), in which LNE was the only method able to rupture fungal mycelia, unlike UAE, MAE, AKE, and HWE. Noteworthy, the efficacy of the extraction methods varied depending on the bioactive compounds. The order of maximal values was LNE > UAE > MAE > AKE > HWE for polyphenols and antioxidants, LNE > AKE > MAE > UAE > HWE for triterpenoids, as well as LNE > MAE > UAE > HWE > AKE for flavonoids. These findings suggested that different methods and optimal conditions should be selected to optimize the extraction process for particular groups of natural products derived from medicinal mushrooms.

CONCLUSION

We studied the efficiency of extracting polyphenols, triterpenoids, and flavonoids from *Coriolis aspera* by ultrasound-assisted extraction (UAE), microwave-assisted extraction (MAE), hot-water extraction (HWE), ultrasound-assisted alkali extraction (AKE), and ultrasound-assisted liquid nitrogen extraction (LNE). The orders of maximal values were LNE > UAE > MAE > AKE > HWE for polyphenols, LNE > AKE > MAE

> UAE > HWE for triterpenoids, and LNE > MAE > UAE > HWE > AKE for flavonoids. Thus, LNE was the most optimal method in all the cases.

Furthermore, the material-to-liquid nitrogen ratio of 1:6 (w/v), ultrasound extraction time of 15 min, and ultrasonic power of 375 W (frequency of 20 kHz; amplitude of 50%) were shown to be the optimal conditions for the LNE method, with the highest concentrations of polyphenols (4.69 ± 0.02 mg GAE/g dry weight), flavonoids (0.88 ± 0.01 mg QE/g dry weight), and triterpenoids (1.28 ± 0.01 mg OAE/g dry weight), as well as high antioxidant activity (3.48 ± 0.01 μ g acid ascorbic/g dry weight). These findings could be used as supportive evidence for the potential application of the extracts from *C. aspera* in functional food production or in the pharmaceutical industry.

CONTRIBUTION

L.M.Thu developed the research concept and methodology, as well as performed the experiments. D.S.Mai designed the study, as well as reviewed and proofread the manuscript. N.N.Thuan collected the data and wrote the draft of the manuscript. L.T.Nguyen reviewed, edited, and proofread the manuscript. D.V.Phuong wrote the abstract, conducted formal analysis, finalized the manuscript and is the corresponding author who submitted the manuscript.

CONFLICT OF INTEREST

The authors declare no conflict of interest regarding the publication of this article.

ACKNOWLEDGEMENTS


The authors would like to thank the Institute of Biotechnology and Food Technology, Industrial University of Ho Chi Minh City (Vietnam) and their co-workers for their technical support.


REFERENCES


1. Chang ST, Wasser SP. The cultivation and environmental impact of mushrooms. Oxford Research Encyclopedia of Environmental Science. 2017. <https://doi.org/10.1093/acrefore/9780199389414.013.231>
2. Ghosh K. A review mushrooms: A source of immunomodulating and antitumor polysaccharides. Journal of Physical Sciences. 2015;20:239–252.
3. Nguyen N-T, Nguyen N-T, Dam S-M, Le T-T, Nguyen T-N, Van H-T, et al. Chemical composition and antioxidant, anti-inflammatory, and anticancer effects of extract from yunzhi mushroom (*Coriolopsis aspera*) in Vietnam. Pharmacophore. 2020;11(4):51–55.
4. Bautista-González JA, Montoya A, Bye R, Esqueda M, Herrera-Campos MA. Traditional knowledge of medicinal mushrooms and lichens of Yuman peoples in Northern Mexico. Journal of Ethnobiology and Ethnomedicine. 2022;18:52. <https://doi.org/10.1186/s13002-022-00550-8>
5. Dantas SBS, Moraes GKA, Araujo AR, Chapla VM. Phenolic compounds and bioactive extract produced by endophytic fungus *Coriolopsis rigida*. Natural Product Research. 2023;37(12):2037–2042. <https://doi.org/10.1080/14786419.2022.2115492>
6. Evana E, Palupi KD, Oktavia L, Fathoni A. Bioprospection of Enggano macroscopic fungi as antibacterial and antioxidant agents. Berita Biologi. 2021;20(2):201–210. <https://doi.org/10.14203/beritabiologi.v20i2.4110>
7. Abascal K, Yarnell E. A Turkey tails polysaccharide as an immunochemotherapy agent in cancer. Alternative and Complementary Therapies. 2007;13(4):178–182. <https://doi.org/10.1089/act.2007.13410>
8. Wasser S. Medicinal mushrooms as a source of antitumor and immunomodulating polysaccharides. Applied Microbiology and Biotechnology. 2002;60:258–274. <https://doi.org/10.1007/s00253-002-1076-7>
9. Haneef M, Ceseracciu L, Canale C, Bayer IS, Heredia-Guerrero JA, et al. Advanced materials from fungal mycelium: Fabrication and tuning of physical properties. Scientific Reports. 2017;7:41292. <https://doi.org/10.1038/srep41292>
10. Chen L, Xu W, Lin S, Cheung PCK. Cell wall structure of mushroom sclerotium (*Pleurotus tuber regium*): Part 1. Fractionation and characterization of soluble cell wall polysaccharides. Food Hydrocolloids. 2014;36:189–195. <https://doi.org/10.1016/j.foodhyd.2013.09.023>
11. Bleha R, Třešnáková L, Sushytskyi L, Capek P, Čopíková J, Klouček P, et al. Polysaccharides from basidiocarps of the polypore fungus *Ganoderma resinaceum*: Isolation and structure. Polymers. 2022;14(2):255. <https://doi.org/10.3390/polym14020255>
12. Ma J, Fu Z, Ma P, Su Y, Zhang Q. Breaking and characteristics of *Ganoderma lucidum* spores by high speed entrifugal shearing pulverizer. Journal of Wuhan University of Technology – Materials Science. 2007;22:617–621. <https://doi.org/10.1007/s11595-006-4617-6>
13. Panda D, Manickam S. Cavitation technology – The future of greener extraction method: A review on the extraction of natural products and process intensification mechanism and perspectives. Applied Sciences. 2019;9(4):766. <https://doi.org/10.3390/app9040766>
14. Trygg J, Beltrame G, Yang B. Rupturing fungal cell walls for higher yield of polysaccharides: Acid treatment of the basidiomycete prior to extraction. Innovative Food Science and Emerging Technologies. 2019;57:102206. <https://doi.org/10.1016/j.ifset.2019.102206>
15. Pinto D, Silva AM, Freitas V, Vallverdú-Queralt A, Delerue-Matos C, Rodrigues F. Microwave-assisted extraction as a green technology approach to recover polyphenols from *Castanea sativa* shells. ACS Food Science and Technology. 2021;1(2):229–241. <https://doi.org/10.1021/acsfoodscitech.0c00055>
16. Sun H, Kang B, Chai Z, Sun H, Du H, Gao J, et al. Characterization of root-associated microbiota in medicinal plants *Astragalus membranaceus* and *Astragalus mongholicus*. Annals of Microbiology. 2017;67:587–599. <https://doi.org/10.1007/s13213-017-1285-z>
17. Liang Z, Du B, Xie L, Jiayi Z, Lin F, Xia Y, et al. Pulverization using liquid nitrogen significantly improves physical properties of powder and extraction yield of polysaccharides of *Astragalus mongholicus*. International Journal of Food Engineering. 2017;13(2):20160034. <https://doi.org/10.1515/ijfe-2016-0034>
18. Thuan NN, Mai DS, Trinh NTN, Thang TD, Tuan NN, Thien LT, et al. Optimization of the extraction process of bioactive compounds from the fruiting bodies of yunzhi mushroom (*Coriolopsis aspera*) in Vietnam by response surface methodology. Malaysian Journal of Chemistry. 2023;25(4):165–175. <https://doi.org/10.55373/mjchem.v25i4.165>
19. Fogarasi M, Socaciu M-I, Sălăgean C-D, Ranga F, Fărcaș AC, Socaci SA, et al. Comparison of different extraction solvents for characterization of antioxidant potential and polyphenolic composition in *Boletus edulis* and *Cantharellus cibarius* mushrooms from Romania. Molecules. 2021;26(24):7508. <https://doi.org/10.3390/molecules26247508>
20. Cai C, Ma J, Han C, Jin Y, Zhao G, He X. Extraction and antioxidant activity of total triterpenoids in the mycelium of a medicinal fungus, *Sanghuangporus sanghuang*. Scientific Reports. 2019;9:7418. <https://doi.org/10.1038/s41598-019-43886-0>


21. Chu M, Khan RD, Zhou Y, Agar OT, Barrow CJ, Dunshea FR, *et al.* LC-ESI-QTOF-MS/MS characterization of phenolic compounds in common commercial mushrooms and their potential antioxidant activities. *Processes*. 2023;11(6):1711. <https://doi.org/10.3390/pr11061711>
22. Machado-Carvalho L, Martins T, Aires A, Saavedra MJ, Marques G. Antioxidant, antibacterial, and cosmeceutical potential of four common edible mushrooms. *Applied Sciences*. 2023;13(13):7357. <https://doi.org/10.3390/app13137357>
23. Zhang J, Wen C, Zhang H, Duan Y, Ma H. Recent advances in the extraction of bioactive compounds with subcritical water: A review. *Trends in Food Science and Technology*. 2020;95:183–195. <https://doi.org/10.1016/j.tifs.2019.11.018>
24. Zheng Y, Cui J, Chen A-H, Zong Z-M, Wei X-Y. Optimization of ultrasonic-microwave assisted extraction and hepatoprotective activities of polysaccharides from *Trametes orientalis*. *Molecules*. 2019;24(1):147. <https://doi.org/10.3390/molecules24010147>
25. Zheng Y, Li Y, Wang W. Optimization of ultrasonic-assisted extraction and in vitro antioxidant activities of polysaccharides from *Trametes orientalis*. *Carbohydrate Polymers*. 2014;111:315–323. <https://doi.org/10.1016/j.carbpol.2014.04.034>
26. Kumar K, Srivastav S, Sharanagat VS. Ultrasound assisted extraction (UAE) of bioactive compounds from fruit and vegetable processing by-products: A review. *Ultrasonics Sonochemistry*. 2021;70:105325. <https://doi.org/10.1016/j.ultsonch.2020.105325>
27. Bagade SB, Patil M. Recent advances in microwave assisted extraction of bioactive compounds from complex herbal samples: A review. *Critical Reviews in Analytical Chemistry*. 2021;51(2):138–149. <https://doi.org/10.1080/10408347.2019.1686966>
28. Maeng J-H, Shahbaz HM, Ameer K, Jo Y, Kwon J-H. Optimization of microwave-assisted extraction of bioactive compounds from *Coriolus versicolor* mushroom using response surface methodology. *Journal of Food Process Engineering*. 2017;40(2):e12421. <https://doi.org/10.1111/jfpe.12421>
29. Smiderle FR, Morales D, Gil-Ramírez A, de Jesus LI, Gilbert-López B, Iacomini M, *et al.* Evaluation of microwave-assisted and pressurized liquid extractions to obtain β -d-glucans from mushrooms. *Carbohydrate Polymers*. 2017;156:165–174. <https://doi.org/10.1016/j.carbpol.2016.09.029>
30. Sharma P, Tulsawani R. Ganoderma lucidum aqueous extract prevents hypobaric hypoxia induced memory deficit by modulating neurotransmission, neuroplasticity and maintaining redox homeostasis. *Scientific Reports*. 2020;10:8944. <https://doi.org/10.1038/s41598-020-65812-5>
31. Ramirez M, Plaza ML, Azeredo A, Balaban MO, Marshall MR. Physicochemical and phytochemical properties of cold and hot water extraction from Hibiscus sabdariffa. *Journal of Food Science*. 2011;76(3):C428–C435. <https://doi.org/10.1111/j.1750-3841.2011.02091.x>
32. Tepsongkroh B, Jangchud K, Trakoontivakorn G. Antioxidant properties and selected phenolic acids of five different tray-dried and freeze-dried mushrooms using methanol and hot water extraction. *Journal of Food Measurement and Characterization*. 2019;13:3097–3105. <https://doi.org/10.1007/s11694-019-00232-2>
33. Leong YK, Yang F-C, Chang J-S. Extraction of polysaccharides from edible mushrooms: Emerging technologies and recent advances. *Carbohydrate Polymers*. 2021;251:117006. <https://doi.org/10.1016/j.carbpol.2020.117006>
34. Zin MIM, Jimat DN, Nawawi WMFW. Physicochemical properties of fungal chitin nanopaper from shiitake (*L. edodes*), enoki (*F. velutipes*) and oyster mushrooms (*P. ostreatus*). *Carbohydrate Polymers*. 2022;281:119038. <https://doi.org/10.1016/j.carbpol.2021.119038>
35. Razumov EYu, Safin RR, Mukhametzyanov ShR, Baigildeeva EI, Safina AV, Lebedev DO. Studies of the composition of the cryogenic ground chaga. *IOP Conference Series: Materials Science and Engineering*. 2020;986:012029. <https://doi.org/10.1088/1757-899X/986/1/012029>
36. Kraljić K, Škevin D, Čukelj Mustač N, Benković M, Drakula S, Balbino S, *et al.* Influence of cryogenic grinding on the nutritional and antinutritional components of rapeseed cake. *Applied Sciences*. 2023;13(10):5841. <https://doi.org/10.3390/app13105841>
37. Thiviya P, Gamage A, Kapilan R, Merah O, Madhujith T. Single cell protein production using different fruit waste: A review. *Separations*. 2022;9(7):178. <https://doi.org/10.3390/separations9070178>


ORCID IDs

Le Minh Thu  <https://orcid.org/0009-0007-2170-4997>

Nguyen Ngoc Thuan  <https://orcid.org/0000-0002-1644-236X>

Luu Thao Nguyen  <https://orcid.org/0000-0002-8146-1102>

Dam Sao Mai  <https://orcid.org/0000-0002-3170-0785>

Do Viet Phuong  <https://orcid.org/0000-0002-0081-0930>



Autumn and winter diet of wood pigeon (*Columba palumbus*) in the Central Ciscaucasia

Anatoly P. Kaledin¹, Lyubov V. Malovichko^{1,*}, Alexander G. Rezanov²,
Lyudmila S. Drozdova¹, Botagoz A. Kentbaeva³

¹ Russian State Agrarian University – Moscow Timiryazev Agricultural Academy^{ROR}, Moscow, Russia

² Moscow City University^{ROR}, Moscow, Russia

³ Kazakh National Agrarian Research University^{ROR}, Almaty, Kazakhstan

* e-mail: l-malovichko@yandex.ru

Received 28.03.2024; Revised 27.05.2024; Accepted 04.06.2024; Published online 02.11.2024

Abstract:

The wood pigeon (*Columba palumbus*) is the largest pigeon in Russia: an adult bird weighs max. 620 g. Its population in Central Ciscaucasia is quite numerous, which makes it a popular object of sports hunting. However, very little is known about its diet and feeding habits. This article describes the seasonal features of *C. palumbus* diet during the hunting season in the Stavropol Region, Russia.

The study relied on the analysis of foods extracted from 66 crops and stomachs of wood pigeons killed by hunters or hit by road vehicles in various biotopes in 25 districts of the Stavropol Region.

In the steppe areas, wood pigeons usually inhabit summer gardens, orchards, vineyards, and green belts along fields, roads, and railways. Wood pigeons are phytophages, which means they feed on plants. Their autumn diet includes sunflower seeds (17.98% occurrence rate, 19.68% total diet), corn grains (15.11 and 9.56%, respectively), wheat (14.39 and 9.98%), flax (6.47 and 10.4%), and millet (2.88 and 4.82%), as well as seeds of wild plants, e.g., wild vetch (7.19 and 3.14%), catchweed (5.75 and 6.25%), trailing bindweed (2.88 and 4.27%), etc.

The wood pigeon inhabits all districts of the Stavropol Region, which makes it a promising game bird species. In addition to cultivated plants, e.g., wheat, sunflower, peas, and corn, wood pigeons feed on a wide range of weeds. The research results contribute to scientific data on *C. palumbus* as a game bird and cast light upon some of its feeding patterns.

Keywords: Wood pigeon, *Columba palumbus*, Central Ciscaucasia, Stavropol Region, diet, gastroliths, distribution, biotope

Please cite this article in press as: Kaledin AP, Malovichko LV, Rezanov AG, Drozdova LS, Kentbaeva BA. Autumn and winter diet of wood pigeon (*Columba palumbus*) in the Central Ciscaucasia. Foods and Raw Materials. 2025;13(2):366–375. <https://doi.org/10.21603/2308-4057-2025-2-652>

INTRODUCTION

Wood pigeon (*Columba palumbus* Linnaeus, 1758) is a large bird species with a wide distribution [1]. The International Union for Conservation of Nature and Natural Resources classifies it as Least Concern [2]. In the Stavropol Region, Russia, wood pigeons are breeding migrants and a wintering species. Research data from 19th and the early 20th centuries give a rather heterogeneous picture of their population and habitat patterns in the Caucasus [3]. These days, wood pigeons are omnipresent in Ciscaucasia, with the exception of open steppes. They entered the Stavropol Region in the 1970s–1980s. Over the next decades, they settled in its northern and central

areas [4]. Early publications, however, scarcely mention them breeding in the Stavropol Region.

This publication is part of a series of articles on the diet of game birds in the Stavropol Region, Russia [5–7].

STUDY OBJECTS AND METHODS

The research material was collected in the Stavropol Region during the hunting seasons (August 25 – October 11) of 2018–2023. It involved the contents of 66 crops and stomachs of wood pigeons (*Columba palumbus*) caught by hunters or hit by vehicles in twelve administrative districts of the Stavropol Region (Fig. 1, Table 1).

The stomach contents were extracted and transferred to paper bags to dry. After 1–2 days, we classified them



Figure 1 Sampling sites of *Columba palumbus* stomachs and crops in Central Ciscaucasia: Stavropol Region, Russia

Table 1 Sampling locations and dates for *Columba palumbus* stomachs and crops in Stavropol Region, Russia

Districts in Stavropol Region	<i>Columba palumbus</i> stomachs and crops, units	Sampling date
Arzgir	7	August 30, 2018 August 25, 2019
Levokumskoye	7	August 31, 2019 August 28, 2020
Grachevka	6	September 4, 2021
Kochubeyevskoye	6	October 11, 2023
Mineralnye Vody	6	September 30, 2022
Petrovsky	6	September 24, 2021
Stepnoye	6	September 27, 2023
Shpakovsky	6	September 29, 2022
Trunovsky	5	August 28, 2018
Izobilny	4	September 25, 2022
Turkmensky	4	August 29, 2019
Aleksandrovskoye	3	September 29, 2021
Total	66	August 25 – October 11

into gastroliths and seeds. The statistical processing followed State Standard ISO 5725-6-2003. The results were presented as mean value (\bar{X}), standard error (SE), limit in the mean (lim.), and standard deviation (SD), with differences considered statistically significant at $p < 0.05$.

To classify stomach and crop contents, we appealed to the classification developed by Prekopov [8]. According to this classification, a food item belonged to primary if it is registered in $\geq 5\%$ cases. Secondary foods occur in 1–5% while random foods are registered in $\leq 1\%$ cases.

These materials update available scientific information about the diet of *C. palumbus* in the Stavropol Region.

RESULTS AND DISCUSSION

Wood pigeons (*Columba palumbus*) are distributed irregularly all over the Stavropol Region and inhabit both crop-farming areas and livestock pastures (Fig. 2).

In the cattle-farming areas, their population growth is constrained by the lack of trees on arid pastures. In the urban areas and villages, their distribution is also irregular as it depends on nesting sites available and man-induced impact on biotopes [9].

The current average annual population of wood pigeons is 2.58 ± 0.57 birds per 10 ha in 25 municipal districts of the Stavropol Region. The calculations took into account the maximal numbers for each region [9]. This count was higher than those reported in earlier studies [10].

The first number in Fig. 2 indicates the lowest count for the entire study period while the second figure represents the most relevant count, i.e., the number of birds in the last research year for that particular area. Single numbers marked with an asterisk* mean that only one count was conducted in this area.

The total population of *C. palumbus* in Fig. 2 is color-coded, with the Kirovsky District colored grey

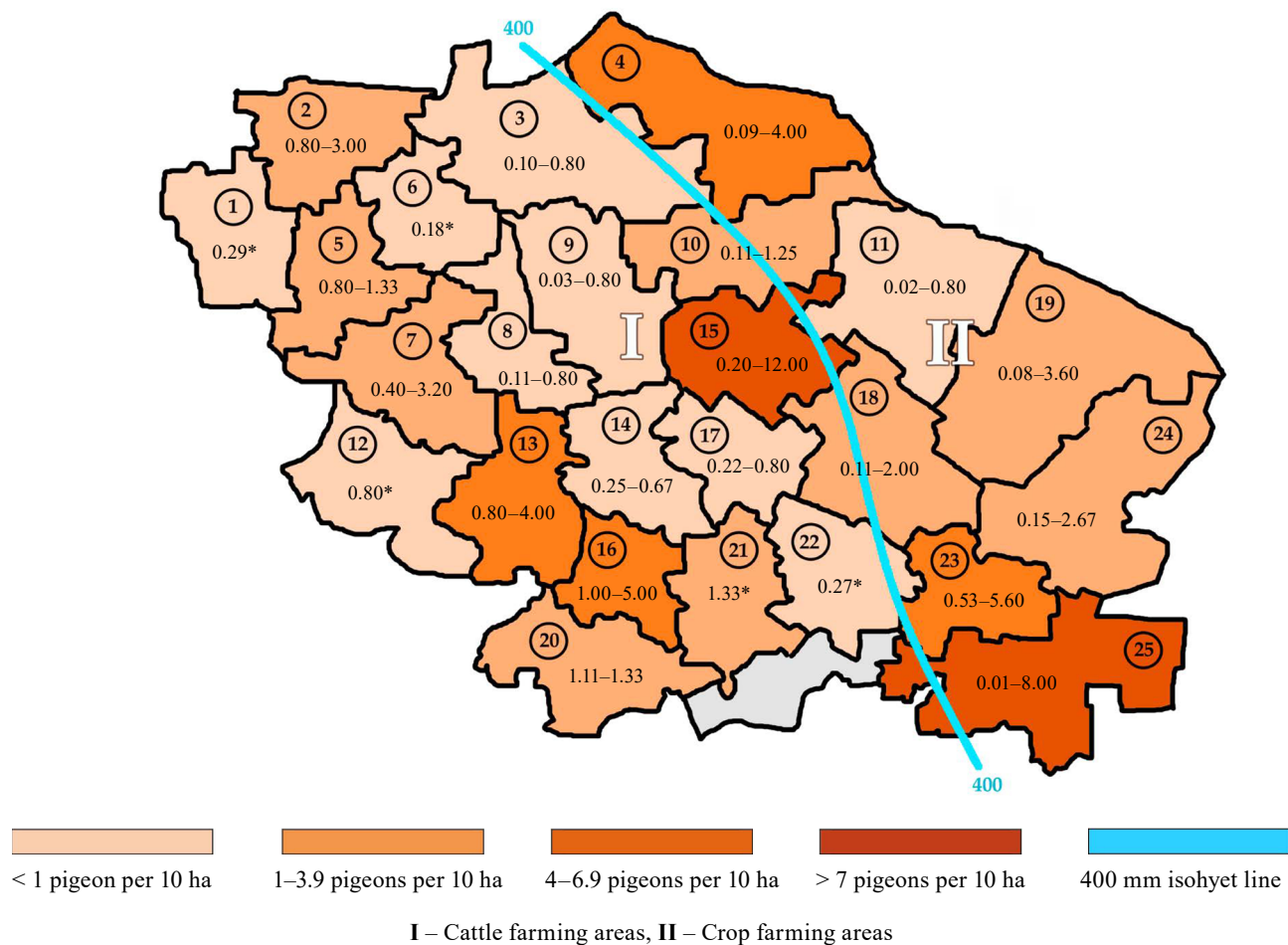


Figure 2 Total population of *Columba palumbus* in 25 districts of Stavropol Region, per 10 ha, 2006–2019: 1 – Novoalexandrovsk, 2 – Krasnogvardeyskoye, 3 – Ipatovo, 4 – Apanasenovsky, 5 – Izobilny, 6 – Trunovsky, 7 – Shpakovsky, 8 – Grachevka, 9 – Petrovsky, 10 – Turkmensky, 11 – Arzgir, 12 – Kochubeevskoye, 13 – Andropovsky, 14 – Aleksandrovskoye, 15 – Blagodarny, 16 – Mineralnye Vody, 17 – Novoselitskoye, 18 – Budennovsk, 19 – Levokumskoye, 20 – Predgorny, 21 – Georgievsk, 22 – Sovetsky, 23 – Stepnoye, 24 – Neftekumsky, 25 – Kurskaya

because no wood pigeon population counts were conducted there in 2006–2019.

The Stavropol Region produces 8–10% all Russia's grain, 4% sugar beets, and 5% sunflower seeds. The local agriculture shows the best results in crop farming, especially in grain production [11].

The Stavropol Region has few forests. The total forest area was 130 100 ha in 2018, with only 15 600 of them growing in urban areas or in rural settlements. Natural forests occupy 51 100 ha whereas man-planted forests make up 41 200 ha [12]. The local steppe afforestation project started in the late 19th century and remained unorganized up to the mid-20th century. The current protective forest belts were planted as part of the so-called Stalin's Plan for Transformation of Nature, adopted in 1948. A real boom in the local green belt policy started in the late 1960s, triggered by severe dust storms.

Wood pigeon diet. Wood pigeons feed on plant foods, i.e., grains, herbal seeds, berries, acorns, beech nuts, buds, and vegetative parts of plants [13–27]. In some areas, they eat foods of animal origin, e.g., terres-

trial mollusks, worms, and insects [13, 23, 28–30]. In general, their diet and food type ration depend on the habitat and season to a large extent.

We discovered 22 species of seeds and grains in the crops and stomachs of *C. palumbus* inhabiting the Stavropol Region: 8 belonged to agricultural crops and 14 were from wild plants. The average number of seeds per crop/stomach was 49.67 ± 12.61 (lim. – 6–153; SD = 31.13; Med. = 37.5; $p = 0.001$; $n = 66$). These calculations were made for all plant species found in the crops and stomachs (Tables 2 and 3).

The statistics revealed an obvious correlation between the occurrence rate of various seeds in the crops and stomachs of wood pigeons and their share in the birds' diet (Figs. 3 and 4). The correlation was of direct nature, i.e., the higher the occurrence rate, the higher their proportion in the diet ($R = 0.8897$; $p < 0.001$).

Gastroliths. We found gastroliths of white, black, gray, dark gray, orange, and brown colors in the crops and stomachs ($n = 66$) of wood pigeons. The mean value for gastroliths of all colors was 9.17 ± 1.92 (lim. 3–21;

Table 2 Seeds in *Columba palumbus* crops and stomachs by plant species, mean value

Plant	Number of crops/stomachs with the seeds	Statistics				
		X ± SE	Lim.	SD	Med.	p
Sunflower (<i>Helianthus cultus</i>)	25	25.80 ± 7.38	9–49	11.21	24	0.001
Sugar corn (<i>Zea mays</i>)	21	16.48 ± 6.59	1–45	11.72	15	0.01
Wheat (<i>Triticum</i> sp.)	20	16.35 ± 6.78	3–34	9.21	14	0.001
Wild vetch (<i>Vicia cracca</i>)	10	10.30 ± 3.89	3–20	6.25	11	0.049
Cotton (<i>Linum usitatissimum</i>)	9	37.89 ± 13.44	11–56	15.66	40	0.01
Catchweed (<i>Galium aparine</i>)	8	25.63 ± 13.70	12–67	19.68	15	0.049
Ragweed (<i>Ambrosia artemisiifolia</i>)	6	42.33 ± 20.05	16–74	24.95	39	0.049
Garden pea (<i>Pisum sativum</i>)	6	14.17 ± 8.82	6–36	10.98	10.5	0.049
Trailing bindweed (<i>Convolvulus arvensis</i>)	4	35.00 ± 13.52	24–45	10.50	35.5	0.001
Knotweed (<i>Fallopia convolvulus</i>)	4	11.25 ± 5.17	4–16	5.25	12.5	0.049
White clover (<i>Trifolium repens</i>)	4	14.75 ± 12.86	5–34	13.07	10	0.049
Millet (<i>Panicum miliaceum</i>)	4	39.50 ± 11.52	29–43	7.00	43	0.001
Meadow pea (<i>Lathyrus pratensis</i>)	4	16.75 ± 11.41	9–34	11.59	12	0.049
Silverberry (<i>Elaeagnus commutata</i>)	3	29.33 ± 16.24	17–45	14.29	26	0.049
Lamb's quarter (<i>Chenopodium album</i>)	3	34.33 ± 1.48	34–35	0.58	34	0.00001
Amaranth (<i>Amaranthus hybridus</i>)	2	16.00 ± 6.74	6–26	14.14	16	0.5
Tare (<i>Vicia sativa</i>)	1	33	33	–	33	< 0.001
Meadow geranium (<i>Geranium pratense</i>)	1	21	21	–	21	< 0.001
Creeping buttercup (<i>Ranunculus repens</i>)	1	45	45	–	45	< 0.001
Oat (<i>Avena sativa</i>)	1	43	4	–	4	< 0.001
Black nightshade (<i>Solanum nigrum</i>)	1	100 (berries)	100	–	100	< 0.001
Field pennycress (<i>Thlaspi arvense</i>)	1	77	77	–	77	< 0.001

Table 3 Primary (> 5%), secondary (1–5%), and random (< 1%) foods in *Columba palumbus* diet

Foods	Total occurrences (n = 139)	Occurrences, % total samples (n = 139)
Primary		
Sunflower (<i>Helianthus cultus</i>)	25	17.98
Sugar corn (<i>Zea mays</i>)	21	15.11
Wheat (<i>Triticum</i> sp.)	20	14.39
Wild vetch (<i>Vicia cracca</i>)	10	7.19
Flax (<i>Linum usitatissimum</i>)	9	6.47
Catchweed (<i>Galium aparine</i>)	8	5.75
Secondary		
Ragweed (<i>Ambrosia artemisiifolia</i>)	6	4.32
Garden pea (<i>Pisum sativum</i>)	6	4.32
Trailing bindweed (<i>Convolvulus arvensis</i>)	4	2.88
Knotweed (<i>Fallopia convolvulus</i>)	4	2.88
White clover (<i>Trifolium repens</i>)	4	2.88
Millet (<i>Panicum miliaceum</i>)	4	2.88
Meadow pea (<i>Lathyrus pratensis</i>)	4	2.88
Silverberry (<i>Elaeagnus commutata</i>)	3	2.16
Lamb's quarter (<i>Chenopodium album</i>)	3	2.16
Amaranth (<i>Amaranthus hybridus</i>)	2	1.44
Random		
Meadow geranium (<i>Geranium pratense</i>)	1	0.72
Tare (<i>Vicia sativa</i>)	1	0.72
Creeping buttercup (<i>Ranunculus repens</i>)	1	0.72
Black nightshade (<i>Solanum nigrum</i>)	1	0.72
Oat (<i>Avena sativa</i>)	1	0.72
Field pennycress (<i>Thlaspi arvense</i>)	1	0.72
Total	139	100.00

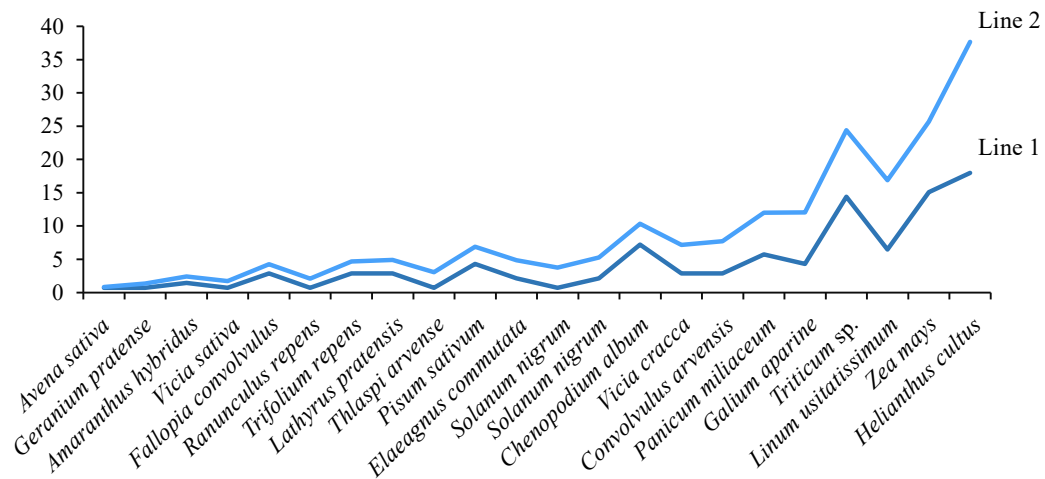


Figure 3 Occurrence rates of various seeds (Line 1) in *Columba palumbus* crops and stomachs vs. their share in *Columba palumbus* diet (Line 2)

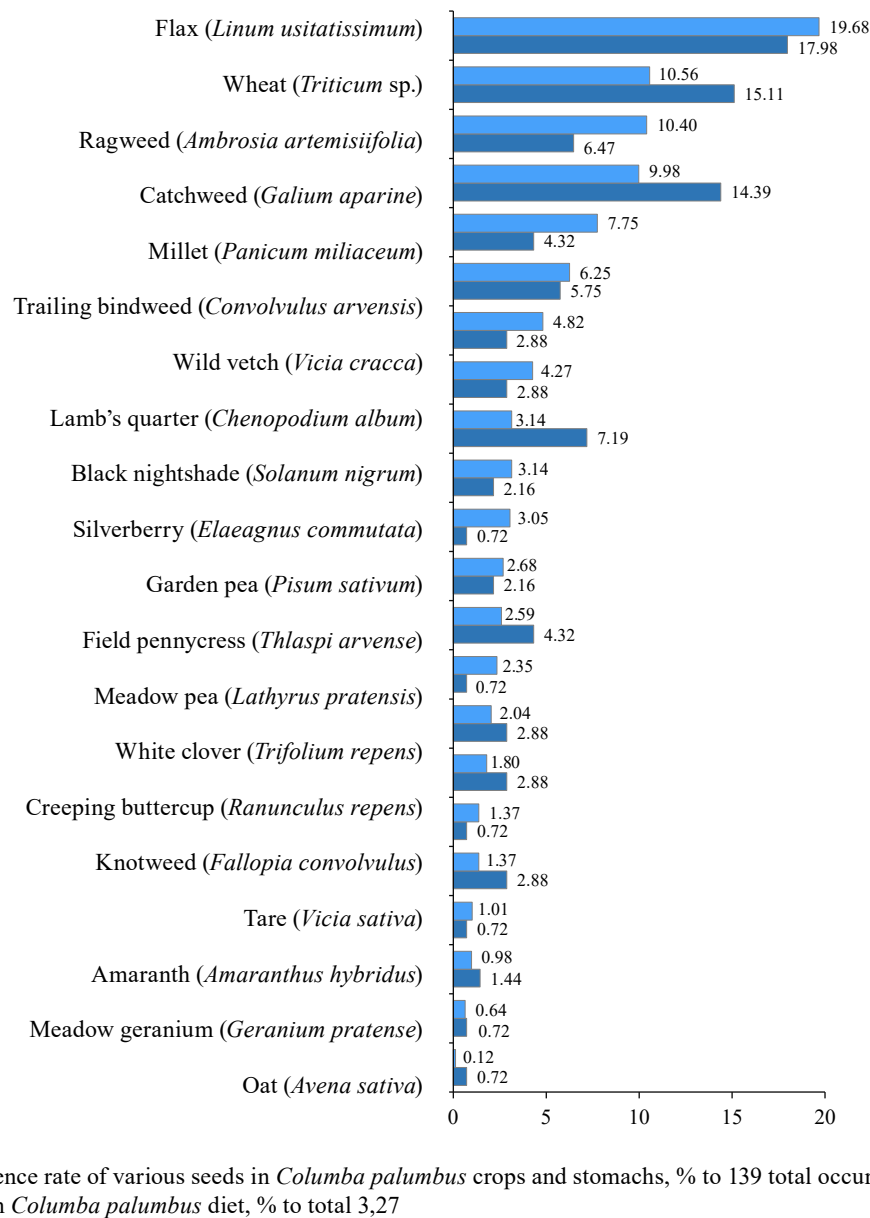


Figure 4 Occurrence rate of seeds in crops and stomachs of *Columba palumbus* vs. their share in *Columba palumbus* diet

SD = 4.74; Med = 8.5; $p = 0.001$; $n = 66$). In 1985, Cramp reported an average of 104 gastroliths per 128 wood pigeon stomachs [29].

Table 4 shows differentiated calculations for gastroliths of each color.

Differences in the number of colored gastroliths in crops and stomachs were not statistically significant ($t_d < 1.7$). We found that the crops and stomachs of wood pigeons from all surveyed areas in the Stavropol Region contained white and black gastroliths. We could not make any assumptions about the pigeons' preference for gastroliths of particular color (Fig. 5) since we had no data on the colors of stones and their ratio in the pigeon feeding areas under analysis.

The average diameter of gastroliths was 1.68–2.16 mm, most being 2 mm across (Table 5).

Gastroliths of different colors demonstrated different patterns in the relationship between their number and diameter. White gastroliths showed a statistically insignificant decrease in number that corresponded with an increase in diameter (Fig. 6). As black gastroliths grew in diameter and reached 2 mm, their number went first up and then down (Fig. 7). We used a polynomial trend for

complex distribution. Orange gastroliths demonstrated an opposite trend (Fig. 8). Grey gastroliths increased in size as they grew in number (Fig. 9). Brown and orange gastroliths demonstrated a similar trend (Fig. 10).

Feeding patterns. In avian studies, feeding patterns are as important as diet. Feeding patterns involve the methods that birds use to obtain food. Wood pigeons are known to feed not only on the ground, but also on trees and shrubs [13, 20, 21]. However, a number of recent publications reported rock pigeons (*Columba livia* var. *urbana*) feeding on trees [31–37]. Rock pigeons seem to have acquired this feeding habit all over Russia, e.g., in the Moscow Region, in Arkhangelsk, in the Crimea, in the Rostov Region, in the Altai mountains, etc.

In the Stavropol Regions, wood pigeons preferred to feed on the ground in the summer and autumn (Fig. 11). In some cases, pigeons flew to sunflower fields and sat on the plants to peck seeds from the anthodium (Fig. 12). We found no evidence of such behavior described in the literature reviewed.

We used our own observations and scientific data from other publications, which we processed by digital coding, to identify the feeding patterns [27, 37].

Table 4 Gastroliths in crops and stomachs of *Columba palumbus*, by color

Color	Crops and stomachs with gastroliths	Total gastroliths	Statistics				
			$X \pm SE$	Lim	SD	Med.	p
White	57	251	4.40 ± 0.89	1–11	2.04	4	0.001
Black	46	117	2.54 ± 0.81	1–8	1.67	2	0.001
Brown	24	66	2.75 ± 0.82	1–6	1.22	3	0.001
Orange	21	92	4.38 ± 1.93	1–10	2.69	4	0.001
Grey	20	79	3.95 ± 1.61	2–11	2.19	3	0.001

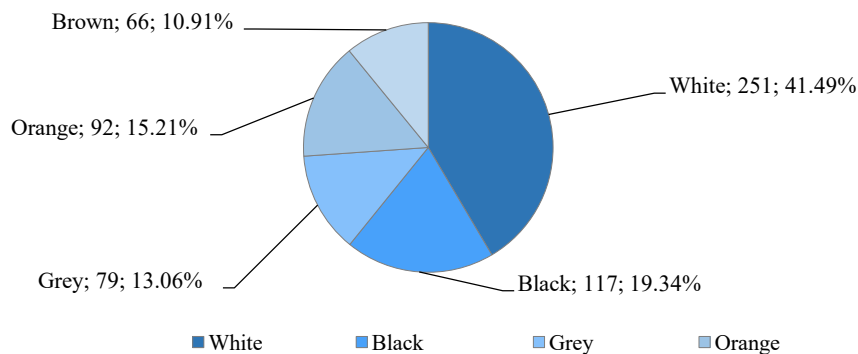


Figure 5 Number and share of gastroliths ($n = 605$) of different colors in crops and stomachs of *Columba palumbus* ($n = 66$)

Table 5 Diameter (mm) of gastroliths in crops and stomachs of *Columba palumbus*, by color

Color	Total gastroliths	Statistics				
		$X \pm SE$	Lim	SD	Med.	p
White	251	2.16 ± 0.23	0.7–6	1.13	2	0.001
Black	117	1.79 ± 0.34	0.7–8	1.11	2	0.001
Orange	92	1.98 ± 0.34	1–4	0.99	2	0.001
Grey	79	2.14 ± 0.37	1–4	1.01	2	0.001
Brown	66	1.68 ± 0.29	1–3	0.71	2	0.001

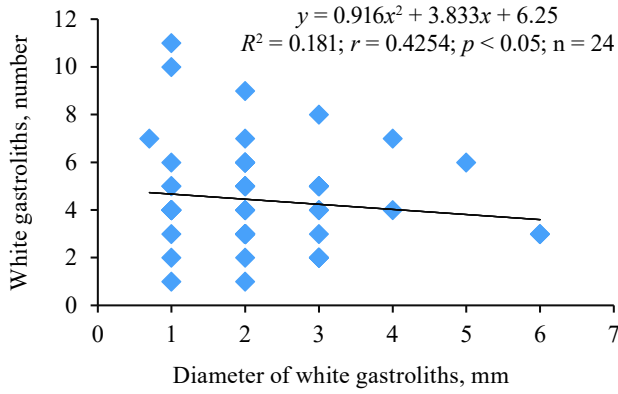


Figure 6 White gastroliths in crops and stomachs of *Columba palumbus*: diameter vs. number

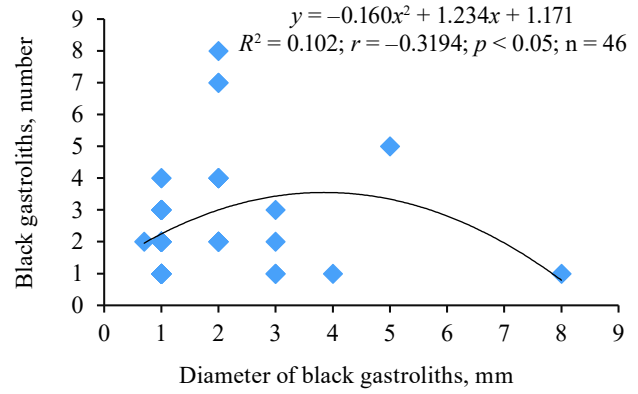


Figure 7 Black gastroliths in crops and stomachs of *Columba palumbus*: diameter vs. number

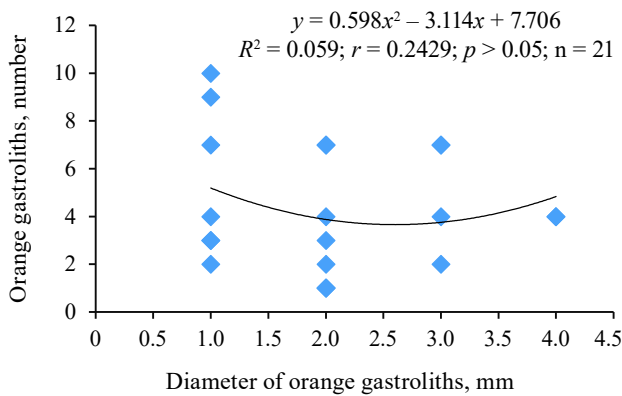


Figure 8 Orange gastroliths in crops and stomachs of *Columba palumbus*: diameter vs. number

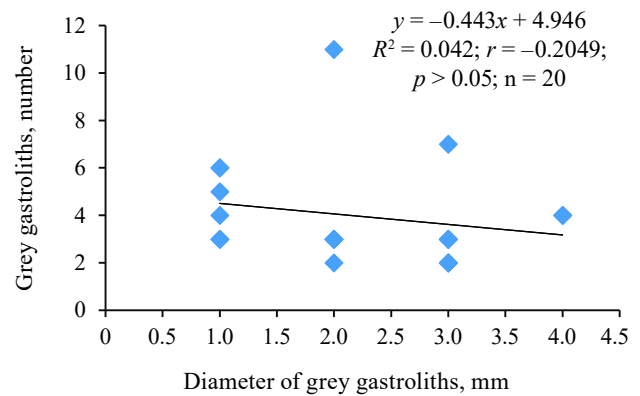


Figure 9 Grey gastroliths in crops and stomachs of *Columba palumbus*: diameter vs. number

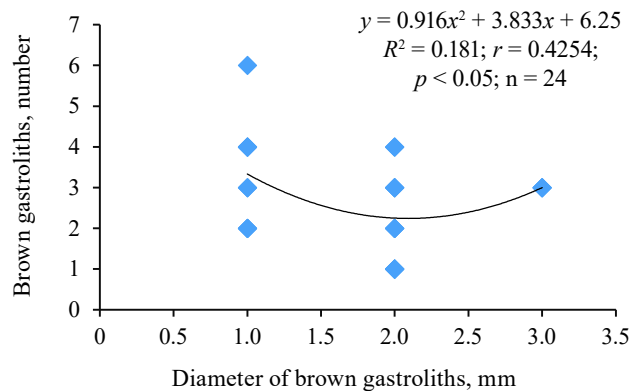


Figure 10 Brown gastroliths in crops and stomachs of *Columba palumbus*: diameter vs. number

Foraging on the ground:

1. Pigeons pick up static seeds, grains, fruits, and terrestrial mollusks from the ground; we collected no information about their behavior while catching moving objects, e.g., insects;
2. They pecked seeds from inflorescences that were close to the ground; and
3. They plucked leaves from herbs while on the ground.

Foraging in tree and bush foliage:

1. Pigeons pecked berries from the bush; and
2. They pecked berries and leave buds on the trees.

Foraging in tall herbal plants:

1. Pigeons pecked sunflower seeds directly from the anthodium while seating on the plant itself, of which nothing was mentioned in scientific literature.



Figure 11 Wood pigeons feeding in a harvested field, July 12, 2021, Mineralnye Vody District, Stavropol Region (photo by L.V. Malovichko)



Figure 12 Wood pigeons feeding on sunflower anthodia, August 27, 2021, Kochubeyevskoye District, Stavropol Region (photo by L.V. Malovichko)

CONCLUSION

During the agricultural crisis of the 1990s, Stavropol fields grew with weeds as the chemical pollution went down. Most fields were not plowed in the autumn, and entire fields of Sudan grass, corn, and sunflowers often stood unharvested. Protective green belts remained uncultivated. These changes were very beneficial for wood pigeons.

These days, agricultural mechanization simplifies the structure of agrocenoses: fields are getting larger; as a result, monoculture areas are growing in size; harvesting and plowing take much less time than before.

Agricultural crops, such as wheat, sunflower and corn, are not the only type of food that attracts wood pigeons

(*Columba palumbus*). They prefer weeds, e.g., wild vetch, meadow pea, white clover, creeping buttercup, lamb's quarters, etc. To support these game birds, agrotechnical practices should alternate crop rotation patterns to increase the mosaic nature of the agricultural landscape.

CONTRIBUTION

All authors have contributed equally to the study and are equally responsible for the information published in this article.

CONFLICT OF INTEREST

The authors declare that there is no conflict of interest regarding the publication of this article.


REFERENCES

1. Stepanyan LS. Conspectus of the ornithological fauna of Russia and adjacent territories (within the borders of the USSR as a historic region). Moscow: Akademkniga; 2003. 808 p. (In Russ.).
2. *Columba palumbus*. The IUCN Red List of Threatened Species 2018. <https://doi.org/10.2305/IUCN.UK.2018-2.RLTS.T22690103A131924602.en>
3. Bostanzhoglo VN. Ornithological fauna of the Aral-Caspian steppes. Moscow: Moscow Society of Nature Explorers; 1911. 410 p. (In Russ.).
4. Khokhlov AN. Increase in wood pigeons breeding in the Stavropol Region. Proceedings of the All-union scientific and methodological meeting of zoologists of pedagogical universities. Makhachkala; 1990. P. 242–244. (In Russ.).
5. Kaledin AP, Malovichko LV, Rezanov AG, Drozdova LS. Autumn and winter diet of *Phasianus colchicus* in the Central Ciscaucasia. Food Processing: Techniques and Technology. 2022;52(1):133–143. (In Russ.). <https://doi.org/10.21603/2074-9414-2022-1-133-143>; <https://www.elibrary.ru/KJONRX>
6. Kaledin AP, Malovichko LV, Rezanov AG, Drozdova LS. Diet of the gray partridge (*Perdix perdix* L.) in the Central Ciscaucasia. Food Processing: Techniques and Technology. 2022;52(2):334–343. (In Russ.). <https://doi.org/10.21603/2074-9414-2022-2-2367>; <https://www.elibrary.ru/SGTLSY>
7. Kaledin AP, Malovichko LV, Rezanov AG, Drozdova LS, Serikbayeva AT. Quails of Stavropol Region: Autumn food habits. Food Processing: Techniques and Technology. 2024;54(1):71–81. (In Russ.). <https://doi.org/10.21603/2074-9414-2024-1-2489>; <https://www.elibrary.ru/KXVHQT>
8. Prekopov AN. The golden bee-eater in Ciscaucasia. Proceedings of the Voroshilov State Pedagogical Institute. 1940;3(2):240–442. (In Russ.).

9. Malovichko LV, Yufereva VV, Tel'pov VA, Yuferev DP. The distribution and dynamics of synanthropisation of the common wood pigeon in the Stavropol region. South of Russia: Ecology, Development. 2021;16(3):33–46. (In Russ.). <https://doi.org/10.18470/1992-1098-2021-3-33-46>; <https://www.elibrary.ru/XNACZW>
10. Bobenko OA, Khokhlov AN, Il'yukh MP. Timing and features of nesting of pigeons in the Stavropol Region. Caucasian Ornithological Bulletin. 2011;(23):9–14. (In Russ.). <https://www.elibrary.ru/XHANVZ>
11. Agriculture [Internet]. [cited 2024 Feb 23]. Available from: <https://stavregion.ru/stat/economics/agriculture>
12. Report on the state of the environment and natural resource management in the Stavropol Region in 2018. Stavropol, 2019. 140 p. (In Russ.).
13. Meklenburtsev RN. Pigeons *Columbae*, or *Columbiformes*. In: Dement'ev GP, Gladkov NA, editors. Birds of the Soviet Union. Vol. II. Moscow: Sovetskaya nauka; 1951. pp. 3–70. (In Russ.).
14. Meklenburtsev RN. Pigeon, family Columbidae. In: Matchanov NM, Sagitov AK. Birds of Uzbekistan. Vol. 2. Tashkent: Fan; 1990. pp. 182–206. (In Russ.).
15. Dolgushin IA. Order Pigeons, Columbidae. In: Gavrinn VF, Dolgushin IA, editors. Birds of Kazakhstan. Vol. 2. Alma-Ata: Nauka; 1962. pp. 328–369. (In Russ.).
16. Ptushenko ES, Inozemtsev AA. Biology and economic importance of birds in the Moscow region and adjacent territories. Moscow: Lomonosov Moscow State University; 1968. 462 p. (In Russ.).
17. Ivanov AI. Birds of the Pamir Alai. Leningrad: Nauka; 1969. 448 p. (In Russ.).
18. Kostin YuV. Birds of Crimea. Moscow: Nauka; 1983. 241 p. (In Russ.).
19. Malchevsky AS, Pukinsky YuB. Birds of the Leningrad Region and adjacent territories. Vol. 1. Leningrad: Leningrad University Publishing House; 1983. 480 p. (In Russ.).
20. Cramp S. Handbook of the birds of Europe, the Middle East and North Africa: The birds of the Western Palearctic. Vol. IV: Terns to woodpeckers. Oxford: Oxford University Press; 1986. 960 p.
21. Kotov AA. Pigeonides. In: Gavrillov EhI, Ivanchev VP, Kotov AA. Birds of Russia and adjacent regions: Pteroclididae, Columbiformes, Cuculiformes, and Strigiformes. Moscow: Nauka; 1993. P. 47–181. (In Russ.).
22. O'Huallachain D, Dunne J. Seasonal variation in the diet and food preference of the Woodpigeon *Columba palumbus* in Ireland. Bird Study. 2013;60(3):417–422. <https://doi.org/10.1080/00063657.2013.798259>
23. Astafieva TV. Characteristics of food of the wood pigeon *Columba palumbus* in the Kaliningrad oblast. The Russian Journal of Ornithology. 2015;24(1158):2231–2234. (In Russ.). <https://www.elibrary.ru/TXOPLH>
24. Gutiérrez-Galán A, González CA, de Mercado JM. Woodpigeon *Columba palumbus* diet composition in mediterranean Southern Spain. Ardeola. 2017;64(1):17–30. <https://doi.org/10.13157/arla.64.1.2017.ra2>
25. Kaouachi A, Menaa M, Rebbah AC, Maazi MC. Diet of wood pigeon (*Columba palumbus*) in forest areas of souk Ahras region (North-Eastern Algeria): Management implications. Pakistan Journal of Zoology. 2021;53(5):1919–1927. <https://doi.org/10.17582/journal.pjz/20190708150749>
26. Berezovikov NN, Kazenas VL. The Turkestan wood pigeon *Columba palumbus casiotis* feeds on the fruits of the bird cherry *Cerasus avium* in the gardens of Almaty. Russian Journal of Ornithology. 2021;30(2103):3912–3914. (In Russ.). <https://www.elibrary.ru/EJQSKC>
27. Fazekas I. First observation in Hungary: the *Columba palumbus* (Linnaeus, 1758) feeding on cherries (Aves). e-Acta Naturalia Pannonica. 2023;25:55–61. <https://doi.org/10.5281/zenodo.8056404>
28. Gorshkov PK. Columbiformes. In: Popov VA, editor. Birds of the Volga-Kama region. Non-passerines. Moscow: Nauka; 1977. P. 221–233. (In Russ.).
29. Gulay VI. Wood pigeon *Columba palumbus* (*Columbiformes*, *Columbidae*) in the anthropogenic landscape of the western forest-steppe of Ukraine. Zoological Journal. 1991;70(5):75–83. (In Russ.).
30. Prokofjeva IV. To breeding ecology of the wood pigeon *Columba palumbus*. Russian Journal of Ornithology. 2003;12(242):1245–1249. (In Russ.). <https://www.elibrary.ru/ICHXGN>
31. Rezanov AA, Rezanov AG. Rock pigeons *Columba livia* feed on berries of *Padus maackii*. Russian Journal of Ornithology. 2004;13(249):18–20. (In Russ.). <https://www.elibrary.ru/IBZCWL>
32. Rezanov AG. Feeding behavior of birds: Digital coding method and database analysis. Moscow: Izdat-shkola; 2000. 223 p. (In Russ.).
33. Andreev VA. Rock pigeons *Columba livia* eat juicy fruits of woody plants in the Arkhangelsk. Russian Journal of Ornithology. 2014;23(1063):3344–3347. (In Russ.). <https://www.elibrary.ru/SXKOGN>
34. Ladygin SI. Rock pigeons *Columba livia* eating apples of the Siberian crabapple *Malus baccata* in Gorno-Altai in winter. Russian Journal of Ornithology. 2014;23(966):408–409. (In Russ.). <https://www.elibrary.ru/RTYKLD>

35. Berezovikov NN, Rozenberg GV. The rock pigeon *Columba livia* eating fruits of the bird cherry *Padus avium* in Altai. Russian Journal of Ornithology. 2019;28(1819):4191–4193. (In Russ.). <https://www.elibrary.ru/WTQSIW>
36. Zabashta AV, Zabashta MV. Feeding of rock pigeons *Columba livia* with fruits of the common hackberry *Celtis occidentalis* in Simferopol and Rostov oblast. Russian Journal of Ornithology. 2019;29(2012):5947–5950. (In Russ.). <https://www.elibrary.ru/KIGQDH>
37. Rezanov AG. Feeding behavior of birds: Generalized method of description and ecological and geographical features. Dr. Sci. Biol. diss. Moscow; 2000. 417 p. (In Russ.).

ORCID IDs

Anatoly P. Kaledin  <https://orcid.org/0000-0002-5744-1363>
Lyubov V. Malovichko  <https://orcid.org/0000-0003-1040-2890>
Alexander G. Rezanov  <https://orcid.org/0009-0002-3433-7624>
Lyudmila S. Drozdova  <https://orcid.org/0000-0003-1150-0134>
Botagoz A. Kentbaeva  <https://orcid.org/0000-0003-0969-9754>



Synergistic interaction between *Azotobacter* and *Pseudomonas* bacteria in a growth-stimulating consortium

Yuliya R. Serazetdinova*, Darya Yu. Chekushkina, Ekaterina E. Borodina,
Daria E. Kolpakova, Varvara I. Minina, Olga G. Altshuler, Lyudmila K. Asyakina

Kemerovo State University, Kemerovo, Russia

* e-mail: serazetdinova2000@mail.ru

Received 07.05.2024; Revised 07.06.2024; Accepted 09.07.2024; Published online 02.11.2024

Abstract:

Intensifying agricultural production involves an active use of agrochemicals, which results in disrupted ecological balance and poor product quality. To address this issue, we need to introduce biologized science-intensive technologies. Bacteria belonging to the genera *Azotobacter* and *Pseudomonas* have complex growth-stimulating properties and therefore can be used as a bioproduct to increase plant productivity. We aimed to create a growth-stimulating consortium based on the strains of the genera *Azotobacter* and *Pseudomonas*, as well as to select optimal cultivation parameters that provide the best synergistic effect. We studied strains *Azotobacter chroococcum* B-4148, *Azotobacter vinelandii* B-932, and *Pseudomonas chlororaphis* subsp. *aurantiaca* B-548, which were obtained from the National Bioresource Center “All-Russian Collection of Industrial Microorganisms” of Kurchatov Institute.

All the test strains solubilized phosphates and produced ACC deaminase. They synthesized 0.98–1.33 mg/mL of gibberellic acid and produced 37.95–49.55% of siderophores. Their nitrogen-fixing capacity ranged from 49.23 to 151.22 µg/mL. The strains had high antagonistic activity against phytopathogens. In particular, *A. chroococcum* B-4148 and *A. vinelandii* B-932 inhibited the growth of *Fusarium graminearum*, *Bipolaris sorokiniana*, and *Erwinia rhapontici*, while *P. chlororaphis* subsp. *aurantiaca* B-548 exhibited antagonism against *F. graminearum* and *B. sorokiniana*. Since all the test strains were biologically compatible, they were used to create several consortia. The greatest synergistic effect was achieved by Consortium No. 6 that contained the strains B-4148, B-932, and B-548 in a ratio of 1:3:1. The optimal nutrient medium for this consortium contained 25.0 g/L of Luria-Bertani medium, 8.0 g/L molasses, 0.1 g/L magnesium sulfate heptahydrate, and 0.01 g/L of aqueous manganese sulfate. The optimal cultivation temperature was 28°C.

The microbial consortium created in our study has high potential for application in agricultural practice. Further research will focus on its effect on the growth and development of plants, in particular cereal crops, under *in vitro* conditions and in field experiments.

Keywords: Biological preparations, sustainable agriculture, growth-stimulating microorganisms, microbial consortium, biocompatibility, phytohormones, siderophores

Funding: This study was part of the state project “Studying the potential of growth-stimulating bacteria to increase the agronomic biofortification of wheat” (FZSR-2024-0009).

Please cite this article in press as: Serazetdinova YuR, Chekushkina DYu, Borodina EE, Kolpakova DE, Minina VI, Altshuler OG, *et al.* Synergistic interaction between *Azotobacter* and *Pseudomonas* bacteria in a growth-stimulating consortium. *Foods and Raw Materials*. 2025;13(2):376–393. <https://doi.org/10.21603/2308-4057-2025-2-651>

INTRODUCTION

In the context of a growing population, food security is becoming a global issue, which calls for a significant increase in agricultural productivity [1–4]. Currently, high crop yields are achieved by using mineral fertilizers, pesticides, as well as chemical and synthetic growth stimulants [5]. They can cause serious harm to the en-

vironment, natural ecosystems, and human health [6, 7]. Residues from fertilizers and other chemicals contribute to air, water, and soil pollution [8]. Intensive use of fertilizers and pesticides leads to significant changes in the physical and chemical properties of the soil. These changes include its contamination with heavy metals and radionuclides, changes in pH, nutrient imbalance,

and soil compaction [9, 10]. Massah and Azadegan found that the long-term application of fertilizers based on nitrogen, phosphorus, and potassium compacted the soil layer [11]. This decreased its porosity, water permeability, and nutrient availability and therefore harmed the growth and development of wheat.

Moreover, the long-term supply of residual nitrogen, phosphorus, and sulfur compounds into the terrestrial ecosystem radically changes the composition and functions of its microbiota. Residues of nutrients in the soil can contribute to the extinction of some species and serve as a selective advantage for others [12]. For example, numerous studies have established a negative correlation between the number of diazotrophic microorganisms and intensive application of nitrogen fertilizers [13–15]. In the long term, this will significantly decrease the efficiency of biological nitrogen fixation and increase the soil's need for additional mineral fertilizers.

Chemical plant protection products have a negative impact on the diversity and number of soil microorganisms, as well as the enzymatic activity of soils [16]. For example, pesticide-treated soil showed decreased abundance and diversity of both fungal and bacterial communities. Moreover, the use of fungicides disturbed the processes of ammonification and nitrification [17]. In other studies, the fungicides benomyl, mancozeb, and tridemorph inhibited the soil enzymatic activity of dehydrogenase, urease, and phosphatase, while captan, trifloxystrobin, and thiram reduced the activity of phosphomonoesterase and urease [18–20].

The ability of agrochemicals to accumulate poses a particular danger. Vegetables, fruits, and grains growing in contaminated agricultural soils accumulate pesticides in their edible and inedible parts at concentrations that are high enough to cause serious health problems in animals and humans [21]. Although acute pesticide poisoning is now virtually unheard of, the long-term consequences of pesticide treatment remain a serious social problem. In particular, chronic toxicity caused by long-term exposure to low doses of pesticides can contribute to diseases such as cancer, asthma, dermatitis, endocrine disorders, reproductive dysfunctions, neurobehavioral disorders, and birth defects [22, 23]. Innovative technological solutions are needed to reduce the environmental load of modern agriculture, as well as ensure high-quality and safe production. Such technologies should aim at transitioning to more sustainable management of soil fertility [24]. Therefore, the development of biological preparations is currently on the rise [25, 26]. Rhizobacteria are a key component of such bioproducts. These microbial inoculants, or biofertilizers, can stimulate plant growth and increase the availability of nutrients. As a result, they reduce the use of chemical fertilizers and minimize their negative impact on the environment [27]. Modern research shows significant potential for the use of rhizobacteria as biological fertilizers for a wide range of agricultural crops [28]. The most important of them are those belonging to the genera *Azotobacter* and *Pseudomonas*.

Azotobacter is a genus of Gram-negative, non-symbiotic nitrogen-fixing aerobic soil bacteria, also known as azotobacteria. Having an oval or spherical shape, they can also form thick-walled cysts, which are dormant cells resistant to adverse environmental conditions. The genus includes about six species, some of which are motile due to the presence of peritrichous flagella, while others are nonmotile. Azotobacteria are known to use atmospheric nitrogen to synthesize cellular protein, which is mineralized in the soil, supplying nitrogen to crops. These bacteria are highly sensitive to environmental pH, high salt concentration, and temperature [29]. Therefore, these cultivation parameters need to be carefully selected to produce azotobacteria on an industrial scale.

Azotobacteria have a beneficial effect on the growth and productivity of agricultural crops. In particular, they synthesize bioactive and growth-stimulating substances, increase the microbial diversity of the rhizosphere, inhibit phytopathogens, improve the availability of nutrients, and enhance biological nitrogen fixation [30]. For example, *Azotobacter chroococcum* improves plant nutrition and increases soil fertility [31]. Other strains of the genus *Azotobacter* can produce amino acids when cultivated on a medium supplemented with various sources of carbon and nitrogen. Azotobacteria can also convert atmospheric nitrogen into ammonia to be absorbed by plants [32]. In addition, these bacteria are highly resistant to oxygen, which is especially important for nitrogen fixation in non-legume crops [33].

Nitrogen fixation plays a very important role in nitrogen homeostasis in the biosphere [34]. Biological nitrogen fixation also helps maintain soil fertility and increase crop yields. According to current research, azotobacteria annually fix about 20 kg of nitrogen per hectare. Therefore, they are successfully used in crop production as an alternative to mineral nitrogen fertilizers [35]. Crops treated with *Azotobacter* strains have been found to need smaller amounts of nitrogen fertilizers. For example, Felipe Romero-Perdomo *et al.* reported that the use of multiple *Azotobacter* strains nearly halved the need for nitrogen fertilizers [35]. Azotobacteria have a direct effect on plant growth by synthesizing plant growth hormones (e.g., auxins, gibberellins, and cytokinins). These hormones not only enhance plant growth and nutrient uptake, but also indirectly protect host plants from phytopathogens, as well as stimulate the development of other beneficial rhizosphere microorganisms [36, 37].

Azotobacteria can efficiently absorb iron from the environment by synthesizing siderophores, low-molecular-weight chelating agents with high affinity for Fe^{3+} ions [38]. Also, they can actively extract sparingly soluble iron salts from the environment by forming an iron-siderophore complex to be absorbed by membrane-bound receptors [39]. Since iron-siderophore complexes cannot be absorbed by other microorganisms, they give *Azotobacter* strains a competitive advantage. In addition, they protect plants from phytopathogens by limiting the availability of iron [39].

Since azotobacteria do not interact with plants symbiotically, they need to be used jointly with other microorganisms for maximum plant productivity. Numerous studies have shown that *Azotobacter* strains increase the activity of other growth-promoting microorganisms in the consortium, such as bacteria of the genus *Pseudomonas* [40, 41]. These rod-shaped, Gram-negative γ -proteobacteria with polar flagella have an extensive habitat [42]. Currently, the genus *Pseudomonas* includes over 100 species, many of which are widely used in biotechnology, biocontrol of phytopathogens, bioremediation, and plant growth stimulation [43, 44].

Pseudomonas bacteria are actively used as an inoculant for agricultural crops. Colonizing the surface and internal tissues of roots and stems, they are able to survive in various ecological niches thanks to highly developed adaptation mechanisms [44]. *Pseudomonas* bacteria promote plant growth by synthesizing ACC deaminase, increasing the availability of nutrients, and enhancing antioxidant activity [45]. Recent advances in the field of biofertilizers have led to the discovery of new strains with high phosphate-solubilizing activity. These include *Pseudomonas plecoglossicida*, a microorganism isolated from the rhizosphere of soybeans. This species can solubilize up to 75.39 mg/L of phosphate. In addition, it can accelerate plant growth by synthesizing an important plant phytohormone, indolyl-3-acetic acid (38.89 ppm) [46]. Another strain, *Pseudomonas* sp. PSB12, had the maximum phosphate solubilization index of 3.86 on Pikovskaya's agar medium. According to Weimin Chen *et al.*, this was mainly due to the synthesis of organic acids [47]. In another study, the presoaking treatment of wheat seeds with phosphate-solubilizing and auxin-producing bacterium *Pseudomonas extremaustralis* IB-Ki-13-1A led to significantly higher yields [48].

In addition, *Pseudomonas* bacteria actively secrete phytohormones and volatile organic compounds [45, 49, 50]. Among them are auxins, phytohormones that stimulate cell division, elongation, and differentiation (particularly, indolyl-3-acetic acid) [51, 52]. *Pseudomonas mendocina* and *Pseudomonas alcaliphila* are auxin-synthesizing strains that stimulate seed germination and increase wheat yield, contributing to longer shoots, roots and ears, as well as higher seed weight [53]. In addition, the plants treated with the strains synthesizing indolyl-3-acetic acid show significant changes in the root system [54]. *Pseudomonas* bacteria also produce cytokinins, phytohormones that stimulate the division of plant cells and seed germination, activate the growth of dormant buds, and increase cell resistance to various unfavorable factors [55, 56]. *Pseudomonas* strains with complex phytohormonal activity include *Pseudomonas stutzeri* MTP40, *Pseudomonas putida* MTP50, and *P. putida* UKM B-398, which secrete indolyl-3-acetic acid, cytokinins, and gibberellins [57].

Pseudomonas species are widely studied to be used in biological control of phytopathogens. They synthesize various antimicrobial substances, including phenazine-1-

carboxamide, ampicillin, tensin, viscosin, massetolide, 2,4-diacetylphloroglucinol, pyrrolnitrin, pyoluteorin, and phenazine-1-carboxylic acid [43]. *Pseudomonas* strains are useful in controlling a number of diseases caused by fungal phytopathogens, including *Pythium* spp., *Fusarium solani*, *Rhizoctonia solani*, and *Phytophthora nicotianae* [58–61]. A partially purified siderophore obtained from the strain *Pseudomonas* JAS-25 completely inhibited the spores of *Fusarium oxysporum* f. sp. *ciceri*, *Fusarium udum*, and *Aspergillus niger*, which destroyed the mycelial hyphae of phytopathogens [62]. Similarly, hydrogen cyanide obtained from *Pseudomonas* strains exhibited bacteriostatic and antifungal effects against phytopathogenic fungi [63]. In particular, hydrogen cyanide derived from *Pseudomonas aeruginosa* (LES4) inhibited *Fusarium oxysporum* f. sp. *radicis-lycopersici* in tomatoes [64]. In addition, *Pseudomonas* bacteria inhibit phytopathogens by competing for nutrients, inducing systemic resistance, producing siderophores, as well as synthesizing enzymes that destroy the cell wall (β -1,3-glucanase, chitinases, cellulases, proteases, etc.) [65]. For example, cyclolipopeptide orphamide induces systemic resistance in rice due to the expression of genes that protect it from the fungal phytopathogen *Cochliobolus miyabeanus* [66]. The siderophore pyoverdine produced by *P. putida* WCS358 induces systemic resistance in eucalyptus to prevent its bacterial wilt caused by *Ralstonia solanacearum* by [67].

Thus, the combined use of *Pseudomonas* and *Azotobacter* bacteria is an effective and environmentally friendly strategy for increasing productivity and sustainability of agricultural production. In addition, using consortia of growth-promoting microorganisms is more effective than using single strains. This is because bacteria naturally exist in taxonomically and metabolically diverse communities, rather than as monocultures of genetically identical strains [68, 69]. Genotypically diverse microbial communities are generally more resilient to various stresses than monocultures. They are also more competitive in the environment, which prevents the development of foreign strains. Further, polymicrobial communities distribute available resources more efficiently than individual genotypes [70]. As a result, they fill all the niches in the environment, preventing the invasion of extraneous microbiota [71]. Finally, diverse microbial communities are more resilient to changes in the abiotic environment, such as oxygen availability or pH levels, than isogenic cultures [72]. All these factors make consortia a promising strategy in agriculture.

There are two ways of creating microbial consortia: bottom-up and top-down. In the first approach, strains with specially selected functions are introduced into the nutrient medium to form an artificial microbial consortium. This approach has been proven to ensure mutually beneficial cooperation between the strains, with an evenly distributed load among them in the system [73]. The second approach is to isolate an already existing microbial consortium from the natural environment and ensure its functioning in a stable system. This method

has a significant drawback since natural microbial consortia have extremely complex compositions, with bacteria having both positive and negative effects on each other [74]. This can make their combined use quite difficult. Therefore, we chose the bottom-up approach for this study. In particular, we aimed to create a growth-stimulating consortium based on bacteria of the genera *Azotobacter* and *Pseudomonas*, as well as to select cultivation parameters that provide the best synergistic effect. The novelty of our research lies in our attempt to develop and optimize the biotechnological process of co-cultivating industrially significant strains available on the domestic market, as well as in the search for technological approaches to ensure maximum biological activity of the constructed consortia.

STUDY OBJECTS AND METHODS

The bacterial strains for this study were obtained from the National Bioresource Center “All-Russian Collection of Industrial Microorganisms” of Kurchatov Institute. They included:

- *Azotobacter chroococcum* B-4148 obtained from a spontaneous mutation of Rif-r and able to fix atmospheric nitrogen;
- *Azotobacter vinelandii* B-932 capable of fixing atmospheric nitrogen; and
- *Pseudomonas chlororaphis* subsp. *aurantiaca* B-548 isolated from *Zea mays*.

Analysis of cultural and morphological characteristics. To study the cultural characteristics of the strains, a low-concentration suspension of microorganisms was inoculated onto meat-peptone agar by the streaking method and cultivated for 18 h at $28 \pm 2^\circ\text{C}$ [75].

The morphological characteristics were examined using an AxioScope A1 upright microscope (Carl Zeiss, Germany) at a total magnification of 1000 \times . A fixed smear of microorganisms was stained using the Gram method [76].

Analysis of growth-stimulating properties and antagonistic activity. Solubilization of phosphates. The test strains were cultivated at $28 \pm 2^\circ\text{C}$ for 4 days on a medium containing (g/L) 5.0 calcium phosphate ($\text{Ca}_3(\text{PO}_4)_2$) (LenReaktiv, Russia), 20.0 glucose (Chem-ex, Russia), 0.2 sodium chloride (NaCl) (LenReaktiv, Russia), 0.1 magnesium sulfate heptahydrate ($\text{MgSO}_4 \times 7\text{H}_2\text{O}$) (Chem-Express, Russia), 0.01 aqueous manganese sulfate ($\text{MnSO}_4 \times \text{H}_2\text{O}$) (Khimplex, Russia), 0.01 iron II sulfate heptahydrate ($\text{FeSO}_4 \times 7\text{H}_2\text{O}$) (LenReaktiv, Russia), and 15.0 bacterial agar (Himmag, Russia). The growth of bacterial culture on Petri dishes indicated the strain's ability to solubilize phosphates [77].

Production of ACC deaminase. The test strains were cultivated on a medium containing (g/L) 2.0 ammonium sulfate ($(\text{NH}_4)_2\text{SO}_4$) (LenReaktiv, Russia), 4.0 monosubstituted potassium phosphate (KH_2PO_4) (ProfSnab, Russia), 6.0 sodium phosphate disubstituted dihydrate ($\text{Na}_2\text{HPO}_4 \times 2\text{H}_2\text{O}$) (Chem-ex, Russia), 0.2 magnesium sulfate heptahydrate, 0.001 iron II sulfate heptahydrate, and 15.0 bacterial agar. The medium also contained 1 mL

of the following solutions: 16 μM boric acid (H_3BO_3) (LenReaktiv, Russia), 66 μM aqueous manganese sulfate, 433 μM zinc sulfate heptahydrate ($\text{ZnSO}_4 \times 7\text{H}_2\text{O}$) (LenReaktiv, Russia), and 313 μM copper sulfate pentahydrate ($\text{CuSO}_4 \times 5\text{H}_2\text{O}$) (LenReaktiv, Russia). The growth of bacterial culture on Petri dishes indicated the strain's ability to produce ACC deaminase [77].

Gibberellic acid. A bacterial suspension of the test strains was prepared on a Luria-Bertani liquid nutrient medium modified by Miller (LB) (Biolight, Russia) to a McFarland optical density of 0.8–1.0 using a Densichek plus densitometer (BioMerieux, France). After that, the suspension (1%) was added to the LB nutrient medium and cultivated in an LSI-3016R shaker-incubator (Daihan Labtech, South Korea) at $28 \pm 2^\circ\text{C}$ and 120 rpm for 24 h. The resulting culture liquid was centrifuged for 15 min at 7500 rpm. Then, 280 mL of a 1 M solution of zinc acetate dihydrate ($\text{Zn}(\text{CH}_3\text{COO})_2 \times 2\text{H}_2\text{O}$) (ProfSnab, Russia) and a 10.6% solution of potassium ferrocyanide III ($\text{K}_3[\text{Fe}(\text{CN})_6]$) (LenReaktiv, Russia) were added to 2 mL of the cell-free culture liquid, quickly mixed and centrifuged at 4500 rpm for 10 min. The resulting supernatant liquid was mixed with 30% hydrochloric acid (HCl) (LenReaktiv, Russia) in a 1:1 ratio and kept for 75 min at $22 \pm 2^\circ\text{C}$. The optical density of the samples was determined in relation to 5% hydrochloric acid using a UV 1800 spectrophotometer (Shimadzu, Japan) at 254 nm. The synthesized gibberellic acid was quantified using a calibration graph of a standard solution of gibberellic acid (Diaem, Russia) in the range from 100 to 700 $\mu\text{g/mL}$ [78].

Production of siderophores. For this, 1 mL of the cell-free culture liquid obtained as described above was mixed with 1 mL of freshly prepared Chorme Azurol S reagent (1.5 mL of a 0.016% solution of iron III chloride hexahydrate ($\text{FeCl}_3 \times 6\text{H}_2\text{O}$) (LenReaktiv, Russia) in a 10 M solution of hydrochloric acid was mixed with 7.5 mL of a 1.21% solution of chromazurol S (Chem-ex, Russia) and then distilled water was added to 100 mL). The resulting solution was kept for 20 min at $22 \pm 2^\circ\text{C}$. The optical density was determined spectrophotometrically at a wavelength of 630 nm. Meanwhile, a control experiment was carried out under the same conditions, with a nutrient medium used as a control. The concentration of siderophores was determined using Eq. [79]:

$$C_{\text{sid}} = \frac{A_s - A_k}{A_k} \times 100$$

where C_{sid} is the concentration of siderophores, %; A_s is the optical density of the test sample; A_k is the optical density of the control sample.

Nitrogen fixation. A bacterial suspension was prepared as described above using a liquid nutrient medium containing (g/L) 20.0 sucrose (LenReaktiv, Russia), 5.0 magnesium sulfate heptahydrate, 1.0 potassium phosphate disubstituted trihydrate ($\text{K}_2\text{HPO}_4 \times 3\text{H}_2\text{O}$) (Chem-ex, Russia), 0.005 sodium molybdate dihydrate ($\text{Na}_2\text{MoO}_4 \times 2\text{H}_2\text{O}$) (LenReaktiv, Russia), 5.0 sodium chloride, 0.01 iron II sulfate heptahydrate, and 2.0 calcium

carbonate (CaCO_3) (LenReaktiv, Russia) [80]. The cultivation was carried out at $28 \pm 2^\circ\text{C}$ and 110 rpm for 48 h. The cells were separated from the culture liquid as described above. The amount of nitrogen in the cell-free culture liquid was determined using a Rapid N Cube nitrogen analyzer (Elementar, Germany) [81].

To determine the bacterial strains' **antagonistic activity**, the phytopathogens *Fusarium graminearum* F-877, *Bipolaris sorokiniana* F-529, and *Erwinia rhapontici* B-9292 were obtained from the National Bioresource Center "All-Russian Collection of Industrial Microorganisms" of Kurchatov Institute. The phytopathogenic fungi and bacteria were cultivated in a test tube with potato-glucose agar and HMF agar, respectively. A daily culture of the test bacteria, which were grown on a liquid Luria-Bertani nutrient medium modified by Miller, was inoculated into Petri dishes on an agar medium using the deep method and incubated for 24 h at $28\text{--}30^\circ\text{C}$. Then, an agar block with the test culture was cut out and inserted into the well of an agar disk of another Petri dish with phytopathogens inoculated superficially using swabs from agar slants. The suspension with a McFarland turbidity of 0.8 (1.5×10^8 CFU/cm³) was inoculated by the lawn method. The Petri dishes were refrigerated for 8 h at 4°C for the diffusion of metabolites of bacterial monocultures from the block into the agar with the test culture. Then, phytopathogenic fungi were incubated in a thermostat at $26\text{--}28^\circ\text{C}$ [82].

Creating a microbial consortium. The **biocompatibility** of the test strains was analyzed by the well method. For this, bacterial suspensions were prepared as described above for gibberellic acid analysis. The test culture was applied with a Drigalski spatula to the surface of a Petri dish with LB agar medium using the spread plate method. Then, a 5-mm well was made for the cell-free culture liquid of the test culture to be cultivated for 24 h at $28 \pm 2^\circ\text{C}$. The cultures were considered biocompatible if there was no inhibition of the test culture growth around the well [83].

Creating a consortium. For this, bacterial suspensions were prepared as described above for gibberellic acid analysis. Next, a certain number of microorganisms (depending on the composition and ratio) were applied to the sterile LB nutrient medium and cultivated under the conditions mentioned above. The supernatant was obtained by the previously described method.

The consortia were analyzed for their ability to produce **gibberellic acid and siderophores**, as well as for their **antagonistic activity** against phytopathogenic microorganisms using the methods described earlier.

Selecting consortium cultivation conditions. The **optimal temperature** for consortium cultivation was determined using an RTS-8 plus personal multichannel bioreactor with non-invasive measurement of optical density in real time (Biosan, Latvia) at temperatures of 20, 24, 28, 32, 35, and 45°C . To cultivate a consortium, 3% of the inoculant composed of the bacterial suspensions in a certain ratio was added to the LB medium.

The **nutrient medium base** was selected from the following options:

- LB (control), 25 g/L;
- GMF broth, 30 g/L (Agat-Med, Russia);
- BTN broth, 30 g/L (Khimmedservis, Russia);
- tryptone-soy broth with yeast extract, 40 g/L (Germeon, Russia); and
- GRM broth, 20 g/L (Chem-ex, Russia)

The bacterial suspensions introduced into the consortium amounted to 3% of the nutrient medium. They were cultivated at the optimal temperature selected at the previous stage.

The **carbon source** was selected from the following options:

- Previously selected base (Control);
- Base + 4.0 g/L sucrose;
- Base + 4.0 g/L glucose;
- Base + 4.0 g/L molasses (Khimiya-express, Russia);
- Base + 8.0 g/L sucrose;
- Base + 8.0 g/L glucose; and
- Base + 8.0 g/L molasses.

The cultivation was carried out under the conditions described above.

The **mineral component** was selected from the following options:

- Control: selected base + selected carbon source;
- Medium No. 1: base + carbon source + 0.1 g/L magnesium sulfate heptahydrate;
- Medium No. 2: base + carbon source + 0.01 g/L aqueous manganese sulfate;
- Medium No. 3: base + carbon source + 0.1 g/L magnesium sulfate heptahydrate + 0.01 g/L aqueous manganese sulfate;
- Medium No. 4: base + carbon source + 0.2 g/L magnesium sulfate heptahydrate;
- Medium No. 5: base + carbon source + 0.02 g/L aqueous manganese sulfate; and
- Medium No. 6: base + carbon source + 0.2 g/L magnesium sulfate heptahydrate + 0.02 g/L aqueous manganese sulfate.

The cultivation was carried out under the conditions described above.

RESULTS AND DISCUSSION

Cultural and morphological characteristics of the strains. Figure 1 shows the cultural characteristics of the test strains. As can be seen, *Azotobacter chroococcum* B-4148, *Azotobacter vinelandii* B-932, and *Pseudomonas chlororaphis* subsp. *aurantiaca* formed 2–3, 3–4, and 1–2 mm round colonies, respectively. All the colonies had a smooth edge and a convex profile. Their color was beige, turning light brown as the culture aged.

Figure 2 shows the morphological characteristics of the test strains.

As can be seen, *A. chroococcum* B-4148 cells were Gram-negative coccobacilli, while the cells of *A. vinelandii* B-932 were Gram-negative, oval in shape, located singly or in pairs, and able to form cysts. The cells

of *P. chlororaphis* subsp. *aurantiaca* were Gram-negative and rod-shaped.

Growth-stimulating properties of the strains. The growth-stimulating activity of the test microorganisms is presented in Table 1.

As can be seen, all the test strains were able to solubilize phosphates and produce ACC deaminase. The amount of gibberellic acid they produced varied from 0.98 to 1.33 mg/mL, while the amount of siderophores ranged from 37.95 to 49.55%. The amount of nitrogen fixed by *A. chroococcum* B-4148, *A. vinelandii* B-932, and *P. chlororaphis* subsp. *aurantiaca* B-548 reached 151.22, 117.53, and 49.23 µg/mL, respectively.

Our results were consistent with those obtained by other scientists. For example, Biello *et al.* found the ability for nitrogen fixation and phosphate solubilization in *A. chroococcum* NCIMB 8003 [84]. In the study by Alsalam, *A. chroococcum* demonstrated the ability to fix atmospheric nitrogen, solubilize phosphates, and synthesize siderophores and indolylacetic acid [85]. In another

study, the isolates of *A. chroococcum* obtained from the rhizosphere of agricultural crops exhibited phosphate-solubilizing activity and produced indolylacetic acid, which changed the root architecture and increased the productivity of wheat [86]. *A. chroococcum* isolated from agricultural soils in China also showed the ability to synthesize indolylacetic acid and transform insoluble forms of phosphorus [87]. Kerečki *et al.* reported the ability of this species to produce ACC deaminase and synthesize indolyl-3-acetic acid [88]. However, the ability of *A. chroococcum* strains to produce gibberellins has been studied much less and is poorly covered in modern literature [89]. Therefore, our data expands the information about their growth-promoting mechanisms.

The growth-promoting activity of *A. vinelandii* has been confirmed by other modern studies. For example, *A. vinelandii* Khsr1 isolated from the rhizosphere of *Chrysopogon aucheri* had the ability to synthesize a number of phytohormones, including indolyl-3-acetic, gibberellic, and abscisic acids [90]. McRose *et al.* reported the

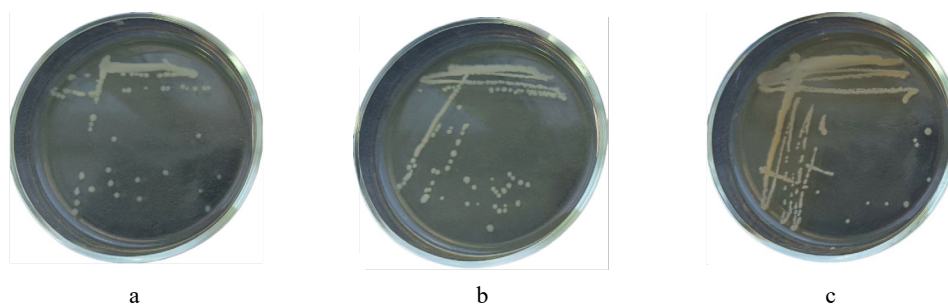


Figure 1 Cultural characteristics of the strains after 24 h of cultivation on meat-peptone agar (MPA): a – *Azotobacter chroococcum* B-4148; b – *Azotobacter vinelandii* B-932; c – *Pseudomonas chlororaphis* subsp. *aurantiaca* B-548

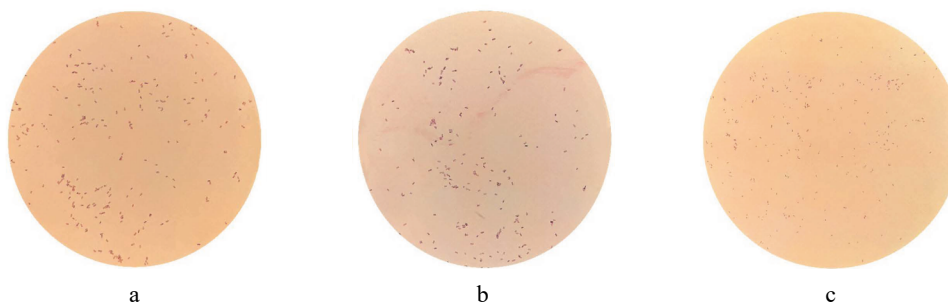


Figure 2 Morphological characteristics of the strains stained by the Gram method (1000×): a – *Azotobacter chroococcum* B-4148; b – *Azotobacter vinelandii* B-932; c – *Pseudomonas chlororaphis* subsp. *aurantiaca* B-548

Table 1 Growth-stimulating properties of the bacterial strains

Indicator	Strain		
	<i>Azotobacter chroococcum</i> B-4148	<i>Azotobacter vinelandii</i> B-932	<i>Pseudomonas chlororaphis</i> subsp. <i>Aurantiaca</i> B-548
Phosphate solubilization	+	+	+
ACC deaminase	+	+	+
Gibberellic acid, mg/mL	0.98 ± 0.03	1.30 ± 0.04	1.33 ± 0.04
Siderophores, %	47.77 ± 2.10	37.95 ± 1.53	49.55 ± 2.06
Nitrogen fixation, µg/mL	151.22 ± 6.23	160.64 ± 6.85	49.23 ± 2.13

strain's ability to produce siderophores under the conditions of iron deficiency [91]. They also noted that this ability reduced under the conditions of molybdenum and vanadium deficiency. Since these trace elements are part of nitrogenases, their deficiency may also limit the strain's nitrogen-fixing ability [92]. In another study, *A. vinelandii* AV7 isolated from the tomato rhizosphere produced indolylacetic acid and siderophores, as well as actively solubilized insoluble phosphates, increasing the plant's dry weight [93]. Shuvro *et al.* also reported this strain's ability to synthesize phytohormones and siderophores, as well as solubilize phosphates [94]. However, its ability to produce ACC deaminase has not been previously reported in literature, although our study showed the presence of this enzyme in the microorganism. Since ACC deaminase is involved in the metabolism of 1-aminocyclopropane-1-carboxylic acid (ACC), a precursor of ethylene in plants, it is an important factor in the plant's response to stress. Our data expands the understanding of the growth-promoting activity of *A. vinelandii*, since ethylene is a hormone that inhibits plant

growth under abiotic stress. Thus, the strain's ACC deaminase activity may contribute to the plant's tolerance to unfavorable environmental factors.

The growth-promoting properties of *P. chlororaphis* subsp. *aurantiaca* were confirmed by a study of Rosas, who established the SR1 strain's ability to produce indolyl-3-acetic acid, hydrogen cyanide, and siderophores [95]. This strain has been reported to stimulate the growth of various crops such as alfalfa, wheat, soybeans, corn, and sugar cane, as well as to improve seed germination. Shi *et al.*, who studied another strain, SPS-41, reported its ability to produce indolyl-3-acetic acid and siderophores, as well as to solubilize phosphates [96].

Our next stage was to assess the antagonistic activity of the test bacteria against the most common fungal and bacterial phytopathogens, namely *Fusarium graminearum* F-877, *Bipolaris sorokiniana* F-529, and *Erwinia rhapontici* B-9292 (Fig. 3 and Table 2).

We found that all the studied strains exhibited antagonistic activity against the phytopathogens. *P. chlororaphis* subsp. *aurantiaca* B-548 had the greatest inhibitory

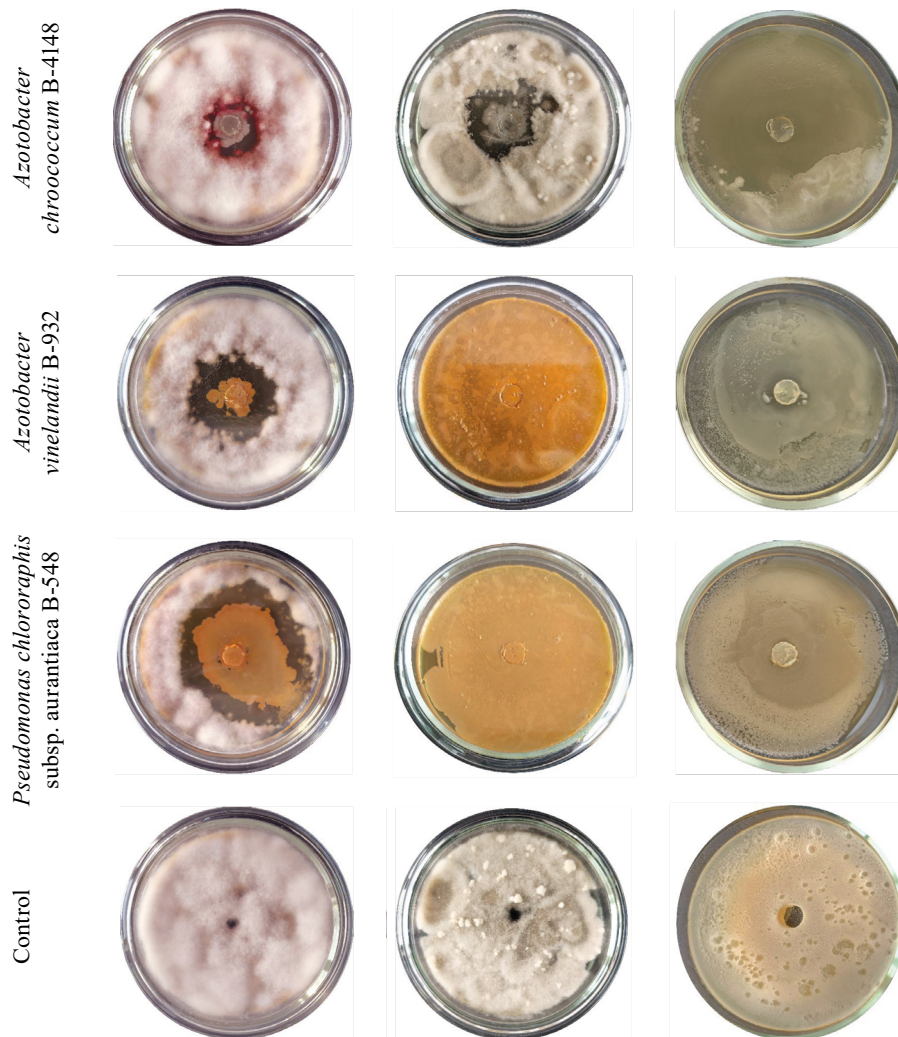


Figure 3 Antagonistic activity of the test strains: a – against *Fusarium graminearum* F-877, b – against *Bipolaris sorokiniana* F-529, c – against *Erwinia rhapontici* B-9292

Table 2 Antagonistic activity of the test bacterial strains

Strain	Phytopathogen inhibition zone, cm		
	<i>Fusarium graminearum</i> F-877	<i>Bipolaris sorokiniana</i> F-529	<i>Erwinia rhapontici</i> B-9292
<i>Azotobacter chroococcum</i> B-4148	2.55 ± 0.01	3.75 ± 0.02	7.50 ± 0.02
<i>Azotobacter vinelandii</i> B-932	4.25 ± 0.02	9.50 ± 0.03	2.00 ± 0.02
<i>Pseudomonas chlororaphis</i> subsp. <i>aurantiaca</i> B-548	6.25 ± 0.02	9.50 ± 0.03	–

Table 3 Consortia of the test strains

Consortium	Strain		
	<i>Azotobacter chroococcum</i> B-4148	<i>Azotobacter vinelandii</i> B-932	<i>Pseudomonas chlororaphis</i> subsp. <i>aurantiaca</i> B-548
No. 1	1	1	1
No. 2	2	1	1
No. 3	1	2	1
No. 4	1	1	2
No. 5	3	1	1
No. 6	1	3	1
No. 7	1	1	3

effect against *F. graminearum* (inhibition zone 6.25 cm) and *B. sorokiniana* (inhibition zone 9.50 cm). However, the strain showed no inhibitory effect against *E. rhapontici*. This may indicate mainly fungicidal properties of its metabolites. *A. vinelandii* showed the highest antagonistic activity against *B. sorokiniana* (inhibition zone 9.50 cm) but weak antibiotic properties against *E. rhapontici* (inhibition zone 2.50 cm). *A. chroococcum* exhibited the greatest inhibitory activity against this bacterial pathogen (inhibition zone 7.50 cm).

The strains' antibacterial and fungicidal properties can be confirmed by other modern studies. *A. chroococcum* is known to successfully suppress root rot [97]. In particular, Muslim *et al.* demonstrated the strain's ability to reduce the severity of tomato *Fusarium* wilt caused by the fungus *Fusarium solani* by more than 70% under greenhouse conditions [98]. Alsudani and Raheem also noted *A. chroococcum*'s ability to inhibit the growth of *F. solani*. The authors also reported its antagonistic activity against another phytopathogen, *Rhizoctonia solani* [99]. Pattaeva *et al.* reported that *A. chroococcum* strains N20, XH2018, and XU1 could synthesize a number of metabolites with fungicidal properties and suppress the growth of *Fusarium oxysporum* f. sp. *vasinfectum* [100].

The antagonistic properties of *A. vinelandii* have also been widely covered in modern literature. For example, Chuiko found that the soil isolate *A. vinelandii* IMV B-7076 exhibited antagonistic properties against a number of phytopathogens, including *Alternaria alternata* 16861, *Fusarium avenaceum* 50720, *Fusarium verticillioides* 50463, *Fusarium lactis* 50719, *Fusarium oxysporum* 54201, *Fusarium poae* 50704, and *F. solani* [101]. Bolaños-Dircio *et al.* also reported the strain's strong fungicidal properties. In particular, the authors showed that the cysts of this microorganism successfully sup-

pressed the growth of *Fusarium brachygibbosum*, *Aspergillus niger*, and *Colletotrichum gloeosporioides* [102]. Since, there has been much less research into the antibacterial activity of *A. vinelandii*, our data on its suppression of *E. rhapontici* open up new possibilities for using the strain to control plant diseases.

Modern studies confirm the ability of *P. chlororaphis* subsp. *aurantiaca* to inhibit the growth of phytopathogenic microorganisms. For example, *Pseudomonas chromoraphis* subsp. *aurantiaca* soja Q16 was reported to produce antibiotic substances that prevented the development of *F. oxysporum* and thus significantly improved potato growth [103]. Tagele *et al.* found that the KNU17Pc1 strain was capable of producing two types of phenazine derivatives and other antimicrobial substances. Due to this, the strain inhibited the growth of *Colletotrichum dematium*, *C. gloeosporioides*, *Fusarium oxysporum* f. sp. *melonis*, *Fusarium subglutinans*, and *Stemphylium lycopersici* [104]. *Pseudomonas chromoraphis* subsp. *aureofaciens* M71, which was studied by Raio *et al.*, produced phenazine-1-carboxylic acid and successfully reduced the development of cancer caused by *Seiridium cardinale* in *Chamaecyparis pisi-fera* Endl [105]. Volatile organic compounds emitted by *P. chromoraphis* subsp. *aureofaciens* SPS-41 successfully inhibited the growth of *Ceratocystis fimbriata* [106].

Creating microbial consortia. All the bacterial strains under study were biocompatible. Their ratios in the consortia are presented in Table 3.

We analyzed the ability of the bacterial consortia to produce gibberellic acid and siderophores (Table 4).

As can be seen, the amount of gibberellic acid varied from 1.23 to 1.44 mg/mL, while that of siderophores ranged from 48.21 to 54.46%. Consortia No. 1, 2, and 3 exhibited lower activity compared to the individual strains. Consortium No. 4 synthesized less gibberellic acid than the strains it was made of. Consortium No. 6 showed the greatest activity, producing 1.44 mg/mL of gibberellic acid and 54.46% of siderophores – 1.17 and 1.30 times as much, respectively, compared to the bacterial strains it contained.

Then, we analyzed the antagonistic activity of the consortia (Table 5).

As can be seen, Consortium No. 6 showed the greatest antagonistic activity against *F. graminearum* F-877 (inhibition zone 7.35 cm, averaging 4.31 cm for individual strains), *B. sorokiniana* F-529 (9.50 cm, averaging 8.35 cm for individual strains), and *E. rhapontici* B-9292 (8.10 cm, averaging 2.70 cm for individual strains). Consortium No. 1 had the lowest activity. Thus, based on

Table 4 The ability of bacterial consortia to produce gibberellic acid and siderophores

Consortium	Gibberellic acid, mg/mL		Siderophores, %	
	Amount	Average for strains	Amount	Average for strains
No. 1	1.23 ± 0.02	1.20	48.21 ± 1.33	45.09
No. 2	1.28 ± 0.02	1.15	48.66 ± 1.20	45.76
No. 3	1.39 ± 0.03	1.23	52.68 ± 1.75	43.31
No. 4	1.20 ± 0.02	1.24	50.45 ± 1.51	46.21
No. 5	1.34 ± 0.03	1.11	49.55 ± 1.49	46.16
No. 6	1.44 ± 0.03	1.24	54.46 ± 1.41	42.23
No. 7	1.32 ± 0.03	1.25	48.66 ± 1.30	46.87

the results, we selected Consortium No. 6 (*A. chroococcum* B-4148, *A. vinelandii* B-932, and *P. chlororaphis* subsp. *aurantiaca* B-548 in a ratio of 1:3:1) for further experiments.

Selecting cultivation parameters. Figure 4 presents the selection of the optimal cultivation temperature for Consortium No. 6.

At 20°C, the exponential phase on the LB nutrient medium began after 9 h of cultivation (optical density 0.33) and the stationary phase began after 22 h (optical density 2.70), with an optical density of 2.91 after 24 h. At 24°C, the exponential phase was observed after 6 h of cultivation (optical density 0.14) and the stationary phase, after 21 h (optical density 2.50), with an optical density of 2.67 after 24 h. At 28°C, the exponential phase started after 4 h of cultivation (optical density 0.10), with an optical density of 3.68 after 24 h. At 32°C, the exponential phase began after 4 h of cultivation (optical density 0.35), while the stationary phase began after 21 h (optical density 3.56), with an optical density of 3.63 after 24 h. At 35°C, the exponential phase was observed after 4 h of cultivation (optical density 0.46), while the stationary phase was noted after 18 h (optical density 2.67), with an optical density of 2.91 after 24 h. At 40°C, the exponential phase began after 4 h of cultivation

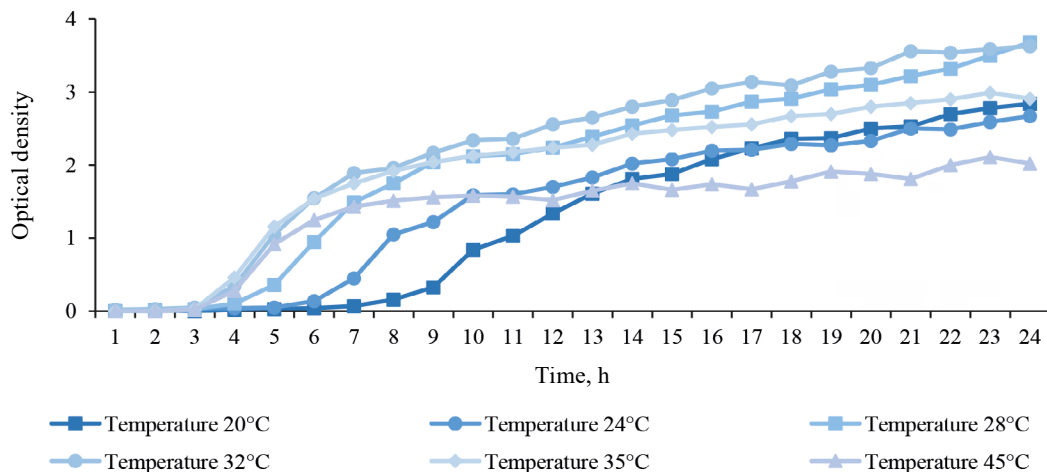
Table 5 The antagonistic activity of bacterial consortia against phytopathogens

Consortium	Phytopathogens		
	<i>Fusarium graminearum</i> F-877	<i>Bipolaris sorokiniana</i> F-529	<i>Erwinia rhapontici</i> B-9292
No. 1	2.00 ± 0.01	2.20 ± 0.02	1.50 ± 0.01
No. 2	3.00 ± 0.02	5.30 ± 0.02	7.55 ± 0.03
No. 3	5.45 ± 0.02	8.05 ± 0.03	4.10 ± 0.02
No. 4	6.60 ± 0.03	6.75 ± 0.02	2.55 ± 0.01
No. 5	4.85 ± 0.02	3.60 ± 0.01	7.25 ± 0.02
No. 6	7.35 ± 0.03	9.50 ± 0.03	8.10 ± 0.03
No. 7	5.40 ± 0.03	9.50 ± 0.03	3.00 ± 0.02

vation (optical density 0.28) and the stationary phase, after 14 h (optical density 1.75), with an optical density of 2.02 after 24 h. Thus, the optimal cultivation temperature was 28°C.

Figure 5 and Table 6 show the selection of a nutrient medium base.

All the experiments were conducted at the optimal cultivation temperature of 28°C (Fig. 5). On the LB nutrient medium (control), the exponential phase began after 2 h of cultivation (optical density 0.93) and the stationary phase, after 21 h (optical density 4.01), with an optical density of 4.01 after 24 h. On the GMF broth, the beginning of the exponential phase was observed after 2 h of cultivation (optical density 0.48) and that of the stationary phase, after 23 h (optical density 6.65), with an optical density of 6.65 after 24 h. On the BTN broth, the exponential phase started after 2 h of cultivation (optical density 0.42), with an optical density of 4.32 after 24 h. On the tryptone-soy broth with yeast extract, the exponential phase was noted after 2 h of cultivation (optical density 0.46), with an optical density of 7.62 after 24 h. On the GRM broth, the exponential phase began after 2 h of cultivation (optical density 0.33), while the stationary phase, after 10 h (optical density 3.04), with an optical density of 3.26 after 24 h.

**Figure 4** Optical density vs. cultivation temperature for Consortium No. 6

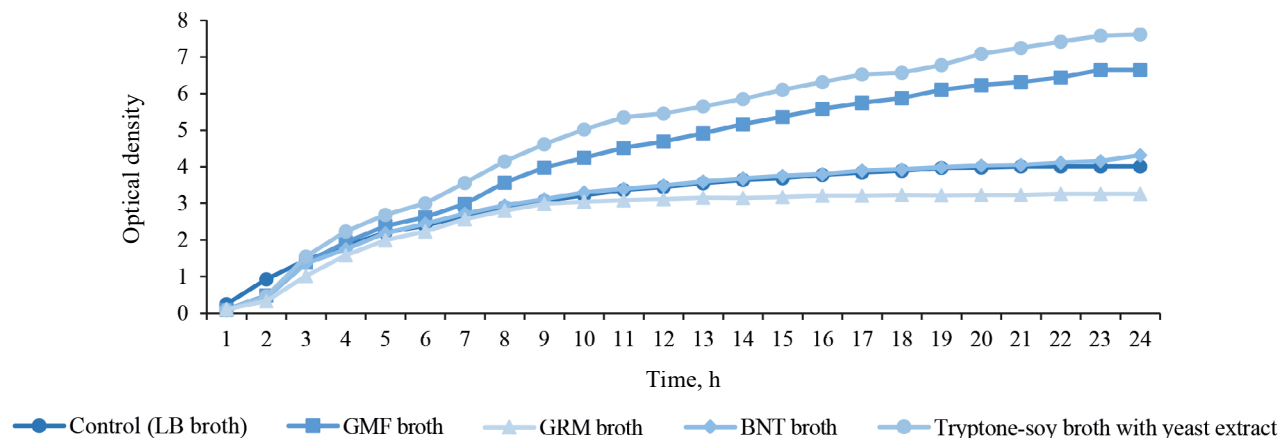


Figure 5 Optical density of Consortium No. 6 depending on the nutrient medium base

Table 6 The ability of bacterial consortia to produce gibberellic acid and siderophores depending on the nutrient medium base

Nutrient medium base	Gibberellic acid, mg/mL	Siderophores, %
LB (control)	1.45 ± 0.06	58.04 ± 2.86
GMF broth	0.96 ± 0.05	17.86 ± 0.81
BTN broth	1.28 ± 0.06	55.36 ± 2.71
Tryptone-soy broth with yeast extract	1.16 ± 0.04	52.68 ± 2.43
GRM broth	0.91 ± 0.04	11.16 ± 0.58

Thus, Consortium No. 6 showed different growth rates and biomass values on different nutrient media. The tryptone-soy broth with yeast extract proved the best medium for bacterial growth, with the highest biomass values (optical density 7.62). The GMF broth also produced high biomass (optical density 6.65), but had a longer exponential growth phase. The GRM broth provided the least favorable conditions for growth, as evidenced by a shorter stationary phase and lower final biomass. However, growth-stimulating preparations require an optimized synthesis of growth-stimulating substances, which does not always correlate with biomass accumulation. Therefore, we carried out additional experiments to study the biochemical parameters of the consortium during its growth on various nutrient media.

As can be seen in Table 4, the amounts of gibberellic acid and siderophores varied from 0.91 to 1.45 mg/mL and from 48.21 to 54.46%, respectively. On the medium based on tryptone-soy broth with yeast extract, the consortium produced 1.16 mg/mL of gibberellic acid (0.29 mg less than on the control medium) and 52.68% of siderophores (5.36% less than on the control medium). Our results showed that the choice of a nutrient medium has a significant effect on both the growth and the biochemical activity of the consortium. The LB medium was considered optimal for cultivating the consortium. Despite the lower biomass observed on this medium, the consortium produced maximum amounts

of gibberellic acid and siderophores, which is crucial for its targeted use.

Figure 6 and Table 7 show the selection of carbon source for the optimal composition of the nutrient medium.

All the experiments were carried out at the optimal cultivation temperature of 28°C (Fig. 6). On the LB medium (control), the exponential phase began after 2 h of cultivation (optical density 0.86) and the stationary phase began after 18 h (optical density 3.94), with an optical density of 4.09 after 24 h. On the LB + 4.0 g/L sucrose medium, the exponential phase started after 5 h of cultivation (optical density 0.59), while the stationary phase, after 22 h (optical density 4.00), with an optical density of 4.13 after 24 h. On the LB + 4.0 g/L glucose medium, the beginning of the exponential phase was observed after 5 h of cultivation (optical density 0.75), while that of the stationary phase, after 21 h (optical density 2.98), with an optical density of 3.04 after 24 h. On the LB + 4.0 g/L molasses medium, the exponential phase began after 5 h of cultivation (optical density 0.67) and the stationary phase, after 22 h (optical density 6.58), with an optical density of 6.75 after 24 h. On the LB + 8.0 g/L sucrose medium, the exponential phase started after 2 h of cultivation (optical density 0.75), while the stationary phase, after 22 h (optical density 4.18), with an optical density of 4.31 after 24 h. On the LB + 8.0 g/L glucose medium, the beginning of the exponential phase was observed after 5 h of cultivation (optical density 0.28), while that of the stationary phase, after 12 h (optical density 2.36), with an optical density of 2.66 after 24 h. On the LB + 8.0 g/L molasses medium, the exponential phase began after 5 h of cultivation (optical density 0.15) and the stationary phase started after 22 h (optical density 7.76), with an optical density of 7.63 after 24 h.

As can be seen in Table 5, the amounts of gibberellic acid and siderophores varied from 1.32 to 1.68 mg/mL and from 44.36 to 61.53%, respectively. The consortium exhibited its greatest activity on the medium containing LB + 8.0 g/L molasses (1.50 mg/mL of gibberellic acid and 61.53% of siderophores). Thus, molasses proved the most effective carbon source for cultivating this

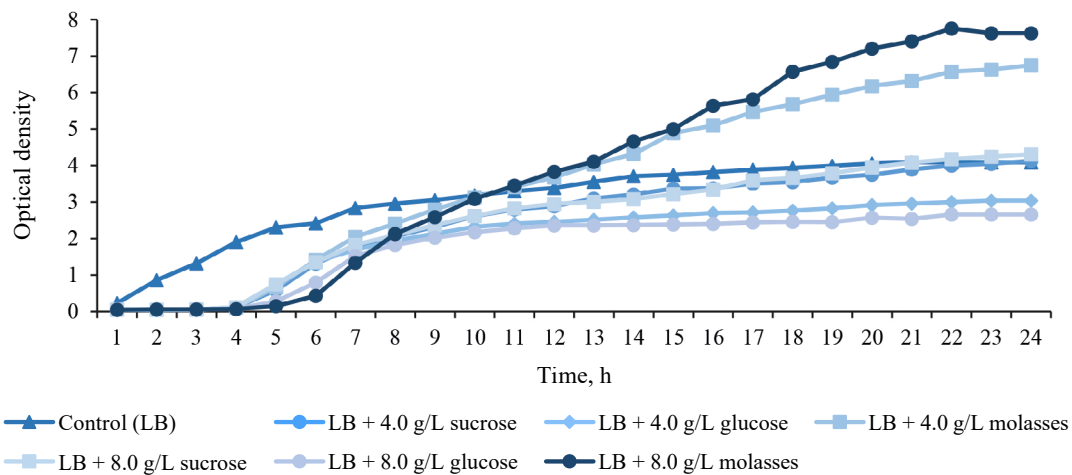


Figure 6 Optical density of Consortium No. 6 versus the composition of the nutrient medium

Table 7 The ability of bacterial consortia to produce gibberellic acid and siderophores depending on the carbon source

Nutrient medium	Gibberellic acid, $\mu\text{g/mL}$	Siderophores, %
LB (control)	1.49 ± 0.06	56.24 ± 2.80
LB + 4.0 g/L sucrose	1.48 ± 0.05	49.86 ± 2.31
LB + 4.0 g/L glucose	1.32 ± 0.04	44.36 ± 2.05
LB + 4.0 g/L molasses	1.53 ± 0.08	59.40 ± 2.93
LB + 8.0 g/L sucrose	1.50 ± 0.06	51.23 ± 2.48
LB + 8.0 g/L glucose	1.39 ± 0.03	47.06 ± 2.20
LB + 8.0 g/L molasses	1.68 ± 0.04	61.53 ± 2.96

consortium, providing the greatest biomass and high production of growth-stimulating substances (gibberellic acid and siderophores). Therefore, molasses was chosen as the main source of carbon.

Figure 7 and Table 8 show the selection of mineral elements for the optimal composition of the nutrient medium.

According to Fig. 7, on the control medium, the exponential phase began after 6 h of cultivation (optical density 0.46) and the stationary phase, after 2 h (optical density 7.69), with an optical density of 7.69 after 24 h. On Medium No. 1, the exponential phase started after 6 h (optical density 0.51) and the stationary phase, after 21 h (optical density 7.53), with an optical density of 8.00 after 24 h. On Medium No. 2, the beginning of the exponential phase was noted after 4 h of cultivation (optical density 0.72), with an optical density of 7.93 after 24 h. On Medium No. 3, the exponential phase began after 5 h of cultivation (optical density 0.49), while the stationary phase, after 21 h (optical density 8.15), with an optical density of 8.31 after 24 h. On Medium No. 4, the exponential phase started after 6 h (optical density 0.31), while the stationary phase, after 21 h (optical density 4.91), with an optical density of 4.91 after 24 h. On Medium No. 5, the beginning of the exponential phase was observed after 5 h (optical density 0.26), while that of the stationary phase, after 17 h (optical

density 5.02), with an optical density of 5.22 after 24 h. On Medium No. 6, the exponential phase began after 6 h of cultivation (optical density 0.21) and the stationary phase, after 15 h (optical density 3.59), with an optical density of 3.60 after 24 h.

As can be seen in Table 6, the amounts of gibberellic acid and siderophores varied from 1.20 to 1.79 mg/mL and from 52.28 to 65.56%, respectively. The consortium exhibited the lowest activity on Medium No. 6 (1.20 mg/mL of gibberellic acid and 52.28% of siderophores) and the highest activity on Medium No. 3 (1.79 mg/mL of gibberellic acid and 65.56% of siderophores).

Based on our results, the optimal composition of the nutrient medium was 25.0 g/L of LB, 8.0 g/L molasses, 0.1 g/L magnesium sulfate heptahydrate, and 0.01 g/L aqueous manganese sulfate. The optimal temperature was 28°C.

CONCLUSION

The bacteria belonging to the genera *Azotobacter* and *Pseudomonas* can be used in biopreparations to increase productivity and protect the plants from pathogens. These microorganisms have complex growth-stimulating properties and are also effective in microbial consortia.

In our study, all the test strains showed the ability to solubilize phosphates and produce ACC deaminase. Our data can clarify the growth-promoting effect of *Azotobacter vinelandii*, since its ability to produce ACC deaminase has been hardly covered in literature. ACC deaminase is involved in the metabolism of 1-aminocyclopropane-1-carboxylic acid (ACC), a precursor of ethylene in plants, which is an important factor in the plant's response to stress. Therefore, *A. vinelandii* can be used to increase plant productivity. The test strains synthesized an important phytohormone, gibberellic acid, in the range from 0.98 to 1.33 mg/mL and produced 37.95–49.55% of siderophores. All the strains showed a high ability to fix atmospheric nitrogen (49.23–151.22 $\mu\text{g/mL}$).

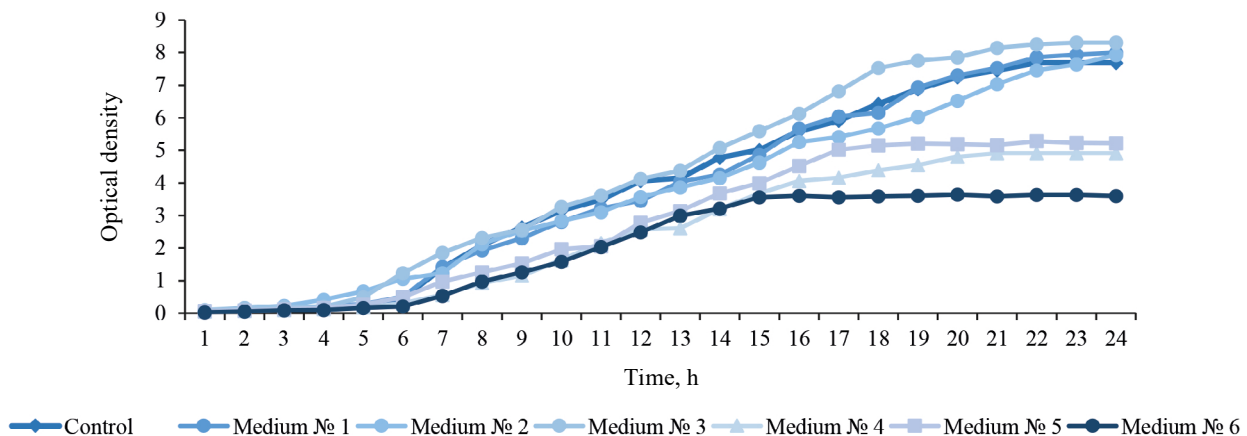


Figure 7 Correlation between the optical density of Consortium No. 6 and the composition of mineral salts in the nutrient medium

Table 8 The ability of bacterial consortia to produce gibberellic acid and siderophores depending on the mineral component in the media

Nutrient medium	Gibberellic acid, $\mu\text{g/mL}$	Siderophores, %
Control	1.66 ± 0.07	60.29 ± 2.76
Medium No. 1 (0.1 g/L magnesium sulfate heptahydrate)	1.70 ± 0.08	62.23 ± 3.06
Medium No. 2 (0.01 g/L aqueous manganese sulfate)	1.69 ± 0.08	61.54 ± 2.89
Medium No. 3 (0.1 g/L magnesium sulfate heptahydrate + 0.01 g/L aqueous manganese sulfate)	1.79 ± 0.05	65.56 ± 3.12
Medium No. 4 (0.2 g/L magnesium sulfate heptahydrate)	1.32 ± 0.04	53.61 ± 2.53
Medium No. 5 (0.02 g/L aqueous manganese sulfate)	1.46 ± 0.06	54.23 ± 2.49
Medium No. 6 (0.2 g/L magnesium sulfate heptahydrate + 0.02 g/L aqueous manganese sulfate)	1.20 ± 0.05	52.28 ± 2.44

The strains also exhibited antagonistic activity against common plant pathogens. In particular, *Azotobacter chroococcum* B-4148 and *A. vinelandii* B-932 inhibited the growth of *Fusarium graminearum*, *Bipolaris sorokiniana*, and *Erwinia raphontici*. *Pseudomonas chlororaphis* subsp. *aurantiaca* B-548 exhibited antagonism against *F. graminearum* and *B. sorokiniana*.

Since all the test strains were biologically compatible, we created a number of microbial consortia from them. The greatest growth-stimulating activity was exhibited by Consortium No. 6 consisting of the strains *A. chroococcum* B-4148, *A. vinelandii* B-932, and *P. chlororaphis* subsp. *aurantiaca* B-548 in a ratio of 1:3:1. This consortium synthesized 1.44 mg/mL of gibberellic acid and 54.46% of siderophores, which was 1.17 and 1.30 times, respectively, as much as the constituent bacterial strains.

Next, we optimized the nutrient medium to ensure maximum efficiency. The LB medium was chosen as a base. Although the consortium had a low increase in biomass on this medium, it intensified the synthesis of gibberellic acid and siderophores (1.45 mg/mL and 58.04%, respectively). Molasses was chosen as the main source of carbon for the consortium since it provided the greatest increase in biomass, with the optical density of the culture liquid being 1.8 times as high as that of the control sample (without molasses). In addition,

molasses contributed to high synthesis of target growth-stimulating substances. The greatest increase in biomass and synthesis of gibberellic acid and siderophores was observed when magnesium and manganese sulfates were added to the nutrient medium. Thus, the optimal composition of the nutrient medium included 25.0 g/L of LB, 8.0 g/L molasses, 0.1 g/L magnesium sulfate heptahydrate, and 0.01 g/L aqueous manganese sulfate. This composition provided the maximum yield of target metabolites. The optimal cultivation temperature for the consortium was 28°C.

Further studies of the created microbial consortium will involve its effect on plant growth and development both *in vitro* and in field experiments. Its effectiveness will be assessed in terms of plant biometric parameters, yield, as well as chlorophyll and nutrient contents. The resulting data will be used to develop a complex biopreparation that can replace chemical fertilizers and pesticides and ensure sustainable development of agriculture.

CONTRIBUTION

The authors were equally involved in writing the manuscript and are equally responsible for plagiarism.

CONFLICT OF INTEREST

The authors declare that there is no conflict of interest regarding this publication.

REFERENCES

1. Godfray HCJ, Beddington JR, Crute IR, Haddad L, Lawrence D, Muir JF, et al. Food security: The challenge of feeding 9 billion people. *Science*. 2010;327(5967):812–818. <https://doi.org/10.1126/science.1185383>
2. Prosekov AYU. Modern aspects of food production. Kemerovo: Kemerovo Institute of Food Science and Technology; 2005. 380 p. (In Russ.). <https://www.elibrary.ru/ZRZGCT>
3. Mardani S, Tabatabaei SH, Pessarakli M, Zareabyaneh H. Physiological responses of pepper plant (*Capsicum annuum* L.) to drought stress. *Journal of Plant Nutrition*. 2017;40(10):1532–1464. <https://doi.org/10.1080/01904167.2016.1269342>
4. Dhar SK, Kaur J, Singh GB, Chauhan A, Tamang J, Lakhara N, et al. Novel *Bacillus* and *Prestia* isolates from Dwarf century plant enhance crop yield and salinity tolerance. *Scientific Reports*. 2024;14:14645. <https://doi.org/10.1038/s41598-024-65632-x>
5. Asyakina LK, Vorob'eva EE, Proskuryakova LA, Zharko MYu. Evaluating extremophilic microorganisms in industrial regions. *Foods and Raw Materials*. 2023;11(1):162–171. <https://doi.org/10.21603/2308-4057-2023-1-556>
6. Mozumder P, Berrens RP. Inorganic fertilizer use and biodiversity risk: An empirical investigation. *Ecological Economics*. 2007;62(3–4):538–543. <https://doi.org/10.1016/j.ecolecon.2006.07.016>
7. Asyakina LK, Serazetdinova YuR, Frolova AS, Fotina NV, Neverova OA, Petrov AN. Antagonistic activity of extremophilic bacteria against phytopathogens in agricultural crops. *Food Processing: Techniques and Technology*. 2023;53(3):565–575. <https://doi.org/10.21603/2074-9414-2023-3-2457>
8. Fonte SJ, Yeboah E, Ofori P, Quansah GW, Vanlauwe B, Six J. Fertilizer and residue quality effects on organic matter stabilization in soil aggregates. *Soil Science Society of America Journal*. 2009;73(3):961–966. <https://doi.org/10.2136/sssaj2008.0204>
9. Mitra B, Chowdhury AR, Dey P, Hazra KK, Sinha AK, Hossain A, et al. Use of agrochemicals in agriculture: Alarming issues and solutions. In: Bhatt R, Meena RS, Hossain A, editors. *Input use efficiency for food and environmental security*. Singapore: Springer; 2021. pp. 85–122. https://doi.org/10.1007/978-981-16-5199-1_4
10. Faskhutdinova ER, Fotina NV, Neverova OA, Golubtsova YuV, Mudgal G, Asyakina LK, et al. Extremophilic bacteria as biofertilizer for agricultural wheat. *Foods and Raw Materials*. 2024;12(2):348–360. <https://doi.org/10.21603/2308-4057-2024-2-613>
11. Massah J, Azadegan B. Effect of chemical fertilizers on soil compaction and degradation. *Agricultural Mechanization in Asia, Africa and Latin America*. 2016;47(1):44–50.
12. Aloo BN, Mbega ER, Makumba BA, Tumuhairwe JB. Effects of agrochemicals on the beneficial plant rhizobacteria in agricultural systems. *Environmental Science and Pollution Research*. 2021;28:60406–60424. <https://doi.org/10.1007/s11356-021-16191-5>
13. Fan K, Delgado-Baquerizo M, Guo X, Wang D, Wu Y, Zhu M, et al. Suppressed N fixation and diazotrophs after four decades of fertilization. *Microbiome*. 2019;7:143. <https://doi.org/10.1186/s40168-019-0757-8>
14. Wang J, Li Q, Shen C, Yang F, Wang J, Ge Y. Significant dose effects of fertilizers on soil diazotrophic diversity, community composition, and assembly processes in a long-term paddy field fertilization experiment. *Land Degradation and Development*. 2020;32. <https://doi.org/10.1002/ldr.3736>
15. Liao H, Li Y, Yao H. Fertilization with inorganic and organic nutrients changes diazotroph community composition and N-fixation rates. *Journal of Soils and Sediments*. 2018;18:1076–1086. <https://doi.org/10.1007/s11368-017-1836-8>
16. Fotina NV, Serazetdinova YuR, Kolpakova DE, Asyakina LK, Atuchin VV, Alotaibi KM, et al. Enhancement of wheat growth by plant growth-stimulating bacteria during phytopathogenic inhibition. *Biocatalysis and Agricultural Biotechnology*. 2024;60:103294. <https://doi.org/10.1016/j.bcab.2024.103294>
17. Abbas Z, Akmal M, Khan KS, Hassan F. Effect of butril super (Bromoxynil) herbicide on soil microbial biomass and bacterial population. *Brazilian Archives of Biology and Technology*. 2014;57(1):9–14. <https://doi.org/10.1590/S1516-89132014000100002>
18. Cycoń M, Piotrowska-Seget Z, Kozdrój J. Dehydrogenase activity as an indicator of different microbial responses to pesticide-treated soils. *Chemistry and Ecology*. 2010;26(4):243–250. <https://doi.org/10.1080/02757540.2010.495062>
19. Carr JF, Gregory ST, Dahlberg AE. Severity of the streptomycin resistance and streptomycin dependence phenotypes of ribosomal protein S12 of *Thermus thermophilus* depends on the identity of highly conserved amino acid residues. *Journal of Bacteriology*. 2005;187(10):3548–3550. <https://doi.org/10.1128/JB.187.10.3548-3550.2005>
20. Meena RS, Kumar S, Datta R, Lal R, Vijayakumar V, Brtnicky M, et al. Impact of agrochemicals on soil microbiota and management: A review. *Land*. 2020;9(2):34. <https://doi.org/10.3390/land9020034>
21. Grewal AS, Singla A, Kamboj P, Dua JS. Pesticide residues in food grains, vegetables and fruits: A hazard to human health. *Journal of Medicinal Chemistry and Toxicology*. 2017;2(1):40–46. <https://doi.org/10.15436/2575-808X.17.1355>

22. Kim K-H, Kabir E, Jahan SA. Exposure to pesticides and the associated human health effects. *Science of The Total Environment*. 2017;575:525–535. <https://doi.org/10.1016/j.scitotenv.2016.09.009>
23. Kalyabina VP, Esimbekova EN, Kopylova KV, Kratasyuk VA. Pesticides: formulants, distribution pathways and effects on human health – A review. *Toxicology Reports*. 2021;8:1179–1192. <https://doi.org/10.1016/j.toxrep.2021.06.004>
24. Faskhutdinova ER, Fotina NV, Neverova OA, Golubtsova YuV, Mudgal G, Asyakina LK, et al. Extremophilic bacteria as biofertilizer for agricultural wheat. *Foods and Raw Materials*. 2024;12(2):348–360. <https://doi.org/10.21603/2308-4057-2024-2-613>
25. García-Fraile P, Menéndez E, Rivas R. Role of bacterial biofertilizers in agriculture and forestry. *AIMS Bioengineering*. 2015;2(3):183–205. <https://doi.org/10.3934/bioeng.2015.3.183>
26. Asyakina LK, Dyshlyuk LS, Prosekov AY. Reclamation of post-technological landscapes: international experience. *Food Processing: Techniques and Technology*. 2021;51(4):805–818. (In Russ.). <https://doi.org/10.21603/2074-9414-2021-4-805-818>; <https://www.elibrary.ru/SANMZI>
27. Andrade MMM, Stamford NP, Santos CERS, Freitas ADS, Sousa CA, Lira Junior MA. Effects of biofertilizer with diazotrophic bacteria and mycorrhizal fungi in soil attribute, cowpea nodulation yield and nutrient uptake in field conditions. *Scientia Horticulturae*. 2013;162:374–379. <https://doi.org/10.1016/j.scienta.2013.08.019>
28. Zvinavashe AT, Lim E, Sun H, Marelli B. A bioinspired approach to engineer seed microenvironment to boost germination and mitigate soil salinity. *Proceedings of the National Academy of Sciences*. 2019;116(51):25555–25561. <https://doi.org/10.1073/pnas.1915902116>
29. Aquilanti L, Favilli F, Clementi F. Comparison of different strategies for isolation and preliminary identification of *Azotobacter* from soil samples. *Soil Biology and Biochemistry*. 2004;36(9):1475–1483. <https://doi.org/10.1016/j.soilbio.2004.04.024>
30. Ansari RA, Rizvi R, Sumbul A, Mahmood I. PGPR: Current vogue in sustainable crop production. In: Kumar V, Kumar M, Sharma S, Prasad R, editors. *Probiotics and plant health*. Singapore: Springer; 2017. pp. 455–472. https://doi.org/10.1007/978-981-10-3473-2_21
31. Kurrey DK, Sharma R, Lahre MK, Kurrey RL. Effect of *Azotobacter* on physio-chemical characteristics of soil in onion field. *The Pharma Innovation*. 2018;7(2):108–113.
32. Prajapati K, Yami KD, Singh A. Plant growth promotional effect of *Azotobacter chroococcum*, *Piriformospora indica* and vermicompost on rice plant. *Nepal Journal of Science and Technology*. 2008;9:85–90. <https://doi.org/10.3126/njst.v9i0.3170>
33. Hakeem KR, Sabir M, Ozturk M, Akhtar MS, Ibrahim FH. Nitrate and nitrogen oxides: Sources, health effects and their remediation. In: De Voogt P, editor. *Reviews of environmental contamination and toxicology*. Volume 242. Cham: Springer; 2016. pp. 183–217. https://doi.org/10.1007/398_2016_11
34. Wani SA, Chand S, Wani MA, Ramzan M, Hakeem KR. *Azotobacter chroococcum* – A potential biofertilizer in agriculture: An overview. In: Hakeem KR, Akhtar J, Sabir M, editors. *Soil science: Agricultural and environmental perspectives*. Cham: Springer; 2016. pp. 333–348. https://doi.org/10.1007/978-3-319-34451-5_15
35. Romero-Perdomo F, Abril J, Camelo M, Moreno-Galván A, Pastrana I, Rojas-Tapias D, et al. *Azotobacter chroococcum* as a potentially useful bacterial biofertilizer for cotton (*Gossypium hirsutum*): Effect in reducing N fertilization. *Revista Argentina de Microbiología*. 2017;49(4):377–383. <https://doi.org/10.1016/j.ram.2017.04.006>
36. Arora M, Saxena P, Abidin MZ, Varma A. Interaction between *Piriformospora indica* and *Azotobacter chroococcum* governs better plant physiological and biochemical parameters in *Artemisia annua* L. plants grown under in vitro conditions. *Symbiosis*. 2018;75:103–112. <https://doi.org/10.1007/s13199-017-0519-y>
37. Singh A, Maji S, Kumar S. Effect of biofertilizers on yield and biomolecules of anti-cancerous vegetable broccoli. *International Journal of Bio-Resource and Stress Management*. 2014;5:262–268. <https://doi.org/10.5958/0976-4038.2014.00565.X>
38. Baars O, Zhang X, Morel FMM, Seyedsayamdost MR. The siderophore metabolome of *Azotobacter vinelandii*. *Applied and Environmental Microbiology*. 2016;82(1):27–39. <https://doi.org/10.1128/AEM.03160-15>
39. Hayat R, Ali S, Amara U, Khalid R, Ahmed I. Soil beneficial bacteria and their role in plant growth promotion: A review. *Annals of Microbiology*. 2010;60:579–598. <https://doi.org/10.1007/s13213-010-0117-1>
40. Zayadan BK, Matorin DN, Baimakhanova GB, Bolathan K, Oraz GD, Sadanov AK. Promising microbial consortia for producing biofertilizers for rice fields. *Microbiology*. 2014;83:391–397. <https://doi.org/10.1134/S0026261714040171>
41. Suryatmana P, Setiawati MR, Hindersah R, Satria A, Fitriatin BN. The potential of the consortium (*Azotobacter* spp. and Phosphate solubilizing bacteria) in increasing plant n uptake, plant nitrogen content, *Azotobacter* spp. population and lettuce (*Lactuca sativa* L) crop yield. *International Journal of Agriculture, Environment and BioResearch*. 2021;06(01):77–86. <https://doi.org/10.35410/IJAEB.2021.5604>




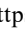
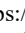


42. Singh A, Jain A, Sarma B, Upadhyay R, Singh HB. Rhizosphere microbes facilitate redox homeostasis in *Cicer arietinum* against biotic stress. *Annals of Applied Biology*. 2013;163:33–46. <https://doi.org/10.1111/aab.12030>
43. Mehmood N, Saeed M, Zafarullah S, Hyder S, Rizvi ZF, Gondal AS, et al. Multifaceted impacts of plant-beneficial *Pseudomonas* spp. in managing various plant diseases and crop yield improvement. *ACS Omega*. 2023;8(25):22296–22315. <https://doi.org/10.1021/acsomega.3c00870>
44. Zhang H, Zheng D, Hu C, Cheng W, Lei P, Xu H, et al. Certain tomato root exudates induced by *Pseudomonas stutzeri* NRCB010 enhance its rhizosphere colonization capability. *Metabolites*. 2023;13(5):664. <https://doi.org/10.3390/metabo13050664>
45. Ortiz-Castro R, Campos-García J, López-Bucio J. *Pseudomonas putida* and *Pseudomonas fluorescens* influence *Arabidopsis* root system architecture through an auxin response mediated by bioactive cyclodipeptides. *Journal of Plant Growth Regulation*. 2020;39:254–265. <https://doi.org/10.1007/s00344-019-09979-w>
46. Astriani M, Zubaidah S, Abadi AL, Suarsini E. *Pseudomonas plecoglossicida* as a novel bacterium for phosphate solubilizing and indole-3-acetic acid-producing from soybean rhizospheric soils of East Java, Indonesia. *Biodiversitas*. 2020;21(2):578–586. <https://doi.org/10.13057/biodiv/d210220>
47. Chen W, Yang F, Zhang L, Wang J. Organic acid secretion and phosphate solubilizing efficiency of *Pseudomonas* sp. PSB12: Effects of phosphorus forms and carbon sources. *Geomicrobiology Journal*. 2016;33(10):870–877. <https://doi.org/10.1080/01490451.2015.1123329>
48. Arkhipova TN, Galimsyanova NF, Kuzmina LYu, Vysotskaya LB, Sidorova LV, Gabbasova IM, et al. Effect of seed bacterization with plant growth-promoting bacteria on wheat productivity and phosphorus mobility in the rhizosphere. *Plant, Soil and Environment*. 2019;65(6):313–319. <https://doi.org/10.17221/752/2018-PSE>
49. Qessaoui R, Bouharroud R, Furze JN, El Aalaoui M, Akroud H, Amarraque A, et al. Applications of new rhizobacteria *Pseudomonas* isolates in agroecology via fundamental processes complementing plant growth. *Scientific Reports*. 2019;9:12832. <https://doi.org/10.1038/s41598-019-49216-8>
50. Jishma P, Hussain N, Chellappan R, Rajendran R, Mathew J, Radhakrishnan EK. Strain-specific variation in plant growth promoting volatile organic compounds production by five different *Pseudomonas* spp. as confirmed by response of *Vigna radiata* seedlings. *Journal of Applied Microbiology*. 2017;123(1):204–216. <https://doi.org/10.1111/jam.13474>
51. Kudoyarova GR, Vysotskaya LB, Arkhipova TN, Kuzmina LYu, Galimsyanova NF, Sidorova LV, et al. Effect of auxin producing and phosphate solubilizing bacteria on mobility of soil phosphorus, growth rate, and P acquisition by wheat plants. *Acta Physiologiae Plantarum*. 2017;39:253. <https://doi.org/10.1007/s11738-017-2556-9>
52. Billah M, Khan M, Bano A, Hassan TU, Munir A, Gurmani AR. Phosphorus and phosphate solubilizing bacteria: Keys for sustainable agriculture. *Geomicrobiology Journal*. 2019;36(10):904–916. <https://doi.org/10.1080/01490451.2019.1654043>
53. Iqbal A, Hasnain S. Auxin producing *Pseudomonas* strains: Biological candidates to modulate the growth of *Triticum aestivum* beneficially. *American Journal of Plant Sciences*. 2013;4(9):1693–1700. <https://doi.org/10.4236/ajps.2013.49206>
54. Ortiz-Castro R, Díaz-Pérez C, Martínez-Trujillo M, del Río RE, Campos-García J, López-Bucio J. Transkingdom signaling based on bacterial cyclodipeptides with auxin activity in plants. *Proceedings of the National Academy of Sciences*. 2011;108(17):7253–7258. <https://doi.org/10.1073/pnas.1006740108>
55. Blaggana A, Grover V, Anjali, Kapoor A, Blaggana V, Tanwar R, et al. Oral health knowledge, attitudes and practice behaviour among secondary school children in Chandigarh. *Journal of Clinical and Diagnostic Research*. 2016;10(10):ZC01–ZC06. <https://doi.org/10.7860/JCDR/2016/23640.8633>
56. Karnwal A, Kaushik P. Cytokinin production by fluorescent *Pseudomonas* in the presence of rice root exudates. *Archives of Phytopathology and Plant Protection*. 2011;44(17):1728–1735. <https://doi.org/10.1080/03235408.2010.526768>
57. Patel T, Saraf M. Biosynthesis of phytohormones from novel rhizobacterial isolates and their in vitro plant growth-promoting efficacy. *Journal of Plant Interactions*. 2017;12(1):480–487. <https://doi.org/10.1080/17429145.2017.1392625>
58. Song Q, Deng X, Song R, Song X. Plant growth-promoting rhizobacteria promote growth of seedlings, regulate soil microbial community, and alleviate damping-off disease caused by *Rhizoctonia solani* on *Pinus sylvestris* var. *mongolica*. *Plant Disease* 2022;106(10):2730–2740. <https://doi.org/10.1094/PDIS-11-21-2562-RE>
59. Sharma H, Haq MA, Koshariya AK, Kumar A, Rout S, Kaliyaperumal K. “*Pseudomonas fluorescens*” as an antagonist to control okra root rotting fungi disease in plants. *Journal of Food Quality* 2022;2022:5608543. <https://doi.org/10.1155/2022/5608543>

60. Anak H, Dönmez MF, Çoruh İ. Biological control of *Rhizoctonia solani* Kühn. with rhizobacteria isolated from different soil and *Calligonum polygonoides* L. subsp. *Comosum* (L'hér.). *Journal of Agriculture*. 2021;4(2):92–107. <https://doi.org/10.46876/ja.986625>
61. Yang X, Hong C. Biological control of Phytophthora blight by *Pseudomonas protegens* strain 14D5. *European Journal of Plant Pathology*. 2020;156:591–601. <https://doi.org/10.1007/s10658-019-01909-6>
62. Sulochana MB, Jayachandra SY, Kumar SKA, Dayanand A. Antifungal attributes of siderophore produced by the *Pseudomonas aeruginosa* JAS-25. *Journal of Basic Microbiology*. 2014;54. <https://doi.org/10.1002/jobm.201200770>
63. Popova AA, Koksharova OA, Lipasova VA, Zaitseva YuV, Katkova-Zhukotskaya OA, Eremina SYu, et al. Inhibitory and toxic effects of volatiles emitted by strains of *Pseudomonas* and *Serratia* on growth and survival of selected microorganisms, *Caenorhabditis elegans*, and *Drosophila melanogaster*. *BioMed Research International*. 2014;2014:125704. <https://doi.org/10.1155/2014/125704>
64. Kumar S, Pandey P, Maheshwari DK. Reduction in dose of chemical fertilizers and growth enhancement of sesame (*Sesamum indicum* L.) with application of rhizospheric competent *Pseudomonas aeruginosa* LES4. *European Journal of Soil Biology*. 2009;45(4):334–340. <https://doi.org/10.1016/j.ejsobi.2009.04.002>
65. Doussoulin Jara HA, Moya Elizondo EA. Root disease suppressive soils: “take all decline (*Gaeumannomyces graminis* var. *tritici*) in wheat”, a case study. *Agro Sur*. 2011;39(2):67–78. <https://doi.org/10.4206/agrosur.2011.v39n2-01>
66. Ma Z, Ongena M, Höfte M. The cyclic lipopeptide orfamide induces systemic resistance in rice to *Cochliobolus miyabeanus* but not to *Magnaporthe oryzae*. *Plant Cell Reports*. 2017;36:1731–1746. <https://doi.org/10.1007/s00299-017-2187-z>
67. Ran LX, Li ZN, Wu GJ, van Loon LC, Bakker PAHM. Induction of systemic resistance against bacterial wilt in *Eucalyptus urophylla* by fluorescent *Pseudomonas* spp. *European Journal of Plant Pathology*. 2005;113:59–70. <https://doi.org/10.1007/s10658-005-0623-3>
68. Morris BEL, Henneberger R, Huber H, Moissl-Eichinger C. Microbial syntrophy: interaction for the common good. *FEMS Microbiology Reviews*. 2013;37(3):384–406. <https://doi.org/10.1111/1574-6976.12019>
69. Fierer N, Jackson RB. The diversity and biogeography of soil bacterial communities. *Proceedings of the National Academy of Sciences*. 2006;103(3):626–631. <https://doi.org/10.1073/pnas.0507535103>
70. Cadotte MW, Cavender-Bares J, Tilman D, Oakley TH. Using phylogenetic, functional and trait diversity to understand patterns of plant community productivity. *PLoS ONE*. 2009;4(5):e5695. <https://doi.org/10.1371/journal.pone.0005695>
71. Jousset A, Schulz W, Scheu S, Eisenhauer N. Intraspecific genotypic richness and relatedness predict the invasibility of microbial communities. *The ISME Journal*. 2011;5(7):1108–1114. <https://doi.org/10.1038/ismej.2011.9>
72. Awasthi A, Singh M, Soni SK, Singh R, Kalra A. Biodiversity acts as insurance of productivity of bacterial communities under abiotic perturbations. *The ISME Journal*. 2014;8(12):2445–2452. <https://doi.org/10.1038/ismej.2014.91>
73. Huang L, Liu C, Liu Y, Jia X. The composition analysis and preliminary cultivation optimization of a PHA-producing microbial consortium with xylose as a sole carbon source. *Waste Management*. 2016;52:77–85. <https://doi.org/10.1016/j.wasman.2016.03.020>
74. Smid EJ, Lacroix C. Microbe-microbe interactions in mixed culture food fermentations. *Current Opinion in Biotechnology*. 2013;24(2):148–154. <https://doi.org/10.1016/j.copbio.2012.11.007>
75. Tarasova IA, Koval'skaya MV. Obtaining a pure culture of saprotrophic bacteria. *Mordovia University Bulletin*. 2008;18(2):129–132. (In Russ.). <https://www.elibrary.ru/SZCGCB>
76. Atuchin VV, Asyakina LK, Serazetdinova YuR, Frolova AS, Velichkovich NS, Prosekov AYU. Microorganisms for bioremediation of soils contaminated with heavy metals. *Microorganisms*. 2023;11(4):864. <https://doi.org/10.3390/microorganisms11040864>
77. Parashar M, Dhar SK, Kaur J, Chauhan A, Tamang J, Singh GB, et al. Two novel plant-growth-promoting *Lelliottia amnigena* isolates from *Euphorbia prostrata* aiton enhance the overall productivity of wheat and tomato. *Plants*. 2023;12(17):3081. <https://doi.org/10.3390/plants12173081>
78. Asyakina LK, Mudgal G, Tikhonov SL, Larichev TA, Fotina NV, Prosekov AYU. Study of the potential of natural microbiota of spring soft wheat to increase yield. *Achievements of Science and Technology in Agro-Industrial Complex*. 2023;37(11):12–17. (In Russ.). <https://www.elibrary.ru/HXXGEC>
79. Kaur J, Mudgal G, Chand K, Singh GB, Perveen K, Bukhari NA, et al. An exopolysaccharide-producing novel *Agrobacterium pusense* strain JAS1 isolated from snake plant enhances plant growth and soil water retention. *Scientific Reports*. 2022;12:21330. <https://doi.org/10.1038/s41598-022-25225-y>
80. Cordova-Rodriguez A, Rentería-Martínez ME, López-Miranda CA, Guzmán-Ortiz JM, Moreno-Salazar SF. Simple and sensitive spectrophotometric method for estimating the nitrogen-fixing capacity of bacterial cultures. *MethodsX*. 2022;9:101917. <https://doi.org/10.1016/j.mex.2022.101917>

81. Das S, De TK. Microbial assay of N₂ fixation rate, a simple alternate for acetylene reduction assay. *MethodsX*. 2018;5:909–914. <https://doi.org/10.1016/j.mex.2017.11.010>
82. Rzhetskaya VS, Semenova EF, Zaitsev GP, Slasya EA, Omelchenko AV, Bugara IA, et al. ANTAGONISTIC effect of lactic acid bacteria and their consortium with yeast on pathogenic microorganisms. *Biotechnology in Russia*. 2021;37(5):96–107. (In Russ.). <https://www.elibrary.ru/AFIKTR>
83. Irkitova AN, Kagan YaR, Sokolova GG. Comparative analysis of the methods to define antagonistic activity of lactic bacteria. *Izvestiya of Altai State University*. 2012;(3–1):41–44. (In Russ.). <https://www.elibrary.ru/PBFQGV>
84. Biello KA, Lucena C, López-Tenllado FJ, Hidalgo-Carrillo J, Rodríguez-Caballero G, Cabello P, et al. Holistic view of biological nitrogen fixation and phosphorus mobilization in *Azotobacter chroococcum* NCIMB 8003. *Frontiers In Microbiology*. 2023;14:1129721. <https://doi.org/10.3389/fmicb.2023.1129721>
85. Alsalim HAA. *Azotobacter chroococcum* and *Rhizobium leguminosarum* inoculums survival in soil and efficiency in enhancing plant growth. *Plant Archives*. 2020;20(1):2851–2859.
86. Kumar V, Behl RK, Narula N. Establishment of phosphate-solubilizing strains of *Azotobacter chroococcum* in the rhizosphere and their effect on wheat cultivars under green house conditions. *Microbiological Research*. 2001;156(1):87–93. <https://doi.org/10.1078/0944-5013-00081>
87. Aung A, Sev TM, Mon AA, Yu SS. Detection of abiotic stress tolerant *Azotobacter* species for enhancing plant growth promoting activities. *Journal of Scientific and Innovative Research*. 2020;9(2):48–53. <https://doi.org/10.31254/jsir.2020.9203>
88. Kerečki S, Pečinar I, Karličić V, Mirković N, Kljujev I, Raičević V, et al. *Azotobacter chroococcum* F8/2: a multitasking bacterial strain in sugar beet biopriming. *Journal of Plant Interactions*. 2022;17(1):719–730. <https://doi.org/10.1080/17429145.2022.2091802>
89. Song Y, Liu J, Chen F. *Azotobacter chroococcum* inoculation can improve plant growth and resistance of maize to armyworm, *Mythimna separata* even under reduced nitrogen fertilizer application. *Pest Management Science*. 2020;76:4131–4140. <https://doi.org/10.1002/ps.5969>
90. Naz I, Bano A, Rehman B, Pervaiz S, Iqbal M, Sarwar A, et al. Potential of *Azotobacter vinelandii* Khsr1 as bio-inoculant. *African Journal of Biotechnology*. 2012;11(45):10368–10372.
91. McRose DL, Baars O, Morel FMM, Kraepiel AML. Siderophore production in *Azotobacter vinelandii* in response to Fe-, Mo- and V-limitation. *Environmental Microbiology*. 2017;19(9):3595–3605. <https://doi.org/10.1111/1462-2920.13857>
92. McRose DL, Lee A, Kopf SH, Baars O, Kraepiel AML, Sigman DM, et al. Effect of iron limitation on the isotopic composition of cellular and released fixed nitrogen in *Azotobacter vinelandii*. *Geochimica et Cosmochimica Acta*. 2019;244:12–23. <https://doi.org/10.1016/j.gca.2018.09.023>
93. Sev TM, Aung A, Mon AA, Yu SS. Assessment for plant growth promoting activities of *Azotobacter vinelandii* AV7 from rhizospheric soil of tomato. *Journal of Materials and Environmental Science*. 2020;11(11):1807–1815.
94. Shuvro SK, Jog R, Morikawa M. Diazotrophic bacterium *Azotobacter vinelandii* as a mutualistic growth promoter of an aquatic plant: *Lemna minor*. *Plant Growth Regulation*. 2023;100:171–180. <https://doi.org/10.1007/s10725-022-00948-0>
95. Rosas SB. *Pseudomonas chlororaphis* subsp. *aurantiaca* SR1: Isolated from rhizosphere and its return as inoculant. A review. *International Biology Review*. 2017;1(3).
96. Shi X-Q, Zhu D-H, Chen J-L, Qin Y-Y, Li X-W, Qin S, et al. Growth promotion and biological control of fungal diseases in tomato by a versatile rhizobacterium, *Pseudomonas chlororaphis* subsp. *aureofaciens* SPS-41. *Physiological and Molecular Plant Pathology*. 2024;131:102274. <https://doi.org/10.1016/j.pmpp.2024.102274>
97. Al-Baldawy MSM, Matloob AAAH, Almammory MKN. The importance of nitrogen-fixing bacteria *Azotobacter chroococcum* in biological control to root rot pathogens (review). *IOP Conference Series: Earth and Environmental Science*. 2023;1259:012110. <https://doi.org/10.1088/1755-1315/1259/1/012110>
98. Muslim SN, Aziz RAR, Al-Hakeem AM. Biological control of *Azotobacter chroococcum* on *Fusarium solani* in tomato plant. *Journal of Physics: Conference Series*. 2021;1879:022018. <https://doi.org/10.1088/1742-6596/1879/2/022018>
99. Alsudani AA, Al-Awsi GRL. Biocontrol of *Rhizoctonia solani* (Kühn) and *Fusarium solani* (Marti) causing damping-off disease in tomato with *Azotobacter chroococcum* and *Pseudomonas fluorescens*. *Pakistan Journal of Biological Sciences*. 2020;23(11):1456–1461. <https://doi.org/10.3923/pjbs.2020.1456.1461>
100. Pattaeva MA, Pattaev AA, Rasulov BA. Analysis of antifungal compounds of bacteria genus *azotobacter*. *Scientific Bulletin of NamSU*. 2023;8:119–124.
101. Chuiko NV, Chobotarov AY, Savchuk YaI, Kurchenko IM, Kurdish IK. Antagonistic activity of *Azotobacter vinelandii* IMV B-7076 against phytopathogenic microorganisms. *Mikrobiologichnii Zhurnal*. 2020;82(5):21–29. <https://doi.org/10.15407/microbiolj82.05.021>

102. Bolaños-Dircio A, Segura D, Toribio-Jiménez J, Toledo-Hernández E, Ortuño-Pineda C, Ortega-Acosta SÁ, et al. Cysts and alkylresorcinols of *Azotobacter vinelandii* inhibit the growth of phytopathogenic fungi. *Chilean Journal of Agricultural Research*. 2022;82(4):658–662. <https://doi.org/10.4067/S0718-58392022000400658>
103. Poštić D, Jošić D, Lepšanović Z, Aleksić G, Latković D, Starović M. The effect of *Pseudomonas chlororaphis* subsp. *aurantiaca* strain Q16 able to inhibit *Fusarium oxysporum* growth on potato yield. *Ratarstvo i Povrtarstvo*. 2019;56(2):41–48. <https://doi.org/10.5937/ratpov56-20428>
104. Tägele SB, Lee HG, Kim SW, Lee YS. Phenazine and 1-undecene producing *Pseudomonas chlororaphis* subsp. *aurantiaca* strain KNU17Pc1 for growth promotion and disease suppression in Korean maize cultivars. *Journal of Microbiology and Biotechnology*. 2019;29(1):66–78. <https://doi.org/10.4014/jmb.1808.08026>
105. Raio A, Reveglia P, Puopolo G, Cimmino A, Danti R, Evidente A. Involvement of phenazine-1-carboxylic acid in the interaction between *Pseudomonas chlororaphis* subsp. *aureofaciens* strain M71 and *Seiridium cardinale* *in vivo*. *Microbiological Research*. 2017;199:49–56. <https://doi.org/10.1016/j.micres.2017.03.003>
106. Zhang Y, Li T, Xu M, Guo J, Zhang C, Feng Z, et al. Antifungal effect of volatile organic compounds produced by *Pseudomonas chlororaphis* subsp. *aureofaciens* SPS-41 on oxidative stress and mitochondrial dysfunction of *Ceratocystis fimbriata*. *Pesticide Biochemistry and Physiology*. 2021;173:104777. <https://doi.org/10.1016/j.pestbp.2021.104777>

ORCID IDs

Yuliya R. Serazetdinova  <https://orcid.org/0000-0002-3044-3529>
 Darya Yu. Chekushkina  <https://orcid.org/0009-0002-3826-8048>
 Ekaterina E. Borodina  <https://orcid.org/0000-0001-6362-7589>
 Daria E. Kolpakova  <https://orcid.org/0000-0002-8508-3372>
 Varvara I. Minina  <https://orcid.org/0000-0003-3485-9123>
 Olga G. Altshuler  <https://orcid.org/0000-0001-7035-673X>
 Lyudmila K. Asyakina  <https://orcid.org/0000-0003-4988-8197>



Barnûf leaves: antioxidant, antimicrobial, antidiabetic, anti-obesity, antithyroid, and anticancer properties

Rowida Y. Essa¹, Essam M. Elsebaie^{1,*}, Wesam M. Abdelrhman², Mohamed R. Badr³

¹ Kafrelsheikh University^{ROR}, Kafr-El-Shiekh, Egypt

² Al-Azhar University, Tanta, Egypt

³ Tanta University^{ROR}, Tanta, Egypt

* e-mail: Essam.ahmed@agr.kfs.edu.eg

Received 09.11.2023; Revised 15.02.2024; Accepted 05.03.2024; Published online 02.11.2024

Abstract:

Barnûf (*Pluchea dioscoridis* L.) is a wild plant that grows in Egypt. Barnûf leaves are utilized as a folk medicine, as well as part of food and drink formulations. Their numerous biological benefits include anti-inflammatory and antioxidant properties. We examined the antioxidant, antidiabetic, anti-obesity, antithyroid, and anticancer activities of methanol, ethanol, and acetone extracts of barnûf leaves.

The methanol extract exhibited the highest total phenolic (241.50 ± 3.71 mg GAE/g extract) and flavonoid (256.18 ± 3.19 mg QE/g extract) contents. All three extracts proved to possess good antioxidant, antimicrobial, antidiabetic, anti-obesity, antithyroid, and anticancer activities. Ellagic acid was the most abundant phenolic acid in the methanolic (30.33%) and ethanolic (24.71%) extracts. The antioxidant experiments revealed that the methanolic extract had potent DPPH[•] ($IC_{50} = 18.21$ µg/mL) and ABTS^{•+} ($IC_{50} = 17.6$ µg/mL) scavenging properties. The acetone extract demonstrated the highest antimicrobial activity against gram-negative bacteria. Regarding α -amylase and α -glucosidase inhibition, the methanolic extract showed the most potent activity with IC_{50} values of 104.28 ± 1.97 and 133.76 ± 2.09 µg/mL, respectively. The methanolic extract also proved to be the strongest inhibitor of lipase and thyroid peroxidase, with IC_{50} values of 127.35 and 211.2 µg/mL, respectively. In addition, the methanolic extract showed the strongest anticancer activity against MCF7-1 and H1299-1 lines with IC_{50} values of 29.3 and 18.4 µg/mL, respectively.

The findings suggest that barnûf leaf extracts could be used in functional foods and pharmaceuticals.

Keywords: *Pluchea dioscoridis* L., medicinal properties, extraction, DPPH, ABTS, herbal medicine

Please cite this article in press as: Essa RY, Elsebaie EM, Abdelrhman WM, Badr MR. Barnûf leaves: antioxidant, antimicrobial, antidiabetic, anti-obesity, antithyroid, and anticancer properties. *Foods and Raw Materials*. 2025;13(2):394–408. <https://doi.org/10.21603/2308-4057-2025-2-647>

INTRODUCTION

People have used herbal medicine since ancient times. Seeds, roots, bark, flowers, and leaves of many plants are known to possess medicinal properties.

Although synthetic drugs are quite efficient against a wide range of diseases, they often produce side effects. As a result, herbal medicine has grown in popularity in the last few decades [1, 2]. Medicinal herbs are, by definition, sources of phytochemical substances with medicinal properties. In many cases, plants owe their beneficial properties to secondary metabolites, e.g., alkaloids, terpenoids, or phenolics [3].

Barnûf (*Pluchea dioscoridis* L.) is a big evergreen shrub that belongs to the *Asteraceae* family. In the wild,

it grows 1–3 m high, with a lot of branches and a rough, hairy surface. Barnûf grows extensively across the Middle East and in the surrounding African countries. According to Shaltout & Slima, this herb is prevalent in Egypt's western desert oases and eastern deserts, in the Nile valley, along the Mediterranean coast, and on the Sinai Peninsula [4]. It proliferates in demolished dwellings, humid environments, along waterways, depressions alongside highways and railroads, on deserted farmlands, solid or liquid wastes, etc. [5].

Food science knows a variety of solvent systems and techniques that optimize the extraction of polyphenols [6, 7]. For instance, Harborne described a well-designed solvent solution that facilitates the best possible extraction of targeted substances without altering their

chemical structure [8]. Liu *et al.* [9] reported that polar solvents could yield better extraction results for polyphenols than non-polar ones. For this reason, acetone, ethanol, and methanol are the organic solvents frequently employed in combination with water to extract plant substances [10]. Methanol (80%) and ethanol (80%) can be used to increase the yield of polyphenols [11]. Aqueous ethanol (80%) was proposed by Wang & Helliwell [12] as a better solvent for polyphenols than methanol and acetone. Other studies promote acetone as a superior solvent for polyphenol extraction or as an alternative to water and chloroform [13].

Thus, polyphenol production depends not only on the physical characteristics of plant materials but also on the type and polarity of the extraction solvent [6]. As of yet, no specific solvent has been advised for efficient plant phenolic extraction [14]. By choosing the optimal solvent, manufacturers can optimize the extraction process because plant extracts vary in quality. Extracts from barnûf leaves are known to demonstrate potent antibacterial properties against some microorganisms and pathogenic bacteria [5, 15]. Historically, the *Pluchea* genus has often been used as a source of hepatoprotectors, antipyretics, muscle relaxants, laxatives, antiinflammatory agents, astringents, nerve tonics, diaphoretics against fevers, etc. These plants are used as part of treatment against lumbago, cachexia, dysuria, dysentery, necrotizing ulcers, hemorrhoids, and leucorrhoea [16]. Uchiyama *et al.* [17] studied *Pluchea* extracts phytochemically, fractionated them, and revealed polyphenolic components, e.g., flavonoids, phenolic acids, phenylpropanoids, tannins, and chalcones, as well as monoterpenes, lignan glycosides, eudesmane-type sesquiterpenoids, and triterpenoids. All these substances render the plants their antioxidant properties and make them natural detoxification agents.

Synergistically, a combination of these components may provide a greater protection than an individual phytoconstituent [18]. All of these substances have indeed been reported to remove free radicals, reduce oxidation stress, and limit the biomolecular oxidation by disrupting the pathogenic interaction cycles that impair human physiological processes. Free radicals in particular produce cell damage and increase the amount of reactive oxygen species, thus causing tissue damage. Reactive oxygen species escape from the mitochondria in a cascade, thus causing oxidative stress. This mechanism has been linked to the development of type 1 diabetes through the death of pancreatic β -cells and type 2 diabetes through insulin opposition. Additionally, insulin insufficiency encourages fatty acid β -oxidation, which increases hydrogen peroxide production. As a result, pancreatic and liver cells are affected by diabetes and suffer from the elevated quantities of reactive oxygen species [19]. Diabetes mellitus is a major health issue that has a negative and permanent effect on individuals, as well as entire families and societies. Over the past three decades, this issue has grown significantly in scope and is expected to affect 439 million elderly patients by 2030 [20]. Due to their tendency to

worsen post-prandial hyperglycemia, α -glucosidase and α -amylase inhibitors are now the most indicated therapies for diabetes. The antioxidant properties of phenolic compounds depend on their characteristics as hydrogen donors, reducing agents, metal ion chelators, and protonated hydrogen quenchers [21]. Natural antioxidants may also be used as a possible treatment for type 2 diabetes mellitus as they reduce postprandial hyperglycemia and block α -glucosidase and α -amylase [22].

Around the world, patients with diabetes show an increased risk of developing such chronic health issues as atherosclerosis, obesity, renal failure, and dyslipidemia [23]. New lipase inhibitors obtained from plant extracts can provide new anti-obesity drugs. Actually, several synthetic medications, including acarbose and orlistat, are often used as inhibitors for these enzymes in people with obesity and type 2 diabetes [24, 25]. However, these inhibitors demonstrated a number of negative side effects [26]. As a result, much effort has been expended in reducing the negative side effects of all of these synthetic hypoglycemia and anti-obesity medications, as well as in discovering safer and natural inhibitors of α -amylase and lipase. Medicinal plants possess photochemically active flavonoids and phenolics with potent antioxidant activities. As a result, they are commonly used to treat diabetes and associated complications [27]. These substances are potent inhibitors of α -amylase and lipase [28].

Environmental elements, e.g., pollution and unhealthy diet, may affect thyroid function [29]. The effects of goitrogenic drugs are a popular research subject [30]. The incidence of goiter is higher if dietary iodine deficiency is caused by thyroid function inhibitors [31].

As the global demand for plant extracts keeps increasing, it triggers an indiscriminate consumption of plants with ambiguous chemical and biological properties. Flavonoids are a class of organic substances that are abundantly present in plants and have been linked to a variety of biological and pharmacological actions in recent years. Thyroid peroxidase is a crucial enzyme for the production and processing of thyroid hormones. It is one of the numerous enzymes that flavonoids can block [32].

According to Bray *et al.* [33], cancer will be the leading cause of mortality in the XXI century. Cancer comes in 36 types that can afflict both women and men. No traditional or contemporary cancer treatment has proved flawless [34]. Numerous variables make it crucial to keep looking for innovative anticancer medications. These concerns include medical procedures that might have serious adverse consequences or that could be rather pricey [35]. Medical scientists are looking for less expensive and more biologically secure options [36]. As far as we know, no comprehensive study has been performed on the therapeutic effect of barnûf leaf extracts, especially their anti-diabetic, anti-obesity, antithyroid, and anticancer properties. This research featured the efficiency of various solvents in the extraction of polyphenols from barnûf leaves, as well as the *in vitro* antioxidant, antimicrobial, antidiabetic, anti-obesity, antithyroid, and anticancer properties of these extracts.

STUDY OBJECTS AND METHODS

Materials. The fresh barnûf (*Pluchea dioscoridis* L.) leaves were procured in March 2019 from an experimental field of the Agriculture Department, Kafrelsheikh University, Egypt. They were identified as such at the Plants Department, Al-Azhar University, Egypt.

The ethanol (80%), methanol (80%), acetone, gallic acid, quercetin, DPPH, ABTS, butylated hydroxyanisole, ciprofloxacin, fluconazole, α -glucosidase, α -amylase, lipase, thyroid peroxidase, and guaiacol were acquired from Sigma-Aldrich Chemical Co., USA. Every chemical employed in this research was of HPLC quality, with 99.9% purity.

The nutritional agar and potato dextrose agar media were purchased from Difco Lab, USA.

The samples of *Salmonella typhimurium* ATCC23851, *Escherichia coli* ATCC25921, *Staphylococcus aureus* ATCC25920, *Pseudomonas aeruginosa* ATCC25004, and *Candida albicans* ATCC10230 came from the Microbiology Department, Kafrelsheikh University, Egypt.

Preparing barnûf leaves. The barnûf leaves were washed with pure water. After gathering surplus water with white towels, we left the leaves to dry for a day in an oven (Memmert, UF) at $45 \pm 3^\circ\text{C}$. After that, we pulverized them in an FX1000 electrical crusher (Black & Decker, England) and sieved the powder to produce particles of ≈ 70 mesh [5].

Preparing barnûf leaf extracts. The barnûf leaf powder was extracted using methanol (80%), ethanol (80%), and acetone as solvents. The solvents were selected based on primary experiments. We extracted 20 g of the dried leaf powder in three separate batches by macerating them for 24 h at room temperature in 100 mL of ethanol, methanol, or acetone. All extracts were then vacuum-concentrated at 40°C after being filtered using Whatman filter paper (No. 4 Chr, UK). The resulting extracts were stored at $4 \pm 1^\circ\text{C}$ for later use.

Quantifying total phenolics and flavonoids. The technique outlined by Waterhouse [37] was used to estimate the total phenolic contents in the barnûf leaf extracts using a UV/Vis spectrophotometer (Shimadzu UV-1800, Kyoto, Japan) at 765 nm and calculated the results as mg gallic acid equivalent (GAE) per 1 g of extract. The flavonoid content was measured using the method of Zhishen *et al.* [38]. Using a UV/Vis spectrophotometer (Shimadzu UV-1800, Kyoto, Japan) at 415 nm and expressed the results as mg of quercetin equivalent (QE) per 1 g of extract.

High-performance liquid chromatography (HPLC) analysis. The barnûf leaf extracts underwent a HPLC analysis in a food chemistry laboratory, National Research Center, Egypt. The phenolic measurements followed the protocol described by Elsebaie & Essa [39] and involved Shimadzu LC-10A HPLC instruments (Kyoto, Japan).

Antioxidant activity. 2,2-diphenyl-1-picrylhydrazyl (DPPH) radical scavenging activity. We used the approach outlined by Fki *et al.* [40] to examine the DPPH radical-scavenging impact. We mixed 5 mL of a 0.004%

methanol DPPH solution with 50 μL of variously diluted extracts (0–100 $\mu\text{g/mL}$) in methanol. After 30 min of room temperature incubation, we measured the absorbance at 517 nm and compared the results with the blank. The percentage of DPPH inhibition, %, was calculated using the following Eq. (1):

$$\text{DPPH inhibition} = \left(\frac{A_b - A_s}{A_b} \right) \times 100 \quad (1)$$

where A_b is the blank absorbance and A_s is the sample absorbance.

By comparing the graph plotting of the inhibition percentage with the extract concentration, we determined the extract concentration that provided 50% inhibition, i.e., IC_{50} . All assays were run in triplicate and used the synthetic antioxidant reagent butylated hydroxyanisole as a positive control.

2,2'-Azinobis-(3-Ethylbenzthiazolin-6-Sulfonic Acid (ABTS) activity. The ABTS^{•+} method to measure the antioxidant activity of the extracts followed the method developed by Sayah *et al.* [41]. First, we mixed a 5 mM solution of ABTS in phosphate buffered saline with pH 7.4. Then, we combined the ABTS stock solution and MnO_2 to create the ABTS radical cation (ABTS^{•+}) and filtered it through a polyvinylidene fluoride membrane. Its absorbance was measured in a 1-cm cuvette after diluting it in phosphate buffered saline (pH 7.4) until equilibrium was reached at 30°C . The mix was then stored at 20°C until use. The final absorbance was measured at 734 nm. After that, we combined 0.05 mL of each extract with 3 mL of the ABTS^{•+} solution at a concentration of 0–100 $\mu\text{g/mL}$. After a violent shaking in an Eppendorf tube, the mix settled in the dark at room temperature for 6 min before the absorbance at 734 nm was measured. Butylated hydroxyanisole served as a positive control while distilled water was applied as a negative control in place of the extract. The results were expressed by the Eq. (2):

$$\% \text{ inhibition ABTS}^{\bullet+} = \left(\frac{A_b - A_s}{A_b} \right) \times 100 \quad (2)$$

where A_b is the blank absorbance and A_s is the sample absorbance.

Determining antimicrobial activity. We assessed the antibacterial activity of the barnûf leaf extracts both quantitatively and qualitatively. To study the growth inhibition zones, we used the disc diffusion test as described by Elsebaie *et al.* [42]. We placed 100 mL of cultured cell suspension on each plate. The amount corresponded to 0.5 McFarland of the isolate. After that, we filled the agar plate wells with 100 μL of each barnûf leaf extract, i.e., ethanol, methanol, and acetone. In the antibacterial and antifungal tests, 100 $\mu\text{g/mL}$ ciprofloxacin and 100 $\mu\text{g/mL}$ fluconazole served as positive controls while dimethyl sulfoxide served as a negative control. The plates stayed at 25°C for 1 h to enable pre-incubation diffusion, which reduced the impact of time variation. The plates were subsequently re-incubated in a DSI-D laboratory incubator (Taichung, Taiwan) for 24 h

at 37°C for bacterial strains and 28°C for fungal strains. After the incubation, we examined the plates for antibacterial activity by measuring inhibition zones for each sample. To prevent errors, each test was triplicated for every strain.

In vitro antidiabetic activity. α -Glucosidase inhibition assay. The α -glucosidase inhibition test followed the protocol developed by Ademiluyi & Oboh [43]. 0.1 mol/L of phosphate buffer with pH of 6.9 contained 0.2 mL of barnûf leaf extracts with concentrations ranging from 0 to 500 g/mL and 100 μ L of α -glucosidase (0.5 mg/mL). It was allowed to settle at $25 \pm 2^\circ\text{C}$ for 10 min. Subsequently, we added 5 mmol/L of *p*-nitrophenyl-D-glucopyranoside solution to the phosphate buffer. After 5 min of incubation at 25°C, the reaction mixes were measured for absorbance at 405 nm using a Bruker 301E spectrophotometer (Rheinstetten, Germany). The α -glucosidase inhibition, %, was determined as follows:

$$\alpha\text{-glucosidase inhibition} = \left(\frac{A_b - A_s}{A_b} \right) \times 100 \quad (3)$$

where A_b is the blank absorbance and A_s is the sample absorbance.

α -amylase inhibiting test. The α -amylase inhibition test followed the method developed by Telagari & Hultatti [44]. We combined 200 μ L of sodium phosphate buffer (0.02 M) with 80 μ L of each barnûf leaf extract at various concentrations that ranged from 0 to 500 μ g/mL. The α -amylase solution (20 μ L) was mixed and kept at room temperature for 10 min. After mixing 200 μ L of soluble starch, we left it to settle for 1 h. After adding the 3,5-dinitrosalicylic acid reagent (400 μ L) and putting it into a boiling water bath for 5 min, we interrupted the enzymatic reaction by cooling it down and adding 15 mL of distilled water. A UV-Vis spectrophotometer (Shimadzu UV-1800, Kyoto, Japan) was used to measure the absorbance at 540 nm and observe the color change. The α -amylase inhibition, %, was calculated by the Eq. (4):

$$\alpha\text{-amylase inhibition} = \left(\frac{A_b - A_s}{A_b} \right) \times 100 \quad (4)$$

where A_b is the blank absorbance and A_s is the sample absorbance.

In vitro anti-obesity activity. Each sample of barnûf leaf extract was dissolved in dimethyl sulfoxide (10%) to yield stock solutions of 500 μ g/mL. These solutions were used to create a concentration dilution series of 0–500 μ g/mL. Right before the experiment, we prepared a new stock solution of lipase in a Tris-HCl buffer. *p*-Nitrophenyl butyrate served as a substrate at a concentration of 41.8 mg in 4 mL acetonitrile. After that, we combined lipase and barnûf leaf extracts (0.2 mL) from each dilution series to make workable solutions. After diluting these operating solutions to a final volume of 1 mL with Tris-HCl, we incubated them at 37°C for 15 min. After incubation, each test tube received 0.1 mL of *p*-nitro-

phenyl butyrate solution. At 37°C, the slurry was incubated again for 30 min. Using a Shimadzu UV-1800 UV/Vis spectrophotometer (Kyoto, Japan), we measured hydrolysis of *p*-nitrophenyl butyrate into *p*-nitrophenolate at 410 nm to evaluate the lipase activity [45]. As before, orlistat served as a standard reference chemical. The lipase inhibition, %, was calculated as follows:

$$\text{Lipase inhibition} = \left(\frac{A_b - A_s}{A_b} \right) \times 100 \quad (5)$$

where A_b is the blank absorbance and A_s is the sample absorbance.

Antithyroid activity. Preparing thyroid peroxidase. We used the method published by Jomaa *et al.* [46], with a few adjustments. The thyroid glands of New Zealand rabbits were purchased from a nearby butcher (Kafrelsheikh, Egypt) and kept at -20°C until needed. We homogenized the material using a Philips homogenizer (Minato-ku, Tokyo, Japan) in a solution that contained 2 mM of Tris-HCl, 0.25 M sucrose, 40 mM NaCl, 100 mM KCl, and 10 mM MgCl_2 . The resulting mass was centrifuged twice at 4000 rpm at 4°C for 15 min, followed by salting out 60% of enzyme protein. The supernatant stayed in an UGH0044N Kiriazi freezer (Cairo, Egypt) at -20°C until utilized for further analysis.

Thyroid peroxidase inhibitory assay. This test, with a few modifications, also followed the procedure developed by Jomaa *et al.* [46]. The measurement was carried out in a cuvette with a light path of 1.0 cm at a wavelength of 470 nm. The test involved a Shimadzu UV-1800 spectrophotometer (Kyoto, Japan). The mix consisted of guaiacol, 0.1 mol/L phosphate buffer, 40 μ L pure material solution, 20 mL thyroid peroxidase enzyme, and 50 μ L H_2O_2 at pH 7.4. The combination had a total volume of 210 L. The buffer replaced the barnûf leaf extracts at various concentrations (0–500 g/mL) in the sample probe. The absorbance values were taken at 37°C for three minutes every one minute. The following formula was used to determine the thyroid peroxidase inhibitory activity, %:

$$\text{Inhibition} = \left(1 - \frac{\Delta A/\text{min for test}}{\Delta A/\text{min for blank}} \right) \times 100 \quad (6)$$

where $\Delta A/\text{min}$ represents the variation in linearity absorbance, minute to minute, of the test samples; and $\Delta A/\text{min}$ stands for the variation in linear blank absorption, minute to minute, for the blank samples. The interpolation of dose dependent curves yielded the IC_{50} value.

Anticancer activity. MCF7-1 (breast) and H1299-1 (lung) drug cytotoxicity assays arrived from the National Institute of Oncology in Cairo, Egypt. The potential cytotoxicity of the barnûf leaf extracts was examined using the Natural Red Uptake (NRU) test at concentrations ranging from 0 to 50 μ g/mL [47].

Statistical analysis. We used the study of variance (ANOVA), the Duncan test, and the SPSS 17.0 software with $p < 0.05$ as significant.

RESULTS AND DISCUSSION

Total phenolics and flavonoids. Table 1 displays the obtained data for total phenolics and flavonoids based on the absorbance values of the different extracts in comparison to the standard solutions of gallic acid and quercetin. The proportion of flavonoids and polyphenols in every extract proved to be high. The methanolic extract contained the highest amount of total phenolics (241.50 ± 3.71 mg GAE/g) and flavonoids (256.18 ± 3.19 mg QE/g), followed by the ethanol extract with 185.15 ± 3.35 mg GAE/g and 194.24 ± 5.02 mg QE/g, and the acetone extract with 123.47 ± 4.15 mg GAE/g and 136.11 ± 2.97 mg QE/g, respectively. These results were found consistent with those reported by Allouche *et al.* [27], who described polar solvents as optimal for polyphenolic extraction. When the extraction solvent polarity rose, the yield of polyphenols extracted also went up. According to Qasim *et al.* [48], methanolic extracts from *Pluchea* leaves contained more polyphenols and flavonoids than ethanolic and acetone extracts.

Identifying polyphenolic acids. Table 2 shows the polyphenolic composition of barnûf leaf extracts measured by high-performance liquid chromatography

Table 1 Total polyphenols and flavonoids in barnûf leaf extracts

Solvent	Total phenolics, mg GAE/g extract	Total flavonoids, mg QE/g extract
Methanol	241.50 ± 3.71^a	256.18 ± 3.19^a
Ethanol	185.15 ± 3.35^b	194.24 ± 5.02^b
Acetone	123.47 ± 4.15^c	136.11 ± 2.97^c

The data are displayed as mean \pm SD

Values followed by different superscripts in each column differed significantly at $p \leq 0.05$

Table 2 Major phenolic compounds, % total, in different barnûf leaf extracts as identified by HPLC

Compounds	Extract type		
	Ethanol	Methanol	Acetone
Gallic acid	6.71	8.13	n.d.
Protocatechuic acid	4.20	6.01	n.d.
Pyrogallol	n.d.	8.24	n.d.
Catechol	n.d.	n.d.	1.06
Chlorogenic acid	8.27	8.20	6.30
<i>p</i> -Coumaric acid	3.76	1.53	1.11
Catechin	15.28	12.80	8.52
Caffeic acid	5.75	4.60	1.96
Vanillic acid	1.90	2.70	n.d.
Ellagic acid	24.71	30.33	22.60
Caffeine	n.d.	0.29	0.86
Salicylic acid	3.91	n.d.	18.22
Ferulic acid	3.72	n.d.	9.34
Cinnamic acid	0.73	n.d.	0.23
B-OH benzoic acid	21.06	15.75	29.80
Colchicine	n.d.	1.40	n.d.
Chrysin	n.d.	0.02	n.d.

n.d. – not detected

(HPLC). The ethanol and methanol extracts contained 12 and 13 phenolic compounds, respectively. Ellagic acid, benzoic acid, catechin, pyrogallol, chlorogenic acid, and gallic acid were the major phenolic compounds presented and identified in the methanolic extract. As for the ethanol extract, the most predominant phenolic compounds were represented by ellagic acid, benzoic acid, catechin, chlorogenic acid, and gallic acid. The acetone extract contained 11 phenolic compounds, the major ones being benzoic acid, ellagic acid, salicylic acid, ferulic acid, and catechin. Pyrogallol, colchicine, and chrysin were found in the methanolic extract only whereas catechol was found in the acetone extract only. These results confirmed those reported by Elsebaie & Essa [5], who found 12 phenolic acids in the barnûf leaf ethanolic extract, ellagic acid and benzoic acid being the most abundant ones.

Antioxidant activity. Free radicals have recently been implicated in a number of medical conditions, including heart disease, cancer, ageing, cataracts, immune system damage, etc. [49]. Antioxidants slow down the oxidation rate and shield cells from harm. As a result, they can get rid of unstable free radicals [49]. Antioxidant medications are employed to prevent and cure various diseases that are caused by oxidative stress, e.g., diabetes, Alzheimer's disease, atherosclerosis, stroke, and cancer [50, 51]. Herbal remedies have recently become very popular as an alternative to synthetic medicines because they have no side effects and are less expensive [52]. Antioxidant activity can be measured both *in vitro* and *in vivo*, but very few quick and accurate techniques cover a wide range of plant extracts [53, 54]. In this research, we investigated the ability of barnûf leaf extracts to scavenge the steady free radical DPPH and the cation ABTS in order to explore their antioxidant activity.

DPPH is a stable free nitrogen-centered radical. It is commercially available and has a distinctive absorbance at 517 nm [55]. It provides a common method for assessing plant extracts for antioxidant standards and ability to scavenge free radicals. By absorbing hydrogen from a matching donor, the DPPH solution loses its typical dark purple hue and transforms into yellow diphenylpicryl hydrazine [56]. The overall *in vitro* antioxidant activity of plant extracts has extensively been assessed using this scavenging activity as a rapid and trustworthy criterion [57].

The DPPH test has been applied to antioxidant activities of various medicinal plants [58–60]. These studies reported many plant compounds that act as antioxidants. Figure 1a illustrates the DPPH radical scavenging capacity of different barnûf leaf extracts at various doses. All barnûf leaf extracts demonstrated scavenging activity, which became stronger as the extract concentration increased. At 100 $\mu\text{g/mL}$ concentration, the methanolic, ethanolic, and acetone barnûf leaf extracts all showed enhanced DPPH radical scavenging activities of 83.17, 70.43, and 64.12%, respectively. The acetone extract demonstrated reduced action at all levels. Barnûf leaves

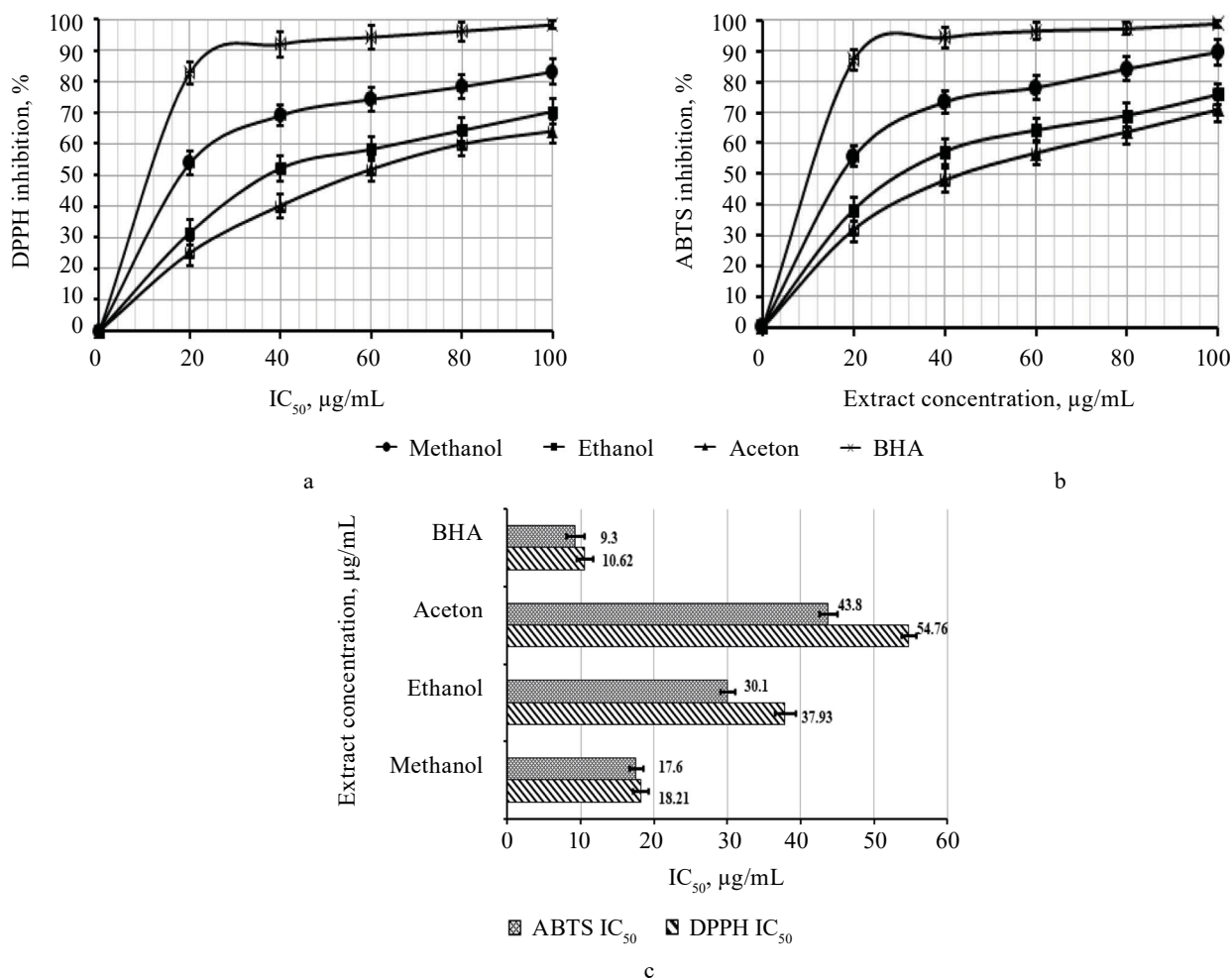
had a significant concentration of phytochemicals that probably donated protons and acted as radical scavengers. Similar findings were reported by Saber [61], who used *Pluchea dioscoridis* leaf extracts to scavenge DPPH radicals in a dose-dependent manner [61].

ABTS stands for 2,2-azino-bis-3-ethylbenzothiazoline-6-sulfonic acid. It has a radical cation that may exist in its free state without losing stability. The concentration of radicals was calculated at 734 nm. When an antioxidant was added to the solution of the radical, both its amount and its absorbance went down. This decline depended on the antioxidant activity of the test compound, as well as on the time and concentration [62]. A more effective ABTS decolorization test was used by Re *et al.* [63].

Figure 1b shows how well the extracts were able to remove the ABTS cation. The methanolic extract demonstrated significant concentration-dependent ABTS radical cation scavenging activity. At a concentration of 100 µg/mL, the ethanolic, methanolic, and acetone extracts of barnûf leaves had 89.7, 75.9, and 70.94% scavenging action on ABTS, respectively. This response may point to the ability of barnûf leaves to reduce oxidative

damage to a few key bodily tissues at the tested amounts [64]. These findings concur with those reported by Vongsak *et al.* [65], who used the same ABTS test in their research. Figure 1c illustrates a comparative analysis of the IC_{50} values. A low IC_{50} value indicated antioxidant activity. In fact, the maximal DPPH radical inhibition value belonged to the methanolic extract (18.21 µg/mL), followed by the ethanolic extract (37.93 µg/mL) and the acetone extract (54.76 µg/mL). Additionally, the methanolic extract also showed the greatest efficiency against the ABTS radical cation (17.6 µg/mL), followed by the ethanolic extract (30.1 µg/mL) and the acetone extract (43.8 µg/mL). For the DPPH and ABTS assays, the butylated hydroxyanisole IC_{50} values were 10.62 and 9.30 µg/mL, respectively. The presence of additional elements in minute amounts or their combination with the primary ingredients may also contribute to the efficiency of the antioxidant. Our results followed the same pattern as those published by Qasim *et al.* [48] and Saber [61].

Antimicrobial activity. Table 3 describes the inhibition zones (mm) to summarize the antibacterial capacity of various barnûf leaf extracts against two gram-negative bacteria (*Escherichia coli* and *Salmonella thyphimu-*



Error bars represent standard deviation (n = 3)

Figure 1 Antioxidant activity of different barnûf leaves extracts by DPPH (a) and ABTS (b); IC_{50} (c)

Table 3 Antimicrobial activity of different Barnûf leaf extracts

Microorganisms	Growth inhibition zone (diameter), mm				
	Barnûf leaf extract			Ciprofloxacin	Fluconazole
	Methanolic	Ethanollic	Acetone		
<i>Escherichia coli</i>	22.3 ± 0.7 ^{ec}	20.4 ± 0.5 ^{dd}	24.2 ± 0.3 ^{eb}	36.1 ± 0.5 ^{ea}	–
<i>Salmonella typhimurium</i>	24.3 ± 0.5 ^{dc}	20.1 ± 0.3 ^{dd}	26.0 ± 0.3 ^{bb}	40.2 ± 0.8 ^{aa}	–
<i>Pseudomonas aeruginosa</i>	29.8 ± 0.4 ^{eb}	26.5 ± 0.7 ^{ec}	20.6 ± 0.4 ^{dd}	38.4 ± 0.3 ^{ba}	–
<i>Staphylococcus aureus</i>	33.2 ± 0.6 ^{ba}	28.1 ± 0.5 ^{bb}	23.2 ± 0.5 ^{cc}	33.3 ± 0.4 ^{da}	–
<i>Candida albicans</i>	39.8 ± 0.3 ^{aA}	35.4 ± 0.6 ^{aB}	27.5 ± 0.7 ^{ac}	–	40.2 ± 0.3 ^A

The data are displayed as mean ± SD

Means with different uppercase superscripts (A–D) in the same row are significantly different at $p \leq 0.05$

Means with different lowercase superscripts (a–d) in the same column are significantly different at $p \leq 0.05$.

rium), two gram-positive bacteria (*Pseudomonas aeruginosa* and *Staphylococcus aureus*), and one strain of yeast (*Candida albicans*).

All extracts were obviously effective against the five microbiological strains under analysis. The methanolic and ethanollic barnûf leaf extracts had the highest inhibitory zones against *S. aureus* (33.2 ± 0.6 and 28.1 ± 0.5 mm, respectively). These actions represented 84.38% of ciprofloxacin activity. *E. coli* and *S. typhimurium* were both successfully inhibited by the acetone extract, with inhibition zones of 24.2 ± 0.3 and 26.0 ± 0.3 mm, respectively. The methanolic extract provided larger inhibition zones against *E. coli* and *S. typhimurium* than the ethanollic one but both values were lower than those demonstrated by the acetone extract. These findings are quite significant because the gram-negative bacteria under investigation cause serious intestinal illnesses.

In contrast, the methanolic and ethanollic barnûf leaf extracts were more effective than the acetone extract in killing *P. aeruginosa* and *S. aureus*. Our extracts demonstrated antibacterial efficacy against gram-positive bacteria that was inferior to that of ciprofloxacin. Overall, the acetone extract inhibited gram-negative bacterial strains whereas the methanolic extract inhibited gram-positive bacteria. The obtained results were in line with those obtained by Elsebaie & Essa [5], Al-Salt [66], and Zalabani *et al.* [67]. These results revealed that gram-positive microbes were more sensitive to hydro alcoholic extracts than gram-negative germs, as previously reported by Aruwa *et al.* [68].

Additionally, the barnûf leaf extracts in methanolic and ethanollic forms were more effective against *C. albicans* than the acetone extract. Our results reconciled with those obtained by El-Ghorab *et al.* [69], who linked the antimicrobial properties of barnûf to its phenolic compounds. Our extracts demonstrated antimicrobial efficacy against all samples, with the exception of the methanolic extract: its activity against *C. albicans* was inferior to fluconazole.

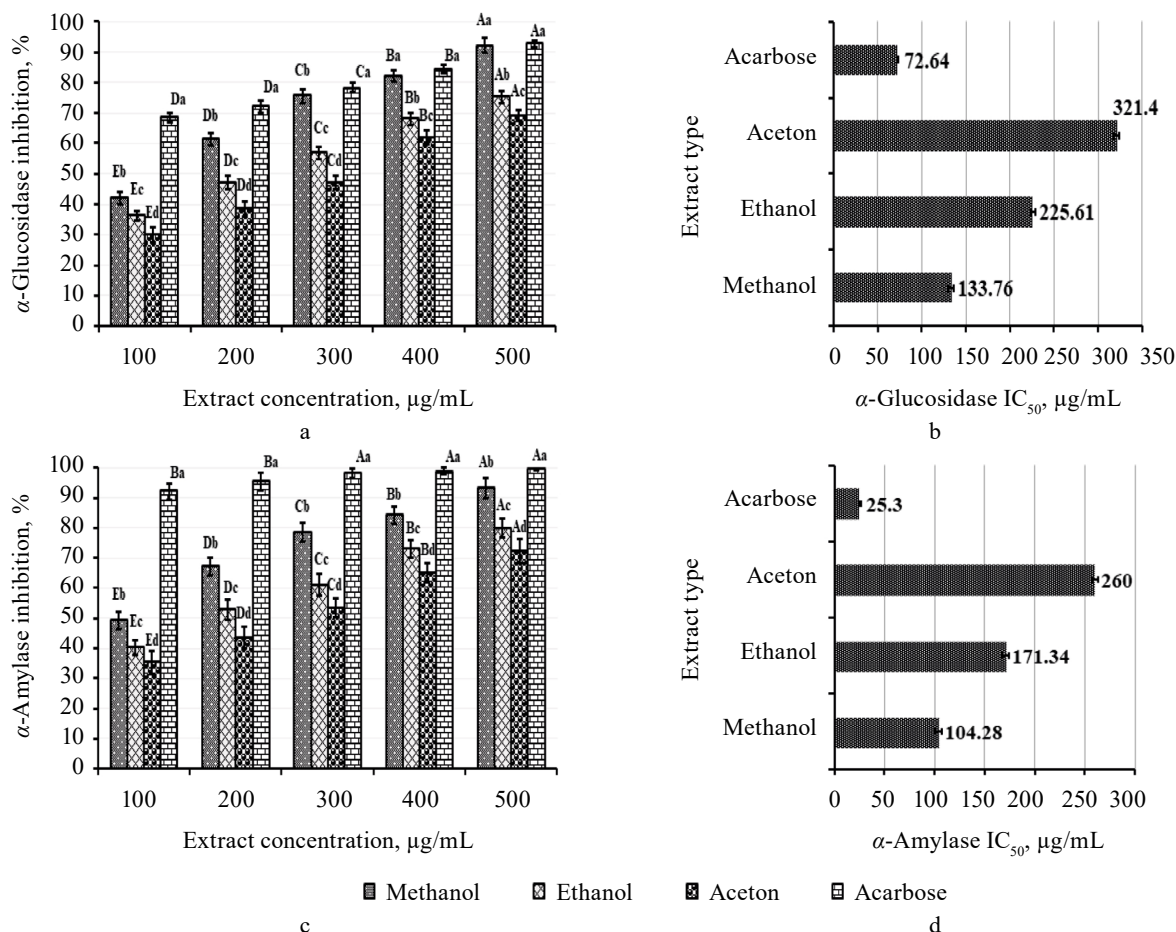
Ciprofloxacin gave larger inhibition zones for *E. coli*, *S. typhimurium*, and *P. aeruginosa* than those obtained by all types of barnûf leaf extracts. The methanolic extract and ciprofloxacin gave similar diameter zones in relation to *S. aureus*. Also, fluconazole and the methanolic

extract gave similar diameter zones in relation to *Ca. albicans*, which exceeded those obtained by the ethanollic and acetone extracts. The antimicrobial activity demonstrated by ciprofloxacin and fluconazole against the bacterial and fungal strains in this research was similar to that reported by Elsebaie & Essa [5], Elsebaie *et al.* [42], and El-Ghorab *et al.* [69].

In vitro antidiabetic activity. α -Glucosidase inhibition assay. A well-known strategy to combat the metabolic changes caused by type 2 diabetes is to inhibit this enzyme [70]. Generally, α -glucosidase inhibitory agents are regarded as oral hypoglycemic medications because they prevent disaccharides from converting into monosaccharides and maintain normal blood sugar levels [19]. We used acarbose, a potent enzyme inhibitor, to compare the results of the α -glucosidase test and calculate the IC_{50} values for the three extracts (Fig. 2a and b). The findings show that all barnûf leaf extracts contained potential α -glucosidase inhibitors. Acarbose, which served as reference, had an IC_{50} of 72.64 ± 1.04 μ g/mL. The methanolic extract demonstrated the strongest inhibitory effect on α -glucosidase (133.76 ± 2.09). The IC_{50} values for the ethanol and acetone extracts were 225.61 ± 2.97 and 321.40 ± 3.12 μ g/mL, respectively, showing only modest α -glucosidase inhibition. The variations in phenolic, flavonoid, and antioxidant activities of barnûf leaf extracts may be responsible for this finding. Gowri *et al.* [71] indicated a positive relationship between the total flavonoid and polyphenol contents and the ability to inhibit α -glucosidase. These results were similar to ours, as demonstrated in Table 2: the barnûf leaf ethanol and methanol extracts contained 12 and 13 phenolic compounds, respectively.

Error bars represent standard deviation ($n = 3$). Different lowercase superscripts indicate significant differences at $p \leq 0.05$ between the extracts at the same concentration. Different uppercase superscripts indicate significant differences at $p \leq 0.05$ between the concentrations for the same extract types

α -Amylase inhibition assay. As a major digestive enzyme, pancreatic α -amylase is implicated in the decomposition of starch into oligosaccharides before freeing glucose into the bloodstream for absorption. The amount of starch that is broken down in the gastro-



Error bars represent standard deviation ($n = 3$). Different lowercase superscripts indicate significant differences at $p \leq 0.05$ between the extracts at the same concentration. Different uppercase superscripts indicate significant differences at $p \leq 0.05$ between the concentrations for the same extract types.

Figure 2 Effect of different barnûf leaf extracts on α -glucosidase inhibition (a), α -glucosidase IC_{50} (b), α -amylase inhibition (c), and α -amylase IC_{50} (d)

intestinal system would decrease if α -amylase was inhibited. As a result, the amount of hyperglycemia may also be decreased [72]. In this test, we used acarbose, a powerful α -amylase inhibitory drug, to test the barnûf leaf extracts for their anti-amylase effectiveness (Fig. 2c and d). All three barnûf leaf extracts inhibited the α -amylase enzyme in a dose-dependent manner (0–500 $\mu\text{g/mL}$). The methanolic extract proved to be the most effective α -amylase inhibitor with an IC_{50} of $104.28 \pm 1.97 \mu\text{g/mL}$, as compared to $25.30 \pm 1.62 \mu\text{g/mL}$ for the reference acarbose. This suggested that barnûf leaf extracts might be an effective herbal treatment against diabetes. The acetone extract exhibited the lowest activity in this assay, with $IC_{50} = 260.00 \pm 1.97 \mu\text{g/mL}$, while the ethanolic extract showed only moderate activity with $IC_{50} = 171.34 \pm 1.50 \mu\text{g/mL}$. Highly polyphenolic herbal extracts demonstrated a stronger potential to block α -amylase, according to Shobana *et al.* [73]. Natural antioxidants and phenolics from plants were reported to possess fewer side effects [74]. The strongest α -amylase inhibitory activity of the methanolic extract may thus be attributed to its high phenolic content and antioxidant capacity.

Our results may be explained by the variation in phenolic, flavonoid, and antioxidant activities of the barnûf leaf extracts. Importantly, some researchers reported a positive relationship between the total flavonoid and polyphenol contents and the ability to inhibit α -glucosidase [71]. These results confirmed our findings presented in Table 2, where the ethanol and methanol extracts contained 12 and 13 phenolic compounds, respectively. Ellagic acid, B-OH benzoic acid, catechin, pyrogallol, chlorogenic acid, and gallic acid were the major phenolic compounds presented and identified in the methanolic extract. Ramkumar *et al.* [75] described ellagic and gallic acids as potent inhibitors of α -glucosidase and α -amylase. The methanolic extract demonstrated the highest content of ellagic and gallic acids, followed by ethanol and acetone. This fact may explain the variations between the inhibitory effects of the three different barnûf leaf extracts against α -glucosidase and α -amylase.

In vitro anti-obesity activity. Lipase is the most crucial digestive enzyme which hydrolyzes dietary lipids into glycerol and fatty acids so that they could be absorbed by the small intestine [76]. As a result, inhibiting this digestive enzyme can help with obesity treat-

ment [45]. As indicated in Fig. 3a and b all extracts in this research inhibited lipase activity. As a result, the IC_{50} values for methanolic, ethanolic, and acetone extracts against lipase activity were 127.35, 194, and 288 $\mu\text{g/mL}$, respectively, showing that the barnûf leaf extracts indeed had a potent anti-obesity action. The anti-hyperlipidemic drug orlistat ($IC_{50} = 14.26 \mu\text{g/mL}$) demonstrated a more powerful suppression of lipase than the other extracts in this research. Additionally, the total phenolics in the various extracts may precisely match their lipase-inhibitory properties. According to McDougall *et al.* [77], the ability to inhibit lipase may come from phenolic components of plant origin, e.g., catechin, gallic acid, epicatechin, myricetin, ellagic acid, kaempferol quercetin, resveratrol, and anthocyanins.

In vitro anti-thyroid activity. Thyroperoxidase (EC1.11.1.14), commonly known as thyroid peroxidase or iodide peroxidase, is an enzyme involved in the production of thyroid hormones [78]. Since the thyroid peroxidase enzyme is a heme peroxidase, the substrate must first undergo oxidation before it can be oxidized. The H_2O_2 molecule is crucial for its oxidation. The H_2O_2 molecule appears only at the apical surface of thyrocytes, activating any thyroid peroxidase molecules that may be there [79]. Figure 4 displays the thyroperoxidase inhibiting activity of the barnûf leaf extracts. All extracts in this research contained potential thyroperoxidase inhibitors. The methanolic extract demonstrated the most prominent inhibitory activity of 85.89%, followed by the ethanolic and acetone extracts

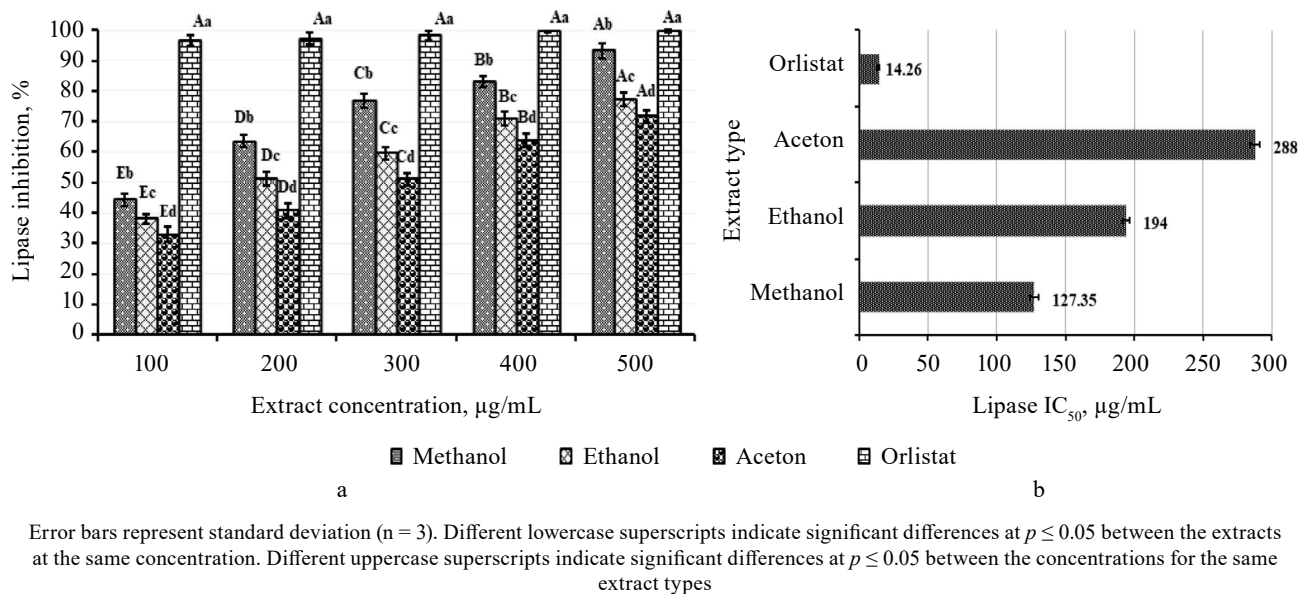


Figure 3 Effect of different barnûf leaf extracts on lipase inhibition (a) and lipase IC_{50} (b)

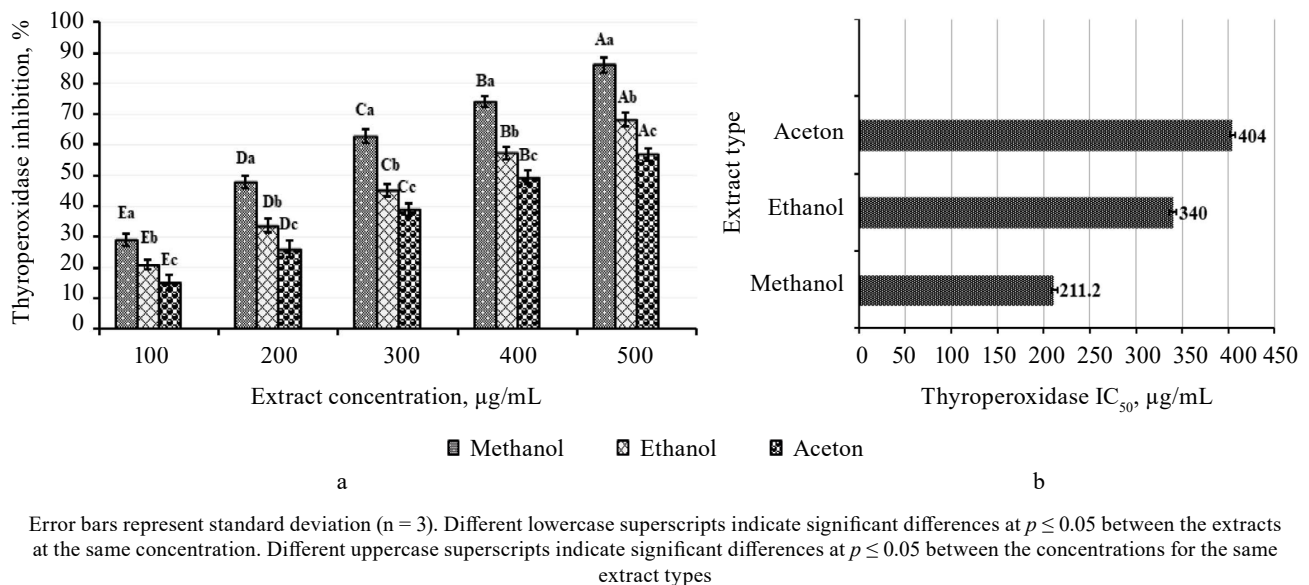
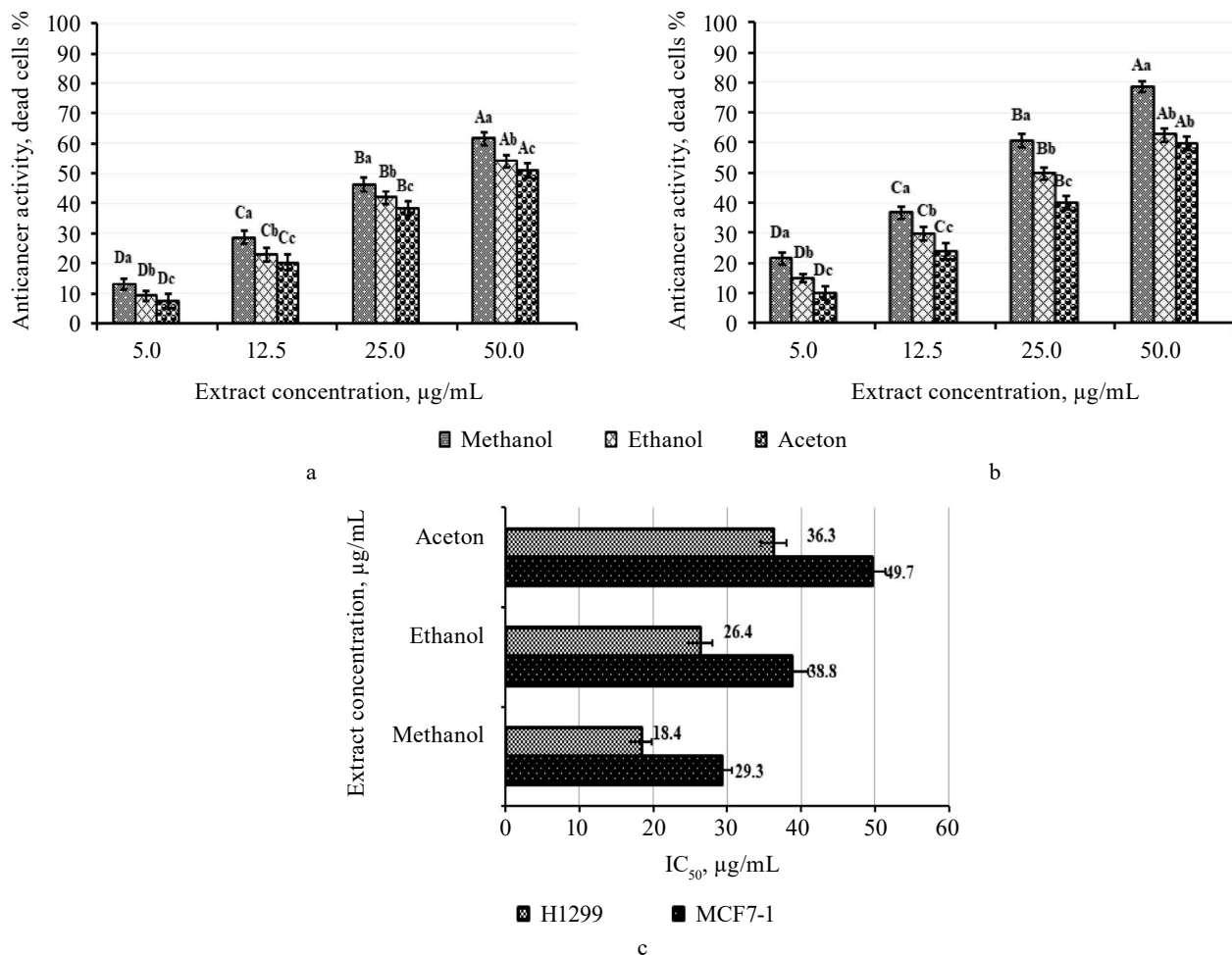


Figure 4 Effect of different barnûf leaf extracts on thyroid peroxidase inhibition (a) and thyroid peroxidase IC_{50} (b)



Error bars represent standard deviation (n = 3). Different lowercase superscripts indicate significant differences at $p \leq 0.05$ between the extracts at the same concentration. Different uppercase superscripts indicate significant differences at $p \leq 0.05$ between the concentrations for the same extract types

Figure 5 Anticancer activity of different barnûf leaf extracts against MCF7-1 (a) and H1299 (b); IC₅₀ (c)

in a dose-dependent manner (0–500 µg/mL). Habza-Kowalska *et al.* [78] linked inhibitory properties to the antioxidant activity power. Their results were in line with ours, as illustrated by Fig. 1, where the methanolic extract demonstrated the highest antioxidant activity against DPPH and ABTS, followed by the ethanol and acetone extracts.

The IC₅₀ values of the methanol, ethanol, and acetone extracts against thyroperoxidase were 211.2, 340, and 404 µg/mL, respectively (Fig. 4b). Such polyphenolic components as chlorogenic acid, rosmarinic acid, and quercetin were probably responsible for thyroperoxidase inhibition [78].

Anticancer activity. We used MCF7-1 (breast) and H1299-1 (lung) cell lines to assess the potential of barnûf leaf extracts to suppress cell proliferation. Both cancer cell lines were treated with varied concentrations of different extracts. Figure 5 shows that the general activity against H1299-1 was superior to that against MCF7-1. At a concentration of 50 µg/mL, the methanolic extract showed strong anticancer activity against both MCF7-1 and H1299-1 with inhibition percentages of

61.47 and 78.66%, respectively. At the same concentration, the ethanolic extract also demonstrated strong anticancer activity against both lines with inhibition percentages of 54.13 and 62.59%. The acetone extract had a cytotoxic impact on both lines, with inhibition percentages of 50.82 and 59.72% at 50 µg/mL acetone extract concentration. In the methanol sample, MCF7-1 and H1299-1 had IC₅₀ values of 29.3 and 18.4 µg/mL, respectively. In the ethanol sample, the IC₅₀ values against MCF7-1 and H1299-1 were 38.8 and 26.4 µg/mL, respectively.

Figure 5 demonstrates an inverse relationship between cell viability and sample concentration, with the cell viability percentage declining as the sample concentration rose. The growth of MCF7-1 and H1299-1 cells was negligible, indicating that the barnûf leaf extracts are safe *in vitro* and may be employed as a component in food products, once clinically evaluated on animals and people. The following investigations support the theory that phytochemicals contribute to anticancer properties. lawsipo *et al.* [80] studied barnûf leaf extracts for anticancer action against breast and cervical cancer cell line. They observed considerable cytotoxicity: the extracts

reduced cancer cell growth even at low doses (15 µg/mL). Bibi *et al.* [81] mentioned about 1000 plant species on Earth as possessing anticancer properties. Our experiment *in vitro* suggests that barnûf is one of these species.

CONCLUSION

The methanolic extract of barnûf (*Pluchea dioscoridis* L.) leaves contained the greatest total phenolics (241.50 ± 3.71 mg GAE/g) and flavonoids (256.18 ± 3.19 mg QE/g), followed by the ethanol extract and the acetone extract. Also, the methanolic extract showed the strongest antioxidant properties against DPPH and ABTS radicals. All barnûf leaf extracts had a potential antimicrobial activity, but the methanolic and ethanolic extracts were more effective than the acetone extract. In addition, gram-positive microbes appeared to be more sensitive to the barnûf leaf extracts than gram-negative bacteria. The extracts demonstrated a powerful suppression of α -glucosidase, α -amylase, lipase, and thyroperoxidase, which suggests that the methanolic extract had good prospects for phytotherapy against diabetes and obesity, as well as an antithyroid agent. Additionally, the methanolic extract inhibited both MCF7-1 and

H1299-1 cell lines. These findings might inspire more *in vivo* research to create all-natural pharmaceutical formulations that would be efficient in the treatment of obesity, diabetes, and certain cancers.

CONTRIBUTION

Essam M. Elsebaie was responsible for conceptualization, data curation, formal analysis, investigation, methodology, validation, drafting, review, and editing. Rowida Y. Essa provided data curation, formal analysis, investigation, methodology, software, and the original draft. Wesam M. Abdelrhman was responsible for validation, drafting, review, and editing. Mohamed R. Badr provided data curation, investigation, methodology, software, validation, formal analysis, review, and editing.

CONFLICT OF INTEREST

The authors declared no conflict of interest regarding the publication of this article.

DATA AVAILABILITY STATEMENT

Data available on request due to privacy/ethical restrictions.

REFERENCES

1. Hlila MB, Mosbah H, Zanina N, Ben Nejma A, Ben Jannet H, Aouni M, *et al.* Characterisation of phenolic antioxidants in *Scabiosa arenaria* flowers by LC-ESI-MS/MS and NMR. *Journal of Pharmacy and Pharmacology*. 2016;68(7):932–940. <https://doi.org/10.1111/jphp.12561>
2. Kumarasingha R, Preston S, Yeo T-C, Lim DSL, Tu C-L, Palombo EA, *et al.* Anthelmintic activity of selected ethnomedicinal plant extracts on parasitic stages of *Haemonchus contortus*. *Parasites and Vectors*. 2016;9:187. <https://doi.org/10.1186/s13071-016-1458-9>
3. Halliwell B. Drug antioxidant effects. A basis for drug selection? *Drugs*. 1991;42:569–605. <https://doi.org/10.2165/00003495-199142040-00003>
4. Shaltout KH, Slima DF. The biology of Egyptian woody perennials. 3. *Pluchea dioscoridis* (L.) DC. *Assuit University Bulletin for Environmental Researches*. 2007;10(1):85–103.
5. Elsebaie EM, Essa RY. Application of barnûf (*Pluchea dioscoridis*) leaves extract as a natural antioxidant and antimicrobial agent for eggs quality and safety improvement during storage. *Journal of Food Processing and Preservation*. 2022;46:e16061. <https://doi.org/10.1111/jfpp.16061>
6. Buhmann A, Papenbrock J. An economic point of view of secondary compounds in halophytes. *Functional Plant Biology*. 2013;40(9):952–967. <https://doi.org/10.1071/FP12342>
7. Falleh H, Trabelsi N, Bonenfant-Magné M, Le Floch G, Abdelly C, Magné C, *et al.* Polyphenol content and biological activities of *Mesembryanthemum edule* organs after fractionation. *Industrial Crops and Products*. 2013;42:145–152. <https://doi.org/10.1016/j.indcrop.2012.05.033>
8. Harborne AJ. *Phytochemical methods a guide to modern techniques of plant analysis*. Dordrecht: Springer; 1998. 302 p.
9. Liu X, Dong M, Chen X, Jiang M, Lv X, Yan G. Antioxidant activity and phenolics of an endophytic *Xylaria* sp. from *Ginkgo biloba*. *Food Chemistry*. 2007;105(2):548–554. <https://doi.org/10.1016/j.foodchem.2007.04.008>
10. Dai J, Mumper RJ. Plant phenolics: Extraction, analysis and their antioxidant and anticancer properties. *Molecules*. 2010;15(10):7313–7352. <https://doi.org/10.3390/molecules15107313>
11. Rubio-Moraga Á, Argandoña J, Mota B, Pérez J, Verde A, Fajardo J, *et al.* Screening for polyphenols, antioxidant and antimicrobial activities of extracts from eleven *Helianthemum* taxa (Cistaceae) used in folk medicine in south-eastern Spain. *Journal of Ethnopharmacology*. 2013;148(1):287–296. <https://doi.org/10.1016/j.jep.2013.04.028>
12. Wang H, Helliwell K. Determination of flavonols in green and black tea leaves and green tea infusions by high-performance liquid chromatography. *Food Research International*. 2001;34(2–3):223–227. [https://doi.org/10.1016/S0963-9969\(00\)00156-3](https://doi.org/10.1016/S0963-9969(00)00156-3)


13. Hayouni EA, Abedrabba M, Bouix M, Hamdi M. The effects of solvents and extraction method on the phenolic contents and biological activities *in vitro* of Tunisian *Quercus coccifera* L. and *Juniperus phoenicea* L. fruit extracts. Food Chemistry. 2007;105(3):1126–1134. <https://doi.org/10.1016/j.foodchem.2007.02.010>
14. Prior RL, Wu X, Schaich K. Standardized methods for the determination of antioxidant capacity and phenolics in foods and dietary supplements. Journal of Agricultural and Food Chemistry. 2005;53(10):4290–4302. <https://doi.org/10.1021/jf0502698>
15. El-Hamouly MA, Ibrahim MT. GC/MS analysis of the volatile constituents of individual organs of *Conyza dioscorides* L. (Desf.), growing in Egypt. Alexandria Journal of Pharmaceutical Sciences. 2003;17:75–81.
16. Kamel EM, Ahemd S. Phenolic constituents and biological activity of the genus *Pluchea*. Der Pharma Chemica. 2013;5(5):109–114.
17. Uchiyama T, Miyase T, Ueno A, Usmanghani K. Terpene and lignan glycosides from *Pluchea indica*. Phytochemistry. 1991;30(2):655–657. [https://doi.org/10.1016/0031-9422\(91\)83746-8](https://doi.org/10.1016/0031-9422(91)83746-8)
18. Bazzano LA, Serdula MK, Liu S. Dietary intake of fruits and vegetables and risk of cardiovascular disease. Current Atherosclerosis Reports. 2003;5:492–499. <https://doi.org/10.1007/s11883-003-0040-z>
19. Saravanan S, Parimelazhagan T. *In vitro* antioxidant, antimicrobial and anti-diabetic properties of polyphenols of *Passiflora ligularis* Juss. fruit pulp. Food Science and Human Wellness. 2014;3(2):56–64.
20. Shaw JE, Sicree RA, Zimmet PZ. Global estimates of the prevalence of diabetes for 2010 and 2030. Diabetes Research and Clinical Practice. 2010;87(1):4–14. <https://doi.org/10.1016/j.diabres.2009.10.007>
21. Zhang R, Zeng Q, Deng Y, Zhang M, Wei Z, Zhang Y, et al. Phenolic profiles and antioxidant activity of litchi pulp of different cultivars cultivated in Southern China. Food Chemistry. 2013;136(3–4):1169–1176. <https://doi.org/10.1016/j.foodchem.2012.09.085>
22. Boaventura BCB, Di Pietro PF, Klein GA, Stefanuto A, de Moraes EC, de Andrade F, et al. Antioxidant potential of mate tea (*Ilex paraguariensis*) in type 2 diabetic mellitus and pre-diabetic individuals. Journal of Functional Foods. 2013;5(3):1057–1064. <https://doi.org/10.1016/j.jff.2013.03.001>
23. Ahmad LA, Crandall JP. Type 2 diabetes prevention: A review. Clinical Diabetes. 2010;28(2):53–59. <https://doi.org/10.2337/diaclin.28.2.53>
24. Yee HS, Fong NT. A review of the safety and efficacy of acarbose in diabetes mellitus. Pharmacotherapy. 1996;16(5):792–805. <https://doi.org/10.1002/j.1875-9114.1996.tb02997.x>
25. Padwal RS, Majumdar SR. Drug treatments for obesity: Orlistat, sibutramine, and rimonabant. The Lancet. 2007;369(9555):71–77. [https://doi.org/10.1016/S0140-6736\(07\)60033-6](https://doi.org/10.1016/S0140-6736(07)60033-6)
26. Tahrani AA, Piya MK, Kennedy A, Barnett AH. Glycaemic control in type 2 diabetes: Targets and new therapies. Pharmacology and Therapeutics. 2010;125(2):328–361. <https://doi.org/10.1016/j.pharmthera.2009.11.001>
27. Allouche N, Fki I, Sayadi S. Toward a high yield recovery of antioxidants and purified hydroxytyrosol from olive mill wastewaters. Journal of Agricultural and Food Chemistry. 2004;52(2):267–273. <https://doi.org/10.1021/jf034944u>
28. Pereira DF, Cazarolli LH, Lavado C, Mengatto V, Figueiredo MSRB, Guedes A, et al. Effects of flavonoids on α -glucosidase activity: Potential targets for glucose homeostasis. Nutrition. 2011;27(11–12):1161–1167. <https://doi.org/10.1016/j.nut.2011.01.008>
29. Doerge DR, Divi RL. Porphyrin π -cation and protein radicals in peroxidase catalysis and inhibition by anti-thyroid chemicals. Xenobiotica. 1995;25(7):761–767. <https://doi.org/10.3109/00498259509061891>
30. Gaitan E. Flavonoids and the thyroid. Nutrition. 1996;12(2):127–129. [https://doi.org/10.1016/S0899-9007\(97\)85052-7](https://doi.org/10.1016/S0899-9007(97)85052-7)
31. Divi RL, Doerge DR. Inhibition of thyroid peroxidase by dietary flavonoids. Chemical Research in Toxicology. 1996;9(1):16–23. <https://doi.org/10.1021/tx950076m>
32. Ferreira ACF, Lisboa PC, Oliveira KJ, Lima LP, Barros IA, Carvalho DP. Inhibition of thyroid type 1 deiodinase activity by flavonoids. Food and Chemical Toxicology. 2002;40(7):913–917. [https://doi.org/10.1016/S0278-6915\(02\)00064-9](https://doi.org/10.1016/S0278-6915(02)00064-9)
33. Bray F, Ferlay J, Soerjomataram I, Siegel RL, Torre LA, Jemal A. Global cancer statistics 2018: GLOBOCAN estimates of incidence and mortality worldwide for 36 cancers in 185 countries. CA: A Cancer Journal for Clinicians. 2018;68:394–424. <https://doi.org/10.3322/caac.21492>
34. Karpuz M, Silindir Gunay M, Ozer AY. Current and future approaches for effective cancer imaging and treatment. Cancer Biotherapy and Radiopharmaceuticals. 2018;33(2):39–51. <https://doi.org/10.1089/cbr.2017.2378>
35. Szablewski L. Diabetes mellitus: Influences on cancer risk. Diabetes/Metabolism Research and Reviews. 2014;30(7):543–553. <https://doi.org/10.1002/dmrr.2573>
36. Moglad EHO, Abdalla OM, Koko WS, Saadabi AM. *In vitro* anticancer activity and cytotoxicity of *Solanum nigrum* on cancers and normal cell lines. International Journal of Cancer Research. 2014;10(2):74–80. <https://doi.org/10.3923/ijcr.2014.74.80>


37. Waterhouse AL. Determination of total phenolics. In: Wrolstad RE, editor. Current protocols in food analytical chemistry. New York: John Wiley and Sons; 2002. Ppp. 11.1.1–11.1.8.
38. Zhishen J, Mengcheng T, Jianming W. The determination of flavonoid contents in mulberry and their scavenging effects on superoxide radicals. *Food Chemistry*. 1999;64(4):555–559. [https://doi.org/10.1016/S0308-8146\(98\)00102-2](https://doi.org/10.1016/S0308-8146(98)00102-2)
39. Elsebaie EM, Essa RY. Microencapsulation of red onion peel polyphenols fractions by freeze drying technicality and its application in cake. *Journal of Food Processing and Preservation*. 2018;42:e13654. <https://doi.org/10.1111/jfpp.13654>
40. Fki I, Allouche N, Sayadi S. The use of polyphenolic extract, purified hydroxytyrosol and 3,4-dihydroxyphenyl acetic acid from olive mill wastewater for the stabilization of refined oils: A potential alternative to synthetic antioxidants. *Food Chemistry*. 2005;93(2):197–204. <https://doi.org/10.1016/j.foodchem.2004.09.014>
41. Sayah K, Marmouzi I, Naceiri Mrabti H, Cherrah Y, Faouzi MEA. Antioxidant activity and inhibitory potential of *Cistus salviifolius* (L.) and *Cistus monspeliensis* (L.) aerial parts extracts against key enzymes linked to hyperglycemia. *BioMed Research International*. 2017;2017:2789482. <https://doi.org/10.1155/2017/2789482>
42. Elsebaie EM, El-Wakeil NHM, Khalil AMM, Bahnasy RM, Asker GA, El-Hassnin MF, et al. Silver nanoparticle synthesis by *Rumex vesicarius* extract and its applicability against foodborne pathogens. *Foods*. 2023;12(9):1746. <https://doi.org/10.3390/foods12091746>
43. Ademiluyi AO, Oboh G. Aqueous extracts of Roselle (*Hibiscus sabdariffa* Linn.) varieties inhibit α -amylase and α -glucosidase activities in vitro. *Journal of Medicinal Food*. 2013;16(1):88–93. <https://doi.org/10.1089/jmf.2012.0004>
44. Telagari M, Hullatti K. *In-vitro* α -amylase and α -glucosidase inhibitory activity of *Adiantum caudatum* Linn. and *Celosia argentea* Linn. extracts and fractions. *Indian Journal of Pharmacology*. 2015;47(4):425–429. <https://doi.org/10.4103/0253-7613.161270>
45. Nakai M, Fukui Y, Asami S, Toyoda-Ono Y, Iwashita T, Shibata H, et al. Inhibitory effects of oolong tea polyphenols on pancreatic lipase in vitro. *Journal of Agricultural and Food Chemistry*. 2005;53(11):4593–4598. <https://doi.org/10.1021/jf047814+>
46. Jomaa B, de Haan LHJ, Peijnenburg AACM, Bovee TFH, Aarts JMMJG, Rietjens IMCM. Simple and rapid *in vitro* assay for detecting human thyroid peroxidase disruption. *ALTEX – Alternatives to Animal Experimentation*. 2015;32(3):191–200. <https://doi.org/10.14573/altex.1412201>
47. Skehan P, Storeng R, Scudiero D, Monks A, McMahon J, Vistica D, et al. New colorimetric cytotoxicity assay for anticancer-drug screening. *JNCI: Journal of the National Cancer Institute*. 1990;82(13):1107–1112. <https://doi.org/10.1093/jnci/82.13.1107>
48. Qasim M, Aziz I, Rasheed M, Gul B, Khan MA. Effect of extraction solvents on polyphenols and antioxidant activity of medicinal halophytes. *Pakistan Journal of Botany*. 2016;48(2):621–627.
49. Asimi O, Sahu NP, Pal AK. Antioxidant activity and antimicrobial property of some Indian spices. *International Journal of Scientific and Research Publications*. 2013;3:1–8.
50. Howlader MSI, Rahman MM, Khalipha ABR, Ahmed F, Rahman MM. Antioxidant and antidiarrhoeal potentiality of *Diospyros blancoi*. *International Journal of Pharmacology*. 2012;8(5):403–409. <https://doi.org/10.3923/ijp.2012.403.409>
51. Sridhar K, Charles AL. *In vitro* antioxidant activity of Kyoho grape extracts in DPPH and ABTS assays: Estimation methods for EC₅₀ using advanced statistical programs. *Food Chemistry*. 2019;275:41–49. <https://doi.org/10.1016/j.foodchem.2018.09.040>
52. Kala CP. Current status of medicinal plants used by traditional Vaidyas in Uttaranchal state of India. *Ethnobotany Research and Applications*. 2005;3:267–278. <https://doi.org/10.17348/era.3.0.267-278>
53. Aruoma OI, Cuppett SL. Antioxidant methodology: in vivo and in vitro concepts. Champaign: The American Oil Chemists Society; 1997. 241 p.
54. Tsai C-E, Lin L-H. DPPH scavenging capacity of extracts from *Camellia* seed dregs using polyol compounds as solvents. *Heliyon*. 2019;5(8):e02315. <https://doi.org/10.1016/j.heliyon.2019.e02315>
55. Helfand SL, Rogina B. Genetics of aging in the fruit fly, *Drosophila melanogaster*. *Annual Review of Genetics*. 2003;37:329–348. <https://doi.org/10.1146/annurev.genet.37.040103.095211>
56. Prashith KTR, Manasa M, Poornima G, Abhipsa V, Rekha C, Upashe SP, et al. Antibacterial, cytotoxic and antioxidant potential of *Vitex negundo* var. *negundo* and *Vitex negundo* var. *purpurascens* – A comparative study. *Science, Technology and Arts Research Journal*. 2013;2(3):59–68. <https://doi.org/10.4314/star.v2i3.98737>
57. Bonina F, Puglia C, Tomaino A, Saija A, Mulinacci N, Romani A, et al. In-vitro antioxidant and in-vivo photoprotective effect of three lyophilized extracts of *Sedum telephium* L. leaves. *Journal of Pharmacy and Pharmacology*. 2000;52(10):1279–1285. <https://doi.org/10.1211/0022357001777261>


58. Ghedadba N, Bousselsela H, Hambaba L, Benbia S, Mouloud Y. Evaluation of antioxidant and antimicrobial activity of leaves and flowering tops of *Marrubium vulgare* L. *Phytothérapie*. 2014;12:15–24. <https://doi.org/10.1007/s10298-014-0832-z> (In French.).
59. Fidrianny I, Rizkiya A, Ruslan K. Antioxidant activities of various fruit extracts from three solanum sp. using DPPH and ABTS method and correlation with phenolic, flavonoid and carotenoid content. *Journal of Chemical and Pharmaceutical Research*. 2015;7(5):666–672.
60. Sarr SO, Fall AD, Gueye R, Diop A, Diatta K, Diop N, et al. Study of the antioxidant activity of extracts from the leaves of *Vitex doniana* (Verbenacea). *International Journal of Biological and Chemical Sciences*. 2015;9(3): 1263–1269.
61. Saber RA. Evaluation of antiurolithiatic and antioxidant activity of the Egyptian *Pluchea dioscoridis* L. leaves extracts in vitro. *African Journal of Biological Sciences*. 2021;17(1):233–249. <https://doi.org/10.21608/ajbs.2021.201676>
62. Cano A, Acosta M, Arnao MB. A method to measure antioxidant activity in organic media: Application to lipophilic vitamins. *Redox Report*. 2000;5(6):365–370. <https://doi.org/10.1179/135100000101535933>
63. Re R, Pellegrini N, Proteggente A, Pannala A, Yang M, Rice-Evans C. Antioxidant activity applying an improved ABTS radical cation decolorization assay. *Free Radical Biology and Medicine*. 1999;26(9–10):1231–1237. [https://doi.org/10.1016/S0891-5849\(98\)00315-3](https://doi.org/10.1016/S0891-5849(98)00315-3)
64. Ndhlala AR, Ncube B, Abdelgadir HA, Du Plooy CP, van Staden, J. Antioxidant potential of African medicinal plants. In: Al-Gubory KH, Laher I, editors. *Nutritional antioxidant therapies: Treatments and perspectives*. Cham: Springer; 2017. pp. 65–88. https://doi.org/10.1007/978-3-319-67625-8_3
65. Vongsak B, Kongkiatpaiboon S, Jaisamut S, Konsap K. Comparison of active constituents, antioxidant capacity, and α -glucosidase inhibition in *Pluchea indica* leaf extracts at different maturity stages. *Food Bioscience*. 2018;25:68–73. <https://doi.org/10.1016/j.fbio.2018.08.006>
66. Obeidat M, Shatnawi M, Al-alawi M, Al-Zu'bi E, Al-Dmoor H, Al-Qudah M, et al. Antimicrobial activity of crude extracts of some plant leaves. *Research Journal of Microbiology*. 2012;7(1):59–67. <https://doi.org/10.3923/jm.2012.59.67>
67. Zalabani SM, Hetta MH, Ismail AS. Anti-inflammatory and antimicrobial activity of the different *Conyza dioscoridis* L. Desf. Organs. *Biosafety*. 2013;2(1):1000106. <https://doi.org/10.4172/2167-0331.1000106>
68. Aruwa CE, Amoo S, Kudanga T. Phenolic compound profile and biological activities of Southern African *Opuntia ficus-indica* fruit pulp and peels. *LWT*. 2019;111:337–344. <https://doi.org/10.1016/j.lwt.2019.05.028>
69. El-Ghorab AH, Ramadan MM, Abd El-Moezc SI, Soliman A-MM. Essential oil, antioxidant, antimicrobial and anticancer activities of Egyptian *Pluchea dioscoridis* extract. *Research Journal of Pharmaceutical, Biological and Chemical Sciences*. 2015;6(2):1255
70. Jhong C-H, Riyaphan J, Lin S-H, Chia Y-C, Weng C-F. Screening alpha-glucosidase and alpha-amylase inhibitors from natural compounds by molecular docking *in silico*. *BioFactors*. 2015;41(4):242–251. <https://doi.org/10.1002/biof.1219>
71. Gowri PM, Tiwari AK, Ali AZ, Rao JM. Inhibition of α -glucosidase and amylase by bartogenic acid isolated from *Barringtonia racemosa* Roxb. seeds. *Phytotherapy Research*. 2007;21(8):796–799. <http://dx.doi.org/10.1002/ptr.2176>
72. Tarling CA, Woods K, Zhang R, Brastianos HC, Brayer GD, Andersen RJ, et al. The search for novel human pancreatic α -amylase inhibitors: High-throughput screening of terrestrial and marine natural product extracts. *ChemBioChem*. 2008;9:433–438. <https://doi.org/10.1002/cbic.200700470>
73. Shobana S, Sreerama YN, Malleshi NG. Composition and enzyme inhibitory properties of finger millet (*Eleusine coracana* L.) seed coat phenolics: Mode of inhibition of α -glucosidase and pancreatic amylase. *Food Chemistry*. 2009;115(4):1268–1273. <https://doi.org/10.1016/j.foodchem.2009.01.042>
74. Apostolidis E, Lee CM. *In vitro* potential of *Ascophyllum nodosum* phenolic antioxidant-mediated α -glucosidase and α -amylase inhibition. *Journal of Food Science*. 2010;75(3):H97–H102. <https://doi.org/10.1111/j.1750-3841.2010.01544.x>
75. Ramkumar KM, Thayumanavan B, Palvannan T, Rajaguru P. Inhibitory effect of *Gymnema montanum* leaves on α -glucosidase activity and α -amylase activity and their relationship with polyphenolic content. *Medicinal Chemistry Research*. 2010;19:948–961. <https://doi.org/10.1007/s00044-009-9241-5>
76. Ali MB, Mnafigui K, Feki A, Damak M, Allouche N. In vitro antidiabetic, anti-obesity and antioxidant proprieties of Rosemary extracts. *Journal of Advances in Chemistry*. 2014;10(2):2305–2316. <https://doi.org/10.24297/jac.v10i2.5497>
77. McDougall GJ, Kulkarni NN, Stewart D. Berry polyphenols inhibit pancreatic lipase activity *in vitro*. *Food Chemistry*. 2009;115(1):193–199. <https://doi.org/10.1016/j.foodchem.2008.11.093>


78. Habza-Kowalska E, Kaczor AA, Żuk J, Matosiuk D, Gawlik-Dziki U. Thyroid peroxidase activity is inhibited by phenolic compounds – Impact of interaction. *Molecules*. 2019;24(15):2766. <https://doi.org/10.3390/molecules24152766>
79. Leonard JA, Tan Y-M, Gilbert M, Isaacs K, El-Masri H. Estimating margin of exposure to thyroid peroxidase inhibitors using high-throughput *in vitro* data, high-throughput exposure modeling, and physiologically based pharmacokinetic/pharmacodynamic modeling. *Toxicological Sciences*. 2016;151(1):57–70. <https://doi.org/10.1093/toxsci/kfw022>
80. Iawsipo P, Poonbud R, Somtragool N, Mutapat P, Meejom A. *Pluchea indica* tea-leaf extracts exert anti-cancer activity by inducing ROS-mediated cytotoxicity on breast and cervical cancer cells. *British Food Journal*. 2022;124(12):4769–4781. <https://doi.org/10.1108/BFJ-05-2021-0497>
81. Bibi Y, Nisa S, Zia M, Waheed A, Ahmed S, Chaudhary MF. In vitro cytotoxic activity of *Aesculus indica* against breast adenocarcinoma cell line (MCF-7) and phytochemical analysis. *Pakistan Journal of Pharmaceutical Sciences*. 2012;25(1):183–187.

ORCID IDs

Rowida Y. Essa  <https://orcid.org/0000-0003-2792-6922>

Essam M. Elsebaie  <https://orcid.org/0000-0002-8507-0694>

Wesam M. Abdelrhman  <https://orcid.org/0000-0003-0920-6729>

Mohamed R. Badr  <https://orcid.org/0009-0000-2083-6444>



Spatial genomic codes

Tatiana T. Glazko^{ID}, Gleb Yu. Kosovsky*^{ID}, Valeriy I. Glazko^{ID}

Scientific Research Institute of Fur-Bearing Animal Breeding and Rabbit Breeding named after V.A. Afanas'ev^{ROR}, Rodniki, Russia

* e-mail: gkosovsky@mail.ru

Received 24.04.2024; Revised 01.08.2024; Accepted 03.09.2024; Published online 20.11.2024

Abstract:

The increasing variability of phenotypic traits in agricultural animal species makes it necessary to search for reliable DNA markers. Due to the poor efficiency of using clustered single-nucleotide polymorphisms (SNP) and individual genomic elements, the hierarchy of gene regulatory networks has become a relevant research area. We summarized available information on different levels of epigenetic regulation, from the linear DNA sequence and its secondary and tertiary structures to the factors outside the cell nucleus, i.e., intercellular contacts and interactions with the extracellular matrix. We also discussed the features of genomic distribution and the role of topologically associated domains (TADs), and architectural protein CTCF in chromatin loop formation. CTCF mediates protein-protein interactions and interacts with various RNA variants. It also involved in epigenetic modifications of the DNA nucleotide sequence, a target of CTCF binding. Such targeted sites are located in transposable elements (TEs). As a result of the evolutionary conservation, they are also to be found in TAD, regardless of the fact that they are delivered by species-specific TEs. CTCF and its binding sites are known to affect the structure of the mitotic spindle. They also have a certain impact on cholesterol biosynthesis, which affects the plasma membrane and cell migration. CTCF indirectly participates in the variability of intercellular contacts and interactions with the extracellular matrix. In animals, CTCF and its binding targets are involved in all levels of gene regulatory networks that maintain or change genomic expression.

Keywords: G4 quadruplexes, DNA-RNA hybrids, CTCF, chromatin loops, topologically associated domains (TAD), extra-nuclear factors, neoplastic transformation

Funding: The study is supported by the Ministry of Science and Higher Education of the Russian Federation (state agreement No. 075-00503-24-01).

Please cite this article in press as: Glazko TT, Kosovsky GYu, Glazko VI. Spatial genomic codes. *Foods and Raw Materials*. 2025;13(2):409–422. <https://doi.org/10.21603/2308-4057-2025-2-653>

EPIGENETIC VARIATIONS AND TRANSCRIPTOME

Natural and artificial selection both target particular genomic elements for each specific biological object. Lack of information on these key genomic elements is a serious problem for molecular genetics, which prevents effective breeding of agricultural plants and animals. Genome-wide association studies (GWAS) make it possible to project phenotypic trait variability onto the genome. As they develop, they accumulate data on the correlation between the genetically complex traits and diseases in both humans and domestic animals and the genomic elements in the non-coding DNA, which control epigenetic variations in relation to coding sequences [1, 2]. Gene expression also depends on such epigenetic mechanisms as the variability of histone methylation

patterns, the DNA, and splicing, as well as movements and expression of mobile genetic elements (MGE) called transposons or transposable elements (TE) [3–8].

Epigenetic modifications in eukaryotic nuclei regulate gene expression programs. Such modifications occur at different organization levels:

- methylation of the linear DNA sequence during imprinting [9];
 - multiple two-way changes in chromatin packaging, e.g., formation of various chromatin loops, G4 quadruplexes, DNA triplexes, hairpin loops, and R-loops (DNA/RNA hybrids); and
 - modifications of histones, i.e., the histone code, with variability in DNA accessibility for transcription [10].
- A three-way organization level includes:
- autonomous chromosome areas in the interphase nucleus;

- formation of topologically associated domains within and between chromosomes; and
- genetic relationships and location in relation to the lamina of the nuclear membrane, nucleoli, and nuclear pores.

The interphase nucleus has two compartments, A and B. Expression-inactive DNA is part of compartment B, where heterochromatin tends to segregate near the nuclear lamina under the nuclear membrane and the nucleoli. The result is specific patterns unique for each cell populations. Heterochromatinization is typical of protein-interacting lamina-associated domains (LAD) enriched in long interspersed nuclear elements (LINE1) [11]. DNA between the LADs is expression-active and forms compartment A, which is believed to be enriched in retrotransposons, i.e., short interspersed nuclear elements (SINEs) [11].

The compartmentalization reflects the three-dimensional (3D) organization of the genome on a mega base scale. However, science knows about 2,000 chromatin domains that range in size from 100 kb to 1 Mb. These topologically associated domains (TADs) correspond to genomic regions with active self-interaction between different genomic elements located at different distances in the primary DNA sequence, i.e., in close physical proximity. Regulatory elements and their target genes are often located within the same TAD. Insulators protect

them from interacting with genomic elements of distal TADs (Fig. 1). The regions between two TADs are enriched in insulator proteins and ubiquitously active housekeeping genes that are present in most tissues of multicellular organisms. In mammals, TAD boundaries are characterized by co-bound cohesin and architectural factor CTCF [12–14]. Accumulating evidence suggests that structural changes within TADs lead to profound variations in the expression and intergenic interactions both inside the TAD and its boundaries [15].

Multicellular organisms have a special level of genetic expression regulation, i.e., intercellular interactions represented by the architectonics of tissues and organs. Intercellular interactions affect cell differentiation, apoptosis, and ontogenesis. The 3D level of genetic organization involves many mechanisms, e.g., extrusion of chromatin loops by cohesin complexes, compartmentalization of heterochromatic domains by phase separation, direct interactions between proteins, etc. [16–17].

CHROMATIN LOOPS

The chromatin loop is an elementary unit of chromatin packaging (Fig. 2). It participates in gene expression. Disruption of chromatin loops is associated with neurological diseases [18–20].

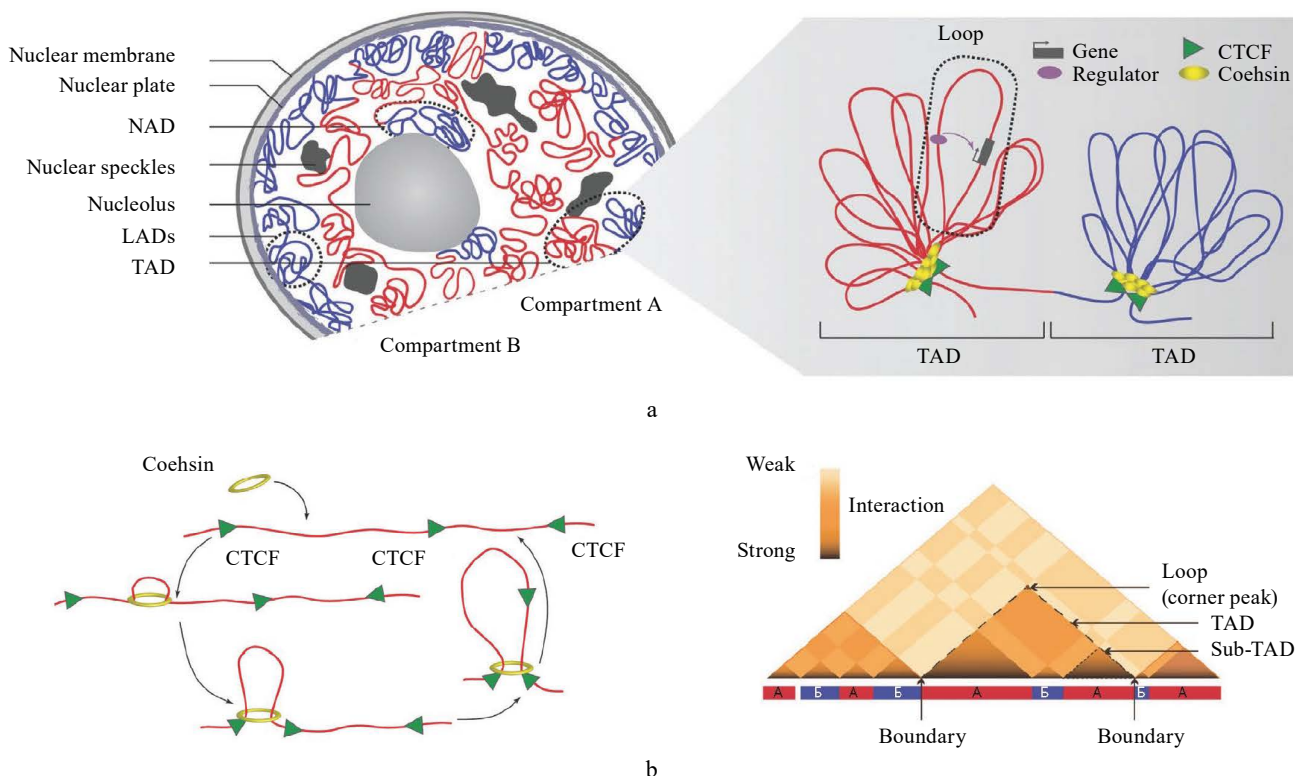


Figure 1 Three-dimensional genomic organization: (a) Compartmentalization into A (red) and B (blue) regions. DNA in compartment A often contacts with nuclear speckles while DNA in compartment B interacts with the nuclear lamina domain (LAD) and the nucleolus-associated domain (NAD). Higher resolution images show topologically associated domains (TADs). Chromatin loops within TADs are formed by cohesin and CTCF binding sites, which brings together regulatory elements (enhancers) and their targets (promoters); (b) Loop extrusion model. Cohesin extrudes chromatin through its ring-shaped structure, thus forming a loop. The loop grows until it reaches two converging CTCFs, which then block cohesin. This process is dynamic and thus can be interrupted; (c) Hi-C visualization of compartments A (red) and B (blue), loops, TADs, and sub-TADs [12].

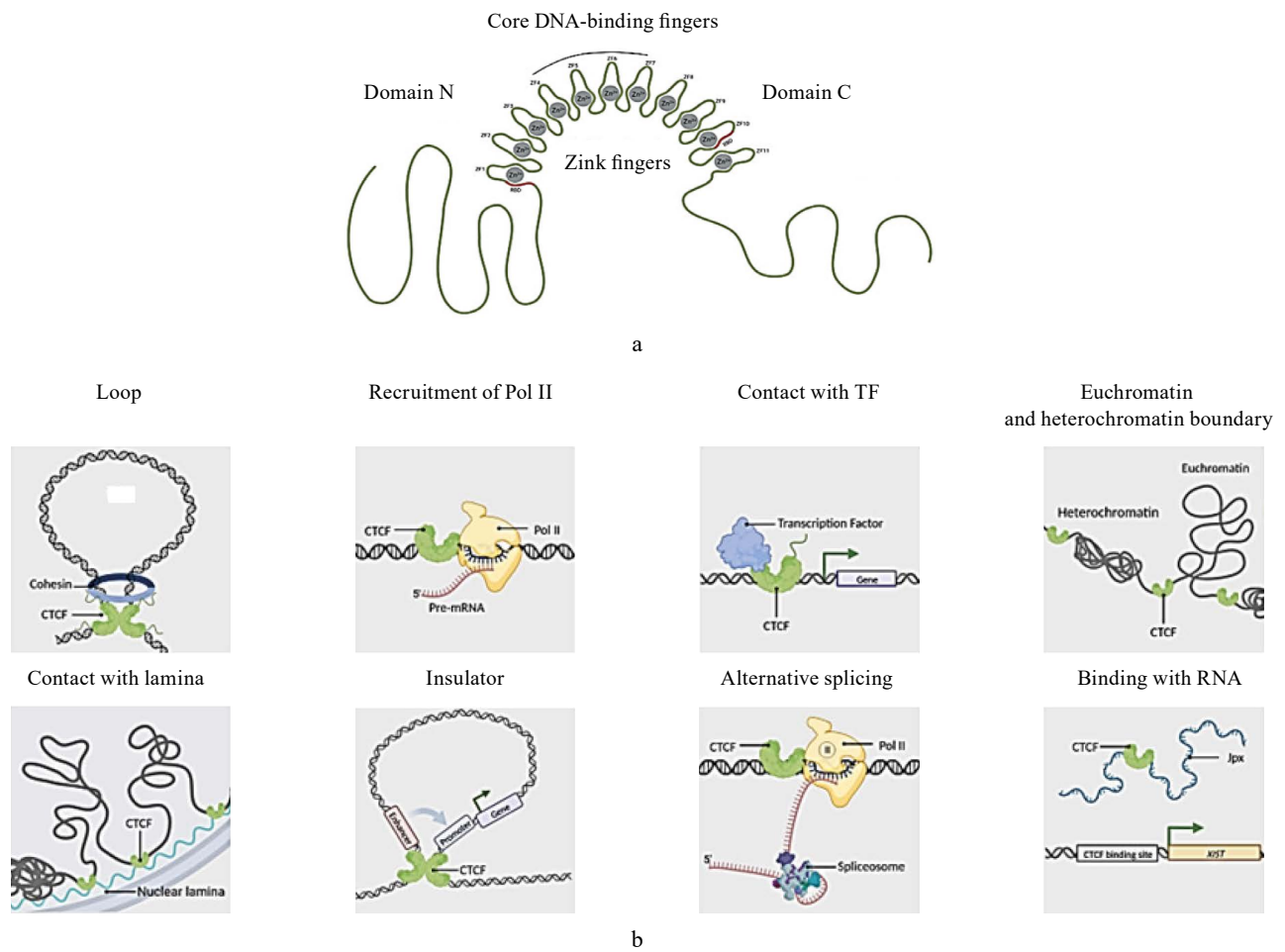


Figure 2 CTCF protein as a gene expression regulator: (a) CTCF is a protein with three domains: N-terminal domain, C-terminal domain, and a central domain with 11 zinc fingers. CTCF uses the zinc finger domain to bind to DNA. RBD – RNA-binding domain; ZF – zinc finger; (b) CTCF mechanisms: chromatin loop, recruitment of RNA polymerase II (Pol II), interaction with transcription factor (TF), defining the boundary between euchromatin and heterochromatin, anchoring the DNA to lamin, insulation, alternative splicing, and binding with RNA [23]

Loop formation usually depends on the CCCTC-binding transcription factor (CTCF), also known as architectural protein. Initially described as a negative regulator of c-Myc expression [21], it is now considered as the best studied transcription factor with C2H2-type zinc finger clusters [22].

A lot of publications report CTCF as a key protein in regulating gene expression because it can mediate between DNA and quite a number of epigenetic factors, even those with no DNA-binding domains (Fig. 3) [23]. Some post-translational modifications, e.g., glycosylation, are also known to affect the binding of CTCF protein to its DNA anchor [24].

While CTCF is a popular factor in chromatin loop formation, the process includes such independent regulatory elements as mammalian-wide interspersed repeats (MIRs) that represent an ancient family of transposable elements (TEs). They are efficient regulators and share some characteristics with tRNA-associated insulators. MIRs are enriched in genes responsible for the T-cell receptor pathway and are located at T-cell-specific boundaries between repressive and active chromatin. In this

family, the anchor sequences bind to RNA Pol III and some histone modifications in a way that depends on the chromatin [25].

Tian *et al.* [26] used the method of DNA methylation dioxygenase Tet-triple knock-out (Tet-TKO) to study the effect of DNA methylation on CTCF functions. In their research, methylation differences between rich and poor domains of CpG islands (CGI) decreased, as did the CTCF binding. As a result, the TAD structure weakened and the long-range chromatin loops depleted.

Apparently, CTCF does not bind to all of its potential targets in different cell types. Not only methylation, but also interactions with various non-coding RNAs may affect this process. Many non-coding RNAs affect chromatin organization and gene expression at different levels [27]. Long non-coding RNAs (lncRNAs) participate in many cellular processes, e.g., regulate nearby and distant genes, recruit chromatin modifiers, splice, translate, etc., as well as form and regulate organelles and nuclear condensates [27–30].

Interactions between DNA and RNA yield hybrids with an R-loop or triplexes. The R-loop results in a

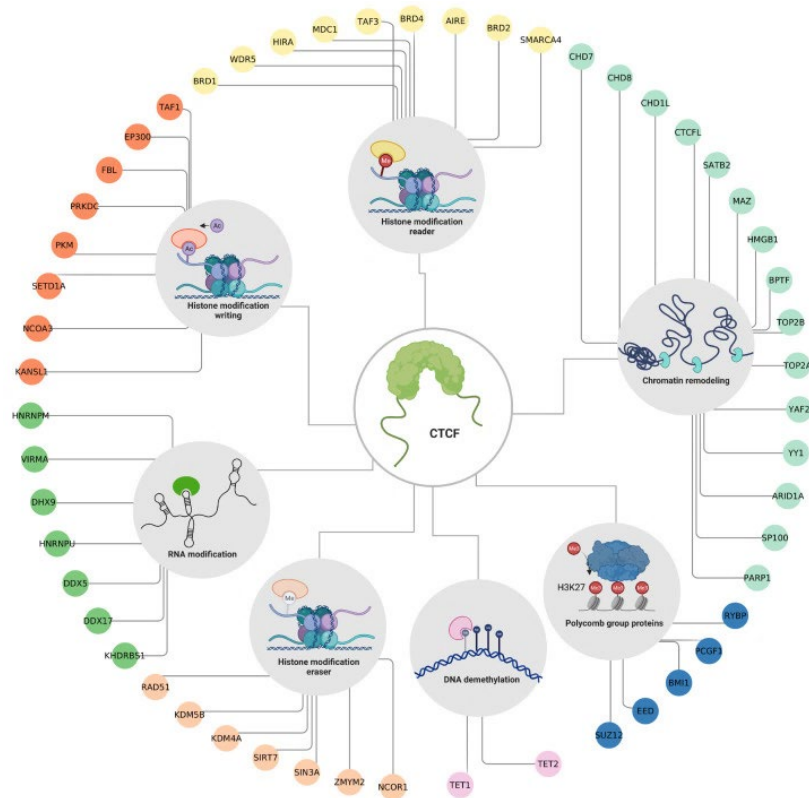


Figure 3 Interactions between CTCF and other epigenetic proteins: histone readers (yellow), chromatin remodelers (light blue), polycomb proteins (dark blue), DNA demethylation proteins (pink), protein that removes histone modifications (beige), RNA-modifying proteins (green), and histone writers (orange) [23]

three-stranded structure that consists of a DNA-RNA hybrid and a displaced DNA strand. The triplex causes a triple-helical structure within the DNA duplex major groove with a marked purine pyrimidine asymmetry across the two strands. The purine-rich DNA strand is available for Hoogsteen pairing with the third RNA strand while the pyrimidine sequence of the RNA binds to the major groove of the target DNA, parallel to the polypurine DNA strand. Should the target DNA site be located in a gene regulatory region, e.g., a promoter or an enhancer, the triplex either modulates local conformational / topological changes or recruits regulatory proteins to the portion of the lncRNA that protrudes from the triplex [31].

R-loops facilitate the anchoring function of CTCF during binding [32]. They form associated structures with G-quadruplexes (G4) in the CTCF binding targets. Wulfridge *et al.* [33] found R-loops and G4 together with CTCF in many regions of the murine embryonic stem cell genome. In their study, a weaker R-loop reduced CTCF binding while a deleted G4-forming motif inhibited CTCF binding and altered gene expression. Hou *et al.* [34] mentioned that sites prone to G4 formation clustered on TAD boundaries and in the transcription, factor binding sites (TFs).

lncRNA GATA6-AS1 is a triplex-forming site with purine-pyrimidine DNA tracks. Its clusters in TAD boundaries rather than in other genomic regions. Some

GATA6-AS1 sites interact with CTCF and are also concentrated in CTCF-enriched genomic regions, e.g., TAD boundaries. GATA6-AS1 may be responsible for transporting CTCF protein to particular sites. Thus, some lncRNAs are able to target different genomic domains via RNA/DNA triplex formation to transport molecules, e.g., CTCF. This ability may be a universal mechanism involved in TAD formation and dynamics in 3D genomic organization [28].

CTCF participates in the sex differentiation of allelic expression during genomic imprinting in mammals. In some imprinted domains, differentially methylated sites exhibit different allelic binding to the CTCF protein with subsequent differences in cohesin retention [35].

Porcine germ cells demonstrated sex differences in the methylation of functionally different genes: 465 in males and 316 in females. The genes had sites that were homologous to retrotransposon sites. In 21%, the first intron demonstrated differentiation in methylation, which could probably affect the regulation of gene transcription [36].

The imprinting mechanism is complex and includes not only CTCF [37], but other regulators as well [37–39], e.g., interactions with long non-coding RNA (lncRNA) [40], microRNA (miRNA) clusters [41], or histone modifications [42].

Imprinting disorders in agricultural animals are known to affect the variability of some economically

valuable traits [9]. Long non-coding RNAs (lncRNAs) are part of the regulome, i.e., a set of non-coding regulatory elements of the genome that are closely associated with TEs. They regulate the dynamics of the interphase nucleus architecture. For instance, NEAT1_2 lncRNA is a granule-forming paraspeckle [29]. The non-coding RNAs, such as lncRNAs, could act as an architectural scaffold in the interphase nucleus [27].

Mammalian TEs also provide binding sites for architectural chromatin proteins, including CTCF. Choudhary *et al.* studied genomes of humans, mice, dogs, and rhesus macaques, i.e., mammalian species that diverged 30–96 million years ago. The share of TE increased from mice to primates, being slightly lower in dogs than in mice. In all four species, however, 8–37% of CTCF loop anchors and TAD boundaries came from TEs. While CTCF at TAD boundaries originated mainly from TEs, the research revealed some species-specific patterns: SINEs in mice, LTRs and DNA in humans, with dogs and rhesus macaques in between [3].

Despite species preferences, a high conservation of orthologous synteny and chromatin loop organization was observed between humans and mice [43]. Most TE-derived loop anchors in mice were generated by a few young TE subfamilies, such as B3, B2_Mm2, B3A, and B2_Mm1t. Human TEs contributed fewer orthologous loops and were distributed across more TE subfamilies than in mice. In fact, 87% of TE-derived orthologous loops in mice were discordant to human TEs and were anchored at putative ancestral CTCF binding sites. In mice, syntenic ancestral CTCF motifs were degraded or deleted, the loops being anchored at CTCF sites derived from the nearby, co-opted TEs. For example, the orthologous loop at the 5' end of Akap81 (A Kinase Anchor Protein 8-Like) is maintained in mice by a MER20 element transposed ~ 1.5 thousand pairs of nucleotides upstream of the degraded ancestral motif, which was conserved in most mammals but not rodents. When the ancestral CTCF motif derived from the 147-million-year-old MIR3 element degraded, it incapacitated the CTCF binding. The younger MER20 element, which inserted about 90 million years ago, harbored strong CTCF binding, thus providing an anchor site to maintain the conserved loop in mice. Therefore, TEs provide redundant CTCF sites and mediate them in switching their binding sites. This way, they promote conserved genome folding events in humans and mice [43].

Buckley *et al.* proposed a model where the density and distribution of genes and regulatory elements catalyzed accumulation of TEs. The conservation of synteny of genomic elements and the nuclear organization make mammalian genomes with dissimilar TEs follow similar evolutionary trajectories. [44]. However, early human embryos demonstrated significant differences in the transcription of different TEs in cell populations [45], as well as in brain cells with cell differentiations – at different stages of normal and pathological development [8].

Phenotypic traits in agricultural animal species are known to be damaged by TE insertion into the exonic, intronic, and promoter regions of various genes [46]. Cattle species demonstrated a correlation between the enrichment of CTCF binding motifs and the major quantitative trait genes (QTLs) associated with gene expression variation (eQTLs) or allele-specific expression (aseQTLs) in the transcriptomes of leukocytes and milk cells of lactating cows [47].

Assessment studies of the variability of CTCF binding motifs as a set of regulatory genomic elements can accelerate artificial selection of complex phenotypic traits [46].

The relationships between chromatin loops are complex. For example, the so-called nested loops may possess and coordinate three convergent anchor sites of the CTCF + cohesin complex in a single TAD domain [17]. Changes in AUTS2 and Calneuron 1 (Caln1) in humans provide a clear example of intra-TAD loop fusion. These two genes are separated by a distance of 1.5 Mb, but this distance changed when experimental rats and mice received cocaine. Cocaine-induced release of the Aut2-Caln1 loop increased the mRNA expression in Aut2 and Caln1 [48]. The process boosted DNA cytosine methylation, which could cause a concomitant loss of CTCF binding. The transcriptional changes could be attributed to the increase in trimethylation of the activating mark H3K4 at the Aut2 and Caln1 sites [48, 49].

Therefore, variations in primary DNA sites affect chromatin loop formation, which is closely related to the variability of gene expression.

INTER-TAD RELATIONSHIPS

The International Nucleome Consortium was initiated almost 10 years ago [50]. One of its latest meetings was held in Greece in September 2023 [51]. The Consortium strives to assess the effect of spatial and temporal genomic organization on phenotypic variability. However, its proceedings show that, to date, several important areas remain largely understudied. The list includes the patterns of TAD spatial interaction, prediction options, and the role of cytoskeletal elements, intercellular contacts, tissue architecture, etc. Apparently, TAD interactions are subject to too many regulatory factors, which may differ significantly even for two TADs and their loops, depending on the exact conditions of gene expression change.

TADs are megabase genomic domains with increased self-interaction density. Sub-TADs are smaller but more dynamic units within TADs. The initial definition of a TAD identifies its boundaries. TAD or subTAD boundaries isolate enhancers and promoters from abnormal contacts and facilitate their interactions across TADs. In addition, they locate replication origins in period S [52].

The human genome includes hundreds of thousands of CTCF binding sites (CBS). For instance, 2898 of human HEC-1-B cells out of total 3881 TAD boundaries contain 2–8 CBS elements. TAD boundaries are

evolutionarily conserved and associated with complex genetic traits. This feature was described by Sandoval-Velasco *et al.* [53], who studied a 52 000-year-old female woolly mammoth, the cells of which retained a certain conservation of TAD organization in Siberian permafrost.

Most interactions between enhancers and promoters occur within TADs; however, a lot of genes are controlled by distal enhancers outside of single TADs. Therefore, distal enhancers can activate target promoters across TAD boundaries. Chen *et al.* [54] reported that 21% of enhancers of key developmental genes acted across TAD boundaries, in cases of both transcription-dependent and pre-formed encounters. This finding suggests different mechanisms of enhancer-promoter interactions. Such differences were described in studies of paralogous genes [55–57]. They are part of common metabolic pathways that may have common or very similar enhancer sites and TF binding sites. Paralogous genes may participate in one and the same transcription factories, e.g., protein speckles enriched in protein-RNA clusters that facilitate the phase separation of nuclear subcompartments.

AI programs make it possible to predict changes in the 3D architecture of the interphase nucleus, e.g., formation of chromatin loops and TADs [58–60]. Keough *et al.* [60] used this method to compare human and chimpanzee genomes in enhancer sites that are active during the prenatal development of nervous system. The structural variants that were specific to humans but not to chimpanzees were associated with the changes in the 3D packaging of the genome. The process made evolutionarily conservative enhancers interact with some new domains that regulate gene expression.

Braunger *et al.* [61] detected changes in intra- and interchromosomal interactions in skin fibroblasts obtained from different age groups. They identified key transcription regulators where target genes rearrange to change their expression during aging. Correction of such changes may potentially rejuvenate cell populations.

Interchromosomal translocations during carcinogenesis receive a lot of scientific attention. They often cause intergenic fusions and chimeric proteins. Interchromosomal translocations usually involve chromosome regions that are part of common gene expression programs. Their transcription depends on the mechanism responsible for formation of transcription factories or on a set of regulatory elements [62]. By detecting such intergenic fusions at the level of nucleotide sites, medics may improve diagnostics and prognosing.

Light microscopy studies revealed that the frequency of associations between non-homologous chromosomes often coincides with typical oncomarker translocations for certain tissues. For example, interchromosomal associations between chromosomes 12 (heavy chains of immunoglobulins) and 15 (c-Myc oncogene) in bone marrow leukocytes of BALB/c mice demonstrated some translocations typical of murine plasmacytomas [63–65].

McStay [66] reported clustered gene superfamilies in different chromosomes, e.g., during nucleolus for-

mation. Human nuclei have about 300 ribosomal genes located on five different acrocentric chromosomes. For comparison, mice have six. They have to physically converge for the preliminary assembly of ribosomes in the nucleus. Monahan *et al.* [67] located olfactory receptor genes on several different chromosomes. They combined in the same nuclear space to create an olfactosome and regulate their expression.

TADs that are located on different chromosomes can interact if assisted by housekeeping genes on TAD boundaries: as they get transcribed, they recruit ribonucleoprotein condensates. Interactions between different TADs are further facilitated by the physical forces that arise from the interaction between transcriptional condensates at these boundaries and subnuclear organelles, especially nuclear speckles [68]. Some oncological studies report a connection between pairwise aneuploidy (loss/gain) between non-homologous chromosomes. This connection emphasizes the complex hierarchy of genetic material [69].

Interchromosomal studies revealed spatial distances for intrachromosomal interactions in the range of 189 ± 95 nm; the range was greater (279 ± 163 nm) in non-homologous chromosomes [70].

GENETIC COMPOSITION OF TADS

Accumulated data on TADs, interchromosomal relationships across boundaries, and the correlations between their disturbances and various pathologies indicate multi-level hierarchical relationships between the 3D genomic organization in ontogenesis. At each level, disturbances affect the expression of many genes within and between TADs, thus leading to phenotypic consequences (Fig. 4) [71].

TAD structure is complex, dynamic, and diverse. It also depends on the functional characteristics of its genes. Abnizova *et al.* [14] studied three germ layers during gastrulation in mice. The genes with the same expression in different layers differed from those genes that varied in expression in such parameters as density and clustering. They also had a larger number of GCs in promoters and belonged to housekeeping genes. The tissue-specific genes had TADs with a relatively smaller number of genes and a reduced GC content in promoters. Their expression was predominantly regulated by distal enhancers. As for the TFs of such genes, species-specific TFs, which the authors called innovative or pioneering, were more common than in housekeeping genes. The genes transcribed in the three murine germ layers were conditionally referred to as housekeeping genes. Their TF binding sites were so close to promoters that they overlapped. The promoters had extensive GC content. The genes in TADs were so clustered that no empty space remained between them. Abnizova *et al.* [14] distinguish two groups of genes that form qualitatively different TADs: those containing developmental genes regulated by innovative TFs and cooperator genes expressed in most tissues.

Numerous studies report the differences in regulatory elements between the housekeeping genes and

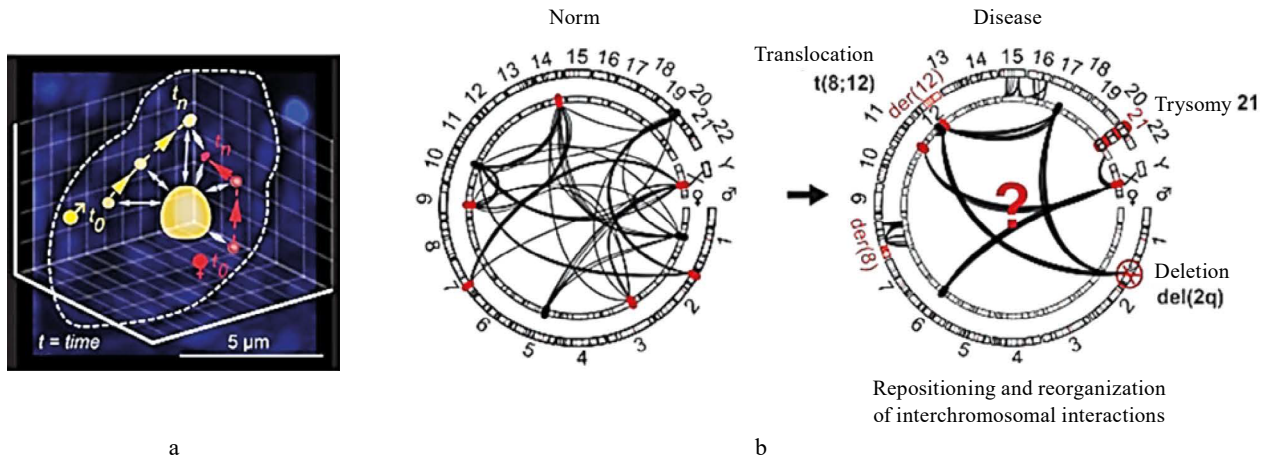


Figure 4 Interactions between non-homologous chromosomes: (a) Allele-specific loci of paternal (yellow) and maternal (red) genomes relative to the nucleolus in primordial embryonic stem cells (ESC); (b, left) Maternal and paternal alleles are in physical proximity and intertwined while they modulate tissue-specific gene regulation in the 3D nucleus space. This interaction contributes to various biological processes, DNA-RNA, proteins, biophysical properties of chromatin, 3D genomic organization, and stochastic factors; (b, right) Structural aberrations involve deletions, translocations, etc., while numerical chromosomal aberrations are represented by trisomies. Both can disrupt and reorganize the complex network of interchromosomal interactions, thus changing transcriptional programs [71].

the tissue-specific genes. Roller *et al.* [72] studied four groups of mammals: primates (macaques and monkeys); rodents (mice, rats, and rabbits); pigs, horses, cats, and dogs; and marsupials (opossum). They took samples of four tissues, i.e., liver, muscles, brain, and testes, as representing three somatic tissues originating from different germ layers. The comparative analysis covered regulatory sites, i.e., promoters and enhancers, in the tissue-specific genes vs. housekeeping genes. The analysis revealed a rather high rate of evolution of tissue-specific genes, where insertions of the LINE1 retrotransposon were quite active. LINE2 as a more ancient variant occurred more often in the regulatory sites of housekeeping genes. The analysis of evolution rate in tissue-specific enhancers and promoters indicated a relatively low rate of evolution of gene expression in the brain whereas the evolution rate in testicles and liver was high. In addition, the study revealed some intraspecific conservation in the variability of regulatory systems with pronounced interspecific differences [72].

Other studies also confirmed important distinctions between TADs with genes of different functions and evolutionary origins. James *et al.* [73] reported that TAD boundaries frequently coincided with breaks in genome. Deleted boundaries depended on negative selection, suggesting that TADs may facilitate genome rearrangements and evolution. The genes co-localized within TADs in a way that depended on their evolutionary age in humans and mice. As a result, TADs were divided into two groups with different shares of older and younger genes. The division was based on whether they arose before or during vertebrate whole-genome duplications (WGDs). Evolutionarily older genes were more frequently expressed in different cell types and were more often classified as essential than younger

genes. Essential genes were found responsible for growth, development, and reproduction at both the cellular and organism levels. The loss of these functions may compromise viability or adaptability. Older genes were more likely to become essential because old genes usually disappear during evolution if they are less essential. However, how some young genes become essential still remains unclear. To answer this question, James *et al.* [73] studied the TAD content ratios in old vs. young genes and essential vs. less essential young genes. In primates and rodents, recently duplicated young genes appeared to be more essential when they were located in TADs enriched in old genes and interacted with those genes that were last duplicated during WGD. Therefore, the evolutionary significance of young genes may increase if they are located in TADs with regulatory networks established by old genes [73].

Thus, the nucleus has different levels that affect the 3D organization of the genetic material, plus the fourth, ontogenetic component: modifications of the linear DNA sequence with methylation and multiple secondary structures; intra- and inter-TAD formation, dynamics, and interactions of chromatin loops; evolutionary and functional features of TAD genes. All these phenomena obviously depend on factors outside the nucleus, especially intercellular interactions.

EXTRANUCLEAR STRUCTURAL ELEMENTS AFFECTING GENE EXPRESSION

Actin is a key element of the cytoskeleton. It is one of the most conservative and widespread proteins in eukaryotic cells. Actin is present as G-actin in a monomeric globular form and as F-actin in polymeric filamentous forms of various length. Actin is highly concentrated at the periphery of the cell, in the cytoplasm.

In low concentrations, it can be found in the nucleus, where it interacts with the lamina to form a network throughout the nuclear membrane [74].

Cytoplasmic actin participates in cell motility, organelle movement, cell signaling systems, etc. The fact that the nucleus has much less actin than the cytoplasm led to discussions about its involvement in the nuclear matrix and interactions with the DNA. However, actin is now known to be part of the control of the nuclear architecture. Nuclear actin interacts with RNA polymerases I, II, and III and ribonucleoprotein transcript complexes. It prolongates transcription and transports polyribosomes. It binds to the lamins of the nuclear membrane either directly or through intermediary proteins. Nuclear actin is involved in the formation of open chromatin and TADs; it repairs DNA breaks, and controls nuclear morphology, e.g., its apical surface [74–80].

Mitotic structure also depends on the chromatin architectural protein CTCF. Targeted mutations of CTCF use clustered regularly interspaced short palindromic repeats (CRISPR) to disorganize the mitotic spindle and disrupt the anaphase chromosome segregation by forming tri- or tetrapolar spindles and chromosomes beyond the spindle pole. Therefore, CTCF is important for both correct metaphase organization and anaphase segregation [81].

The correlation between 3D chromatin organization and cell morphology can be ensured by the variability of the plasma membrane state. A targeted mutation of architectural proteins CTCF and CTCF pLoF was reported to affect cell migration because this mutation increased the RNA level of cholesterol biosynthesis enzymes. Migrasomes, which are extracellular vesicles on the retraction fibers of migrating cells, slowed down

in their formation in CTCF pLoF cells. Hmgcs1 promoter, which encodes the cholesterol biosynthesis enzyme, did not bind with CTCF directly. However, CTCF could affect at least two key features, i.e., spatial organization and histone modification [82].

Intercellular interactions are another long-standing source of gene expression program. The epithelial-mesenchymal transition (EMT) is a good example of cell plasticity as it renders the epithelium its mesenchymal phenotypes (Fig. 5) [83].

Epithelial cells contain specialized junctional proteins, exhibit apicobasal polarity, and have limited dissociation and migration potential. In contrast, mesenchymal cells are irregular and do not form specialized adhesion complexes. Their end-to-end polarity and focal adhesions increase migratory capacity. During EMT, epithelial cells acquire mesenchymal features, which include changes in the expression of epithelial and mesenchymal markers [83].

α -Smooth muscle actin (α -SMA) is an actin isoform that predominates in vascular smooth muscle cells and is important for fibrogenesis. α -SMA expression is lower in cells during contact inhibition than in during serum starvation [84].

AIFM2 is a mitochondrion-associated apoptosis-inducing factor. It was renamed from an unidentified anti-ferroptosis gene into ferroptosis suppressor protein 1 (FSP1). It is known to protect against ferroptosis induced by deletion of glutathione peroxidase 4 (GPX4), which controls phospholipid oxidation [85].

Gene expression programs depend on the cellular environment. This fact was established on classical models of cellular differentiation gradients, e.g., trabeculae of mammalian liver lobules. They consist of two layers of

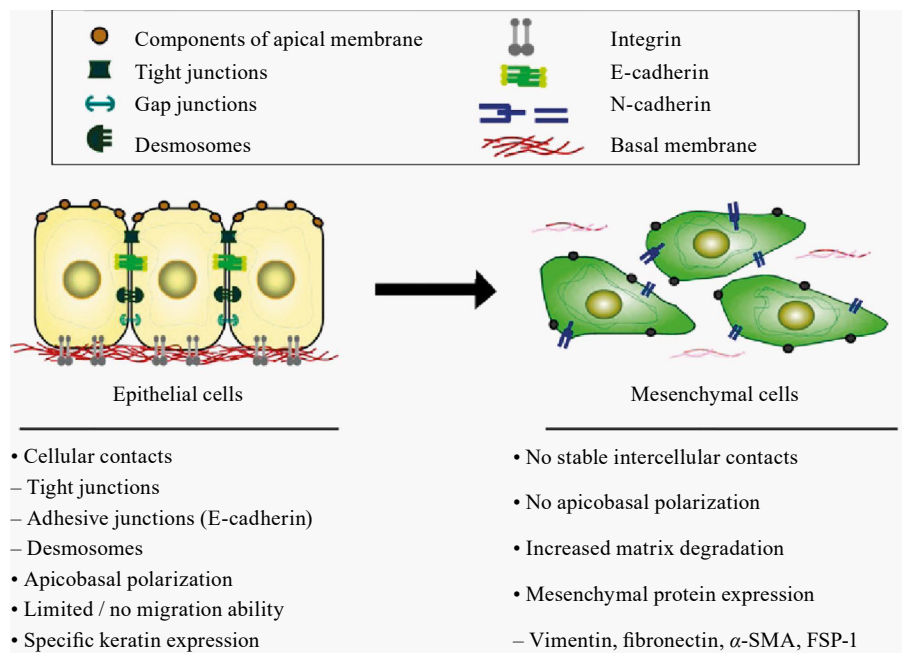


Figure 5 Key features of epithelial and mesenchymal cells

hepatocytes that polyploidize from diploids to decaploids as they move toward the central venule and change the enzymic expression. Small intestine villi are another example. They grow from a stem cell; daughter cells move to the apical apex by asymmetric differentiation, upon which they die and are exfoliated into the intestinal lumen. Based on our own unpublished research result, we know that hepatectomy of one lobule in the liver leads to polyploidization of the rest while a CH4 poisoning causes necrosis of hepatocytes around the central venule and proliferation of peripheral diploid hepatocytes. To sum it up, each cell receives differentiated signals depending on its position in the tissue architecture.

Internal and external factors that affect the asymmetry by the level of cellular differentiation of stem cell progeny in different tissues. Two daughters of one stem cell behave asymmetrically: one remains a stem cell while the other differentiates. The same happens every time they divide: one remains young while the other specializes. The process includes the state of the mitotic spindle. The transfer of old and young chromatids, histones, and cellular organelles to daughter cells is asymmetric. Thus, the gene expression of each cell depends on its position in the structure of the tissue or organ [86].

Embryonic cells can undergo neoplastic transformation in a non-embryonic environment. Tumor cells can spread out and acquire contact inhibition when placed in an embryonic environment or on a substrate that increases their adhesiveness. Sarcomas could be induced by embedding pieces of quartz glass into murine muscles. Probably, it happens because conditional morphostats stop entering cells, which prevents neoplastic transformation [87]. Inherited oncogenic traits are encoded not only by gene sequences, but also by DNA or chromosomal structures that can be changed by non-mutational mechanisms, e.g., methylation, chromatin packaging with architectural proteins and RNA, or post-translational modifications of nuclear proteins [88]. I. Berenblum, who authored the theory of two-stage carcinogenesis, reported that benign tumors develop each at its own rate under the same influences, going malignant at their own rate as well [89]. That is, each founder cell has an individual response to the same impact [90].

The individual character of the 3D cellular organization follows from the long-discussed heterogeneity of cells in the architectonics of the interphase nucleus, as well as from the potential differences in genomic organization in different sexes. Severe individual heterogeneity at the molecular level was described, in particular, in the spatial positioning of alleles of the same gene [91]. Studies in allele expression during the production of induced pluripotent stem cells revealed three groups of genes that differed in the way they coordinated their expression. They were classified as highly coordinated, semi-coordinated, or independent. Two alleles of highly coordinated genes have a similar accessibility of chromatin, enriched in such accessibility regulators as H3K4me3, H3K4me1, H3K36me3, and H3K27ac. The

genes themselves have denser binding sites with enhancers, unlike the other two variants [92].

We obtained data that suggested independent segregation of haploid sets of chromosomes in mammalian somatic cells, which could change positions relative to each other in bone marrow cell populations [93]. This finding was further confirmed by data obtained after nuclear transfer of unreplicated nuclei of somatic cells at the G0/G1 stage into the metaphase cytoplasm of enucleated murine oocytes [94]. A genome sequencing analysis revealed correct segregation of homologous chromosomes into the polar body, resulting in cells with complete haploid sets of chromosomes. This, however, occurred only in the nuclei of inbred mice and never in interstrain hybrids. This finding emphasizes the importance of sequence homology between homologs. However, the same finding might indicate that haploid sets “remember” that they used to be one. The destruction of this unity in zygotes from interlinear murine crossings may reflect the organization of the cytoskeleton and the division spindle. The process is similar to chromosome ejection from the metaphase plates of one species when obtaining interspecific hybridomas.

Thus, haploid segregation is preserved in somatic cells, which indicates another level of 3D genomic organization, where haploid sets of chromosomes behave as autonomous units.

Undifferentiated stem cells are believed to be the only ones responsible for the formation of all other cells and the cause of neoplastic transformation [95]. However, tumor cells differ from the original cells by a combination of expression of both highly specialized genes and embryonic ones, e.g., in melanomas. According to C. L. Markert, neoplastic transformation is a disease of cellular differentiation, as a result of which a tumor cell differs from a normal one by an “abnormal combination of normal components” [96]. Apparently, genetic or epigenetic changes leading to neoplastic transformation must affect the cellular mechanisms involved in the organization and change of gene expression.

Some mammal species are resistant to cancer – from such large mammals as elephants and whales to such small rodents as naked mole rats, blind mole rats, and bats [97]. Naked mole rats have early two-level contact inhibition whereas blind mole rats have adapted to hypoxia and low heparanase, an endoglycosidase enzyme that breaks down heparan sulfate, which is involved in contacts between cells and their interactions with the extracellular matrix. Other cancer-resistant species differ in the activity of genes involved in other metabolic pathways but associated with the impact on intercellular contacts and relationships with the extracellular matrix.

CONCLUSION

The genetic code is a triplet encoding of amino acid sequences of proteins. It is the basic heredity component, but it is a very small component that occupies, for example, $\leq 2\%$ nucleotides of the entire mammal genome. It contributes to phenotypic variability by

different levels of internal packaging, i.e., secondary DNA structures, e.g., hairpins, G4 quadruplexes, triplexes, packaging in nucleosomes, histone code, etc. The interactions between enhancers and promoters, DNA and proteins, DNA and RNA hybrids belong to genome organization level two. Level three is associated with loops, topologically associated domains (TAD), non-random integration, writing of mobile genetic elements in the genome, subdivision into hetero- and euchromatin compartments, autonomy of chromosome territories, interactions between TADs of different chromosomes, and a certain autonomy of haploid sets of chromosomes in diploid species. Level four usually implies the abovementioned characteristics in dynamics during ontogenesis. However, it very seldom includes factors outside the nucleus, e.g., cytoskeleton, extracellular matrix, plasma membrane, intercellular contacts, etc., which affect all other levels. CTCF is an element that unifies the levels. This architectural protein possesses evolutionary conservation; its densi-

ty is different on the loop boundaries and TADs of the nucleotide binding sites to this protein. CTCF is dynamic in the epigenetic variability of CTCF binding targets and post-transcriptional modifications. It is part of transcription and translation factories; it participates directly and indirectly in intercellular interactions with the extracellular matrix. All these features indicate that, apparently, its targets can create a certain framework for regulating gene expression. Studies in this sphere could contribute to a better understanding of phenotypic variability and yield approaches to manage it.

CONTRIBUTION

All the authors were equally involved in the manuscript and are equally responsible for any potential plagiarism.

CONFLICT OF INTEREST

The authors declared no conflict of interests regarding the publication of this article.

REFERENCES

1. Glazko VI, Kosovskiy GYu, Glazko TT. The Sources of Genome Variability as Domestication Drivers (Review). *Agricultural Biology*. 2022;57(5):832–851. (In Russ.). <https://doi.org/10.15389/agrobiology.2022.5.832rus>
2. Glazko VI, Kosovskiy GYu, Glazko TT, Fedorova LM. DNA Markers and Microsatellite Code (Review). *Agricultural Biology*. 2023;58(2):223–248. (In Russ.). <https://doi.org/10.15389/agrobiology.2023.2.223rus>
3. Choudhary MNK, Quaid K, Xing X, Schmidt H, Wang T. Widespread Contribution of Transposable Elements to The Rewiring of Mammalian 3D Genomes. *Nature Communications*. 2023;14:634. <https://doi.org/10.1038/s41467-023-36364-9>
4. Gebrie A. Transposable Elements as Essential Elements in The Control of Gene Expression. *Mobile DNA*. 2023;14:9. <https://doi.org/10.1186/s13100-023-00297-3>
5. Lawson HA, Liang Y, Wang T. Transposable Elements in Mammalian Chromatin Organization. *Nature Reviews Genetics*. 2023;24:712–723. <https://doi.org/10.1038/S41576-023-00609-6>
6. Lu JY, Chang L, Li T, Wang T, Yin Y, Zhan G, et al. Homotypic Clustering of L1 and B1/Alu Repeats Compartmentalizes the 3D Genome. *Cell Research*. 2021;31:613–630. <https://doi.org/10.1038/s41422-020-00466-6>
7. Glazko TT, Glazko GV, Kosovskiy GYu, Zybaylov VL, Glazko VI. Interphase Nucleus and Transposable Elements (Review). *Biogeosystem Technique*. 2022;(9):62–76. (In Russ.). <https://doi.org/10.13187/bgt.2022.2.62>
8. Mustafin RN. A Hypothesis about Interrelations of Epigenetic Factors and Transposable Elements in Memory Formation. *Vavilov Journal of Genetics and Breeding*. 2024;28(5):476–486. (In Russ.). <https://doi.org/10.18699/vjgb-24-54>
9. Hubert JN, Perret M, Riquet J, Demars J. Livestock Species as Emerging Models for Genomic Imprinting. *Frontiers in Cell and Developmental Biology*. 2024;12:1348036. <https://doi.org/10.3389/fcell.2024.1348036>
10. Strahl BD, Allis CD. The Language of Covalent Histone Modifications. *Nature*. 2000;403:41–45. <https://doi.org/10.1038/47412>
11. Falk M, Feodorova Y, Naumova N, Imakaev M, Lajoie BR, Leonhardt H, et al. Heterochromatin Drives Compartmentalization of Inverted and Conventional Nuclei. *Nature*. 2018;570:395–399. <https://doi.org/10.1101/244038>
12. Glaser J, Mundlos S. 3D or Not 3D: Shaping the Genome during Development. *Cold Spring Harbor Perspectives in Biology*. 2022;14:a040188. <https://doi.org/10.1101/cshperspect.a040188>
13. Gamliel A, Meluzzi D, Oh S, Jiang N, Destici E, Rosenfeld MG, et al. Long-Distance Association of Topological Boundaries Through Nuclear Condensates. *Proceedings of the National Academy of Sciences*. 2022;119(32):e2206216119. <https://doi.org/10.1073/pnas.2206216119>
14. Abnizova I, Stapel C, Boekhorst RT, Lee JTH, Hemberg M. Integrative Analysis of Transcriptomic and Epigenomic Data Reveals Distinct Patterns for Developmental and Housekeeping Gene Regulation. *BMC Biology*. 2024;22:78. <https://doi.org/10.1186/s12915-024-01869-2>


15. Gheldof N, Witwicki RM, Migliavacca E, Leleu M, Didelot G, Harewood L, *et al.* Structural Variation-Associated Expression Changes are Paralleled by Chromatin Architecture Modifications. *PLoS One*. 2013;8(11):e79973. <https://doi.org/10.1371/journal.pone.0079973>
16. Magnitov M, de Wit E. (2024) Attraction and Disruption: How Loop Extrusion and Compartmentalisation Shape the Nuclear Genome. *Current Opinion in Genetics and Development*. 2024;86:102194. <https://doi.org/10.1016/j.gde.2024.102194>
17. Logie C. The Role of CTCF-Mediated Chromatin Looping in Enhancer-Promoter Communication. In: Witzany G, editor. *Epigenetics in Biological Communication*. Springer: Cham; 2024. pp. 333–355. https://doi.org/10.1007/978-3-031-59286-7_16
18. Behrends M, Engmann O. Loop Interrupted: Dysfunctional Chromatin Relations in Neurological Diseases. *Frontiers in Genetics*. 2021;12:732033. <https://doi.org/10.3389/fgene.2021.732033>
19. Osman N, Shawky AE, Brylinski M. Exploring the Effects of Genetic Variation on Gene Regulation in Cancer in The Context Of 3D Genome Structure. *BMC Genomic Data*. 2022;23:13. <https://doi.org/10.1186/s12863-021-01021-x>
20. Mitchell AC, Bharadwaj R, Whittle C, Krueger W, Mirnics K, Hurd Y, *et al.* The Genome in Three Dimensions: A New Frontier in Human Brain Research. *Biological Psychiatry*. 2014;75(12):961–969. <https://doi.org/10.1016/j.biopsych.2013.07.015>
21. Lobanenko VV, Nicolas RH, Adler VV, Paterson H, Klenova EM, Polotskaja AV, *et al.* A Novel Sequence-Specific DNA Binding Protein Which Interacts with Three Regularly Spaced Direct Repeats of the CCCTC-Motif in the 5'-Flanking Sequence of the Chicken C-Myc Gene. *Oncogene*. 1990;5(12):1743–1753.
22. Maksimenko OG, Fursenko DV, Belova EV, Georgiev PG. CTCF As an Example of DNA-Binding Transcription Factors Containing Clusters of C₂H₂-Type Zinc Fingers. *Acta Naturae*. 2021;13(1):31–46. (In Russ.). <https://doi.org/10.32607/actanaturae.11206>
23. Del Moral-Morales A, Salgado-Albarrán M, Sánchez-Pérez Y, Wenke NK, Baumbach J, Soto-Reyes E. CTCF and Its Multi-Partner Network for Chromatin Regulation. *Cells*. 2023;12(10):1357. <https://doi.org/10.3390/cells12101357>
24. Tang X, Zeng P, Liu K, Qing L, Sun Y, Liu X, *et al.* The PTM Profiling of CTCF Reveals the Regulation of 3D Chromatin Structure by O-GlcNacylation. *Nature Communications*. 2024;15:2813. <https://doi.org/10.1038/s41467-024-47048-3>
25. Wang J, Vicente-García C, Seruggia D, Moltó E, Fernandez-Miñán A, Neto A, *et al.* MIR Retrotransposon Sequences Provide Insulators to the Human Genome. *Proceedings of the National Academy of Sciences*. 2015; 112(32):E4428–E4437. <https://doi.org/10.1073/pnas.1507253112>
26. Tian H, Luan P, Liu Y, Li G. Tet-mediated DNA Methylation Dynamics Affect Chromosome Organization. *Nucleic Acids Research*. 2024;52(4):3654–3666. <https://doi.org/10.1093/nar/gkae054>
27. Razin SV, Gavrillov AA. Non-coding RNAs in Chromatin Folding and Nuclear Organization. *Cellular and Molecular Life Sciences*. 2021;78:5489–5504. <https://doi.org/10.1007/s00018-021-03876-w>
28. Soibam B. Association between Triplex-Forming Sites of Cardiac Long Noncoding RNA *GATA6-AS1* and Chromatin Organization. *Non-coding RNA*. 2022;8(13):41. <https://doi.org/10.3390/ncrna8030041>
29. Zacco E, Broglia L, Kurihara M, Monti M, Gustincich S, Pastore A, Plath K, *et al.* RNA: The Unsuspected Conductor in the Orchestra of Macromolecular Crowding. *Chemical Reviews*. 2024;124(8):4734–4777. <https://doi.org/10.1021/acs.chemrev.3c00575>
30. Poller W, Sahoo S, Hajjar R, Landmesser U, Krichevsky AM. Exploration of the Noncoding Genome for Human-Specific Therapeutic Targets-Recent Insights at Molecular and Cellular Level. *Cells*. 2023;12(22):2660. <https://doi.org/10.3390/cells12222660>
31. Merici G, Amidani D, Dieci G, Rivetti C. A New Strategy to Investigate RNA: DNA Triplex Using Atomic Force Microscopy. *International Journal of Molecular Sciences*. 2024;25(5):3035. <https://doi.org/10.3390/ijms25053035>
32. Zhang H, Shi Z, Banigan EJ, Kim Y, Yu H, Bai XC, *et al.* CTCF and R-loops are Boundaries of Cohesin-Mediated DNA Looping. *Molecular Cell*. 2023;83(16):2856–2871. <https://doi.org/10.1016/j.molcel.2023.07.006>
33. Wulfridge P, Yan Q, Rell N, Doherty J, Jacobson S, Offley S, *et al.* G-quadruplexes Associated with R-loops Promote CTCF Binding. *Molecular Cell*. 2023;83(17):3064–3079. <https://doi.org/10.1016/j.molcel.2023.07.009>
34. Hou Y, Li F, Zhang R, Li S, Liu H, Qin ZS, Sun X. Integrative Characterization of G-Quadruplexes in the Three-Dimensional Chromatin Structure. *Epigenetics*. 2019;14(9):894–911. <https://doi.org/10.1080/15592294.2019.1621140>
35. Moindrot B, Imaizumi Y, Feil R. Differential 3D Genome Architecture and Imprinted Gene Expression: Cause or Consequence? *Biochemical Society Transactions*. 2024;52(3):973–986. <https://doi.org/10.1042/BST20230143>
36. Gómez-Redondo I, Planells B, Cánovas S, Ivanova E, Kelsey G, Gutiérrez-Adán A. Genome-wide DNA Methylation Dynamics During Epigenetic Reprogramming in The Porcine Germline. *Clinical Epigenetics*. 2021;13:27. <https://doi.org/10.1186/s13148-021-01003-x>


37. Noordermeer D, Feil R. Differential 3D Chromatin Organization and Gene Activity in Genomic Imprinting. *Current Opinion in Genetics and Development*. 2020;61:17–24. <https://doi.org/10.1016/j.gde.2020.03.004>
38. Monk, D, Mackay DJG, Eggermann T, Maher ER, Riccio A. Genomic Imprinting Disorders: Lessons on How Genome, Epigenome and Environment Interact. *Nature Reviews Genetics*. 2019;20:235–248. <https://doi.org/10.1038/s41576-018-0092-0>
39. Hubert J-N, Demars J. Genomic Imprinting in The New Omics Era: A Model for Systems-Level Approaches. *Frontiers in Genetics*. 2022;13:838534. <https://doi.org/10.3389/fgene.2022.838534>
40. MacDonald WA, Mann MRW. Long Noncoding RNA Functionality in Imprinted Domain Regulation. *PLOS Genetics*. 2020;16(8):e1008930. <https://doi.org/10.1371/journal.pgen.1008930>
41. Malnou EC, Umlauf D, Mouysset M, Cavaillé J. Imprinted MicroRNA Gene Clusters in The Evolution, Development, and Functions of Mammalian Placenta. *Frontiers in Genetics*. 2019;9:706. <https://doi.org/10.3389/fgene.2018.00706>
42. Sanli I, Feil R. Chromatin Mechanisms in the Developmental Control of Imprinted Gene Expression. *The International Journal of Biochemistry and Cell Biology*. 2015;67:139–147. <https://doi.org/10.1016/j.biocel.2015.04.004>
43. Choudhary MN, Friedman RZ, Wang JT, Jang HS, Zhuo X, Wang T. Co-opted Transposons Help Perpetuate Conserved Higher-Order Chromosomal Structures. *Genome Biology*. 2020;21:16. <https://doi.org/10.1186/s13059-019-1916-8>
44. Buckley RM, Kortschak RD, Raison JM, Adelson DL. Similar Evolutionary Trajectories for Retrotransposon Accumulation in Mammals. *Genome Biology and Evolution*. 2017;9(9):2336–2353. <https://doi.org/10.1093/gbe/evx179>
45. DiRusso JA, Clark AT. Transposable Elements in Early Human Embryo Development and Embryo Models. *Current Opinion in Genetics and Development*. 2023;81:102086. <https://doi.org/10.1016/j.gde.2023.102086>
46. Zhao P, Peng C, Fang L, Wang Z, Liu GE. Taming Transposable Elements in Livestock and Poultry: A Review of Their Roles and Applications. *Genetics Selection Evolution*. 2023;55:50. <https://doi.org/10.1186/s12711-023-00821-2>
47. Wang M, Hancock TP, Chamberlain AJ, Vander Jagt CJ, Pryce JE, Cocks BG, *et al.* Putative bovine topological association domains and CTCF binding motifs can reduce the search space for causative regulatory variants of complex traits. *BMC Genomics*. 2018;19:395. <https://doi.org/10.1101/242792>
48. Engmann O, Labonté B, Mitchell A, Bashtrykov P, Calipari ES, Rosenbluh C, *et al.* Cocaine-Induced Chromatin Modifications Associate with Increased Expression and Three-Dimensional Looping of *Auts2*. *Biological Psychiatry*. 2017;82(11):794–805. <https://doi.org/10.1016/j.biopsych.2017.04.013>
49. Szabó D, Franke V, Bianco S, Batiuk MY, Paul EJ, Kukalev A, *et al.* A Single Dose of Cocaine Rewires The 3D Genome Structure of Midbrain Dopamine Neurons. 2024. <https://doi.org/10.1101/2024.05.10.593308>
50. Tashiro S, Lanctôt C. The International Nucleome Consortium. *Nucleus*. 2015;6(2):89–92. <https://doi.org/10.1080/19491034.2015.1022703>
51. Rey-Millet M, Bystricky K. International Nucleome Consortium. The Genome in Space and Time Comes of Age. *Nucleus*. 2024;15(2):2307665. <https://doi.org/10.1080/19491034.2024.2307665>
52. Huang H, Wu Q. Pushing the TAD Boundary: Decoding Insulator Codes of Clustered CTCF Sites in 3D Genomes. *BioEssays*. 2024;46(10):2400121. <https://doi.org/10.1002/bies.202400121>
53. Sandoval-Velasco M, Dudchenko O, Rodríguez JA, Pérez Estrada C, Dehasque M, Fonsere C, *et al.* Three-Dimensional Genome Architecture Persists in a 52,000-Year-Old Woolly Mammoth Skin Sample. *Cell*. 2024;187(14):3541–3562. <https://doi.org/10.1016/j.cell.2024.06.002>
54. Chen Z, Snetkova V, Bower G, Jacinto S, Clock B, Dizhechi A, *et al.* Increased Enhancer-Promoter Interactions During Developmental Enhancer Activation in Mammals. *Nature Genetics*. 2024;56:675–685. <https://doi.org/10.1038/s41588-024-01681-2>
55. Schoenfelder S, Sexton T, Chakalova L, Cope NF, Horton A, Andrews S, *et al.* Preferential Associations between Co-Regulated Genes Reveal a Transcriptional Interactome in Erythroid Cells. *Nature Genetics*. 2010;42:53–61. <https://doi.org/10.1038/ng.496>
56. Yan Y, Tian Y, Wu Z, Zhang K, Yang R. Interchromosomal Colocalization with Parental Genes Is Linked to the Function and Evolution of Mammalian Retrocopies. *Molecular Biology and Evolution*. 2023;40(12):msad265. <https://doi.org/10.1093/molbev/msad265>
57. Pollex T, Marco-Ferreres R, Ciglar L, Ghavi-Helm Y, Rabinowitz A, Viales RR, *et al.* Chromatin Gene-Gene Loops Support the Cross-Regulation of Genes with Related Function. *Molecular Cell*. 2024;84(15):822–838. <https://doi.org/10.1016/j.molcel.2023.12.023>
58. Fudenberg G, Kelley DR, Pollard KS. Predicting 3D Genome Folding from DNA Sequence with Akita. *Nature Methods*. 2020;17:1111–1117. <https://doi.org/10.1038/s41592-020-0958-x>


59. Liu T, Zhu H, Wang Z. Learning Micro-C from Hi-C with Diffusion Models. *PLoS Computational Biology*. 2024;20(5):e1012136. <https://doi.org/10.1371/journal.pcbi.1012136>
60. Keough KC, Whalen S, Inoue F, Przytycki PF, Fair T, Deng C, et al. Three-Dimensional Genome Rewiring in Loci with Human Accelerated Regions. *Science*. 2023;380:(6643):eabm1696. <https://doi.org/10.1126/science.abm1696>
61. Braunger JM, Cammarata LV, Sornapudi TR, Uhler C, Shivashankar GV. Transcriptional Changes Are Tightly Coupled to Chromatin Reorganization During Cellular Aging. *Aging Cell*. 2024;23(3):e14056. <https://doi.org/10.1111/ace1.14056>
62. Schmitt AD, Sikkink K, Ahmed AA, Melnyk S, Reid D, Van Meter L, et al. Evaluation of Hi-C Sequencing for the Detection of Gene Fusions in Hematologic and Solid Pediatric Cancer Samples. *Cancers*. 2024;16(170):2936. <https://doi.org/10.3390/cancers16172936>
63. Glazko TT. Approaches to the Analysis of Reciprocal Chromosome Distribution in the Bone Marrow Cells of Mice. *Tsitologiya*. 1988;30(5):597–605. (In Russ.). <https://elibrary.ru/UWLSHL>
64. Righolt CH, Wiener F, Taylor-Kashton C, Harizanova J, Vermolen BJ, Garini Y, et al. Translocation Frequencies and Chromosomal Proximities for Selected Mouse Chromosomes in Primary B Lymphocytes. *Cytometry*. 2011;79A(4):276–283. <https://doi.org/10.1002/cyto.a.21038>
65. Kovalchuk AL, Kim JS, Janz S. *Emu/Su* Transposition into *Myc* is Sometimes a Precursor for T(12;15) Translocation in Mouse B Cells. *Oncogene*. 2003;22:2842–2850. <https://doi.org/10.1038/sj.onc.1206345>
66. McStay B. Nucleolar Organizer Regions: Genomic ‘Dark Matter’ Requiring Illumination. *Genes Development*. 2016;30:1598–1610. <https://doi.org/10.1101/gad.283838.116>
67. Monahan K, Schieren I, Cheung J, Mumbey-Wafula A, Monuki ES, Lomvardas S. Cooperative Interactions Enable Singular Olfactory Receptor Expression in Mouse Olfactory Neurons. *Elife*. 2017;6:e28620. <https://doi.org/10.7554/eLife.28620>
68. Gamliel A, Meluzzi D, Oh S, Jiang N, Destici E, Rosenfeld MG, et al. Long-distance association of Topological Boundaries Through Nuclear Condensates. *Proceedings of the National Academy of Sciences*. 2022;119:320:e2206216119. <https://doi.org/10.1073/pnas.2206216119>
69. Ozery-Flato M, Linhart C, Trakhtenbrot L, Israeli S, Shamir R. Large-Scale Analysis of Chromosomal Aberrations in Cancer Karyotypes Reveals Two Distinct Paths to Aneuploidy. *Genome Biology*. 2011;12:R61. <https://doi.org/10.1186/gb-2011-12-6-r61>
70. Maass PG, Barutcu AR, Weiner CL, Rinn JL. Inter-chromosomal Contact Properties in Live-Cell Imaging and in Hi-C. *Molecular Cell*. 2018;69(15):1039–1045. <https://doi.org/10.1016/j.molcel.2018.02.007>
71. Maass PG, Barutcu AR, Rinn JL. Interchromosomal Interactions: A Genomic Love Story of Kissing Chromosomes. *Journal of Cell Biology*. 2019;218(1):27–38. <https://doi.org/10.1083/jcb.201806052>
72. Roller M, Stamper E, Villar D, Izuogu O, Martin F, Redmond AM, et al. LINE Retrotransposons Characterize Mammalian Tissue-Specific and Evolutionarily Dynamic Regulatory Regions. *Genome Biology*. 2021;22:62. <https://doi.org/10.1186/s13059-021-02260-y>
73. James C, Trevisan-Herraz M, Juan D, Rico D. Evolutionary Analysis of Gene Ages Across Tads Associates Chromatin Topology with Whole-Genome Duplications. *Cell Reports*. 2024;43(4):113895. <https://doi.org/10.1016/j.celrep.2024.113895>
74. Fernandez MK, Sinha M, Zidan M, Renz M. Nuclear Actin Filaments – a Historical Perspective. *Nucleus*. 2024;15(1):2320656. <https://doi.org/10.1080/19491034.2024.2320656>
75. Venit T, Xie X, Percipalle P. Actin in the Cell Nucleus. In: Victor JM, editor. *Nuclear Architecture and Dynamics*. Boston: Academic Press; 2018. p 345–367.
76. Mahmood SR, Xie X, Hosny El Said N, Venit T, Gunsalus KC, Percipalle P. β -actin Dependent Chromatin Remodeling Mediates Compartment Level Changes in 3D Genome Architecture. *Nature Communications*. 2021;12:5240. <https://doi.org/10.1038/s41467-021-25596-2>
77. Wollscheid HP, Ulrich HD. Chromatin Meets the Cytoskeleton: The Importance of Nuclear Actin Dynamics and Associated Motors for Genome Stability. *DNA Repair*. 2023;131:103571. <https://doi.org/10.1016/j.dnarep.2023.103571>
78. Sen B, Xie Z, Thomas MD, Pattenden SG, Howard S, McGrath C, et al. Nuclear Actin Structure Regulates Chromatin Accessibility. *Nature Communications*. 2024;15:4095. <https://doi.org/10.1038/s41467-024-48580-y>
79. Zhuo L, Stöckl JB, Fröhlich T, Moser S, Vollmar AM, Zahler S. A Novel Interaction of Slug (SNAI2) and Nuclear Actin. *Cells*. 2024;13(8):696. <https://doi.org/10.3390/cells13080696>
80. Marshall-Burghardt S, Migueles-Ramírez RA, Lin Q, El Baba N, Saada R, Umar M, Mavalwala K, et al. Excitable Rho Dynamics Control Cell Shape and Motility by Sequentially Activating ERM Proteins and Actomyosin Contractility. *Science Advances*. 2024;10(36):eadn6858. <https://doi.org/10.1126/sciadv.adn6858>

81. Chiu K, Berrada Y, Eskndir N, Song D, Fong C, Naughton S, *et al.* CTCF is Essential for Proper Mitotic Spindle Structure and Anaphase Segregation. *Chromosoma*. 2024;133:183–194. <https://doi.org/10.1007/s00412-023-00810-w>
82. Kaczmarczyk LS, Levi N, Salmon-Divon M, Gerlitz G. The CTCF-H3K27me3 Axis Supports Melanoma Cell Migration by Repressing Cholesterol Biosynthesis. 2023. <https://doi.org/10.1101/2023.02.23.529650>
83. Lee K, Nelson CM. New Insights into The Regulation of Epithelial-Mesenchymal Transition and Tissue Fibrosis. *International Review of Cell and Molecular Biology*. 2012;294:171–221. <https://doi.org/10.1016/B978-0-12-394305-7.00004-5>
84. Andrianto A, Sudiana IK, Suprabawati DGA. α -Smooth Muscle Actin as Predictors of Early Recurrence in Early-Stage Ductal Type Breast Cancer After Mastectomy and Chemotherapy. *Iranian Journal Pathology*. 2024;19(1):67–74. <https://doi.org/10.30699/ijp.2023.2004468.3126>
85. Doll S, Freitas FP, Shah R, Aldrovandi M, da Silva MC, Ingold I, *et al.* FSP1 is a glutathione-independent ferroptosis suppressor. *Nature*. 2019;575:693–698. <https://doi.org/10.1038/s41586-019-1707-0>
86. Chao S, Yan H, Bu P. Asymmetric Division of Stem Cells and its Cancer Relevance. *Cell Regeneration*. 2024;13:5. <https://doi.org/10.1186/s13619-024-00188-9>
87. Baker SG, Soto AM, Sonnenschein C, Cappuccio A, Potter JD, Kramer BS. Plausibility of Stromal Initiation of Epithelial Cancers Without a Mutation in The Epithelium: A Computer Simulation of Morphostats. *BMC Cancer*. 2009;9:89. <https://doi.org/10.1186/1471-2407-9-89>
88. Zhu S, Wang J, Zellmer L, Xu N, Liu M, Hu Y, *et al.* Mutation or Not, What Directly Establishes a Neoplastic State, Namely Cellular Immortality and Autonomy, Still Remains Unknown and Should Be Prioritized in Our Research. *Journal of Cancer*. 2022;13(9):2810–2843. <https://doi.org/10.7150/jca.72628>
89. Berenblum I, Shubik P. An Experimental Study of The Initiating State of Carcinogenesis, and a Re-Examination of The Somatic Cell Mutation Theory of Cancer. *British Journal of Cancer*. 1949;3(1):109–118. <https://doi.org/10.1038/bjc.1949.13>
90. Foulds L. Multiple etiologic factors in neoplastic development. *Cancer Research*. 1965;25(8):1339–1347.
91. Finn EH, Pegoraro G, Brandão HB, Valton AL, Oomen ME, Dekker J, *et al.* Extensive Heterogeneity and Intrinsic Variation in Spatial Genome Organization. *Cell*. 2019;176(6):1502–1515. <https://doi.org/10.1016/j.cell.2019.01.020>
92. Ayyamperumal P, Naik HC, Naskar AJ, Bammidi LS, Gayen S. Epigenomic States Contribute to Coordinated Allelic Transcriptional Bursting in iPSC reprogramming. *Life Science Alliance*. 2024;7(4):e202302337. <https://doi.org/10.26508/lsa.202302337>
93. Glazko TT, Glazko VI. Segregation Of Haploid Sets of Chromosomes in Diploid Cells of a Number of Mammalian Species. *Cifra. Biology*. 2024;2:2. (In Russ.). <https://doi.org/10.60797/BIO.2024.2.1>
94. Mikhachenko A, Gutierrez NM, Frana D, Safaei Z, Van Dyken C, Li Y, *et al.* Induction of Somatic Cell Haploidy by Premature Cell Division. *Science Advances*. 2024;10(10):eadk9001. <https://doi.org/10.1126/sciadv.adk9001>
95. Cho CJ, Brown JW, Mills JC. Origins of Cancer: Ain't It Just Mature Cells Misbehaving? *EMBO Journal*. 2024;43(13):2530–2551.
96. Markert CL. Neoplasia: a disease of cell differentiation. *Cancer Research*. 1968;28(9):1908–1914.
97. Trivedi DD, Dalai SK, Bakshi SR. The Mystery of Cancer Resistance: A Revelation Within Nature. *Journal of Molecular Evolution*. 2023;91:133–155. <https://doi.org/10.1007/s00239-023-10092-6>

ORCID IDs

Tatiana T. Glazko  <https://orcid.org/0000-0002-3879-6935>

Gleb Yu. Kosovsky  <https://orcid.org/0000-0003-3808-3086>

Valeriy I. Glazko  <https://orcid.org/0000-0002-8566-8717>

GUIDE FOR AUTHORS FORMATTING REQUIREMENTS FOR ARTICLES

We publish original, previously unpublished English language articles that possess scientific novelty in the field of food industry and related branches of science. The Journal publishes scientific papers, peer reviews, brief scientific communications, letters to the editor, and related news items.

The main requirements for submitted articles are: validity of factual material, clarity and brevity, reproducibility of experimental data. The manuscript should meet the specified formatting standards. Please make sure that the section "Results and discussion" of your article states the novelty of your research.

All manuscripts submitted to the *Foods and Raw Materials* should be written in US English. The manuscript should contain no less than 10 pages in Microsoft Word text editor, abstract, tables, figures, and references included.

Format instructions

- 20 mm margins;
- single line spacing without automatic hyphenation;
- no extra interspaces between words or gaps between paragraphs;
- Times New Roman, size 10.

Structure

(1) **The type of your manuscript** should be clarified in the upper left corner (scientific article, review article, short message, note or letter, etc).

(2) **Title** (< 10 words) should be informative and reflect the main results of the research. The title of the article should be in lowercase letters, with the exception of the first letter and proper names. Please avoid abbreviations.

(3) **First and last names of the authors** are separated by commas. Paternal and middle names should be contracted to the first letter. Spelling should coincide with your ORCID id. Please mark the name of the author responsible for correspondence with an asterisk*.

(4) **Affiliation** is a formal name of the institution, city, postal address with postal code. The names and locations of institutions or companies should be given for all authors. If several institutions are listed, match the institution and the corresponding author with superscript numbers. Please include the e-mail address of the author responsible for correspondence.

(5) **Abstract** (200–250 words) cannot exceed 2000 characters with spaces. The abstract should be original and completely reflect the main results and novelty of the article. The best way to structure your abstract is to let it follow the structure of the article itself: relevance, tasks and objectives, methods, results, and conclusions. Please avoid meaningless introductory phrases and vague, general statements.

(6) **Keywords** provide < 10 keywords identifying the subject and the result of the research. Remember that it is key words that enable your potential readers to find your article on the Internet.

(7) **Introduction** gives a brief review of the publications related to the matter and proves its relevance. Referenced sources should be indexed in international scientific databases. In-text references should be given in square brackets and numbered [beginning with №1] in order of their appearance in the text. If several sources are quoted, they are given in chronological order. Make sure your introduction reflects the objectives of your research.

(8) Study objects and methods:

– Experimental research papers should contain a full description of the subject of the study, consecutive stages of the experiment, equipment, and reagents. Do not forget to specify the original company names of equipment and reagents manufacturers in brackets. If the method you use is not widely known or has been considerably modified, please provide a brief description.

– Theoretical research papers should specify objectives, approximations and assumptions, conclusions and equations. Please do not overload your text with intermediate data and description of well-known methods (such as numerical methods of solving equations) unless you have introduced some novelty into them.

(9) **Results and discussion** should provide a concise description of experimental data. Rather than repeating the data given in tables and graphs, the text should seek to reveal the principles detected. While describing your research results, it is recommended to use the Past Indefinite verb tense. The discussion should not reiterate the results. The discussion should contain an interpretation of the obtained research results (compliance of the results with the research hypothesis, generalisation of the research results, suggestions for practical application and future research).

Each **table** should be made in MS Word (Table – Add Table) or MS Excel and contain no less than three columns. Provide a number and a title for each table.

The Journal publishes color photographs and diagrams.

Mathematical equations should start with a separate line and be typed in the MathType frame as a whole. Mind that it is not allowed to compile formulae from composite elements (e.g. one part of the formula is a table, another part is a text, and some other part is an embedded frame). Please maintain the common settings for fonts, the size of characters and their placement in MathType formulas. Please avoid manual change for individual symbols or formula elements.

(10) **Conclusion** briefly summarises the main results of your research. Naturally, the conclusion should contain the answer to the question posed by the introduction.

(11) **Contribution** should indicate the actual contribution of each author in the research process. *Foods and Raw Materials* observes the CRediT taxonomy of the authors' contributions.

(12) **Conflict of interest** should indicate a real or potential conflict of interest. If there is no conflict of interests, you should write that "the author declares that there is no conflict of interest".

(13) **Acknowledgements** contains expression of gratitude to those who contributed to the research.

(14) **Funding** indicates how the research and the publication of this article were funded. If the study was performed with the support of a grant, specify the number of the grant and its name. State the name of your employer if the study was performed as part of your routine work and did not receive additional funding.

(15) **References** should be formatted according to the standard defined by the editors. The references are given in the order of their appearance in the text. Make sure you have included the DOI, if available.

Please avoid references to publications that are not readily available, e.g. institutional regulations, state standards, technical requirements, unpublished works, proceedings of conferences, extended abstracts of dissertation, and dissertations. Make sure you do not cite unpublished articles. It is not recommended to use more than three references to web resources. Please avoid citing publications that are more than 10 years old.

Self-citation should be well-justified and cannot exceed 10% of the references. Please make sure that at least 50% of the works you cite are less than 5 years old and published in periodicals registered in such data bases as Scopus, Web of Science, etc.

If you mention no references to fresh, 2–3-year-old papers, it might reduce your chances for publication. The references should reflect the actual impact of representatives of the international scientific community on the issue.

The manuscript should be carefully checked and signed by all authors on the first page of the main text. The article will not be published if it fails to meet the requirements. All articles are subject to general editing.

Correspondence and submission of all documents is done by e-mail: fjournal@mail.ru or www.jfrm.ru/en

The editors expect to receive the following documents, in Russian or English:

(1) an e-version of your article in MS Word named by the first author's last name (e.g. SmithJ.doc).

(2) a scanned PDF version of your article, the first page signed by all the authors (SmithJ.pdf);

(3) a form with personal information about the author(s). Please do not forget to mark the name of the author responsible for correspondence with an asterisk*. Name the file by the first author's name, e.g., SmithJ_Form.doc;

(4) a scanned PDF version of a cover letter to the editor-in-chief from the responsible organisation with the conclusion about the relevance of the research and recommendations for its publishing. The document should contain the date, reference number, and the signature of the head of the organisation;

(5) a standard copyright agreement.

Please mind that all the files should contain a single document.

For submission instructions, subscription and all other information visit this journals online at jfrm.ru/en/

CONTENTS

Editor's column.....	ii
Reshetnik Ekaterina I., Griбанova Svetlana L., Derzhapolskaya Yulia I., Li Chun, Liu Libo, Zhang Guofang, Korneva Nadezhda Yu., Shkolnikov Pavel N. Fermented buttermilk drinks fortified by plant raw materials.....	211
Velichkovich Natalia S., Dunchenko Nina I., Stepanova Anna A., Kozlova Oksana V., Faskhutdinova Elizaveta R., Yustratov Vladimir P., Luzyanin Sergey L. The phytochemical composition of Kuzbass medicinal plants studied by spectrophotometry and chromatography.....	219
Budianto, Suparmi Anik, Susanti Dewi Optimizing the utilization of pomelo (<i>Citrus maxima</i> (Brum.) Merr.) seeds as a quality dietary fiber.....	233
Daiaeddine Mohamed Jibril, Badrouss Sara, Harti Abderrazak El, Bachaoui El Mostafa, Biniz Mohamed, Mouncif Hicham UAV imagery, advanced deep learning, and YOLOv7 object detection model in enhancing citrus yield estimation.....	242
Matbo Atefeh, Ghanbari Mohammad Mehdi, Sekhavatizadeh Seyed Saeed, Nikkha Mehdi Stabilizing fish oil during storage with <i>Satureja bachtiarica</i> Bunge.....	254
Maurice Bilung Lesley, Radzi Ernie Suhaiza, Tahar Ahmad Syatir, Zulharnain Azham, Ngu Romano, Apun Kasing BOX-PCR and ERIC-PCR evaluation for genotyping Shiga toxin-producing <i>Escherichia coli</i> and <i>Salmonella enterica</i> serovar Typhimurium in raw milk.....	264
Mohamed Rasha K., Ahmed Zahra S., Abozed Safaa S. Multi-objective development of novel egg free cakes using quinoa protein and its quality attributes.....	276
Aksu Muhammet Irfan, Halil İbrahim Erkovan, Sule Erkovan Ultra-high-pressure homogenization in chicory root juice production.....	287
Barzkar Noora, Sukhikh Stanislav A., Zhikhreva Anastasiia V., Cheliubeeva Elizaveta Yu., Kapitonova Anastasia I., Malkov Danil I., Babich Olga O., Kulikova Yuliya V. <i>Aurelia aurita</i> jellyfish collagen: Recovery properties.....	296
Jovanović-Cvetković Tatjana, Savić Aleksandar, Topalić-Trivunović Ljiljana, Velemir Ana, Grbić Rada Red wines from the Mostar area: Physicochemical, antioxidative, and antimicrobial properties.....	306
Albay Zehra, Çelebi Mehmet, Şimşek Bedia Physicochemical, rheological, and microbiological properties of honey-fortified probiotic drinkable yogurt.....	320
Murillo Vázquez Rosa Nallely, Pacheco Moisés Fermín Paul, Nardello-Rataj Verónica, Carbajal Arizaga Gregorio Lycopene from tomato biomass: Extraction and stabilization.....	330
Andreeva Oksana I., Shorstkii Ivan A. Innovative physical techniques in freeze-drying.....	341
Thu Le Minh, Thuan Nguyen Ngoc, Nguyen Luu Thao, Mai Dam Sao, Phuong Do Viet Extraction methods: Effects on the contents of bioactive compounds and anti-oxidant activity of <i>Coriopsis aspera</i> mycelia.....	355
Kaledin Anatoly P., Malovichko Lyubov V., Rezanov Alexander G., Drozdova Lyudmila S., Kentbaeva Botagoz A. Autumn and winter diet of wood pigeon (<i>Columba palumbus</i>) in the Central Ciscaucasia.....	366
Serazetdinova Yuliya R., Chekushkina Darya Yu., Borodina Ekaterina E., Kolpakova Daria E., Minina Varvara I., Altshuler Olga G., Asyakina Lyudmila K. Synergistic interaction between <i>Azotobacter</i> and <i>Pseudomonas</i> bacteria in a growth-stimulating consortium.....	376
Essa Rowida Y., Elsebaie Essam M., Abdelrhman Wesam M., Badr Mohamed R. Barnûf leaves: antioxidant, antimicrobial, antidiabetic, anti-obesity, antithyroid, and anticancer properties.....	394
Glazko Tatiana T., Kosovskiy Gleb Yu., Glazko Valeriy I. Spatial genomic codes.....	409